frontiers | Research Topics

A new frontier for traditional medicine research - multi-omics approaches

Edited by
Xian-Jun Fu, Kah Keng Wong and Yiider Tseng

Published in
Frontiers in Pharmacology

ISSN 1664-8714
ISBN 978-2-8325-2511-1
DOI 10.3389/978-2-8325-2511-1

About Frontiers

Frontiers is more than just an open access publisher of scholarly articles: it is a pioneering approach to the world of academia, radically improving the way scholarly research is managed. The grand vision of Frontiers is a world where all people have an equal opportunity to seek, share and generate knowledge. Frontiers provides immediate and permanent online open access to all its publications, but this alone is not enough to realize our grand goals.

Frontiers journal series

The Frontiers journal series is a multi-tier and interdisciplinary set of open-access, online journals, promising a paradigm shift from the current review, selection and dissemination processes in academic publishing. All Frontiers journals are driven by researchers for researchers; therefore, they constitute a service to the scholarly community. At the same time, the *Frontiers journal series* operates on a revolutionary invention, the tiered publishing system, initially addressing specific communities of scholars, and gradually climbing up to broader public understanding, thus serving the interests of the lay society, too.

Dedication to quality

Each Frontiers article is a landmark of the highest quality, thanks to genuinely collaborative interactions between authors and review editors, who include some of the world's best academicians. Research must be certified by peers before entering a stream of knowledge that may eventually reach the public - and shape society; therefore, Frontiers only applies the most rigorous and unbiased reviews. Frontiers revolutionizes research publishing by freely delivering the most outstanding research, evaluated with no bias from both the academic and social point of view. By applying the most advanced information technologies, Frontiers is catapulting scholarly publishing into a new generation.

What are Frontiers Research Topics?

Frontiers Research Topics are very popular trademarks of the *Frontiers journals series*: they are collections of at least ten articles, all centered on a particular subject. With their unique mix of varied contributions from Original Research to Review Articles, Frontiers Research Topics unify the most influential researchers, the latest key findings and historical advances in a hot research area.

Find out more on how to host your own Frontiers Research Topic or contribute to one as an author by contacting the Frontiers editorial office: frontiersin.org/about/contact

A new frontier for traditional medicine research - multi-omics approaches

Topic editors

Xian-Jun Fu — Shandong University of Traditional Chinese Medicine, China

Kah Keng Wong — Universiti Sains Malaysia Health Campus, Malaysia

Yiider Tseng — Shandong University of Traditional Chinese Medicine, China

Citation

Fu, X.-J., Wong, K. K., Tseng, Y., eds. (2023). *A new frontier for traditional medicine research - multi-omics approaches*. Lausanne: Frontiers Media SA. doi: 10.3389/978-2-8325-2511-1

Table of contents

frontiers | Frontiers in Pharmacology

TYPE Editorial
PUBLISHED 09 May 2023
DOI 10.3389/fphar.2023.1203097

OPEN ACCESS

EDITED BY
Javier Echeverria,
University of Santiago, Chile

REVIEWED BY
Adolfo Andrade-Cetto,
National Autonomous University of Mexico, Mexico

*CORRESPONDENCE
Xianjun Fu,
xianxiu@hotmail.com

RECEIVED 10 April 2023
ACCEPTED 26 April 2023
PUBLISHED 09 May 2023

CITATION
Fu X, Wong KK and Tseng Y (2023), Editorial: A new frontier for traditional medicine research—Multi-omics approaches.
Front. Pharmacol. 14:1203097.
doi: 10.3389/fphar.2023.1203097

Editorial: A new frontier for traditional medicine research—Multi-omics approaches

Xianjun Fu[1,2]*, Kah Keng Wong[3] and Yiider Tseng[1]

[1]Shandong University of Traditional Chinese Medicine, Jinan, China, [2]Qingdao Key Laboratory of Research in Marine Traditional Chinese Medicine, Shandong University of Traditional Chinese Medicine Qingdao Academy of Traditional Chinese Medicine, Qingdao, China, [3]Universiti Sains Malaysia, School of Medical Sciences, Kota Bharu, Malaysia

KEYWORDS

traditional medicine, multi-omics approaches, TCM syndrome, therapeutic mechanism of TCM, biological processes

Editorial on the Research Topic
A new frontier for traditional medicine research—Multi-omics approaches

Traditional medicine accumulates cultural theories, beliefs, and experiences that are unique to different populations, whether scientifically explicable or not. It is used in the maintenance of health as well as in the prevention, diagnosis, improvement, or treatment of physical and mental illness (Che, et al., 2017). However, the lack of scientific exploration, empirical diagnosis, and rigorous therapeutic strategy hinders greater access to better understanding these healthcare services (Patwardhan and Patwardhan, 2005). To address these issues, multi-omics experimental designs analyze pharmacological action and biological mechanisms at the molecular level by integrating multiple omics such as the genome, transcriptome, proteome, metabolome, epigenome, and microbiome, thus shifting the paradigm of "single omic" research (Menyhárt and Gyorffy, 2021). Multi-omics provides a powerful approach to gathering further hereditary information of the organism and illustrating a wide range of biological phenomenon, such as identifying the bioactive components, action targets and biological pathways of various traditional Chinese medicine. This integration of modern scientific insights with the role of traditional Chinese medicine in a variety of diseases, including cardiovascular diseases, infectious diseases, metabolic diseases, and neurodegenerative diseases, (Zhu et al.).

In this Research Topic, we have collected twelve research papers and review articles focusing on multi-omics research related traditional Chinese medicine to biological mechanisms, and the complex biological processes in traditional therapies.

This Research Topic comprises a variety of article types, including animal experiments (6 papers), clinical research (2 papers), reviews (2 papers), meta-analysis (1 paper), and comparative metabolic profiling and its substituents in traditional Chinese medicine (1 paper). The related Multi-Omics Approaches range from proteomics to metabolomics, intestinal microbiomics, and lipomics. These articles cover diseases such as COVID-19, cardiomyopathy, triple-negative breast cancer, depression, fatty liver related to metabolic dysfunction, coronary heart disease, chronic liver disease, and stroke. Traditional Chinese Medicine (TCM) syndromes, such as phlegm stasis and damp heat, as well as research on toxicity and metabolic substances of TCM, are also included. The 108 authors who contributed to these papers are from 43 institutes located in China.

Six contributions in this Research Topic focus on the effect of traditional Chinese medicine on different diseases using a multi-omics research approach. The first two contributions address depression. Qiao et al. evaluated the effects of Tibetan medicine, metacinnabar (β-HgS) combined with imipramine or sertraline (SER) on depression-like symptoms in mice. They revealed that β-HgS promotes the antidepressant effect of SER on depression-like behavior in mice by promoting glucocorticoid receptor (GR) expression and neuronal proliferation in key hippocampal subregions. Liang et al. evaluated the antidepressant efficacy of Yang-Xin-Jie-Yu Decoction (YXJYD) in a chronic unpredictable mild stress (CUMS)-induced depression rat model and investigated the underlying mechanisms by using metabolomics and intestinal microbiomics methods. They identified the pathway of the tricarboxylic acid cycle (TCA cycle) and propanoate metabolism as the regulated target of YXJYD on host-microbiome interaction. He et al. found that *Poria cocos* extract can affect metabolic dysfunction-associated fatty liver disease via the FXR/PPARα-SREBPs pathway. Wang et al. presented a study revealing that Dandelion extract inhibits triple-negative breast cancer cell proliferation by interfering with glycerophospholipids and unsaturated fatty acids metabolism. Liu et al. revealed that astragaloside IV significantly promotes pharmacological effect of *Descurainia sophia* seeds on isoproterenol-induced cardiomyopathy in rats by complementarily reversing myosin motor MYH6/7, and further downregulating NPPA and MYL4. Chien et al. presented a systematic review and meta-analysis of randomized controlled trials about the therapeutic effects of herbal-medicine combined therapy for COVID-19.

Three contributions focus on using the multi-omics research approach to explore the biological basis of TCM syndrome. Yang et al.revealed that coronary heart disease with phlegm and blood stasis syndrome is characterized by low levels of FOS, AP-1, CCL2, CXCL8, and JNK1, and elevated levels of PTGS2 and CSF1 by using a strategy that integrated RNA-seq, DIA-based proteomics, and untargeted metabolomics on 90 clinical samples. Pan et al.found distinct common signatures of gut microbiota associated with damp-heat syndrome, a status of disharmony that often occurs when dampness binds with heat evil, in patients with different chronic liver diseases. Liu et al. summarized and highlighted the latest significant progress in the crucial value of applying multi-omics approaches to reveal TCM syndromes of stroke in a new horizon.

Two contributions focus on the toxicity and metabolic substances of TCM. Miao et al. revealed novel insights into the mechanism of hepatotoxicity induced by *Tripterygium wilfordii* multiglycoside in mice via proteomics analysis and demonstrate that the gut-liver axis may play a vital role in the progression of *Tripterygium wilfordii* multiglycoside-induced hepatotoxicity. Guo et al. comprehensively profiled the metabolites in wild Chinese Cordyceps species from Naqu (NCs) and Yushu (YCs) and their substituents including artificially cultivated Cordyceps species (CCs) and mycelia, by using liquid chromatography-tandem mass spectrometry (LC-MS/MS)-based metabolomics analysis. They analyzed quantitatively seventy amino acid-relevant metabolites in four samples for the first time.

The remaining contribution, Zhu et al. presented a review of multi-omics approaches for an in-depth understanding of the therapeutic mechanism of TCM. They evaluated and compared several TCM databases for storing multi-omics data in terms of completeness and reliability.

As a summary, we believe that the papers we have collected contain a wide range of multiple-omics methods which can help us systematically understand the biological basis of TCM syndromes, the mechanisms by which TCM treats diseases, as well as the spectrum-effect relationship of TCM components.

Author contributions

The initial idea of and concept of this Research Topic originated from XF. The discussions among the guest editors lead to the maturation of the ideas for this Research Topic. XF drafted the initial version of this editorial. All authors contributed to the writing process of the editorial and approved the final version.

Acknowledgments

We thank the various authors for submitting their work to this Research Topic and the reviewers who agreed to review individual contributions.

Conflict of interest

The authors declare that the research was conducted in the absence of any commercial or financial relationships that could be construed as a potential conflict of interest.

Publisher's note

References

Che, C. T., George, V., Ijinu, T. P., Pushpangadan, P., and Andrae-Marobela, K. (2017). "Traditional medicine," in *Pharmacognosy* (Cambridge: Academic Press).

Menyhárt, O., and Győrffy, B. (2021). Multi-omics approaches in cancer research with applications in tumor subtyping, prognosis, and diagnosis. *Comput. Struct. Biotechnol. J.* 19, 949–960. doi:10.1016/j.csbj.2021.01.009

Patwardhan, B., and Partwardhan, A. (2005). *Traditional medicine: Modern approach for affordable global health*. Switzerland: World Health Organization.

frontiers | Frontiers in Pharmacology

TYPE Original Research
PUBLISHED 11 August 2022
DOI 10.3389/fphar.2022.939483

OPEN ACCESS

EDITED BY
Kah Keng Wong,
Universiti Sains Malaysia Health Campus, Malaysia

REVIEWED BY
Gobinath Shanmugam,
University of Alabama at Birmingham, United States
Meili Lu,
Jinzhou Medical University, China
Lamiaa A. Ahmed,
Cairo University, Egypt

*CORRESPONDENCE
Qun Luo,
qunluo@iccas.ac.cn
Shijun Wang,
wsj@sdutcm.edu.cn
Fuyi Wang,
fuyi.wang@iccas.ac.cn

†These authors have contributed equally to this work

SPECIALTY SECTION
This article was submitted to Ethnopharmacology, a section of the journal Frontiers in Pharmacology

RECEIVED 09 May 2022
ACCEPTED 12 July 2022
PUBLISHED 11 August 2022

CITATION
Liu X, Chen Q, Ji X, Yu W, Wang T, Han J, Li S, Liu J, Zeng F, Zhao Y, Zhang Y, Luo Q, Wang S and Wang F (2022), Astragaloside IV promotes pharmacological effect of Descurainia sophia seeds on isoproterenol-induced cardiomyopathy in rats by synergistically modulating the myosin motor. *Front. Pharmacol.* 13:939483. doi: 10.3389/fphar.2022.939483

Astragaloside IV promotes pharmacological effect of *Descurainia sophia* seeds on isoproterenol-induced cardiomyopathy in rats by synergistically modulating the myosin motor

Xingkai Liu[1,2†], Qian Chen[3†], Xuming Ji[4†], Wanchen Yu[3], Tong Wang[3], Juanjuan Han[1], Shumu Li[1], Jianan Liu[1], Fangang Zeng[5], Yao Zhao[1], Yanyan Zhang[1], Qun Luo[1,2*], Shijun Wang[3*] and Fuyi Wang[1,2,3*]

[1]Beijing National Laboratory for Molecular Sciences, CAS Research/Education Center for Excellence in Molecular Sciences, National Centre for Mass Spectrometry in Beijing, CAS Key Laboratory of Analytical Chemistry for Living Biosystems, Institute of Chemistry, Chinese Academy of Sciences, Beijing, China, [2]University of Chinese Academy of Sciences, Beijing, China, [3]College of Traditional Chinese Medicine, Shandong University of Traditional Chinese Medicine, Jinan, China, [4]Academy of Chinese Medical Science, School of Basic Medical Science, Zhejiang Chinese Medical University, Hangzhou, China, [5]School of Environment and Natural Resources, Renmin University of China, Beijing, China

Descurainia sophia seeds (DS), *Astragalus mongholicus* (AM), and their formulas are widely used to treat heart failure caused by various cardiac diseases in traditional Chinese medicine practice. However, the molecular mechanism of action of DS and AM has not been completely understood. Herein, we first used mass spectrometry coupled to UPLC to characterize the chemical components of DS and AM decoctions, then applied MS-based quantitative proteomic analysis to profile protein expression in the heart of rats with isoproterenol-induced cardiomyopathy (ISO-iCM) before and after treated with DS alone or combined with AM, astragaloside IV (AS4), calycosin-7-glucoside (C7G), and Astragalus polysaccharides (APS) from AM. We demonstrated for the first time that DS decoction alone could reverse the most of differentially expressed proteins in the heart of the rats with ISO-iCM, including the commonly recognized biomarkers natriuretic peptides (NPPA) of cardiomyopathy and sarcomeric myosin light chain 4 (MYL4), relieving ISO-iCM in rats, but AM did not pronouncedly improve the pharmacological efficiency of DS. Significantly, we revealed that AS4 remarkably promoted the pharmacological potency of DS by complementarily reversing myosin motor MYH6/7, and further downregulating NPPA and MYL4. In contrast, APS reduced the efficiency of DS due to upregulating NPPA and MYL4. These findings not only provide novel insights to better understanding in the combination principle of traditional Chinese medicine but also highlight the power of mass

spectrometric proteomics strategy combined with conventional pathological approaches for the traditional medicine research.

KEYWORDS

astragaloside IV, cardiomyopathy, myosin, quantitative proteomics, *Descurainia sophia* seed, traditional Chinese medicine

Introduction

Cardiomyopathy is one of the leading causes of heart failure, and dilated cardiomyopathy (DCM) and hypertrophic cardiomyopathy (HCM) are the two most common cardiomyopathies (Yamada and Nomura, 2021). HCM is a genetic disease, to which hundreds of mutations in genes encoding cardiac myosin and sarcomere-related proteins are linked (Lehman et al., 2022). However, various factors, such as ischemia, viral infection, and alcohol toxicity, could cause DCM, though the variants in genes encoding sarcomeric proteins, for example, myosin heavy chain-β and -α (*MYH7* and *MYH6*), and the myosin light chain *MYL2* were also implicated in DCM (Kamisago et al., 2000; Yuan et al., 2018). Sarcomeric myosins act as the molecular accelerator/brake, modulating cardiac contractility (Daniels et al., 2021). The inherited HCM and DCM are both attributable to pathogenic variants in the myosin motor, which alters the proportion of the myosin accelerator and brake (Daniels et al., 2021). Therefore, directly targeting sarcomere in genetic cardiomyopathies has been thought to be a root-eradicating strategy for the treatment of these diseases without side effects on other organs. Both myosin activators and inhibitors have been developed and shown great promise for therapeutics of HCM and/or DCM (Lehman et al., 2022). For example, danicamtiv, a promising cardiac myosin activator, also known as MYK-491, was reported to selectively promote cardiac actomyosin activity by increasing myosin head availability and phosphate release rates (Shen et al., 2021), reversing respective contractile disordered in engineered heart tissue models of HCM and DCM (Halder et al., 2021). In contrast, mavacamten, a myosin inhibitor, also known as MYK-461, was shown to reduce sarcomere contractility in HCM by binding to myosin and decreasing phosphate release rates (Anderson et al., 2018; Lehman et al., 2022).

Traditional Chinese medicines (TCMs) have been used for long time to treat cardiac diseases including DCM and HCM (Yu et al., 2019; Li et al., 2020; Tan et al., 2020). Among them, *Descurainia sophia* seeds (DS; Brassicaceae; *Descurainia sophia* (L.) Webb ex Prantl. seed) and *Astragalus mongholicus Bunge* (AM; Leguminosae*; Astragalus mongholicus Bunge* radix) and their combination are widely used to treat heart failure caused by various cardiac diseases (Ma et al., 1998; Chen et al., 2006a; Zhou et al., 2016; Yu et al., 2019; Liu et al., 2020; Huang et al., 2021; Yu et al., 2021). Quercetin and kaempferol were identified by a network pharmacology study, to be the main active components in the DS–AM formula. They were believed to relieve heart injury by regulating PI3K-Akt, VEGF, and erbB signaling pathways, and insulin resistance (Yu et al., 2021). Quercetin is one of the active flavone components in many Chinese herbal medicines. Our pharmacological studies showed that DS decoction could alleviate heart failure by inhibiting excessive activation of the neuroendocrine system, strengthening myocardial contractility, and reducing end-diastolic volume and pressure to improve cardiac hemodynamics. However, quercetin alone produced less pharmacological effect than DS used in the whole (unpublished data). In TCM practices AM is believed to be an important Qi tonic medicine and can replenish Qi and Yang, promoting diuresis and detumescence and enhancing myocardial muscle strength. More studies on the mechanism of action of AM, in particular the three major active components astragaloside IV (AS4) (Liu et al., 2018; Lin et al., 2019; Tan et al., 2020; Zang et al., 2020), calycosin-7-glucoside (C7G), and Astragalus polysaccharides (APS), have also been reported. The major bioactive components astragalosides, in particular astragaloside IV (AS4), from AM have been extensively studied (Zhang et al., 2015; Xu et al., 2016; Tan et al., 2020; Du et al., 2022) were shown to exert a beneficial effect on myocardial lesion by regulating ATP consumption and preserving intracellular Ca^{2+} homeostasis (Chen et al., 2006b). Wang et al. reported that AS4 reduced cardiac hypertrophy induced by aortic banding surgery in mice *via* inactivating the TBK1/PI3K/AKT signaling pathway (Liu et al., 2018). Zhang et al. (2015)demonstrated that AS4 released ISO-induced cardiac hypertrophy *via* regulating NF-κB/PGC-1α signaling and improved the ISO-induced vascular dysfuntion by regulating eNOS uncoupling-mediated oxidative stress and retarding ROS-NF-κB signaling (Xu et al., 2016). Xiao et el. showed that AS4 acting as an antioxidant relieved doxorubicin-induced cardiomyopathy *in vitro* and *in vivo* by suppressing NADPH oxidase expression (Lin et al., 2019). AS4 was also revealed to ameliorate isoprenaline-induced cardiac fibrosis in mice by modulating gut microbiota and fecal metabolites (Du et al., 2022). Calycosin is another major active component in AM and was shown to attenuate oxidative stress-induced cardiomyocyte apoptosis by activating estrogen receptors and promoting AKT phosphorylation (Liu et al., 2016). Very recently, calysosin was reported to act as a PI3K activator to ameliorate inflammation and fibrosis in heart failure *via* the AKT-IKK-STAT3 axis (Wang et al., 2022). Astragalus polysaccharide was revealed to be able to inhibit diabetic cardiomyopathy in hamsters by suppressing chymase activation (Chen et al.,

2010a; Chen et al., 2010b). However, despite DS and AM and their active components have been extensively studied, the molecular mechanism of action of them has not been completely understood. For instance, how DS and AM or their active components regulate PI3K/AKT phosphorylation signaling pathway? How DS and AM or their active components regulate ATP consumption and maintain intracellular Ca^{2+} homeostasis?

To address these issues, in the present work, we applied a mass spectrometry (MS)-based quantitative proteomics strategy to explore the mechanism of action of DS combined with AM or the major active components, astragaloside IV and calysosin-7-glucoside, of AM. The studies were performed on rats with isoproterenol-induced cardiomyopathy (ISO-iCM) (Xie et al., 2015). With quantitatively comparing the protein expression levels in the heart of the sacrificed control, model, and treated rats, we demonstrated for the first time that DS decoction ameliorates ISO-iDM in rats by significantly downregulating the typical biomarkers of cardiomyopathy, including natriuretic peptides A (NPPA) and myosin light chain 4 (MYL4) (Tripathi et al., 2017). More importantly, we provided molecular evidence for that AM did not improve the pharmacological effect of DS on ISO-iDM, but astragaloside IV (AS4) in AM remarkably promoted the pharmacological efficacy of DS by reversing the expression of the sarcomeric motor myosin heavy chain 7 (MYH7) (Daniels et al., 2021), and further downregulating NPPA and MYL4. The combination of DS with AS4 interestingly showed a similar beneficial effect on cardiac contractibility to the myosin inhibitor mavacamten under clinical trial (Anderson et al., 2018; Lehman et al., 2022).

Materials and method

Reagents

Descurainia sophia seeds (DS; Brassicaceae; *Descurainia Sophia* (L.) Webb ex Prantl. seed) and *Astragalus mongholicus Bunge* (AM; *Leguminosae; Astragalus mongholicus Bunge* radix) were purchased from Baiweitang Decoction Pieces Co. (China). The two plant materials were identified by the affiliated hospital of Shandong University of Traditional Chinese Medicine, with Specimen Nos. SUTCM/PHAR/HRB/21/05/17 and SUTCM/PHAR/HRB/20/03/18, respectively. *Astragalus* polysaccharides (P/N: 7105MC, w/w 99%) was provided by Medicass Biological Products Co. (China). Astragaloside IV and calycosin-7-glucoside were obtained from Nature Standard Technical Service Co. (China). The low protein binding microcentrifuge tube was purchased from Thermo Fisher Scientific Ltd. (United States). Sodium chloride obtained from Sinopharm Chemical Reagent Co., Tris base from BioDee (China), and Tween-20 from Solarbio (China) were used to prepare TBST buffer. HPLC grade water (Fisher Chemical) was used throughout all experiments.

Animals and models

In primary experiments, we did not find significant difference in the pharmacological efficiency of DS and AM and various combinations between male and female rats with isoproterenol-induced cardiomyopathy (ISO-iCM). Therefore, in the present work, we selected 1:1 of male and female rats to establish of ISO-iCM models. To this end, 77 specific-pathogen-free, Sprague–Dawley rats (half male and half female), weighing 260 ± 20 g, were purchased from Beijing Vital River Laboratory Animal Technology Co. Ltd (Beijing, China), with a certification number of SCXK (Jing) 2012-0001. The rats were acclimated for 3 days in the animal facility of the Shandong University of Traditional Chinese Medicine and then randomly divided into seven groups, designated as control group (CG), model group (MG), and treated groups with DS decoction alone (DS), DS combined with AM (DSAM), astragaloside IV (DSAS4), calycosin-7-glucoside (DSC7G), or Astragalus polysaccharides (DSAPS) decoction, respectively, with 11 rats in each group. Isoproterenol was used to induce cardiomyopathy, following the procedure reported previously (Xie et al., 2015). In brief, isoproterenol (3 mg kg^{-1}•d^{-1}) was subcutaneously injected into the scapular region of each rat for 10 days. After 2 weeks of observation, an endotracheal tube was implanted in each rat by using an endotracheal intubation device. The catheter was retained for 7 days prior to further experiments. Notably, the endotracheal tube was used to establish the models with the Upper Energizer Stage patterns (Code: SG70 in the International Statistical Classification of Diseases and Related Health Problems (ICD-11)) with the fluid disturbance pattern (ICD Code: SF11), accompanied with isoproterenol stimulus. However, in the present work, the pharmacological benefits of all formulas were evaluated only based on the heart of the models. All animal experiments were approved by the Ethics Committee of Shandong University of Traditional Chinese Medicine and carried out in accordance with the Laboratory Animal-Guideline for Ethical Review of Animal Welfare (GB/T 35892-2018).

Preparation and administration of drugs

The DS and AM decoctions were prepared following the traditional clinical medication method described in Chinese Pharmacopoeia (2010 Edition, p283 and p313). In brief, an aliquot of purchased DS seeds and AM slices were individually put into a casserole, followed by the addition of 10-fold tap water to obtain a final concentration of 0.18 g/ml for DS and 0.54 g/ml for AM, and stilled at room temperature for 0.5 h and then boiled for 1 h. The raw decoction was filtered, and

the filtrate was collected. The boiling and filtration were repeated three times, and the filtrates were merged. The merged decoctions were evaporated to the initial values, of which the final concentrations of total extracts were 2.18 mg/ml (DS) and 6.53 mg/ml (AM), respectively. The mixed decoction of DS and AM (1:3, w/w) was prepared following the procedure described earlier, of the final concentration of total extract was 8.73 mg/ML. Aliquots of AS4, C7G, and APS were individually dissolved in 0.5% sodium carboxymethyl cellulose solution to prepare the suspensions of 3 mg/ml for AS4, 1.5 mg/ml for C7G, and 141 mg/ml for APS, which were stored at 4°C before use.

After pathological assessments of all rats with ISO-iDM, DS decoction and the various combinations were administrated. Based on the Chinese Pharmacopoeia (2010 Edition), 10 ml kg^{-1}•d^{-1} of DS decoction (containing 21.8 mg of extract in total) was administrated to each rat of the DS group, 10 ml kg^{-1}•d^{-1} of mixed decoction of DS and AM (containing 87.3 mg of extract in total) to each rat of the DSAM group, and 10 ml g•kg^{-1}•d^{-1} of DS decoction plus 50 mg kg^{-1}•d^{-1} of AS4, 30 mg kg^{-1}•d^{-1} of C7G, or 41 mg kg^{-1}•d^{-1} of APS, were administrated to each rat of the DSAS4, DSC7G, or DSAPS group, respectively, by gavage once a day for 14 days. While the rats in the control and model groups were given normal saline at the same dose.

Characterization of components in *Descurainia sophia* seeds and *Astragalus mongholicus*

Preparation of *Descurainia sophia* seeds (DS) and *Astragalus mongholicus* (AM) samples

Aliquot (100 μL) of DS or AM decoction prepared as described earlier was diluted by 900 μL method chloroform (3:2) mixture, and then 200 μL deionized water was added. The resulting mixture was centrifuged at 15,000 g, 4°C for 15 min. The up-layer was then transferred to a new tube and dried in a vacuum centrifuge. The residue was re-dissolved by 150 μL 80% MeOH/H_2O containing 0.25% formic acid (FA) and 80% MeOH/H_2O containing 20 mM ammonium acetate for positive and negative ESI-MS/MS analyses, respectively.

UPLC–MS/MS

The UPLC–MS/MS characterization of components in DS and AM decoctions was performed on a SYNAPT XS mass spectrometer coupled with the Waters ACQUITY Class I UPLC PLUS and an ACQUITY UPLC® HSS T3 column (i.d. 1.8 μm, 100 mm × 2.1 mm) (Waters, United States). The mobile phases were water containing 0.25% FA (A) and methanol containing 0.25% FA (B) for positive mode, and water containing 20 mM ammonium acetate (A) and methanol containing 20 mM ammonium (B) for negative mode, respectively. For both positive and negative detections, the mobile phase B started at 2% and increased to 5% at 1 min, and further increase to 45% at 7 min, to 85% at 10 min, and to 95% at 17 min, with a flow rate of 0.17 ml/min.

The mass spectrum data were collected in $HDMS_e$ mode, and the detection parameters were set as follows: acquiring mass range from 95-1000 Da under sensitivity acquisition mode; scan time 1.5 s; low transfer collision energy 15 V; and high ramp transfer collision energy 60–80 V. The lock-mass compound was leucine enkephalin (0.2 ng/ml).

Data analysis

Progenesis QI was used to interpret MS raw data. The mixture of DS and AM (1:1) decoction was used to align the chromatographic peaks for each mass spectrum file. For positive ion detection, the adduct ions including $[M + H]^+$, $[M + Na]^+$, $[M + K]^+$, $[M\text{-}H_2O + H]^+$, and $[M+2H]^{2+}$ were selected. The adduct ions $[M\text{-}2H]^{2-}$, $[M\text{-}H_2O\text{-}H]^-$, $[M\text{-}H]^-$, and $[M + Cl]^-$ were selected for the negative mode. The compounds which have the highest abundance in the blank group or Anova(p) value larger than 0.0001 were filtered out for future analysis. KEGG, Human Metabolome Database, BroadPharm, Food and Agriculture Organization, xPharm, AQ BioPharma, AxisPharm, BLDpharm, abcr, and PubMed metabolite databases, and Nature Chemical Biology, Nature Chemistry, Nature Communications, and Springer Nature databases, were used to identify compounds detected by MS. The precursor tolerances and fragmentation tolerances were set 10 and 5 ppm, respectively. After identification, the compounds with Anova(p) value <0.0001, abundance >5000, and abundance ratio between AM and DS > 25 or <0.04 were considered as the main contents for AM and DS, respectively.

Echocardiography

After the intervention described earlier, rats in all groups were examined by high-frequency echocardiography with a pb207 probe (20 MHz). The left ventricular ejection fraction (LVEF) and the left ventricular short-axis shortening fraction (LVFS) were measured by ultrasonic measurement.

Determination of cardiac index and left ventricular mass index

Rats were weighed, then injected intraperitoneally with 10% chloral hydrate (3 ml/kg), anesthetized, and fixed. Blood was collected from the main abdominal vein and placed in an anticoagulant tube at room temperature for 2 h, centrifuged at 4°C, and 4,000 g for 10 min. The supernatant was stored at −80°C for determination of the creatine kinase (CK) level by enzyme-linked immunosorbent assay kit (Jiancheng Bioengineering

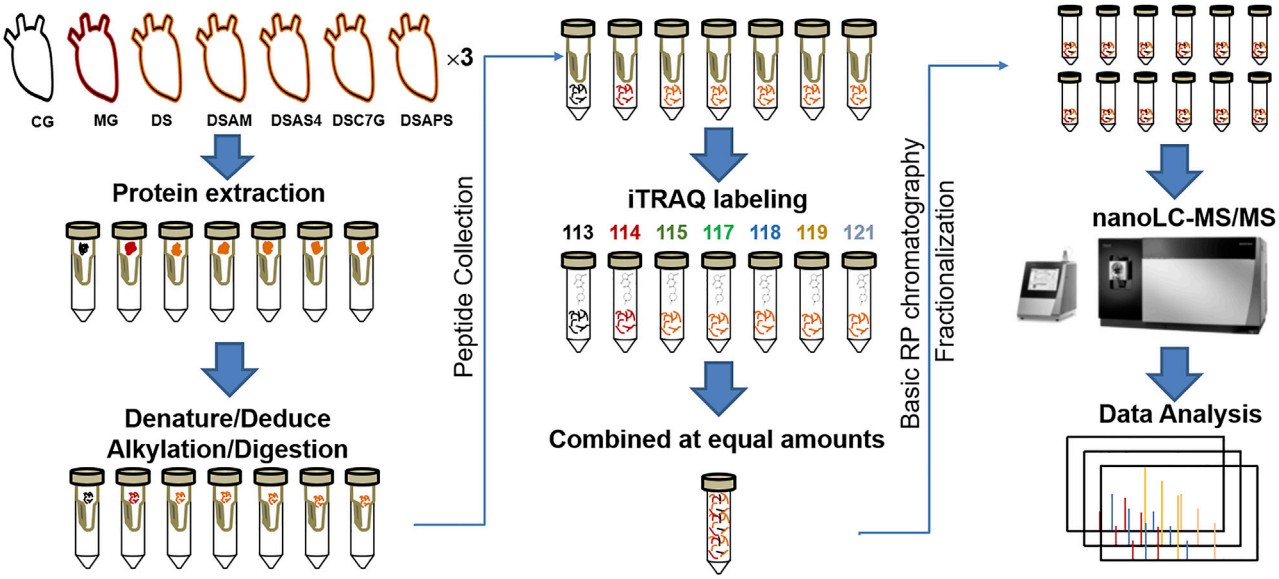

FIGURE 1
Workflow of quantitative proteomics analysis. The heart tissues of rats from seven groups are designated as the control group (CM), ISO-iCM model group (MG), and treated groups with *Descurainia sophia* seed decoction alone (DS), and combined with *Astragalus mongholicus* (DSAM), astragaloside IV (DSAS4), astragalus calycosin-7-glucoside (DSC7G), or astragalus polysaccharides (DSAPS), respectively.

Institute, China). Then, the rats were sacrificed to remove hearts, which washed off the residual blood with 0.9% ice normal saline, dried with filter paper, and weighed. The left atrium was cut off along the coronary sulcus, and the right ventricle was removed along the interventricular sulcus. The left ventricular was weighed, and the cardiac index (cardiac weight/body weight, HWI) and left ventricular weight index (left ventricular weight/body weight, LVWI) were thereby calculated.

Histopathological assays

The left ventricular myocardial tissue of each rat was fixed with 10% paraformaldehyde for 24 h and then embedded in paraffin. The tissue sections were stained with hematoxylin–eosin and Masson (Wuhan Google Biotechnology, China) for pathological assays on a Nikon Eclipse optical microscope (Nikon, Japan). The collagen fiber volume fraction (CVF) of Masson's stained sections was calculated by the ipp6.0 image analysis system (Media Cybernetics).

Quantitative proteomics analysis

The workflow of quantitative proteomics analysis is shown in Figure 1, and the detailed procedures are described as follows.

Protein extraction and digestion

RIPA lysis buffer (Beyotime, China) was added to ca. 0.5 g of rat heart tissue at 100 μL:10 mg ratio, the tissue was then lysed for 30 s by a homogenate machine (JXFSTPRP-24, Shanghai Jingxin Industrial Development Co., Ltd.) at 50% pulse for 5 times. The raw protein extract was centrifuged at 12,000 g for 15 min, and then the supernatant was transferred to a PE tube. After the measurement of protein concentration by BCA kit (Beyotime), an aliquot (100 μg) of each extract was transferred to a 10 kD centrifugal filter (Merck Millipore), and 200 μL of 0.1 M triethylammonium bicarbonate (TEAB, Thermo Scientific) buffer was added to wash off lysis buffer twice at 14,000 g for 30 min at 4°C. Thereafter, 50 μL of 0.5 M TEAB was used to re-dissolve the protein residues in the ultrafilter, and then the proteins were denatured and reduced by incubating in a buffer, containing 0.1% SDS, 5.3 mM TCEP, and 0.5 M TEAB for 1 h at 60°C, followed by alkylation of cysteinyl thiols with 3 μL of 200 mM MMTS at 25°C for 15 min. The excess of denaturing, reducing, and alkylation reagents were washed off by centrifuging twice at 14,000 g for 30 min at 4°C with 200 μL of 0.1 M TEAB buffer, and the protein residue was re-dissolved with 30 μL of 0.5 M TEAB and digested by adding 2 μL of 1 μg/μL MS grade rAc-Trypsin (Bei-Er-Li, China) and incubating at 37°C for 16 h. The resulting tryptic peptides were collected by adding 200 μL 0.1 M TEAB buffer into the 10-kD centrifugal filter, spinning at 14,000 g for 30 min at 4°C, followed by desalting by a C18 cartridge (Waters Sep-Pak). The C18 cartridge was first

activated by 1 ml of 0.1% formic acid (Honeywell Fluka™)/80% acetonitrile (Fisher Chemical) and 1 ml of 0.1% formic acid (FA)/50% acetonitrile (ACN) sequentially, and then equilibrated by 1 ml of 0.1% trifluoroacetic acid (Alfa Aesar) twice. The collected peptides were loaded into the equilibrated column and washed twice with 1 ml of 0.1% trifluoroacetic acid (TFA), and then eluted with 1 ml of 0.1% FA/50% ACN and 1 ml of 0.1% FA 80% ACN sequentially. Finally, the desalted peptides were merged and dried in a vacuum centrifuge for further use.

iTRAQ labeling

Each desalted peptide mixture was re-dissolved in 20 μL of 0.5 M TEAB buffer, and mixed with 70 μL of iTRAQ labeling reagent (SCIEX) dissolved in isopropanol (Cairn Pharmaceutical Technology Co.). The resulting mixture was adjusted to pH = 7.6 and then incubated at room temperature for 2 h. The labeling reaction was then quenched by adding 150 μL of deionized water and incubating for 15 min at room temperature. Thereafter, each labeled peptide mixture with different isotopic patterns from six groups were equivalently mixed and desalted by a C18 cartridge again following the same procedure described earlier.

HPLC pre-fractionation

The labeled and desalted peptide mixture was dried by vacuum centrifuge, and then re-dissolved in 100 uL 4.5 mM ammonium formate in 2% ACN aqueous solution (pH 10). An aliquot (95 uL) of each labeled peptide mixture was loaded into HPLC (Agilent Technologies 1260 infinity) with a C18 column (CAPCELL PAK MG II S-5, 4.6 × 150 mm, 5 μm, Shiseido), and eluted by basic (pH = 10) mobile phases A (4.5 mM HCOONH4 in 2% ACN) and B (4.5 mM HCOONH4 in 90% ACN). The gradient started with 0% B until 9 min and continuously increased to 6% B at 13 min, 28.5% B at 63 min, 34% B at 68.5 min, 60% B at 81.5 min, and maintained until 90 min with a flow rate of 1 ml/min. The fractions were collected chronologically into 12 tubes from 3 to 90 min, individually lyophilized and re-dissolved in 10 μL of 0.1% formic acid for NanoLC–MS/MS analysis.

NanoLC–MS/MS analysis

The NanoLC–MS/MS analysis was performed on an Orbitrap Fusion Lumos mass spectrometer (Thermo Fisher Scientific) coupled with an EASY-nLC 1200 nanoHPLC system equipped with an Acclaim™ PepMap™ 100 pre-column (20 mm × 75 μm, 3 μm) and an Acclaim™ PepMap™ RSLC C18 analytical column (150 mm × 75 μm, 2 μm). The mobile phases for the NanoLC separation were 0.1% FA in H2O (A) and 80% ACN/20% H2O (B), respectively, with a flow rate of 300 nL/min. The mobile phase B started at 2% and increased to 6% at 1 min, and then to 30% at 85 min, 60% at 94 min, and sharply to 90% within 1 min and remained at 90% for 5 min, and then decreased to 50% within 1 min and remained at 50% for 9 min, finally dropped down to 2% within 1 min and remained 3 min. An aliquot (1 μL) of each HPLC fraction containing 0.1% formic acid was loaded, and elution from the analytical column was directly infused into the mass spectrometer for MS/MS analysis. The details of the parameters of the MS/MS analysis are listed in Supplementary Table S1.

Protein identification and quantification

Acquired MS/MS spectra were analyzed by Proteome Discoverer 2.2 (Thermo Fisher Scientific) to identify and quantify proteins based on the protein database (Version 10/25/2017, 42,252 sequences) downloaded from the UniPort database. The taxonomy was *Rattus norvegicus*, and the taxon identifier was 10116. Sequest HT 2.2 search engine was used for peptide matching. The dynamic modifications were oxidation at methionine and phosphorylation at serine and threonine. The static modifications were carbamidomethylation at cystine, iTRAQ labeling at lysine, tyrosine, and N-terminus of all peptides. The quantitative results were normalized based on the abundance of total peptides in each set. Abundance ratios were calculated for each protein identified in all groups other than controls by comparing the value of each protein to that of the same protein in the control group. The other settings are the defaults of PD software.

Western blotting

The expression levels of the NPPA, TPM1, and TPM2 in the control and model groups were measured by Western blotting with glyceraldehyde phosphate dehydrogenase (GAPDH) as an internal control protein. An aliquot (40 μg) of protein extract from the heart tissue of each group was boiled at 95°C for 5 min in SDS-loading buffer and separated over 4–12% polyacrylamide gel (GeneScript) at 140 V for 1 h with Tris-MOPS-SDS running buffer (GeneScript). The proteins were then transferred to the PVDF membrane by semi-dry transfer blotting at 20 V for 1 h. The PVDF membrane (Millipore) with proteins was cut into two parts along ca. 30 kD, and then blocked in 5% milk TBST buffer for 120 min. Anti-NPPA antibody (Abcam), anti-TPM2 (Abcam), anti-TPM1 (Abcam), and anti-GAPDH (Abcam) were diluted at 1:1000, 1:300, 1:1000, and 1:5000, respectively, to blot PVDF membrane by incubation at 4°C for 10 h, and then washed three times by 5% milk TBST for 5 min each. The PVDF membrane was then incubated with horseradish peroxidase-conjugated second antibodies, goat antirabbit antibody (Abcam) for NPPA, TPM2, and TPM1 and goat antimouse antibody (Abcam) for GAPDH, respectively, for 1 h at 25°C. After washing with TBST, the protein bands were visualized by enhanced chemiluminescence (Tanon 5200Multi, China), and the optical densities were quantified using ImageJ.

Bioinformatics analysis

The proteins identified and quantified by MS/MS, of which false-discovery rates (FDRs) are <0.01, *p*-values <0.05, and abundance ratios (model vs. control) ≥ 1.5 or ≤0.67, were uploaded into the STRING 10.0 data pool for Gene Ontology (GO) and protein–protein interaction (PPI) network analysis. The UniPort accession ID of the differentially expressed proteins (DEPs) in the heart tissues of the model and treated groups were inputted into the list of gene name box, and *Rattus norvegicus* organism was selected for the analysis. The confidence option was selected for the meaning of network edge, and textmining, experiments, databases, co-expression, neighborhood, gene fusion, and co-occurrence options were chosen for active interaction sources.

Statistical analysis

All data were analyzed with Origin 8.0 and Microsoft Office Excel 2010 software and are expressed as mean ± SEM. The between-group differences in physiological and/or pathological indexes were analyzed by one-way ANOVA. A two-sided *p* value <0.05 represents statistically significant. * indicates $p < 0.05$, ** $p < 0.01$, and *** $p < 0.001$. Principal component analysis (PCA) was performed on MATLAB(Version 8.4.0.150421, MathWorks Inc.).

Results

Characterization of components in *Descurainia sophia* seeds and *Astragalus mongholicus*

To investigate the mechanism of action of *Descurainia sophia* seeds (DS) and *Astragalus mongholicus* (AM), we first characterize the main components in DS and AM decoctions, individually, by UPLC–MS/MS. As shown in Supplementary Figure S1, both the decoctions display complicated composition. We collected all ion peaks detected by MS in DS and AM decoctions under both positive and negative modes into the Progenesis QI program for principal component analysis (PCA). In total, 10,078 positive ion peaks and 6,710 negative ion peaks were selected by Progenesis QI. The results showed that under the positive mode, the first principal component (PC1) can distinguish DS and AM, and under the negative mode, the second principal component (PC2) can separate DS and AM (Supplementary Figure S2). The 10,078 positive ion peaks and 6,710 negative ion peaks enabled the identification of 90 compounds commonly existing in DS and AM decoctions, of which the abundance (A) ratios calculated on A_{DS}/A_{AM} or A_{AM}/A_{DS} are >1 and <25 (Supplementary Figure S2). Furthermore, after data filtering, 48 and 23 compounds were exclusively identified for DS with the A_{DS}/A_{AM} values > 25, and for AM with the A_{AM}/A_{DS} >25, respectively (Tables 1, 2, Supplementary Tables S3, S4). The identification was verified further by checking the MS^2 fragment patterns and the isotope similarity of each compound to the standard. For example, one of the main components in DS is quercetin-7-O-β-D-glucopyranosyl (1→6)-β-D-glucopyranoside (Figure 2A), according to the integrative pharmacology-based network computational research platform of traditional Chinese medicine database (TCMIP v2.0, http://www.tcmip.cn/). The hydrolytic product of this component, quercetin (Figure 2B), was identified under positive mode with a retention time of 7.66 min at the extraction chromatogram (EIC) (DS-11 in Supplementary Figure S3A), and the fragment pattern is depicted in Supplementary Figure S4A, which shows that the MS/MS fragments of quercetin were observed at *m/z* 153.0183, 121.0284 and 137.0234, being consistent with Makarov's report (Scigelova et al., 2011). The well-known major component in AM, astragaloside IV (Figure 2C), was detected at 13.13 min (AM-23 in Supplementary Figure S3C), of which the MS/MS fragment ions were detected at *m/z* 669.3967, 627.3853, and 203.0526 (Supplementary Figure S4B).

Phenotypic and pathological characterization of isoproterenol-induced cardiomyopathy in rats

Isoproterenol (ISO) as a β-adrenergic receptor (β-AR) agonist is often used to induce cardiomyopathy in the mouse (Shanmugam et al., 2019; Houson et al., 2020; Zhu et al., 2020). We have previously constructed rat models with the upper energizer stage (ICD code: SG70) and fluid retention patterns (ICD code: SF11) by injecting subcutaneously into the abdomen of rats, accompanied by the endotracheal intubation. The established models included disorders in both the heart and lung of rats (Xie et al., 2015). We have also primarily evaluated the effects of DS, AM, and DS/AM formula on the lung and heart functions of the model rats and found that the combined use of DS with AM produced better pharmacological effects on the lung and cardiac functions evidenced by the reversion of the lung weight index (LWI), the lung permeability index (LPI), left ventricular weight index (LVWI), and left ventricular ejection fraction (LVEF) (Chen et al., 2019). In the present work, we only evaluate the phenotypes and pharmacological benefits of DS and AM as well as each combination on the disorders in the heart of the rat models induced by isoproterenol.

As echocardiographic left ventricular ejection fraction (LVEF) and left ventricular fraction shortening (LVFS) accurately reflect the cardiac function, for example, systolic and diastolic functions (Cho et al., 2018; Rieth et al., 2019), we first performed a high-frequency echocardiographic

TABLE 1 Components identified in *Descurainia sophia* seed decoction.

Compound no.	Accepted description	Retention time/min	m/z	Adducts	Formula	Abundance	Fold change[a]
DS-1	(5Z)-3-Ethyl-5-{4-[(4-fluorobenzyl)oxy] benzylidene}-2-thioxo-1,3-thiazolidin-4-one	3.82	372.0534	M-H	$C_{19}H_{16}FNO_2S_2$	2306842	120.8
DS-2	1-[(Benzyloxy)carbonyl]-3-(carboxymethyl)-3-pyrrolidinecarboxylic acid	7.04	308.1125	M + H	$C_{15}H_{17}NO_6$	1018277	31.0
DS-3	1-Nitro-7-hydroxy-8-glutathionyl-7,8-dihydronaphthalene	10.30	477.1080	M-H_2O-H	$C_{20}H_{24}N_4O_9S$	963011	162.1
DS-4	(8Z,22Z)-4-Methoxy-2-oxa-11,16,20-triazatricyclo [22.2.2.1–3.7~]nonacosa-1(26),3(29),4,6,8,22,24,27-octaene-10,21-dione	5.68	472.2168	M + Na	$C_{26}H_{31}N_3O_4$	875325	2199.6
DS-5	Methyl 5-({(4-carbamoyl-2,6-dimethyl-N-{[(2-methyl-2-propanyl)oxy]carbonyl}-L-phenylalanyl) [(1S)-1-(5-phenyl-1H-imidazol-2-yl)ethyl]amino} methyl)-2-methoxybenzoate	8.94	718.3035	M + Cl	$C_{38}H_{45}N_5O_7$	841332	2231.0
DS-6	1-(1-Ethyl-1H-pyrrol-3-yl)-7,7-difluoro-2-azaspiro [3.5]nonane	9.87	289.1266	M + Cl	$C_{14}H_{20}F_2N_2$	831149	1688.2
DS-7	Nepetin	7.79	317.0653	M + H	$C_{16}H_{12}O_7$	803804	268.4
DS-8	Isorhamnetin	8.27	317.0654	M + H	$C_{16}H_{12}O_7$	722166	160.2
DS-9	(−)-Epothilone A	9.33	532.2177	M + K	$C_{26}H_{39}NO_6S$	671218	33.8
DS-10	4,4-Difluoro-2-({[(2-methyl-2-propanyl)oxy] carbonyl}amino)cyclopentanecarboxylic acid	7.71	264.1039	M-H	$C_{11}H_{17}F_2NO_4$	561303	6441.1
DS-11	Quercetin	7.66	303.0493	M + H	$C_{15}H_{10}O_7$	503905	203.8
DS-12	(8E,22E)-4-Methoxy-2-oxa-11,16,20-triazatricyclo [22.2.2.1–3.7~]nonacosa-1(26),3(29),4,6,8,22,24,27-octaene-10,21-dione	5.98	472.2164	M + Na	$C_{26}H_{31}N_3O_4$	382457	35.9
DS-13	Lawsone	6.91	175.0377	M + H	$C_{10}H_6O_3$	327344	25.0
DS-14	Ethyl 3-amino-5-methoxy-4.5,6,7-tetrahydro-1-benzofuran-2-carboxylate	7.04	262.1069	M + Na	$C_{12}H_{17}NO_4$	323375	33.0
DS-15	Kaempferol	10.31	287.0550	M + H	$C_{15}H_{10}O_6$	315159	25.8
DS-16	4(1H)-Isoquinolinone	6.16	146.0589	M + H	C_9H_7NO	308144	58.1
DS-17	DSS	9.56	777.2218	M + Na	$C_{34}H_{42}O_{19}$	272640	280.6
DS-18	Tozadenant	8.45	429.1548	M + Na	$C_{19}H_{26}N_4O_4S$	261991	126.7
DS-19	Hypolaetin	7.09	303.0491	M + H	$C_{15}H_{10}O_7$	247943	157.2
DS-20	1,2-indandione	6.96	147.0431	M + H	$C_9H_6O_2$	212572	29.4
DS-21	1-O-trans-cinnamoyl-Î²-D-glucopyranose	5.85	291.0898	M-H_2O-H	$C_{15}H_{18}O_7$	205788	3514.0
DS-22	SAMe	8.63	381.1330	M + H-H_2O	$C_{15}H_{22}N_6O_5S$	196306	29.1
DS-23	(3-Isopropoxy-2-thienyl) (phenyl)methanol	6.96	247.0778	M-H	$C_{14}H_{16}O_2S$	192040	257871.9
DS-24	Methyl (2Z)-4-(2,3-dihydro-1,4-benzodioxin-6-yl)-2-hydroxy-4-oxo-2-butenoate	8.20	287.0505	M + Na	$C_{13}H_{12}O_6$	187762	43.9
DS-25	(2S,3Z)-5-{[(2R,3R,5S,6S)-6-{(2E,4E)-5-[(3R,4R,5R)-4-Hydroxy-7,7-dimethyl-1,6-dioxaspiro [2.5]oct-5-yl]-3-methyl-2,4-pentadien-1-yl}-2,5-dimethyltetrahydro-2H-pyran-3-yl]amino}-5-oxo-3-penten-2-yl acetate	4.39	506.3137	M + H	$C_{28}H_{43}NO_7$	157104	419.8
DS-26	(4-Methoxy-3,5-dimethyl-2-thienyl) (phenyl) methanol	8.63	247.0780	M-H	$C_{14}H_{16}O_2S$	148151	2318.7
DS-27	(2E)-N-(6-Amino-1,3-diethyl-2,4-dioxo-1.2,3,4-tetrahydro-5-pyrimidinyl)-3-(3,4-dimethoxyphenyl) acrylamide	8.89	427.1389	M + K	$C_{19}H_{24}N_4O_5$	122759	85.2
DS-28	1-[(4-Methoxyphenyl)sulfonyl]-3-(4.4,5,5-tetramethyl-1,3-dioxolan-2-yl)-1H-pyrrolo [2,3-b] pyridine	9.87	451.1124	M + Cl	$C_{21}H_{24}N_2O_5S$	115812	Infinity
DS-29	Hexamethylolmelamine	9.74	287.1109	M-H_2O-H	$C_9H_{18}N_6O_6$	94535	1208.7
DS-30	2-Methyl-2-propanyl [5-(6-hydroxy-2-naphthyl)-2,2-dimethyl-1,3-dioxan-5-yl]carbamate	7.71	354.1675	M-H_2O-H	$C_{21}H_{27}NO_5$	92513	Infinity

(Continued on following page)

TABLE 1 (*Continued*) Components identified in *Descurainia sophia* seed decoction.

Compound no.	Accepted description	Retention time/min	m/z	Adducts	Formula	Abundance	Fold change[a]
DS-31	Convalloside	11.28	735.3238	M + Na	$C_{35}H_{52}O_{15}$	81129	28.1
DS-32	Mirificin	6.86	547.1655	M-H	$C_{26}H_{28}O_{13}$	78320	2798.7
DS-33	Bis [(3R,4S,5S,6R)-3,4,5-trihydroxy-6-(hydroxymethyl)tetrahydro-2H-pyran-2-yl] malonate	7.48	427.1103	M-H	$C_{15}H_{24}O_{14}$	70481	1752.4
DS-34	4-Hydroxy-3-methyl-6-(trifluoromethyl)-4.5,6,7-tetrahydro-1-benzofuran-2-carboxylic acid	7.66	287.0493	M + Na	$C_{11}H_{11}F_3O_4$	68140	144.5
DS-35	N-Hydroxy-2-(4-phenyl-1,3-thiazol-2-yl) ethanimidamide	8.63	232.0549	M-H	$C_{11}H_{11}N_3OS$	66872	2358.5
DS-36	(6E)-4-Hydroxy-1,7-diphenyl-6-hepten-3-one	9.95	303.1333	M + Na	$C_{19}H_{20}O_2$	59840	43.1
DS-37	5-[2-(Ethylsulfanyl)phenyl]-3-methyl-5-oxopentanoic acid	8.58	265.0878	M-H	$C_{14}H_{18}O_3S$	48253	12299.5
DS-38	(3Z)-2,10-Diamino-4-(phosphonomethyl)-3-decenoic acid	8.63	329.1039	M + Cl	$C_{11}H_{23}N_2O_5P$	46056	214.8
DS-39	1,2-O-Cyclohexylidene-a-D-glucofuranose	8.58	295.0971	M + Cl	$C_{12}H_{20}O_6$	46002	Infinity
DS-40	Benzyl 5-[(acetylsulfanyl)methyl]-4-(1,3-benzodioxol-5-yl)-1-hydroxy-L-prolylglycinate	6.65	467.1278	M-H_2O-H	$C_{24}H_{26}N_2O_7S$	42389	2324.0
DS-41	GDC-0152	6.60	479.2189	M-H_2O-H	$C_{25}H_{34}N_6O_3S$	42040	172.2
DS-42	Sakuranin	10.74	471.1286	M + Na	$C_{22}H_{24}O_{10}$	36290	38.4
DS-43	Aklaviketone	8.58	411.1090	M + H	$C_{22}H_{18}O_8$	19893	25.9
DS-44	1-[4-({(1R)-1-[(6S,7S)-2-Amino-7-methyl-4-oxo-1,4,5,6,7,8-hexahydro-6-pteridinyl]ethyl}amino) phenyl]-1-deoxy-5-O-(5-O-{[(1S)-1,3-dicarboxypropoxy](hydroxy)phosphoryl}-alpha-D-ribofuranosyl)-D-ribitol	8.81	799.2547	M + Na	$C_{30}H_{45}N_6O_{16}P$	11051	33.2
DS-45	Neohesperidin dihydrochalcone	8.45	635.1893	M + Na	$C_{28}H_{36}O_{15}$	7239	42.8
DS-46	N-[(9H-Fluoren-9-ylmethoxy)carbonyl]-N-methyl-1-{[(2-methyl-2-propanyl)oxy]carbonyl}histidine	9.56	530.1665	M + K	$C_{27}H_{29}N_3O_6$	6166	51.8

[a]Fold change = (abundance)DS/(abundance)AM

examination on rats in all groups. As shown in Supplementary Figure S5, significant changes were observed between the ventricular cavity size and wall motion coordination of the heart of rats in the control group and model group. Compared with the control group (CG), the average (n = 6) LVEF and LVES of the model group (MG) reduced from 76.4 to 51.6%, and 48.2 to 31.5%, respectively (Figures 3A,B). Although the changes in LVEF and LVES between the controls and models were not as significant as those observed in patients with newly diagnosed DCM and heart failure (Cho et al., 2018), the alterations in LVEF and LVES together with the changes in the cardiac index (HWI) and left ventricular mass index (LVWI) between the controls and the models (Figures 3C,D), demonstrated that the models had developed pseudo-cardiomyopathy, termed as isoproterenol-induced cardiomyopathy (ISO-iCM) (Zhu et al., 2020).

Next, we evaluate the pharmacological effects of *Descurainia sophia* seeds (DS) and the combination of DS with *Astragalus mongholicus* (AM), astragaloside IV (AS4), calycosin-7-glucoside (C7G), and Astragalus polysaccharides (APS) on ISO-iCM in rats, based on the effect of various treatments on LVEF, LVFS, LVWI, and HWI levels of models. We found that AM and C7G slightly improved the pharmacological efficacy of DS, and AS4 significantly promoted the pharmacological effect of DS, whereas PLS showed little benefit for the pharmacological efficiency of DS on ISO-iCM (Figures 3A–D).

To evaluate further pharmacological efficiency of various combinations of DS with AM and the three active components of AM, we performed histopathological assays on the left ventricular myocardial tissues. The H&E staining results (Figures 3G,H) indicated that compared to the controls, the myocardial cells in the heart of models were significantly enlarged and hypertrophic and disorderly arranged accompanied with increased intercellular substances. Moreover, the inflammatory cell infiltration in the heart of the model was obvious. After treatment with DS or the combinations, these pathological phenotypes were diminished to a different extent (Figure 3I-M). Notably, the

TABLE 2 Components identified in *Astragalus mongholicus* decoction.

Compound No.	Accepted description	Retention time/min	m/z	Adducts	Formula	Abundance	Fold change[a]
AM-1	Deslanoside	11.90	941.4749	M-H	$C_{47}H_{74}O_{19}$	987131	270.0
AM-2	2′-Methyl-1H,1′H-2.5′-bibenzimidazole	9.20	283.0763	M + Cl	$C_{15}H_{12}N_4$	973789	1673.7
AM-3	(11R,23R)-14,17,20-Trihydroxy-14,20-dioxido-8,26-dioxo-9,13,15,19,21,25-hexaoxa-14lambda~5~,20lambda~5~-diphosphatritriacontane-11,23-diyl dioctanoate	13.26	885.4538	M-H_2O-H	$C_{41}H_{78}O_{17}P_2$	948470	385.7
AM-4	9,10-Dihydrobenzo [e]acephenanthrylene-5,9,10-triol	8.94	283.0764	M-H_2O-H	$C_{20}H_{14}O_3$	890204	304.5
AM-5	8-Azaadenosine	9.95	267.0823	M-H	$C_9H_{12}N_6O_4$	857889	458.3
AM-6	Decursinol	10.66	269.0800	M + Na	$C_{14}H_{14}O_4$	829194	37.0
AM-7	Seocalcitol	13.08	437.3415	M + H-H_2O	$C_{30}H_{46}O_3$	723031	43.9
AM-8	(2E)-3-[2-(3-Ethylphenoxy)-5-fluorophenyl]acrylic acid	11.67	267.0823	M-H_2O-H	$C_{17}H_{15}FO_3$	690119	43.6
AM-9	8′-apo-beta-carotenol	13.08	419.3309	M + H	$C_{30}H_{42}O$	630918	94.6
AM-10	2-Ammonio-5-[(1-carboxy-2-{[(1Z)-N-hydroxy-2-phenylethanimidoyl]sulfanyl}ethyl)amino]-5-oxopentanoate	2.64	382.1102	M-H	$C_{16}H_{21}N_3O_6S$	594536	142.8
AM-11	2-Phenyl-7-quinolinecarbaldehyde	8.94	268.0536	M + Cl	$C_{16}H_{11}NO$	541619	Infinity
AM-12	OLMESARTAN LACTONE	10.61	463.1659	M + Cl	$C_{24}H_{24}N_6O_2$	430921	123.8
AM-13	(6S,9S,9aS)-N-Benzyl-6-(4-hydroxybenzyl)-2,9-dimethyl-4,7-dioxo-8-(8-quinolinylmethyl) hexahydro-2H-pyrazino [2,1-c][1,2,4]triazine-1(6H)-carboxamide	9.02	577.2606	M-H	$C_{33}H_{34}N_6O_4$	306730	244.4
AM-14	3-Hydroxylup-18-en-21-one	12.77	423.3613	M + H-H_2O	$C_{30}H_{48}O_2$	292174	55.0
AM-15	Dicyclohexyl [2-(2,6-dimethoxybenzyl)benzyl] phosphine	7.40	461.2595	M + Na	$C_{28}H_{39}O_2P$	110198	52.7
AM-16	Ganoderal A	12.11	437.3410	M + H	$C_{30}H_{44}O_2$	106769	107.5
AM-17	Astragaloside III	12.95	807.4493	M + Na	$C_{41}H_{68}O_{14}$	95644	30.2
AM-18	Astragaloside II	13.08	849.4615	M + Na	$C_{43}H_{70}O_{15}$	92457	43.1
AM-19	Metoprolol succinate	13.83	653.4049	M + H	$C_{34}H_{56}N_2O_{10}$	83919	1307.8
AM-20	Soyasaponin I	12.77	965.5083	M + Na	$C_{48}H_{78}O_{18}$	75689	152.5
AM-21	N~2~-[(8-Fluoro-6-{5-[(2-methyl-2-propanyl) sulfamoyl]-3-pyridinyl}[1,2,4]triazolo [1,5-a]pyridin-2-yl)carbamoyl]-N,N-dimethylglycinamide	2.02	473.1553	M-H_2O-H	$C_{20}H_{25}FN_8O_4S$	75544	28.4
AM-22	(5R)-2,4-Dideoxy-1-C-{(2S,3R,4S)-3-hydroxy-4-[(2R,3S,4E,6E,9R,10S,11R,12E,14Z)-10-hydroxy-3,15-dimethoxy-7.9,11,13-tetramethyl-16-oxooxacyclohexadeca-4.6,12,14-tetraen-2-yl]-2-pentanyl}-5-isopropyl-4-methyl-alpha-D-threo-pentopyranose	13.26	645.3974	M + Na	$C_{35}H_{58}O_9$	49716	70.1
AM-23	Astragaloside IV	13.13	807.4506	M + Na	$C_{41}H_{68}O_{14}$	42693	34.4

aFold change = (abundance)AM/(abundance)DS

combined uses of DS with AS4 or C7G again resulted in further reduction in the severity of hypertrophy of myocardial cells and the content of intercellular substances in the hearts, compared with that treated with DS alone (Figures 3I,K, L), implying better pharmacological benefits on the heart injury in the model rats. However, the combination of DS with APS did not produce an improvement in the pharmacological efficiency of DS to ISO-iCM in rats (Figure 3M).

We also performed Masson's staining on the heart tissues of all groups (Figures 3N–P), where collagen fibers were stained in blue and myocardial cells in dark red. Based on Masson's staining, the average cardiac collagen volume fractions (CVFs) of each group were calculated and depicted in Figure 3E. The results indicate that compared to the controls, the CVF value of model rats significantly increased ($p < 0.01$) but decreased to a large content after treatments, though the treatments did not reverse completely the CVF level of models. Again, we found that

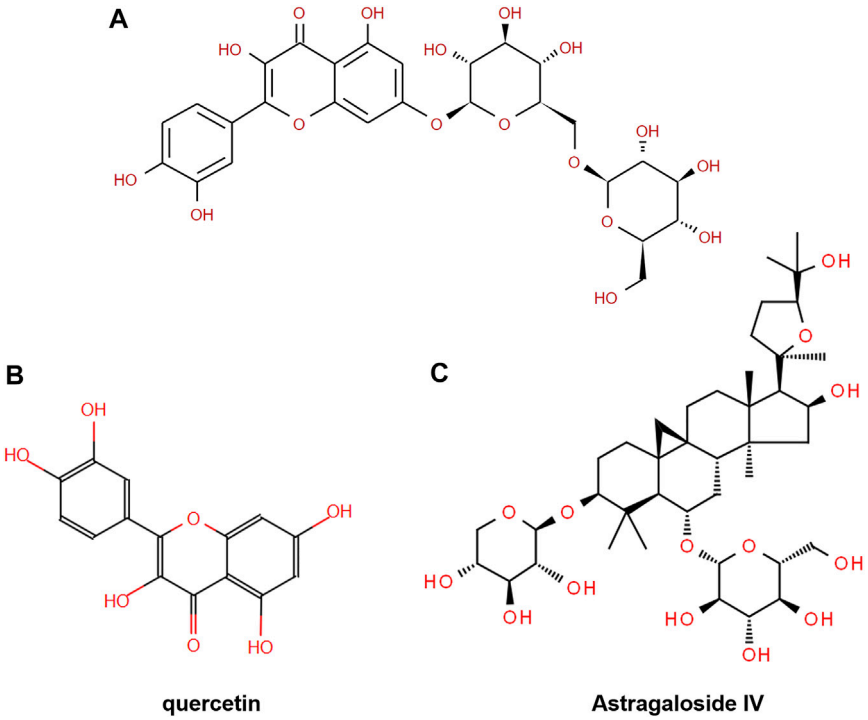

FIGURE 2
Chemical structure of **(A)** quercetin-7-O-β-D-glucopyranosyl (1→6)-β-D-glucopyranoside, **(B)** quercetin, and **(C)** astragaloside IV.

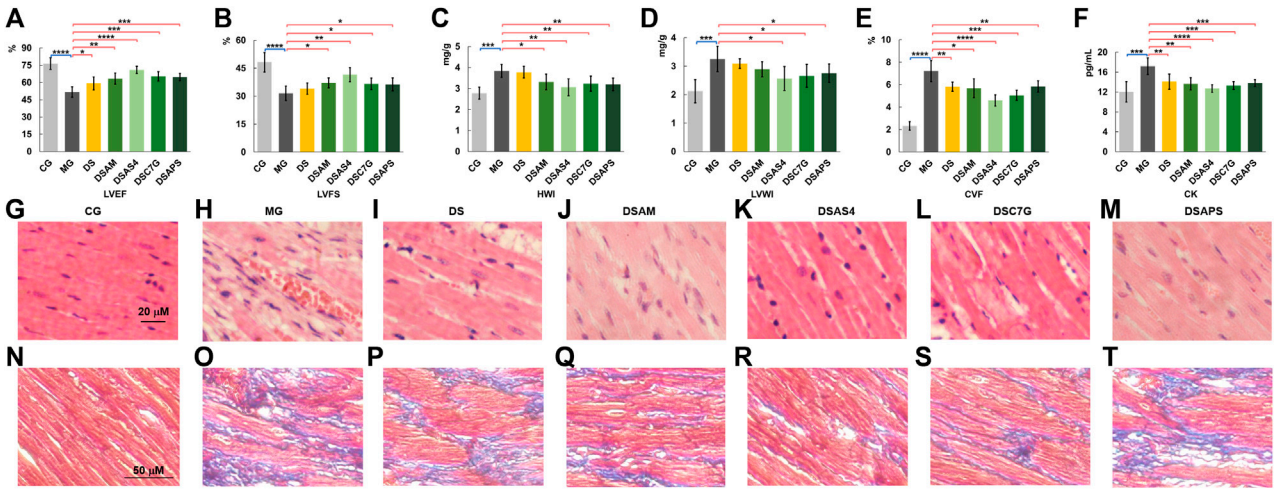

FIGURE 3
Phenotypic and pathological characterization **(A–F),** left ventricular ejection fraction (LVEF, **(A)**, left ventricular fraction shortening (LVFS, **(B)**, heart index (HWI, **(C)**, left ventricular mass index (LVWI, **(D)**, collagen volume fraction (CVF, **(E)** of myocardial cells, and plasma CK levels **(F)** of rats of the control (CG), model (MG), and treated groups with *Descurainia sophia* seed decoction alone (DS), and *Descurainia sophia* seeds plus *Astragalus mongholicus* decoction (DSAM), *Descurainia sophia* seeds decoction plus astragaloside IV (DSAS4), calycosin-7-glucoside (DSC7G), or Astragalus polysaccharides (DSAPS). The results of LVEF, LVFS, HWI, LVWI, CVF, and CK were measured by randomly selecting six rats (n = 6) from each group and are represented as mean ± SD. *$p < 0.05$ and **$p < 0.01$, ***$p < 0.001$ and ****$p < 0.0001$, represent statistical significance and high significance, respectively. **(G–M)** H&E (400×) and **(N–T)** Masson's (200×) trichrome staining of heart tissues of all groups. For Masson's staining, collagen fibers were stained in blue, and myocardial cell in dark red.

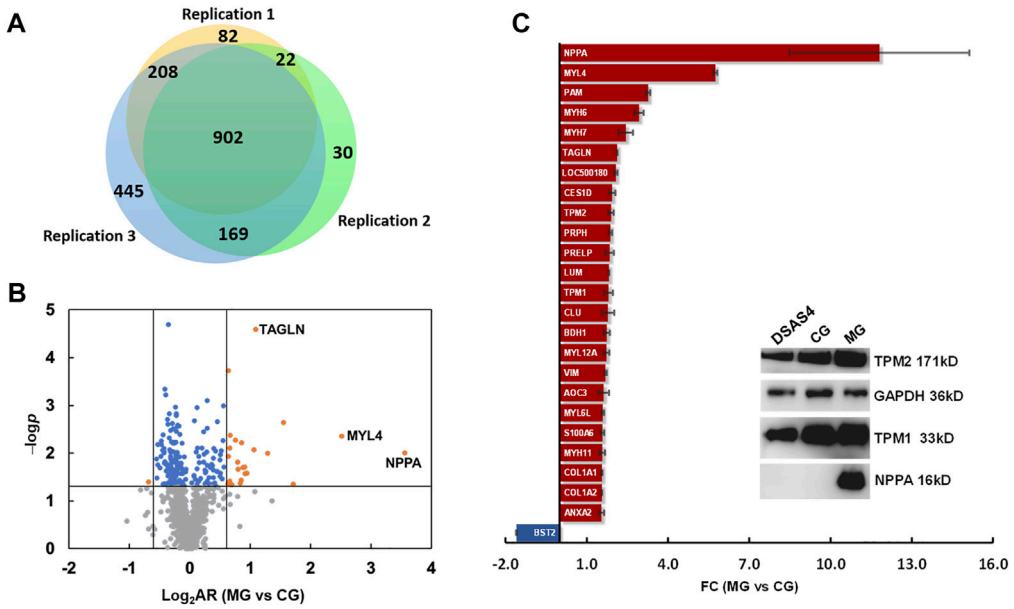

FIGURE 4
Differential expression proteomics of the heart of rats in the control group (CG) and ISO-iCM model group (MG). **(A)** Number of proteins identified in three parallel replicates. **(B)** Volcanic map of the proteins identified in both the control (CG) and model (MG) groups with various abundance ratios (ARs) and *p*-values. Orange point refers to a protein with a $\log_2$AR (MG vs. CG) of ≥0.59 or ≤ −0.59 and a *p*-value of <0.05; blue to a protein with a $\log_2$AR of > −0.59 or <0.59 and a *p*-value of <0.05, gray to a protein with a *p*-value of >0.05. **(C)** Fold changes (FCs) of 25 differentially expressed proteins in the heart of the model group (MG) compared to those in the control group (CG). The insert is the Western blotting bands of the representatives of DEPs, NPPA, TMP1, and TMP2 in the heart of rats in CG, MG, and the treated group with *Descurainia sophia* seeds decoction plus astragaloside IV (DSAS4). GAPDH was used as an internal reference.

the treatment with DS combined with AS4 exhibited the highest effectiveness to reverse the CVF level (Figure 3R). Meanwhile, this combined treatment also reverses the plasma myocardial enzyme creatine kinase (CK) level of model rats to close to that of controls (Figure 3F). Given the increased expression of CK in plasma is an important diagnostic marker of myocardial ischemia (Holmvang et al., 1998), these results indicate that the treatment with DS and AS4 significantly alleviated myocardial cell necrosis, resulting from myocardial ischemia in rats with ISO-iCM.

Identification of differential expressed proteins

After phenotypic characterization and physiological evaluation of rats with ISO-iCM before and after various treatments, we performed mass spectrometry (MS)-based quantitative proteomics analysis on the heart of rats to investigate the pharmacological efficiency of various treatments at a molecular level. The protein extraction from heart tissues and the subsequent MS/MS analysis were carried out in three independent replicates. In total, peptide matching spectrum maps allowed us to identify 55,307 peptides and 10,418 peptide groups, corresponding to 1,858 proteins. Of these 902 proteins were detected in three parallel sets, and 213 proteins were considered statistically reliable with a *p*-value <0.05 (Figures 4A,B, Supplementary Table S5). Among the 213 proteins were 24 proteins upregulated by more than 1.5-fold and 1 protein downregulated by more than 1.5-fold in the model rats compared to the counterparts in the controls (Figure 4C).

Among the 25 differentially expressed proteins (DEPs) (Figure 4C), the most significantly upregulated protein in the rats with ISO-iCM was natriuretic peptides A (NPPA), of which the fold-change (FC), designated as the abundance ratio of an upregulated protein in MG vs CG, but as negative reciprocal of abundance ratio of a downregulated proteins in MG vs CG, was 11.8. All 25 DEPs were grouped by the Proteome Discoverer (PD) software into extracellular matrix proteins, myosin family, intermediated filament family, actin or actin filament binding proteins, metabolism-related proteins, immune-related proteins, and calcium sensors (Table 3). It is worth to point out that the members of the myosin family, intermediated filaments, and actin filament binding proteins are all related to sarcomere modulation of the heart (Anderson et al., 2018; Daniels et al., 2021; Lehman et al., 2022). More importantly, the myosin proteins MYL4, MYH6, and MYH7, which work with actin to

TABLE 3 Differentially expressed proteins in the heart of rats with ISO-iCM.

Category	Accession	Gene symbol	Protein name (abbreviation)
Extracellular matrix protein	O08590	*Aoc3*	Membrane primary amine oxidase (AOC3)
	Q07936-1	*Anxa2*	Annexin A2 (ANXA2)
	P02466	*Col1a2*	Collagen alpha-2(I) chain (COL1A2)
	P02454	*Col1a1*	Collagen alpha-1(I) chain (COL1A1)
	P05371	*Clu*	Clusterin (CLU)
	P51886	*Lum*	Lumican (LUM)
	Q9EQP5	*Prelp*	Prolargin (PRELP)
	P14925-1	*Pam*	Peptidyl-glycine alpha-amidating monooxygenase (PAM)
Myosin family protein	Q63862-1	*Myh11*	Myosin-11 (MYH11)
	P13832	*Myl12a*	Myosin regulatory light chain RLC-A (MYL12A)
	Q64119-2	*Myl6l*	Myosin light polypeptide 6 (MYL6L)
	P02564	*Myh7*	Myosin-7 (MYH7)
	P02563	*Myh6*	Myosin-6 (MYH6)
	P17209	*Myl4*	Myosin light chain 4 (MYL4)
Intermediated filaments	P31000	*Vim*	Vimentin (VIM)
	P21807	*Prph*	Peripherin (PRPH)
Actin filament binding protein	P31232	*Tagln*	Transgelin (TAGLN)
	P04692-2	*Tpm1*	Isoform 2 of tropomyosin alpha-1 chain (TPM1)
	P58775-2	*Tpm2*	Isoform 2 of tropomyosin beta chain (TPM2)
Metabolism-related protein	P29147	*Bdh1*	D-beta-hydroxybutyrate dehydrogenase (BDH1)
	P16303	*Ces1d*	Carboxylesterase 1D (CES1D)
	P01161	*Nppa*	Natriuretic peptides A (NPPA)
Immunity-related protein	Q811A2	*Bst2*	Bone marrow stromal antigen 2 (BST2)
	P01835	Igkc	Ig kippa chain C (LOC500180)
Calcium sensor	P05964	*S100a6*	Protein S100-A6 (S100A6)

regulate the myocardial contraction (Daniels et al., 2021), were remarkably upregulated in the heart of the rats with ISO-iCM. This with the most significant upregulation of the commonly accepted biomarker NPPA to cardiomyopathy confirms the successful establishment of the ISO-iCM models at the molecular level.

Next, we performed MS quantitative proteomics analysis on the heart of the five treated groups. As shown in Figure 5A and the Supplementary Table S5, subjected to the treatment with DS alone, the expression of the most 25 DEPs were reversed to a different extent except for COL1A2, COL1A1, BDH1, MYH7, and MYH6, among which COL1A1, COL1A2, MYH6, and MYH7, especially MYH7, were further regulated, but D-β-hydroxybutyrate dehydrogenase (BDH1) in mitochondrion was downregulated, compared to the models. In TCM practices, DS is often used in combination with AM to treat cardiac diseases (Yu et al., 2021). However, our proteomic data showed that this combination did not pronouncedly improve the pharmacological effectiveness, though AM appeared to reverse the expression of BDH1, which was downregulated by DS, to the control level (Figure 5A). This may be contributable to the upregulation of NPPA and MYL4 by AM, compared to the DS treated group (Figure 5A). Interestingly, the major active component of AM, AS4 not only reversed the further expression of NPPA and myosin such as MYH6 and MYL4 closer to the control level but also reversed the expression of MYH7 and BDH1, which were upregulated and downregulated, respectively, by DS (Figure 5A). We also noticed that APS significantly upregulated MYL4 and NPPA, which were the most and the second upregulated proteins in the heart of model rats with ISO-iCM, compared with the DS-treated group. These results indicate that the upregulation of NPPA and MYL4, resulting from AM may be attributed to its active component APS (Figure 5A).

To verify the expression of the DEPs identified by quantitative proteomics analysis, we selected three NPPA, TPM1, and TPM2, the molecular weights of which locate at the low, medium, and high levels, respectively, to perform the traditional Western blot assays. As shown in the inset of Figure 4C, the results confirmed that compared to the control group (CG), NPPA, TPM1, and TPM2 were all significantly upregulated, and the combination of DS with AS4 remarkably reversed the expression of the three proteins.

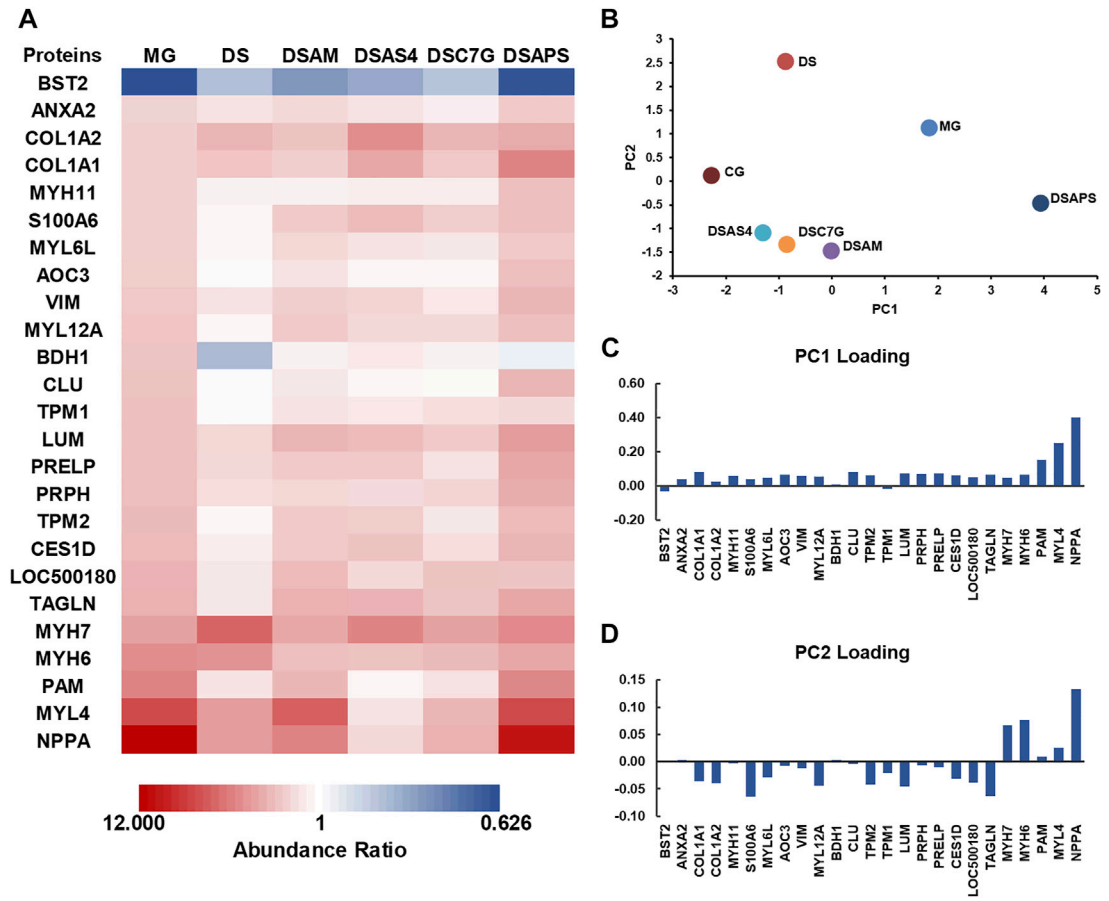

FIGURE 5
Differentially expressed proteins (DEPs) were detected in the heart of rats with ISO-iCM before and after treatments, compared to the controls. **(A)** Abundance ratios (model or treated groups vs. control group) of 25 DEPs in the model group (MG), treated group with Descurainia *sophia* seed decoction alone (DS), and *Descurainia sophia* seeds plus *Astragalus mongholicus* decoction (DSAM), *Descurainia sophia* seed decoction plus astragaloside IV (DSAS4), calycosin-7-glucoside (DSC7G), or astragalus polysaccharides (DSAPS). **(B)** Principal component analysis (PCA) is based on 213 proteins identified in all groups with a p-value <0.05. **(C,D)** Loading scores discriminate the model (MG) and treated groups, DS, DSAM, DSAS4, DSC7G, and DSAPS, over the control group (CG).

We performed principal component analysis (PCA) based on the protein profiling, including all 213 proteins detected in the heart of all six groups. The results indicated that among the five treated groups, the combination of DS with AS4 (DSAS4) made the treated group closer to the control group in the PC1 direction (Figure 5B), suggesting the highest pharmacological effect of this combination on ISO-iCM in rats. This is most likely contributable to the reversion of expression of NPPA, MYL4, and PAM, which contributes the most to PC loading in the positive direction (Figures 5A–C). In contrast, the treatment with DS and APS (DSAPS) made the treated group further away from the control one in the PC1 positive direction (Figure 5B) because this treatment further upregulated the expression of NPPA, MYL4, and PAM (Figure 5C). In other words, NPPA, MYL4, and PAM may serve as potential predictors and biomarkers for the diagnosis and prognosis of cardiomyopathy.

Bioinformatics analysis

To further dissect the functions and roles of the 25 DEPs (Table 3) in the heart of rats with ISO-iCM, we next performed bioinformatics analysis on these proteins. First, the 25 DEPs were uploaded into STRING 11.0 for protein–protein interaction (PPI) analysis. As shown in Figure 6A, the PPI network of the 25 DEPs consists of 25 nodes (genes/proteins) and 54 edges (interactions), which indicates that 18 of the 25 DEPs interact with each other and that the interactions could be grouped at four levels based on the edge confidence scores. One interaction group with high confidence level covers four extracellular matrix (ECM) proteins, PRELP, LUM, COL1A1, and COL1A2, of which the primary function is cell connecting. Another interaction group with a high confidence level contains VIM, MYL4, MYH7, MYH11, MYH6, MYL12a, TAGLN, TPM2, and

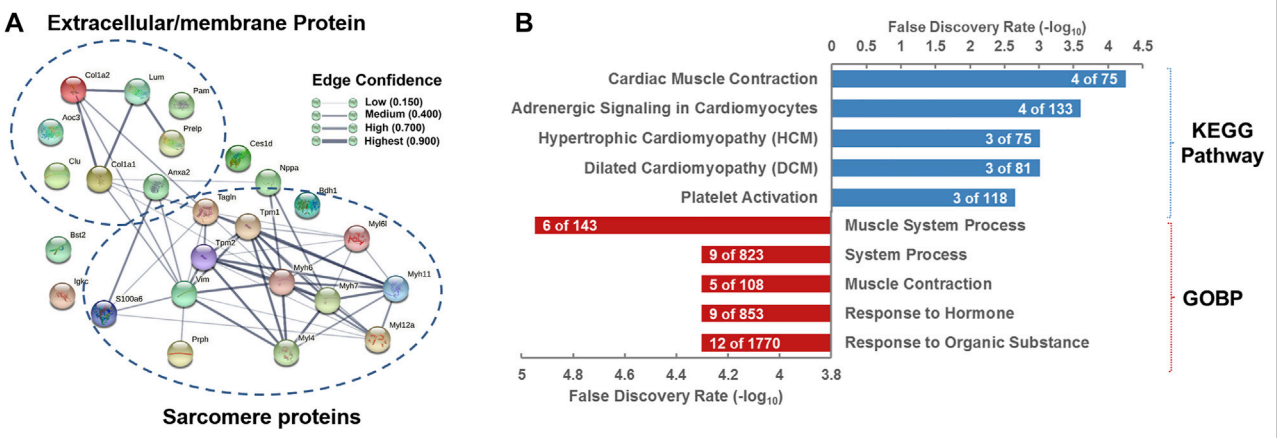

FIGURE 6
Bioinformatics analysis of differentially expressed proteins (DEPs) in the hearts of rats with ISO-iCM compared to the controls **(A)** Protein–protein interaction network of the 25 DEPs. **(B)** KEGG pathways and biological processes in which the 25 DEPs are associated with.

TPM1, which are all located in the cytoplasm and mainly regulate the structure and function of the sarcomere (Toepfer et al., 2020). Interestingly, being a member of type III intermediate filament proteins VIM directly interacts with the members of both the myosin family and ECM family. This suggests that VIM plays an essential role in ISO-iCM *via* involvement in the development of cytoskeleton and sarcomere, which are modulated by ECM proteins and myosin motor, respectively, associating with actin and/or actin-filament binding proteins such as TAGLN, TPM2, and TPM1.

Natriuretic peptides A (NPPA) is an energy metabolism-related protein and mediates cardio-renal homeostasis by binding to and stimulating NPR1 to produce cGMP (Ogawa et al., 2004). As shown in Figure 6A, NPPA directly interacts not only with the myosin proteins such as MYH6 and MYH7, of which both are molecular motors of the sarcomere (Toepfer et al., 2020; Daniels et al., 2021) but also with actin cross-linking/gelling protein TAGLN (Huang et al., 2018b), actin filament binding proteins TPM1/2 (Rani et al., 2015), and the intermediate filament protein VIM (Hol and Capetanaki, 2017), which are all involved in the binding of myosin to actin, modulating the myosin motor (Anderson et al., 2018; Lehman et al., 2022). In addition, NPPA directly interacts with ECM protein COL1A1 weakly. These implicate that NPPA plays a crucial role in the development of ISO-iCM by participating regulation of sarcomere structure and function of cardiomyocytes. As mentioned earlier, we induced cardiomyopathy in rats by isoproterenol, which is a non-specific β-AR agonist and can increase inotropy, chronotropy, and systemic vasodilation (Verma et al., 2012). It is commonly accepted that isoproterenol binds to the β2 adrenergic receptor, ADRB2, of cardiomyocytes, which in turn regulates the function of the proteins such as SLC9A3R2, CD36, and STAT3 (Yin et al., 2003; Verma et al., 2012; Stapel et al., 2017). The activation of the signal transducer and activator of transcription 3 (STAT3) can rapidly upregulate the expression of some cellular proteins, including NPPA and MYH7 (Figure 7), which were significantly upregulated in rats with ISO-iCM (*vide supra*) and in the patients with DCM (Chan et al., 2020; Toepfer et al., 2020). On the other hand, STAT3 activates the transcription regulator GATA4 (Snyder et al., 2010; Wang et al., 2018), thereby upregulating the expression of NPPA, MYH7, and MYH6 (Figure 7), which interacted with each other to regulate the structure and function of the sarcomere, resulting in heart failure and arrhythmias (Toepfer et al., 2020).

It is worth pointing out that similar to VIM and NPPA, the calcium sensor and modulator S100A6 is also upregulated in the heart of rats with ISO-iCM. Given that S100A6 is involved in the regulation of cytoskeleton and sarcomere structures by interacting with ANXA2, TAGLN, and MYL12a, which are all upregulated in the model rats, the elevated level of S100A6 may contribute to the disorder in cytoskeleton and cardiomyocyte motility *via* modulating the homeostasis of calcium ions (Breen and Tang, 2003; Nowotny et al., 2003).

Being a member of the myosin family and molecular motors of the sarcomere, Myosin 11 (MYH11) is a protein complex contributing to cell contraction by hydrolysis of ATP (Zhu et al., 2006). The mutation of the *Myh11* gene may cause familial thoracic aortic aneurysm and dissection heart, in which the aortic was enlarged near the heart (El-Hamamsy and Yacoub, 2009). There have been so far few reports on the relationship of MYL12a with heart-related diseases, but Park et al. (2011) found that this protein could influence cell morphology and dynamics by sustaining the stability of the Myosin 11. In *Myl12a* knockout cells, the MYH9, MYH10, and MYH6 expressions were significantly reduced. Taking together, our work suggests that

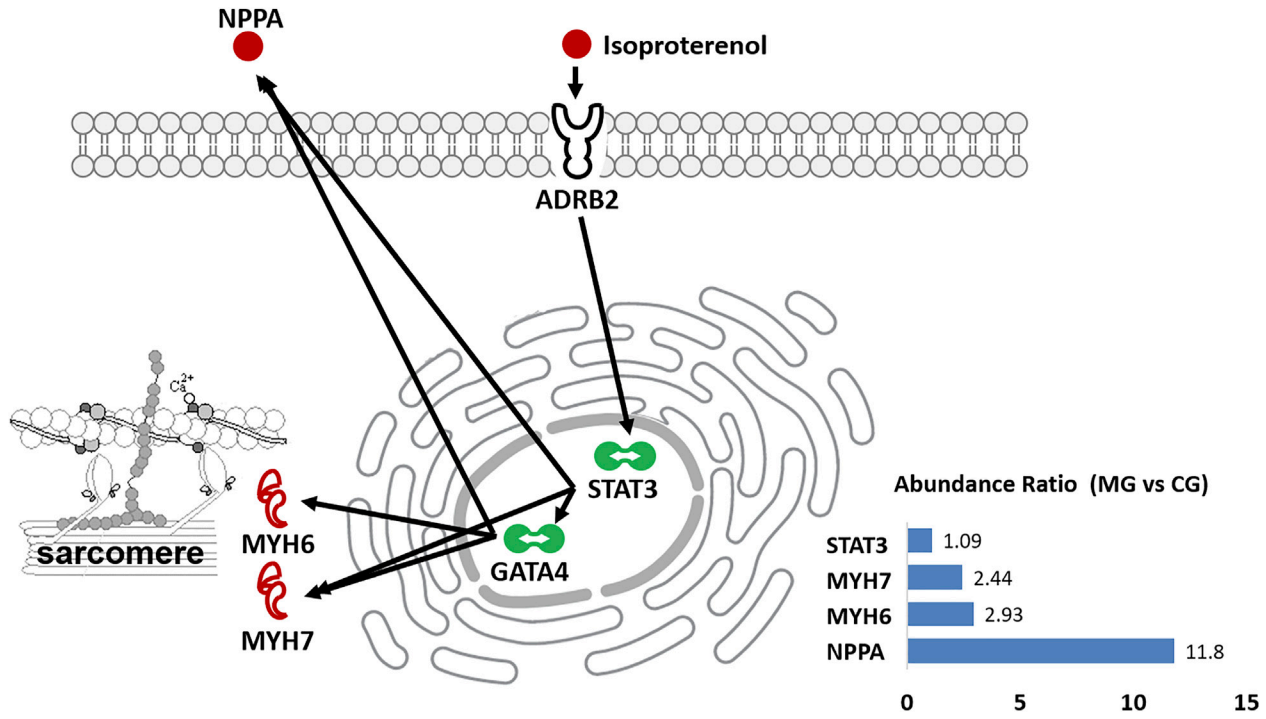

FIGURE 7
Diagrammatic process of isoproterenol-induced heart dysfunction in rats. It shows that isoproterenol binds to ADRB2 and upregulates the expression of NPPA, MYH6, and MYH7 *via* activating the transcriptional regulators STAT3 and GATA4. The inset shows the abundance ratio of the selected proteins expressed in the heart of controls (CG) and models (MG).

MYH11 and MYH12a are also implicated in the development of ISO-iCM in rats in addition to other members, MYL4, MYH6/7, and MYL6L, of the myosin family.

Both PRPH and VIM belong to the type III intermediate filament family. PRPH is primarily expressed in peripheral neurons. The expression of *Prph* is upregulated during neuron development or regeneration when axons were injured (Hol and Capetanaki, 2017). With regard to this, the upregulation of PRPH in rats with ISO-iCM may suggest damage to the nervous system of the heart. VIM is mainly expressed in undifferentiated mesenchymal origin cells and regulates the functions of the lysosome, Golgi complex, and mitochondria organelles. Moreover, VIM can also influence the transportation of the integrins to the plasm membrane, and may then impact cell-extracellular matrix adhesion (Hol and Capetanaki, 2017). Taking this into account, the intermediate filament family proteins PRPH and VIM may be involved in the development of ISO-iCM in rats *via* damaging heart nerves and regulating cytoskeleton and myofibril structure.

Transgelin (TAGLN) is an actin filament binding protein and is also named smooth muscle protein 22-α (SM22-α). It was reported to be associated with tumorigenesis (Yu et al., 2013). Studies on patients with pulmonary arterial hypertension (PAH) in congenital heart disease (CHD) showed that TAGLN overexpression may promote the proliferation, migration, and cytoskeleton strengthening of pulmonary arterial smooth muscle cells (PASMCs) (Huang et al., 2018a). The upregulation of TAGLN in the heart of rats with ISO-iCM implicates its participation in cardiomyopathy by functioning as smooth muscle protein.

The membrane primary amine oxidase (AOC3) is an extracellular matrix protein. Although there is no evidence for direct association of AOC3 with heart failure, this protein has been identified as a new marker of myofibroblasts (Hsia et al., 2016). Hence, the protein is likely to be involved in the process of cardiomyocyte fibrosis and has a close relationship with ISO-iCM.

Two immune-related proteins, the Ig kappa chain C region (LOC500180) and BST2 were unraveled to be significantly upregulated and downregulated, respectively, in the heart of rats with ISO-iCM. A clinical study suggested that combined free light chains (cFLCs), which include both kappa and lambda FLCs, could be a marker of heart failure prognosis (Jackson et al., 2015). However, another report argued that a more mechanistic understanding of heart failure pathophysiology is needed to support the conclusion (Januzzi and Mann, 2015). Our results herein verified that Ig kappa chain C may play an important role in cardiomyopathy, perhaps *via* involvement in the

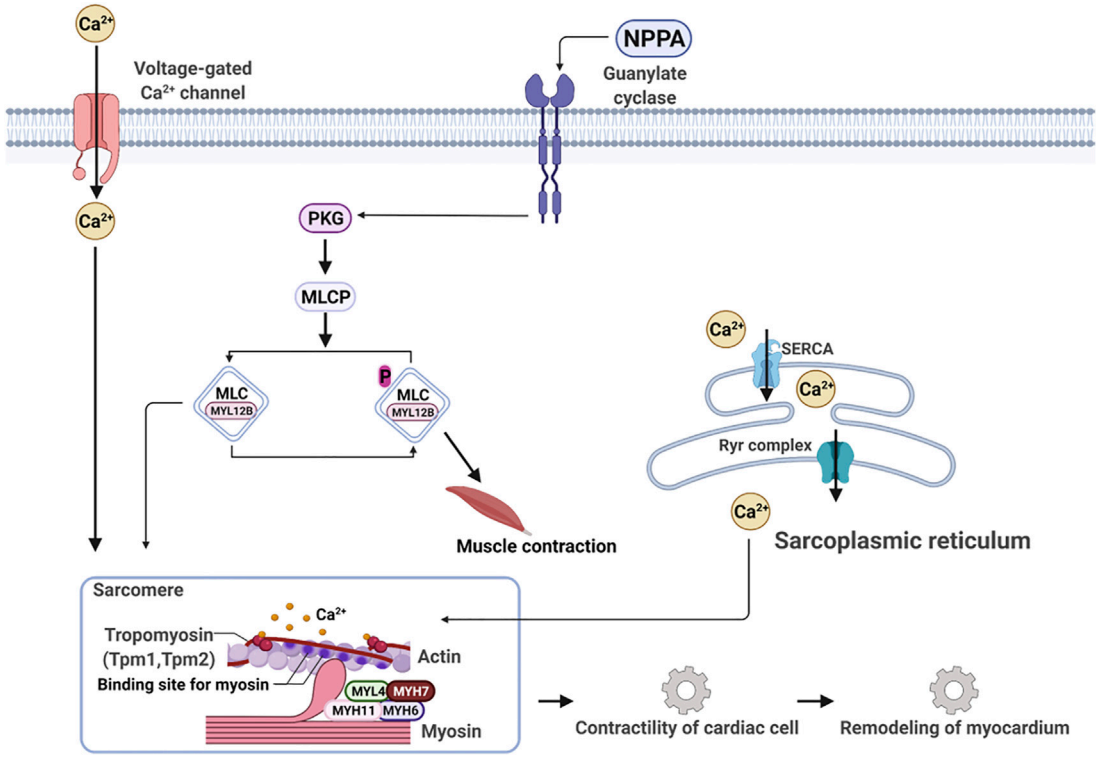

FIGURE 8
NPPA-triggered signaling pathway works together with the calcium signaling pathway to modulate contractility and remodeling of the myocardium.

inflammatory pathway (Kang et al., 2009). BST2 is the only protein that was downregulated in rats with ISO-iCM. It is an antiviral antigen implicated in the regulation of viral infection (Evans et al., 2010). Despite its antiviral functions, BST2 may be involved in some disease manifestations, for example, cancer and autoimmune diseases (Mahauad-Fernandez and Okeoma, 2016). Recently, the research found that circulating healing (CH) cells expressing BST2 are functionally activated by the injury-regulated systemic factor hepatocyte growth factor-activator (HGFA), which could participate in tissue repair (Lo Sicco et al., 2018). With regard to this, our finding that BST2 was downregulated in rats with ISO-iCM implies myocardial inflammatory damage in the rats.

The gene ontology (GO) enrichment showed that the most associated Kyoto Encyclopedia of Genes and Genomes (KEGG) pathways and biological process (BP) of the 25 DEPs are cardiac muscle contraction and muscle system process, respectively (Figure 6B). Since the most of the 25 DEPs, including eight extracellular matrix proteins and six myosin family proteins, and five actin-binding proteins, are involved in the cytoskeleton and myofibril structure and function, the disorders in cardiac muscle contraction, in particular structure and function of sarcomeric myosin motor, is most likely the main pathogenic elements of ISO-iCM in rats, similar to DCM and HCM in human.

The functional enrichment by STRING added 100 proteins (nodes) and 1,437 interactions (edges) to the initial 25 DEPs by matching the best interactor criteria (Supplementary Figure S6A). Notably, GO analysis annotated the most associated KEGG pathway and the biological process (GOBP) of the 125 proteins to be focal adhesion and muscle system process (Supplementary Figure S6B), again indicating that abnormality in structures of cytoskeleton and sarcomere are the characteristic phenotypes of ISO-iCM in rats.

Next, we applied the Ingenuity Pathway Analysis (IPA) program to enrich the core signaling pathways, which the 25 DEPs are associated with. The top 20 core signaling pathways of which the 25 DEPs are most associated with are depicted in Supplementary Figure S7. We can see that the myosins, for example, MYH6 and MYH7, and tropomyosins (TPM1 and TPM2) are deeply implicated in the dilated cardiomyopathy signaling pathway (Supplementary Figure S8) and the calcium signaling pathway (Supplementary Figure S9), of which both play a crucial role in the contractility of cardiac cell and the remodeling of the myocardium (Figure 8).

Discussion

The occurrence and development of heart failure are closely related to the disorder of water and electrolyte metabolism (Chobanian et al., 1957), which are mainly modulated by natriuretic peptides A (NPPA) and GMP signaling (Moro and Lafontan, 2013; Song et al., 2015). In this work, we used isoproterenol to induce cardiomyopathy in rats. Our results indicated that isoproterenol is bound to β2-adrenergic receptor, and indeed upregulated NPPA expression by activating STA3 and GATA4 in the heart of rats. Meanwhile, the activation of STAT3 and GATA4 also promoted remarkably the expression of myosins MYH6, MYH7, MYH11, and MYL4, and tropomyosins TPM1 and TPM2. The myocardial contraction requires two proteins, myosin, and actin (Daniels et al., 2021). Sarcomeric myosin is the molecular engine of the heart, which converts the chemical energy of ATP into movement and regulates force production for contractibility of the whole heart. Myosin acts as a molecular accelerator or brake depending on whether and how it binds to actin. Actin is controlled by fluctuating calcium levels, which regulate a molecular clutch shielding actin *via* the troponin complex (TPM1 and TPM2) from myosin in a low diastolic Ca^{2+} level and exposing actin at a high systolic Ca^{2+} level (Daniels et al., 2021) to myosin binding, thereby activating myosin-ATPase activity to power heart movement. Therefore, any changes in ATP consumption and force production caused by genetic mutations on myosin and/or abnormal activation/suppression of myosin motor could lead to cardiac diseases, for example, hypertrophic cardiomyopathy (HCM) and dilated cardiomyopathy (DCM). With regard to this, several small molecule inhibitors and activators of myosin have been developed for treating inherited cardiomyopathies with genetic variants in myosin and entered different phases of clinic trails (Lehman et al., 2022). The drug candidates, for example, mavacamten, were demonstrated to have a spatially distinct effect in the sarcomere and are thought to be root-targeting therapeutics without harmfulness to other organs (Lehman et al., 2022).

Our quantitative proteomics data demonstrated that apart from about 12-fold increase in the NPPA level, the expression levels of myosin family proteins, MYL4, MYH6, MYH7, MYL12A, MYL6L, and MYH11, and actin filament binding proteins TAGLN, TPM1, and TPM2, were all elevated in the heart of the model rats with ISO-iCM. This remarkably indicates the upregulation of myosin-ATPase activity. Taking the increase in the expression of calcium sensor S100A6 into account, the model rats appeared to have similar characteristics to the inherited HCM, in which the genetic variants in sarcomeric myosin and myofilament increase the proportion of active myosin, that is, more accelerator and less brake, leading to diastolic dysfunction and hypercontractility (Daniels et al., 2021). Also, thanks to the precise MS quantification of proteins, we demonstrated that DS significantly reversed the expression of the myosin family proteins and actin filament binding proteins, except for MYH6 and MYH7, showing a good pharmacological effect on ISO-iCM in rats. More importantly, our study revealed that the major active component AS4 in AM remarkably improved the pharmacological efficiency of DS on ISO-iCM in rats by complementarily reversing the expression of MYH6 and MYH7, and further downregulating NPPA, MYK4, and PAM. These results strongly suggest that the combination of DS with AS4 exerted pharmacological benefits on ISO-iCM in rats by synergistically modulating the myosin motor. Another active component calycosin-7-glucoside (C7G) was also shown to improve the pharmacological efficacy of DS on ISO-iCM. However, the improvement was less than AS4, most likely due to the weaker ability of C7G to downregulate NPPA, MYL4, and PAM.

As mentioned earlier, AM is often used in combination with DS. However, in the present work, we did not find that the combination of DS and AM produced a pronouncedly higher pharmacological potential for ISO-iCM in rats than the use of DS alone. We have also investigated the pharmacological efficiency of AM used alone and found that the pharmacological effect of AM alone on ISO-iCM in rats was poor (data now showed). To sort out why the combination of DS and AM could not provide better pharmacological benefits on ISO-iCM, we further studied the effect of Astragalus polysaccharides (APS) on the pharmacological efficiency of DS. Surprisingly, we found that APS upregulated NPPA, MYL4, and PAM, which are the most contributors to the development of ISO-iCM in rats, thereby reducing the pharmacological efficiency of DS on ISO-iCM. This suggests that it is the presence of APS in AM that reduced the pharmacological effect of DS combined with AM on ISO-iCM in rats. These findings imply that the combination of TCMs is highly necessary, but that the simple combination may not produce expected outcomes.

On the other hand, our quantitative proteomics results showed that DS decoction significantly upregulated the expression of MYH7, which as mentioned earlier plays a vital role in development of cardiomyopathy, and downregulated the expression of BDH1, which acts as an actin filament binding protein and is involved in cardiac diseases (Brahma et al., 2020). However, we herein did not identify which components in DS caused the differential expression of these two proteins. To address this issue, it is necessary to perform the proteomics analysis after treating the ISO-iCM model rats with purified active components, for example, quercetin and kaempferol, from DS. This work will be undertaken in the near future in our laboratory.

Conclusion

In this work, with the use of quantitative mass spectrometric proteomics analysis, we revealed for the first time that the classic traditional Chinese medicine, *Descurainia sophia* seeds (DS) relieved isoproterenol-induced cardiomyopathy (ISO-iCM) in rats by reversing the most of differentially expressed proteins (DEPs), including molecular motor MYL4 and the well-known biomarker NPPA of cardiomyopathy. Importantly, we demonstrated that the combined use of DS with *Astragalus mongholicus* (AM) did not provide better pharmacological benefit to ISO-iCM, while astragaloside IV (AS4), a major active component in AM, significantly improved the pharmacological effect of DS on ISO-iCM *via* complementarily or further reversing myosins MYH6/7, and NPPA and MYL4. This suggests that DS and AS4 synergistically work on modulating the myosin motor in sarcomere to achieve better pharmacological benefit to cardiomyopathy. In contrast, the combination of DS with *Astragalus* polysaccharides (APS) from AM even reduced the pharmacological efficiency of DS to ISO-iCM in rats, most likely contributing to the less improvement of AM on the pharmacological efficiency of DS. This work highlights the power of mass spectrometric proteomics strategy combined with conventional pathological approaches for the development and modernization of TCM. Significantly, our findings provide novel insights to better understanding and improving the combination pharmacological principle of traditional Chinese medicine.

Data availability statement

The datasets of proteomics analysis presented in this study can be found in online Proteomics Identification Database at ebi.ac.uk/pride/ with a reference number of 1-20220509-37752.

Ethics statement

The animal study was reviewed and approved by Ethics Committee of Shandong University of Traditional Chinese Medicine.

Author contributions

FWand SW conceived and supervised the project. SW, FW, QL, and QC obtained the fundings. XL, QL, JH, SL, JL, YZ, and YZ performed mass spectrometry and data analysis. QC, XJ, WY, and TW conducted animal experiments and pathological assays. FW, SL, XL, FZ, and QC wrote and revised the manuscript. All authors approved the final version of the manuscript.

Funding

This work was partially supported by the National Natural Science Foundation of China (Nos. 81673852 (SW), 82104554 (QC)), Beijing Municipal Natural Science Foundation (No. 7182190 (QL)), Natural Science Foundation of Shandong Province (ZR2021MH313 (QC)), Shandong Province TCM Science and Technology Development Plan Project (NO.2019-0048, (QC)) and the National Key Research and Development Program of China (No. 2013CB531805 (FW)).

Conflict of interest

The authors declare that the research was conducted in the absence of any commercial or financial relationships that could be construed as a potential conflict of interest.

Publisher's note

Supplementary material

The Supplementary Material for this article can be found online at: https://www.frontiersin.org/articles/10.3389/fphar.2022.939483/full#supplementary-material

References

Anderson, R. L., Trivedi, D. V., Sarkar, S. S., Henze, M., Ma, W. K., Gong, H., et al. (2018). Deciphering the super relaxed state of human beta-cardiac myosin and the mode of action of mavacamten from myosin molecules to muscle fibers. *Proc. Natl. Acad. Sci. U. S. A.* 115 (35), E8143–E8152. doi:10.1073/pnas.1809540115

Brahma, M. K., Ha, C. M., Pepin, M. E., Mia, S., Sun, Z., Chatham, J. C., et al. (2020). Increased glucose availability attenuates myocardial ketone body utilization. *J. Am. Heart Assoc.* 9 (15), e013039. doi:10.1161/jaha.119.013039

Breen, E. C., and Tang, K. (2003). Calcyclin (S100A6) regulates pulmonary fibroblast proliferation, morphology, and cytoskeletal organization *in vitro*. *J. Cell. Biochem.* 88 (4), 848–854. doi:10.1002/jcb.10398

Chan, M. Y., Efthymios, M., Tan, S. H., Pickering, J. W., Troughton, R., Pemberton, C., et al. (2020). Prioritizing candidates of post-myocardial infarction heart failure using plasma proteomics and single-cell transcriptomics. *Circulation* 142 (15), 1408–1421. doi:10.1161/circulationaha.119.045158

Chen, Q., Ji, X.-M., Wang, Y.-F., Kan, D.-F., Han, X.-C., and Wang, S.-J. (2019). Effects of compatibility of Radix Astragali seu Hedysari and Semen Lepidii on the rats with harmful fluid retention in the upper jiao. *China J. Tradit. China. Med. Pharm.* 34 (3), 952–956.

Chen, W., Li, Y. M., and Yu, M. H. (2010a). Astragalus polysaccharides inhibited diabetic cardiomyopathy in hamsters depending on suppression of heart chymase activation. *J. Diabetes Complicat.* 24 (3), 199–208. doi:10.1016/j.jdiacomp.2008.12.003

Chen, W., Yu, M.-H., Li, Y.-M., Chen, W.-J., and Xia, Y.-P. (2010b). Beneficial effects of astragalus polysaccharides treatment on cardiac chymase activities and cardiomyopathy in diabetic hamsters. *Acta Diabetol.* 47 (S1), 35–46. doi:10.1007/s00592-009-0116-5

Chen, X. J., Bian, Z. P., Lu, S., Xu, J. D., Gu, C. R., Yang, D., et al. (2006a). Cardiac protective effect of astragalus on viral myocarditis mice: comparison with perindopril. *Am. J. Chin. Med.* 34 (3), 493–502. doi:10.1142/S0192415X06004028

Chen, X. J., Meng, D., Feng, L., Bian, Y. Y., Li, P., Yang, D., et al. (2006b). Protective effect of astragalosides on myocardial injury by isoproterenol in SD rats. *Am. J. Chin. Med.* 34 (6), 1015–1025. doi:10.1142/S0192415X0600448X

Cho, J. Y., Kim, K. H., Song, J. E., Kim, J. E., Park, H., Yoon, H. J., et al. (2018). Predictors of left ventricular functional recovery and their impact on clinical outcomes in patients with newly diagnosed dilated cardiomyopathy and heart failure. *Heart Lung Circ.* 27 (1), 41–49. doi:10.1016/j.hlc.2017.02.013

Chobanian, A. V., Burrows, B. A., and Hollander, W. (1957). Electrolyte and water metabolism in cardiac patients with early congestive heart failure. *Circulation* 16 (5), 866.

Daniels, M. J., Fusi, L., Semsarian, C., and Naidu, S. S. (2021). Myosin modulation in hypertrophic cardiomyopathy and systolic heart failure getting inside the engine. *Circulation* 144 (10), 759–762. doi:10.1161/circulationaha.121.056324

Du, X. Q., Shi, L. P., Chen, Z. W., Hu, J. Y., Zuo, B., Xiong, Y., et al. (2022). Astragaloside IV ameliorates isoprenaline-induced cardiac fibrosis in mice via modulating gut microbiota and fecal metabolites. *Front. Cell. Infect. Microbiol.* 12, 836150. doi:10.3389/fcimb.2022.836150

El-Hamamsy, I., and Yacoub, M. H. (2009). Cellular and molecular mechanisms of thoracic aortic aneurysms. *Nat. Rev. Cardiol.* 6 (12), 771–786. doi:10.1038/nrcardio.2009.191

Evans, D. T., Serra-Moreno, R., Singh, R. K., and Guatelli, J. C. (2010). BST-2/tetherin: a new component of the innate immune response to enveloped viruses. *Trends Microbiol.* 18 (9), 388–396. doi:10.1016/j.tim.2010.06.010

Halder, S. S., Sewanan, L. R., Rynkiewicz, M. J., Moore, J. R., Lehman, W. J., and Campbell, S. G. (2021). Abstract P459: mavacamten and danicamtiv reverse respective contractile abnormalities in engineered heart tissue models of hypertrophic and dilated cardiomyopathy. *Circ. Res.* 129. doi:10.1161/res.129.suppl_1.p459

Hol, E. M., and Capetanaki, Y. (2017). Type III intermediate filaments desmin, glial fibrillary acidic protein (GFAP), vimentin, and peripherin. *Cold Spring Harb. Perspect. Biol.* 9 (12), a021642. doi:10.1101/cshperspect.a021642

Holmvang, L., Luscher, M. S., Clemmensen, P., Thygesen, K., Grande, P., and Grp, T. S. (1998). Very early risk stratification using combined ECG and biochemical assessment in patients with unstable coronary artery disease (A thrombin inhibition in myocardial ischemia [TRIM] substudy). The TRIM Study Group. *Circulation* 98 (19), 2004–2009. doi:10.1161/01.cir.98.19.2004

Houson, H., Hedrick, A., and Awasthi, V. (2020). Drug-induced cardiomyopathy: Characterization of a rat model by [^{18} F]FDG/PET and [^{99m} Tc]MIBI/SPECT. *Anim. Model. Exp. Med.* 3 (4), 295–303. doi:10.1002/ame2.12136

Hsia, L. T., Ashley, N., Ouaret, D., Wang, L. M., Wilding, J., and Bodmer, W. F. (2016). Myofibroblasts are distinguished from activated skin fibroblasts by the expression of AOC3 and other associated markers. *Proc. Natl. Acad. Sci. U. S. A.* 113 (15), E2162–E2171. doi:10.1073/pnas.1603534113

Huang, C. Y., Qiu, S., Fan, X. C., Jiao, G. Y., Zhou, X., Sun, M., et al. (2021). Evaluation of the effect of Shengxian Decoction on doxorubicin-induced chronic heart failure model rats and a multicomponent comparative pharmacokinetic study after oral administration in normal and model rats. *Biomed. Pharmacother.* 144, 112354. doi:10.1016/j.biopha.2021.112354

Huang, L., Li, L., Yang, T., Li, W., Song, L., Meng, X., et al. (2018a). Transgelin as a potential target in the reversibility of pulmonary arterial hypertension secondary to congenital heart disease. *J. Cell. Mol. Med.* 22 (12), 6249–6261. doi:10.1111/jcmm.13912

Huang, L., Li, L., Yang, T., Li, W., Song, L., Meng, X. M., et al. (2018b). Transgelin as a potential target in the reversibility of pulmonary arterial hypertension secondary to congenital heart disease. *J. Cell. Mol. Med.* 22 (12), 6249–6261. doi:10.1111/jcmm.13912

Jackson, C. E., Haig, C., Welsh, P., Dalzell, J. R., Tsorlalis, I. K., McConnachie, A., et al. (2015). Combined free light chains are novel predictors of prognosis in heart failure. *JACC. Heart Fail.* 3 (8), 618–625. doi:10.1016/j.jchf.2015.03.014

Januzzi, J. L., Jr., and Mann, D. L. (2015). Light chains and the failing heart: important mechanistic link or fifty shades of gray? *JACC. Heart Fail.* 3 (8), 626–628. doi:10.1016/j.jchf.2015.03.012

Kamisago, M., Sharma, S. D., Depalma, S. R., Solomon, S., Sharma, P., McDonough, B., et al. (2000). Mutations in sarcomere protein genes as a cause of dilated cardiomyopathy. *N. Engl. J. Med.* 343 (23), 1688–1696. doi:10.1056/nejm200012073432304

Kang, B. Y., Hu, C., Prayaga, S., Khaidakov, M., Sawamura, T., Seung, K. B., et al. (2009). LOX-1 dependent overexpression of immunoglobulins in cardiomyocytes in response to angiotensin II. *Biochem. Biophys. Res. Commun.* 379 (2), 395–399. doi:10.1016/j.bbrc.2008.12.143

Lehman, S. J., Crocini, C., and Leinwand, L. A. (2022). Targeting the sarcomere in inherited cardiomyopathies. *Nat. Rev. Cardiol.* 19, 353–363. doi:10.1038/s41569-022-00682-0

Li, F., Li, J., Li, S., Guo, S., and Li, P. (2020). Modulatory effects of Chinese herbal medicines on energy metabolism in ischemic Heart Diseases. *Front. Pharmacol.* 11, 995. doi:10.3389/fphar.2020.00995

Lin, J., Fang, L., Li, H., Li, Z., Lyu, L., Wang, H., et al. (2019). Astragaloside IV alleviates doxorubicin induced cardiomyopathy by inhibiting NADPH oxidase derived oxidative stress. *Eur. J. Pharmacol.* 859, 172490. doi:10.1016/j.ejphar.2019.172490

Liu, B., Zhang, J., Liu, W., Liu, N., Fu, X., Kwan, H., et al. (2016). Calycosin inhibits oxidative stress-induced cardiomyocyte apoptosis via activating estrogen receptor-α/β. *Bioorg. Med. Chem. Lett.* 26 (1), 181–185. doi:10.1016/j.bmcl.2015.11.005

Liu, Q., Qu, H. Y., Zhou, H., Rong, J. F., Yang, T. S., Xu, J. J., et al. (2020). Luhong formula has a cardioprotective effect on left ventricular remodeling in pressure-overloaded rats. *Evid. Based. Complement. Altern. Med.* 2020, 4095967. doi:10.1155/2020/4095967

Liu, Z.-H., Liu, H.-B., and Wang, J. (2018). Astragaloside IV protects against the pathological cardiac hypertrophy in mice. *Biomed. Pharmacother.* 97, 1468–1478. doi:10.1016/j.biopha.2017.09.092

Lo Sicco, C., Reverberi, D., Villa, F., Pfeffer, U., Quarto, R., Cancedda, R., et al. (2018). Circulating healing (CH) cells expressing BST2 are functionally activated by the injury-regulated systemic factor HGFA. *Stem Cell Res. Ther.* 9 (1), 300. doi:10.1186/s13287-018-1056-1

Ma, J., Peng, A., and Lin, S. Y. (1998). Mechanisms of the therapeutic effect of astragalus membranaceus on sodium and water retention in experimental heart failure. *Chin. Med. J.* 111 (1), 17–23.

Mahauad-Fernandez, W. D., and Okeoma, C. M. (2016). The role of BST-2/Tetherin in host protection and disease manifestation. *Immun. Inflamm. Dis.* 4 (1), 4–23. doi:10.1002/iid3.92

Moro, C., and Lafontan, M. (2013). Natriuretic peptides and cGMP signaling control of energy homeostasis. *Am. J. Physiol. Heart Circ. Physiol.* 304 (3), H358–H368. doi:10.1152/ajpheart.00704.2012

Nowotny, M., Spiechowicz, M., Jastrzebska, B., Filipek, A., Kitagawa, K., and Kuznicki, J. (2003). Calcium-regulated interaction of Sgt1 with S100A6 (calcyclin) and other S100 proteins. *J. Biol. Chem.* 278 (29), 26923–26928. doi:10.1074/jbc.M211518200

Ogawa, H., Qiu, Y., Ogata, C. M., and Misono, K. S. (2004). Crystal structure of hormone-bound atrial natriuretic peptide receptor extracellular domain - rotation mechanism for transmembrane signal transduction. *J. Biol. Chem.* 279 (27), 28625–28631. doi:10.1074/jbc.M313222200

Park, I., Han, C., Jin, S., Lee, B., Choi, H., Kwon, J. T., et al. (2011). Myosin regulatory light chains are required to maintain the stability of myosin II and cellular integrity. *Biochem. J.* 434 (1), 171–180. doi:10.1042/bj20101473

Rani, D. S., Nallari, P., Dhandapany, P. S., Rani, J., Meraj, K., Ganesan, M., et al. (2015). Coexistence of digenic mutations in both thin (TPM1) and thick (MYH7) filaments of sarcomeric genes leads to severe hypertrophic cardiomyopathy in a south Indian FHCM. *DNA Cell Biol.* 34 (5), 350–359. doi:10.1089/dna.2014.2650

Rieth, A. J., Jung, C., Gall, H., Rolf, A., Mitrovic, V., Hamm, C. W., et al. (2019). Association of galectin-3 with changes in left ventricular function in recent-onset dilated cardiomyopathy. *Biomarkers* 24 (7), 652–658. doi:10.1080/1354750x.2019.1642959

Scigelova, M., Hornshaw, M., Giannakopulos, A., and Makarov, A. (2011). Fourier transform mass spectrometry. *Mol. Cell. Proteomics* 10 (7), M111.009431. doi:10.1074/mcp.M111.009431

Shanmugam, G., Challa, A. K., Litovsky, S. H., Devarajan, A., Wang, D., Jones, D. P., et al. (2019). Enhanced Keap1-Nrf2 signaling protects the myocardium from

isoproterenol-induced pathological remodeling in mice. *Redox Biol.* 27, 101212. doi:10.1016/j.redox.2019.101212

Shen, S., Sewanan, L. R., Jacoby, D. L., and Campbell, S. G. (2021). Danicamtiv enhances systolic function and frank-starling behavior at minimal diastolic cost in engineered human myocardium. *J. Am. Heart Assoc.* 10 (12), e020860. doi:10.1161/JAHA.121.020860

Snyder, M., Huang, X. Y., and Zhang, J. J. (2010). Stat3 directly controls the expression of Tbx5, Nkx2.5, and GATA4 and is essential for cardiomyocyte differentiation of P19CL6 cells. *J. Biol. Chem.* 285 (31), 23639–23646. doi:10.1074/jbc.M110.101063

Song, W., Wang, H., and Wu, Q. Y. (2015). Atrial natriuretic peptide in cardiovascular biology and disease (NPPA). *Gene* 569 (1), 1–6. doi:10.1016/j.gene.2015.06.029

Stapel, B., Kohlhaas, M., Ricke-Hoch, M., Haghikia, A., Erschow, S., Knuuti, J., et al. (2017). Low STAT3 expression sensitizes to toxic effects of beta-adrenergic receptor stimulation in peripartum cardiomyopathy. *Eur. Heart J.* 38 (5), 349–361. doi:10.1093/eurheartj/ehw086

Tan, Y. Q., Chen, H. W., and Li, J. (2020). Astragaloside IV: an effective drug for the treatment of cardiovascular diseases. *Drug Des. Devel. Ther.* 14, 3731–3746. doi:10.2147/dddt.S272355

Toepfer, C. N., Garfinkel, A. C., Venturini, G., Wakimoto, H., Repetti, G., Alamo, L., et al. (2020). Myosin sequestration regulates sarcomere function, cardiomyocyte energetics, and metabolism, informing the pathogenesis of hypertrophic cardiomyopathy. *Circulation* 141 (10), 828–842. doi:10.1161/CIRCULATIONAHA.119.042339

Tripathi, R., Sullivan, R., Fan, T. M., Wang, D., Sun, Y., Reed, G. L., et al. (2017). Enhanced heart failure, mortality and renin activation in female mice with experimental dilated cardiomyopathy. *PLoS One* 12 (12), e0189315. doi:10.1371/journal.pone.0189315

Verma, S. K., Krishnamurthy, P., Barefield, D., Singh, N., Gupta, R., Lambers, E., et al. (2012). Interleukin-10 treatment attenuates pressure overload-induced hypertrophic remodeling and improves heart function via signal transducers and activators of transcription 3-dependent inhibition of nuclear factor-kappa B. *Circulation* 126 (4), 418–429. doi:10.1161/CIRCULATIONAHA.112.112185

Wang, K. K., Ding, R. R., Ha, Y. P., Jia, Y. A., Liao, X. M., Wang, S. S., et al. (2018). Hypoxia-stressed cardiomyocytes promote early cardiac differentiation of cardiac stem cells through HIF-1α/Jagged1/Notch1 signaling. *Acta Pharm. Sin. B* 8 (5), 795–804. doi:10.1016/j.apsb.2018.06.003

Wang, X. P., Li, W. L., Zhang, Y. W., Sun, Q. B., Cao, J., Tan, N. N., et al. (2022). Calycosin as a novel PI3K activator reduces inflammation and fibrosis in heart failure through AKT-IKK/STAT3 Axis. *Front. Pharmacol.* 13, 828061. doi:10.3389/fphar.2022.828061

Xie, W. J. X., Pang, Z., and Wang, S. (2015). Establishment and evaluation of the rat model of harmful fluid retention in the upper jiao. *World J. Integr. Traditional West. Med.* 10, 767–770.

Xu, C., Tang, F., Lu, M., Yang, J., Han, R., Mei, M., et al. (2016). Astragaloside IV improves the isoproterenol-induced vascular dysfunction via attenuating eNOS uncoupling-mediated oxidative stress and inhibiting ROS-NF-κB pathways. *Int. Immunopharmacol.* 33, 119–127. doi:10.1016/j.intimp.2016.02.009

Yamada, T., and Nomura, S. (2021). Recent findings related to cardiomyopathy and genetics. *Int. J. Mol. Sci.* 22 (22), 12522. doi:10.3390/ijms222212522

Yin, F., Li, P., Zheng, M., Chen, L., Xu, Q., Chen, K., et al. (2003). Interleukin-6 family of cytokines mediates isoproterenol-induced delayed STAT3 activation in mouse heart. *J. Biol. Chem.* 278 (23), 21070–21075. doi:10.1074/jbc.M211028200

Yu, B., Chen, X., Li, J., Qu, Y., Su, L., Peng, Y., et al. (2013). Stromal fibroblasts in the microenvironment of gastric carcinomas promote tumor metastasis via upregulating TAGLN expression. *BMC Cell Biol.* 14, 17. doi:10.1186/1471-2121-14-17

Yu, Y. D., Xiu, Y. P., Li, Y. F., Zhang, J., Xue, Y. T., and Li, Y. (2021). To explore the mechanism and equivalent molecular group of radix astragali and semen Lepidii in treating heart failure based on network pharmacology. *Evid. Based. Complement. Altern. Med.* 2021, 5518192. doi:10.1155/2021/5518192

Yu, Y., Spatz, E. S., Tan, Q., Liu, S., Lu, Y., Masoudi, F. A., et al. (2019). Traditional Chinese medicine use in the treatment of acute heart failure in western medicine hospitals in China: analysis from the China PEACE retrospective heart failure study. *J. Am. Heart Assoc.* 8 (15), e012776. doi:10.1161/jaha.119.012776

Yuan, C. C., Kazmierczak, K., Liang, J. S., Zhou, Z. Q., Yadav, S., Gomes, A. V., et al. (2018). Sarcomeric perturbations of myosin motors lead to dilated cardiomyopathy in genetically modified MYL2 mice. *Proc. Natl. Acad. Sci. U. S. A.* 115 (10), E2338–E2347. doi:10.1073/pnas.1716925115

Zang, Y. B., Wan, J. J., Zhang, Z., Huang, S., Liu, X., Zhang, W. D., et al. (2020). An updated role of astragaloside IV in heart failure. *Biomed. Pharmacother.* 126, 110012. doi:10.1016/j.biopha.2020.110012

Zhang, S., Tang, F., Yang, Y., Lu, M., Luan, A., Zhang, J., et al. (2015). Astragaloside IV protects against isoproterenol-induced cardiac hypertrophy by regulating NF-κB/PGC-1α signaling mediated energy biosynthesis. *PLoS One* 10 (3), e0118759. doi:10.1371/journal.pone.0118759

Zhou, X. M., Xin, Q., Wang, Y. L., Zhao, Y. J., Chai, H., Huang, X., et al. (2016). Total flavonoids of Astragalus plays a cardioprotective role in viral myocarditis. *Acta Cardiol. Sin.* 32 (1), 81–88. doi:10.6515/acs20150424h

Zhu, L. M., Vranckx, R., Van Kien, P. K., Lalande, A., Boisset, N., Mathieu, F., et al. (2006). Mutations in myosin heavy chain 11 cause a syndrome associating thoracic aortic aneurysm/aortic dissection and patent ductus arteriosus. *Nat. Genet.* 38 (3), 343–349. doi:10.1038/ng1721

Zhu, Z., Li, H., Chen, W., Cui, Y., Huang, A., and Qi, X. (2020). Perindopril improves cardiac function by enhancing the expression of SIRT3 and PGC-1 alpha in a rat model of isoproterenol-induced cardiomyopathy. *Front. Pharmacol.* 11, 94. doi:10.3389/fphar.2020.00094

frontiers | Frontiers in Pharmacology

TYPE Systematic Review
PUBLISHED 01 September 2022
DOI 10.3389/fphar.2022.950012

OPEN ACCESS

EDITED BY
Xian-Jun Fu,
Shandong University of Traditional Chinese Medicine, China

REVIEWED BY
Ibrahim C. Haznedaroglu,
Hacettepe University Hospital, Turkey
Hee Geun Jo,
BS Healthcare Co., Ltd., South Korea

*CORRESPONDENCE
Tsai-Ju Chien,
silence021@gmail.com

SPECIALTY SECTION
This article was submitted to Ethnopharmacology, a section of the journal Frontiers in Pharmacology

RECEIVED 22 May 2022
ACCEPTED 08 August 2022
PUBLISHED 01 September 2022

CITATION
Chien T-J, Liu C-Y, Chang Y-I, Fang C-J, Pai J-H, Wu Y-X and Chen S-W (2022), Therapeutic effects of herbal-medicine combined therapy for COVID-19: A systematic review and meta-analysis of randomized controlled trials. *Front. Pharmacol.* 13:950012. doi: 10.3389/fphar.2022.950012

Therapeutic effects of herbal-medicine combined therapy for COVID-19: A systematic review and meta-analysis of randomized controlled trials

Tsai-Ju Chien[1,2]*, Chia-Yu Liu[2], Yuan-I Chang[3], Ching-Ju Fang[4,5], Juo-Hsiang Pai[1], Yu-Xuan Wu[3] and Shuoh-Wen Chen[3]

[1]Division of Hemato-Oncology, Department of Internal Medicine, Branch of Zhong-Zhou, Taipei City Hospital, Taipei, Taiwan, [2]Institute of Traditional Medicine, National Yang Ming Chiao Tung University, Taipei, Taiwan, [3]Department and Institute of Physiology, College of Medicine, National Yang Ming Chiao Tung University, Taipei, Taiwan, [4]Medical Library, National Cheng Kung University, Tainan, Taiwan, [5]Department of Secretariat, National Cheng Kung University Hospital, College of Medicine, National Cheng Kung University, Tainan, Taiwan

Background/Aim: Since 2019, the COVID-19 pandemic has been a devastating disease affecting global health to a great extent. Some countries have added on herbal medicines as a complementary treatment for combating COVID-19 due to the urgency of stopping the spread of this viral disease. However, whether these herbal medicines are effective is uncertain. This systematic review and meta-analysis aimed to evaluate the effects of herbal medicine combined therapy in the treatment of COVID-19.

Methods: A literature search was performed following the PRISMA Statement and without language restrictions. Seven databases were searched from inception through December 2021. All selected studies were randomized clinical trials (RCTs). Comparing the effects of herbal medicine combined therapy with conventional western medicine, including improvement of clinical symptoms, chest CT images, viral conversion rate, C-reactive protein (CRP) and interleukin 6. Cochrane criteria were applied to examine the methodological quality of the enrolled trials; and meta-analysis software (RevMan 5.4.1) was used for data analysis.

Results: In total, the data of 5,417 participants from 40 trials were included in this systematic review; and 28 trials were qualified for meta-analysis. The trials had medium-to-high quality based on GRADE system. Meta-analysis showed that combining herbal medicine vs conventional treatment in 1) coughing (1.43

Abbreviations: HM, Herbal medicine; CWM, conventional western medicine; WHO, World Health Organization; RoB 2, Risk of Bias version 2; RCTs, randomized controlled trials; AE, adverse events; RR, risk ratio; ACE2, angiotensin converting enzyme2.

95% CI:1.21, 1.71, p = 0.0001), 2) fever (1.09 95% CI:1.00, 1.19, p = 0.06), 3) fatigue (1.21 95% CI:1.10, 1.33, p = 0.0001); 4) CT images (1.26 95% CI:1.19, 1.34, $P \leq 0.00001$), 5) viral conversion rates (1.22 95% CI:1.06, 1.40, p = 0.005) and 6) viral conversion times (−3.72 95% CI: −6.05, −1.40, p = 0.002), 7) IL6 change (1.97 95% CI: −0.72, 4.66, p = 0.15) and 8) CRP change (−7.92 95% CI: −11.30, −4.53, $P \leq 0.00001$).

Conclusion: Herbal medicine combined therapy significantly reduces COVID-19 clinical symptoms, improving CT images and viral conversion rates. Reported adverse events are mild. However, for certain biases in the included studies, and the need for further study on effective components of herbal medicine. Further large trials with better randomized design are warranted to definite a more definite role of herbal medicine.

KEYWORDS

herbal medicine, COVID-19, systematic (Literature) review, meta-analysis, complementary therapy, traditional chinese medicine

1 Introduction

Since December 2019, the outbreak of the COVID-19 pandemic has had devastating effects on global health systems and economic growth, and has affected the lifestyle of human populations on a large scale (Sreepadmanabh et al., 2020). In March 2020, the World Health Organization (WHO) declared that COVID-19 was a global pandemic because the viral infection had spread rapidly within a growing number of countries.

The causative agent of COVID-19, severe acute respiratory syndrome coronavirus 2 (SARS-CoV-2), distressed not only the respiratory tract system (Zhu et al., 2020), but also presented as a systemic disease associated with vascular inflammation; this affected multiple organs and eventually led to multi-organ failure in severely affected individuals (Ding et al., 2020; Smadja et al., 2021). Therefore, it became urgent to prevent or treat COVID-19 early and effectively.

Currently, treatment of COVID-19 includes administering antiviral and symptomatic support in mild cases; whereas no definitively effective drugs are available to treat this viral infection even though some non-specific therapeutic options exist and vaccination is ongoing (Mirtaleb et al., 2021). Since August 2021, the delta variant has exhibited high capability of invading the host's immune system and appears to be more transmissible than other variants, making people more anxious (Harder et al., 2021; Shiehzadegan et al., 2021). In November 2021, the appearance of the Omicron (B.1.1.529) variant expressed high enhanced transmissibility and immune evasion and was shown to re-infect individuals previously infected with other SARS-CoV-2 variants (Kannan et al., 2021). In this scenario, beyond the conventional western medicine (CWM) approach, which includes antiviral drugs such as interferon, ribavirin, lopinavir-ritonavir, and chloroquine phosphate (Negrut et al., 2021; Wong et al., 2021), there is widespread use of antibacterial drugs, antitussives, expectorants and supportive therapy, while Herbal -medicine combined therapy is also flourishing in many countries. Since the origin of the COVID-19 outbreak in China in 2019, herbal medicine (HM) has been used to help combat COVID infection along with modern anti-infective agents because no vaccine or definitive antiviral treatment was available for COVID-19 at that time. In Asian countries such as China, Taiwan and Hong-Kong, HM has played a critical role in both treating and preventing COVID-19; the inclusion of traditional Chinese medicine (TCM) in the Chinese protocol is based on its long, successful historic experience in fighting against pestilence (Ni et al., 2020). To have a successful experience combating COVID-19, the TCM therapeutic schedule was included in the guidelines for diagnosis and treatment of COVID-19 (Jin Y. H. et al., 2020). Broadly speaking, many other countries such as India and Japan have also applied HM to alleviate the effects of infectious diseases in the context of SARS-CoV-2 (Ang et al., 2020a; Ang et al., 2020b). The volume of existing reports and systematic reviews provide irrefutable evidence that HM combined therapy possesses a potential antiviral capability against SARS-CoV-2 (Fan et al., 2020; Du et al., 2021), yet the lack of solid evidence-based trials makes the value of herbs vague (Panyod et al., 2020). Furthermore, no grading was performed on the certainty of evidence for their results also easily skew the result directions if not handled properly.

In addition to herbal medicine, some natural products were also under investigation, more and more studies applied network pharmacology in exploring the related pathways and mechanisms of these herbs and natural compounds (Fan et al., 2020; Ang et al., 2021). The more research focus on this field, the more appealing and potential of these herbs were found.

To date, many HM-related trials (not only TCM) have been published on aspects of COVID-19; however, the high heterogeneity and loose trial design made it hard for previous studies to draw definitive conclusions. To further understand the efficacy of HM combined therapy in treating the COVID-19, we

conducted a systematic review and meta-analysis to evaluate the efficacy of HM in the treatment of COVID-19 objectively.

2 Methods

The protocol for this review and meta-analysis has been registered on the International Prospective Register of Systematic Reviews (PROSPERO) with the registration number CRD42021287021. This review was reported according to the updated Preferred Reporting Items for Systematic Reviews and Meta-Analyses (PRISMA) (Page et al., 2021).

2.1 Data sources and search strategy

This systematic review was conducted in compliance with the PRISMA Statement ensure transparent and complete reporting. The following 7 databases were searched for relevant randomized clinical trials, with no language restrictions, from their inception dates to 30 December 2021: Embase (Elsevier), Medline (Ovid, including epub ahead of print, in-process, and other nonindexed citations), Cochrane Library (including clinical registers from WHO ICTRP and US ClinicalTrials.gov), CINAHL Complete (EBSCOhost), Scopus, China National Knowledge Infrastructure (CNKI) and Wanfang Data. The reference lists of eligible articles were also reviewed to identify additional studies for possible inclusion. We also manually retrieved relevant studies and clinical trials to acquire as many studies as possible. E-mail alerts were established to identify newly released studies from the different databases that fell within the scope of our review.

The key concepts – COVID-19 and Traditional Chinese Medicine–used in the search included their 216 synonyms in total and controlled vocabulary (12 Emtree terms, 13 MeSH terms, etc.). Highly sensitive search filters were applied to identify randomized clinical trials. Supplementary Appendix A1 displays the full search strategy for the individual databases.

2.2 Eligibility criteria and data extraction

All eligible studies examined studies that fulfilled the inclusion criteria, as follows: 1) Studies designed as randomized clinical trials (RCTs); 2) Adult patients (aged 18 years and older) with an established diagnosis of COVID-19 in evaluable status. The criteria of mild and moderate is according to the Clinical Spectrum of SARS -CoV-2 Infection from National Institutes of Health(Maier et al., 2021), which set mild illness as individuals who have any of the various signs and symptoms of COVID-19 (e.g., fever, cough, sore throat, malaise, headache, muscle pain, nausea, vomiting, diarrhea, loss of taste and smell) but who do not have shortness of breath, dyspnea, or abnormal chest imaging; and moderate illness as individuals who show evidence of lower respiratory disease during clinical assessment or imaging and who have an oxygen saturation (SpO2) ≥94% on room air at sea level. 3) The intervention group was treated with HM combined therapy. Patients in the control group were required to be treated with CWM or a combination of HM placebo and CWM. We excluded studies designed as retrospective studies, observational studies, repeated data studies and cross-sectional studies. Studies which set outcomes only with TCM syndromes evaluation, sample size less than 30; or if the full text cannot be obtained were also excluded. The selection of studies and data extraction were performed independently by two reviewers (Chien and Liu) according to the inclusion and exclusion criteria.

2.3 Risk of bias and quality assessment

Two reviewers (Chien and Liu) assessed the methodological quality of studies by using the Cochrane Collaboration's tool (Higgins et al., 2022)and the new version of this tool, Risk of Bias version 2 (RoB 2). Six items of ROB 2 were evaluated as follows: Randomization, Deviations from intended interventions, Missing outcome data, Measurement of the outcome, Selective Outcome reporting, overall bias (Cochrane Collaboration, 2021). Once the disagreements were noted, discussions were held with the other investigators (Chang; Wu) to make a consensus decision.

2.4 Assessment of evidence certainty

We assessed the outcomes by using GRADE methodology (Guyatt et al., 2008). The overall evidence certainty was evaluated by using five downgrading domains which included considerations of study limitation, inconsistency, indirectness, imprecision, and publication bias. The level of evidence was classified as high, moderate, low, or very low. Grading was performed using GRADE pro software (Diekemper et al., 2018) (available from http://www.gradepro.org).

2.5 Outcome measures assessment

In the review, the outcome measures in the enrolled studies included chest CT scan; blood tests and cytokines, including CRP, interleukin 6, lymphocytes, etc; symptom evaluation; virus nuclei acid tests; hospitalization time, adverse events (AE) and mortality; and TCM syndrome score. In this SR, we chose data that were more objective, consistent in the unit and completeness for analysis. Therefore, we did not analyze the TCM syndrome

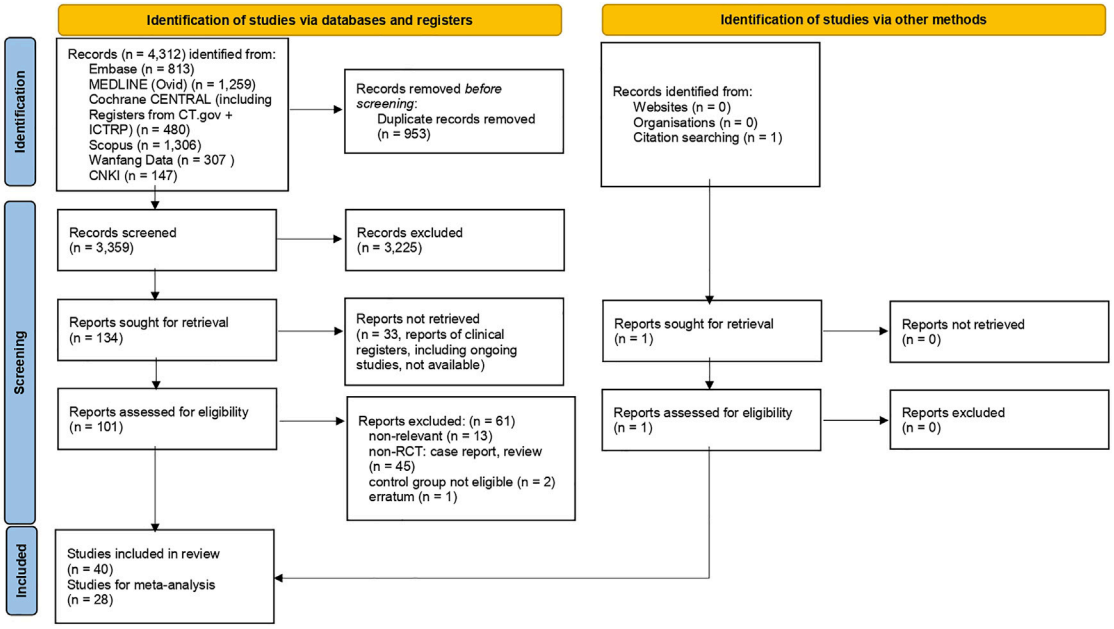

FIGURE 1
Study selection flow diagram based on the PRISMA 2020 statement.

score or hospitalization days since the method of evaluation of TCM syndrome is different, and factors affect hospitalization time might be bias. The targeted outcomes we chose were: 1) Clinical symptoms (fever; cough; fatigue, which were measured as percentage decreased %); 2) Chest CT manifestations (the percentage of consolidations in the whole lung or improved rate %); 3) Viral nucleic conversion rates (%) and duration (days); 4) Serum interleukin-6 (pg/ml) and CRP (mg/L), and the effect estimates were re-calculated using data extracted from the qualified studies.

2.6 Meta-analysis

To analyze the effects of combining herbal medicines on targeted outcomes after treatment compared with baseline values, we applied Review Manager software (RevMan, Version 5.4.1, Copenhagen: The Nordic Cochrane Centre, The Cochrane Collaboration, 2014) to analyze dichotomous and continuous outcome measures extracted from the original studies. Weighted mean difference (WMD) was utilized for data measurement of continuous outcomes, while risk ratio (RR) was used for dichotomous outcomes. Statistical heterogeneity was assessed using the Chi-square test ($p < 0.1$). The I2 statistic was also calculated, and we considered $I^2 > 50\%$ to indicate significant heterogeneity across studies (Higgins et al., 2003). A random-effects model was used if significant heterogeneity was shown among trials. Otherwise, results were obtained from a fixed-effects model. Funnel plot was also used to evaluate the publication bias (Sterne et al., 2011).

3 Results

3.1 Eligible studies

Figure 1 is the flow diagram of the literature search and screening, which complies with PRISMA guidelines (Page et al., 2021). Figure 2 demonstrates the risk of bias by applying low ROB, high ROB or some concern to each item. We also consulted the third reviewer if any disagreement occurred for risk of bias.

3.2 Study characteristics

In total, 40 studies that fulfilled the inclusion criteria were included for systematic review; yet 28 randomized clinical trials were eligible for meta-analysis for targeted outcome measures; Table 1 summarizes the characteristics of the 40 randomized clinical trials.

Among these 40 randomized clinical trials, 33 trials were conducted in China with Chinese herbal medicine; of these, 13 were published in English (Wang J. B. et al., 2020; Xiong W. Z. et al., 2020; Xiao et al., 2020; An et al., 2021; Zhao C. et al., 2021;

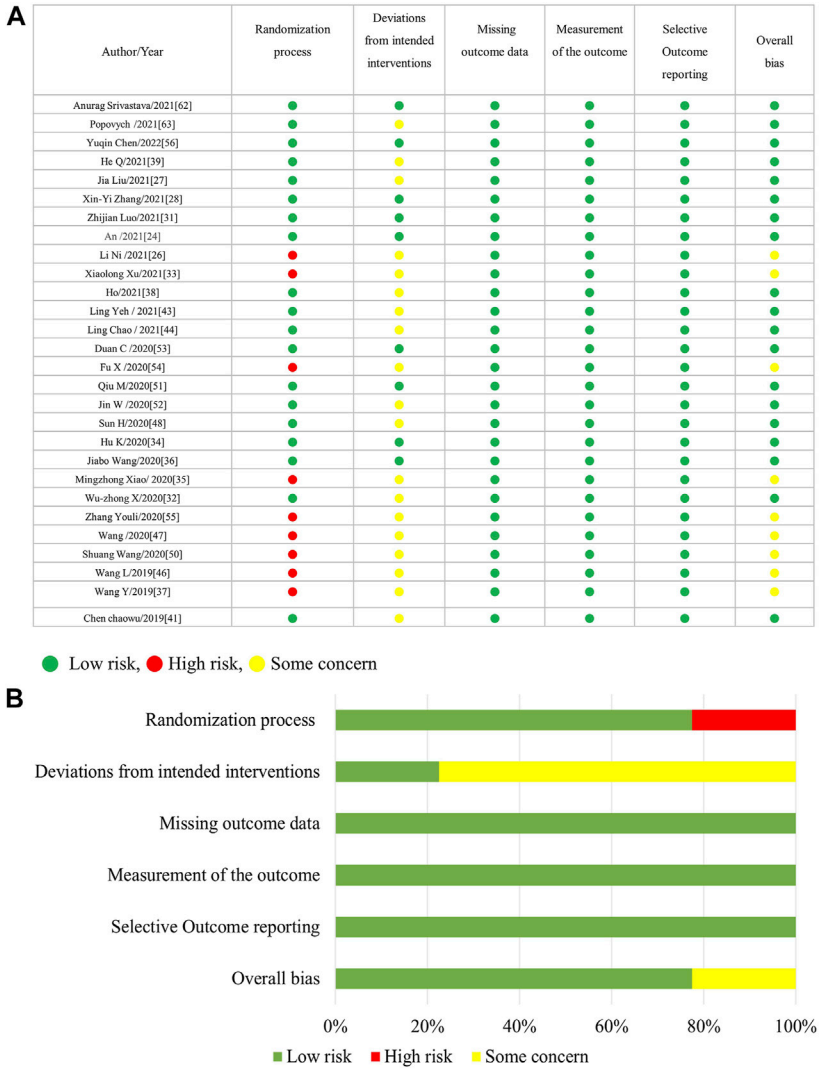

FIGURE 2
(A): Risk of bias summary (ROB2). **(B)**: Risk of bias graph.

Liu J. et al., 2021; Xu X. et al., 2021; Zhang X. Y. et al., 2021; Hu et al., 2021; Luo et al., 2021; Ni et al., 2021; Zeng et al., 2021; Zhou et al., 2021), while 20 were published in Chinese (Jin W. et al., 2020; Wang et al., 2020b; Wang et al., 2020c; Duan et al., 2020; Wang S. et al., 2020; Fu et al., 2020; Mou et al., 2020; Qiu et al., 2020; Sun et al., 2020; Zhang et al., 2020; Chen C. et al., 2021; Liu A. et al., 2021; Chen Y. et al., 2021; Zhao J. et al., 2021; Wang Y. et al., 2021; He et al., 2021; He and Zhang, 2021; Ping et al., 2021; Ye et al., 2021; Zhang, 2021). In addition, 3 studies were conducted in Iran (Karimi et al., 2021; Kosari et al., 2021; Borujerdi et al., 2022), 3 in India (Majeed et al., 2021; Pawar et al., 2021; Srivastava et al., 2021) and 1 in Ukraine (Popovych et al., 2021). Twelve randomized clinical trials (30%) were multi-center trials whereas others were conducted in a single site. In total, 5,417 study participants were included in this systematic review, with sample sizes ranging from 15 to 384. Treatment duration ranged from 6 to 90 days.

3.3 Assessment of methodological quality

Figure 2 shows that 33% of the included trials (13/40 randomized clinical trials) did not appropriately address the process of randomization, and more than 75% (31/40 trials) have the deviations from intended interventions. Regarding selective outcome reporting and incomplete

TABLE 1 The characteristics of the included study.

References	Sample size (intervention: Control)	Age	Type of COVID 19	Intervention	Control	Treatment days	Outcomes	Adverse report (V or no report--)
Mehrdad Karimi et al., 2021(Iran)	I:184 C:174	I:48.7 C:50.8	—	Persian medicine + *c*	Conventional western medicine	7	#131413 C, E,F	V (Gastro-intestine events)
Morteza Kosari et al., 2021(Iran)	I:25 C:25	I:43.5 C:41.5	—	Propolis plus Hyoscyamus niger L. methanolic extract	Conventional western medicine	6	C	no report
Borujerdi et al., 2021(Iran)	I:59 C:57	I:44.3 C:44.0	Mild to moderate	Zufa syrup	Conventional western medicine + placebo	10	C,F	no AE
Kirti S Pawar, et al., 2021 (India)	I:70 C:70	I:18–85 C:25–84	Mild to severe	Curcumin and piperine	Conventional western medicine + placebo	14	A, B, C, E, F	no AE
Muhammed Majeed et al., 2021 (India)	I:50 C:50	I:39.0 C:37.3	—	ImmuActiveTM 500 mg capsule	Placebo (same appearance)	28	C, D, E, F	no AE
Anurag Srivastava et al., 2021 (India)	I1:40 I2:40 C:40	I1: 44.4 I2: 42.8 I3: 39.5	Mild to moderate	I2:Nilavembu Kudineer + allopathy treatment I3:Kaba Sura Kudineer + allopathy treatment	Placebo + allopathy treatment	10	B, C, D,E, F	V (vomiting and diarrhea)
Popovych et al., 2021 (Ukraine)	I:49 C:47	I:33.1 C:3.6	Mild	BNO 1030 (a standardized extract of seven medicinalplants (Imupret®)	Conventional western medicine	14	C, E, F	no AE
Yuqin Chen et al., 2022(China)	I:64 C:65	I:54.2 C:52.5	—	Bufei Huoxue capsules	Placebo	90	A, C, F, G	V (Abnormal liver function)
He Q, et al., 2021(China)	I:36 C:35	—	Mild	Buzhong Yiqi decoction + *c*	Conventional western medicine	10	A, B, C,D,F	V (1 with arrthymia)
Jia Liu et al., 2021(China)	I:99 C:96	I:56.0 C:56.5	Mild to severe stages	Huashi Baidu granule + *c*	Conventional western medicine	14	A, B, C, D, F	V (diarrhea)
Xin-Yi Zhang et al., 2021(China)	I:65 C:65	I:44.3 C:48.3	Mild to moderate	Xiyanping injection + *c*	Conventional western medicine	14	C,D,F	V (mild)
Zhijian Luo et al., 2021(China	I:29 C:28	I:60.3 C:56.4	Severe	Xuebijing	Conventional western medicine	14	B,C,E,F	V (no AI)
Shuang Zhou et al., 2021(China)	I:57 C:54	66 (median)	Severe/ Critical	Standard care (Table 1)+shenhuang granule	Conventional western medicine	14	B, F	**V** (Increased neutrophil)
An et al., 2021(China)	I:92 C:31	I:50.2 C:44.7	—	Jinhua Qinggan granules	Conventional western medicine	14	C,D, F	no AE
Li Ni et al., 2021(China)	I:56/61/59 C:59	I:54/ 56/53 C:51	—	Shuanghuanglian oral liquids	Conventional western medicine	14	A, C, D, F	No serious adverse events occurred
Xiaolong Xu et al., 2021(China)	I:77 C:80	I:49.1 C:50.4	—	Reduning injection	Conventional western medicine	14	C, D, E, F	V
Congcong Zeng et al., 2021(China)	I:30 C:29	I:50.7 C:53.3	Mild to moderate	Maxingshigan-Weijing Decoction	Conventional western medicine	14	B, C, D, E, G, F	no AE

(Continued on following page)

TABLE 1 (*Continued*) The characteristics of the included study.

References	Sample size (intervention: Control)	Age	Type of COVID 19	Intervention	Control	Treatment days	Outcomes	Adverse report (V or no report--)
Chen Zhao et al., 2021(China)	I:358 C:384	I:52.0 C:50	Mild	Huashibaidu Granule	Conventional treatment	7	C, E, F	V (Mild diarrhea)
Ping Xianghua et al., 2021(China)	I:30 C:24	I:40.8 C:41.2	Mild to severe	Jiawei Yupingfeng powder	Conventional western medicine	14	A, B, C, D, E, F	V (vomiting, chest distress diarrhea)
Ho et al., 2021(China)	I:34 C:30	I:15–80 C:15–80	Moderate to severe	Shengmai Powder	Conventional western medicine	7	A, B, D, G	no report
Zhang Dan et al., 2021(China)	I:240 C:240	—	High risk	Fuzheng Gubiao Fangggan Decoction	Conventional western medicine	14	C	no report
Ling Yeh et al., 2021(China)	I:50 C:50	I:43.3 C:42.6	Ordinary	Modified Shengjiang Powder	Conventional western medicine treatment	6	B, C, F	no AE
Ling Chao et al., 2021(China)	I:51 C:45	I:46.8 C:45.1	Ordinary	Antivirus No. 1 + *c*	Conventional western medicine treatment	9	A, B, C, G	no report
Liu et al., 2021(China)	I:15 C:15	I:41.6 C:44.5	Mild to moderate	Jiawei Sang Ju drink	Conventional western medicine	10	A, B, C, D, F	V (no AI)
Duan C et al., 2020 (China)	I:82 C:41	I:52.0 C:50.3	Mild	jinhua qinggan granules	Conventional western medicine	5	C, G,F	V (diarrhea)
Fu X, et al., 2020(China)	I:37 C:36	I:45.3 C:44.7	Ordinary	Toujie Quwen granule	Conventional western medicine	15	B, C, F	no AE
Qiu M et al., 2020(China)	I:25 C:25	I: 53.4 C:51.3	Ordinary	Maxing Xuanfei Jiedu decoction	Conventional western medicine	10	A, C, G	no report
Jin W et al., 2020(China)	I:20; C:18	I:43.6 C:41.3	Ordinary	Compound Yin Chai granule + Qingqiao detoxification granule	Routine western medicine	21	A, B, C, E, F	no report
Sun H et al., 2020(China)	I:32 C:25	I:45.4 C:42.0	Mild, Ordinary	Lianhua Qingke granule + C	Antiviral medications	14	A, C, F	no AE
Hu K et al., 2021 (China)	142:142	I:50.4; C:50.8	Ordinary	Lianhua Qingwen capsules (1.4 g,tid)+C	Antiviral medications	14	A, C, D, F	V (liver function)
Jiabo Wang et al., 2020(China)	I:24 ; C:23	I:46.8 C:51.4	—	Keguan-1 (ARDS-suppressing drug)+C	Antiviral drugs	14	A, D, F	V (diarrhea, anorexia, vomiting)
Mingzhong Xiao et al., 2020(China)	I:119 (58/61) ; C:63	I: 52.6/56.7 C:53.9	—	1)Huoxiang Zhengqi dropping pills and Lianhua Qingwen granules or 2) Linahua granules	Antiviral drugs Anti-infective drug	14	C, F	no AE
Wu-zhong **Xiong** et al., 2020(China)	I:22 C:20	I:57.1; C:62.4	Mild to ordinary	Xuanfei Baidu decoction + *c*	Conventional western medicine	7	B, C, F	no AE
Zhang Youli et al., 2020(China)	I:80 C:40	I:53.4 C:52.0	Ordinary	Jinyinhua Oral Liquid + C	Conventional western medicine	10	A, C, D	V (diarrhea)
Wang LQ et al., 2020(China)	I:58 C:60	I:66 C:57.5	Mild to severe	Gegen Qinlian pill	Routine treatment	—	A,B, C, D, F	no AE
	I:37	I:47.4				—	C	no report

(Continued on following page)

TABLE 1 (*Continued*) The characteristics of the included study.

References	Sample size (intervention: Control)	Age	Type of COVID 19	Intervention	Control	Treatment days	Outcomes	Adverse report (V or no report--)
Mou et al., 2020(China)	C:37	C:42.2	Mild to severe	Maxing Shigan Sanren Decoction	Conventional treatment			
Shuang Wang et al., 2020(China)	I:45 C:45	I:43.8 C:42.6	Ordinary	Tablets Combined with Sanren Decoction	Western medicine	15	B, C	no report
Wang L et al., 2020(China)	I:40 C:40	—	Ordinary	Shengmai powder + Shenling Baizhu powder	Conventional western medicine	—	A, B, C, D, G, F	no AE
Wang Y et al., 2021(China)	I:70; C:70	I:48.0 C:49.4	Ordinary	Qingfei Paidu decoction + *c*	Conventional western medicine	10	B, E, F, G	V (fatigue)
Chen chaowu, et al., 2021(China)	I:28 C:29	I:49.5 C:50.2	Mild	Lianhua Qingwen capsule + *c*	Conventional western medicine	—	B, C, D, F	V (vomiting, diarrhea, liver)

Outcomes: A: Chest CT, or other imaging; B: blood test and cytokine; C: symptom evaluation; D: virus nuclei acid tests; E: hospitalization time; F: AE, and mortality; G: TCM, syndrome score.

TABLE 2 Grade evidence Profile.

Certainty assessment							Risk difference 95% CI
Outcomes (no of studies)	Study limitation	Inconsistency	Indirectness	Imprecision	Publication bias	Overall certainty of evidence	
Fever (12 randomized clinical trials)	No serious limitation	No serious inconsistency	No Serious indirectness	No serious	Undetected	Moderate ⊕⊕◯◯	1.09 (1.1.19)
Cough (13)	Serious	Serious inconsistency	Serious indirectness	Serious	Undetected	Low ⊕◯◯◯	1.43 (1.21, 1.71)
Fatigue (11)	Serious	Serious inconsistency	Serious indirectness	Serious	Serious	Low ⊕◯◯◯	1.21 (1.10.1.33)
Chest CT (16)	No serious	No serious	No Serious indirectness	No serious	Undetected	High ◯⊕⊕⊕	1.26 (1.19.1.34)
Virus conversion time (10)	No serious	No serious	No Serious indirectness	No serious	Undetected	High ◯⊕⊕⊕	1.22 (1.06.1.40)
Virus conversion rate (5)	No serious	No serious	No Serious indirectness	No serious	Undetected	High ◯⊕⊕⊕	−3.72 (−6.05, −1.40)
Interleukin -6 (4)	No serious	No serious	No Serious indirectness	No serious	Undetected	High ◯⊕⊕⊕	1.97 (−0.72.4.66)
CRP (10)	No serious	No serious	No Serious indirectness	No serious	Undetected	High ◯⊕⊕⊕	−7.92 (−11.3,−4.53)

GRADE: grading of recommendations assessment, Development, and Evaluation; RCT: randomized clinical trials; CI: confidence interval.

outcome measures data, all included trials were within low risk; however, some trials were within unclear risk of allocation concealment. Generally speaking, the included trials were of medium quality, while details of randomization and blinding were the most frequent problems.

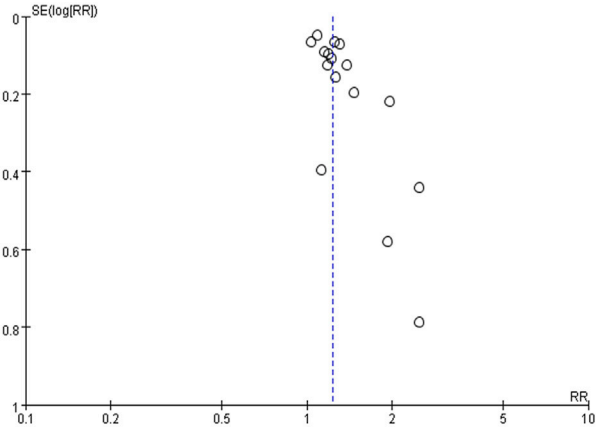

FIGURE 3
Funnel plots for included studies.

3.3.1 Grading of recommendations assessment development evaluation assessment

Table 2 summarizes the evidence certainty of outcomes. Considering that more than half of the enrolled randomized clinical trials were rated as some-concerned of bias (RoB), we downgraded the evidence certainty in the domain of study limitation. The domain of inconsistency was downgraded because of the varied heterogeneity in outcomes as how to evaluate the severity of cough and fever. Publication bias was not considered based on no asymmetry in funnel plots.

3.4 Publication bias

The funnel plot was used to explore potential publication bias (Figure 3). The funnel plot is symmetrical, indicating no obvious deviation and that publication bias is unlikely. Thirty-four trials (85%) reported "No" adverse events (AE), indicating little bias in this systematic review.

3.5 Main traditional chinese medicine and herbal components included in data analysis

This meta-analysis includes not only TCM but also HM, and 90% of the included trials used TCM formulas or granules. The complexity of TCM or HM components is evident; the most popular components are ***honeysuckle- and forsythia-***based (which is a concept of ***couplet medicines*** in TCM theory), such as Jinhua qinggan granules (An et al., 2021), Jinyinhua liquid (Duan et al., 2020; Zhang et al., 2020), Toujie Quwen Granules, and Lianhua qingwen capsules (Duan et al., 2020; Yu et al., 2020; Chen C. et al., 2021; Hu et al., 2021). Another popular couplet medicines applied in these studies is ***ephedra sinica-*** and ***almond***-based, such as Huashi Baidu granules (Zhao C. et al., 2021), Qingfei Paidu decoction (Wang Y. et al., 2021), Maxingshigan-Weijing decoction, Maxing Xuanfei Jiedu decoction (Qiu et al., 2020), Lianhua qingwen capsules (Chen et al., 2020; Yu et al., 2020; Chen C. et al., 2021; Hu et al., 2021) and Guangwenyilun. Other herbs are applied in India, Iran and Ukraine, including curcuminoids (Pawar et al., 2021), Propolis (Kosari et al., 2021), Rheum palmatum (Karimi et al., 2021) and polyherbal formulas (Borujerdi et al., 2022). The components of herbal medicine used in each trial are listed in Supplementary Appendix A2.

3.6 Outcomes and efficacy assessment

3.6.1 Effects of combined -herbal medicines on COVID-19 clinical symptoms (fever; cough; fatigue)

Significant between-study heterogeneity was observed in the effects of combined herbal medicines on COVID-19-related fever and cough (I2 = 80%, and 73%, respectively), but no significant between-study heterogeneity was noted in the effects of combined herbal medicines on fatigue (I2 = 39%). For the 12 trials that reported data on fever reduction cases, no significant differences were observed in subjects treated with combined HM and CWM (1.09 95% CI:1.00, 1.19, p = 0.06; Figure 4A) as compared with control intervention. In the 13 trials that reported data on cough reduction cases, significant improvement was observed in subjects treated with add-on herbs (1.43 95% CI:1.21, 1.71, p = 0.0001; Figure 4B) as compared with control subjects. In the 11 trials that reported data on fatigue reduction cases, significant differences in patient benefits were found when they were treated with combined HM and CWM (1.21 95% CI:1.10, 1.33, p = 0.0001; Figure 4C).

3.6.2 Effects of combined -herbal medicines on chest CT manifestations in COVID-19 patients

No significant between-study heterogeneity in chest CT manifestations were noted between studies in terms of combining HM and CWM (I2 = 49%). As for the 16 trials that reported chest CT data, significant improvement in CT images was observed in subjects receiving add-on herbal medicine (1.26 95% CI: 1.19, 1.34, $P \leq$ 0.00001; Figure 5) as compared with those of control subjects. We provide additional random model effect in Supplementary Appendix A3.

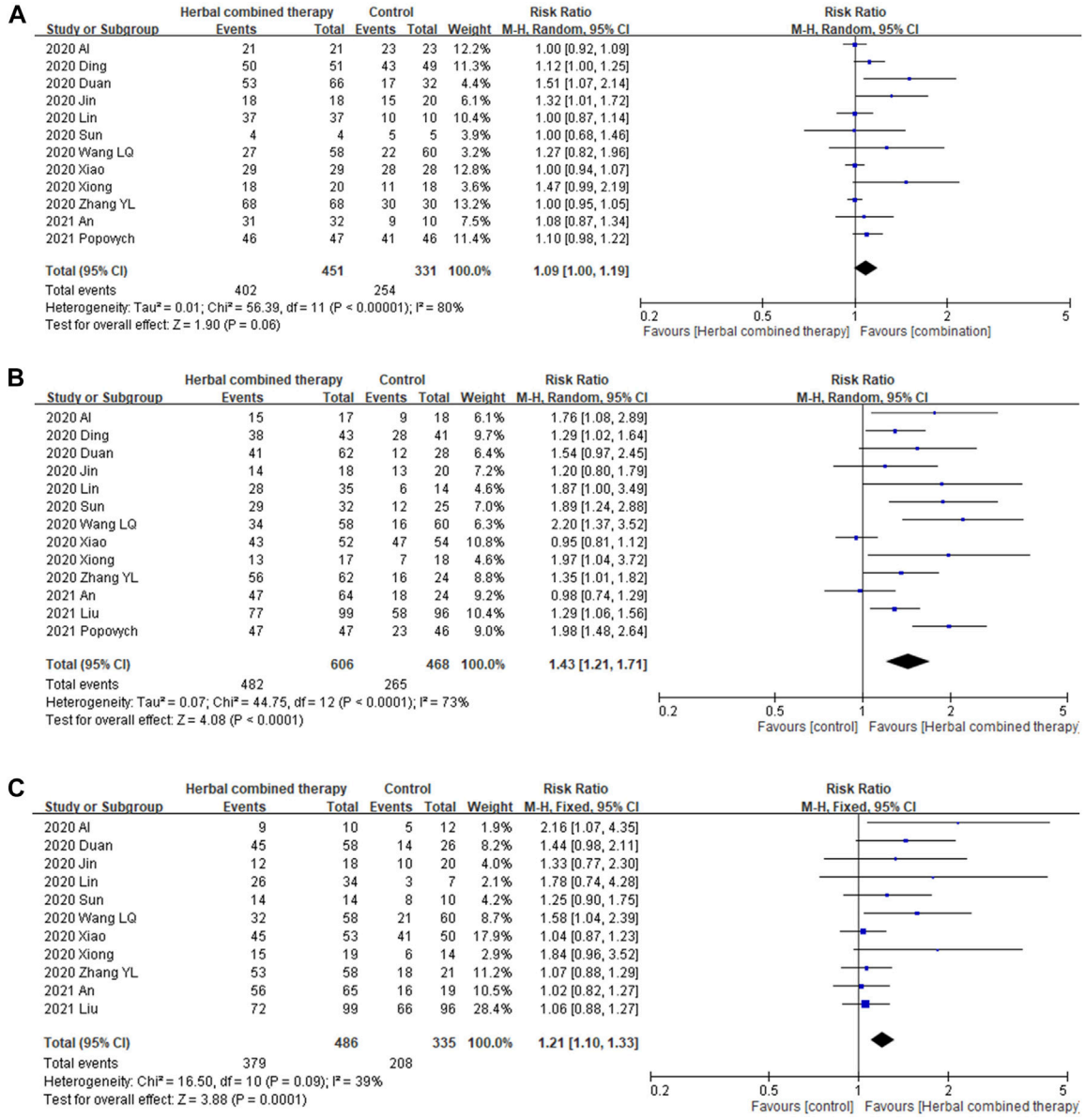

FIGURE 4
Forrest plot of the effects of HM combined therapy in symptom relief. **(A)**: comparison of HM combined therapy in fever reduction. **(B)**: Comparison of HM combined therapy in cough reduction. **(C)**: Comparison of HM combined therapy in fatigue reduction.

3.6.3 Effects of combined -herbal medicines on viral nucleic test, and viral negative conversion time (days)

Significant between-study heterogeneity was observed in the effects of alternative medicines on viral conversion rate and viral conversion time (I^2 = 74%, and 93%, respectively). For the 10 trials that reported data on viral negative conversion rates, more significant improvements were observed in subjects whose treatment included with add-on herbs (1.22 95% CI:1.06, 1.40, p = 0.005; Figure 6A). In the 5 trials that reported data on viral negative conversion time (days), significant improvement was noted in subjects whose treatment included combined herbs (−3.72 95% CI: −6.05, −1.40, p = 0.002; Figure 6B) as compared with CWM alone.

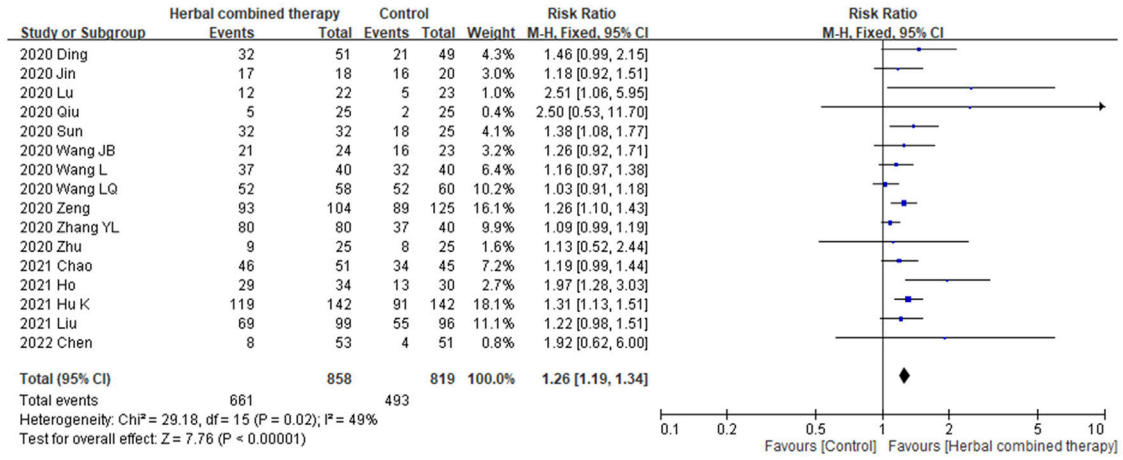

FIGURE 5
Forrest plot of the effects of HM combined therapy in chest CT improvement.

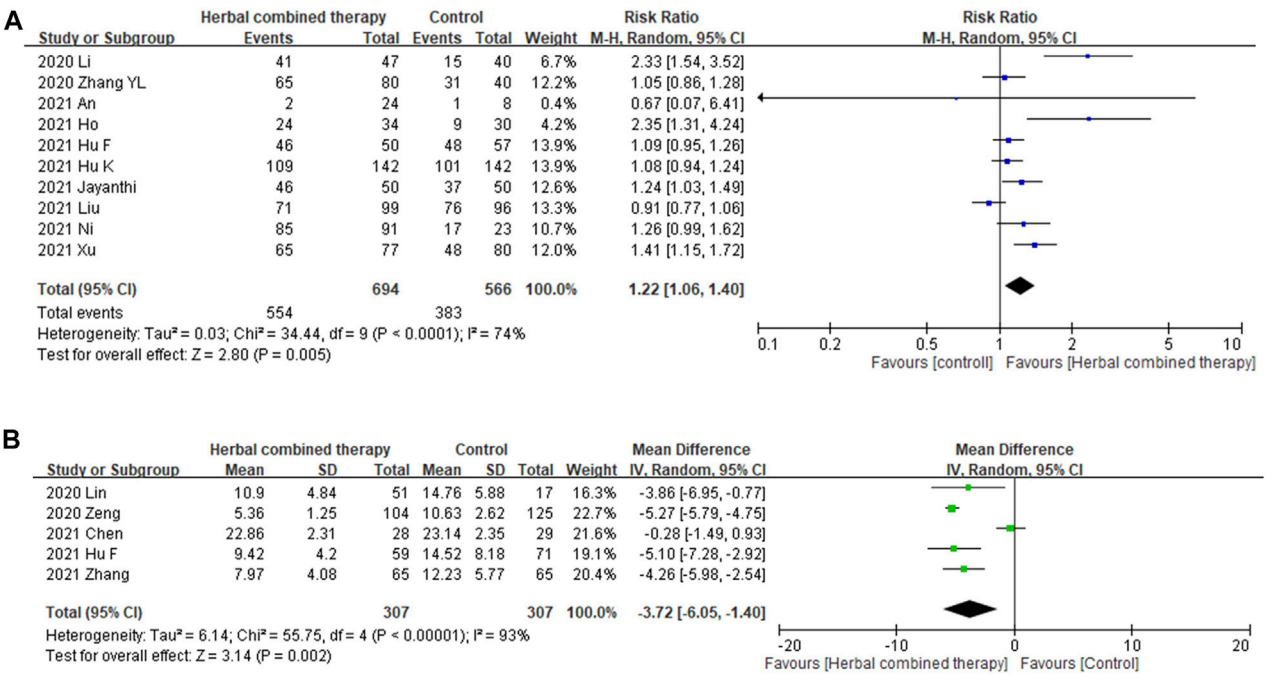

FIGURE 6
(A): Forrest plot of the effects of HM combined therapy in viral conversion rate. **(B)**: Forrest plot of the effects of HM combined therapy in viral conversion time (day).

3.6.4 Effects of combined -herbal medicines on serum interleukin-6 (IL-6), and C reactive protein

Significant between-study heterogeneity was observed in the effects of alternative medicines on serum interleukin-6 level and CRP level (I^2 = 78%, and 93%, respectively). In 4 trials that reported data on serum interleukin-6 level, no significant differences were observed in subjects treated with add-on herbs (1.97 95% CI: −0.72, 4.66, p = 0.15; Figure 7A). Regarding serum CRP levels,

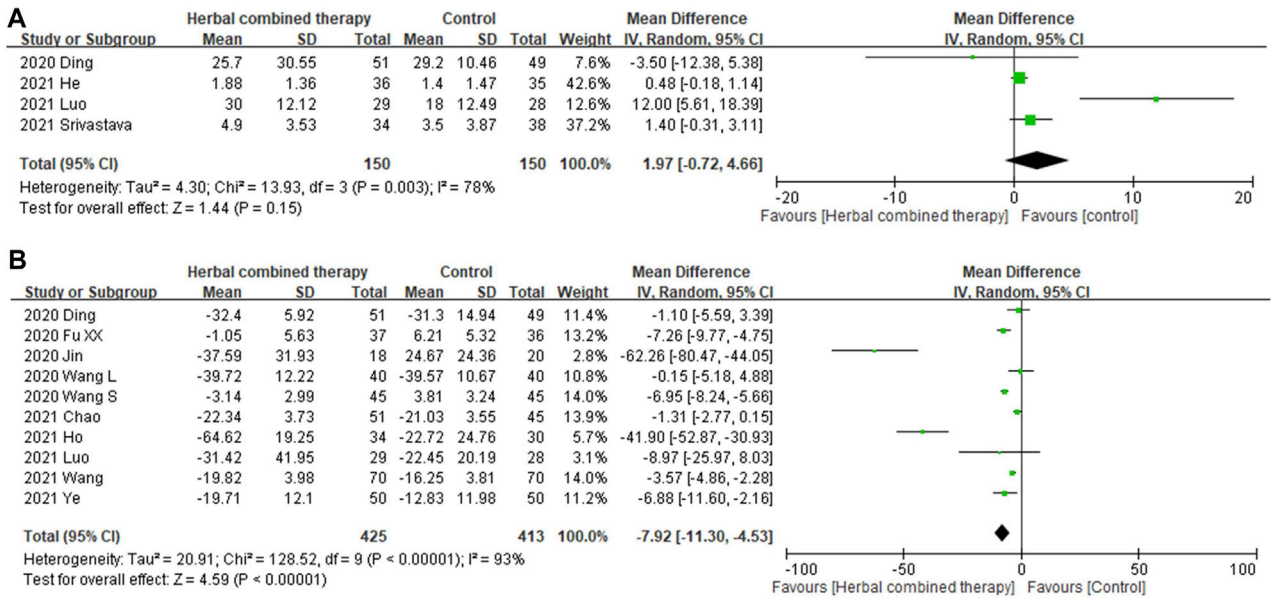

FIGURE 7
(A): Forrest plot of the effects of HM combined therapy in interleukin-6 (ng/ml) in COVID19 patient. **(B)**: Forrest plot of the effects of HM combined therapy in C-reactive protein (ng/ml)in COVID19 patient.

significant decreases were noted in the analysis of 10 enrolled trials that treated with combined HM (−7.92 95% CI: −11.30, −4.53, p = 0.000; Figure 7B) as compared with control subjects.

3.6.5 Safety concern

No serious adverse events were noted in all included randomized clinical trials, except few trials mentioned that participants might have some nausea or GI upset which not directly related to the herbal formula. Accordingly, no quantitative analysis was applied targeted the safety concern or adverse events.

4 Discussion

To our knowledge, this meta-analysis has the advantages of recruiting 2-years trials, and that outcomes selection was not only confined to subjective constitution scores or subjective symptom improvement but also included the objective measurement of changes in CT images, virus conversion rate and time and cytokines such as IL6, as well as changes in CRP levels. Except for IL6 changes, the results favored HM combined therapy by its add-on effect, which shortened virus conversion time and rate and improved clinical symptoms and CRP better than CWM alone. The mechanism of HM is hard to confirm since the components of these formulas are complicated, ranging from a single herb to more than ten herbs added into the treatment regimen in these trials.

Furthermore, the dosage and the course of treatment can always be adjusted according to the patient's condition, for which sensitivity analysis shows increased heterogeneity. One study even tried to identify the most frequently-used herb associated with this issue (Xiong X. et al., 2020), but as each herb's proportion varies between different formulas, and the use of HM or TCM emphasizes the synergistic effect between multiple herbs in individual formulas, it remains difficult to identify a specific single herb as a potential drug for COVID-19 treatment. However, Indian trials applied Zingiber officinale-based (Srivastava et al., 2021) or curcumin-based (Pawar et al., 2021) polyherbal formulas, which are also popularly used in Asian countries. Several TCM studies focused on "Lian-Hua Qing-Wen granules" (Hu et al., 2020; Shi M. et al., 2021) and Qingfei Paidu decoction (Li X. et al., 2021; Li Y. et al., 2021; Wang Q. et al., 2021; Wu et al., 2022), which are recognized as Chinese patent medicines and are now available in western countries. In the real world, HM emphasizes the synergistic effect based on holistic theory, which appeals to people who prefer natural products. In the academic field, some scholars have applied modern pharmacologic methods in analyzing TCM formulas and noted that they have similar mechanisms, including the

regulation of apoptosis and immune response (Shi et al., 2021c), and anti-inflammatory effects, which tend to benefit lung function in patients with COVID-19 (Yan et al., 2020; Zhang F. et al., 2021). For example, a deep study proposed that "Rheum palmatum L (Da Huang)," a common component of these formulas, can directly block the viral life cycle (Shi et al., 2020), and inhibit viral transcription and replication (Galasiti Kankanamalage et al., 2018). The meta-analysis noted that combining HM therapy decreases CRP significantly, but does not decrease Il-6, indicating that HM helps to reduce the inflammatory status through an uncertain pathway. In a previous study, the CRP level correlated with the severity of lung involvement and prognosis (Beydogan and Yuruk Atasoy, 2021). In this context, it makes sense that many Chinese herbal medicines utilized in these trials targeted the lung meridian and anti-inflammatory effects are especially valuable. Similar studies investigated the potential herbs by utilizing information medicine and precision medicine (Balkrishna et al., 2021; Dzobo et al., 2021). While the present study has confirmed the efficacy of HM, further studies are needed to connect the potential drugs with precision medicine.

Additionally, some of the outcomes in the enrolled trials such as TCM syndrome, hospitalization days, or adverse events were not analyzed is due to the evaluation methods of TCM syndrome are not consistent or well addressed in original manuscripts. We didn't analyze the hospitalization days owing to it was probably affected by some other medical, social, and medical rules problems which not directly related to COVID-19 infection. Furthermore, most studies address the adverse events in description without quantitative comparison; therefore, some outcomes were mentioned in the enrolled trials yet cannot be analyzed. Generally speaking, since the COVID-19 pandemic started in 2019, and researchers are still very much at a groping stage. Some consensuses are under modified during this period; thus, we only chose the presentive clinical symptom (fever, cough, fatigue), image improvements, and quantitative outcomes as cytokine change and reliable virus conversion times and rate for analysis. Further detailed analysis towards other items could be considered depend on how scholars treat the COVID related issues.

Regarding the basic mechanism about these herbs or potential of the plants' extracts, more and more research focus on the network pharmacology analysis and cross-talks between signaling pathways (Qi et al., 2022). Take some formulas, which have been included in this meta-analysis, Lian Hua Qing Wen has been proved with regulating angiotensin converting enzyme 2 (ACE2) expression-disorder-caused symptoms and relieve the cytokine storm (Zheng et al., 2020). Some study revealed that acacetin, wogonin, and isorhamnetin were the main active ingredients in Qing Fei Pai Du decoction, (Li et al., 2022); while the target network model noted that some compounds such as licochalcone B acted on multiple targets, and multiple components interacted with the same target such as GPR35, reflecting the synergistic mechanism of Chinese medicine (Xu F. et al., 2021). Another special agent which not included in this trial is a potential mucosal topical agent "Ankaferd hemostat (ABS)", which was approved with effect of antagonizing proteinase-activated receptors (PARs), mainly PAR-1. By activation of the PAR-1, mediators and hormones impact on the hemostasis, endothelial activation, alveolar epithelial cells and mucosal inflammatory responses which are the essentials of the COVID-19. The mucosal problem is an issue which has been ignored for most study focused on oral form and systematic treatment (Beyazit et al., 2020).

The basic research of herbs confronts the problems that in-depth studies are not available to precisely define bioactive compounds of plant origin and their mechanism of action as many cross-talks between target pathway network and protein-protein interaction (PPI) network (Wang L. et al., 2021); this underlines the need for studying the synthetic molecules to circumvent the viral load in the host system (Prasad et al., 2020). Additional trials or basic research may be designed on the hypothetically established plant extracts as add-on herbal medicines in the COVID-19 treatment field and there is a lot space for exploration.

Lastly, although some between -study heterogenicity was noted; we didn't perform additional heterogeneity analysis as no more than 10 trials among these indicators are included and we still need to hold a conservative view point towards the results. Furthermore, no un-tolerable side effects were reported by 80% of the studies in the present meta-analysis. Among the enrolled trials, the treatment goals primarily targeted respiratory distress and symptoms. In the present review, the most common AEs were diarrhea or other gastrointestinal upset, which may also be associated with anti-inflammatory effects of the specific herbal medicines applied for treating COVID-19 (Luo et al., 2020). Therefore, the side effects were similar to those of antibiotics or associated with combining the herbs with the use of western medicines (anti-viral, antimicrobial agent); nevertheless, the events were mild and tolerable, we didn't analyze since there were no quantitative report from the enrolled trials. However, another study advocated cautious use of HM in patients with prominent gastrointestinal symptoms (Shi et al., 2021b). We suggest that in the process of HM research, drug-drug interactions remain a concern in mainstream medicine, which prompts us to explore new drugs, not only those confined to herbal medicine. Therefore, the best way is to record AEs carefully, and the present review has revealed that HM is safe and the side effects are easily manageable. Accordingly, in this meta-analysis, patients with mild to moderate COVID-19 infection who received conventional therapy combined with HM benefited more than those receiving only CWM. From an

epidemiological view, because COVID-19 is caused by rapid viral emission, shortening the disease is meaningful toward decreasing the spread of the pandemic and lowering the medical and economic burden (Pak et al., 2020; Zhang et al., 2022). Since the global population has paid a heavy price for this pandemic, it is worthwhile to make the best use of herbal medicines in treating infected patients worldwide.

4.1 Limitations

The present review has several limitations. First, many included trials lack details of methodology such as the randomization process, allocation or blinding. Secondly, the composition of herbal formulas varied considerably between studies and some even had overlapping components. Thirdly, most of the trials were conducted in a single center, which limits generalizability of results to other populations and may also compromise comparisons with multicenter studies. Lastly, more consensus about the reliable endpoints were in need to be reached about herbal medicine related study before we can make any further precise analysis and conclusion. As COVID-19 is an emergent infective disease, double blinding is difficult, yet in further study, more consistent herbal formulas and solid methodologies are required to make a powerful conclusion. We also expect more and more herbal medicine related COVID-19 research will published, and we might extract some studies which are qualified for sub-group analysis and provide valuable information for future scholars who has interests in mechanism exploration; and this is our preliminary meta-analysis on this issue.

5 Conclusion

This systematic review has demonstrated that herbal medicine is a viable complementary therapy for COVID-19 and the application of herbal medicine to COVID-19 patients in certain circumstances is recommended. It has the benefit of mitigating clinical symptoms (fever, cough, fatigue) and shortening the disease duration; yet for the complicated components in varied formulas, of which herb exert its effect need to be further investigated and clarified. The definitive herb or mechanism remains uncertain and related studies are ongoing. The merge of existing studies and further identify potential herb for following studies with scientific method is in emergent. Further large and rigorous multicenter trials or basic research integrating informative and precision medicine are warranted in order to clarify role of add-on herbal medicine in the COVID-19 regimen.

Data availability statement

The original contributions presented in the study are included in the article/Supplementary Material, further inquiries can be directed to the corresponding author.

Author contributions

Conception and design: T-JC Collection and assembly of data: T-JC; C-YL; C-JF Statistical analysis: J-HP; Y-IC literature research: Y-XW; S-WC Manuscript writing: All authors Final approval of manuscript.

Funding

The study is supported by Ministry of Science and Technology – MOST, Taiwan grant 108–2320-B-532–001 -MY3.

Acknowledgments

We thank all authors and participants in this study and the authors we have contacted who provided us with the information of their trials.

Conflict of interest

The authors declare that the research was conducted in the absence of any commercial or financial relationships that could be construed as a potential conflict of interest.

Publisher's note

All claims expressed in this article are solely those of the authors and do not necessarily represent those of their affiliated organizations, or those of the publisher, the editors and the reviewers. Any product that may be evaluated in this article, or claim that may be made by its manufacturer, is not guaranteed or endorsed by the publisher.

Supplementary material

The Supplementary Material for this article can be found online at: https://www.frontiersin.org/articles/10.3389/fphar.2022.950012/full#supplementary-material

References

An, X., Xu, X., Xiao, M., Min, X., Lyu, Y., Tian, J., et al. (2021). Efficacy of Jinhua qinggan granules combined with western medicine in the treatment of confirmed and suspected COVID-19: A randomized controlled trial. *Front. Med.* 8, 728055. doi:10.3389/fmed.2021.728055

Ang, L., Lee, H. W., Kim, A., Choi, J. Y., and Lee, M. S. (2021). Network analysis of herbs recommended for the treatment of COVID-19. *Infect. Drug Resist.* 14, 1833–1844. doi:10.2147/IDR.S305176

Ang, L., Lee, H. W., Kim, A., and Lee, M. S. (2020a). Herbal medicine for the management of COVID-19 during the medical observation period: A review of guidelines. *Integr. Med. Res.* 9, 100465. doi:10.1016/j.imr.2020.100465

Ang, L., Song, E., Lee, H. W., and Lee, M. S. (2020b). Herbal medicine for the treatment of coronavirus disease 2019 (COVID-19): A systematic review and meta-analysis of randomized controlled trials. *J. Clin. Med.* 9, 1583. doi:10.3390/jcm9051583

Balkrishna, A., Verma, S., Sharma, P., Tomer, M., Srivastava, J., and Varshney, A. (2021). Comprehensive and rapid quality evaluation method for the ayurvedic medicine divya-swasari-vati using two analytical techniques: UPLC/QToF MS and HPLC-DAD. *Pharm. (Basel)* 14, 297. doi:10.3390/ph14040297

Beyazit, F., Beyazit, Y., Tanoglu, A., and Haznedaroglu, I. C. (2020). Ankaferd hemostat (ABS) as a potential mucosal topical agent for the management of COVID-19 syndrome based on its PAR-1 inhibitory effect and oestrogen content. *Med. Hypotheses* 143, 110150. doi:10.1016/j.mehy.2020.110150

Beydogan, E., and Yuruk Atasoy, P. (2021). The relationship between CRP at admission and thorax CT findings in patients diagnosed with COVID-19. *Int. J. Clin. Pract.* 75, e14962. doi:10.1111/ijcp.14962

Borujerdi, R., Adeli, S. H., Mohammadbeigi, A., Aliasl, F., Asghari, A., Hormati, A., et al. (2022). Effects of Iranian polyherbal syrup (zufa syrup) on oxygen saturation and clinical symptoms in suspected patients with COVID-19: A triple-blinded, randomized, placebo-controlled trial. *Med. Gas. Res.* 12, 44–50. doi:10.4103/2045-9912.325991

Chen, C., Li, X., Liu, Y., and Chen, S. (2021a). [Clinical study of Lianhua qingwen capsule in the treatment of corona virus disease 2019]. *Res. Integr. Tradit. Chin. West. Med.* 13, 1–4. doi:10.3969/j.issn.1674-4616.2021.01.001

Chen, J., Zhou, Y., Chen, F., Liu, X., Chen, Y., and Wang, S. (2020). [Clinical study on treatment of COVID-19 in convalescent period treated with Lianhua Qingwen Capsule combined with Interferon α-2b]. *Adv. Clin. Med.* 10, 1144–1149. doi:10.12677/acm.2020.106174

Chen, Y., Liu, C., Wang, T., Qi, J., Jia, X., Zeng, X., et al. (2021b). Efficacy and safety of bufei huoxue capsules in the management of convalescent patients with COVID-19 infection: A multicentre, double-blind, and randomised controlled trial. *J. Ethnopharmacol.* 284, 114830. doi:10.1016/j.jep.2021.114830

Cochrane Collaboration (2021). *Risk of bias 2 (RoB 2) tool*. Available at: https://methods.cochrane.org/risk-bias-2 (Accessed July 15, 2022).

Diekemper, R. L., Patel, S., Mette, S. A., Ornelas, J., Ouellette, D. R., and Casey, K. R. (2018). Making the GRADE: CHEST updates its methodology. *Chest* 153, 756–759. doi:10.1016/j.chest.2016.04.018

Ding, Q., Lu, P., Fan, Y., Xia, Y., and Liu, M. (2020). The clinical characteristics of pneumonia patients coinfected with 2019 novel coronavirus and influenza virus in Wuhan, China. *J. Med. Virol.* 92, 1549–1555. doi:10.1002/jmv.25781

Du, X., Shi, L., Cao, W., Zuo, B., and Zhou, A. (2021). Add-on effect of Chinese herbal medicine in the treatment of mild to moderate COVID-19: A systematic review and meta-analysis. *PLoS One* 16, e0256429. doi:10.1371/journal.pone.0256429

Duan, C., Xia, W., Zheng, C., Sun, G., Li, Z., Li, Q., et al. (2020). [Clinical observation on Jinhua Qinggan Granule combined with conventional western medicine therapy in treating mild cases of Coronavirus Disease 2019]. *J. Tradit. Chin. Med.* 61, 1473–1477. doi:10.13288/j.11-2166/r.2020.17.001

Dzobo, K., Chiririwa, H., Dandara, C., and Dzobo, W. (2021). Coronavirus disease-2019 treatment strategies targeting interleukin-6 signaling and herbal medicine. *OMICS* 25, 13–22. doi:10.1089/omi.2020.0122

Fan, A. Y., Gu, S., Alemi, S. F., and Research Group for Evidence-based Chinese, M. (2020). Chinese herbal medicine for COVID-19: Current evidence with systematic review and meta-analysis. *J. Integr. Med.* 18, 385–394. doi:10.1016/j.joim.2020.07.008

Fu, X., Lin, L., and Tan, X. (2020). [Clinical study on 37 case of COVID-19 treated with integrated traditional Chinese and western medicine]. *Tradit. Chin. Drug Res. Clin. Pharm.* 31, 600–604. doi:10.19378/j.issn.1003-9783.2020.05.016

Galasiti Kankanamalage, A. C., Kim, Y., Damalanka, V. C., Rathnayake, A. D., Fehr, A. R., Mehzabeen, N., et al. (2018). Structure-guided design of potent and permeable inhibitors of MERS coronavirus 3CL protease that utilize a piperidine moiety as a novel design element. *Eur. J. Med. Chem.* 150, 334–346. doi:10.1016/j.ejmech.2018.03.004

Guyatt, G. H., Oxman, A. D., Vist, G. E., Kunz, R., Falck-Ytter, Y., Alonso-Coello, P., et al. (2008). Grade: An emerging consensus on rating quality of evidence and strength of recommendations. *BMJ* 336, 924–926. doi:10.1136/bmj.39489.470347.AD

Harder, T., Kulper-Schiek, W., Reda, S., Treskova-Schwarzbach, M., Koch, J., Vygen-Bonnet, S., et al. (2021). 2) variant: Second interim results of a living systematic review and meta-analysis, 1 january to 25 august 2021. *Eff. COVID-19 vaccines against SARS-CoV-2 Infect. Delta (B.1.617.Euro Surveill* 26, 2100920. doi:10.2807/1560-7917.ES.2021.26.41.2100920

He, Q., and Zhang, Q. (2021). [Clinical efficacy analysis of ShengMai San in the treatment of Qi-Yin deficiency syndrome in convalescent stage of COVID-19]. *ActaChin. Med. Pharm.* 49, 84–86. doi:10.19664/j.cnki.1002-2392.210069

He, Q., Zhang, Q., Gan, X., and Li, X. (2021). [Clinical efficacy analysis of Buzhong Yiqi Decoction in the treatment of mild new coronavirus pneumonia]. *J. Emerg. Tradit. Chin. Med.* 30, 385–387. doi:10.3969/j.issn.1004-745X.2021.03.003

Higgins, J. P., Thompson, S. G., Deeks, J. J., and Altman, D. G. (2003). Measuring inconsistency in meta-analyses. *BMJ* 327, 557–560. doi:10.1136/bmj.327.7414.557

Higgins, J. P. T., Thomas, J., Chandler, J., Cumpston, M., Li, T., Page, M. J., et al. (2022). *Cochrane handbook for systematic reviews of interventions version 6.3*. Available at: https://training.cochrane.org/handbookrob (Accessed July 15, 2022).

Hu, K., Guan, W. J., Bi, Y., Zhang, W., Li, L., Zhang, B., et al. (2021). Efficacy and safety of lianhuaqingwen capsules, a repurposed Chinese herb, in patients with coronavirus disease 2019: A multicenter, prospective, randomized controlled trial. *Phytomedicine* 85, 153242. doi:10.1016/j.phymed.2020.153242

Hu, Z., Yang, M., and Xie, C. (2020). Efficacy and safety of lian-hua qing-wen granule for COVID-2019: A protocol for systematic review and meta-analysis. *Med. Baltim.* 99, e20203. doi:10.1097/MD.0000000000020203

Jin, W., Lu, Y., Zhao, W., Tang, S., Sang, X., Zhang, L., et al. (2020a). [The efficacy of recommended treatments with integrated Chinese and western medicine on coronavirus disease 2019 (COVID-19) in sichuan: A clinical trial observation]. *Pharm. Clin. Chin. Mat. Med.* 36, 6–10.

Jin, Y. H., Cai, L., Cheng, Z. S., Cheng, H., Deng, T., Fan, Y. P., et al. (2020b). A rapid advice guideline for the diagnosis and treatment of 2019 novel coronavirus (2019-nCoV) infected pneumonia (standard version). *Mil. Med. Res.* 7, 4. doi:10.1186/s40779-020-0233-6

Kannan, S., Shaik Syed Ali, P., and Sheeza, A. (2021). Omicron (B.1.1.529) - variant of concern - molecular profile and epidemiology: A mini review. *Eur. Rev. Med. Pharmacol. Sci.* 25, 8019–8022. doi:10.26355/eurrev_202112_27653

Karimi, M., Zarei, A., Soleymani, S., Jamalimoghadamsiahkali, S., Asadi, A., Shati, M., et al. (2021). Efficacy of Persian medicine herbal formulations (capsules and decoction) compared to standard care in patients with COVID-19, a multicenter open-labeled, randomized, controlled clinical trial. *Phytother. Res.* 35, 6295–6309. doi:10.1002/ptr.7277

Kosari, M., Noureddini, M., Khamechi, S. P., Najafi, A., Ghaderi, A., Sehat, M., et al. (2021). The effect of propolis plus hyoscyamus Niger L. methanolic extract on clinical symptoms in patients with acute respiratory syndrome suspected to COVID-19: A clinical trial. *Phytother. Res.* 35, 4000–4006. doi:10.1002/ptr.7116

Li, J., Zhang, K., Bao, J., Yang, J., and Wu, C. (2022). Potential mechanism of action of Jing Fang Bai Du San in the treatment of COVID-19 using docking and network pharmacology. *Int. J. Med. Sci.* 19, 213–224. doi:10.7150/ijms.67116

Li, X., Xiang, L., Lin, Y., Tang, Q., Meng, F., and Chen, W. (2021a). Computational analysis illustrates the mechanism of Qingfei Paidu decoction in blocking the transition of COVID-19 patients from mild to severe stage. *Curr. Gene Ther.* 22, 277–289. doi:10.2174/1566523221666210907162005

Li, Y., Li, B., Wang, P., and Wang, Q. (2021b). Traditional Chinese medicine, Qingfei Paidu decoction and Xuanfei Baidu decoction, inhibited cytokine production via NF-kappaB signaling pathway in macrophages: Implications for coronavirus disease 2019 (COVID-19) therapy. *Front. Pharmacol.* 12, 722126. doi:10.3389/fphar.2021.722126

Liu, A., Wang, W., Liao, J., Wang, X., Liu, X., Zeng, Y., et al. (2021a). [Observation on the curative effect of Jia Wei Sang Ju Decoction in the treatment of novel coronavirus pneumonia with wind-heat invading the lung (Jia Wei Sang Ju Yin zhi liao Feng Re Fan Fei zheng xin xing guan Zhuang bing du fei yan liao xiao guan cha)]. *Mod. J. Integ Tradit. Chin. West Med.* 30, 2395–2399. doi:10.3969/j.issn.1008-8849.2021.22.001

Liu, J., Yang, W., Liu, Y., Lu, C., Ruan, L., Zhao, C., et al. (2021b). Combination of Hua Shi Bai du granule (Q-14) and standard care in the treatment of patients with coronavirus disease 2019 (COVID-19): A single-center, open-label,

randomized controlled trial. *Phytomedicine* 91, 153671. doi:10.1016/j.phymed.2021.153671

Luo, C. H., Ma, L. L., Liu, H. M., Liao, W., Xu, R. C., Ci, Z. M., et al. (2020). Research progress on main symptoms of novel coronavirus pneumonia improved by traditional Chinese medicine. *Front. Pharmacol.* 11, 556885. doi:10.3389/fphar.2020.556885

Luo, Z., Chen, W., Xiang, M., Wang, H., Xiao, W., Xu, C., et al. (2021). The preventive effect of xuebijing injection against cytokine storm for severe patients with COVID-19: A prospective randomized controlled trial. *Eur. J. Integr. Med.* 42, 101305. doi:10.1016/j.eujim.2021.101305

Maier, H. E., Kuan, G., Saborio, S., Bustos Carrillo, F. A., Plazaola, M., Barilla, C., et al. (2021). Clinical spectrum of SARS-CoV-2 infection and protection from symptomatic re-infection. *Clin. Infect. Dis.* 1, ciab717. doi:10.1093/cid/ciab717

Majeed, M., Nagabhushanam, K., Shah, K., and Mundkur, L. (2021). A randomized, double-blind, placebo-controlled study to assess the efficacy and safety of a nutritional supplement (ImmuActive™) for COVID-19 patients. *Evid. Based Complement. Altern. Med.* 2021, 8447545. doi:10.1155/2021/8447545

Mirtaleb, M. S., Mirtaleb, A. H., Nosrati, H., Heshmatnia, J., Falak, R., and Zolfaghari Emameh, R. (2021). Potential therapeutic agents to COVID-19: An update review on antiviral therapy, immunotherapy, and cell therapy. *Biomed. Pharmacother.* 138, 111518. doi:10.1016/j.biopha.2021.111518

Mou, F., Gong, X., Wei, D., Gong, X., Wang, T., Xiong, Y., et al. (2020). [Observation on curative effect of maxing shigan sanren decoction in the treatment of new coronavirus pneumonia]. *J. Emerg. Tradit. Chin. Med.* 36, 1259–1260.

Negrut, N., Codrean, A., Hodisan, I., Bungau, S., Tit, D. M., Marin, R., et al. (2021). Efficiency of antiviral treatment in COVID-19. *Exp. Ther. Med.* 21, 648. doi:10.3892/etm.2021.10080

Ni, L., Chen, L., Huang, X., Han, C., Xu, J., Zhang, H., et al. (2020). Combating COVID-19 with integrated traditional Chinese and Western medicine in China. *Acta Pharm. Sin. B* 10, 1149–1162. doi:10.1016/j.apsb.2020.06.009

Ni, L., Wen, Z., Hu, X., Tang, W., Wang, H., Zhou, L., et al. (2021). Effects of shuanghuanglian oral liquids on patients with COVID-19: A randomized, open-label, parallel-controlled, multicenter clinical trial. *Front. Med.* 15, 704–717. doi:10.1007/s11684-021-0853-6

Page, M. J., McKenzie, J. E., Bossuyt, P. M., Boutron, I., Hoffmann, T. C., Mulrow, C. D., et al. (2021). The PRISMA 2020 statement: An updated guideline for reporting systematic reviews. *Int. J. Surg.* 88, 105906. doi:10.1016/j.ijsu.2021.105906

Pak, A., Adegboye, O. A., Adekunle, A. I., Rahman, K. M., McBryde, E. S., and Eisen, D. P. (2020). Economic consequences of the COVID-19 outbreak: The need for epidemic preparedness. *Front. Public Health* 8, 241. doi:10.3389/fpubh.2020.00241

Panyod, S., Ho, C. T., and Sheen, L. Y. (2020). Dietary therapy and herbal medicine for COVID-19 prevention: A review and perspective. *J. Tradit. Chin. Med.* 10, 420–427. doi:10.1016/j.jtcme.2020.05.004

Pawar, K. S., Mastud, R. N., Pawar, S. K., Pawar, S. S., Bhoite, R. R., Bhoite, R. R., et al. (2021). Oral curcumin with piperine as adjuvant therapy for the treatment of COVID-19: A randomized clinical trial. *Front. Pharmacol.* 12, 669362. doi:10.3389/fphar.2021.669362

Ping, X.-H., Xu, H.-L., Fu, D.-F., Liu, L., and Xu, H.-X. (2021). [Clinical observation of Jiawei Yupingfeng Powder combined with western medicine in the treatment of the novel coronavirus pneumonia]. *Med. Forum* 25, 149–151.

Popovych, V., Koshel, I., Haman, Y., Leschak, V., Malofiichuk, O., Kapustina, N., et al. (2021). A randomized, open-label, multicentre, comparative study of therapeutic efficacy, safety, and tolerability of BNO 1030 extract, containing marshmallow root, chamomile flowers, horsetail herb, walnut leaves, yarrow herb, oak bark, dandelion herb, in the treatment of mild forms of COVID-19. *Clin. Phytoscience* 7, 72. doi:10.1186/s40816-021-00308-x

Prasad, A., Muthamilarasan, M., and Prasad, M. (2020). Synergistic antiviral effects against SARS-CoV-2 by plant-based molecules. *Plant Cell Rep.* 39, 1109–1114. doi:10.1007/s00299-020-02560-w

Qi, J. H., Dong, F. X., Wang, K., Zhang, S. Y., Liu, Z. M., Wang, W. J., et al. (2022). Feasibility analysis and mechanism exploration of Rhei Radix et Rhizome-Schisandrae Sphenantherae Fructus (RS) against COVID-19. *J. Med. Microbiol.* 71, 1. doi:10.1099/jmm.0.001528

Qiu, M., Li, Q., Zhu, D., Wang, C., Sun, Q., Qian, C., et al. (2020). [Efficacy observation of maxing Xuanfei Jiedu decoction on moderate COVID-19 patients]. *J Emerg Tradit Chin Med* 29, 1129–1132. doi:10.3969/j.issn.1004-745X.2020.07.001

Shi, M., Peng, B., Li, A., Li, Z., Song, P., Li, J., et al. (2021a). Broad anti-viral capacities of lian-hua-qing-wen capsule and jin-hua-qing-Gan granule and rational use against COVID-19 based on literature mining. *Front. Pharmacol.* 12, 640782. doi:10.3389/fphar.2021.640782

Shi, N., Liu, B., Liang, N., Ma, Y., Ge, Y., Yi, H., et al. (2020). Association between early treatment with Qingfei Paidu decoction and favorable clinical outcomes in patients with COVID-19: A retrospective multicenter cohort study. *Pharmacol. Res.* 161, 105290. doi:10.1016/j.phrs.2020.105290

Shi, S., Wang, F., Li, J., Li, Y., Li, W., Wu, X., et al. (2021b). The effect of Chinese herbal medicine on digestive system and liver functions should not be neglected in COVID-19: An updated systematic review and meta-analysis. *IUBMB Life* 73, 739–760. doi:10.1002/iub.2467

Shi, S., Wang, F., Yao, H., Kou, S., Li, W., Chen, B., et al. (2021c). Oral Chinese herbal medicine on immune responses during coronavirus disease 2019: A systematic review and meta-analysis. *Front. Med. (Lausanne)* 8, 685734. doi:10.3389/fmed.2021.685734

Shiehzadegan, S., Alaghemand, N., Fox, M., and Venketaraman, V. (2021). Analysis of the delta variant B.1.617.2 COVID-19. *Clin. Pract.* 11, 778–784. doi:10.3390/clinpract11040093

Smadja, D. M., Mentzer, S. J., Fontenay, M., Laffan, M. A., Ackermann, M., Helms, J., et al. (2021). COVID-19 is a systemic vascular hemopathy: Insight for mechanistic and clinical aspects. *Angiogenesis* 24, 755–788. doi:10.1007/s10456-021-09805-6

Sreepadmanabh, M., Sahu, A. K., and Chande, A. (2020). COVID-19: Advances in diagnostic tools, treatment strategies, and vaccine development. *J. Biosci.* 45, 148. doi:10.1007/s12038-020-00114-6

Srivastava, A., Rengaraju, M., Srivastava, S., Narayanan, V., Gupta, V., Upadhayay, R., et al. (2021). Efficacy of two siddha polyherbal decoctions, Nilavembu Kudineer and Kaba Sura Kudineer, along with standard allopathy treatment in the management of mild to moderate symptomatic COVID-19 patients-a double-blind, placebo-controlled, clinical trial. *Trials* 22, 570. doi:10.1186/s13063-021-05478-0

Sterne, J. A., Sutton, A. J., Ioannidis, J. P., Terrin, N., Jones, D. R., Lau, J., et al. (2011). Recommendations for examining and interpreting funnel plot asymmetry in meta-analyses of randomised controlled trials. *BMJ* 343, d4002. doi:10.1136/bmj.d4002

Sun, H., Xu, F., Zhang, L., Wei, C., Chen, J., Wang, Q., et al. (2020). Study on clinical efficacy of Lianhua Qingke Granule in treatment of mild and ordinary COVID-19. *Chin. J. Exp. Tradit. Med. Formulae* 26, 29–34. doi:10.13422/j.cnki.syfjx.20201438

Wang, J. B., Wang, Z. X., Jing, J., Zhao, P., Dong, J. H., Zhou, Y. F., et al. (2020a). Exploring an integrative therapy for treating COVID-19: A randomized controlled trial. *Chin. J. Integr. Med.* 26, 648–655. doi:10.1007/s11655-020-3426-7

Wang, L., Li, W., Huang, W., Zhou, Z., Deng, Y., Hu, Y., et al. (2020b). [Clinical study of Gegen Qinlian pill in treating COVID-19]. *Mod. Tradit. Chin. Med. Mater Mater-World Sci. Technol.* 22, 3509–3514. doi:10.11842/wst.20200430002

Wang, L., Wang, Y., Yang, W., He, X., Xu, S., Liu, X., et al. (2021a). Network pharmacology and molecular docking analysis on mechanisms of Tibetan Hongjingtian (Rhodiola crenulata) in the treatment of COVID-19. *J. Med. Microbiol.* 70, 001374. doi:10.1099/jmm.0.001374

Wang, L., Xu, M., Wang, Y., Li, H.-B., Liu, N., and Zuo, J.-L. (2020c). [Clinical study on shengmai powder combined with shenling baizhu powder in the treatment of common corona virus disease 2019]. *China J. Traditl Chin. Med. Pharm.* 35, 4268–4271.

Wang, Q., Zhu, H., Li, M., Liu, Y., Lai, H., Yang, Q., et al. (2021b). Efficacy and safety of Qingfei Paidu decoction for treating COVID-19: A systematic review and meta-analysis. *Front. Pharmacol.* 12, 688857. doi:10.3389/fphar.2021.688857

Wang, S., Liu, X., Ran, G., Liu, M., and Chen, J. (2020d). [Clinical study on treatment of cases of COVID-19 treated with viable bifidobacterium tablets combined with sanren decoction]. *Tradit. Chin. Med.* 9, 288–292. doi:10.12677/tcm.2020.93043

Wang, Y., Chen, L., Zheng, L., Ku, B.-Q., Yu, R., and Zhang, X.-F. (2021c). [Clinical effects of Qingfei Paidu Decoction combined with conventional treatment on patients with coronavirus disease 2019]. *Chin. Tradit. Pat. Med.* 43, 656–659. doi:10.3969/j.issn.1001-1528.2021.03.017

Wong, C. K. H., Lau, K. T. K., Au, I. C. H., Xiong, X., Lau, E. H. Y., and Cowling, B. J. (2021). Clinical improvement, outcomes, antiviral activity, and costs associated with early treatment with remdesivir for patients with COVID-19. *Clin. Infect. Dis.* 7, 1450–1458. doi:10.1093/cid/ciab631

Wu, Y., Xu, L., Cao, G., Min, L., and Dong, T. (2022). Effect and mechanism of Qingfei Paidu decoction in the management of pulmonary fibrosis and COVID-19. *Am. J. Chin. Med.* 50, 33–51. doi:10.1142/S0192415X22500021

Xiao, M., Tian, J., Zhou, Y., Xu, X., Min, X., Lv, Y., et al. (2020). Efficacy of huoxiang zhengqi dropping pills and Lianhua qingwen granules in treatment of COVID-19: A randomized controlled trial. *Pharmacol. Res.* 161, 105126. doi:10.1016/j.phrs.2020.105126

Xiong, W. Z., Wang, G., Du, J., and Ai, W. (2020a). Efficacy of herbal medicine (Xuanfei Baidu decoction) combined with conventional drug in treating COVID-19:A pilot randomized clinical trial. *Integr. Med. Res.* 9, 100489. doi:10.1016/j.imr.2020.100489

Xiong, X., Wang, P., Su, K., Cho, W. C., and Xing, Y. (2020b). Chinese herbal medicine for coronavirus disease 2019: A systematic review and meta-analysis. *Pharmacol. Res.* 160, 105056. doi:10.1016/j.phrs.2020.105056

Xu, F., Hou, T., Shen, A., Jin, H., Xiao, Y., Yu, W., et al. (2021a). Mechanism deconvolution of Qing Fei Pai Du decoction for treatment of Coronavirus Disease 2019 (COVID-19) by label-free integrative pharmacology assays. *J. Ethnopharmacol.* 280, 114488. doi:10.1016/j.jep.2021.114488

Xu, X., Zhang, J., Zheng, W., Yang, Z., Zhao, X., Wang, C., et al. (2021b). Efficacy and safety of reduning injection in the treatment of covid-19: A randomized, multicenter clinical study. *Ann. Palliat. Med.* 10, 5146–5155. doi:10.21037/apm-20-2121

Yan, H., Zou, Y., and Zou, C. (2020). [Mechanism of Qingfei Paidu decoction for treatment of COVID-19: Analysis based on network pharmacology and molecular docking technology]. *Nan Fang. Yi Ke Da Xue Xue Bao* 40, 616–623. doi:10.12122/j.issn.1673-4254.2020.05.02

Ye, L., Zhao, H., Xu, S., and Chen, W. (2021). [Clinical study of modified shengjiang powder in the treatment of ordinary COVID-19]. *Chin. Foreign Med. Res.* 19, 9–13.

Yu, P., Li, Y. Z., Wan, S. B., and Wang, Y. (2020). Effects of Lianhua qingwen granules plus arbidol on treatment of mild corona virus disease-19. *Chin. Pharm. J.* 55, 1042–1045. doi:10.11669/cpj.2020.12.014

Zeng, C., Yuan, Z., Zhu, J., Wang, Y., Xie, Y., Ye, R., et al. (2021). Therapeutic effects of traditional Chinese medicine (Maxingshigan-Weijing Decoction) on COVID-19: An open-label randomized controlled trial. *Integr. Med. Res.* 10, 100782. doi:10.1016/j.imr.2021.100782

Zhang, D. (2021). [A randomized controlled study of Fuzheng Gubiao Fanggan Decoction intervention in high risk group of Corona Virus Disease 2019]. *Pharm. Clin. Chin. Mat. Med.* 12, 26–29. doi:10.3969/j.issn.1674-926X.2021.01.00710.1007/s12671-021-01618-4

Zhang, F., Huang, J., Liu, W., Wang, C. R., Liu, Y. F., Tu, D. Z., et al. (2021a). Inhibition of drug-metabolizing enzymes by Qingfei Paidu decoction: Implication of herb-drug interactions in COVID-19 pharmacotherapy. *Food Chem. Toxicol.* 149, 111998. doi:10.1016/j.fct.2021.111998

Zhang, H., Li, P., Zhang, Z., Li, W., Chen, J., Song, X., et al. (2022). Epidemic versus economic performances of the COVID-19 lockdown: A big data driven analysis. *Cities* 120, 103502. doi:10.1016/j.cities.2021.103502

Zhang, X. Y., Lv, L., Zhou, Y. L., Xie, L. D., Xu, Q., Zou, X. F., et al. (2021b). Efficacy and safety of xiyanping injection in the treatment of COVID-19: A multicenter, prospective, open-label and randomized controlled trial. *Phytother. Res.* 35, 4401–4410. doi:10.1002/ptr.7141

Zhang, Y., Lei, L., Xu, Y., Wei, D., and Hu, F. (2020). [Clinical efficacy of Jinyinhua oral liquid in the treatment of 80 patients with coronavirus disease 2019]. *China Pharm.* 29, 23–26.

Zhao, C., Li, L., Yang, W., Lv, W., Wang, J., Guo, J., et al. (2021a). Chinese Medicine Formula Huashibaidu Granule early treatment for mild COVID-19 patients: An unblinded, cluster-randomized clinical trial. *Front. Med. (Lausanne)* 8, 696976. doi:10.3389/fmed.2021.696976

Zhao, J., Yang, S., Ke, D., Qiu, L., and Jiang, L. (2021b). [Clinical observation of the Antiviral Formula-1 in the treatment of novel coronavirus pneumonia in early and middle stage with cold damp and depressed lung type]. *Forum Tradit. Chin. Med.* 36, 20–22. doi:10.13913/j.cnki.41-1110/r.2021.06.008

Zheng, S., Baak, J. P., Li, S., Xiao, W., Ren, H., Yang, H., et al. (2020). Network pharmacology analysis of the therapeutic mechanisms of the traditional Chinese herbal formula Lian Hua Qing Wen in Corona virus disease 2019 (COVID-19), gives fundamental support to the clinical use of LHQW. *Phytomedicine* 79, 153336. doi:10.1016/j.phymed.2020.153336

Zhou, S., Feng, J., Xie, Q., Huang, T., Xu, X., Zhou, D., et al. (2021). Traditional Chinese medicine shenhuang granule in patients with severe/critical COVID-19: A randomized controlled multicenter trial. *Phytomedicine* 89, 153612. doi:10.1016/j.phymed.2021.153612

Zhu, N., Zhang, D., Wang, W., Li, X., Yang, B., Song, J., et al. (2020). A novel coronavirus from patients with pneumonia in China, 2019. *N. Engl. J. Med.* 382, 727–733. doi:10.1056/NEJMoa2001017

frontiers | Frontiers in Pharmacology

TYPE Original Research
PUBLISHED 02 September 2022
DOI 10.3389/fphar.2022.971243

OPEN ACCESS

EDITED BY
Kah Keng Wong,
Universiti Sains Malaysia Health Campus, Malaysia

REVIEWED BY
Thangaraj Devadoss,
KVSR Siddhartha College of Pharmaceutical Sciences, India
Qiong Wang,
Institute of Food Science and Technology (CAAS), China
Ansab Akhtar,
University of Petroleum and Energy Studies, India

*CORRESPONDENCE
Hongtao Bi,
bihongtao@hotmail.com
Lixin Wei,
lxwei@nwipb.cas.cn
Tingting Gao,
gaott646@hotmail.com

SPECIALTY SECTION
This article was submitted to Ethnopharmacology, a section of the journal Frontiers in Pharmacology

RECEIVED 16 June 2022
ACCEPTED 05 August 2022
PUBLISHED 02 September 2022

CITATION
Qiao Y, Li C, Zhang M, Zhang X, Wei L, Cao K, Zhang X, Bi H and Gao T (2022), Effects of Tibetan medicine metacinnabar (β-HgS) combined with imipramine or sertraline on depression-like symptoms in mice.
Front. Pharmacol. 13:971243.
doi: 10.3389/fphar.2022.971243

Effects of Tibetan medicine metacinnabar (β-HgS) combined with imipramine or sertraline on depression-like symptoms in mice

Yajun Qiao[1,2,3], Cen Li[2,4], Ming Zhang[2,4], Xingfang Zhang[2,5], Lixin Wei[2,4]*, Keshen Cao[1], Xiaoyuan Zhang[3], Hongtao Bi[2]* and Tingting Gao[1,3]*

[1]Department of Psychiatry, The People's Hospital of Jiangmen, Southern Medical University, Jiangmen, China, [2]Qinghai Provincial Key Laboratory of Tibetan Medicine Pharmacology and Safety Evaluation, Northwest Institute of Plateau Biology, Chinese Academy of Science, Xining, China, [3]Department of Psychology, School of Public Health, Southern Medical University, Guangzhou, China, [4]CAS Key Laboratory of Tibetan Medicine Research, Northwest Institute of Plateau Biology, Chinese Academy of Sciences, Xining, China, [5]Medical College, Qinghai University, Xining, China

Depression is a common mood disorder that has exhibited an increased incidence rate worldwide, but the overall clinical efficacy of antidepressants remains unsatisfactory. In traditional Ayurveda and Tibetan medicines, β-HgS-containing medicines have been used to treat neurological diseases for thousands of years, and our previous study found that β-HgS ameliorated depression-like behaviors in chronic restraint stress (CRS)-treated or chronic unpredictable mild stress (CUMS)-treated mice. Hence, present study investigated the effects of β-HgS combined with the clinical first-line antidepressants, imipramine (IMI) and sertraline (SER), on depression-like symptoms in CRS- and CUMS-co-treated mice. Our results revealed that β-HgS promoted the antidepressant effect of SER on depression-like behavior in mice, and enhanced its effects on promoting glucocorticoid receptor (GR) expression and neuronal proliferation in key hippocampal subregions, as well as increasing interleukin 10 (IL-10) levels and decreasing malondialdehyde levels in the sera of stress-stimulated mice. As for IMI, β-HgS enhanced its effects on preventing atrophy and severe structural damage in the hippocampus, as well as in promoting hippocampal GR levels and neuronal proliferation and serum IL-10 and superoxide dismutase (SOD) levels. Additionally, combination therapy resulted in the increased diversity of important intestinal microbiota compared to that of monotherapy, which may help sustain the health of the digestive tract and reduce inflammation to further enhance the antidepressant effects of IMI and SER in mice.

KEYWORDS

depression, β-HgS, imipramine, sertraline, combination therapy

1 Introduction

The most intuitive manifestation of depression is a persistent sense of sadness and loss of interest. This emotional disorder can even affect the way an individual feels, thinks, and behaves, and can lead to various psychological and physical problems (Ferrari et al., 2013). With lifestyle and psychosocial environmental changes in modern society, the incidence of depression has continued to increase worldwide. At present, about 350 million people in the world suffer from depression of varying degrees, and depression is expected to become the world's major disease burden by 2030 (data from the World Health Organization 2012) (WHO, 2012; Gigantesco et al., 2019; Hamel et al., 2019).

Antidepressants are the initial treatment choice for patients with mild-to-moderate depression and the definitive choice for patients with major depression. At present, the clinical use of antidepressants consists of four classes of drugs: tricyclic antidepressants (TCAs), serotonin reuptake inhibitors (SSRIs), selective serotonin noradrenaline reuptake inhibitors (SNRIs), and monoamine oxidase inhibitors (MAOIs) (Cosgrove et al., 2012). Additionally, drugs with other mechanisms of action—including bupropion, nefazodone, ketones of letrozole, and rice nitrogen equality are also used. Among clinical first-line antidepressants, imipramine (IMI) and sertraline (SER) are two of the most commonly used antidepressants in China. IMI, a milestone in the development of antidepressants, represents the first clinically available TCA and has been widely used to treat endogenous depression and functional or reactive depression since it was first successfully synthesized in 1957. SER is commonly used to treat major depressive disorder (MDD), obsessive-compulsive disorder (OCD), panic disorder, post-traumatic stress disorder (PTSD), premenstrual dysphoric disorder (PMDD), and social anxiety disorder. The SER belongs to SSRI, which is a common psychotropic drug (López-Muñoz and Álamo, 2009). Although some studies have suggested that some mechanisms of action of antidepressants are superior to those of others, there have been no repeatable findings to confirm the clinical significance of these claims (Bayes and Parker, 2019). For most patients, antidepressant efficacy is similar between different types of drugs and among different drugs of the same class. Despite these findings, studies of sequential treatment of depression suggest that some residual symptoms, such as sadness, impaired functioning, and negative self-perceptions, persist in patients with complete remission after treatment (Steven and Maurizio, 2011). Therefore, these residual symptoms can make patients in complete remission more likely to relapse into depression (Nil et al., 2016; Bressington et al., 2019). Therefore, the identification and development of adjuvant therapies for existing antidepressants have become a major focus of research on the treatment of depression.

In traditional Ayurveda and Tibetan medicines, the cubic form of mercury sulfide (metacinnabar, also known as β-HgS) and β-HgS-containing medicines have been used to treat various chronic ailments for thousands of years, especially neurological diseases such as neuroinflammation, brain trauma, and stroke (Liu et al., 2018). Recently, we revealed that the Tibetan medicine, Zuotai (containing 54.5% β-HgS), and β-HgS significantly relieve depression-like behaviors in CRS-treated or CUMS-treated mice (Niu et al., 2016; Zhao et al., 2016; Zhao J. et al., 2018). However, the antidepressant effects of β-HgS as an adjuvant therapy for existing antidepressants remain unknown. Therefore, in this study, to investigate the effect of β-HgS combined with clinical first-line antidepressants on depression-like symptoms, we chose two types of antidepressants, IMI and SER, for use in combined pharmacotherapies to evaluate the antidepressant-like ability of β-HgS as an adjuvant therapy in CRS- and CUMS-treated mice. Additionally, through behavioral testing, we analyzed the effect of these different treatment modalities on depression-like symptoms in mice, and by analyzing some physiological indicators of depression (including neurotransmitters, brain-derived neurotrophic factors, inflammatory factors, and antioxidants), receptors in various subregions of the hippocampus, and gut microbiota to explore the corresponding underlying mechanisms.

2 Materials and methods

2.1 Animals

The experimental animals were 8-week-old male Kunming (KM) mice obtained from Gansu University of Traditional Chinese Medicine, China [Animal Production License No. SCXK (Gan) 2015-0005). Mice were placed in standard cages with wood shavings. The rearing environment was a closed an imal room with an ambient temperature of 22 ± 1°C, artificial lighting from 7:00 am to 19:00 pm, and mice were fed standard laboratory chow and distilled water ad libitum. Animal experiments in this study were in accordance with ARRIVE guidelines and were approved by the Animal Experimentation Committee of the Institute of Plateau Biology, Chinese Academy of Sciences (Lot: NWIPB20171106-01), and strict accordance with the National Institutes of Health Guide for the Care and Use of Laboratory Animals (NIH Publication No. 8023) , revised in 1978.

2.2 Drugs and reagents

β-HgS was purchased from Alfa Aesar Chemical Co., Ltd. (Haverhill, MA, United States) with a purity of 98%. IMI hydrochloride was obtained from the National Institutes for Food and Drug Control (Bejing, China). SER hydrochloride was purchased from Shanghai Yuanye Bio-Technology Co., Ltd. (Shanghai, China).

Enzyme-linked immunosorbent assay (ELISA) kits for 5-hydroxytryptamine(5-HT), norepinephrine (NE), and brain-

derived neurotrophic factor (BDNF) for neurotransmitter detection; corticosterone (CORH), corticotropin-releasing hormone (CRH), and adrenocorticotropic hormone (ACTH) ELISA kits for the detection of HPA axis core indicators; interleukin-6 (IL-6), IL-10 and tumor necrosis factor-α (TNF-α) ELISA kits to detect cellular immune factors, the above ELISA kits were purchased from Jianglai Biotechnology Co., Ltd. (Shanghai, China); purchased from Nanjing Jiancheng Bioengineering Institute (Nanjing, China) detection kit for the detection of SOD, catalase (CAT) and malondialdehyde (MDA). Antibodies used in fluorescence immunohistochemistry were purchased from Abcam, Inc. (Cambridge, Cambridgeshire, United Kingdom), including anti-GR antibody (ab3578), anti-Proliferating Cell Nuclear Antigen (PCNA) antibody (ab18197), anti-Neuronal Nuclei (NeuN) antibody (ab128886), anti-NG2 antibody (ab129051) and anti-Olig2 antibody (ab136253). The chemicals in other laboratory tests are of analytical grade and manufactured in China.

2.3 Chronic predictable and unpredictable stress procedures and drug treatments

After 1 week of acclimatization, mice were randomly divided into the following seven groups ($n = 10$): 1) normal, 2) model, 3) β-HgS, 4) IMI, 5) SER, 6) IMI+β-HgS, and 7) SER+β-HgS. Mice in the normal and model groups were intragastrically administrated 2% (w/v) starch solution. β-HgS, IMI, and SER were separately dissolved in 2% (w/v) starch solutions and were then intragastrically administrated to mice in the drug-treatment groups (β-HgS, IMI, SER, IMI+β-HgS, and SER+β-HgS groups) at dosages of 0.014 $mmol.kg^{-1}$ (β-HgS) (Zhao J. et al., 2018), 15 $mg.kg^{-1}$ (IMI) (Furukawa et al., 2022), and 7.6 $mg.kg^{-1}$ (SER) (Weilburg et al., 2003) per day for 3 weeks. Drugs were prepared the day before the experiment and stored in a 4°C refrigerator. Additionally, the mice exposed to chronic predictable and unpredictable stressors included a predictable chronic restraint stressor and a total of seven unpredictable mild stressors per day for 3 weeks, with the exception of the normal group. The predictable chronic restraint stressor consisted of placing the mice into tubes from 8:30 to 14:30 each day (Ding et al., 2016). The experiment used seven different stimuli to simulate an unpredictable stressor [1): 5 min of heat stress at 42°C; 2): 2 min of cold stress at 10°C; 3): 2 min of reciprocating swing; 4): 24 h of 45° tilt; 5): 24 h of fasting; 6): 24 h of water deprivation; 7): 24 h of day-night reversal], and each stimulus occurred randomly, with three stimulations per day (Ma et al., 2018). In addition, the body weight of each group of mice was measured weekly (Figure 1).

2.4 Behavioral tests

The behavioral tests—including the sucrose preference test (SPT), open field test (OFT), tail suspension test (TST), and forced swimming test (FST)—were conducted before the stress procedures and drug treatments began (0 days) and at the end of the 3-week stress period (21 days). The SPT was performed out following the procedures described by Yan et al. (2015), and the sucrose preference ratio (SPR) was calculated as follows: SPR (%) = sucrose intake/total fluid intake (including sucrose and water intake); 2 h-food consumption = the amount of food before the test minus the amount of food after the test. The OFT was performed following the procedures described by Choleris et al. (2001). TST was performed following the procedures described by O'Leary and Cryan (2009). Finally, the FST was carried out following the procedures described by Porsolt et al. (1977), Qiao et al. (2020).

2.5 Determination of biomarkers related to depression, immune function, and oxidative stress

After the behavioral test, mouse blood was collected through the retro-orbital venous plexus, and the collected mouse blood was placed in coagulation tubes, respectively, and serum was obtained by centrifugation at 4°C and 4,000 RPM for 10 min. Immediately after blood collection, the animals were sacrificed, and the cortex, hippocampus, and hypothalamus were collected from the brain and mixed with phosphate-buffered saline (pH 7.2) in proportion to each, and these tissues were homogenized using a tissue homogenizer (frequency: 60 Hz), rotation rate: 1,800 times/min, duration: 2 min). The supernatant was then extracted after centrifugation for 10 min at 4°C and 5,000 RPM. According to the kit manufacturer's instructions, 5-HT and NE content in the cortical supernatant, BDNF content in the hippocampal supernatant, CRH level in hypothalamic supernatant, as well as CORT, ACTH, TNF-α, IL-6, IL-10, MDA, CAT, and SOD levels in serum were determined, respectively.

2.6 Immunohistochemistry

Whole brains were collected from the control and stress-stimulation groups after the stress stimulations were completed. Briefly, the brains were fixed in 4% paraformaldehyde solution, paraffin-embedded, and serially sectioned at a slice thickness of 5 μm. Then, the paraffin-embedded sections were deparaffinized, and non-specific binding was blocked by incubation with 3% BSA for 30 min. Subsequently, brain sections were incubated with primary antibodies against PCNA (1:500), GR (1:500), NG2 (1:500), NeuN (1:200), and Olig-2 (1:250) overnight at 4°C. After incubation and washing, FITC-conjugated and Cy3-conjugated secondary antibodies were added. Following incubation with these antibodies (4°C, 24 h for primary antibodies; and room temperature, 45 min for secondary antibodies), the sections were

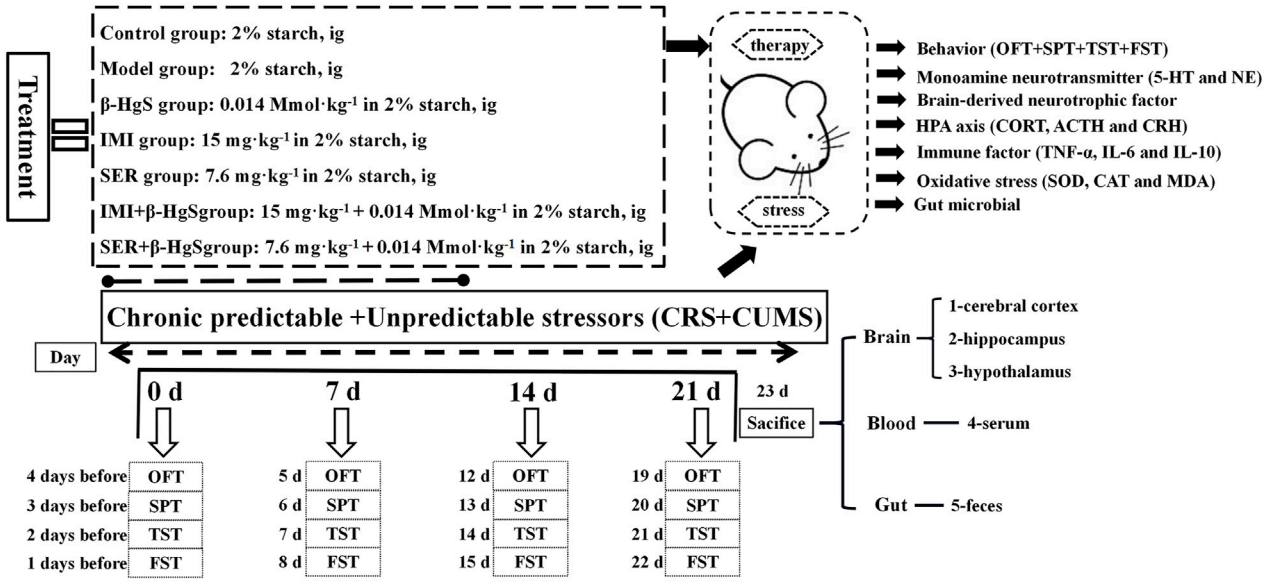

FIGURE 1
Experimental flowchart.

embedded in Fluoroshield mounting medium with DAPI (ab104139, Abcam). Images were acquired using a fluorescence microscope (IX73, Olympus, Japan) (Qiao et al., 2020).

2.7 Intestinal microbial-diversity analysis

After the stress stimulations, fresh rectal contents of the mice were collected, frozen quickly in liquid nitrogen, and placed in a refrigerator at −80°C for subsequent DNA extraction. Microbial DNA was extracted using the E.Z.N.A. Stool DNA Kit (Omega Bio-tek, Norcross, GA, United States) according to the manufacturer's protocols, after which the extracted DNA was stored at −80°C until further use.

The primers, 338F (5′-CTCCTACGGGAGGCAGCAG-3′) and 806R (5′-GGACTACHVGGGTWTCTAAT-3′), were used to amplify the V3–V4 region of the bacterial 16S rDNA gene. The amplification procedure of PCR reactions was 95°C for 3 min, followed by 27 cycles at 95°C for 30 s, 55°C for 30 s, and 72°C for 45 s, as well as a final extension at 72°C for 10 min. Approximately 420 bp of amplified fragments was obtained per sample. PCR reactions were performed in 20 μl volumes containing 4 μl of 5 × FastPfu Buffer, 2 μl of 2.5 mM dNTPs, 0.8 μl of 5 μM primers, 0.4 μl of FastPfu Polymerase, and 10 ng of template DNA *via* a PCR system (ABI GeneAmp 9700, Applied Biosystems, Inc., MA, United States). Using the MiSeq platform, paired-end data of 2 × 300 bp were obtained *via* sequencing. Long sequences were obtained by splicing, and 16S analysis was performed. The raw reads were deposited into the NCBI Sequence Read Archive (SRA) database (https://www.ncbi.nlm.nih.gov/sra/?term=PRJNA850836).

The original sequence was quality-filtered using Trimmomatic software (version 0.39) and was spliced by FLASH software with the following criteria: 1) setting a 50 bp sliding window, the 300 bp reads were truncated at any site receiving an average quality score < 20 over this window, discarding the truncated reads that were shorter than 50 bp; 2) barcodes matching exactly 2-nucleotide mismatches in primer matching were allowed, and reads containing ambiguous characters were removed; and 3) two end sequences were spliced according to base overlap, whereas overlaps longer than 10 bp and unspliced sequences were removed. Reads that could not be assembled were discarded. Operational taxonomic units (OTUs) were clustered with a 97% similarity cutoff using UPARSE (version 7.1 http://drive5.com/uparse/), and chimeric sequences were identified and removed using UCHIME. The taxonomy of each 16S rRNA gene sequence was analyzed by RDP Classifier (http://rdp.cme.msu.edu/) against the Silva (SSU123) 16S rRNA database using a confidence threshold of 70% (Amato et al., 2013; Qiao et al., 2020).

2.8 Statistical analysis

Experimental data for all tests are presented as the mean ± standard deviation (SD) of six replicates and an analysis of variance was performed for a completely randomized

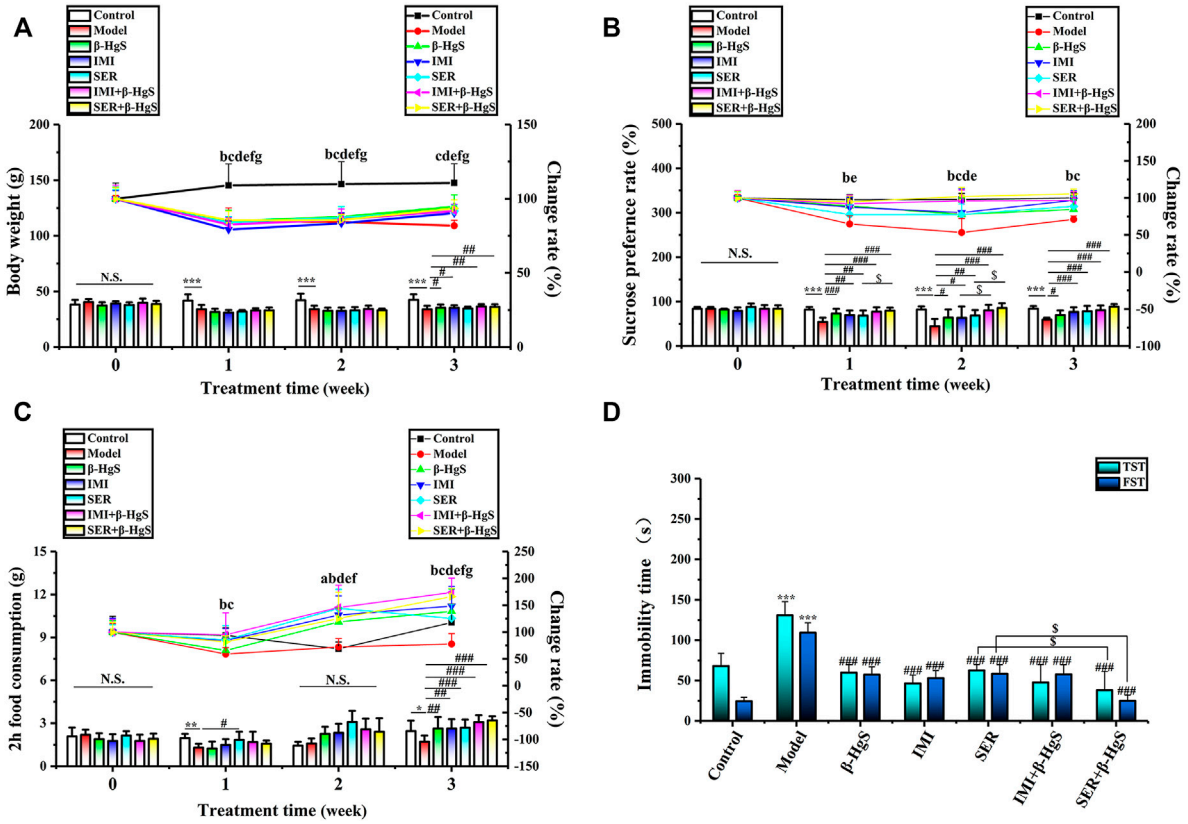

FIGURE 2
The effects of drug treatments on **(A)** body weight, **(B)** sucrose preference ratio, **(C)** 2 h-food consumption, and **(D)** immobility time in the tail suspension test (TST) and forced swimming test (FST) of stress-stimulated mice. Data are shown as the mean ± *SD* (n = 10). $^{**}p < 0.01$ and $^{***}p < 0.001$ denote a significant difference from the control group. $^{\#}p < 0.05$, $^{\#\#}p < 0.01$, and $^{\#\#\#}p < 0.001$ denote significant differences from the model group. $^{\$}p < 0.05$ denotes a significant difference from the relative monotherapy group. Intra-group comparison of each group, the letters indicate significant differences compared with 0 days $p < 0.05$.

experimental design. Data were subjected to multiple t-tests using SPSS 22.0 software to identify differences between means (without assuming consistent SD) and "Pearson" correlation analysis. p-Value < 0.05 was considered statistically significant.

3 Results

3.1 Effect on body weight

As shown in Figure 2A, mice in the model group significantly lost body weight due to experiencing stress stimuli, as their body weight losses were 19.52%, 20.85%, and 23.82% on days 7, 14, and 21, respectively, compared to those of the control group. In contrast, the body weights of the mice in the drug-treated groups all initially decreased, but then increased during the 3-week treatment and yielded significantly higher body weights compared those of the model group on day 21 ($p < 0.05$ or $p < 0.01$), except for the SER group. The mice in the IMI+β-HgS group had the highest body weights among all drug-treated groups on day 21.

3.2 Effects on sucrose preference ratio and two h-food consumption

SPR and food consumption are usually used to evaluate anhedonia levels (a core symptom of depression) in mice, and corresponding results in this study are shown in Figures 2B,C. Compared to those of the normal group, the SPR and 2 h-food consumption of mice in the model group were both dramatically decreased by 3-week stress stimulation, as these decreases were 28.96% and 30.46%, respectively. Compared with those of the model group, the SPR and 2 h-food consumption of mice in all drug-treated groups were increased significantly on day 21 ($p < 0.05$, $p < 0.01$, or $p < 0.001$). Moreover, the SPR of mice in the IMI+β-HgS group was significantly higher than that of the IMI

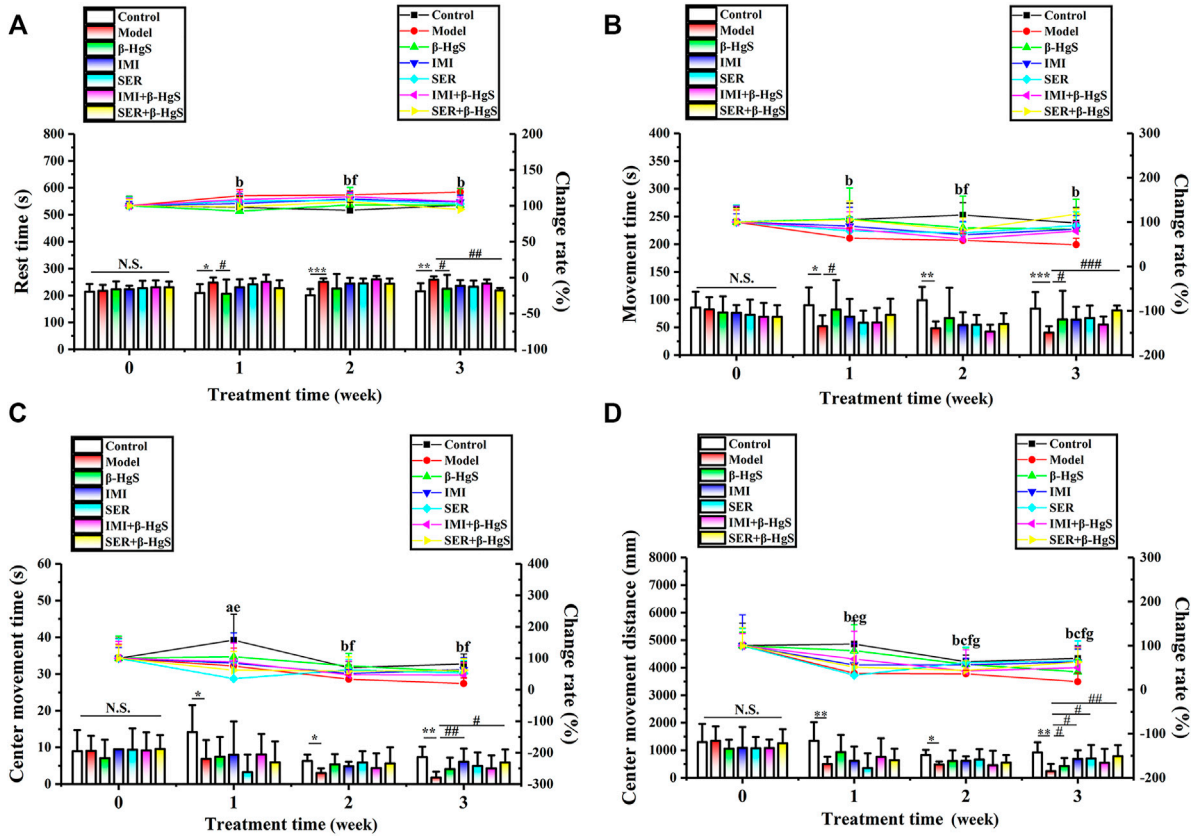

FIGURE 3
Effects of drug treatments on **(A)** rest time, **(B)** movement time, **(C)** center movement time, and **(D)** center movement distance in stress-stimulated mice in the open-field test. Data are shown as the mean ± *SD* (n = 10). $^{*}p < 0.05$, $^{**}p < 0.01$, and $^{***}p < 0.001$ denote a significant difference from the control group. $^{\#}p < 0.05$, $^{\#\#}p < 0.01$, and $^{\#\#\#}p < 0.001$ denote significant differences from the model group. Intra-group comparison of each group, the letters indicate significant differences compared with 0 days $p < 0.05$.

group on day 14 ($p < 0.05$), and the SPR of mice in the SER+β-HgS group was significantly higher than that of the SER group on days 7 and 14 ($p < 0.05$).

3.3 Effects on immobility time in the TST and FST

The TST and FST are two of the primary methods for evaluating depression-like behavior in mice, in which the corresponding immobility time reflects the level of depression-like behavior. As shown in Figure 2D, 3-week stress stimulations significantly increased the immobility time of mice in the TST and FST in the model group ($p < 0.001$). Compared with that of the model group, the immobility time of mice in all drug-treated groups was significantly shorter in both the TST and FST ($p < 0.001$). In particular, the mice in the SER+β-HgS group had much shorter immobility times than those in the SER group in both the TST and FST ($p < 0.001$).

3.4 Effects on rest time, movement time, center residence time, and movement distance in the open field test

The activities of mice were tested using the OFT during the 3-week stress stimuli and drug treatments. As shown in Figure 3, compared to the parameters in the control group, the mice in the model group exhibited a marked increase in the rest time (RT) and dramatic decreases in movement time (MT), center residence time (CRT), and movement distance (CMD) on day 7 onward. Compared with parameters in the model group, mice had less RT and more MT and CMT in the β-HgS and SER+β-HgS groups ($p < 0.05$, $p < 0.01$, or $p < 0.001$), as well as more CMD in the β-HgS, IMI, SER, and SER+β-HgS groups ($p < 0.05$ or $p < 0.01$) on day 21. These results suggest that mice in the SER+β-HgS and β-HgS groups were the most active among all drug-treated groups.

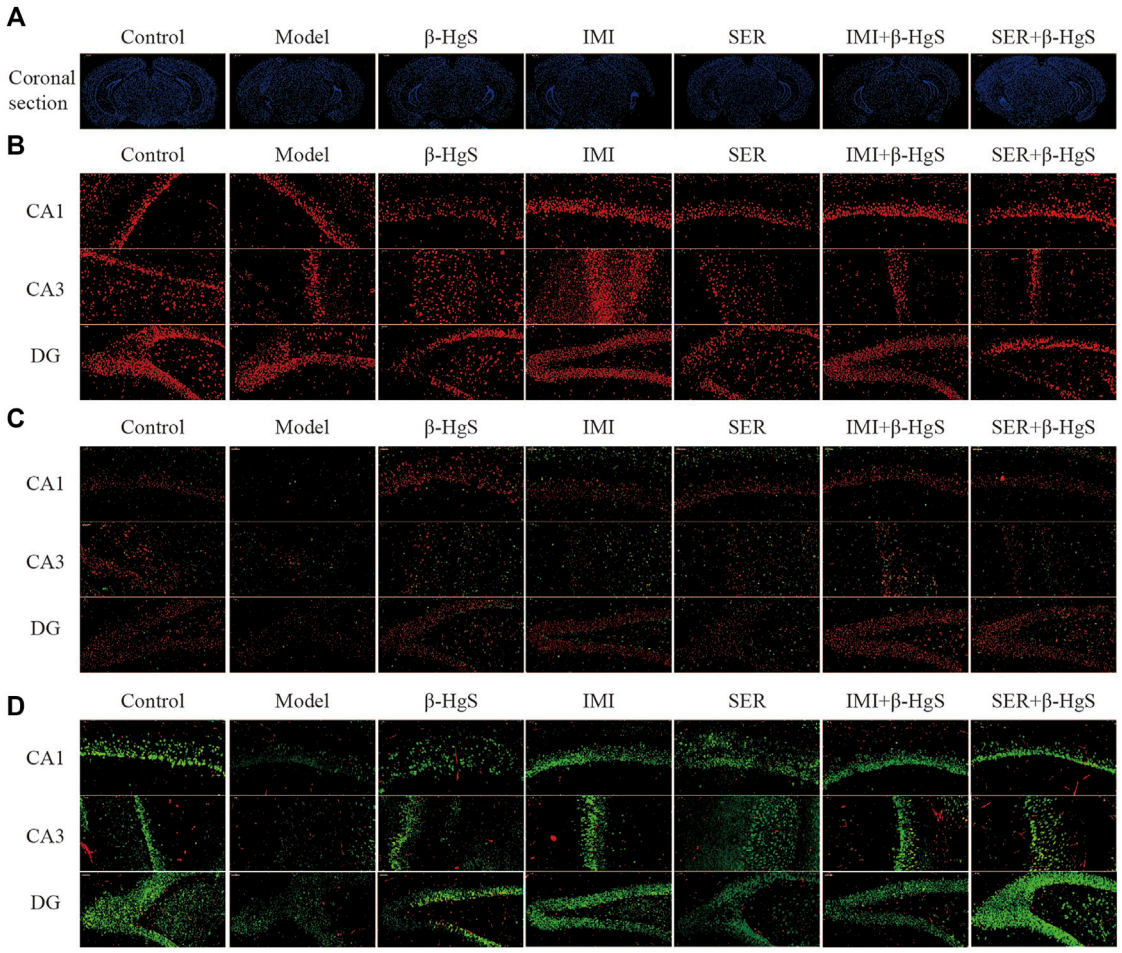

FIGURE 4
Effects of drug treatments on the structure, expression of GRs and oligodendrocytes, and neuronal proliferation in key hippocampal subregions of stress-stimulated mice. **(A)** Coronal sections, **(B)** immunofluorescent images of GRs (red), **(C)** immunofluorescent images of NG+ cells (red) and Olig2+ glial cells (green), and **(D)** immunofluorescent images of NeuN+ cells (green) and PCNA+ cells (red).

3.5 Effects on morphological structure, GR levels, oligodendrocyte numbers, and neuronal proliferation in key hippocampal subregions

The effects of stress and drug treatments on morphological structure, GR levels, oligodendrocyte numbers, and neuronal proliferation in key hippocampal subregions were assessed via immunohistochemistry (Figures 4, 5). As shown in Figure 4A, the representative coronal section of the mouse brain shows the complete morphology and clear structure, and the hippocampal cells are arranged orderly in each subregion of the hippocampus of mice in the control group. Compared with those of the control group, the hippocampus of the mice in the model was atrophied and the hippocampal cells were disorganized and fewer in number, suggesting severe structural damage in the hippocampus of the mice in the model group. Compared with the characteristics in the model group, there was much less structural damage in the hippocampi of the mice in all drug-treatment groups, among which the structural damage of the hippocampus in the IMI+β-HgS group was less than that found in the other drug-treatment groups.

Immunofluorescent staining of GRs in key hippocampal subregions is shown in Figure 4B, and the corresponding fluorescence densities are shown in Figure 5A. Compared with features of the control group, the distribution of GR-positive cells was narrower, the cellular morphology was irregular and disorderly, and the fluorescence intensities were significantly weakened ($p < 0.01$ or $p < 0.001$) in all key subregions of the hippocampus in the model groups. Compared with properties of the model group, GR-positive cells exhibited a larger distribution range and significantly higher fluorescence intensities in key subregions of the hippocampus in drug-treatment groups,

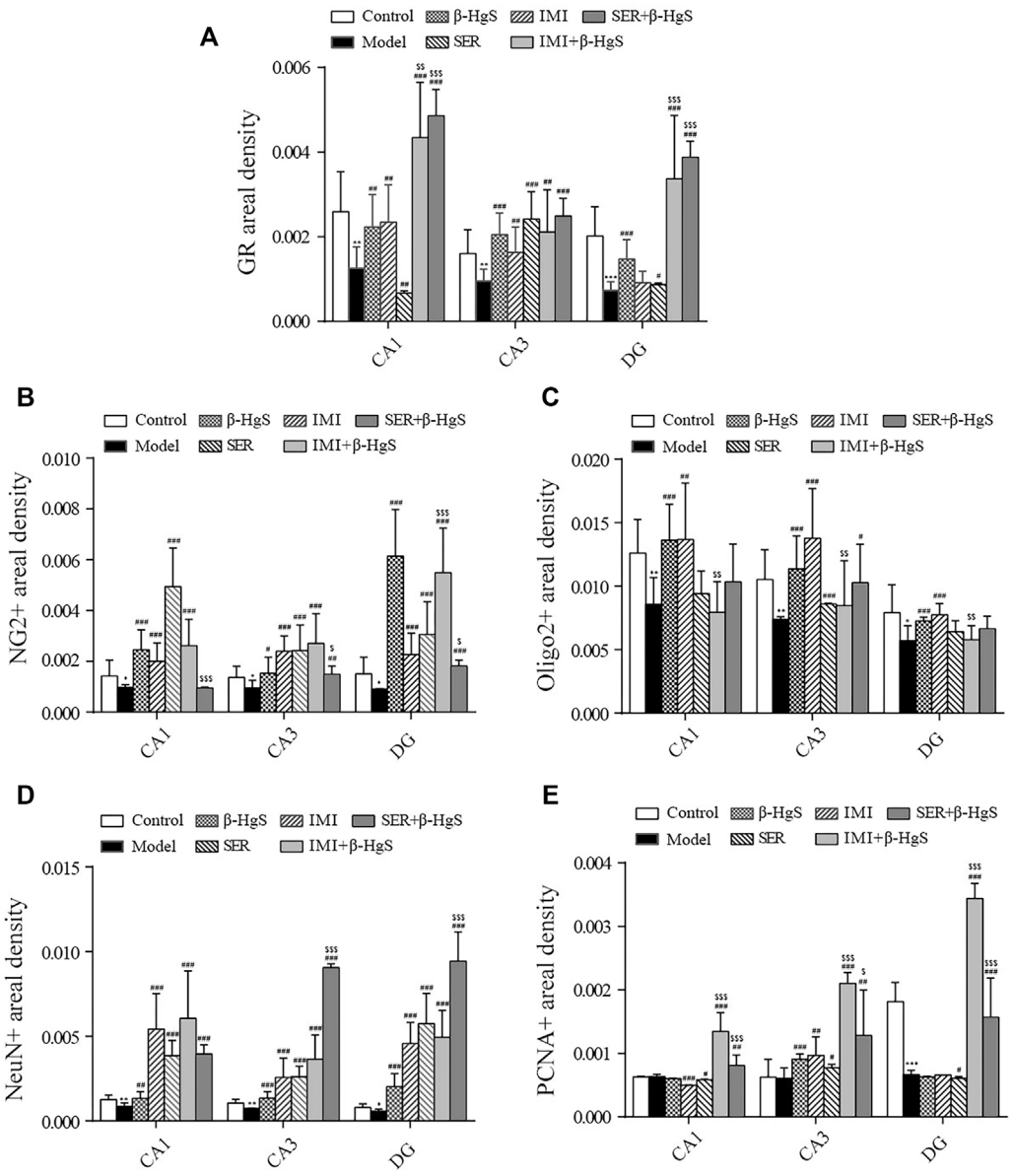

FIGURE 5
Effects of drug treatments on fluorescence intensities of GRs and oligodendrocytes, and neuronal proliferation in key hippocampal subregions of stress-stimulated mice. **(A)** Fluorescence intensity of GRs, **(B)** fluorescence intensity of NG2+ glial cells, **(C)** fluorescence intensity of Olig2+ glial cells, **(D)** fluorescence intensity of NeuN+ cells, and **(E)** fluorescence intensity of PCNA+ cells in subregions of the hippocampus. Data are shown as the mean ± *SD* ($n = 4$). *$p < 0.05$, **$p < 0.01$, and ***$p < 0.001$ denote significant differences from the control group. $^{\#}p < 0.05$, $^{\#\#}p < 0.01$, and $^{\#\#\#}p < 0.001$ denote significant differences from the model group. $^{\$}p < 0.05$, $^{\$\$}p < 0.01$, and $^{\$\$\$}p < 0.001$ denote significant differences from the relative monotherapy group.

with the exceptions of CA1 in the SER group and the dentate gyrus (DG) in the IMI group. The fluorescence intensity of GR-positive cells in the combined pharmacotherapy groups was 84.83% and 267.97% (IMI+β-HgS group), and 629.71% and 343.33% (SER+β-HgS group) higher than those of their corresponding single antidepressant-treated groups (IMI or SER group) in CA1 and DG regions ($p < 0.01$ or $p < 0.001$).

Next, the effects of stress and drug treatment on oligodendrocytes in the hippocampus were assessed. We measured the levels of NG2 (a marker for oligodendrocyte progenitors) and Olig2 (a pan-oligodendrocyte marker), respectively Compared with those in the control group, there was a dramatic loss of NG2+ and Olig2+ cells in the CA1, CA3, and DG regions of the hippocampus of mice in the

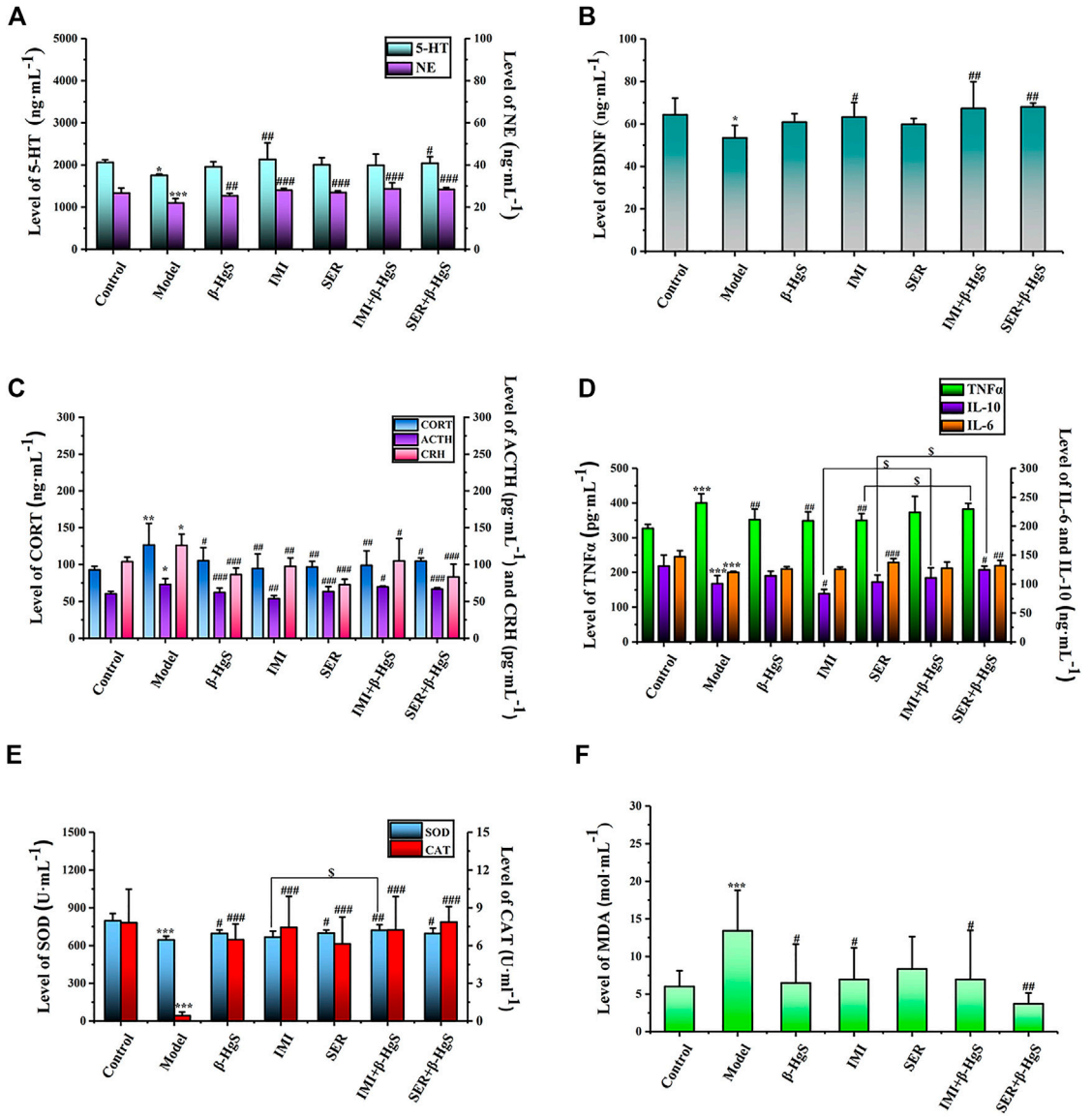

FIGURE 6
The effects of drug treatments on the levels of monoamine neurotransmitters **(A)** and BDNF **(B)**, and the biomarkers of HPA axis **(C)**, and the biomarkers of immune factors **(D)**, and **(E, F)** oxidative stress in stress-stimulated mice. Data are shown as the mean ± *SD* (n = 10). $^{*}p < 0.05$, $^{**}p < 0.01$, and $^{***}p < 0.001$ denote significant differences from the control group. $^{\#}p < 0.05$, $^{\#\#}p < 0.01$, and $^{\#\#\#}p < 0.001$ denote significant differences from the model group. $^{\$}p < 0.05$ denotes a significant difference from the relative monotherapy group.

model group (Figure 4D), and the fluorescence intensities of NG2+ and Olig2+ cells were both remarkably decreased (Figures 5B,C). Compared with those in the model group, NG2+ and Olig2+ cells had a larger distribution range in the hippocampal CA1, CA3, and DG regions in all drug-treatment groups. The fluorescence intensities of NG2+ cells were significantly higher than those in the control group in the hippocampal CA1, CA3, and DG regions in all drug-treatment groups, except the CA1 region in the SER+β-HgS group. The fluorescence intensities of Olig2+ cells were significantly higher than those of the control group in all three hippocampal subregions in both the β-HgS and IMI groups. Notably, the fluorescence intensity of NG2+ cells in the DG region of the IMI+β-HgS group was 142.56% higher than that in the IMI group ($p < 0.001$).

Neuronal proliferation in key hippocampal subregions was evaluated using a cell-cycle marker proliferating cell nuclear antigen (PCNA) and neuronal nuclear antigen neuron marker (NeuN). As shown in Figure 4D, the mice in the model group showed significantly weaker responses to

PCNA and NeuN immunoreactivity in the hippocampal CA1, CA3, and DG regions compared with those in the control group. Compared with those in the model group, the fluorescence intensities of NeuN+ cells were significantly increased in all three hippocampal subregions in all drug-treatment groups ($p < 0.05$, $p < 0.01$, or $p < 0.001$). For the combined pharmacotherapy groups (IMI+β-HgS and SER+β-HgS groups), the fluorescence intensities of PCNA+ cells were significantly increased in all three hippocampal subregions ($p < 0.01$ or $p < 0.001$) compared with those in the model group. Furthermore, the fluorescence intensities of NeuN+ cells in the CA3 and DG regions, as well as PCNA+ cells in all three hippocampal subregions, in the SER+β-HgS group were significantly higher than those of the SER group ($p < 0.05$ or $p < 0.001$). Additionally, the fluorescence intensities of PCNA+ cells in all three hippocampal subregions of the IMI+β-HgS group were significantly higher than those of the IMI group ($p < 0.001$).

3.6 Effects on the contents of monoamine neurotransmitters, BDNF, and neuroendocrine hormone content in the hypothalamic-pituitary-adrenal axis

Cortical levels of monoamine neurotransmitters (5-HT and NE), hippocampal levels of BDNF, and levels of three core neuroendocrine hormones (CRH, ACTH, and CORT) in the hypothalamic-pituitary-adrenal (HPA) axis were determined (Figures 6A–C). After three-week stress stimulation, cortical levels of 5-HT/NE and hippocampal levels of BDNF in model mice were significantly lower—whereas levels of CRH, ACTH, and CORT in the HPA axis were remarkably higher—than those in normal control mice ($p < 0.05$ or $p < 0.01$). Compared with those in the model group, the cortical levels NE, as well as the CRH, ACTH, and CORT levels in the HPA axis, were significantly increased in all drug-treated groups ($p < 0.01$ or $p < 0.001$). However, 5-HT levels were only significantly increased in the IMI and SER+β-HgS groups ($p < 0.05$ or $p < 0.01$), whereas BDNF levels were only significantly increased in the IMI, IMI+β-HgS, and SER+β-HgS groups ($p < 0.05$ or $p < 0.01$).

Among all groups, cortical 5-HT levels were the highest in the IMI group, cortical NE levels were the highest in the IMI+β-HgS group, and hippocampal BDNF levels were the highest in the SER+β-HgS group. Additionally, among all drug-treated groups, SER and IMI were the most effective at inhibiting the increases in levels of three core neuroendocrine hormones (CRH, ACTH, and CORT) induced by stress. Compared with those in the model group, CRH, ACTH, and CORT levels in the SER and IMI groups were decreased by 42.25%, 13.40%, and 23.63%, and by 22.67%, 26.31%, and 25.18%, respectively.

3.7 Effects on the contents of TNF-α, IL-6, and IL-10 content in serum

The effects of stress and drug treatments on immune inflammatory responses in mice were preliminarily investigated according to serum levels of TNF-α, IL-6, and IL-10. As shown in Figure 6D, after three-week stress stimulation, TNF-α levels in the model group were significantly higher—while IL-6 and IL-10 levels were both significantly lower—compared to those in the control group ($p < 0.001$). Compared with those in the model group, TNF-α levels were significantly decreased in the β-HgS, IMI, and SER groups ($p < 0.01$); IL-10 levels were significantly increased in the SER+β-HgS group ($p < 0.05$) but decreased in the IMI group ($p < 0.05$); IL-6 levels were significantly increased in the SER and SER+β-HgS groups ($p < 0.01$ or $p < 0.001$). Moreover, IL-10 levels in the IMI+β-HgS and SER+β-HgS groups were significantly higher than those in their corresponding IMI and SER groups ($p < 0.05$), whereas TNF-α levels in the SER+β-HgS group were significantly higher than those in the SER group ($p < 0.05$).

3.8 Effect on oxidative stress

To evaluate the oxidative stress levels of mice induced by three-week stress and drug treatments, serum levels of MDA, SOD, and CAT were determined (Figures 6E,F). Compared with those of the control group, MDA levels were significantly higher—whereas SOD and CAT levels were significantly lower—in the model group ($p < 0.05$). Compared with those of the model group, the MDA levels were significantly decreased after 3 weeks of drug treatment (except for the SER group), and CAT and SOD levels were significantly increased (except for the SOD content in the IMI group). Moreover, the MDA levels of the SER+β-HgS group were significantly lower than those of the SER group ($p < 0.05$), while SOD levels of the IMI+ β-HgS group were much higher than those of the IMI group ($p < 0.05$).

3.9 Effect on gut microbiota

3.9.1 Diversity of gut microbiota

In the Alpha diversity analysis (Figures 7A–C), the differences between Chao1, PD whole tree index, and observed species were statistically significant ($p < 0.05$; $p < 0.05$; $p < 0.05$). The analysis of beta diversity was calculated from the unweighted and weighted UniFrac distances, as well as the Bray–Curtis dissimilarity (Figures 7D–F; and Table 1). The results revealed that the bacterial microbiota of stress-treated mice were clustered apart from that of normal mice ($p < 0.05$, multi-response permutation procedure analysis), and the diversity of gut microbiota also differed significantly among the drug-treatment groups ($A >$

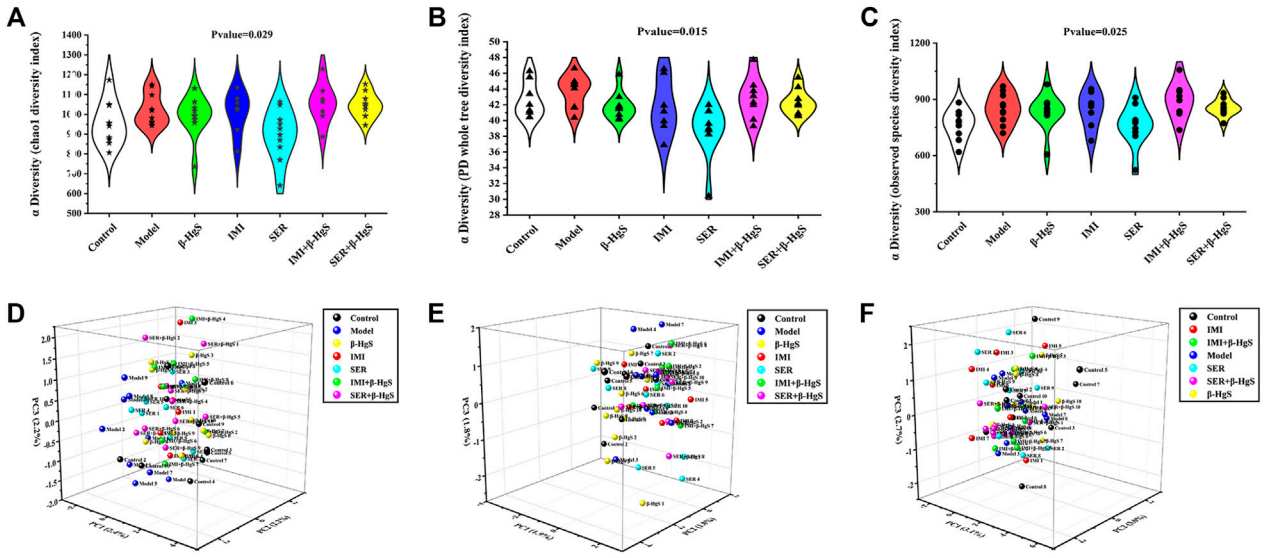

FIGURE 7
The diversity of gut microbiota. **(A)** Chao1 index, **(B)** PD whole tree index, **(C)** observed species, **(D)** Bray curtis distance, **(E)** Weighted Unifrac distance, **(F)** Unweighted Unifrac distance.

TABLE 1 PCoA of gut microbiota beta diversity.

Beta diversity	*A* Value	Observed delta	Expected delta	*p* Value
Weighted unifrac distance	0.019097	0.263322	0.268449	0.064
Unweighted_unifrac distance	0.042404	0.335139	0.34998	0.001
Bray-Curtis dissimilarity	0.043234	0.537801	0.562103	0.001

0 and $p < 0.05$), indicating the varying degrees of significant effects on the diversity of gut microbiota induced by the five drug treatments.

3.9.2 Altered composition in gut microbiota at the phylum level

Next, the phylum-level compositions of gut microbiota were identified (Figure 8A), and the differences in gut-microbiota abundances among the groups were analyzed by *t* tests (Figures 8B–E). The results showed that stress induced a significant increase in the relative abundance of *Firmicutes* and a significant decrease in the relative abundance of *Verrucomicrobia* in the model group ($p < 0.05$). Compared to that of the model group, the relative abundance of *Verrucomicrobia* was significantly increased in the SER and IMI+β-HgS groups ($p < 0.05$). Furthermore, the relative abundance of *Patescibacteria* in the SER+β-HgS group was significantly higher than that in the SER group ($p < 0.05$). However, the β-HgS, IMI, and SER+β-HgS groups showed no differences compared to the model group in terms of the phylum level of gut microbiota.

3.9.3 Altered composition in gut microbiota at the order level

Next, the order levels of gut microbiota were investigated (Figure 9A). *Clostridiales*, *Rhodospirillales*, and *Bifidobacteriales* levels were significantly higher and *Verrucomicrobiales* and *Erysipelotrichales* levels were significantly lower in the model group than those in the control group ($p < 0.05$) (Figure 9B). Compared with those in the model group, the relative abundances of two orders (*Pseudomonadales* and *Micrococcales*), one order (*Micrococcales*), two orders (*Micrococcales* and *Verrucomicrobiales*), two orders (*Micrococcales* and *Verrucomicrobiales*) and one order (*Micrococcales*) of bacteria were significantly higher ($p < 0.05$ or $p < 0.01$) in the β-HgS, IMI, SER, IMI+β-HgS, and SER+β-HgS groups, respectively (Figures 9D–G), whereas the relative abundances of two orders (*Betaproteobacteriales* and *Bifidobacteriales*), one order (*Bacteroidales*), and three orders (*Erysipelotrichales*, *Bifidobacteriales*, and *Flavobacteriales*) of bacteria were

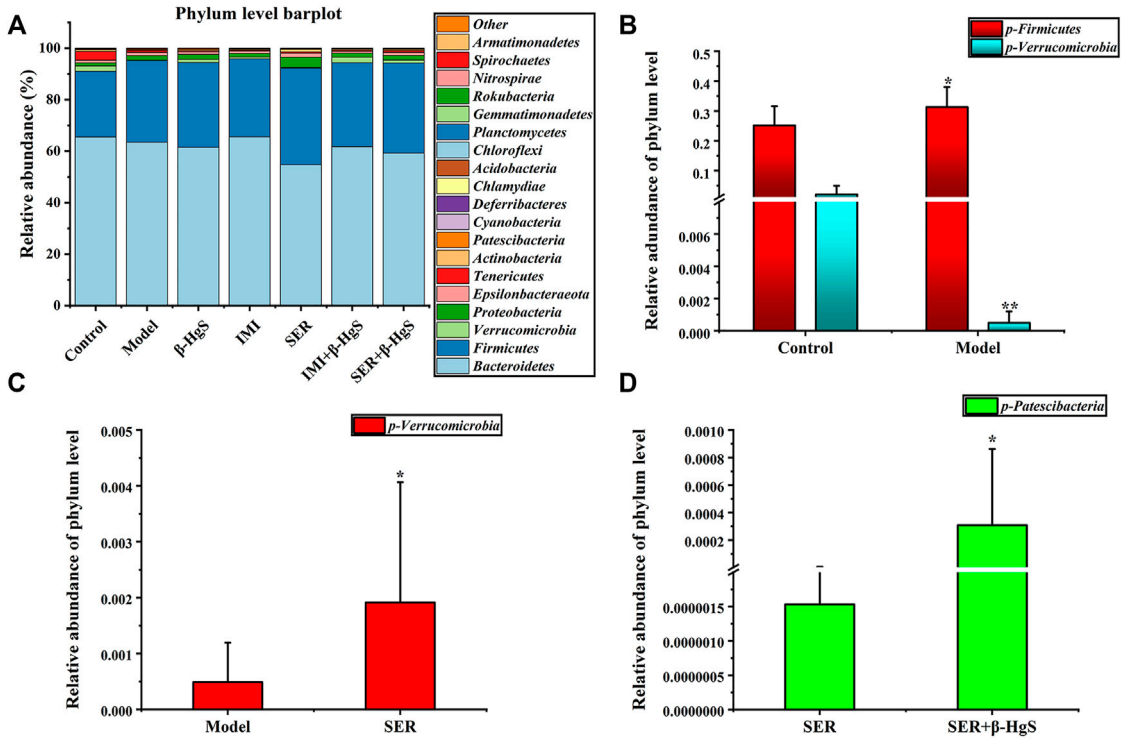

FIGURE 8
The effects of drug treatments on the composition of gut microbiota at the phylum level in stress-stimulated mice. **(A)** The relative abundances of phylum in intestinal contents of mice after 3 weeks of treatment. **(B)** Relative abundances of the gut microbiota with significant differences at the phylum level in the model group, compared with those in the control group. **(C)** Relative abundances of the gut microbiota with significant differences at the phylum level in the drug-treated groups, compared with those in the model group. **(D)** Relative abundances of gut microbiota with significant differences at the phylum level in the combination therapy group, compared with those of the relative monotherapy group. Data are shown as the mean ± *SD* (n = 10). *p < 0.05 and **p < 0.01 denote significant differences from the compared group.

significantly lower ($p < 0.05$) in the IMI, SER, and SER+β-HgS groups, respectively. Notably, the relative abundances of *Betaproteobacteriales* in the IMI+β-HgS group and *Chlamydiales* in the SER+β-HgS group were significantly higher while that of *Bifidobacteriales* in the SER+β-HgS group was significantly lower—compared to those in the corresponding single antidepressant-treated groups (IMI or SER group) ($p < 0.05$).

3.9.4 Altered composition of gut microbiota at the family level

Next, the family levels of gut microbiota were investigated (Figure 10A). The results showed that *Ruminococcaceae*, *Marinifilaceae*, and *Clostridialesvadin BB60* presented at significantly higher levels, while *Bacteroidaceae*, *Akkermansiaceae*, *Erysipelotrichaceae*, and *Peptostreptococcaceae* presented at significantly lower levels in the model group than those in the control group ($p < 0.05$) (Figure 10B). Compared with those in the model group, the relative abundances of three families (*Bacteroidaceae*, *Moraxellaceae*, and *Micrococcaceae*), one family (*Bacteroidaceae*), three families (*Bacteroidaceae*, *Micrococcaceae*, and *Akkermansiaceae*), two families (*Micrococcaceae* and *Akkermansiaceae*), and one family (*Micrococcaceae*) of bacteria were significantly higher ($p < 0.05$, $p < 0.01$, or $p < 0.001$) in the β-HgS, IMI, SER, IMI+β-HgS, and SER+β-HgS groups, respectively, whereas three families (*Peptococcaceae*, *Burkholderiaceae*, and *Bifidobacteriaceae*), two families (*Muribaculaceae* and *Peptococcaceae*), and three families (*Erysipelotrichaceae*, *Bifidobacteriaceae*, and *Flavobacteriaceae*) of bacteria were significantly lower ($p < 0.05$) in the IMI, SER, and SER+β-HgS groups, respectively (Figures 10D–G). Compared with those in the corresponding single antidepressant-treated groups (IMI or SER group), the relative abundances of *Burkholderiaceae* in the IMI+β-HgS group and *Mycoplasmataceae*, *Peptococcaceae*, *Christensenellaceae*, *Defluviitaleaceae*, and *Chlamydiaceae* in the SER+β-HgS group were significantly higher ($p < 0.05$ or $p < 0.01$), whereas *Bacteroidaceae* in the IMI+β-HgS and SER+β-HgS groups was significantly lower ($p < 0.05$).

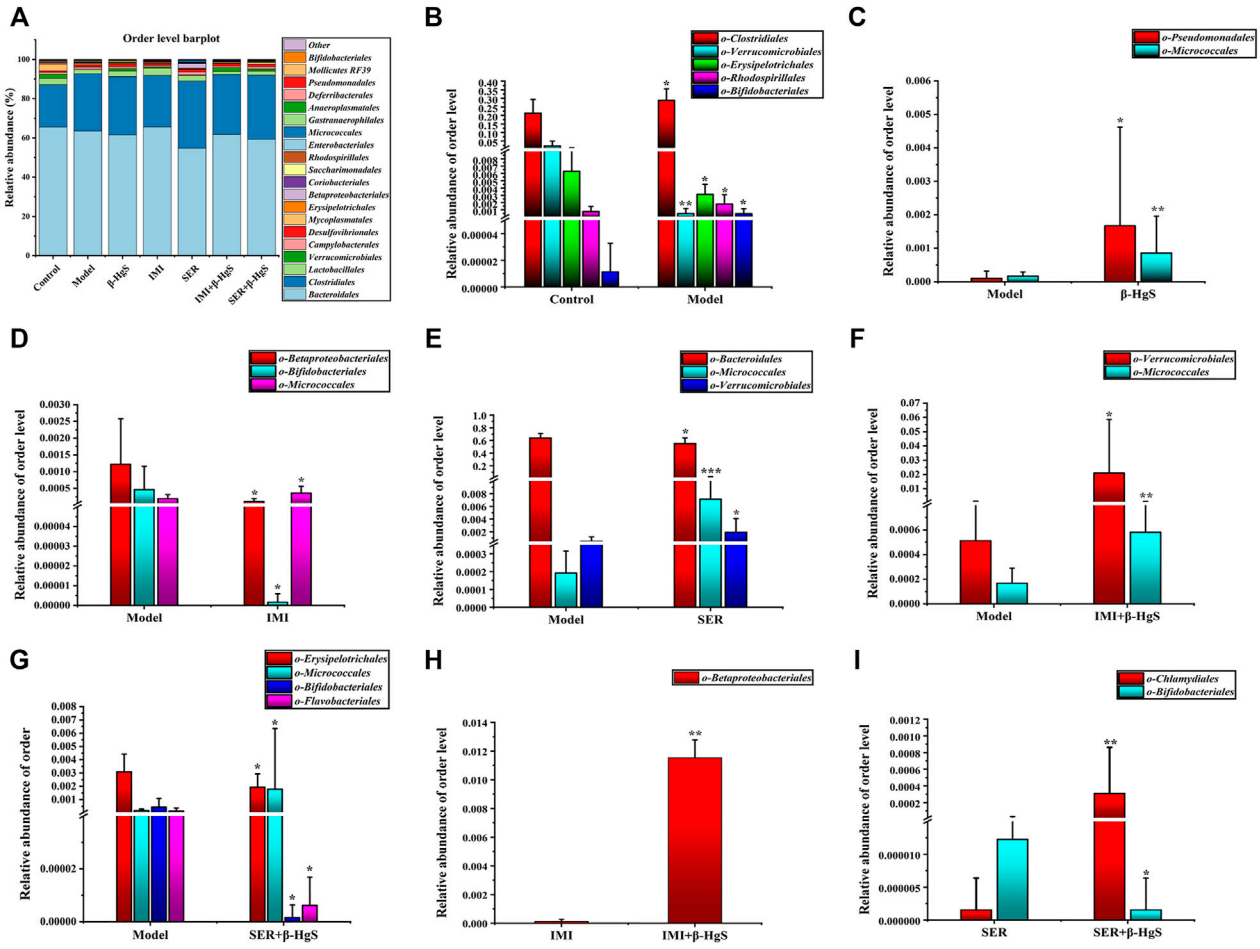

FIGURE 9
The effects of drug treatments on the composition of gut microbiota at the order level in stress-stimulated mice. **(A)** The relative abundances of constituents of gut microbiota at the order level in the intestinal contents of mice after 3 weeks of treatment. **(B)** Relative abundances of the gut microbiota with significant differences at the order level in the model group, compared with those in the control group. **(C–G)** Relative abundances of the gut microbiota with significant differences at the order level in the drug-treated groups, compared with those in the model group. **(H–I)** Relative abundances of the gut microbiota with significant differences at the order level in the combination therapy group, compared with those in the relative monotherapy group. Data are shown as the mean ± *SD* ($n = 10$). *$p < 0.05$, **$p < 0.01$, and ***$p < 0.001$ denote significant differences from the same kind of gut microbiota in the compared group.

3.9.5 Altered composition of gut microbiota at the genus level

Next, the compositions of the gut microbiota at the genus level were investigated (Figure 11A). Compared with those of the control group, 11 genera of gut microbiota were significantly different in terms of their relative abundances in the model group ($p < 0.05$, $p < 0.001$, or $p < 0.01$). Specifically, the relative abundances of *Bacteroides*, *Akkermansia*, *Blautia*, and *Erysipelatoclostridium* were lower and those of *Odoribacter*, *Ruminococcaceae UCG-010*, *Rikenella*, *Family XIIIAD3011 group*, *Lachnospiraceae FCS020 group*, *Bilophila*, and *Bifidobacterium* were higher than those of the control group (Figure 11B). Compared with those of the model group, the relative abundances of five genera (*Bacteroides*, *Lachnoclostridium*, *Muribaculum*, *Acinetobacter*, and *Renibacterium*), two genera (*Prevotellal* and *Bacteroides*), four genera (*Bacteroides*, *Muribaculum*, *Renibacterium*, and *Akkermansia*), three genera (*Akkermansia*, *Ruminococcaceae UCC-009*, and *Renibacterium*), and three genera (*Renibacterium*, *Ruminococcaceael UCC-004*, and *Ruminococcaceae UCC-009*) were significantly higher ($p < 0.05$, $p < 0.01$ or $p < 0.001$), whereas those of two genera (*Bilophila* and *Parasutterella*), seven genera (*Ruminiclotridium9*, *[Eubacterium]coprostanoligenes group*, *Lachnoclostridium*, *Parasutterella*, *Family XIIIAD3011 group*, *Candidatus Stoquefichus*, and *Bifidobacterium*), seven genera

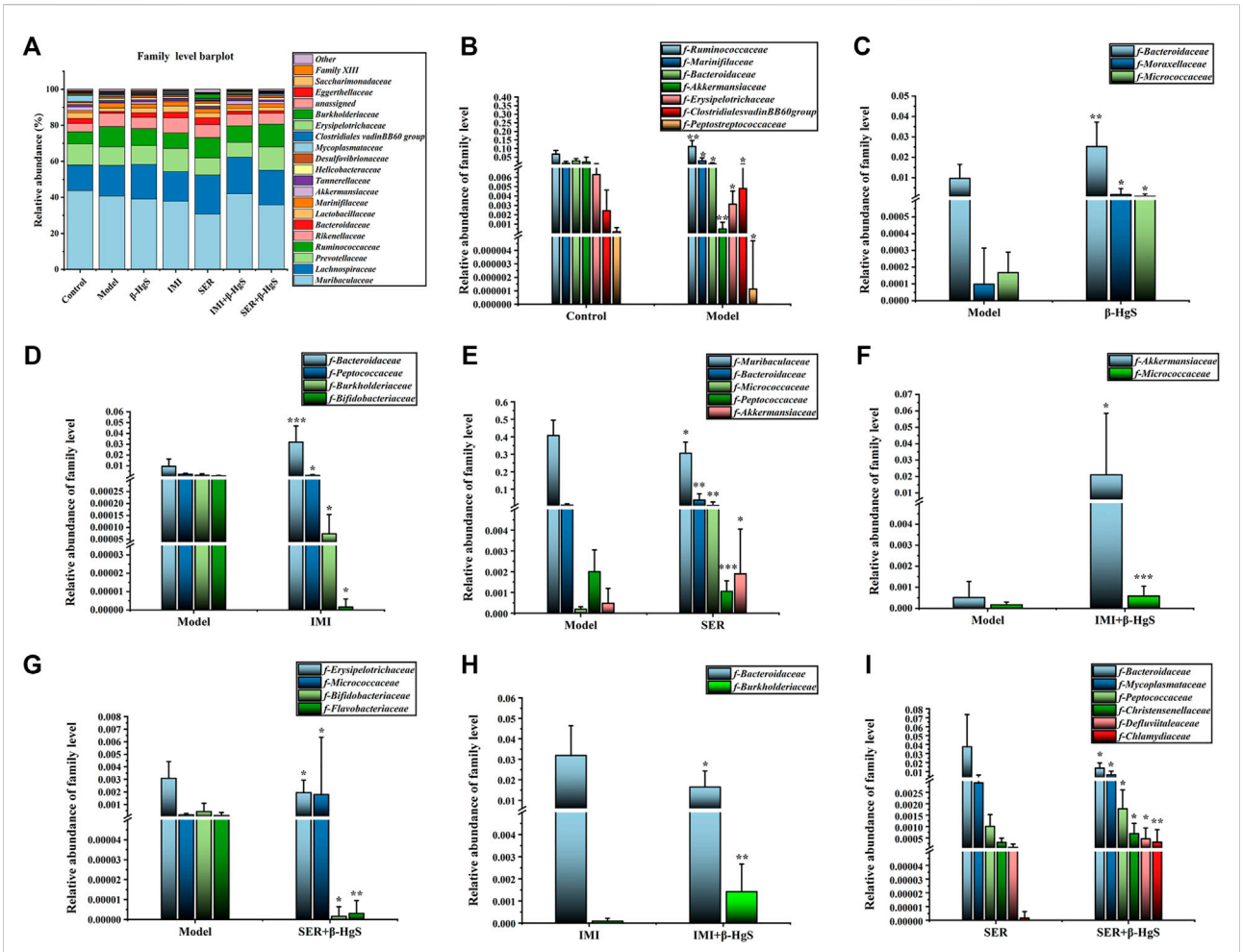

FIGURE 10
The effects of drug treatments on the composition of gut microbiota at the family level in stress-stimulated mice. **(A)** The relative abundances of constituents of gut microbiota at the family level in the intestinal contents of mice after 3 weeks of treatment. **(B)** The relative abundances of the gut microbiota with significant differences at the family level in the model group, compared with those in the control group. **(C–G)** The relative abundances of the gut microbiota with significant differences at the family level in the drug-treated groups, compared with those in the model group. **(H–I)** The relative abundances of gut microbiota with significant differences at the family level in the combination therapy group, compared with those in the relative monotherapy group. Data are shown as the mean ± *SD* ($n = 10$). *$p < 0.05$, **$p < 0.01$, and ***$p < 0.001$ denote significant differences from the same kind of gut microbiota in the compared group.

(*Ruminococcaceae* UCG-010, *Christensenellaceae R-7 group*, *Family XIIIAD 3011 group*, *Defluviitaleaceae UCG-011*, *Lachnospiraceae FCS020 group*, *Ruminiclostridium1*, and *Bifidobacterium*), three genera (*Rikenellaceae RC9gut group*, *[Eubacterium] coprostanoligenes group*, and *Lachnospiracee UCG-006*), and four genera (*Ruminiclostridium*1, *Bifidobacterium*, *[Eubacterium] brachy group*, and *Macrococcus*) were significantly lower ($p < 0.05$, $p < 0.01$ or $p < 0.001$) in the β-HgS, IMI, SER, IMI+β-HgS, and SER+β-HgS groups, respectively (Figures 11C–G). Compared with those of the corresponding single antidepressant-treated groups (IMI or SER group), the relative abundances of *Ruminiclostridium9*, *[Eubacterium] coprostanoligenes group*, and *Parasutterella* in the IMI+β-HgS group as well as *Ruminococcaceae UCG-010*, *Family XIIIAD3011 group*, *Christensenellaceae R-7 group*, *Defluviitaleaceae UCG-011*, and *Chlamydia* in the SER+β-HgS group was significantly higher ($p < 0.05$ or $p < 0.01$), whereas those of *Bacteroides* and *Rikenellaceae RC9gut group* in IMI+β-HgS group and *Bacteroides* and *Muribaculum* in the SER+β-HgS group were significantly lower ($p < 0.05$) (Figures 11H,I).

3.9.6 LDA Effect size analysis and functional prediction

As shown in Figure 12A, the microbial groups that play an important role in the grouping are separately displayed in the Cladogram. According to genus-level species statistical analysis, *Allobaculums*, *Dubosiella*, *Erysipelatoclostridium*, *Holdemania*, *Corynebacterium*, *Papillibacter*, *Devosia*, and *Parasutterella* are

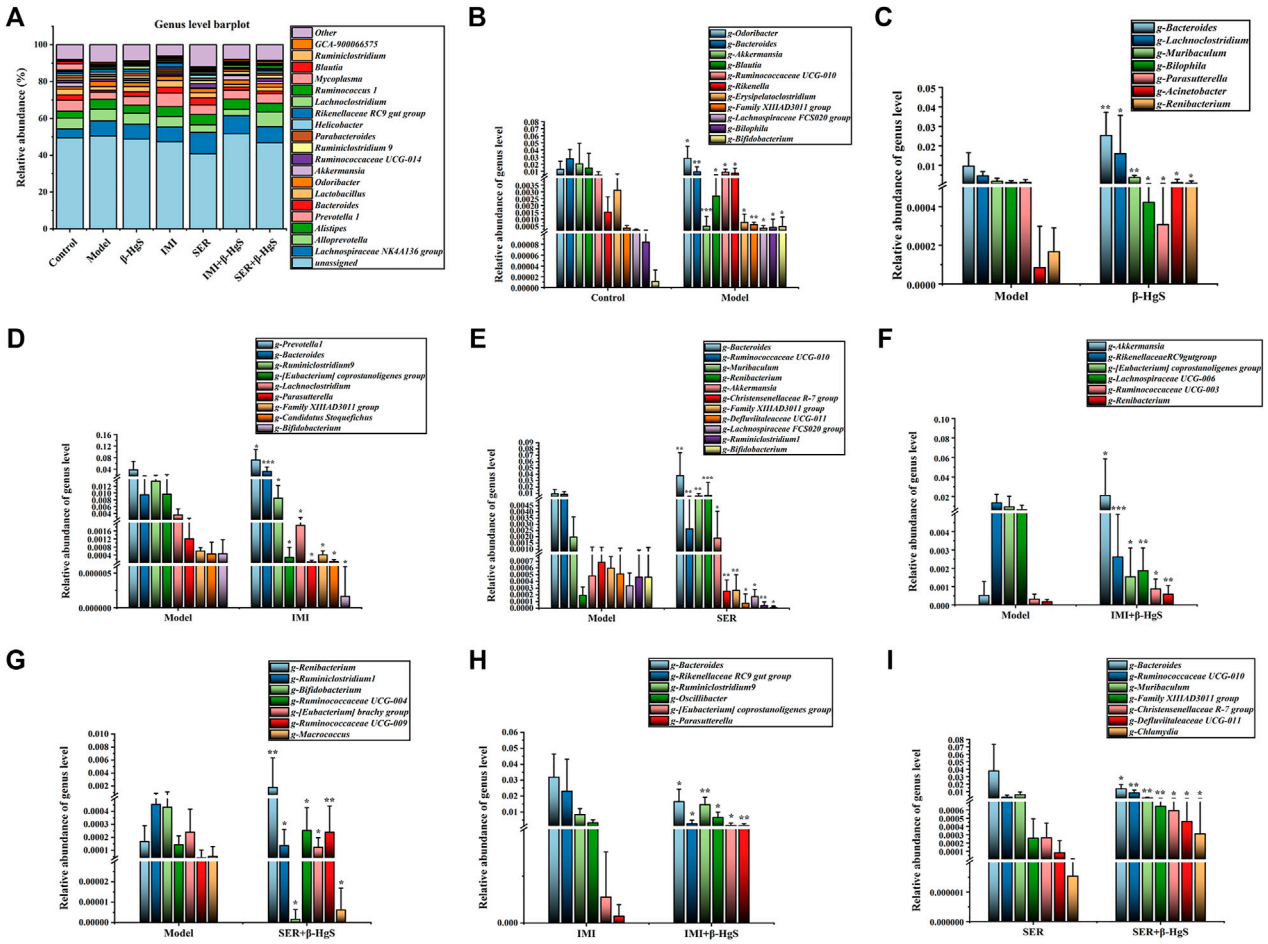

FIGURE 11
The effects of drug treatments on the composition of gut microbiota at the genus level in stress-stimulated mice. **(A)** The relative abundances of constituents of gut microbiota at the genus level in intestinal contents of mice after 3 weeks of treatment. **(B)** The relative abundances of the gut microbiota with significant differences at the genus level in the model group, compared with those of the control group. **(C–G)** The relative abundances of the gut microbiota with significant differences at the genus level in the drug-treated groups, compared with those of the model group. **(H–I)** The relative abundances of the gut microbiota with a significant difference at the genus level in the combination therapy group, compared with those of the relative monotherapy group. Data are shown as the mean ± *SD* (n = 10). *p < 0.05, **p < 0.01, and ***p < 0.001 denote significant differences from the same kind of gut microbiota in the compared group.

important gut microbiota for differentiation the control group; *Coprococcus2*, *UBA1819*, and *Bilophila* are important gut microbiota that differentiate the Model group; *Ruminiclostridium 5* was important gut microbiota that differentiated the β-HgS group; *DNF 00809*, *Rikenellaceae RC9 gut group*, and *Ureaplasma* are important gut microbiota that allow differentiation pressure in the IMI group; *Renibacterium*, *Bacteroides*, *Muribaculum*, and *Rikenella* are important gut microbiota that differentiate pressure in the SER group; *Ruminococcaceae* UCG-004 and *Turicibacter* are important gut microbiota that allow differentiation pressure in the IMI+β-HgS group; *Chlamydia*, *Family IIIAD3011 group*, *Ruminococcaceae UCG-003*, *Ruminococcaceae UCG-010* and *Ruminococcus1* are important gut microbiota that differentiate pressure in the SER+β-HgS group.

Moreover, according to the histogram of linear discriminant analysis (LDA) scores computed for differentially abundant features among the groups (Figure 12B), there were 8, 3, 1, 3, 4, 2, and 5 types of gut microbes with LDA values >3 in the Control, Model, β-HgS, IMI, SER, IMI+β-HgS, and SER+β-HgS groups, respectively. As shown in Figure 12C, the one-level pathways annotating gut microbiota are mainly distributed in Cellular Processes, Environmental Information Processing, Genetic Information Processing, Human Diseases, Metabolism, and Organismal Systems; the two-level pathway annotation (Figure 12D) distribution of the main pathways of gut flora Carbohydrate metabolism (14.4%–14.7%), Membrane

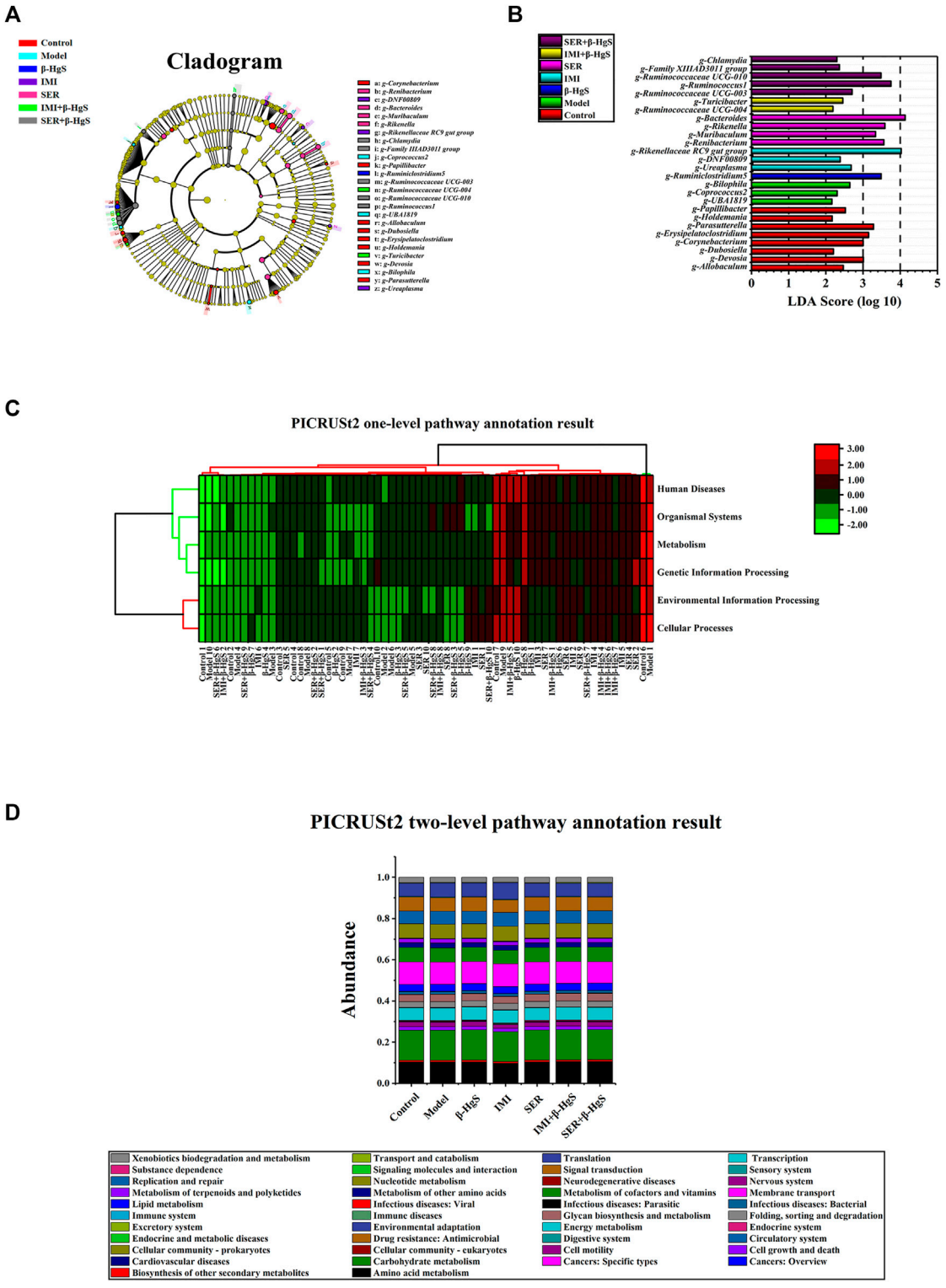

FIGURE 12
LEfSe analysis and functional prediction. **(A)** Cladogram representing taxa with different abundances of gut microbiota at baseline, and **(B)** histogram of linear discriminant analysis scores computed for differentially abundant features among groups, as well as **(C)** PICRUSt2 one-level pathway annotation results and **(D)** PICRUSt2 two-level pathway annotation results. The LDA score on the log10 scale is indicated at the bottom. The greater the LDA score, the more significant the phylotype biomarker is in the comparison.

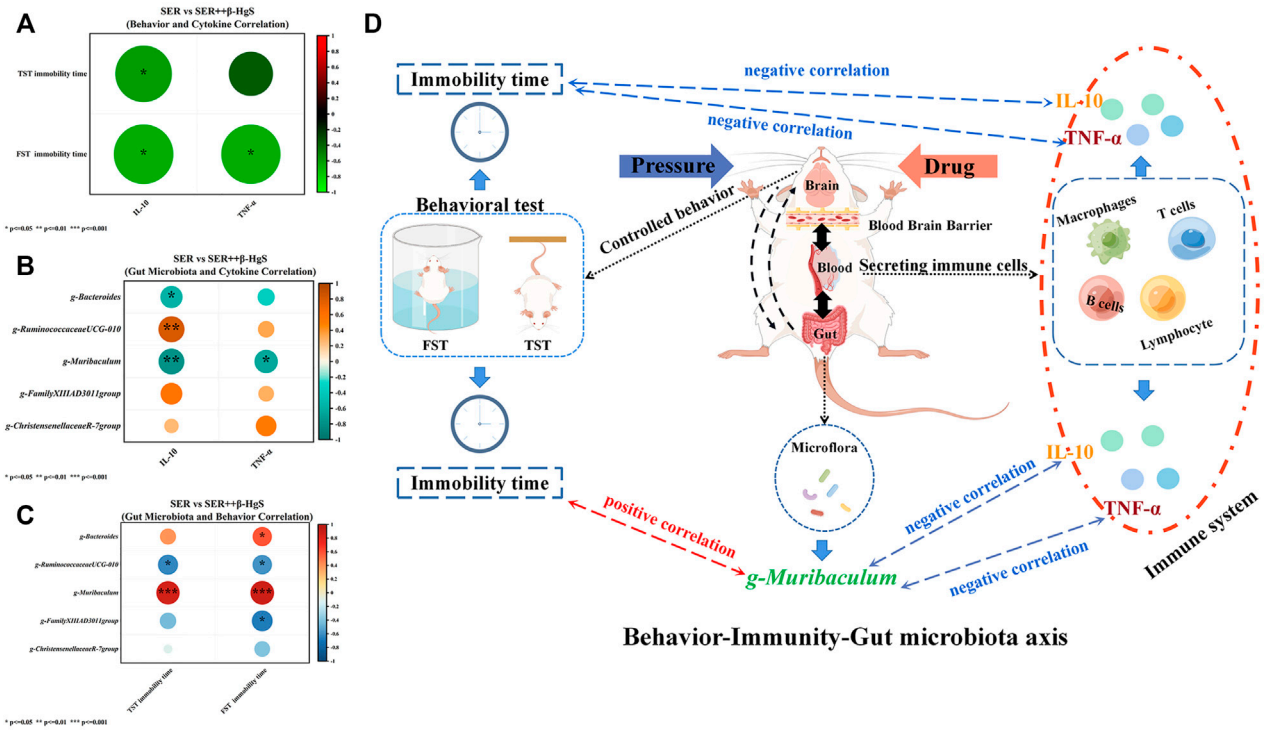

FIGURE 13
Pearson correlation analysis was performed on the differential physiological indicators, behavior and bacterial flora of SER vs. SER+β-HgS. **(A)** Behavior and Cytokine Correlation, **(B)** Gut Microbiota and Cytokine Correlation, **(C)** Gut Microbiota and Behavioral Correlation, **(D)** Behavior-Immunity-Gut microbiota axis.

transport (10.4%–10.9%), Amino acid metabolism (9.8%–10.6%), Translation (6.4%–7.9%), Nucleotide metabolism (7.0%–7.2%), Metabolism of cofactors and vitamins (6.6%–7.0%), Signal transduction (6.1%–6.7%) , Replication and repair (6.1%–6.6%) Energy metabolism (6.0%–6.2%).

3.10 Association analysis of differences between monotherapy and combination therapy

Pearson correlation analysis was performed on the differential physiological indicators, behavior and bacterial flora of SER vs. SER+β-HgS, respectively, as shown in Figure 13. In behavior and cytokine correlation (Figure 13A), TST immobility time was negatively correlated with IL-10 ($p < 0.05$); FST immobility time was negatively correlated with IL-10 and TNF-α levels ($p < 0.05$; $p < 0.05$). IL-10 was negatively correlated with *Muribaculum* and *Bacteroides* ($p < 0.01$; $p < 0.05$) in differential microbiota and cytokine correlation (Figure 13B), and negatively correlated with *Ruminococccaceae UCG-010* ($p < 0.01$). In differential microbiota and behavioral correlation (Figure 13C), TST immobility time was positively correlated with *Muribaculum* ($p < 0.001$) and negatively correlated with *Ruminococccaceae UCG-010* ($p < 0.01$); FST immobility time was positively correlated with *Muribaculum*, *Bacteroides* ($p < 0.001$; $p < 0.05$), and negatively correlated with *Ruminococccaceae UCG-010* and *Family XIIIAD3011 group* ($p < 0.05$; $p < 0.05$).

4 Discussion

According to existing studies, depression is mainly caused by mental stress, physical diseases and genetic factors, and most of the cases are caused by persistent mental stress (Marsay et al., 2018). In daily life, mental stress consists of two kinds of different stressors, predictable persistent stress and unpredictable short-term stress. Therefore, we used a combination of predictable and unpredictable stressors to simulate the depression-like environment of the mice used in this study. The results showed that the three-week combined action of predictable and unpredictable stressors induced depression-like symptoms in mice according to decreases in body weight, SPR, and 2 h-food consumption, as well as increases in immobility times in the FST and TST. Furthermore, these stressors inhibited exploratory behavior based on significant increases in RT and decreases in

MT, CMT, and CMD in the OFT, all of which are typical depression-like behaviors (Harvey and Bouwer, 2000; Chourbaji et al., 2005; Peng et al., 2007; Rizvi et al., 2016). Additionally, mice in all drug-treatment groups had significantly higher body weights and SPRs (except for the body weights in the SER group), much more 2 h-food consumption, and less immobility times in the FST and TST compared with those of the model group, indicating less pleasure deficiency and learned helplessness compared to those in the model group. In particular, the combined therapy of SER and β-HgS showed more of an advantage than the single therapy of SER in preventing the learned helplessness induced by stress stimulation, according to significantly fewer immobility times in the FST and TST in the SER+β-HgS group. Additionally, mice in the SER+β-HgS group were the most active among all drug-treatment groups since only the SER+β-HgS group exhibited significantly less RT and more MT, CMT, and CMD in the OFT compared with these parameters in the model group. The above findings suggest that the depression-like symptoms of mice in the SER+β-HgS group were most relieved among those of all drug-treatment groups.

Over the past decade, a series of compelling studies have reported that long-term major depressive disorder is associated with central nervous system atrophy in the hippocampus. The hippocampus plays a crucial role in learning and memory, and changes in hippocampal volume are associated with cognitive deficits in major depression (Bremner et al., 2000; Sahay and Hen, 2007; Chen et al., 2015). These studies were careful and well-controlled, demonstrating hippocampal atrophy after controlling for total brain volume, independent of variables such as history of antidepressant treatment, electroconvulsive therapy, or alcohol consumption. In addition, patients with persistent depression have more severe atrophic hippocampus (Robert, 2001). In this study, after stimulation *via* predictable and unpredictable stressors for 3 weeks, mice in the model group exhibited significant atrophy in the hippocampus and structural damage in key hippocampal subregions. Moreover, compared with those in the control group, the GR levels and the number of oligodendrocytes (NG2 and Olig2 cells) were remarkably decreased, and neuronal proliferation (PCNA+ and NeuN+ expression) was significantly inhibited via stress stimulation in the model group. Compared with parameters in the model group, all drug-treatment groups showed less atrophy and structural damage in key hippocampal subregions. Compared with the effects of the corresponding single-antidepressant treatments, the combined therapy groups better promoted GR and neuronal proliferation levels in most key hippocampal subregions. It is worth noting that only the fluorescence intensity of NG2+ oligodendrocytes in the DG area of the IMI+β-HgS group was 142.56% higher than that of the IMI group ($p < 0.001$), but did not significantly increase the number of oligodendrocytes in other areas. Oligodendrocyte precursor cells (OPCs, also known as NG2-glia) are located in the adult gray and white matter parenchyma and constitute approximately 6% of the total number of cells in the central nervous system. Inflammation is a hallmark feature of many neurological diseases, and existing studies have found that OPCs have the ability to sense and respond to inflammation (Boccazzi et al., 2022). Under physiological conditions, OPCs play a crucial role in maintaining microglia homeostasis, and it has been demonstrated that depletion of OPCs can cause a decrease in the stability of microglia (Zhang et al., 2019; Liu and Aguzzi, 2020). Furthermore, NG2-glia ablation induced hippocampal neuronal cell death while increasing microglial activation and mRNA levels of interleukin-1β, interleukin-6, and tumor necrosis factor (TNF), pro-inflammatory factors that exacerbate inflammation , affecting the decline of neuroprotective hepatocyte growth factor (HGF) levels (Nakano et al., 2017). Therefore, it is believed that β-HgS may enhance the recovery of inflammation in the brain hippocampus of depressed mice by IMI by increasing NG2+ oligodendrocytes in the DG area.

Currently, several theories have been proposed about the mechanism of depression. The most common is monoamine transmitter deficiency, especially 5-HT and NE (Liu et al., 2017). Second, the HPA axis is over-excited, leading to dysfunction of the body (Thomas et al., 2019). Neurogenesis and neurodegeneration hypotheses are also important theories to explain the pathogenesis of depression (Sapolsky, 2004; Czéh and Lucassen, 2007). Finally, inflammatory response, a feature of many psychiatric diseases, also has a clear correlation with depression (Loftis et al., 2010). Furthermore, BDNF and GRs are generally considered to underlie the pathophysiology of MDD. BDNF plays a major role in neuronal growth and survival and is considered a neuromodulator (Popova and Naumenko, 2019). BDNF is also involved in neural plasticity, whereas decreases in GRs can result in HPA-axis dysfunction and hyperactivity. Finally, both BDNF and GFs show that neuroendocrine function is unusual in depressed individuals (Pariante and Lightman, 2008). Recent studies have found that oxidative stress plays an important role in the pathophysiological process of major depression through the action of free radicals, non-free radicals, reactive oxygen species, and reactive nitrogen; hence, oxidative stress products are important parameters for the measurement and prediction of depressive states (Chen et al., 2018; Miller et al., 2018). In this study, our data showed that three-week stress treatments in mice induced defects in the biogenic amine system, dysfunction of HPA axis and peripheral immune system, reduced neurogenesis, and aggravation of oxidative stress. Compared with those of the model group, the above features were alleviated in mice in the drug-treatment groups. In the drug-treatment groups, mice in the SER+β-HgS group had the largest effects of significantly alleviated aspects compared with those in the model group. In particular, the TNF-α and IL-10 content in the SER+β-HgS group was significantly lower than that in the SER group, indicating the superiority of the combined therapy of SER and β-HgS in increasing inflammation levels in mice. IL-10 is a potent anti-inflammatory cytokine released by immune and glial cells that drives the regulation of multiple anti-inflammatory processes (Roque et al., 2009; Kwilasz et al., 2015), and increasing evidence that pro-inflammatory cytokines are associated with psychiatric disorders, namely depression. Notably, recent studies have shown that anti-

inflammatory cytokines, such as IL-10, can also modulate depressive-like behaviors, specifically, mice lacking IL-10 expression were shown to remain immobile for longer in FST (Mesquita et al., 2008). These results suggest that mice lacking IL-10 display more helplessness. Our behavioral test also showed this phenomenon, β-HgS can promote SRE to increase the level of IL-10, and IL-10 is negatively correlated with desperate behavior. Meanwhile, the direct effect of IL-10 in the central nervous system may be mediated by its role in regulating cell survival. IL10 prevents glial cell death (Molina-Holgado et al., 2001; Strle et al., 2002) and increases the survival of cerebellar neurons (Bachis et al., 2001), however, we also found that β-HgS enhanced effects on IMI and SER restore neuronal proliferation in the hippocampus, and this phenomenon may also be related to the elevated level of IL-10, which needs further verification. Additionally, decreased IL-10 promotes an imbalance in the cytokine milieu that further activates the HPA axis, which induces the release of glucocorticoids to trigger pro-inflammatory effects (Sorrells and Sapolsky, 2007). Interestingly, we found that TNF-α was increased and IL-6 and IL-10 were decreased in stressed mice compared with unstressed mice. The results of this experiment showed that pressure stimulation caused an inflammatory response. Although IL-6 is a pro-inflammatory factor, the biological activity of IL-6 is not limited to this. In the current study, it was found that activated microglia produced IL-6, a pleiotropic cytokine, which plays an important role in the cytokine network. It can regulate the growth and differentiation of various cells, regulate immune response, acute phase response, and hematopoietic function, and play an important role in the body's anti-infection immune response. As a neurotrophic factor related to neuroimmunity and neuroendocrine, IL-6 can stimulate neuronal process growth and neuron regeneration. Meanwhile, many studies have reported that IL-6 increases the prevalence of schizophrenia, and that IL-6 levels in serum of schizophrenia patients are higher than those of healthy controls. Elevated IL-6 induces enhanced activity of DA and 5-HT in hippocampus and prefrontal cortex. IL-6 was significantly elevated and highly correlated with major depressive disorder. Several studies noted that veterans with post-traumatic stress disorder (PTSD) had elevated levels of IL-6 in cerebrospinal fluid (CSF) but not in plasma compared to controls (Erta et al., 2012). Both IL-6 and TNF-α can increase the permeability of the blood-brain barrier, and blocking the effects of IL-6 and TNF-α can reduce stress-induced opening of the blood-brain barrier. On the contrary, the increase of IL-6 and TNF-α increases the permeability of the blood-brain barrier, which may help to accelerate the excretion of harmful substances in the brain and strengthen the two-way communication at the brain-blood level (Beurel et al., 2020). Therefore, we speculate that the decrease of IL-6 and TNF-α, under the dual stress stimulation of CRS + CUMS, is mostly manifested as a weakened neuroprotective effect, and at the same time, it reduces the stress-induced opening of the blood-brain barrier. After drug treatment, the levels of IL-6 and TNF-α increased, the permeability of the blood-brain barrier was increased, the two-way communication at the brain-blood level was enhanced, and the harmful substances in the brain were excreted faster. At the same time, IL-6 promotes neuron proliferation and protects nerves. Our experimental results showed that the levels of 5-HT and BDNF were increased in the combined treatment, which also supported our speculation. In addition, because the relationship between cellular immune factors and depression is not clear, in the drug treatment, the experimental results show that pro-inflammatory factors and anti-inflammatory factors are on the rise, but the stress group is one high and one low. We speculate that on the one hand, the levels of brain inflammation, serum inflammation and intestinal inflammation may not match in space and time, resulting in abnormal expression of pro-inflammatory and anti-inflammatory factors in serum. On the other hand, it may be related to the side effects of drugs Reaction-related, long-term use of antidepressant drugs, there is also the possibility of inducing inflammatory reactions.

Recently, the gut microbiome has been revealed to be crucial to human health *via* the bidirectional communication between the gut and the brain (known as the visceral-brain axis). Furthermore, many recent studies have demonstrated that some intestinal florae are associated with major depression (Evrensel and Ceylan, 2015); hence, the diversity of intestinal flora is considered to be helpful in understanding depression (Pusceddu et al., 2015). In this study, the relative abundances of gut microbes in mice in the model group exhibited significant changes in two, five, seven, and eleven categories at the phylum, order, family, and genus levels, respectively, compared with those of the control group. Among the gut microbiota with decreased relative abundances in the model group, *Bacteroides* are symbiotic bacteria in the intestine that produce short-chain fatty acids (SCFAs), such as butyrates, which can aid in maintaining normal intestinal permeability while suppressing mucosal inflammation. *Akkermansia* promotes the barrier function of the gut and the effectiveness of cancer immunotherapy. *Blautia* can help clear the intestinal tract of gas and may be associated with irritable bowel syndrome. *Erysipelatoclostridium* can be effective for treating and preventing diseases and conditions mediated by the IL-17 or Th17 pathways (Levine et al., 2018; Ansaldo et al., 2019; Schirmer et al., 2019). Among the gut microbiota with increased relative abundances in the model group, *Odoribacter* can produce acetic acid, propionic acid, and butyric acid in the gut. *Rikenellaceae* has been increased in septic rats, and the increasing amount of *Bilophila* may increase the risk of inflammatory bowel disease (IBD) and hepatobiliary disease (Hyland and Stanton, 2016; Li et al., 2017; Zheng et al., 2019).

Compared with those of the model group, the diversities of intestinal flora of mice in the drug-treatment groups were significantly altered, especially in the SER, IMI+β-HgS, and SER+β-HgS groups. Moreover, the diversities of intestinal flora of mice in the combined therapy groups were also different from those in the corresponding single antidepressant-treated groups. Compared with those in the corresponding single antidepressant-treated groups, mice in the IMI+β-HgS group had more *Ruminiclostridium* and

Ruminococcu (two anaerobic bacteria that metabolize plant cell-wall polysaccharides and may play a positive role in treating Th17-driven inflammation) and *Parasutterella* (a member of the core gut microbiota that may play a role in microbial interactions and infection resistance, especially early in life) and less *Rikenellaceae* bacteria; mice in the SER+β-HgS group had more *Christensenellaceae* and *Defluviitaleaceae* (two probiotics that may negatively correlate with metabolic diseases such as fat deposition, IBD, and metabolic syndrome) and less *Muribaculaceae* bacteria (an anaerobic bacteria that produces succinate, acetate, and propionate, and its family is composed of metabolic guilds, each specializing in the degradation of particular types of polysaccharides) (Halfvarson et al., 2017; Ma et al., 2019; Smith et al., 2019). These changes in the gut microbiota may therefore represent one of the mechanisms by which β-HgS enhances the therapeutic effects of antidepressants in mice. Moreover, the relative abundance of *Bacteroides* in mice in the combined therapy groups was significantly lower than that in the corresponding single antidepressant-treated groups, indicating that β-HgS had an inhibiting effect on *Bacteroides*. We performed association analysis on the differences in physiological indicators, behavioral indicators and differential flora compared with the monotherapy and combination treatment groups. In SER vs. SER+β-HgS, gut microbiota *Muribaculum* was negatively correlated with despair behavior (TST and FST immobility time), and positively correlated with IL-10 and TNF-α. Meanwhile, IL-10 and TNF-α were negatively and positively associated with desperate behavior. This may indicate that β-HgS may enhance and improve the immune level and restore despair behavior abilities of depressed mice by affecting the abundance of the intestinal flora *Muribaculum*. Interestingly, in the time-honored Traditional Chinese Medicine (TCM), there are many ancient recipes that intentionally added mercury-containing ingredients for therapeutic purposes. Cinnabar (mercury sulfide, >96% HgS) is a representative mercury-containing mineral material used in traditional Chinese medicine formulations. Cinnabar is a naturally occurring mineral element with calming properties. According to the Chinese Pharmacopoeia (Halfvarson et al., 2017), traditional Chinese medicine formulations contain cinnabar (Zhao H. et al., 2018). Wansheng Huafengdan (WSHFD) is a traditional Chinese medicine used to treat nervous system diseases (Zhang et al., 2012). Cinnabar (HgS) is contained in WSHFD, and which can significantly attenuate LPS-induced DA uptake capacity and decrease in the number of TH-positive neurons, inhibit microglial activation, and improve LPS-induced TNFα, iNOS, IL-1β, and COX-2. However, WSHFD removal or reduction of cinnabar and realgar failed to prevent LPS-induced neurotoxicity, thus cinnabar and realgar have protective effects against LPS-induced neurotoxicity. Simultaneously, Angong Niuhuang Pill (AGNHW) is also a representative traditional Chinese medicine formulation containing realgar and cinnabar for treating acute ischemic stroke (Tsoi et al., 2019). Studies have found that AGNHW can reduce infarct volume, maintain blood-brain barrier integrity, and improve cerebral ischemia-reperfusion injury. However, removal of realgar and/or cinnabar from AGNHW abolished the neuroprotective effects, suggesting that realgar and cinnabar are essential elements for neuroprotective effects of AGNHW and synergistically act with other herbs. However, due to the complexity of the composition of Zuotai and the theory of Tibetan medicine, we acknowledge the limitations of this study and only explored the effects of clinically equivalent doses of the main components of the drug against antidepressants. The relationship between β-HgS and depression-related gut microbiota, behavior, and immune system remains unknown and requires further research.

5 Conclusion

Our present results suggest that β-HgS may promote the antidepressant effects of SER on depression-like symptoms in mice, possibly *via* ameliorating learned helplessness, as well as atrophy and severe structural damage of the hippocampus, induced by stress stimulation. Our pathogenic studies showed that β-HgS enhanced the effects of SER on promoting GR and neuronal proliferation levels in key hippocampal subregions, as well as increased serum IL-10 and TNF-α levels in stress-stimulated mice. As for IMI, β-HgS enhanced its effects in preventing atrophy and severe structural damage in the hippocampus, promoting GR and neuronal proliferation levels in key hippocampal subregions and increasing serum IL-10 and SOD levels, whereas β-HgS did not significantly enhance the ameliorating effect of IMI on depression-like behavior in stress-stimulated mice. Furthermore, these combination therapies resulted in increased changes in the diversity of important gut microbiota compared to corresponding monotherapies, with associations between *Muribaculum* relative abundance and desperate behavior and cytokine levels (Figure 12D), which may be a factor in the enhancement of such combination therapies. Important factors in the efficacy of these combination therapies include SER or IMI for β-HgS.

Data availability statement

The raw data supporting the conclusions of this article will be made available by the authors, without undue reservation.

Ethics statement

The animal study was reviewed and approved by the Northwest Plateau Institute of Biology, CAS, for animal experiments.

Author contributions

All authors have materially participated in the research and article preparation. The roles for all authors are follows: HB and TG designed the study; YQ, CL, and MZ performed the experiments; YQ, LW, and HB analyzed the data and wrote the manuscript; XFZ, KC, and XYZ contributed to the interpretation of data and critically revised the manuscript. All authors have approved the final version of the manuscript.

Funding

This work was supported by the Natural Science Foundation of China (Grant Nos. 82171863), National Key R&D Program of China (2018YFC1708006), China Postdoctoral Science Foundation funded project (2021M701642), the Innovation Platform Program of Qinghai Province (2021-ZJ-T02), the Key project of Basic and applied Basic Research of Jiangmen (20210301030000007455), the Applied Basic Research Project of Qinghai Province (2019-ZJ-7030) and the Central Asian Drug Discovery and Development Center of CAS (CAM201903).

Acknowledgments

Thanks to Nanjing Jisihuiyuan Company (Nanjing, China) for the technical support provided in the detection of intestinal flora.

Conflict of interest

The authors declare that the research was conducted in the absence of any commercial or financial relationships that could be construed as a potential conflict of interest.

Publisher's note

All claims expressed in this article are solely those of the authors and do not necessarily represent those of their affiliated organizations, or those of the publisher, the editors and the reviewers. Any product that may be evaluated in this article, or claim that may be made by its manufacturer, is not guaranteed or endorsed by the publisher.

References

Amato, K. R., Yeoman, C. J., Kent, A., Righini, N., Carbonero, F., Estrada, A., et al. (2013). Habitat degradation impacts black howler monkey (*Alouatta pigra*) gastrointestinal microbiomes. *Isme. J.* 7, 1344–1353. doi:10.1038/ismej.2013.16

Ansaldo, E., Slayden, L. C., Ching, K. L., Koch, M. A., Wolf, N. K., Plichta, D. R., et al. (2019). *Akkermansia muciniphila* induces intestinal adaptive immune responses during homeostasis. *Science* 364, 1179–1184. doi:10.1126/science.aaw7479

Bachis, A., Colangelo, A. M., Vicini, S., Doe, P. P., De Bernardi, M. A., Brooker, G., et al. (2001). Interleukin-10 prevents glutamate-mediated cerebellar granule cell death by blocking caspase-3-like activity. *J. Neurosci.* 21 (9), 3104–3112. doi:10.1523/JNEUROSCI.21-09-03104.2001

Bayes, A., and Parker, G. (2019). How to choose an antidepressant medication. *Acta Psychiatr. Scand.* 139, 280–291. doi:10.1111/acps.13001

Beurel, E., Toups, M., and Nemeroff, C. B. (2020). The bidirectional relationship of depression and inflammation: Double trouble. *Neuron* 1072, 234–256. doi:10.1016/j.neuron.2020.06.002

Boccazzi, M., Raffaele, S., and Fumagalli, M. (2022). Not only myelination: The immune-inflammatory functions of oligodendrocytes. *Neural Regen. Res.* 1712, 2661–2663. doi:10.4103/1673-5374.342678

Bremner, J. D., Narayan, M., Anderson, E. R., Staib, L. H., Miller, H. L., and Charney, D. S. (2000). Hippocampal volume reduction in major depression. *Am. J. Psychiatry* 157, 115–118. doi:10.1176/ajp.157.1.115

Bressington, D., Mui, J., Yu, C., Leung, S. F., Cheung, K., Wu, C. S. T., et al. (2019). Feasibility of a group-based laughter yoga intervention as an adjunctive treatment for residual symptoms of depression, anxiety and stress in people with depression. *J. Affect. Disord.* 248, 42–51. doi:10.1016/j.jad.2019.01.030

Chen, B., Luo, M., Liang, J., Zhang, C., Gao, C., Wang, J., et al. (2018). Surface modification of PGP for a neutrophil–nanoparticle co-vehicle to enhance the antidepressant effect of baicalein. *Acta Pharm. Sin. B* 8, 64–73. doi:10.1016/j.apsb.2017.11.012

Chen, C., Wang, L., Rong, X., and Wang, W. (2015). Effects of fluoxetine on protein expression of potassium ion channels in the brain of chronic mild stress rats. *Acta Pharm. Sin. B* 5, 55–61. doi:10.1016/j.apsb.2014.12.004

Choleris, E., Thomas, A. W., Kavaliers, M., and Prato, F. S. (2001). A detailed ethological analysis of the mouse open field test: Effects of diazepam, chlordiazepoxide and an extremely low frequency pulsed magnetic field. *Neurosci. Biobehav. Rev.* 25, 235–260. doi:10.1016/s0149-7634(01)00011-2

Chourbaji, S., Zacher, C., Sanchis-Segura, C., Dormann, C., Vollmayr, B., and Gass, P. (2005). Learned helplessness: Validity and reliability of depressive-like states in mice. *Brain Res. Brain Res. Protoc.* 16, 70–78. doi:10.1016/j.brainresprot.2005.09.002

Cosgrove, L., F Shaughnessy, A., Wheeler, E. E., Austad, K. E., Kirsch, I., and Bursztajn, H. J. (2012). The American psychiatric association's guideline for major depressive disorder: A commentary. *Psychother. Psychosom.* 81, 186–188. doi:10.1159/000335523

Czéh, B., and Lucassen, P. J. (2007). What causes the hippocampal volume decrease in depression? *Eur. Arch. Psychiatry Clin. Neurosci.* 257, 250–260. doi:10.1007/s00406-007-0728-0

Ding, Q., Li, H., Tian, X., Shen, Z., Wang, X., Mo, F., et al. (2016). Zinc and imipramine reverse the depression-like behavior in mice induced by chronic restraint stress. *J. Affect. Disord.* 197, 100–106. doi:10.1016/j.jad.2016.03.017

Erta, M., Albert, Q., and Hidalgo, J. (2012). Interleukin-6, a major cytokine in the central nervous system. *Int. J. Biol. Sci.* 89, 1254–1266. doi:10.7150/ijbs.4679

Evrensel, A., and Ceylan, M. E. (2015). The gut-brain Axis: The missing link in depression. *Clin. Psychopharmacol. Neurosci.* 13, 239–244. doi:10.9758/cpn.2015.13.3.239

Ferrari, A. J., Charlson, F. J., Norman, R. E., Murray, Christopher J. L., Freedman, G., Murray, C. J. L., et al. (2013). Burden of depressive disorders by country, sex, age, and year: Findings from the global burden of disease study 2010. *PLoS Med.* 10, e1001547–12. doi:10.1371/journal.pmed.1001547

Furukawa, T. A., Mcguire, H., and Barbui, C. (2022). Meta-analysis of effects and side effects of low dosage tricyclic antidepressants in depression: Systematic review. *BMJ Br. Med. J.* 325, 7371–7995. doi:10.1136/bmj.325.7371.991

Gigantesco, A., Fagnani, C., Toccaceli, V., Stazi, M. A., Lucidi, F., Violani, C., et al. (2019). The relationship between satisfaction with life and depression symptoms by gender. *Front. Psychiatry* 10, 419. doi:10.3389/fpsyt.2019.00419

Halfvarson, J., Brislawn, C. J., Lamendella, R., Vazquez-Baeza, Y., Walters, W. A., Bramer, L. M., et al. (2017). Dynamics of the human gut microbiome in inflammatory bowel disease. *Nat. Microbiol.* 2, 17004–17007. doi:10.1038/nmicrobiol.2017.4

Hamel, C., Lang, E., Morissette, K., Beck, A., Stevens, A., Skidmore, B., et al. (2019). Screening for depression in women during pregnancy or the first year postpartum and in the general adult population: A protocol for two systematic reviews to update a guideline of the Canadian task force on preventive health Care. *Syst. Rev.* 18, 27–13. doi:10.1186/s13643-018-0930-3

Harvey, B. H., and Bouwer, C. D. (2000). Neuropharmacology of paradoxic weight gain with selective serotonin reuptake inhibitors. *Clin. Neuropharmacol.* 23, 90–97. doi:10.1097/00002826-200003000-00006

Hyland, N., and Stanton, C. (2016). *The gut-brain Axis dietary, probiotic, and prebiotic interventions on the microbiota*. 1st ed. Pittsburgh: Academic Press.

Kwilasz, A. J., Grace, P. M., Serbedzija, P., Maier, S. F., and Watkins, L. R. (2015). The therapeutic potential of interleukin-10 in neuroimmune diseases. *Neuropharmacology* 96, 55–69. doi:10.1016/j.neuropharm.2014.10.020

Levine, A., Sigall, R. B., and Wine, E. (2018). Evolving role of diet in the pathogenesis and treatment of inflammatory bowel diseases. *Gut* 67, 1726–1738. doi:10.1136/gutjnl-2017-315866

Li, S., Lv, J., Li, J., Zhao, Z., Guo, H., Zhang, Y., et al. (2017). Intestinal microbiota impact sepsis associated encephalopathy via the vagus nerve. *Neurosci. Lett.* 662, 98–104. doi:10.1016/j.neulet.2017.10.008

Liu, B., Liu, J., Wang, M., Zhang, Y., and Li, L. (2017). From serotonin to neuroplasticity: Evolvement of theories for major depressive disorder. *Front. Cell. Neurosci.* 11, 305–309. doi:10.3389/fncel.2017.00305

Liu, J., Wei, L., Wang, Q., Lu, Y. F., Zhang, F., Shi, J. Z., et al. (2018). A review of cinnabar (HgS) and/or realgar (As4S4)-containing traditional medicines. *J. Ethnopharmacol.* 210, 340–350. doi:10.1016/j.jep.2017.08.037

Liu, Y., and Aguzzi, A. (2020). NG2 glia are required for maintaining microglia homeostatic state. *Glia* 682, 345–355. doi:10.1002/glia.23721

Loftis, J. M., Huckans, M., and Morasco, B. J. (2010). Neuroimmune mechanisms of cytokine-induced depression: Current theories and novel treatment strategies. *Neurobiol. Dis.* 37, 519–533. doi:10.1016/j.nbd.2009.11.015

López-Muñoz, F., and Álamo, C. (2009). Monoaminergic neurotransmission: The history of the discovery of antidepressants from 1950s until today. *Curr. Pharm. Des.* 15, 1563–1586. doi:10.2174/138161209788168001

Ma, H., Wang, W., Xu, S., Wang, L., and Wang, X. (2018). Potassium 2-(1-hydroxypentyl)-benzoate improves depressive-like behaviors in rat model. *Acta Pharm. Sin. B* 8, 881–888. http://en.cnki.com.cn/Article_en/CJFDTotal-YXBY201806006. doi:10.1016/j.apsb.2018.08.004

Ma, S., Jiang, Y., Zhang, B., Pang, J., Xu, X., Sun, J., et al. (2019). Comparison of the modulatory effect on intestinal microbiota between raw and bran-fried atractylodis rhizoma in the rat model of spleen-deficiency syndrome. *Int. J. Environ. Res. Public Health* 16, 3183. doi:10.3390/ijerph16173183

Marsay, C., Manderson, L., and Subramaney, U. (2018). Changes in mood after screening for antenatal anxiety and depression. *J. Reprod. Infant Psychol.* 36, 347–362. doi:10.1080/02646838.2018.1453601

Mesquita, A. R., Correia-Neves, M., Roque, S., Castro, A. G., Vieira, P., Pedrosa, J., et al. (2008). IL-10 modulates depressive-like behavior. *J. Psychiatr. Res.* 43 (2), 89–97. doi:10.1016/j.jpsychires.2008.02.004

Miller, M. W., Lin, A. P., Wolf, E. J., and Miller, D. R. (2018). Oxidative stress, inflammation, and neuroprogression in chronic PTSD. *Harv. Rev. Psychiatry* 26, 57–69. doi:10.1097/HRP.0000000000000167

Molina-Holgado, Eduardo, Vela, J. M., ArevAlo-MArtin, A., and Guaza, C. (2001). LPS/IFN-γ cytotoxicity in oligodendroglial cells: Role of nitric oxide and protection by the anti-inflammatory cytokine IL-10. *Eur. J. Neurosci.* 133, 493–502. doi:10.1046/j.0953-816x.2000.01412.x

Nakano, M., Tamura, Y., Yamato, M., Kume, S., Eguchi, A., Takata, K., et al. (2017). NG2 glial cells regulate neuroimmunological responses to maintain neuronal function and survival. *Sci. Rep.* 71, 42041. doi:10.1038/srep42041

Nil, R., Lütolf, S., and Seifritz, E. (2016). Residual symptoms and functionality in depressed outpatients: A one-year observational study in Switzerland with escitalopram. *J. Affect. Disord.* 197, 245–250. doi:10.1016/j.jad.2016.02.062

Niu, C., Zhao, J., Geng, L., Tan, Q., Zhang, J., Li, C., et al. (2016). Zuotai effects on chronic restrained stress depression model mice's behavioral. *Pharmacol. Clin. Chin. Mat. Med.* 32, 179–183. http://www.cnki.com.cn/Article/CJFDTOTAL-ZYYL201606049.

O'Leary, O. F., and Cryan, J. F. (2009). The tail-suspension test: A model for characterizing antidepressant activity in mice. *Neuromethods* 42, 119–137. doi:10.1007/978-1-60761-303-9_7

Pariante, C. M., and Lightman, S. L. (2008). The HPA axis in major depression: Classical theories and new developments. *Trends Neurosci.* 31, 464–468. doi:10.1016/j.tins.2008.06.006

Peng, W., Lo, K., Lee, Y., Hung, T. H., and Lin, Y. C. (2007). Berberine produces antidepressant-like effects in the forced swim test and in the tail suspension test in mice. *Life Sci.* 81, 933–938. doi:10.1016/j.lfs.2007.08.003

Popova, N. K., and Naumenko, V. S. (2019). Neuronal and behavioral plasticity: The role of serotonin and BDNF systems tandem. *Expert Opin. Ther. Targets* 23, 227–239. doi:10.1080/14728222.2019.1572747

Porsolt, R. D., Pichon, M. L., and Jalfre, M. (1977). Depression: A new animal model sensitive to antidepressant treatments. *Nature* 266, 730–732. doi:10.1038/266730a0

Pusceddu, M. M., Aidy, S. E., Crispie, F., O'Sullivan, O., Cotter, P., Stanton, C., et al. (2015). N-3 polyunsaturated fatty acids (PUFAs) reverse the impact of early-life stress on the gut microbiota. *Plos One* 10, e0139721–13. doi:10.1371/journal.pone.0139721

Qiao, Y., Zhao, J., Li, C., Zhang, M., Wei, L., Zhang, X., et al. (2020). Effect of combined chronic predictable and unpredictable stress on depression-like symptoms in mice. *Ann. Transl. Med.* 158, 942. doi:10.21037/atm-20-5168

Rizvi, S. J., Pizzagalli, D. A., Sproule, B. A., and Kennedy, S. H. (2016). Assessing anhedonia in depression: Potentials and pitfalls. *Neurosci. Biobehav. Rev.* 65, 21–35. doi:10.1016/j.neubiorev.2016.03.004

Robert, M. (2001). Depression, antidepressants, and the shrinking hippocampus. *Proc. Natl. Acad. Sci. U. S. A.* 98, 12320–12322. doi:10.1073/pnas.231475998

Roque, S., Correia-Neves, M., Mesquita, A. R., Palha, J. A., and Sousa, N. (2009). Interleukin-10: A key cytokine in depression? *Cardiovasc. Psychiatry Neurol.* 6, 187894–187895. doi:10.1155/2009/187894

Sahay, A., and Hen, R. (2007). Adult hippocampal neurogenesis in depression. *Nat. Neurosci.* 10, 1110–1115. doi:10.1038/nn1969

Sapolsky, R. M. (2004). Is impaired neurogenesis relevant to the affective symptoms of depression? *Biol. Psychiatry* 56, 137–139. doi:10.1016/j.biopsych.2004.04.012

Schirmer, M., Garner, A., Vlamakis, H., and Xavier, R. J. (2019). Microbial genes and pathways in inflammatory bowel disease. *Nat. Rev. Microbiol.* 17, 497–511. doi:10.1038/s41579-019-0213-6

Smith, B. J., Miller, R. A., Ericsson, A. C., Harrison, D. C., Strong, R., and Schmidt, T. M. (2019). Changes in the gut microbiome and fermentation products concurrent with enhanced longevity in acarbose-treated mice. *BMC Microbiol.* 19, 130. doi:10.1186/s12866-019-1494-7

Sorrells, S. F., and Sapolsky, R. M. (2007). An inflammatory review of glucocorticoid actions in the CNS. *Brain Behav. Immun.* 213, 259–272. doi:10.1016/j.bbi.2006.11.006

Steven, D. T., and Maurizio, F. (2011). Fatigue as a residual symptom of depression. *Innov. Clin. Neurosci.* 8, 40–43. https://www.ncbi.nlm.nih.gov/pmc/articles/PMC3225130.

Strle, K., Zhou, J. H., Broussard, S. R., Venters, H. D., Johnson, R. W., Freund, G. G., et al. (2002). IL-10 promotes survival of microglia without activating Akt. *J. Neuroimmunol.* 122 (1-2), 9–19. doi:10.1016/S0165-5728(01)00444-1

Thomas, N., Gurvich, C., Hudaib, A., Gavrilidis, E., and Kulkarni, J. (2019). Systematic review and meta-analysis of basal cortisol levels in Borderline Personality Disorder compared to non-psychiatric controls. *Psychoneuroendocrinology* 102, 149–157. doi:10.1016/j.psyneuen.2018.12.009

Tsoi, B., Wang, S., Gao, C., Luo, Y., Li, W., Yang, D., et al. (2019). Realgar and cinnabar are essential components contributing to neuroprotection of Angong Niuhuang Wan with no hepatorenal toxicity in transient ischemic brain injury. *Toxicol. Appl. Pharmacol.* 377, 114613. doi:10.1016/j.taap.2019.114613

Weilburg, J. B., Meigs, J. B., Hennen, J., and Stafford, R. S. (2003). Evaluation of the adequacy of outpatient antidepressant treatment. *Psychiatr. Serv.* 549, 1233–1239. doi:10.1176/appi.ps.54.9.1233

WHO (2012). World mental health day celebration 2012. theme: Depression, a global crisis. Available at: https://www.afro.who.int/news/world-mental-health-day-celebration-2012.

Yan, S., You, Z., Zhao, Q., Peng, C., He, G., Gou, X. J., et al. (2015). Antidepressant-like effects of Sanyuansan in the mouse forced swim test, tail suspension test, and chronic mild stress model. *Kaohsiung J. Med. Sci.* 31, 605–612. doi:10.1016/j.kjms.2015.10.009

Zhang, F., Lu, Y., Wu, Q., Yan, J., Shi, J., and Liu, J. (2012). Role of cinnabar and realgar of WSHFD in protecting against LPS-induced neurotoxicity. *J. Ethnopharmacol.* 139, 822–828. doi:10.1016/j.jep.2011.12.026

Zhang, S.-Z., Wang, Q. Q., Yang, Q. Q., Gu, H. Y., Yin, Y. Q., Li, Y. D., et al. (2019). NG2 glia regulate brain innate immunity via TGF-β2/TGFBR2 axis. *BMC Med.* 171, 204–222. doi:10.1186/s12916-019-1439-x

Zhao, H., Feng, Y., and Mao, M. (2018). Application of toxic Chinese medicine in Chinese Pharmacopoeia. *IOP Conf. Ser. Mat. Sci. Eng.* 301, 012068. doi:10.1088/1757-899X/301/1/012068

Zhao, J., Niu, C., Wang, J., Yang, H., Du, Y., Wei, L., et al. (2018). The depressive-like behaviors of chronic unpredictable mild stress-treated mice ameliorated by Tibetan medicine Zuotai: Involvement in the hypothalamic–pituitary–adrenal (HPA) axis pathway. *Neuropsych. Dis. Treat.* 14, 129–141. doi:10.2147/NDT.S151107

Zhao, J., Zhang, M., Geng, L., Li, C., Du, Y., Wei, L., et al. (2016). Antidepressant activities of Tibetan medicine Zuotai in two mouse depression models. *Chin. Trad. Pat. Med.* 38, 1461–1467. http://www.cnki.com.cn/Article/CJFDTotal-ZCYA201607005. doi:10.3969/j.issn.1001-1528.2016.07.005

Zheng, P., Zeng, B., Liu, M., Chen, J., Pan, J., Han, Y., et al. (2019). The gut microbiome from patients with schizophrenia modulates the glutamate-glutamine-GABA cycle and schizophrenia-relevant behaviors in mice. *Sci. Adv.* 5, eaau8317–11. doi:10.1126/sciadv.aau8317

frontiers | Frontiers in Pharmacology

TYPE Original Research
PUBLISHED 06 September 2022
DOI 10.3389/fphar.2022.942996

OPEN ACCESS

EDITED BY
Xian-Jun Fu,
Shandong University of Traditional Chinese Medicine, China

REVIEWED BY
Shao Li,
Tsinghua University, China
Pamela Ovadje,
Innovate Calgary, Canada

*CORRESPONDENCE
Shu-yan Han,
shuyanhan@bjmu.edu.cn
Ping-ping Li,
lppma123@sina.com

SPECIALTY SECTION
This article was submitted to Ethnopharmacology, a section of the journal Frontiers in Pharmacology

RECEIVED 13 May 2022
ACCEPTED 17 August 2022
PUBLISHED 06 September 2022

CITATION
Wang S, Hao H-f, Jiao Y-n, Fu J-l, Guo Z-w, Guo Y, Yuan Y, Li P-p and Han S-y (2022), Dandelion extract inhibits triple-negative breast cancer cell proliferation by interfering with glycerophospholipids and unsaturated fatty acids metabolism.
Front. Pharmacol. 13:942996.
doi: 10.3389/fphar.2022.942996

Dandelion extract inhibits triple-negative breast cancer cell proliferation by interfering with glycerophospholipids and unsaturated fatty acids metabolism

Shan Wang[1,2], Hui-feng Hao[2], Yan-na Jiao[2], Jia-lei Fu[2], Zheng-wang Guo[2], Yang Guo[2], Yuan Yuan[2], Ping-ping Li[1,2]* and Shu-yan Han[1,2]*

[1]Department of Integration of Chinese and Western Medicine, School of Basic Medical Sciences, Peking University, Beijing, China, [2]Key Laboratory of Carcinogenesis and Translational Research (Ministry of Education), Department of Integration of Chinese and Western Medicine, Peking University Cancer Hospital and Institute, Beijing, China

Triple-negative breast cancer (TNBC) is the most aggressive breast cancer subtype with limited treatment options and a poor prognosis. TNBC exists widely reprogrammed lipid metabolism, and its metabolic-associated proteins and oncometabolites are promising as potential therapeutic targets. Dandelion (*Taraxacum mongolicum*) is a classical herbal medicine used to treat breast diseases based on traditional Chinese medicine theory and was reported to have antitumor effects and lipid regulatory capacities. Our previous study showed that dandelion extract was effective against TNBC. However, whether dandelion extract could regulate the lipid metabolisms of TNBC and exert its antitumor effects via interfering with lipids metabolism remained unclear. In this study, an integrated approach combined with network pharmacology and multi-omics techniques (including proteomics, metabolomics, and lipidomics) was performed to investigate the potential regulatory mechanisms of dandelion extract against TNBC. We first determined the antitumor effects of dandelion extract *in vitro* and *in vivo*. Then, network pharmacology analysis speculated the antitumor effects involving various metabolic processes, and the multi-omics results of the cells, tumor tissues, and plasma revealed the changes in the metabolites and metabolic-associated proteins after dandelion extract treatment. The alteration of glycerophospholipids and unsaturated fatty acids were the most remarkable types of metabolites. Therefore, the metabolism of glycerophospholipids and

Abbreviations: TNBC, triple-negative breast cancer; ER, estrogen receptor; SREBP, sterol-regulatory element-binding proteins; FASN, fatty acid synthase; FADS2, fatty acid desaturase 2; LPC, lysophosphatidylcholine; AMPK, AMP-activated protein kinase; PC, phosphatidylcholine; PE, phosphatidylethanolamine; LPE, lysophosphatidylethanolamine; TG, triglyceride; SM, sphingomyelin; Cer, ceramide; CE, cholesteryl ester; LA, linoleic acid; OA, oleic acid.

unsaturated fatty acids, and their corresponding proteins CHKA and FADS2, were considered the primary regulatory pathways and biomarkers of dandelion extract against TNBC. Subsequently, experimental validation showed that dandelion extract decreased CHKA expression, leading to the inhibition of the PI3K/AKT pathway and its downstream targets, SREBP and FADS2. Finally, the molecular docking simulation suggested that picrasinoside F and luteolin in dandelion extract had the most highly binding scores with CHKA, indicating they may be the potential CHKA inhibitors to regulate glycerophospholipids metabolisms of TNBC. In conclusion, we confirmed the antitumor effects of dandelion extract against TNBC cells *in vitro* and demonstrated that dandelion extract could interfere with glycerophospholipids and unsaturated fatty acids metabolism via downregulating the CHKA expression and inhibiting PI3K/AKT/SREBP/FADS2 axis.

KEYWORDS

triple-negative breast cancer, dandelion extract, multi-omics, glycerophospholipid metabolism, choline kinase α

Introduction

Breast cancer has surpassed lung cancer as the most commonly diagnosed cancer worldwide with high incidence and mortality in the light of the latest global cancer data in 2020 by the International Agency for Research on Cancer. Approximately 15%–20% of primary breast cancers are triple-negative breast cancers (TNBC), characterized by the absence of estrogen receptor (ER), progesterone receptor, and human epidermal growth factor receptor-2. TNBC has specific clinical features with high invasiveness, high metastatic potential, proneness to relapse, and poor prognosis (Wang et al., 2018; Yin et al., 2020). Due to its molecular and clinical heterogeneity, TNBC lacks highly effective targeted drugs and treatment strategies (Burstein et al., 2015; Bianchini et al., 2016). Consequently, it is necessary and urgent to discover newly specific biomarkers and excavate novel and efficacious alternative medications for TNBC treatment.

Deregulated metabolism frequently exists in primary malignant cancers, and several metabolic pathways underlie cancer initiation and progression (Yoshida, 2015). Breast cancer has metabolic heterogeneity, and its reprogrammed metabolic patterns are different between TNBC and ER^+ subtypes (Yamashita et al., 2017; Gandhi and Das, 2019). Notably, TNBC also has inherent metabolic heterogeneity (Sun et al., 2020), and a clinical study revealed that 60% of TNBC tumor samples existed significantly upregulated lipids metabolism pathways (Gong et al., 2021). Abnormal lipid metabolism in TNBC could provide biomolecules such as unsaturated fatty acids for phospholipid synthesis and cell membrane formation and generate energy, synergistically promoting and sustaining TNBC progression and survival (Hopperton et al., 2014). Simultaneously, multiple lipid metabolism-associated enzymes and metabolites have significantly altered in TNBC (Hilvo et al., 2011; Tonje et al., 2017). For example, sterol-regulatory element-binding protein (SREBP), a critical regulatory molecule in lipid metabolism, and its downstream fatty acid synthase (FASN), fatty acid desaturase 2 (FADS2) were dramatically increased in the TNBC tissues (Griffiths et al., 2013). Compared to the health, lipids analysis of peripheral blood in TNBC patients suggested prominent metabolic disturbances in choline, sphingolipids, and glycerophospholipids. Among them, triglycerides and lysophosphatidylcholine (LPC) levels were significantly downregulated (Eghlimi et al., 2020). The changed metabolic-associated proteins and metabolites reflected the metabolic vulnerabilities of TNBC. Therefore, they could be considered promising biomarkers for discovering and developing novel therapeutic targets and effective alternative treatments.

Natural products and their derivatives are important sources for discovering new small-molecule compounds for cancer treatment (Li and Weng, 2017). Dandelion, termed *Taraxacum mongolicum*, had been used as a classical herbal medicine based on the traditional Chinese medicine theory in treating mammary diseases, including mammary abscess and hyperplasia of mammary glands (Martinez et al., 2015). Sizeable evidence indicated that dandelion and its components have significant inhibitory effects against various tumor cells (Gauhar et al., 2017; Zhu et al., 2017; Duan et al., 2021)and lipids regulatory impact on normal cells and fat animal models, which is closely related to activating the AMP-activated protein kinase (AMPK) pathway (Liu et al., 2014; Gauhar et al., 2017). For example, dandelion extract significantly reduced adipogenesis and lipid accumulation in 3T3-L1 (González-Castejón et al., 2013), as well as decreased serum levels of cholesterol and triglyceride and liver lipid accumulation in high-fat-fed rabbits (Choi et al., 2010) and rats (Davaatseren et al., 2013). A recent study uncovered the mechanisms of the

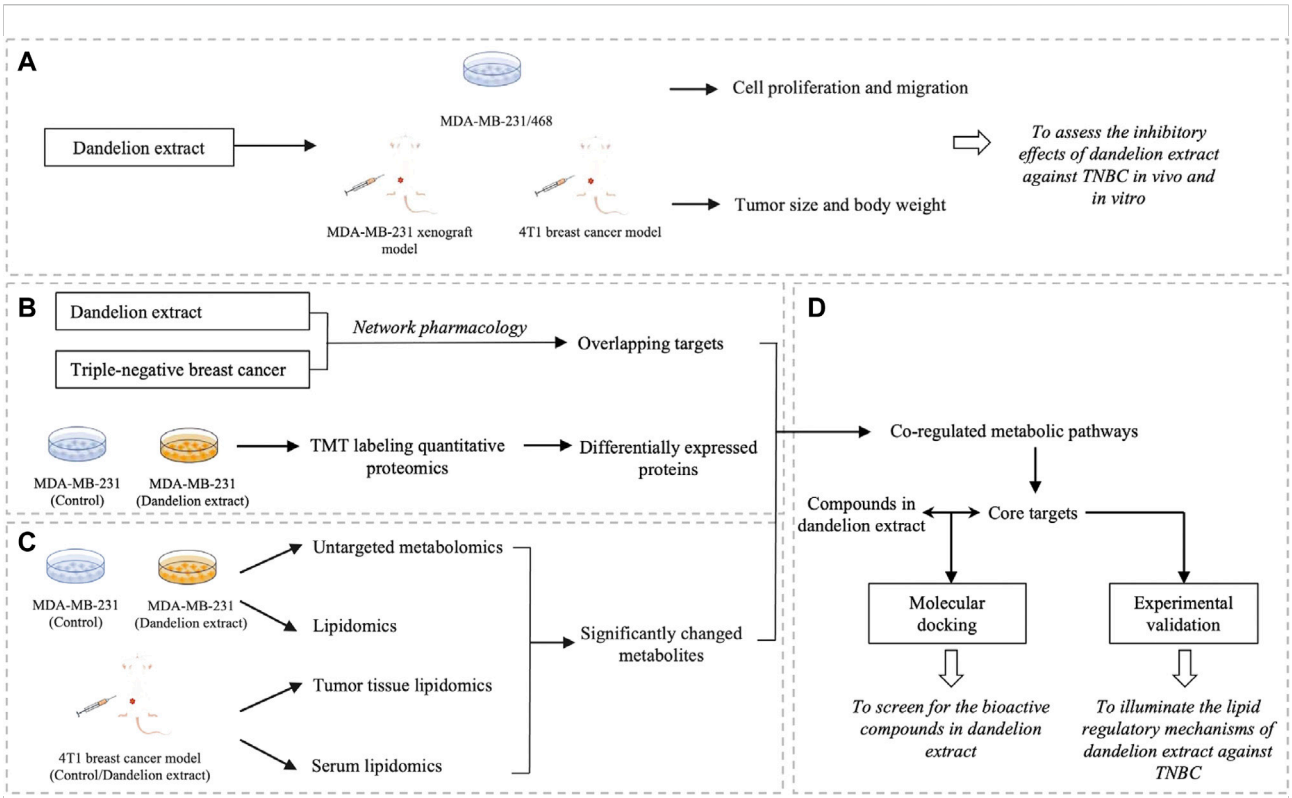

FIGURE 1
The schematic flowchart of the integrated analysis for dandelion extract against TNBC. **(A)** The inhibitory effects of dandelion extract against TNBC *in vivo* and *in vitro*. **(B)** The Network pharmacology analysis and quantitative proteomic analysis. **(C)** The metabolomics and lipidomics analysis using the TNBC cell, tumor tissue, and plasmas specimens. **(D)** The experimental verification of key targets and the screening for the bioactive compound in dandelion extract via molecular docking.

aqueous extract of dandelion against TNBC via the regulation of a series of biological processes involving cell cycle and metabolism (Qu et al., 2022). Our previous studies revealed that dandelion extract could decrease TNBC cell growth via inducing endoplasmic reticulum stress associated-apoptosis (Li et al., 2017)and inhibit TNBC cell malignant phenotype in tumor-associated macrophages microenvironment (Deng et al., 2021). However, whether dandelion extract could regulate the lipid metabolisms of TNBC and exert its antitumor effects via interfering with lipids metabolism remain unclear and need to elucidate.

Network pharmacology is a multidisciplinary approach combining computational biology, network analysis, and experimental verification. It is a promising approach to discovering the underlying mechanisms between the multiple-component drug such as herbal extract and their putative targets (Li and Zhang, 2013; Wang et al., 2021a). Besides, the multi-omics techniques, including genomics, transcriptomics, proteomics, and metabolomics, could directly reflect the changes after drug treatment and have become effective tools to discover potential targets of natural products or TCM (Zhang et al., 2021). Therefore, in the current study, we first demonstrated the antitumor effects of dandelion extract against TNBC *in vitro* and *in vivo*. Subsequently, we conducted an integrated analysis combined with network pharmacology analysis, multi-omics techniques (quantitative proteomics, untargeted metabolomics, and untargeted lipidomics), experimental validation, and molecular docking to investigate the potential regulatory mechanisms of dandelion extract against TNBC *in silico* and *in vitro* and screen for the main bioactive components in dandelion extract. The research flowchart is shown in Figure 1.

Materials and methods

Materials and reagents

Fetal bovine serum (FBS), phosphate-buffered saline (PBS, pH 7.2), trypsin, and Dulbecco's Modified Eagle Medium (DMEM) were purchased from Gibco (Grand Island, NY, United States).3-(4,5-dimethyl thiazol-2-yl-)-2, 5-diphenyl tetrazolium bromide (MTT), and dimethyl sulfoxide (DMSO) were purchased from Sigma-Aldrich (St. Louis, MO,

United States). Choline and phosphorylcholine were purchased from TOP SCIENCE (Shanghai, China).

Cell culture

TNBC cell lines MDA-MB-231 and MDA-MB-468 and human normal mammary epithelial cell MCF-10A were obtained from Peking Union Medical College Cell Bank (Beijing, China). MDA-MB-231 and MDA-MB-468 were cultured in DMEM supplemented with 10% FBS, penicillin (100 units/mL), and streptomycin (100 μg/ml). All cells were maintained in a 5% CO_2 incubator at 37°C. MCF-10A were cultured in the dedicated medium (Procell, CM-0525, China) with 5%cholera toxin (Macgene, CC104, China).

Dandelion extract preparation

The dandelion used in this study was identified as *Taraxacum mongolicum* Hand. Mazz, and its extract was produced as the previous report (Li et al., 2017). In brief, the whole dried plant of dandelion was extracted with 50% ethanol three times, concentrated under vacuum, and then purified by macroporous resin column chromatography. The water eluent was discarded, and the 30% ethanol eluent portion was collected, evaporated, and sprayed to dryness. In cell experiments, dandelion extract was dissolved in 50% DMSO to prepare a stock solution and diluted with the culture medium. The final concentration of DMSO is 0.5%. UHPLC-ESI-Orbitrap MS/MS analysis results showed 20 compounds were identified in dandelion extract and most of them are flavonoids and phenolic acids (Supplementary Figure S1) (Li et al., 2017).

Transfection of CHKA siRNA

MDA-MB-231 cells at a density of 1.5×10^5 were transfected withCHKA siRNA (5′- CAUGCUGUUCCA GUGCUCC-3′) (RiboBio Co., Ltd. Guangzhou, China) using Lipofectamine 2000. The scrambled siRNAwas used as the negative control. The final concentration of CHKAsiRNA and scramble siRNA is 50 nM. The transfected cells withscramble or CHKA siRNA were cultured for 24 h and then assessed using Western blotting.

MTT assay

MTT assay was performed to measure the cell viability. Briefly, MCF-10A, MDA-MB-231, and MDA-MB-468 cells were plated in 96-well plates (7×10^3 cells/well) and cultured overnight, and then treated with dandelion extract (0, 10, 20, 40, 80, and 160 μg/ml) in DMEM with 1% FBS for 24 h. After washing with 1×PBS, cells were incubated with 0.5 mg/ml MTT solution (100 μl per well) at 37°C for 4 h. Afterward, the supernatant was discarded, and 100 μl of DMSO was added to dissolve the formazan crystals. The optical density was determined at 570 nm using Tecan Infinite 200 pro. The data was analyzed and visualized by GraphPad Prism 9.0.

Wound-healing assay

The cell migration was performed using a wound-healing assay. MDA-MB-231 and MDA-MB-468 cells were plated in 6-well plates at 4×10^5 cells per well and incubated to grow for 90% confluence. Afterward, the yellow pipette tips were used to make linear scratches, and the cell debris was removed by washing with 1×PBS. Then the cells were cultured in DMEM with 1% FBS and treated with dandelion extract at different concentrations (0, 10, 20, 40, 80, and 160 μg/ml). The images were captured by Leica DMi8 inverted microscope. The scratch width was measured by ImageJ software, and the rate of wound closure was calculated and analyzed by GraphPad Prism 9.0.

Animal model construction

To evaluate the antitumor effects of dandelion extract *in vivo*, we constructed the MDA-MB-231 xenograft model and the 4T1 breast cancer model using NOG mice and BALB/C mice, respectively. Female NOG mice and BALB/C mice (6–8 weeks old) were purchased from Beijing HFK Bioscience Co. Ltd. (Beijing, China) and housed in a specific pathogen-free environment with a 12-h light/dark cycle and adequate food and water. All procedures involving mice were followed by the animal ethics guidelines and were approved by the Peking University Animal Research Committee. Briefly, after a 1-week acclimation, 2.5×10^6MDA-MB-231 cells (resuspended in 100 μl Matrigel to NOG mice) and 2×10^4 4T1 cells (resuspended in 100 μl PBS to BALB/C mice) were implanted into the fourth inguinal mammary gland. When the tumor was palpable, the mice were randomized into three groups (n = 6 in the MDA-MB-231 xenograft model per group, n = 8 in the 4T1 model per group), including control (intraperitoneal injection with 0.1%sodium carboxymethylcellulose) and dandelion extract group (intraperitoneal injection with 50 and 100 mg/kg dandelion extract dissolved 0.1%sodium carboxymethylcellulose). Tumor volume was measured every 2–3 days and calculated by the following formula: tumor volume (mm^3) = $0.5\times d_1\times d_2^2$, where d_1 is the longest diameter and d_2 is the shortest diameter. At the end point of animal experiments (depending on the tumor sizes), the resected tumors were weighed, and the plasma was harvested.

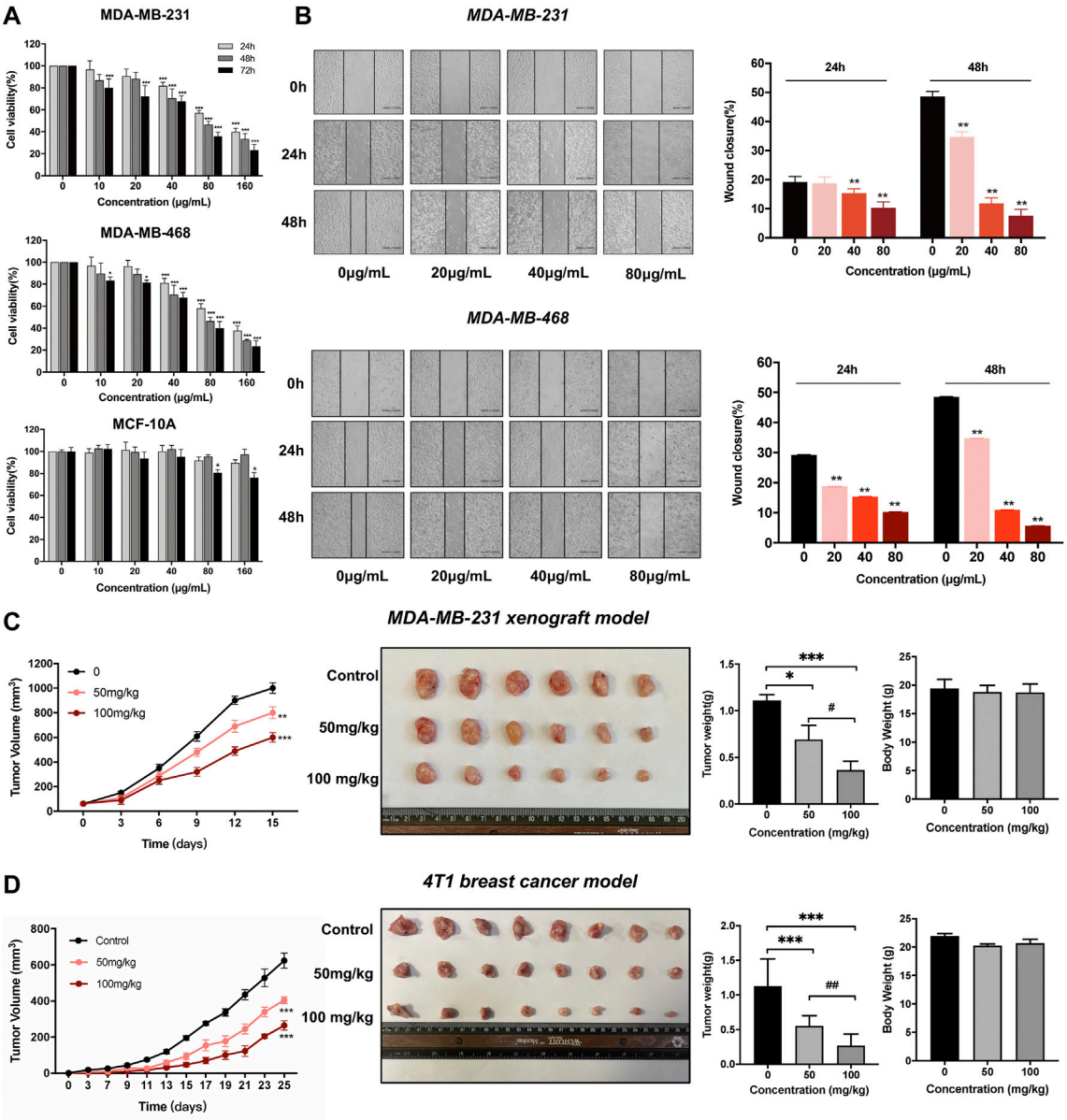

FIGURE 2
Dandelion extract inhibited TNBC cells malignant phenotypes and tumor growth in breast cancer mice model. **(A)** Dandelion extract inhibited cell proliferation on MDA-MB-231, MDA-MB-468, and MCF-10A. *$p < 0.05$, **$p < 0.01$, ***$p < 0.005$ vs. 24 h. **(B)** Dandelion extract inhibited TNBC cell migration in a dose-dependent manner. *$p < 0.05$, **$p < 0.01$, ***$p < 0.005$ vs. 0 μg/ml **(C)**Dandelion extract reduced the tumor growth in MDA-MB-231 xenograft model. **(D)** Dandelion extract reduced the tumor growth in 4T1BALB/C mice model. *$p < 0.05$, **$p < 0.01$, ***$p < 0.001$vs. control group (0 mg/kg), $^{\#}p < 0.05$, $^{\#\#}p < 0.01$, $^{\#\#\#}p < 0.001$ vs. dandelion extract (50 mg/kg).

Network pharmacology analysis

The chemical ingredients from dandelion extract were identified by liquid chromatography-mass spectrometry in our previous study (Li et al., 2017). Their chemical structures and SMILES ID were obtained from the PubChem database (Kim et al., 2019). The corresponding putative targets of the chemical components were predicted by three different databases, including SwissTargetPrediction (Daina et al., 2019), SEA (Keiser et al., 2007), and PharmMapper (Wang et al., 2017). TNBC-associated targets were collected from DisGeNET (Piñero et al., 2017) and GeneCards (Stelzer et al., 2016) databases with the keyword"triple-negative breast cancer". To evaluate the reliability of our method, we validated the precision of the predicted targets based on recall via the means of literature mining. The precision rate is calculated by (the number of the

intersection of the predicted targets and reported biomolecules)/(the number of predicted targets) × 100%. The overlapping genes between the chemical components of dandelion extract and TNBC were virtualized by the Venn diagram. Notably, only human genes were retained. The "compound-disease-targets" network and its topological analysis were performed via Cytoscape software (version 3.6.1). Gene Ontology (GO) functional enrichment and Kyoto Encyclopedia of Genes and Genomes (KEGG) pathway enrichment were performed using the DAVID database. Their results were visualized by the ggplots package in R software.

Multi-omics analysis

In this study, we performed quantitative proteomics, untargeted metabolomics, and untargeted lipidomic analysis on cell samples to reveal the metabolic vulnerabilities of TNBC after dandelion extract treatment. Three batches of MDA-MB-231 cell samples with equal treatment were used for multi-omics analysis. And the tumor tissue and plasma from the 4T1 mice model were used for the lipidomics. Briefly, MDA-MB-231 cells were divided into two groups that were treated with vehicle (50% DMSO) or dandelion extract (40 μg/ml) with a sublethal concentration (40 μg/ml) based on its IC50 value, respectively. The cells were cultured in DMEM supplemented with 1% FBS (triplicate for each group) for 24 h. Then, the cell samples were washed with 1×PBS and collected into different centrifuge tubes for LC-MS/MS analysis. The differentially expressed proteins were obtained by Tandem Mass Tag (TMT) labeling quantitative proteomics via HPLC-MS/MS. And the significantly changed metabolites were identified by untargeted metabolomics and lipidomic via UPLC-MS/MS. The specific conditions and processes of multi-omics were shown in Supplementary Materials.

Quantitative real-time polymerase chain reaction

Total RNA was extracted from cells using Trizol reagent (Invitrogen, United States), and its concentration was measured via NanoDrop 2000 (Thermo, United States). cDNAs were synthesized using a Hifair II 1st Strand cDNA Synthesis Kit (Yeasen Biotech, China). qRT-PCR was performed using SYBR Green qPCR Supermix (Applied Biosystems, United States) on 7,500 Fast Real-Time PCR Systems (Thermo, United States). The primers were from Sangon Biotech (Shanghai, China), and their sequences are listed in Supplementary Table S1. The qRT-PCR procedure for quantitative amplification was 95°C for 5 min, followed by 40 cycles of 15 s at 95°C, the 20 s at 60°C, and 40 s at 72°C. The data was analyzed and visualized via GraphPad 9.0.

Western blotting

Western blotting was performed to confirm the results of the integrated analysis. Briefly, protein concentrations were determined by a BCA Kit (Thermo, United States). Protein samples (20 μg) were separated by SDS-PAGE and transferred onto PVDF membrane (Millipore, United States). Then the membranes were blocked with 5% skim milk in TBS solution supplemented with 0.1% Tween-20 (TBST) for 1 h at room temperature and subsequently incubated overnight at 4°C with specific primary antibodies. After that, membranes were washed with TBST and incubated with horseradish peroxidase-conjugated secondary antibodies at room temperature for 1 h. Finally, the protein bands were visualized by an enhanced chemiluminescence reagent kit (Millipore, MA). The specific information of antibodies used in this study is shown in Supplementary Table S2. Densitometry was quantitated using ImageJ software and normalized to GAPDH expression.

Molecular modeling analysis

The molecular structures of compounds were obtained from the PubChem database, and the protein crystal structure of the candidate target was obtained from the RCSB Protein Data Bank (PDB) database. The protein structures were processed via AutoDockTools to remove ligand and water molecules, compute Gasteiger charges, add polar hydrogens, and merge non-polar hydrogens. The prepared protein structures and compounds were saved in PDBQT format. The binding box was set to contain all protein 3D structures, and other docking parameters followed the default value in AutoDock Vina. Next, the structure potential energy diagram and hydrogen bonds were shown in PyMOL.24.

Statistical analysis

Data were shown as the mean ± standard error (SD) from three independent experiments. Evaluation of the data was performed by a two-tailed Student's t-test. $p < 0.05$ was considered a statistically significant difference.

Results

Dandelion extract inhibited TNBC cell proliferation and migration *in vitro* and *in vivo*

In this study, we performed the MTT and wound-healing assay on MCF-10A, MDA-MB-231, and MDA-MB-468 cells to assess the antitumor effects of dandelion extract. As shown in

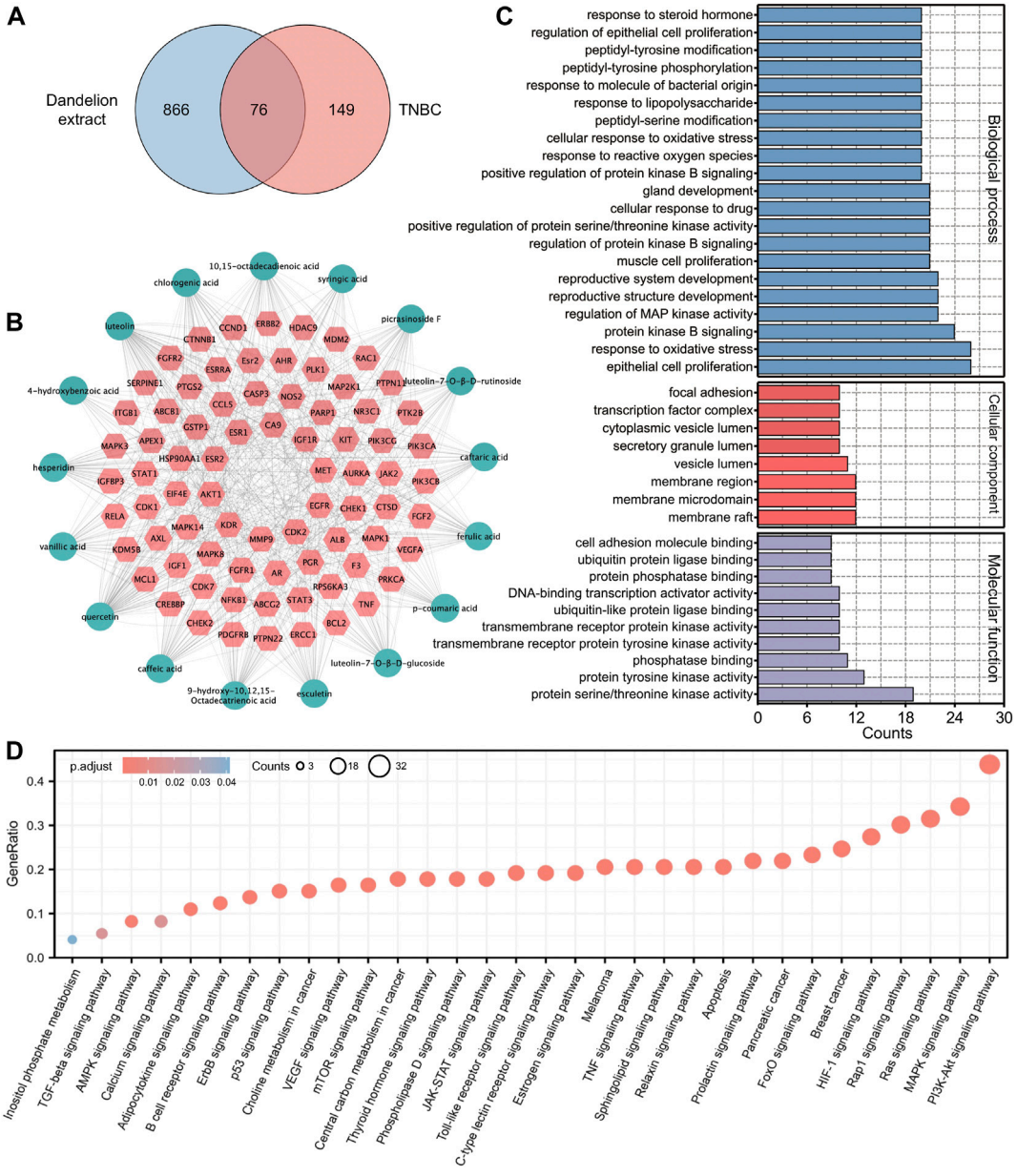

FIGURE 3
Network pharmacology analysis predicted the underlying regulatory mechanisms of dandelion extract against TNBC. **(A)** Venny diagram of the overlapping targets of dandelion extract and TNBC. **(B)** Compounds-disease-targets network. The pink diamond indicated the overlapping genes and the light green circles indicated the compounds in dandelion extract. **(C)** GO analysis for the overlapping genes. The *x*-axis represents the gene counts, and the *y*-axis represents the enriched terms. ($p < 0.05$). **(D)** KEGG pathway enrichment for the overlapping genes. The *x*-axis represents the enriched terms, and the *y*-axis represents the gene ratio ($p < 0.05$).

Figure 2A, TNBC cell viability was reduced in a dose-and time-dependent manner after dandelion extract treatment. The IC_{50} values of dandelion extract on MDA-MB-231 and MDA-MB-468 were 110.8 ± 9.2 μg/ml and 107.9 ± 5.6 μg/ml for 24 h, respectively. However, dandelion extract only showed its inhibitory effect on MCF-10A at the highest concentration (160 μg/ml) at 48 and 72 h. Moreover, the wound closure ability of TNBC cells was significantly decreased by dandelion extract in a dose- and time-dependent manner (Figure 2B). These results suggested that dandelion extract could preferably inhibit proliferation and migration in TNBC cells rather than normal breast cells. To further determine whether dandelion extract could suppress tumor growth in the MDA-MB-231 xenograft model and 4T1 mice model, mice were given dandelion extract

TABLE1 The topological parameters of compounds from the dandelion extract ranked Top 8.

Ranking	Compounds	Degree	Betweenness centrality	Closeness centrality
1	luteolin	44	0.07947041	0.53142857
2	quercetin	43	0.07417193	0.52542373
3	10,15-octadecadienoic acid	41	0.0716824	0.51381215
4	9-hydroxy-10,12,15- octadecatrienoic acid	40	0.10063292	0.50819672
5	caffeic acid	39	0.07271655	0.5027027
6	ferulic acid	39	0.08650739	0.5027027
7	picrasinoside F	38	0.07415693	0.4973262
8	vanillic acid	36	0.13189874	0.48691099

(50 and 100 mg/kg) daily for15 and 20 days, respectively. We found that dandelion extract could significantly reduce the tumor volume and weight in a dose-dependent manner in the MDA-MB-231 xenograft model and 4T1 mice model. Notably, there were no obvious differences in body weights after dandelion extract treatment (Figures 2C,D). These results indicated that dandelion has potent inhibitory effects against TNBC *in vivo* and *in vitro*.

Network pharmacology speculated the possible regulatory mechanisms of dandelion extract against TNBC

Network pharmacology could exhibit the complexities among compounds, diseases, and biological systems from a network perspective and thus predict their interacted mechanisms (Zhang et al., 2019). Hence, the network pharmacology analysis was used to conjecture the potential mechanisms of dandelion extract against TNBC and screen for the main bioactive compounds in dandelion extract. Our previous studies identified 22 bioactive compounds from dandelion extract via LC-MS, among which 17 compounds obtained their SMILE IDs from the PubChem database to perform network pharmacology analysis. The chemical structures and detailed information are shown in Supplementary Figures S1, S2, and Supplementary Table S3, respectively. Finally, a total of 942 compound-related putative targets and 225 TNBC-associated targets were collected after discarding the replicate, and 76 overlapped targets were merged (Figure 3A). All targets were put in the UniProt database to obtain their standard gene synonyms (Supplementary Table S4), and the precision rates of predicted targets were high.

Subsequently, we constructed a "compounds-disease-targets" network comprised of 11 nodes and 22 edges and analyzed its topological parameters, including degree, betweenness centrality, and closeness centrality (Figure 3B). The parameter values could reflect the importance of each compound in the network. Table 1 showed eight compounds with parameter values greater than the average, like luteolin, quercetin, and 10,15-octadecadienoic acid, which could be considered the major bioactive components in dandelion extract. The detailed parameters information was displayed in Supplementary Table S5. Then, GO functional analysis and KEGG pathway enrichment were used to speculate the possible regulatory pathways of dandelion extract against TNBC. Figure 3C showed multiple enriched terms, including cell proliferation, oxidative stress, membrane microdomain, and protein tyrosine kinase activity, suggesting that dandelion extract might function its anti-TNBC effects by acting on these biological processes. Moreover, as shown in Figure 3D, multiple signaling pathways involved in tumorigeneses and tumor progression were enriched, and the PI3K/AKT signaling pathway ranked first, indicating that it might play an important role in the inhibitory effects of dandelion extract against TNBC. Besides, metabolic-associated pathways, such as the AMPK signaling pathway and the choline metabolism in cancer, suggested the possible lipid regulatory effects of dandelion extract on TNBC. In general, the network pharmacology provided a systematic predictive analysis of the regulatory mechanisms of dandelion extract against TNBC *in silico*.

Proteome and metabolome profiles of MDA-MB-231 cells after dandelion extract treatment

In order to further explore the regulatory mechanisms of dandelion extract against TNBC, TMT-based quantitative proteomics and untargeted metabolomics were performed on cell samples. The unsupervised principal component analysis (PCA) showed significant differences between the two groups (Supplementary Figure S3A). As a result, a total of 5,049 proteins were identified, and 3,932 proteins were quantitated. Based on the screen criteria of fold change >1.2 and p-value ($p < 0.05$), we finally identified144 differentially expressed proteins, including 82 upregulated proteins and 62 downregulated proteins (Supplementary Figure S3B). Then, GO function enrichment

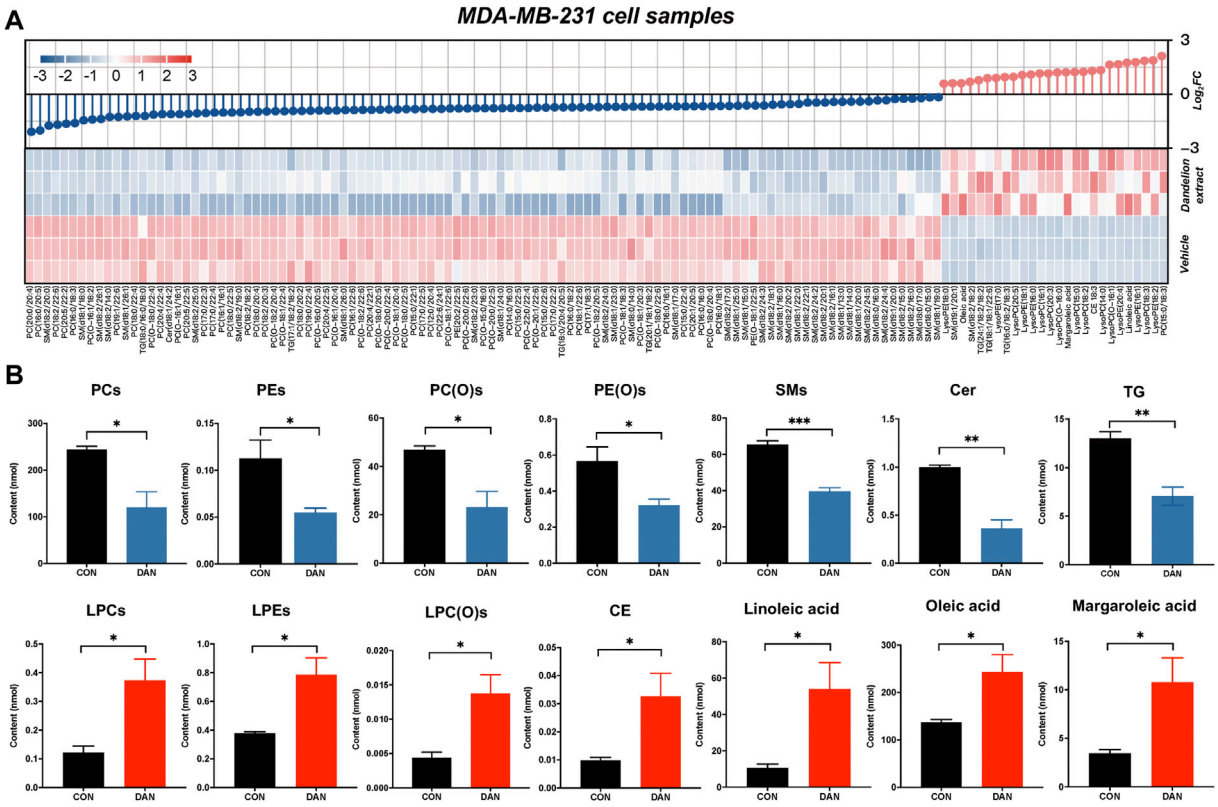

FIGURE 4
The lipidomics profiles of MDA-MB-231 cells after dandelion extract treatment. **(A)** The heatmap and change dumbbell charts of the significantly changed metabolites of untargeted lipidomics. **(B)** The changes of the significantly differential metabolites of untargeted lipidomics.

analysis indicated that the differentially expressed proteins involved multiple biological functions, including metabolic processes (Supplementary Figure S3C). Besides, by using clusters of orthologous groups (COG) annotation, differentially expressed proteins could be divided into three different functional categories involved in metabolism, cellular process and signaling, and information storage and processing, accounting for 24.6, 19.3, and 43.0%, respectively (Supplementary Figure S3D).

As for metabolome profiles, the cell samples from two groups could be distinguished well by the PCA and OSPL-DA (Supplementary Figures S3E,F). Totally, based on the screen criteria with VIP ≥1, fold change≥ 2, and *p*-value ($p < 0.05$), we determined 33 significantly changed metabolites (28 upregulated and 5 downregulated) that belonged to 9 categories, including glycerophospholipids, amino acids, carboxylic acids, heterocyclic compounds, coenzyme and vitamins, etc. (Supplementary Figure S3G). Notably, glycerophospholipids spices were the majority metabolites that accounted for 54.5%. The results of proteomics and untargeted metabolomics suggested that dandelion extract exerted its antitumor effects on TNBC by primarily interfering with the lipid metabolic processes, especially in glycerophospholipid metabolism.

Lipidome profiling of MDA-MB-231 after dandelion extract treatment revealed its primary metabolic regulatory processes

To further address the lipid regulatory mechanisms of dandelion extract on TNBC, untargeted lipidomic was performed using TNBC cell, tumor tissue and plasma samples to find out more significantly changed lipid metabolites and their related metabolic pathways. The MDA-MB-231 cell samples treatment was consistent with proteomics and untargeted metabolomics, and the tumor tissue and plasma samples were obtained from the mice model. The unsupervised PCA and OSPL-DA indicated that all the samples from the two groups were significantly separated (Supplementary Figures S4–S6). The significantly changed lipid metabolites were identified by the screen criteria with VIP ≥1 and *p*-value ($p < 0.05$). Finally, we obtained 1,331 significantly changed lipid metabolites (26 upregulated and 105 downregulated) in cell lipidomics that could be classified into glycerophospholipids, sphingolipids,

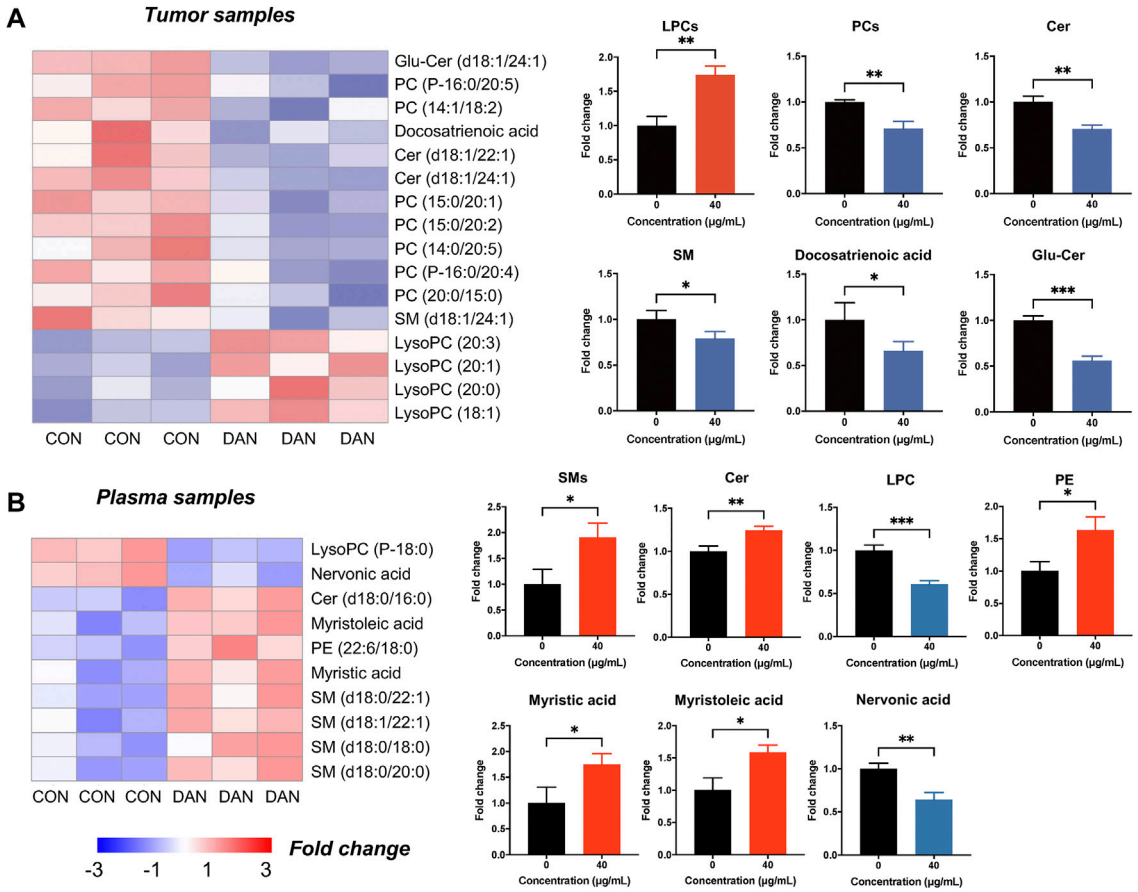

FIGURE 5
The lipidomics profiles of TNBC tumor tissue and plasma after dandelion extract treatment. **(A)** The heatmap charts of the significantly changed metabolites in tumor tissue lipidomics. **(B)** The heatmap charts of the significantly changed metabolites in plasma lipidomics.

cholesterol, and unsaturated fatty acids (Figure 4A). The primarily disrupted lipids were glycerophospholipids, including phosphatidylcholine (PC), phosphatidylethanolamine (PE), lysophosphatidylcholine (LPC), alkyl phosphatidylcholine, alkyl phosphatidylethanolamine, and lysophosphatidylethanolamine (LPE). The total relative abundance of each lipid species was visualized in Figure 4B. Specifically, the contents of PC, PE, alkyl phosphatidylcholine, alkyl phosphatidylethanolamine, triglyceride (TG), sphingomyelin (SM), and ceramide (Cer) were significantly decreased after dandelion extract treatment. Inversely, the total relative levels of LPC, LPE, cholesteryl ester (CE), linoleic acid (LA), oleic acid (OA), and margaroleic acid were increased.

Furthermore, a total of 16 lipid metabolites were changed significantly in tumor tissue lipidomics (12 upregulated and 4 downregulated). PC, SM, Cer, and docosatrienoic acid were decreased, and LPC was increased in tumor tissues (Figure 5A). Notably, the variation trends of PC, LPC, SM, and Cer in tumor tissue were consistent with the cell lipidomics, indicating that dandelion extract interfered with the synthesis of phospholipids and sphingolipids of TNBC both *in vitro* and *in vivo*. Besides, a total of 10 significantly changed lipid metabolites were identified by plasma lipidomics (8 upregulated and 2 downregulated) (Figure 5B). Sphingolipid metabolites such as SM and Cer, PE, and the unsaturated fatty acids like myristoleic acid and myristic acid were increased in plasma. LPC and nervonic acid were decreased in plasma. In addition, the KEGG pathway enrichment indicated glycerophospholipid metabolism, sphingolipid metabolism, and unsaturated fatty acid metabolism were the primary regulatory processes (Supplementary Figure S7).

Integrated analysis identified the primary metabolic pathways and biomarkers in the regulation of dandelion extract on TNBC

Afterward, we performed an integrated analysis based on the results of multi-omics and network pharmacology to find out the

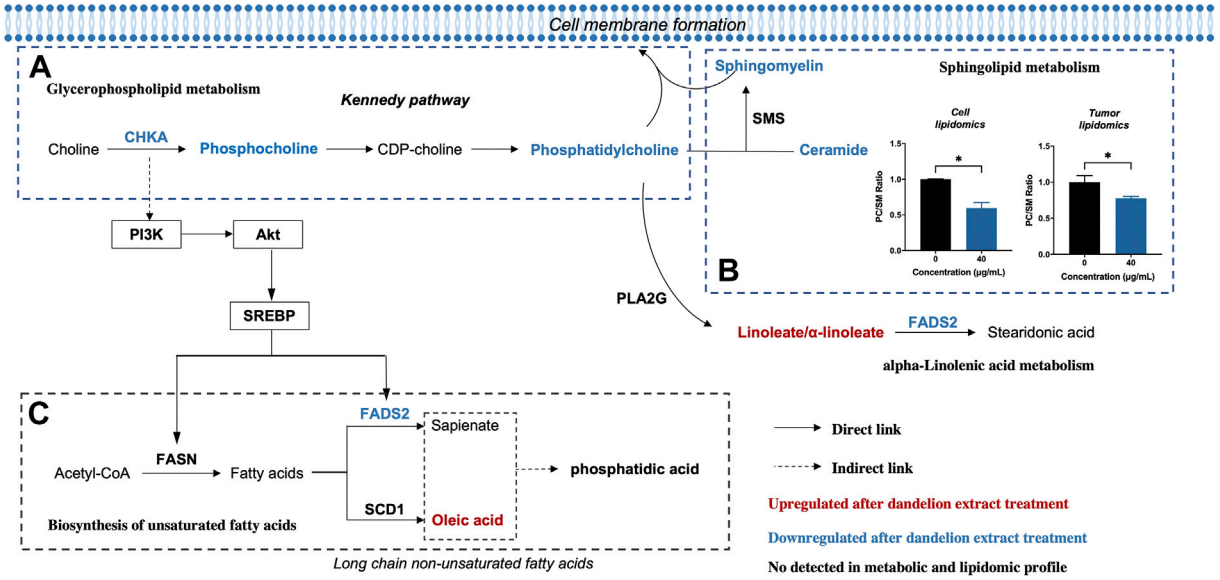

FIGURE 6
Altered metabolic pathways of MDA-MB-231 cell after dandelion extract treatment. **(A)** The Glycerophospholipid metabolism. **(B)** The Sphingolipid metabolism. **(C)** The biosynthesis of unsaturated fatty acids.

co-regulated lipid metabolic pathways and identified the primary regulatory processes and biomarkers in the regulation of dandelion extract against TNBC. As shown in Figure 6, the co-regulated pathways included linoleic acid metabolism (map02591), glycerophospholipid metabolism (map00564), biosynthesis of unsaturated fatty acids (map01040), alpha-linolenic acid metabolism (map00592), and sphingolipid metabolism (map00600). By matching the changed metabolic-associated proteins identified in proteomics, we found that choline kinase α (CHKA) and FADS2 were highly connected with the metabolites in glycerophospholipid metabolism and the biosynthesis of unsaturated fatty acids, respectively. In the glycerophospholipid metabolism, CHKA expression was decreased, and the levels of its downstream metabolites PCho, PC, and PE were decreased simultaneously (Figure 6A). Besides, the content levels of SM and Cer were also reduced. Notably, both SM and PC are important components of cell membranes, and the PC/SM ratio could reflect the fluidity of cell membranes (Mao et al., 2022), which is closely related to the invasive and migrative capacities of tumor cells (Li et al., 2021a). Our results showed that the PC/SM ratio was reduced both in the TNBC cells and tissues (Figure 6B) and demonstrated that dandelion extract could impede cell membrane formation and reduce the cell membrane fluidity via disrupting the biosynthesis of PC and SM, ultimately leading the inhibition of TNBC cell growth and migration.

On the other hand, in the biosynthesis of unsaturated fatty acids, the protein expression levels of FADS2 were decreased, and meanwhile, linoleic acid and oleic acid were increased (Figure 6C). Therefore, CHKA and FADS2 were considered the critical biomarkers that accounted for lipids regulatory effects of dandelion extract against TNBC. Based on the KEGG enrichment in network pharmacology, CHKA might interact with the PI3K/AKT pathway, which plays a vital role in tumor growth, proliferation, and metabolism (Alzahrani, 2019). Besides, SREBP and FADS2 were the downstream molecules of the PI3K/AKT pathway (Griffiths et al., 2013; Zhang et al., 2020). Next, we would perform experimental validations on the above molecules.

Dandelion extract disrupted metabolic-associated pathways *in vitro*

To further demonstrate the accuracy of the integrated analysis results, we performed experimental validations on the identified biomarkers CHKA and FADS2, as well as their related regulatory pathways. First, we compared the mRNA expression levels based on a transcriptome profile with130 breast cancer samples (41 TNBC and 89 ER^+ BC) and 11 normal breast tissue samples (GSE65194 dataset from Gene Expression Omnibus database). These data indicated that mRNA expression levels of *CHKA*, *FADS2*, and *SREBF1*werehigher in breast cancer samples than in normal breast tissue, and their levels in TNBC were significantly changed compared to ER^+ breast cancer samples (Figure 7A). Then, qRT-PCR results confirmed that the mRNA levels of *CHKA* and *FADS2* were higher in TNBC cells than in MCF-10A, but there were no

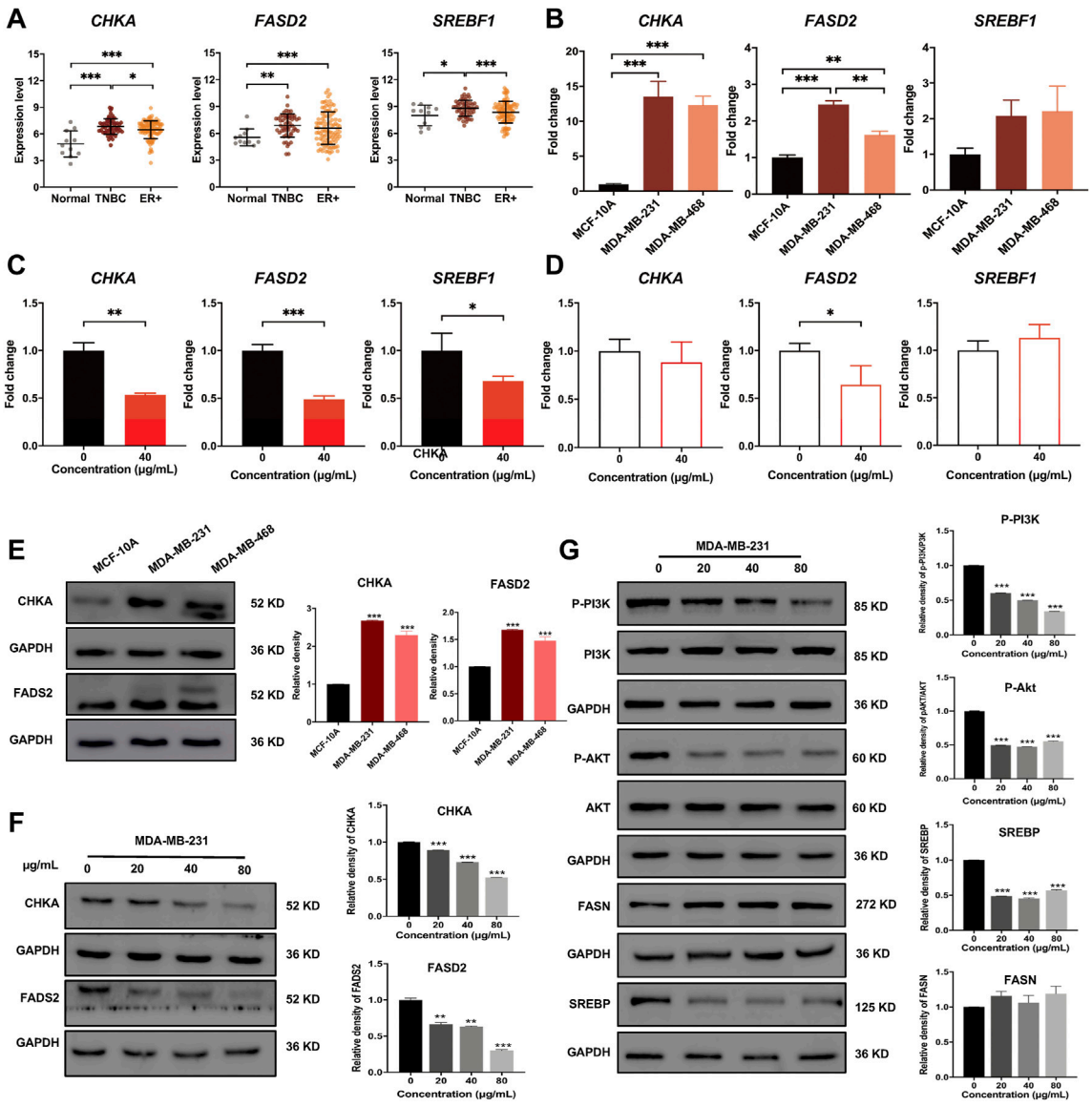

FIGURE 7
Dandelion extract inhibited mRNA and protein expression levels of metabolic-associated proteins and pathways. **(A)** The mRNA expression levels of *CHKA, FADS2*, and*SREBF1* in normal, TNBC, and ER$^+$ breast cancer tissues based on the GSE65194 dataset. **(B)** The mRNA expression levels of *CHKA, FADS2*, and*SREBF1* in TNBC and normal cells by RT-PCR. **(C)** The mRNA expression levels of *CHKA, FADS2*, and*SREBF1* after dandelion extract treatment in MDA-MB-231 cells by RT-PCR. **(D)** The mRNA expression levels of *CHKA, FADS2*, and*SREBF1* after dandelion extract treatment in MCF-10A cells by RT-PCR. **(E)** The protein expression levels of CHKA and FADS2 in MCF-10A and TNBC cells. **(F)** The protein expression levels of CHKA and FADS2 in MDA-MB-231 cells after dandelion extract treatment. **(G)** The expression levels of p-PI3K, p-AKT, SREBP, and FASN in MDA-MB-231 cells after dandelion extract treatment. *$p < 0.05$, **$p < 0.01$, ***$p < 0.001$.

significant differences in *SREBF1* mRNA levels (Figure 7B). After dandelion extract treatment, the mRNA expression levels of *CHKA*, *FADS2*, and *SREBF1*in MDA-MB-231 were both decreased (Figure 7C). For MCF-10A cells, dandelion extract only reduced the mRNA level of *FADS2*but with no significant effect on the *CHKA* and *SREBF1*(Figure 7D).

Subsequently, western blot results showed that the expression levels of CHKA and FADS2 in TNBC cells were higher than in MCF-10A (Figure 7E). After dandelion extract treatment, the expression of CHKA and FADS2 were reduced in a dose-dependent manner in TNBC cells (Figure 7F). Moreover, the phosphorylation levels of PI3K and AKT were also reduced, suggesting that the PI3K/AKT pathway was inhibited by dandelion extract (Figure 7G). And the expression of SREBP, a downstream target of the PI3K/AKT pathway, was reduced accordingly. It is demonstrated

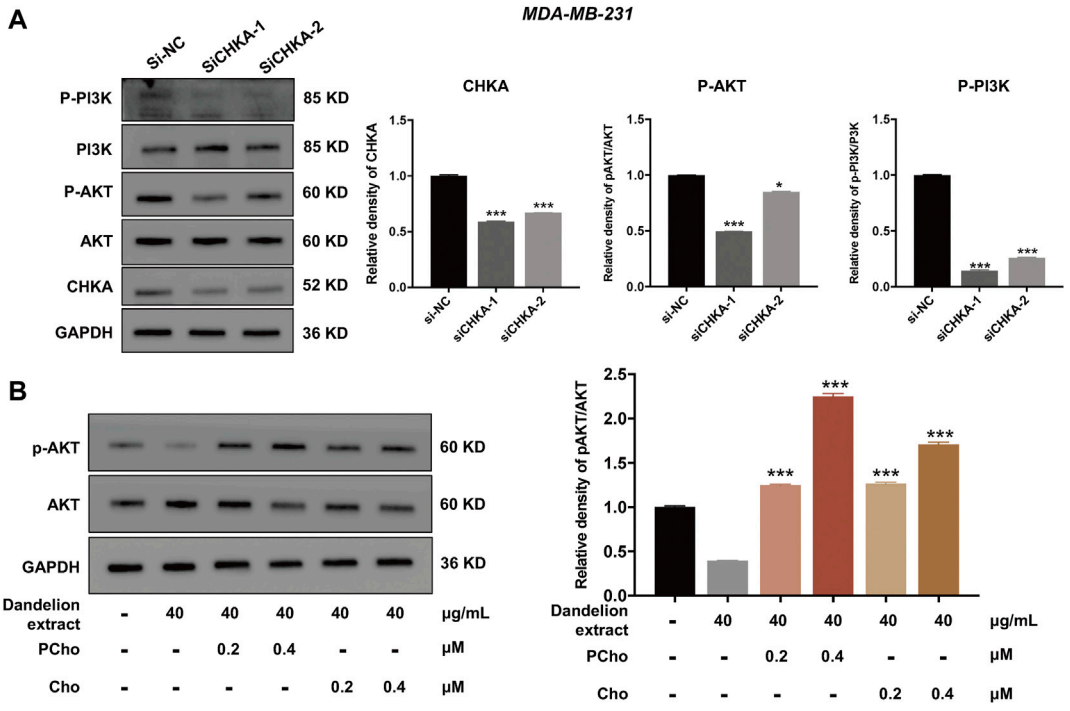

FIGURE 8
Dandelion extract inhibited mRNA and protein expression levels of metabolic-associated proteins and pathways. **(A)** Inhibition of CHKA expression decreased the phosphorylation levels of PI3K and AKT. *$p < 0.05$, **$p < 0.01$, ***$p < 0.001$ vs. si-NC. **(B)**The exogenous addition of Cho and PCho reversed the decreased phosphorylation levels of AKT in MDA-MB-231 cells. *$p < 0.05$, **$p < 0.01$, ***$p < 0.001$ vs. dandelion extract (40 μg/kg).

that FASN and FADS2 were the targets of SREBP, accounting for the fatty acid synthesis and desaturation, respectively (Griffiths et al., 2013). However, our results showed that dandelion extract could inhibit the expression of SREBP and FADS2, but did not have apparent inhibitory effects on FASN (Figure 7G). The above results confirmed that dandelion extract could reduce the mRNA and protein expression levels of CHKA and FADS2 and inhibit the PI3K/AKT pathway in TNBC cells.

Furthermore, our previous results showed that the content of PCho was decreased due to the inhibition of CHKA by dandelion extract. It is reported that PCho, the direct metabolite of CHKA, is abnormally elevated in various cancers and is able to provide phosphate molecules for AKT activation, thus promoting tumor proliferation (Venkatesh et al., 2012). To explore the interaction between CHKA and PI3K/ATK signaling pathway, MDA-MB-231 cells were transfection with CHKA siRNA. Western blot results showed CHKA expression in MDA-MB-231 cells was significantly inhibited by CHKA siRNA, and the phosphorylation levels of PI3K and AKT were similarly reduced after endogenous inhibition of CHKA expression (Figure 8A). In contrast, exogenous addition of Cho and PCho could reverse the decreased AKT phosphorylation levels in MDA-MB-231 cells by dandelion extract (Figure 8B). The above results suggest that dandelion extract could inhibit the PI3K/AKT signaling pathway by reducing the CHKA expression and reducing the synthesis of Cho into PCho, thereby reducing the phosphorylation level of AKT.

Luteolin might be the primary bioactive compound in dandelion extract via inhibiting CHKA

Integrated analysis and experimental validation revealed that CHKA played a vital role in the inhibition of dandelion extract on TNBC. And the network pharmacology analysis speculated eight compounds that were essential for dandelion's multi-pharmacological effects. To address whether the compounds could interact with CHKA directly, molecular docking simulation was performed to calculate the binding scores between CHKA and compounds. The binding scores of CHKA and its specific inhibitors rabusertib or AZD7762 were the baseline. The molecular structures of compounds were obtained from the PubChem database. The 3D crystal structure of CHKA and hemicholinium-3 complex (PDB code: 3F2R) was derived from the PDB. Notably, hemicholinium-3 should be removed from the

TABLE 2 The binding scores between CHKA andthe compounds from dandelion extract.

Ranking	Target	Ligands	Binding score (kcal/mol)
-	CHKA	rabusertib	−7.98
-	CHKA	AZD7762	−7.32
1	CHKA	picrasinoside F	−7.5
2	CHKA	luteolin	−6.94
3	CHKA	quercetin	−5.47
4	CHKA	caffeic acid	−4.82
5	CHKA	9-hydroxy-10,12,15-octadecatrienoic acid 7	−4.44
6	CHKA	ferulic acid	−4.39
7	CHKA	vanillic acid	−4.3
8	CHKA	10,15-octadecadienoic acid	−3.73

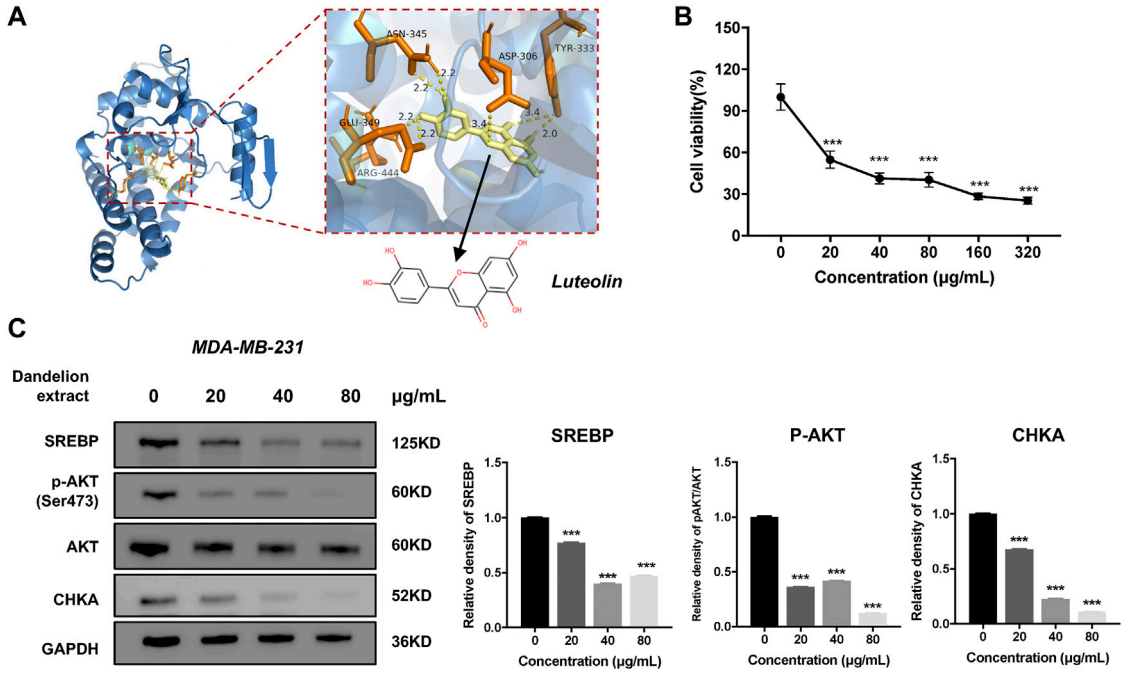

FIGURE 9
The luteolin could inhibit TNBC cell proliferation and reduce the expression level of CHKA. **(A)** The interactions of the potential crystal structure of CHKA domain in complex with luteolin based on the molecular docking simulation. The dotted line between the compound and the protein refers to the hydrogen bond. TYR, tyrosine; CLU, glutamic acid; SER, serine; LEU, leucine; ASN, Asparagine; ASP, Aspartic acid; ARG, Arginine.**(B)**. Luteolin inhibited MDA-MB-231 cell proliferation by MTT assays. **(C)**. Luteolin reduced the expression levels of SREBP, CHKA, and p-AKT. *$p < 0.05$, **$p < 0.01$, ***$p < 0.001$ vs. 0 μg/ml.

complex with the PyMOL, and the pure 3D crystal structure of CHKA only remained. Molecular docking was processed via AutoDock Vina, and the results were viewed and analyzed using PyMOL. The results showed that eight compounds exhibited inconsistent binding capacities with CHKA (Table 2 and Figure 9A), and picrasinoside F, luteolin, and esculetin possess the strongest binding capacity to CHKA. Subsequently, we performed the MTT assays using luteolin on the TNBC cells, and it showed a potent inhibitory effect against MDA-MB-231 cells (Figure 9B). Western blot results demonstrated that luteolin could decrease the expression levels of CHKA, SREBP, and p-AKT, which were consistent with the tendency after dandelion extract treatment (Figure 9C), suggesting it might be a novel CHKA inhibitor and the primary bioactive compound in dandelion extract.

Discussion

Metabolic reprogramming is a prominent hallmark of cancer cells (Deberardinis and Chandel, 2016). The alterations in lipid metabolic activities provide energy and the building stocks of the cell membrane to meet the increased needs for tumor cell proliferation (Peck and Schulze, 2016). Simultaneously, it had been reported that certain Chinese herbal medicines and their components could disrupt the reprogrammed metabolic processes, enhancing the antitumor efficacies of conventional therapeutics or leading to tumor cell death directly (Zhong et al., 2016; Wang et al., 2021b). Dandelion is a classic herbal medicine in treating mammary diseases and has been demonstrated to possess antitumor and lipid regulatory effects. In the present study, dandelion extract was confirmed to inhibit the proliferation and migration of TNBC cells in a time- and dose-dependent manner, and it could significantly suppress the tumor growth in the MDA-MB-231 xenograft and 4T1 mice model. TNBC has wide reprogrammed lipid metabolisms that contribute to its malignancy (Sun et al., 2020). To address the question of whether dandelion extract possesses lipid regulatory effects on TNBC and elucidate the potential mechanisms, an integrated approach composed of network pharmacology, quantitative proteomics, untargeted metabolomics, and untargeted lipidomics was performed in this study.

Network pharmacology could analyze the molecular association between compounds and diseases and predict systematic pharmacological mechanisms in a holistic manner (Gu et al., 2013). The topological analysis of network pharmacology suggested that luteolin, quercetin, 10,15-octadecadienoic acid, and other five compounds were the main bioactive component in dandelion extract and played key roles in dandelion's antitumor effects. Besides, the enrichment analysis of network pharmacology speculated that dandelion extract regulated various biological processes and metabolic-associated pathways of TNBC. The PI3K/AKT pathway was the most remarkable among them (Figure 3).

Next, the multiple-omics technique was used to obtain the changed protein and metabolites and reveal metabolic vulnerabilities of TNBC after dandelion extract treatment. Totally, 144 differential expressed proteins and 43 significantly changed metabolites were identified by quantitative proteomics and untargeted metabolomics, respectively. These results suggested that the primary regulatory effect of dandelion extract was involved in lipid metabolism. Therefore, the untargeted lipidomics was performed subsequently, and we obtained 131 significantly changed lipid metabolites, including glycerophospholipids, sphingolipids, cholesterol, and unsaturated fatty acids. Then, through the integrated analysis of the multi-omics results and network pharmacology, we identified five co-regulated metabolic pathways, and the glycerophospholipid metabolism, linolenic acid metabolism, and biosynthesis of unsaturated fatty acids were the most significant and considered CHKA and FADS2 as the critical targets for further experimental validation *in vitro* (Figure 6).

In glycerophospholipid metabolism, multiple metabolic-associated proteins and metabolites were changed after dandelion extract treatment. Among them, CHKA is a crucial rate-limiting enzyme that converts intracellular free choline to phosphorylcholine in the *de novo* synthesis of PC (Kennedy pathway) (Andrejeva et al., 2020). CHKA and its related metabolites, including phosphorylcholine, PC, PE, LPC, and LPE, are overexpressed in primary tumor tissues of the breast, colorectal, prostate, and lung and could be considered the prognostic and diagnostic markers (Gibellini and Smith, 2010; Grinde et al., 2014) In this study, we confirmed that the mRNA and protein levels of CHKA were higher than normal and reduced after dandelion extract treatment. More importantly, the decreased CHKA expression led to the reduction of the content of its metabolites like PCho, PC, and PE. The decreased PC reduced the SM biosynthesis accordingly. PC, PE, and SM are essential components of cell membranes, and the PC/SM ratio could reflect its fluidity, which is closely related to the invasive and migrative capacities of tumor cells. Our results demonstrated that dandelion extract could disrupt the glycerophospholipids metabolism via inhibiting CHKA expression, impeding cell membrane formation, and reducing the cell membrane fluidity, ultimately leading to the inhibition of TNBC cell growth and migration. Moreover, the content of LPC and LPE were increased inversely, and thus the ratio of PC/LPC was decreased after dandelion extract treatment. The higher content of LPC is beneficial for a better prognosis (Li et al., 2021b).

In addition to the catalytic effect, CHKA could act as a mediator in regulating cell signaling transduction and promoting tumor initiation and progression (Cheng et al., 2016). For example, the c-Src-dependent link between CHKA and EGFR promoted breast cancer cell proliferation and tumorigenesis (Miyake and Parsons, 2012). Down-regulation of CHKA expression elicited the endoplasmic reticulum stress and induced apoptosis via CHOP in breast cancer (Sanchez-Lopez et al., 2013), and it is reported that CHKA could promote glioma development via activating PI3K/AKT pathways (Zou et al., 2021). In this study, the network pharmacology analysis spectacled that CHKA may interact with the P13K/AKT pathway, which is abnormally active in various tumor cells and is closely related to tumor growth, proliferation, and metabolism (Hoxhaj and Manning, 2020). The western blot results showed that the phosphorylation levels of PI3K and AKT were reduced after dandelion extract treatment, which is according to the decrease in CHKA expression. Besides, the phosphorylation levels of PI3K and AKT were similarly reduced after endogenous inhibition of CHKA expression. It is reported that PCho, the direct metabolite of CHKA, is abnormally elevated in various cancers and is able to provide

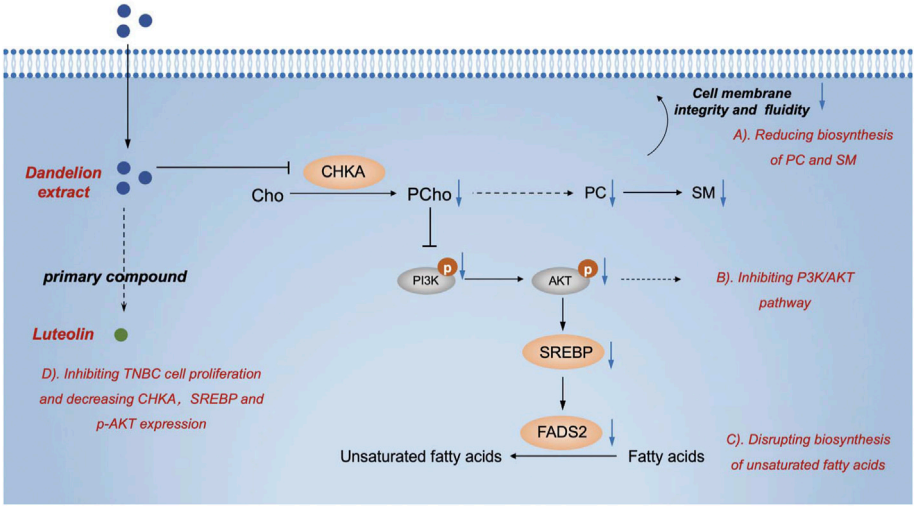

FIGURE 10
The graphic abstract of the lipid regulatory effects of dandelion extract against TNBC.

phosphate molecules for AKT activation, thus promoting tumor proliferation. The content of PCho was decreased due to the inhibition of CHKA by dandelion extract based on the metabolomics results. Then, we found that the exogenous addition of Cho and PCho could reverse the decreased AKT phosphorylation levels by inhibiting CHKA in MDA-MB-231 cells. The above results indicated that dandelion extract could inhibit the PI3K/AKT signaling pathway by reducing the CHKA expression and the biosynthesis of PCho, ultimately decreasing the phosphorylation level of AKT. The exogenous addition of Cho and PCho could reverse the phosphorylation levels of PI3K and AKT, thus suggesting that the antitumor effects of dandelion extract are partially mediated by the CHKA/PI3K/AKT pathway.

On the other hand, we found that dandelion extract could disrupt the unsaturated fatty acids metabolism, enhancing the content of oleic acid and linoleic acids but decreasing FADS2 expression. The unsaturated fatty acids are the integral macromolecules for phospholipid synthesis and cell membrane formation, and inhibition of fatty acids synthesis and desaturation is detrimental to tumor cell survival and contributes to antitumor properties (Saati and Archer, 2011; Peck et al., 2016). Some cancers rely on two desaturation pathways mediated by stearoyl-coenzyme A desaturase (SCD) and FADS2 to generate unsaturated fatty acids (Vriens et al., 2019). FADS2 is regulated by SREBP and generates unusual fatty acid sapienate, which could replace palmitoleate or oleate produced by SCD in cell membrane synthesis (Li et al., 2021b). Hence, only dual inhibition of SCD and FADS2 could result in tumor cell death directly. In this study, we confirmed that the mRNA and proteins expression levels of FADS2 were higher in TNBC cells and tissues than normal, suggesting that TNBC existed the abnormal FADS2-dependent fatty acids desaturation. After dandelion extract treatment, the mRNA and protein expression of FADS2 were decreased and SREBP expression was also reduced accordingly (Triki et al., 2020). However, we did not detect the changes of sapienate via metabolomics or lipidomics, and we speculated the content of sapienate would be reduced in theory, causing the compensatory increase of other unsaturated fatty acids, such as oleic acid and linoleic acids. Besides, the expression of FASN, another downstream target of SREBP, had no significant changes after dandelion extract treatment. Taken together, our results indicated that dandelion extract could decrease fatty acids desaturation via inhibiting the SREBP/FADS2 axis but has no apparent effects on fatty acids synthesis (Figure 10).

Notably, a recent study indicated that the aqueous extract of dandelion could exhibit therapeutic effects on TNBC by inhibiting CDK6 expression and regulating arginine and proline metabolism pathway based on its results of untargeted metabolomics (Qu et al., 2022). However, the dandelion extract in our study was extracted via 50% ethanol and purified by macroporous resin. Therefore, different extraction processes led to the differences in the types and contents of bioactive compounds in dandelion extract and the regulatory mechanisms of aqueous or ethanol extract of dandelion were not entirely consistent. Our results suggested that dandelion ethanol extract inhibited TNBC by interfering with glycerophospholipids and unsaturated fatty acids metabolism.

Furthermore, we performed the molecular docking simulation to screen the potential anti-cancer compounds from dandelion extract, which could exert its pharmacological effects by binding CHKA. The topological analysis of network pharmacology identified eight essential compounds and their

binding scores between CHKA wound compared to the scores of CHKA-specific inhibitors to evaluate the binding capacity. The results indicated that picrasinoside F and luteolin possessed a high binding capacity with hydrogen bond and might consider novel potential CHKA inhibitors. Besides, we preliminary showed that luteolin had a potent inhibitory effect against MDA-MB-231 cells and inhibited the CHKA/AKT/SREBP axis, which might be the main bioactive compound in dandelion extract.

Conclusion

In conclusion, we confirmed the antitumor effects of dandelion extract on TNBC *in vitro* and found that dandelion extract could suppress tumor growth in the MDA-MB-231 xenograft and 4T1 model. We also exhibited the proteomic and lipidomic characteristics of TNBC cells, tumor tissue, and plasma after dandelion extract treatment. Through integrated analysis and experimental invalidation *in vitro*. We demonstrated that dandelion extract could interfere with glycerophospholipids and unsaturated fatty acids metabolism by inhibiting CHKA/PI3K/AKT/FADS2 axis, ultimately resulting in the blockage of cell membrane formation and tumor cell death (Figure 10). Additionally, we speculated that picrasinoside F and luteolin were the main bioactive components in dandelion extract and might function their pharmacological effects against TNBC via binding CHKA *in silicon*.

Data availability statement

The original contributions presented in the study are publicly available. This data can be found here: https://www.ebi.ac.uk/pride/archive/, PXD035797.

Ethics statement

The animal study was reviewed and approved by the Experimental Animal Ethics Committee, Peking university cancer hospital.

Author contributions

SW and S-YH conceived and designed the study. SW and Z-WG performed the network pharmacology and multi-omics analysis. H-FH, Y-NJ, J-LF, and YG performed phenotypic experiments on tumor cells and the Western blotting, qRT-PCR assays. SW and YY performed the molecular docking simulation. SW drafted the manuscript, and S-YH reviewed the revised manuscript. S-YH and P-PL funded this study.Confirm if the edit made in the "Author Contributions" section is correct.

Funding

This work was supported by the National Natural Science Foundation of China (Grant No. 81873054 and 82074062).

Conflict of interest

The authors declare that the research was conducted in the absence of any commercial or financial relationships that could be construed as a potential conflict of interest.

Publisher's note

Supplementary material

The Supplementary Material for this article can be found online at: https://www.frontiersin.org/articles/10.3389/fphar.2022.942996/full#supplementary-material

References

Alzahrani, A. S. (2019). PI3K/Akt/mTOR inhibitors in cancer: At the bench and bedside. *Semin. Cancer Biol.* 59, 125–132. doi:10.1016/j.semcancer.2019.07.009

Andrejeva, G., Gowan, S., Lin, G., Wong Te Fong, A. C. L., Shamsaei, E., Parkes, H. G., et al. (2020). De novo phosphatidylcholine synthesis is required for autophagosome membrane formation and maintenance during autophagy. *Autophagy* 16, 1044–1060. doi:10.1080/15548627.2019.1659608

Bianchini, G., Balko, J. M., Mayer, I. A., Sanders, M. E., and Gianni, L. (2016). Triple-negative breast cancer: Challenges and opportunities of a heterogeneous disease. *Nat. Rev. Clin. Oncol.* 13, 674–690. doi:10.1038/nrclinonc.2016.66

Burstein, M., Tsimelzon, A., Poage, G. M., Covington, K. R., Brown, P. H., Fuqua, S. A. W., et al. (2015). Comprehensive genomic analysis identifies novel subtypes and targets of triple-negative breast cancer. *Clin. Cancer Res.* 21, 1688–1698. doi:10.1158/1078-0432.CCR-14-0432

Cheng, M., Bhujwalla, Z. M., and Glunde, K. (2016). Targeting phospholipid metabolism in cancer. *Front. Oncol.* 6, 266. doi:10.3389/fonc.2016.00266

Choi, U. K., Lee, O. H., Yim, J. H., Cho, C. W., Rhee, Y. K., Lim, S. I., et al. (2010). Hypolipidemic and antioxidant effects of dandelion (*Taraxacum officinale*) root and leaf on cholesterol-fed rabbits. *Int. J. Mol. Sci.* 11, 67–78. doi:10.3390/ijms11010067

Daina, A., Michielin, O., and Zoete, V. (2019). SwissTargetPrediction: Updated data and new features for efficient prediction of protein targets of small molecules. *Nucleic Acids Res.* 47, W357–W364. doi:10.1093/nar/gkz382

Davaatseren, M., Hur, H. J., Yang, H. J., Hwang, J. T., Park, J. H., Kim, H. J., et al. (2013). Taraxacum official (dandelion) leaf extract alleviates high-fat diet-induced nonalcoholic fatty liver. *Food Chem. Toxicol.* 58, 30–36. doi:10.1016/j.fct.2013.04.023

Deberardinis, R. J., and Chandel, N. S. (2016). Fundamentals of cancer metabolism. *Sci. Adv.* 2, e1600200. doi:10.1126/sciadv.1600200

Deng, X. X., Jiao, Y. N., Hao, H. F., Xue, D., Bai, C. C., and Han, S. Y. (2021). Taraxacum mongolicum extract inhibited malignant phenotype of triple-negative breast cancer cells in tumor-associated macrophages microenvironment through suppressing IL-10/STAT3/PD-L1 signaling pathways. *J. Ethnopharmacol.* 274, 113978. doi:10.1016/j.jep.2021.113978

Duan, X., Pan, L., Deng, Y., Liu, Y., Han, X., Fu, H., et al. (2021). Dandelion root extract affects ESCC progression via regulating multiple signal pathways. *Food Funct.* 12, 9486–9502. doi:10.1039/d1fo01093j

Eghlimi, R., Shi, X., Hrovat, J., Xi, B., and Gu, H. (2020). Triple negative breast cancer detection using LC-MS/MS lipidomic profiling. *J. Proteome Res.* 19, 2367–2378. doi:10.1021/acs.jproteome.0c00038

Gandhi, N., and Das, G. M. (2019). Metabolic reprogramming in breast cancer and its therapeutic implications. *Cells* 8, E89. doi:10.3390/cells8020089

Gauhar, R., Hamayun, M., Iqbal, A., Khan, S. A., Khan, H., Shehzad, A., et al. (2017). Effect of methanolic extract of dandelion roots on cancer cell lines and AMP-activated protein kinase pathway. *Front. Pharmacol.* 8, 875. doi:10.3389/fphar.2017.00875

Gibellini, F., and Smith, T. K. (2010). The Kennedy pathway--De novo synthesis of phosphatidylethanolamine and phosphatidylcholine. *IUBMB Life* 62, 414–428. doi:10.1002/iub.337

Gong, Y., Ji, P., Yang, Y. S., Xie, S., Yu, T. J., Xiao, Y., et al. (2021). Metabolic-pathway-based subtyping of triple-negative breast cancer reveals potential therapeutic targets. *Cell Metab.* 33, 51–64.e9. doi:10.1016/j.cmet.2020.10.012

Griffiths, B., Lewis, C. A., Bensaad, K., Ros, S., Zhang, Q., Ferber, E. C., et al. (2013). Sterol regulatory element binding protein-dependent regulation of lipid synthesis supports cell survival and tumor growth. *Cancer Metab.* 1, 3. doi:10.1186/2049-3002-1-3

Grinde, M. T., Skrbo, N., Moestue, S. A., Rodland, E. A., Borgan, E., Kristian, A., et al. (2014). Interplay of choline metabolites and genes in patient-derived breast cancer xenografts. *Breast Cancer Res.* 16, R5. doi:10.1186/bcr3597

Gu, J., Gui, Y., Chen, L., Yuan, G., Lu, H. Z., and Xu, X. (2013). Use of natural products as chemical library for drug discovery and network pharmacology. *Plos One* 8, e62839. doi:10.1371/journal.pone.0062839

Hilvo, M., Denkert, C., Lehtinen, L., Muller, B., Brockmoller, S., Seppanen-Laakso, T., et al. (2011). Novel theranostic opportunities offered by characterization of altered membrane lipid metabolism in breast cancer progression. *Cancer Res.* 71, 3236–3245. doi:10.1158/0008-5472.CAN-10-3894

Hoxhaj, G., and Manning, B. D. (2020). The PI3K-AKT network at the interface of oncogenic signalling and cancer metabolism. *Nat. Rev. Cancer* 20, 74–88. doi:10.1038/s41568-019-0216-7

Hopperton, K. E., Duncan, R. E., Bazinet, R. P., and Archer, M. C. (2014). Fatty acid synthase plays a role in cancer metabolism beyond providing fatty acids for phospholipid synthesis or sustaining elevations in glycolytic activity. *Exp. Cell Res.* 320, 302–310. doi:10.1016/j.yexcr.2013.10.016

Keiser, M. J., Roth, B. L., Armbruster, B. N., Ernsberger, P., and Shoichet, B. K. (2007). Relating protein pharmacology by ligand chemistry. *Nat. Biotechnol.* 25, 197–206. doi:10.1038/nbt1284

Kim, S., Chen, J., Cheng, T., Gindulyte, A., He, J., He, S., et al. (2019). PubChem 2019 update: Improved access to chemical data. *Nucleic Acids Res.* 47, D1102–D1109. doi:10.1093/nar/gky1033

Li, F. S., and Weng, J. K. (2017). Demystifying traditional herbal medicine with modern approach. *Nat. Plants* 3, 17109. doi:10.1038/nplants.2017.109

Li, S., and Zhang, B. (2013). Traditional Chinese medicine network pharmacology: Theory, methodology and application. *Chin. J. Nat. Med.* 11, 110–120. doi:10.1016/s1875-5364(13)60037-0

Li, X., Chen, Z., Li, Y., Liang, H., Wang, H., and Li, M. (2021). Optical tweezers study of membrane fluidity in small cell lung cancer cells. *Opt. Express* 29, 11976–11986. doi:10.1364/oe.420288

Li, X. H., He, X. R., Zhou, Y. Y., Zhao, H. Y., Zheng, W. X., Jiang, S. T., et al. (2017). Taraxacum mongolicum extract induced endoplasmic reticulum stress associated-apoptosis in triple-negative breast cancer cells. *J. Ethnopharmacol.* 206, 55–64. doi:10.1016/j.jep.2017.04.025

Li, X., Nakayama, K., Goto, T., Kimura, H., Akamatsu, S., Hayashi, Y., et al. (2021). High level of phosphatidylcholines/lysophosphatidylcholine ratio in urine is associated with prostate cancer. *Cancer Sci.* 112, 4292–4302. doi:10.1111/cas.15093

Liu, Y.-J., Shieh, P.-C., Lee, J.-C., Chen, F.-A., Lee, C.-H., Kuo, S.-C., et al. (2014). Hypolipidemic activity of Taraxacum mongolicum associated with the activation of AMP-activated protein kinase in human HepG2 cells. *Food & Funct.* 5, 1744–1762. doi:10.1039/c4fo00183d

Mao, X., Lei, H., Yi, T., Su, P., Tang, S., Tong, Y., et al. (2022). Lipid reprogramming induced by the TFEB-ERRα axis enhanced membrane fluidity to promote EC progression. *J. Exp. Clin. Cancer Res.* 41, 28. doi:10.1186/s13046-021-02211-2

Martinez, M., Poirrier, P., Chamy, R., Prufer, D., SChulze-Gronover, C., Jorquera, L., et al. (2015). *Taraxacum officinale* and related species-An ethnopharmacological review and its potential as a commercial medicinal plant. *J. Ethnopharmacol.* 169, 244–262. doi:10.1016/j.jep.2015.03.067

González-Castejón, M., Garcia-Carrasco, B., Fernandez-Dacosta, R., Davalos, A., and Rodriguez-Casado, A. (2013). Reduction of adipogenesis and lipid accumulation byTaraxacum officinale(dandelion) extracts in 3T3L1 adipocytes: Anin vitroStudy. *Phytother. Res.* 28, 745–752. doi:10.1002/ptr.5059

Miyake, T., and Parsons, S. J. (2012). Functional interactions between Choline kinase α, epidermal growth factor receptor and c-Src in breast cancer cell proliferation. *Oncogene* 31, 1431–1441. doi:10.1038/onc.2011.332

Peck, B., Schug, Z. T., Zhang, Q., Dankworth, B., Jones, D. T., Smethurst, E., et al. (2016). Inhibition of fatty acid desaturation is detrimental to cancer cell survival in metabolically compromised environments. *Cancer Metab.* 4, 6. doi:10.1186/s40170-016-0146-8

Peck, B., and Schulze, A. (2016). Lipid desaturation - the next step in targeting lipogenesis in cancer? *FEBS J.* 283, 2767–2778. doi:10.1111/febs.13681

Piñero, J., Bravo, A., Queralt-Rosinach, N., Gutierrez-Sacristan, A., Deu-Pons, J., Centeno, E., et al. (2017). DisGeNET: A comprehensive platform integrating information on human disease-associated genes and variants. *Nucleic Acids Res.* 45, D833–D839. doi:10.1093/nar/gkw943

Qu, J., Ke, F., Liu, Z., Yang, X., Li, X., Xu, H., et al. (2022). Uncovering the mechanisms of dandelion against triple-negative breast cancer using a combined network pharmacology, molecular pharmacology and metabolomics approach. *Phytomedicine.* 99, 153986. doi:10.1016/j.phymed.2022.153986

Saati, G. E., and Archer, M. C. (2011). Inhibition of fatty acid synthase and Sp1 expression by 3, 3′-diindolylmethane in human breast cancer cells. *Nutr. Cancer* 63, 790–794. doi:10.1080/01635581.2011.570896

Sanchez-Lopez, E., Zimmerman, T., Gomez del Pulgar, T., Moyer, M. P., Lacal Sanjuan, J. C., and CebriAn, A. (2013). Choline kinase inhibition induces exacerbated endoplasmic reticulum stress and triggers apoptosis via CHOP in cancer cells. *Cell Death Dis.* 4, e933. doi:10.1038/cddis.2013.453

Stelzer, G., Rosen, N., Plaschkes, I., Zimmerman, S., Twik, M., Fishilevich, S., et al. (2016). The GeneCards suite: From gene data mining to disease genome sequence analyses. *Curr. Protoc. Bioinforma.* 54, 1.30.1–1.30.33. doi:10.1002/cpbi.5

Sun, X., Wang, M., Wang, M., Yu, X., Guo, J., Sun, T., et al. (2020). Metabolic reprogramming in triple-negative breast cancer. *Front. Oncol.* 10, 428. doi:10.3389/fonc.2020.00428

Tonje, H., Leslie, E., Guro, G., and Tone, B. (2017). Metabolic portraits of breast cancer by HR MAS MR spectroscopy of intact tissue samples. *Metabolites* 7, 18. doi:10.3390/metabo7020018

Triki, M., Rinaldi, G., Planque, M., Broekaert, D., Fendt, S. M., Maier, C. R., et al. (2020). mTOR signaling and SREBP activity increase FADS2 expression and can activate sapienate biosynthesis. *Cell Rep.* 31, 107806. doi:10.1016/j.celrep.2020.107806

Venkatesh, H. S., Chaumeil, M. M., Ward, C. S., Haas-Kogan, D. A., James, C. D., and Ronen, S. M. (2012). Reduced phosphocholine and hyperpolarized lactate provide magnetic resonance biomarkers of PI3K/Akt/mTOR inhibition in glioblastoma. *Neuro. Oncol.* 14, 315–325. doi:10.1093/neuonc/nor209

Vriens, K., Christen, S., Parik, S., Broekaert, D., Yoshinaga, K., Talebi, A., et al. (2019). Evidence for an alternative fatty acid desaturation pathway increasing cancer plasticity. *Nature* 566, 403–406. doi:10.1038/s41586-019-0904-1

Wang, C., Kar, S., Lai, X., Cai, W., Arfuso, F., Sethi, G., et al. (2018). Triple negative breast cancer in Asia: An insider's view. *Cancer Treat. Rev.* 62, 29–38. doi:10.1016/j.ctrv.2017.10.014

Wang, S., Fu, J. L., Hao, H. F., Jiao, Y. N., Li, P. P., and Han, S. Y. (2021). Metabolic reprogramming by traditional Chinese medicine and its role in effective cancer therapy. *Pharmacol. Res.* 170, 105728. doi:10.1016/j.phrs.2021.105728

Wang, X., Shen, Y., Wang, S., Li, S., Zhang, W., Liu, X., et al. (2017). PharmMapper 2017 update: A web server for potential drug target identification

with a comprehensive target pharmacophore database. *Nucleic Acids Res.* 45, W356–W360. doi:10.1093/nar/gkx374

Wang, X., Wang, Z. Y., Zheng, J. H., and Li, S. (2021). TCM network pharmacology: A new trend towards combining computational, experimental and clinical approaches. *Chin. J. Nat. Med.* 1919, 1–11. doi:10.1016/s1875-5364(21)60001-8

Yamashita, Y., Nishiumi, S., Kono, S., Takao, S., Azuma, T., and Yoshida, M. (2017). Differences in elongation of very long chain fatty acids and fatty acid metabolism between triple-negative and hormone receptor-positive breast cancer. *Bmc Cancer* 17, 589. doi:10.1186/s12885-017-3554-4

Yin, L., Duan, J. J., Bian, X. W., and Yu, S. C. (2020). Triple-negative breast cancer molecular subtyping and treatment progress. *Breast Cancer Res.* 22, 61. doi:10.1186/s13058-020-01296-5

Yoshida, G. J., (2015). Metabolic reprogramming: The emerging concept and associated therapeutic strategies. *J. Exp. Clin. Cancer Res.* 34, 111–210. doi:10.1186/s13046-015-0221-y

Zhang, B., Wu, J., Guo, P., Wang, Y., Fang, Z., Tian, J., et al. (2020). Down-regulation of SREBP via PI3K/AKT/mTOR pathway inhibits the proliferation and invasion of non-small-cell lung cancer cells. *Onco. Targets. Ther.* 13, 8951–8961. doi:10.2147/ott.S266073

Zhang, H. W., Lv, C., Zhang, L. J., Guo, X., Shen, Y. W., Nagle, D. G., et al. (2021). Application of omics- and multi-omics-based techniques for natural product target discovery. *Biomed. Pharmacother.* 141, 111833. doi:10.1016/j.biopha.2021.111833

Zhang, R., Zhu, X., Bai, H., and Ning, K. (2019). Network pharmacology databases for traditional Chinese medicine: Review and assessment. *Front. Pharmacol.* 10, 123. doi:10.3389/fphar.2019.00123

Zhong, Z., Qiang, W. W., Tan, W., Zhang, H., Wang, S., Wang, C., et al. (2016). Chinese herbs interfering with cancer reprogramming metabolism. *Evid. Based. Complement. Altern. Med.* 2016, 9282813–9282910. doi:10.1155/2016/9282813

Zhu, H., Zhao, H., Zhang, L., Xu, J., Zhu, C., Zhao, H., et al. (2017). Dandelion root extract suppressed gastric cancer cells proliferation and migration through targeting lncRNA-CCAT1. *Biomed. Pharmacother.* 93, 1010–1017. doi:10.1016/j.biopha.2017.07.007

Zou, Y., Huang, L., Sun, S., Yue, F., Li, Z., Ma, Y., et al. (2021). Choline kinase alpha promoted glioma development by activating PI3K/AKT signaling pathway. *Cancer Biother. Radiopharm.* doi:10.1089/cbr.2021.0294

frontiers | Frontiers in Pharmacology

TYPE Systematic Review
PUBLISHED 06 September 2022
DOI 10.3389/fphar.2022.980650

OPEN ACCESS

EDITED BY
Xian-Jun Fu,
Shandong University of Traditional Chinese Medicine, China

REVIEWED BY
Dong Bai,
China Academy of Chinese Medical Science, China
Yunhui Chen,
Chengdu University of Traditional Chinese Medicine, China
Xuezhong Zhou,
Beijing Jiaotong University, China

*CORRESPONDENCE
Ying Gao,
gaoying973@163.com
Xinxing Lai,
new-star@163.com

SPECIALTY SECTION
This article was submitted to Ethnopharmacology, a section of the journal Frontiers in Pharmacology

RECEIVED 28 June 2022
ACCEPTED 08 August 2022
PUBLISHED 06 September 2022

CITATION
Liu T, Qin M, Xiong X, Lai X and Gao Y (2022), Multi-omics approaches for deciphering the complexity of traditional Chinese medicine syndromes in stroke: A systematic review.
Front. Pharmacol. 13:980650.
doi: 10.3389/fphar.2022.980650

Multi-omics approaches for deciphering the complexity of traditional Chinese medicine syndromes in stroke: A systematic review

Tingting Liu[1,2,3], Mingzhen Qin[1,2,3], Xuejiao Xiong[1,2,3], Xinxing Lai[1,2]* and Ying Gao[1,2,4]*

[1]Institute for Brain Disorders, Beijing University of Chinese Medicine, Beijing, China, [2]Department of Neurology, Dongzhimen Hospital, Beijing University of Chinese Medicine, Beijing, China, [3]Beijing University of Chinese Medicine, Beijing, China, [4]Chinese Medicine Key Research Room of Brain Disorders Syndrome and Treatment of the National Administration of Traditional Chinese Medicine, Beijing, China

Background: Deciphering the biological basis of traditional Chinese medicine (TCM) syndromes in complex diseases is challenging. Rapid advances in multi-omics approaches provide new opportunities to unveil the biological basis of TCM syndromes. We intend to summarize the latest significant progress and highlight the crucial value of applying multi-omics approaches to reveal TCM syndromes of stroke in a new horizon.

Methods: We systematically searched PubMed, EMBASE, Web of Science Core Collection (WOSCC), Cochrane Library, China National Knowledge Infrastructure (CNKI), Chinese Science and Technology Periodical Database (VIP), Wanfang database and China Biology Medicine Database (SinoMed) for relevant studies from their inception to 31 March 2022, and conducted a comprehensive systematic review (PROSPERO registration number: CRD42021285922).

Results: A total of 43 relevant studies were included in the final systematic review, genomics, transcriptomics, proteomics, and metabolomics were all involved. Some gene polymorphisms, differential lncRNAs, mRNAs, miRNAs, proteins, and metabolites may be associated with TCM syndromes of stroke. In addition, some studies conducted a preliminary exploration on the different diseases with the same TCM syndrome. The results showed that thioredoxin-dependent peroxidase reductase may be the specific marker protein of Liver-

Abbreviations: CHD, coronary atherosclerotic heart disease; CNKI, China National Knowledge Infrastructure; DE, dimensional gel electrophoresis; DEGs, differentially expressed genes; GP, glycoprotein; ICH, intracerebral hemorrhage; IS, ischemic stroke; MALDI-TOF-MS, matrix-assisted laser desorption/ionization time-of-flight mass spectrometry; NMR, nuclear magnetic resonance; PCR, polymerase chain reaction; SinoMed, China Biology Medicine Database; SNP, single nucleotide polymorphism; SOP, strict standard operating procedure; TCM, traditional Chinese medicine; TRAF6, tumor necrosis factor receptor-associated factor 6; UPLC-MS, ultra-performance liquid chromatography-mass spectrometry; VIP, Chinese Science and Technology Periodical Database; WOSCC, Web of Science Core Collection.

yang transforming into wind syndrome, and the network formed by mir-146b-5p, -199a-5p, and 23 targeted mRNAs may be the biomarker of Blood-stasis syndrome.

Conclusion: Multi-omics technologies have served as powerful tools to investigate the complexity of TCM syndromes and may hold the promise of promoting the modernization of TCM as well as personalized medicine of TCM in stroke.

KEYWORDS

stroke, traditional Chinese medicine, syndromes, multi-omics, systematic review

1 Introduction

Traditional Chinese medicine (TCM) has accumulated valuable medical experience over thousands of years, which has played an important role in maintaining people's health (Cheung, 2011). TCM syndrome, as one of the key concepts in TCM, is a generalization of the cause, location, nature, and developmental tendency of a disease at a specific stage and is identified through a comprehensive analysis of the clinical symptoms and signs gathered by a practitioner using inspection, auscultation, olfaction, interrogation, and palpation of the pulses (Wang and Xu, 2014; Wang and Dong, 2017). Usually, the same disease has variable TCM syndromes. Correctly identifying the TCM syndrome is the cornerstone for TCM practitioners to understand diseases and guide individualized clinical medication (Wang and Xu, 2014). However, TCM syndrome differentiation has a certain degree of complexity, ambiguity, and subjectivity (Jiang et al., 2012; Gu and Chen, 2014). Deciphering the biological basis of TCM syndromes will be conducive to objectively diagnosing syndromes, discovering the potential targets of Chinese herbal medicine, and ultimately leading to the discovery of new therapeutic drugs and promoting precision medicine in TCM.

In recent years, a series of studies have been conducted to elucidate the biological basis of TCM syndromes using low-throughput sequencing methods; however, this is insufficient due to the complexity of TCM syndromes (Hou et al., 2014; Liu et al., 2014; Han et al., 2015). With the advent of systems biology era, high-throughput, high-content genomics, transcriptomics, proteomics, and metabolomics methods, combined with robust bioinformatics and computational tools have been widely and effectively applied in the biological basis research of TCM syndromes, which have provided unparalleled information about quantities and interactions of different biomolecules at the system and whole organism levels (Gu and Chen, 2014; Guo et al., 2020). Simultaneously, considerable achievements have been made, such as the biological basis of two TCM syndromes (Cold-congealing and qi-stagnation, Qi-stagnation and blood-stasis) in coronary heart disease, transcriptomic research on two TCM syndromes (Spleen-qi deficiency, Spleen-stomach damp-heat) in chronic atrophic gastritis, and the dynamic biological network of TCM syndromes in chronic hepatitis B (Lu et al., 2019; Wu et al., 2021; You et al., 2021).

It is worth noting that stroke, as the second leading cause of death in the world and ranks first in China, has made great advances in understanding the pathophysiology with omics technology, generating a large amount of data and information at the multi-omics level (Collaborators, 2021). It is encouraging that potential biomarkers associated with etiological classification and prognosis, as well as new therapeutic targets, have been identified (Montaner et al., 2020). Notably, the application of multi-omics technology has also provided new opportunities for the elucidation of TCM syndromes for stroke, including metabolomics research on Phlegm-heat syndrome and Blood-stasis syndrome, as well as transcriptomics research on Yin syndrome and Yang syndrome (Cha et al., 2013; Cha et al., 2015; Zhao et al., 2019).

Considering that there is no comprehensive review on the current status of applying multi-omics approaches to reveal the biological basis of TCM syndromes in stroke, we conducted this systematic review to summarize the related progress, analyze the challenges that need to be addressed, and provide important insights into the biological complexity of TCM syndromes for future research.

2 Methods

This systematic review was registered in PROSPERO (CRD42021285922).

2.1 Search strategy and selection criteria

Eight electronic databases were searched without language limitation (from their inception to 31 March 2022): PubMed, EMBASE, Web of Science Core Collection (WOSCC), Cochrane Library, China National Knowledge Infrastructure (CNKI), Chinese Science and Technology Periodical Database (VIP), Wanfang database, and China Biology Medicine Database (SinoMed). All searches were conducted by combining free-

text and MESH terms, including *stroke, omics, genomics, transcriptomics, proteomics, metabolomics, multi-omics, syndrome, ZHENG,* and *traditional Chinese medicine* (Supplementary Table S1).

Two reviewers (MQ and XX) independently screened titles and abstracts and selected potential full texts for further analysis. Studies that fulfilled our pre-defined eligibility criteria were included in the review. Any disagreements were resolved through consensus or consultation with a third reviewer (XL). The detailed inclusion criteria were as follows: 1) stroke patients with specific TCM syndromes, 2) application of omics approaches to study TCM syndromes of stroke, and 3) experimental or observational studies. The exclusion criteria were as follows: 1) abstracts, editorials, letters, comments, case reports, and review papers; 2) articles on subarachnoid hemorrhage; and 3) intracerebral hemorrhage (ICH) caused by traumatic injury.

2.2 Data extraction

Data were independently extracted by two reviewers (MQ and XX) using a preformulated data collection form. A narrative summary of the results was produced according to specific data subjects: 1) the article's author and publication year; 2) study characteristics, including the study site, disease, TCM syndromes, sample size, stroke onset time, omics type, omics technology, and specimen; and 3) the main findings. For each study, all relevant data were extracted from the tables, figures, text, and supplemental materials.

2.3 Quality assessment

The quality of included studies was assessed using an 11-item checklist recommended by the Agency for Healthcare Research and Quality. If an item was answered with "No" or "Unclear," the item was scored as "0;" if the answer was "Yes," the item was scored as "1." Based on the total score (ranging from 0 to 11 points), the quality of the study was divided into high (8–11 points), fair (4–7 points), or low (< 4 points) (Hu et al., 2015; Zeng et al., 2015).

3 Results

Our systematic search yielded 2973 studies through eight electronic databases, 516 of which were excluded after duplication and 2268 were excluded after abstract review. A total of 43 relevant studies were included in the final data set after a full-text review (Figure 1) (Xiong et al., 2007; Huang et al., 2008; Jia et al., 2008; Xiao et al., 2008; Zeng et al., 2008; Zhao et al., 2008; Hu et al., 2009; Xiong et al., 2011; Shang et al., 2012; Wang et al., 2012; Cha et al., 2013; Chen et al., 2013; Xie et al., 2013; Li et al., 2014; Yang et al., 2014; Cha et al., 2015; Shen et al., 2015; Gu et al., 2016a; Gu et al., 2016b; Gu et al., 2016c; Gu et al., 2016d; Huo and Tan, 2016; Liao et al., 2016; Wang et al., 2016; Gu et al., 2017; Zhao et al., 2018; Gu et al., 2019a; Gu et al., 2019b; Gu et al., 2019c; Gu et al., 2019d; Li et al., 2019; Liu et al., 2019; Wei et al., 2019; Yang et al., 2019; Zhang et al., 2019; Zhao et al., 2019; Zhu et al., 2019; Gu et al., 2020a; Gu et al., 2020b; Rong and Li, 2020; Zhang et al., 2020; Gu et al., 2021; Li et al., 2022).

Overall, 43 studies ranged in size from eight to 1802 participants, of which 41 studies were conducted in China (Xiong et al., 2007; Huang et al., 2008; Jia et al., 2008; Xiao et al., 2008; Zeng et al., 2008; Zhao et al., 2008; Hu et al., 2009; Xiong et al., 2011; Shang et al., 2012; Wang et al., 2012; Chen et al., 2013; Xie et al., 2013; Li et al., 2014; Yang et al., 2014; Shen et al., 2015; Gu et al., 2016a; Gu et al., 2016b; Gu et al., 2016c; Gu et al., 2016d; Huo and Tan, 2016; Liao et al., 2016; Wang et al., 2016; Gu et al., 2017; Zhao et al., 2018; Gu et al., 2019a; Gu et al., 2019b; Gu et al., 2019c; Gu et al., 2019d; Li et al., 2019; Liu et al., 2019; Wei et al., 2019; Yang et al., 2019; Zhang et al., 2019; Zhao et al., 2019; Zhu et al., 2019; Gu et al., 2020a; Gu et al., 2020b; Rong and Li, 2020; Zhang et al., 2020; Gu et al., 2021; Li et al., 2022), and two in South Korea (Cha et al., 2013; Cha et al., 2015). Of these, 32 studies enrolled patients with ischemic stroke (IS) (Huang et al., 2008; Jia et al., 2008; Zeng et al., 2008; Hu et al., 2009; Shang et al., 2012; Wang et al., 2012; Cha et al., 2013; Xie et al., 2013; Li et al., 2014; Cha et al., 2015; Shen et al., 2015; Gu et al., 2016a; Gu et al., 2016b; Gu et al., 2016c; Gu et al., 2016d; Huo and Tan, 2016; Liao et al., 2016; Wang et al., 2016; Gu et al., 2017; Gu et al., 2019a; Gu et al., 2019b; Gu et al., 2019c; Gu et al., 2019d; Liu et al., 2019; Zhao et al., 2019; Zhu et al., 2019; Gu et al., 2020a; Gu et al., 2020b; Rong and Li, 2020; Zhang et al., 2020; Gu et al., 2021; Li et al., 2022), nine with ICH (Xiong et al., 2007; Xiao et al., 2008; Zhao et al., 2008; Chen et al., 2013; Yang et al., 2014; Zhao et al., 2018; Li et al., 2019; Yang et al., 2019; Zhang et al., 2019), one with stroke complications (Wei et al., 2019), and one with both IS and ICH (Tables 1–T4) (Xiong et al., 2011). Genomics, transcriptomics, proteomics, and metabolomics were involved in the omics approaches (Table 5). The quality of all the studies was fair (Supplementary Table S2).

3.1 Genomic studies on traditional Chinese medicine syndromes of stroke

Human genomics, the study of the structure, function, and interactions of all genes in the human genome, are widely used to elucidate the scientific basis of TCM syndrome differentiation (Lazaridis and Petersen, 2005). In this section, 25 studies (Huang et al., 2008; Jia et al., 2008; Hu et al., 2009; Shang et al., 2012; Xie et al., 2013; Shen et al., 2015; Gu et al., 2016a; Gu et al., 2016b; Gu et al., 2016c; Gu et al., 2016d; Huo and Tan, 2016; Wang et al.,

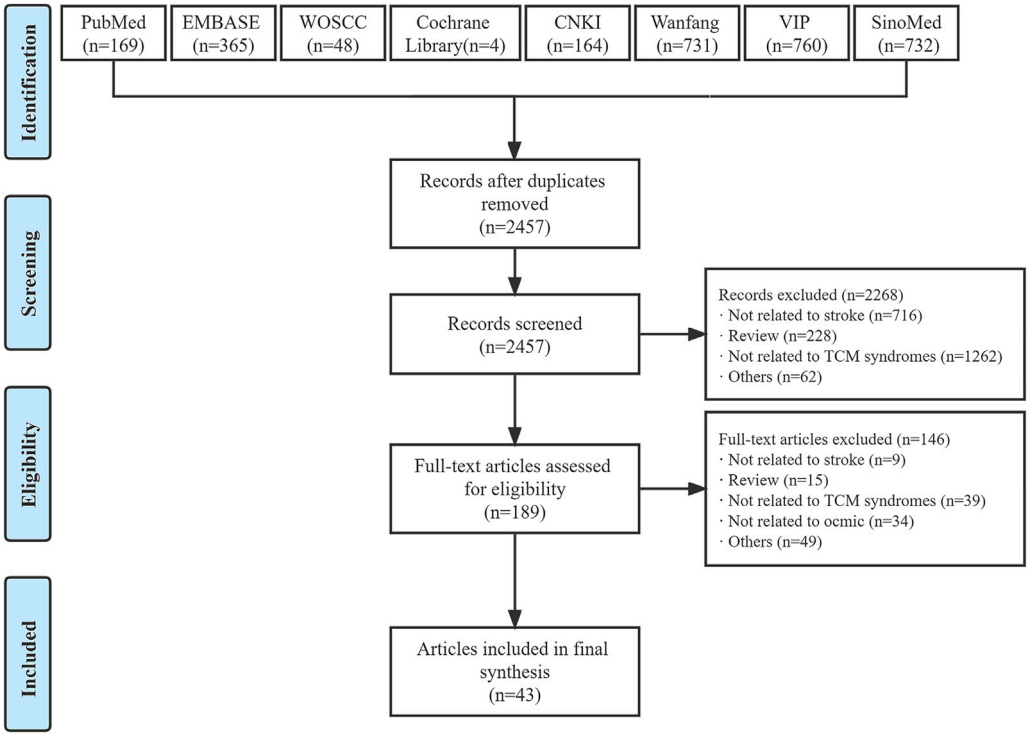

FIGURE 1
Flow diagram of study selection. CNKI, China National Knowledge Infrastructure; TCM, traditional Chinese medicine; VIP, Chinese Science and Technology Periodical Database; WOSCC, Web of Science Core Collection.

2016; Gu et al., 2017; Zhao et al., 2018; Gu et al., 2019a; Gu et al., 2019b; Gu et al., 2019c; Gu et al., 2019d; Li et al., 2019; Wei et al., 2019; Zhu et al., 2019; Gu et al., 2020a; Gu et al., 2020b; Zhang et al., 2020; Gu et al., 2021), containing IS, ICH and post-stroke cognitive impairment, mainly covered research on single nucleotide polymorphisms (SNP) and differentially expressed genes (DEGs) (Table 1).

3.1.1 Ischemic stroke

Genomics studies on TCM syndromes of IS have focused on SNP, which are the most common cause of DNA sequence polymorphism (Griffin and Smith, 2000). To some extent, SNP has few similarities with the "Innate Endowmentt" of TCM, which may affect an individual's susceptibility to a specific TCM syndrome (Yang et al., 2021). All included studies collected peripheral venous blood at baseline to extract DNA, and then carried out primer design, synthesis, and polymerase chain reaction (PCR) amplification. Finally, specific technology was used for SNP genotyping.

Most studies found that some gene polymorphisms may be pivotal in the occurrence of Wind-phlegm stagnation syndrome of IS, including the platelet glycoprotein Iba (GP Iba) gene *VNTR*, toll-like receptor 5 gene *rs5744174*, toll-like receptor 7 gene *rs2897827*, and tumor necrosis factor receptor-associated factor 6 (*TRAF6*) gene *rs5030416* (Shang et al., 2012; 2016; Gu et al., 2016c; Wang et al., 2016; Gu et al., 2017). Likewise, some gene polymorphisms, such as the GP Iba gene *VNTR* and *CYP2C19* gene may be associated with Qi-deficiency and blood-stasis syndrome in IS (Shang et al., 2012; Zhang et al., 2020). Additionally, methylenetetrahydrofolate reductase *C677T* and selenocysteine insertion sequence binding protein 2 gene *rs3211703* may be related to the pathogenesis of Blood-stasis syndrome of IS (Hu et al., 2009).

In addition to elucidating the scientific basis of TCM syndromes, researchers also revealed the relationships between gene polymorphisms and bodily functions in IS patients with specific TCM syndromes, including coagulation function, immunity, and blood lipid metabolism. The findings included the linkage between fibrinogen β-148C/T and coagulation function in patients with Wind-phlegm obstructing the meridians syndrome (Huo and Tan, 2016), between *TRAF6* gene *rs5030411* and inflammatory reaction in patients with Wind-phlegm stasis syndrome (Gu et al., 2017), and between myeloid differentiation factor 88 gene *rs7744*, histone deacetylase 9 gene *rs2107595* and coagulation function in patients with

TABLE 1 Summary of the main findings of the included genomics studies.

Source	Sites	Disease	TCM syndromes	Sample size	Onset time	Specimen	Technology	Main findings
Genomics								
Jia et al. (2008)	China	IS	Phlegm; Qi-deficiency	226	≤7 days	Plasma	ARMS-PCR	Angiotensin converting enzyme gene D allele may be related to Phlegm, I allele may be related to Qi-deficiency
Huang et al. (2008)	China	IS	Hyperactive liver-yang; Wind-phlegm and blood-stasis	104	NA	PVB	PCR-RFLP	Angiotensinogen gene M235T No correlation with TCM syndromes
Hu et al. (2009)	China	IS	Blood-stasis	227	NA	PVB	PCR-RFLP	Methylenetetrahydrofolate reductase gene C677T TT genotype may be related to Blood-stasis
Shang et al. (2012)	China	IS	Phlegm-heat and fu-organ excess; Qi-deficiency and blood-stasis; Wind-phlegm and fire-hyperactivity; Wind-phlegm stagnation; Wind-stirring due to yin-deficiency	390	NA	PVB	PCR-RFLP	Platelet membrane glycoprotein Iba ·VNTRBC CD genotype may be related to Qi-deficiency and blood-stasis; BC, BD, AC genotype and B allele may be related to Wind-phlegm stagnation ·HPA-2 No correlation with TCM syndromes
Xie et al. (2013)	China	IS	Blood-stasis; Phlegm-stasis	340	NA	PVB	TaqMan	Chromosome 12p13 rs12425791 No correlation with TCM syndromes
Shen et al. (2015)	China	IS	Qi-deficiency and blood-stasis	889	NA	Leucocyte	Sequenom MassARRAY	rs2107595 May be related to blood lipid metabolism of patients with Qi-deficiency and blood-stasis
Huo and Tan, (2016)	China	IS	Hyperactive liver-yang; Qi-deficiency and blood-stasis; Wind-stirring due to yin-deficiency; Wind-phlegm obstructing the meridians	110	<7 days	PVB	PCR-RELP	Fibrinogen β-148C/T gene May be related to the fibrinogen level of TT genotype carriers with Wind-phlegm obstructing the meridians
Wang et al. (2016)	China	IS	Qi-deficiency and blood-stasis; Wind-phlegm stagnation	1200	NA	PVB	Sequenom MassARRAY	Toll-like receptor 5 gene rs5744174 The recessive model may be related to Wind-phlegm stagnation
Gu et al. (2016a)	China	IS	Wind-phlegm stagnation	916	NA	PVB	Sequenom MassARRAY	Histone deacetylase 9 gene rs2107595 May be related to blood lipid metabolism of patients with Wind-phlegm stasis
Gu et al. (2016b)	China	IS	Qi-deficiency and blood-stasis; Wind-phlegm stagnation	1200	≤7 days	PVB	Sequenom MassARRAY	MAP2K1 gene ·rs9340 May be related to Wind-phlegm stagnation in men, and levels of TG in patients with Qi-deficiency and blood-stasis ·rs6928 May be related to levels of TG and HDL in patients with Qi-deficiency and blood-stasis MAPK4 gene No correlation with TCM syndromes
Gu et al. (2016c)	China	IS	Qi-deficiency and blood-stasis; Wind-phlegm stagnation	1200	≤7 days	PVB	Sequenom MassARRAY	Toll-like receptor 7 gene rs2897827 May be related to Wind-phlegm stagnation
Gu et al. (2016d)	China	IS	Qi-deficiency and blood-stasis; Wind-phlegm stagnation	1200	NA	PVB	Sequenom MassARRAY	Myeloid differentiation factor 88 gene rs7744 May be related to blood lipid metabolism in patients with Wind-phlegm stagnation

(Continued on following page)

TABLE 1 (*Continued*) Summary of the main findings of the included genomics studies.

Source	Sites	Disease	TCM syndromes	Sample size	Onset time	Specimen	Technology	Main findings
Gu et al. (2017)	China	IS	Qi-deficiency and blood-stasis; Wind-phlegm stagnation	1200	NA	PBMCs	Sequenom MassARRAY	Tumor necrosis factor receptor-associated factor 6 gene ·rs5030416 The recessive model may be related to Wind-phlegm stagnation ·rs5030411 May engage in the inflammatory reaction of patients with Wind-phlegm stagnation
Zhu et al. (2019)	China	IS	Blood-stasis; Phlegm; Wind	527	NA	PVB	Sanger	Histone deacetylase 9 gene rs2240419 No correlation with TCM syndromes
Gu et al. (2019a)	China	IS	Phlegm-stasis	1100	NA	PVB	Sequenom MassARRAY	Signal transducer and activator of transcription 5 gene rs319502 May be related to coagulation and inflammatory reaction in patients with Phlegm-stasis
Gu et al. (2020a)	China	IS	Blood-stasis; Fire-heat; Phlegm; Qi-deficiency; Wind	1802	≤7 days	PVB	Sequenom MassARRAY	Selenocysteine insertion sequence binding protein 2 gene rs3211703 May be related to 2 TCM syndromes (Blood-stasis, Qi-deficiency)
Zhang et al. (2020)	China	IS	Phlegm-heat and fu-organ excess; Qi-deficiency and blood-stasis; Wind-stirring due to yin-deficiency; Wind-phlegm obstructing the meridians	70	NA	PVB	NA	CYP2C19 gene CYP2C19 * 2 gene mutation may be related to Qi-deficiency and blood-stasis
Gu et al. (2021)	China	IS	Blood-stasis; Fire-heat; Phlegm; Qi-deficiency; Wind	1756	≤72 h	PVB	Sequenom MassARRAY	DNA polymerase kappa gene rs5744724 May be related to 2 TCM syndromes (Blood-stasis, Qi-deficiency)
Gu et al. (2019b)	China	IS; CHD	Phlegm-stasis	1650	NA	PVB	Sequenom MassARRAY	Coagulation factor X gene ·rs3093261 May be related to coagulation function in Phlegm-stasis both IS and CHD ·rs563964 No correlation with TCM syndromes
Gu et al. (2019c)	China	IS; CHD	Phlegm-stasis	1650	NA	PVB	Sequenom MassARRAY	EP300gene rs20551 May be related to coagulation function in Phlegm-stasis both IS and CHD
Gu et al. (2019d)	China	IS; CHD	Phlegm-stasis	1650	NA	PVB	Sequenom MassARRAY	Kinase insert domain receptor gene rs2305948, rs2239702 May be related to the coagulation function in Phlegm-stasis both IS and CHD
Gu et al. (2020b)	China	IS, CHD	Phlegm-stasis	1650	NA	PVB	Sequenom MassARRAY	Decorin gene rs7441 May be related to the lipid metabolism in patients with Phlegm-stasis of IS and the coagulation function in patients with Phlegm-stasis of CHD
Zhao et al. (2018)	China	ICH	Stasis-heat	18	≤48 h	Lymphocytes	Microarray chips	Identified 4,744 differential genes: 2867↑, 1877↓ The essence of Stasis-heat was related to coagulation and inflammatory pathology
Li et al. (2019)	China	ICH	Hyperactive liver-yang	15	NA	Fecal samples	16S rRNA	Decrease in relative abundance of prevotella and ackermann Myxobacteria

(Continued on following page)

TABLE 1 (*Continued*) Summary of the main findings of the included genomics studies.

Source	Sites	Disease	TCM syndromes	Sample size	Onset time	Specimen	Technology	Main findings
Wei et al. (2019)	China	PSCI	Blood-stasis obstructing the meridians; Fu-organ turbidness stagnation; Heat-toxin exuberance; Hyperactive liver-yang; Kidney-essence deficiency; Phlegm-turbidity obstructing the orifices; Qi-blood deficiency	190	NA	Leucocytes	PCR-RFLP	Methyl-tetrahydrofolate reductase gene G677T CT genotype may be related to Phlegm-turbidity obstructing the orifices and Blood-stasis obstructing the meridians, TT genotype may be related to Kidney-essence deficiency

ARMS-PCR, amplification refractory mutation system-polymerase chain reaction; CHD, coronary atherosclerotic heart disease; HDL, high density lipoprotein; ICH, intracerebral hemorrhage; IS, ischemic stroke; NA, not available; PBMCs, peripheral blood mononuclear cells; PCR-RFLP, polymerase chain reaction-restriction fragment length polymorphism; PSCI, post-stroke cognitive impairment; PVB, peripheral venous blood; TG, triglyceride; TCM, traditional Chinese medicine; UA, unstable angina.

TABLE 2 Summary of the main findings of the included transcriptomics studies.

Source	Sites	Disease	TCM syndromes	Sample size	Onset time	Specimen	Technology	Main findings
Zhao et al. (2018)	China	IS	Yang; Yin	22	≤6 h	Lymphocytes	Microarray chips	Yang related miRNAs: hsa-miR-93-5p, miR-320b, miR-320a, miR-128, and miR-181a-5p; Yin related miRNAs: hsa-miR-424-5p, miR-7-5p, miR-106b-5p, miR-19a-3p, and miR-301a-3p
Liu et al. (2019)	China	IS	Yang; Yin	30	NA	Serum	Microarray chips	Yang: identified 227 lncRNAs (73↑, 154↓), 54 mRNAs (21↑, 33↓), and 4 miRNAs; Yin: identified 394 lncRNAs (283↑, 111↓), 206 mRNAs (177↑, 29↓)
Liao et al. (2016)	China	IS; UA	Blood-stasis	15	≤48 h	PBMCs	Microarray chips	MiR-146b-5p, -199a-5p and 23 targeted mRNAs formed network-type biomarkers for Blood-stasis

(↑) upregulated; (↓) downregulated; IS, ischemic stroke; NA, not available; PBMCs, peripheral blood mononuclear cells; UA, unstable angina.

Wind-phlegm stagnation syndrome (Gu et al., 2016a; Zhu et al., 2019).

In particular, three studies focused on different diseases with the same TCM syndrome, including Phlegm-stasis syndrome in patients with IS or coronary atherosclerotic heart disease (CHD). The results showed that coagulation factor X gene *rs3093261*, *EP300* gene *rs20551*, and kinase insert domain receptor genes *rs2305948* and *rs2239702* may be related to the coagulation function in patients with Phlegm-stasis syndrome of IS and CHD, which indicated that different diseases with the same TCM syndrome may have the same biological basis (Gu et al., 2019b; Gu et al., 2019c; Gu et al., 2019d).

3.1.2 Intracerebral hemorrhage

Stasis-heat syndrome and Hyperactive liver-yang syndrome were the main syndromes of ICH in the two included studies, wherein the biological basis of TCM syndromes was investigated using DEGs. On the one hand, a total of 4,744 DEGs were identified in patients with Stasis-heat syndrome by using microarray chips to analyze lymphocytes (Zhao et al., 2018). Among these DEGs, few were further verified by real-time quantitative PCR, indicating that the Stasis-heat syndrome was intrinsically associated with coagulation and inflammatory pathology. On the other hand, fecal samples from patients were tested using the Illumina MiSeq platform, indicating that the Hyperactive liver-yang syndrome was related to the structural disorder of intestinal flora, with a reduced relative abundance of *Prevotella* and *Ackermann myxobacteria* (Li et al., 2019).

3.1.3 Post-stroke cognitive impairment

One study investigated the relationship between gene polymorphisms and TCM syndromes of post-stroke cognitive impairment using PCR-restriction fragment length polymorphism technology (Wei et al., 2019). Kidney-essence deficiency syndrome, Phlegm-turbidity obstructing the orifice syndrome, and Blood-stasis obstructing the meridians syndrome, all had a significant correlation with *MTHFR* gene *C677T* locus polymorphisms. Further correlation analysis showed that the former TCM syndrome was associated with the TT genotype, and the two latter TCM syndromes were associated with the CT genotype.

TABLE 3 Summary of the main findings of the included proteomics studies.

Source	Sites	Disease	TCM syndromes	Sample size	Onset time	Specimen	Technology	Main findings
Zeng et al. (2008)	China	IS	Liver-yang transforming into wind; Wind-stirring due to yin-deficiency	45	NA	Lymphocytes	2-DE; MALDI-TOF-MS	Identified 15 differential proteins, including capping protein, adenylyl cyclase-associated protein 1 and platelet thrombin sensitive protein-1
Xiong et al. (2011)	China	ICH; IS; CS; PD	Liver-yang transforming into wind; Hyperactive liver-yang; Wind-stirring due to yin-deficiency; Wind-stirring due to blood-deficiency	135	NA	PBMCs	2-DE; MALDI-TOF-MS	Thioredoxin-dependent peroxide reductase may be a specific marker protein of Liver yang transforming into wind
Wang et al. (2012)	China	IS	Liver-yang transforming into wind; Wind-stirring due to yin-deficiency	42	NA	Serum	2-DE; MALDI-TOF-MS	Liver-yang transforming into wind: 7 proteins↑ (ceruloplasmin, monocyte chemotaxis protein-1, c-reactive protein, etc.); Wind-stirring due to yin-deficiency: 5 proteins↑ (neuronspecific enolase, glycoprotein, signaling protein, etc.)
Li et al. (2014)	China	IS	Blood-stasis	27	≤72 h	Plasma	2-DE; MALDI-TOF-MS	Identified 6 differential proteins: 5↑ (haptoglobin, fibrinogen gamma chain, gamma-actin, SP40/40, vascular Rab-GAP/TBC-containing protein), 1↓ (TROVE domain family, member 2)
Zhao et al. (2008)	China	ICH	Liver-yang transforming into wind	20	NA	Lymphocytes	2-DE; MALDI-TOF-MS	Identified 8 differential proteins: 6↓ (alpha-enolase, apolipoprotein A-1, fibrinogen alpha chain, etc.),1↑ (hypothetical protein), 1 missing
Xiong et al. (2007)	China	HICH; HTN	HICH: liver-yang transforming into wind; HTN: hyperactive liver-yang	50	NA	Serum	2-DE; MALDI-TOF-MS	Identified 5 differential proteins, such as amyloid precursor protein, ceruloplasmin and vitamin D-binding protein
Xiao et al. (2008)	China	HICH; HTN	HICH: liver-yang transforming into wind; HTN: hyperactive liver-yang	45	NA	Lymphocytes	2-DE; MALDI-TOF-MS	Identified 16 differential proteins: 3↑ (gamma-actin, glutathione s-transferase omega-1, filamentous actin), 13↓ (zinc-binding protein, capping protein, thioredoxin-dependent peroxide reductase, etc.)
Chen et al. (2013)	China	ICH	Wind-stirring due to yin-deficiency	30	NA	Lymphocytes	2-DE; MALDI-TOF-MS	Identified 10 differential proteins: 5↑ (FilaminA, glucose-regulated protein, Zyxin protein, etc.), 4↓ (fibrinogen beta chain precursor, cofilin-1, hypothetical protein, glyceraldehyde-3-phosphate dehydrogenase), 1 missing
Yang et al. (2014)	China	ICH	Liver-yang transforming into wind	20	≤72 h	Lymphocytes	2-DE; MALDI-TOF-MS	Identified 3 differential proteins: actin, hypothetical protein and fibrinogen alpha chain precursor
Zhang et al. (2019)	China	ICH	Stasis-heat	8	≤48 h	Plasma	Tandem Mass Tag; UPLC-MS	Identified 7 differential proteins, such as ceruloplasmin, alpha-1B-glycoprotein, and carbonic anhydrase-1. Stasis-heat was related to inflammatory reaction and coagulation related to dysfunction

(↑) upregulated; (↓) downregulated; CS, cervical spondylosis; HICH, hypertensive intracerebral hemorrhage; HTN, hypertension; ICH, intracerebral hemorrhage; IS, ischemic stroke; MALDI-TOF-MS, matrix-assisted laser desorption/ionization time-of-flight mass spectrometry; NA, not available; PBMCs, peripheral blood mononuclear cells; PD, Parkinson's disease; 2-DE, two-dimensional gel electrophoresis; UPLC-MS, ultra-performance liquid chromatography-mass spectrometry.

TABLE 4 Summary of the main findings of the included metabolomics studies.

Source	Sites	Disease	TCM syndromes	Sample size	Onset time	Specimen	Technology	Main findings
Cha et al. (2013)	Korean	IS	Phlegm-dampness	141	≤72 h	Plasma	UHPLC-MS	Plasma lysophosphatidylcholines with polyunsaturated fatty acid groups were associated with Phlegm-dampness
Cha et al. (2015)	Korean	IS	Blood-stasis	62	≤30 days	Plasma	UPLC-Q-TOF-MS	7 metabolites were related to Blood-stasis, including acyl-carnitines, creatinine and kynureninem
Rong and Li, (2020)	China	IS	Phlegm-dampness	31	≤72 h	Serum	NMR	30 metabolites were potential biomarkers for Phlegm-dampness, including 1-methyl histidine, alanine and acetic acid
Li et al. (2022)	China	IS	Yang-deficiency	20	>4 w	Serum	GC-TOF-MS	27 metabolites were related to Yang-deficiency, including glycine, fumaric acid, and aspartic acid
Yang et al. (2019)	China	ICH	Stasis-heat	120	≤48 h	Plasma	UPLC-MS	Cortisone 21 acetate, methyl acetate and triglyceride were potential biomarkers for Stasis-heat

GC-TOF-MS, gas chromatography-time of flight-mass spectrometry; ICH, intracerebral hemorrhage; IS, ischemic stroke; NMR, nuclear magnetic resonance; UHPLC-MS, ultra-high performance liquid chromatography-mass spectrometry; UPLC-MS, ultra-performance liquid chromatography-mass spectrometry; UPLC-Q-TOF-MS, ultra-performance liquid chromatography-quadrupole-time offlight-mass spectrometry.

3.2 Transcriptomic studies on traditional Chinese medicine syndromes of stroke

Transcriptomics is the study of all transcripts in cells using microarray or RNA sequencing, including coding and non-coding RNAs, which is beneficial for revealing the intrinsic regulatory mechanisms of TCM syndromes (Manzoni et al., 2018; Montaner et al., 2020). Microarray technology is limited by the amount of RNA, quantification of transcript levels, and sequence information, however, it can still reveal the biological basis of TCM syndromes to a certain extent (Mutz et al., 2013). Microarray chips were used to investigate the transcriptomic characteristics of TCM syndromes of IS in the three included studies (Table 2) (Liao et al., 2016; Liu et al., 2019; Zhao et al., 2019).

Liu et al. (2019) and Zhao et al. (2019) focused on two TCM syndromes (Yin and Yang) of IS. The former found that there were some differences in the expression profiles of lncRNA, mRNA, and miRNA between the Yin syndrome and Yang syndrome. Further enrichment analysis revealed that the phenotypic differences between the Yin syndrome and Yang syndrome may be caused by blood pressure regulation, adrenergic receptor regulation, the renin-angiotensin system, and other pathways. The latter also identified some differentially expressed miRNAs; further enrichment analysis indicated that the key regulatory miRNAs, genes and pathways in Yang syndrome were hsa-miR-93-5p and -320b, enabled homologs, metabolic pathways, and mitogen-activated protein kinase signaling pathways, respectively, while those in Yin syndrome were hsa-miR-424-5p and -106b-5p, CNOT4, hepatitis B and pathways in cancer, respectively. Liao et al. (2016) found that 401 mRNAs and 11 miRNAs were differentially expressed in two conditions (IS and unstable angina) with the same TCM syndrome (Blood-stasis). Further bioinformatics analysis with validation by real-time quantitative PCR in an independent cohort demonstrated that miR-146b-5p, -199a-5p and 23 targeted mRNAs formed network-type biomarkers for the Blood-stasis syndrome.

3.3 Proteomic studies on traditional Chinese medicine syndromes of stroke

The aim of proteomics in modern biology is to understand the expression, function, and regulation of the entire set of proteins encoded by an organism, the information of which will be invaluable for understanding how complex biological processes occur at a molecular level (Zhu et al., 2003). Proteomics research is conducive to exploring the microscopic material basis of TCM syndromes at the surface level (Zhou et al., 2012; Yang et al., 2021). At present, proteomic studies on TCM syndromes of stroke have mainly focused on exploring differential proteins (Table 3) (Xiong et al., 2007; Xiao et al., 2008; Zeng et al., 2008; Zhao et al., 2008; Xiong et al., 2011; Wang et al., 2012; Chen et al., 2013; Li et al., 2014; Yang et al., 2014; Zhang et al., 2019).

3.3.1 Ischemic stroke

A total of three studies were conducted by using two-dimensional gel electrophoresis (2DE) combined with matrix-assisted laser desorption/ionization time-of-flight mass spectrometry (MALDI-TOF-MS) analyses, in which Blood-stasis syndrome and Liver-yang transforming into wind syndrome of IS were investigated (Zeng et al., 2008; Wang et al., 2012; Li et al., 2014). Six differentially expressed proteins were identified in Blood-stasis syndrome of IS, of which one protein (TROVE domain family, member 2) was

TABLE 5 Summary of TCM syndromes and omics methods in studies included.

TCM syndromes of stroke	Number of genomics studies		Number of transcriptomics studies	Number of proteomics studies	Number of metabonomics studies
	SNP	DEGs			
IS					
Blood-stasis	5	0	1	1	1
Fire-heat	2	0	0	0	0
Hyperactive liver-yang	2	0	0	0	0
Liver-yang transforming into wind	0	0	0	2	0
Phlegm	4	0	0	0	0
Phlegm-dampness	0	0	0	0	2
Phlegm-heat and fu-organ excess	2	0	0	0	0
Phlegm-stasis	6	0	0	0	0
Qi-deficiency	3	0	0	0	0
Qi-deficiency and blood-stasis	9	0	0	0	0
Wind	3	0	0	0	0
Wind-phlegm and blood-stasis	1	0	0	0	0
Wind-phlegm and fire-hyperactivity	1	0	0	0	0
Wind-phlegm obstructing the meridians	2	0	0	0	0
Wind-phlegm stagnation	7	0	0	0	0
Wind-stirring due to yin-deficiency	3	0	0	2	0
Yang	0	0	2	0	0
Yang-deficiency	0	0	0	0	1
Yin	0	0	2	0	0
ICH					
Hyperactive liver-yang	0	0	1	0	0
Liver-yang transforming into wind	0	0	0	4	0
Stasis-heat	0	0	1	1	1
Wind-stirring due to yin-deficiency	0	0	0	2	0
PSCI					
Blood-stasis obstructing the meridians	1	0	0	0	0
Fu-organ turbidness stagnation	1	0	0	0	0
Hyperactive liver-yang	1	0	0	0	0
Heat-toxin exuberance	1	0	0	0	0
Kidney-essence deficiency	1	0	0	0	0
Phlegm-turbidity obstructing the orifices	1	0	0	0	0
Qi-blood deficiency	1	0	0	0	0

DEGs, differential expression genes; ICH, intracerebral hemorrhage; IS, ischemic stroke; PSCI, post-stroke cognitive impairment; SNP, single nucleotide polymorphism; TCM, traditional Chinese medicine.

downregulated, while the others, such as haptoglobin, fibrinogen gamma chain, and gamma-actin, were upregulated (Li et al., 2014). Interestingly, Zeng et al. (2008) and Wang et al. (2012) compared the Liver-yang transforming into wind syndrome with Wind-stirring due to yin-deficiency syndrome of IS, but their results were different. The former identified 15 differentially expressed proteins, including capping protein, adenylyl cyclase-associated protein 1, and platelet thrombin sensitive protein-1. The latter identified seven upregulated proteins in the Liver-yang transforming into wind syndrome, including ceruloplasmin, monocyte chemotaxis protein-1, and c-reactive protein, and five upregulated proteins in Wind-stirring due to yin-deficiency syndrome, including neuron-specific enolase, glycoprotein, and signaling proteins.

In addition, Xiong et al. (2011) tried to reveal the biological mechanism of Liver-yang transforming into wind syndrome in four different diseases: including ICH, IS, Parkinson's disease, and cervical spondylosis. Through the application of 2DE

combined with MALDI-TOF-MS technology and further comparative analysis, the results demonstrated that thioredoxin-dependent peroxide reductase may be a common marker protein of Liver-yang transforming into wind syndrome in multiple diseases.

3.3.2 Intracerebral hemorrhage

Similar to proteomic studies on TCM syndromes of IS, there were five other studies using 2DE combined with MALDI-TOF-MS technology to carry out related TCM syndromes of ICH, including Wind-stirring due to yin-deficiency syndrome and Live-yang transforming wind syndrome (Xiong et al., 2007; Xiao et al., 2008; Zhao et al., 2008; Chen et al., 2013; Yang et al., 2014). Ten differential proteins were finally identified in Wind-stirring due to yin-deficiency syndrome, five of which were upregulated, including FilaminA, Zyxin protein, and glucose-regulated protein, while four were downregulated, including fibrinogen beta chain precursor, cofilin-1, and hypothetical protein (Chen et al., 2013). Eight differential proteins were identified in the Live-yang transforming wind syndrome, among which the hypothetical protein was upregulated, and six were downregulated, including alpha-enolase, apolipoprotein A-1, and fibrinogen alpha chain (Zhao et al., 2008). Moreover, two studies also focused on Liver-Yang transforming wind syndrome; however, they only concentrated on ICH caused by hypertension (Xiong et al., 2007; Xiao et al., 2008). In comparison with hypertensive patients with Hyperactive liver-yang syndrome and healthy individuals, one study identified five differentially expressed, including amyloid precursor protein, ceruloplasmin, and vitamin D-binding protein (Xiong et al., 2007); the other identified 16 differential proteins, three of which were upregulated, such as gamma-actin, glutathione s-transferase omega-1, and filamentous actin, while 13 were downregulated, such as zinc-binding protein, capping protein, and thioredoxin-dependent peroxide reductase (Xiao et al., 2008).

Of note, one study included 10 patients with Liver-yang transforming into wind syndrome of ICH within 3 days of onset, and thereafter observed patients whose TCM syndrome changed to Wind-stirring due to yin-deficiency syndrome within 3 months (Yang et al., 2014). Through comparative analysis before and after, actin, hypothetical protein, and fibrinogen alpha chain precursor may be closely related to the dynamic evolution of these two TCM syndromes. Furthermore, through Tandem Mass Tag combined with ultra-performance liquid chromatography-mass spectrometry (UPLC-MS), Zhang et al. (2019) finally identified seven differential proteins, such as ceruloplasmin, alpha-1B-glycoprotein, and carbonic anhydrase-1, which proved that the basis of Stasis-heat syndrome may be related to inflammatory reactions and coagulation related to dysfunctions.

3.4 Metabolomic studies on traditional Chinese medicine syndromes of stroke

Metabolomics is defined as the comprehensive analysis in which all the metabolites of a biological system are identified and quantified (Lindon and Nicholson, 2008). Unlike genes and proteins, metabolites serve as direct signatures of biochemical activity and are therefore, easier to correlate with phenotypes (Ussher et al., 2016). Nuclear magnetic resonance (NMR) spectroscopy and mass spectrometry combined with chromatography are the main primary analytical methods. In this section, five studies were included, four of which focused on TCM syndromes of IS (Cha et al., 2013; Cha et al., 2015; Rong and Li, 2020; Li et al., 2022), whereas the rest focused on TCM syndromes of ICH (Table 4) (Yang et al., 2019).

3.4.1 Ischemic stroke

Metabolomic studies on the TCM syndromes of IS carried out by different groups have helped elucidate the biological basis of TCM syndromes. Phlegm-dampness syndrome, Yang-deficiency syndrome, and Blood-stasis syndrome were the main syndromes investigated in the four included studies. There were two studies on Phlegm-dampness syndrome using different metabolomics technologies (Cha et al., 2013; Rong and Li, 2020). The former used NMR and found 30 different metabolites, including 1-methylhistidine, alanine, and acetic acid, which were potential biomarkers for the Phlegm-dampness syndrome of IS (Cha et al., 2013). The latter used UPLC-MS and found that the levels of lysophosphatidylcholine (18:2) and lysophosphatidylcholine (20:3) in the Phlegm dampness syndrome were low, suggesting that the variation in plasma lipid profiles may serve as a potential biomarker for its diagnosis (Rong and Li, 2020). In addition, Seven differential metabolites, including acyl-carnitines, creatinine, and kynureninem, were identified to be associated with Blood-stasis syndrome by using ultra-high performance liquid chromatography-quadrupole-time of flight-mass spectrometry (Yang et al., 2019). In addition, the gas chromatography-time of flight-mass spectrometry method was applied in the study of Yang-deficiency syndrome, with 27 metabolites as potential markers (Li et al., 2022).

3.4.2 Intracerebral hemorrhage

Metabolomics has also been used to gain insights into the biological basis of TCM syndromes in ICH. Yang et al. (2019) investigated the metabolomic characteristics of the Stasis-heat syndrome of ICH by analyzing peripheral blood using UPLC-

MS. The results showed that the pathogenesis of Stasis-heat syndrome of ICH was related to excess oxidative stress, inflammatory response, vascular sclerosis, and apoptosis. Moreover, the obtained cortisone 21 acetate, methyl acetate, and triglycerides could be used as potential biomarkers for the Stasis-heat syndrome of ICH.

4 Discussion

This systematic review provided a summary of the application of multi-omics approaches to reveal the biological basis of TCM syndromes in stroke. Omics data have prompted elucidation of the remarkable complexity of TCM syndromes. The current results demonstrated that some gene polymorphisms, differential lncRNAs, mRNAs, miRNAs, proteins, and metabolites may all be associated with TCM syndromes of stroke. Of note, some studies conducted a preliminary exploration of different diseases with the same TCM syndrome. The results showed that thioredoxin-dependent peroxidase reductase may be a common marker protein of Liver-yang transforming into wind syndrome, and the network formed by mir-146b-5p, -199a-5p, and 23 targeted mRNAs may be the biomarker of Blood-stasis syndrome. These results brought us closer to deciphering the biological basis of TCM syndromes in stroke, and even uncovered some potential biomarkers, especially for Liver-yang transforming into wind syndrome and Blood-stasis syndrome. With further validation, these findings may be applied to the objective diagnosis of TCM syndromes in future clinical practice and may also be potential targets of Chinese herbal medicine, which will facilitate the discovery of new therapeutic drugs. However, these results should be interpreted with caution because of the moderate quality of the included studies.

In addition to the omics methods used in the included studies, there are also epigenomics, glycomics, and lipidomics, which generate a large amount of information at the sample level but neglect the characteristics within individual cells concurrently. As new omics technologies continue to emerge, single-cell omics technologies, including single-cell genomes, transcriptomes, epigenomes, proteomes, and metabolomes, may be able to address cellular level heterogeneities and further discover new diagnostic and therapeutic targets (Islam et al., 2020). Currently, it has been used in the exploration of TCM syndromes. For example, Lu et al. (2021) used single-cell RNA sequencing technology to explore the significance of tumor heterogeneity in the classification of TCM syndromes of colorectal cancer and finally found that Excess syndrome and Deficiency syndrome may be related to tumor heterogeneity.

Notably, none of these included studies performed multi-omics integrated analysis. These included studies only stayed at a single omics level, ignoring the crosstalk between different molecular entities at different omics levels, which may have led to the omission of biologically relevant information. We did not perform an integrated analysis in this review due to significant heterogeneity among participants from different studies as well as the limited data from these included original articles. The main goal of omics research is not merely to find identifiable differences at the single-omics level but also to decipher the complexity of TCM syndromes at multiple layers at the molecular-level. Consequently, the integration of multi-omics data is becoming crucial for in-depth understanding of the biological basis of TCM syndromes in stroke, which ultimately leads to the discovery of biomarkers and novel therapeutic drugs, and promotes the modernization of TCM and personalized medicine of TCM in stroke (Gu and Chen, 2014; Guo et al., 2020). Future omics research on TCM syndromes should focus on the multi-omics levels and get the utmost out of high-precision algorithms. The best strategy to conduct integrated multi-omics analysis would rely on proteomics, genomics, transcriptomics, and metabolomics data which are acquired simultaneously from participants with low heterogeneity.

Fortunately, it was encouraging to see some promising findings recently, in which Li et al. (2007) established a network research paradigm integrating high-precision computational prediction, multi-omics data and experimental validation. Using this network strategy, we successfully discovered the molecular network characteristics of Spleen-deficiency syndrome at multiple molecular levels, and revealed that this TCM syndrome was closely related to insufficient immune response, including decreased macrophage activity and decreased lymphocyte proliferation (Wang et al., 2020).

Despite promising findings and advances in this field, multi-omics research related to TCM syndromes of stroke still needs to be improved in future studies. First, a recognized and consistent standard for TCM syndrome diagnosis or identification is fundamental for further uncovering the biological mechanism of TCM syndromes. Second, the control group should be set reasonably and strictly matched with the group of interest TCM syndrome to eliminate confounding factors. Third, to ensure data quality, strict standard operating procedures (SOP) should be set for sample collection, storage, processing and acquisition, such as SOP for the collection, storage, and transportation of fecal samples that conform to the unique features of TCM for fecal samples (Su et al., 2022). Fourth, external validation of biomarkers for potential TCM syndromes should be performed before incorporating them into clinical practice.

5 Conclusion

In facing the great challenge of research on TCM syndromes, multi-omics technologies combined with high-precision computational algorithms have served as powerful tools to investigate the complexity of TCM syndromes and may hold

the promise of promoting the modernization of TCM as well as personalized medicine of TCM in stroke.

Data availability statement

The original contributions presented in the study are included in the article/Supplementary Material, further inquiries can be directed to the corresponding authors.

Author contributions

YG and XL contributed to the concept and design. TL contributed to the systematic search of studies. MQ and XX contributed to study screening and data extraction. TL and XL drafted the manuscript. YG and XL contributed to the critical revision of the manuscript.

Funding

This work was supported by the the National Key Research and Development Project (2018YFC1705000), the National Science Foundation of China (82104823), Beijing Nova Program of Science and Technology (Z211100002121061) and the Young Elite Scientist Sponsorship Program by the China Association for Science and Technology (2021-QNRC1-04).

Acknowledgments

The authors acknowledge contributions from all the included studies.

Conflict of interest

The authors declare that the research was conducted in the absence of any commercial or financial relationships that could be construed as a potential conflict of interest.

Publisher's note

Supplementary material

The Supplementary Material for this article can be found online at: https://www.frontiersin.org/articles/10.3389/fphar.2022.980650/full#supplementary-material

References

Cha, M. H., Jones, A. D., Ko, M. M., Zhang, C., and Lee, M. S. (2013). Metabolic profiles distinguish non-dampness-phlegm and dampness-phlegm patterns among Korean patients with acute cerebral infarction. *Evid. Based. Complement. Altern. Med.* 2013, 517018. doi:10.1155/2013/517018

Cha, M. H., Kim, M. J., Jung, J., Kim, J. H., Lee, M. S., and Kim, M. S. (2015). Metabolomic analysis of clinical plasma from cerebral infarction patients presenting with blood stasis. *Evid. Based. Complement. Altern. Med.* 2015, 453423. doi:10.1155/2015/453423

Chen, J., Zhang, Y., Xiong, X., Liang, Q., and Zhao, Y. (2013). Proteomics study on the syndrome-effect relationship of Dading Fengzhu decoction for intracerebral hemorrhage patients with Wind-stirring due to yin-deficiency syndrome in recovery stage. *J. Hunan Univ. traditional Chin. Med.* 33 (11), 57–62.

Cheung, F. (2011). TCM: Made in China. *Nature* 480 (7378), S82–S83. doi:10.1038/480S82a

Collaborators, G. S., Stark, B. A., Johnson, C. O., Roth, G. A., Bisignano, C., Abady, G. G., et al. (2021). Global, regional, and national burden of stroke and its risk factors, 1990-2019: A systematic analysis for the global burden of disease study 2019. *Lancet Neurol.* 20 (10), 795–820. doi:10.1016/S1474-4422(21)00252-0

Griffin, T. J., and Smith, L. M. (2000). Single-nucleotide polymorphism analysis by MALDI-TOF mass spectrometry. *Trends Biotechnol.* 18 (2), 77–84. doi:10.1016/s0167-7799(99)01401-8

Gu, L., Chen, Z., Li, M., Yan, Y., Liang, B., Yang, J., et al. (2019d). Correlation between KDR gene rs2305948, rs2239702 polymorphism and coagulation function of ischemic stroke, coronary heart disease with Phlegm-stasis syndrome. *J. Beijing Univ. Traditional Chin. Med.* 32 (4), 345–352.

Gu, L., Chen, Z., Long, J., Zhu, L., and Su, L. (2021). Correlation between rs5744724 polymorphism of DNA polymerase kappa (Polk) gene and ischemic stroke with Qi-deficiency syndrome and Blood-stasis syndrome. *Chin. Archives Traditional Chin. Med.* 39 (6), 8–13.

Gu, L., Chen, Z., Su, L., Yan, Y., Wu, G., Liang, B., et al. (2017). Association between TRAF6 gene polymorphisms and risk and inflammatory reactions of stroke with Wind-phlegm stagnation syndrome. *J. Beijing Univ. Traditional Chin. Med.* 40 (12), 1030–1036.

Gu, L., Chen, Z., Yan, Y., Long, J., Zhu, L., and Su, L. (2020a). Selenocysteine insertion sequence binding protein 2 gene rs3211703 polymorphism is significantly associated with Blood-stasis syndrome and Qi-deficiency syndrome in ischemic stroke. *Chin. Archives Traditional Chin. Med.* 38 (6), 34–38+65.

Gu, L., Gong, L., Huang, S., Li, J., Li, M., Li, T., et al. (2019a). Correlation analysis of STAT5A gene polymorphism rs319502 between coagulation function and inflammatory reaction in ischemic stroke of Phlegm-stasis syndrome. *Liaoning J. Traditional Chin. Med.* 46 (11), 2241–2245.

Gu, L., Huang, S., Li, M., Li, J., Li, T., Gong, L., et al. (2020b). Association analyses between decorin gene rs7441 polymorphism and Phlegm-Stasis syndrome of ischemic stroke and coronary atherosclerotic heart disease. *Chin. Archives Traditional Chin. Med.* 38 (2), 130–134.

Gu, L., Li, M., Li, J., Liang, B., Huang, S., and Su, L. (2019b). Correlation between genetic polymorphisms of F10 gene and coagulation markers of Phlegm-stasis syndrome in ischemic stroke and Phlegm-stasis syndrome in coronary heart disease. *Chin. J. Gerontology* 39 (16), 3878–3884.

Gu, L., Li, T., Li, M., Huang, S., Gong, L., Li, J., et al. (2019c). Relationship of EP300 gene rs20551 polymorphism with Phlegm-stasis syndrome and blood coagulation function in patients with ischemic stroke and coronary atherosclerotic heart disease. *Chin. J. Geriatric Heart Brain Vessel Dis.* 21 (7), 720–724.

Gu, L., Shen, T., Liang, B., Tan, J., Yan, Y., and Tang, N. (2016a). GWAS-supported variant rs2107595 polymorphism influence the serum lipid metabolism of ischemic stroke patients with Wind-phlegm stagnation syndrome. *China J. Traditional Chin. Med. Pharm.* 31 (11), 4484–4487.

Gu, L., Wu, Y., Liang, B., Tan, J., Chen, Q., Wei, Q., et al. (2016b). Association analysis of gene polymorphism of MAP2K4and MAPK1 and different traditional Chinese medicine syndromes and serum lipid levels in patients with ischemic stroke. *J. Tradit. Chin. Med.* 57 (10), 864–869.

Gu, L., Wei, Q., Xie, J., Chen, Q., Liang, B., and Tang, N. (2016d). Myeloid differentiation factor gene (MYD88) polymorphism affects blood lipid metabolism in stroke with Phlegm-Stasis syndrome. *Lishizhen Med. Materia Medica Res.* 27 (5), 1266–1288.

Gu, L., Zhou, J., Chen, Q., Xie, J., Yan, Y., Liang, B., et al. (2016c). TOLL-like receptor-7 gene rs2897827 polymorphism increase the risk on stroke with Wind-phlegm stagnation syndrome in Han nationality females. *China J. Traditional Chin. Med. Pharm.* 31 (10), 4219–4222.

Gu, P., and Chen, H. (2014). Modern bioinformatics meets traditional Chinese medicine. *Brief. Bioinform.* 15 (6), 984–1003. doi:10.1093/bib/bbt063

Guo, R., Luo, X., Liu, J., Liu, L., Wang, X., and Lu, H. (2020). Omics strategies decipher therapeutic discoveries of traditional Chinese medicine against different diseases at multiple layers molecular-level. *Pharmacol. Res.* 152, 104627. doi:10.1016/j.phrs.2020.104627

Han, X., Gao, Y., Ma, B., Gao, Y., Sun, Y., Jiang, R., et al. (2015). The clinical relevance of serum NDKA, NMDA, PARK7, and UFDP levels with phlegm-heat syndrome and treatment efficacy evaluation of traditional Chinese medicine in acute ischemic stroke. *Evid. Based. Complement. Altern. Med.* 2015, 270498. doi:10.1155/2015/270498

Hou, J., Wang, J., Lin, C., Fu, J., Ren, J., Li, L., et al. (2014). Circulating MicroRNA profiles differ between qi-stagnation and qi-deficiency in coronary heart disease patients with blood stasis syndrome. *Evid. Based. Complement. Altern. Med.* 2014, 926962. doi:10.1155/2014/926962

Hu, J., Dong, Y., Chen, X., Liu, Y., Ma, D., Liu, X., et al. (2015). Prevalence of suicide attempts among Chinese adolescents: A meta-analysis of cross-sectional studies. *Compr. Psychiatry* 61, 78–89. doi:10.1016/j.comppsych.2015.05.001

Hu, M., Wang, Z., Li, T., Zhang, X., Xing, Z., Zhou, C., et al. (2009). Study on MTHFR C677T polymorphism in ischemic stroke with Blood-stasis syndrome. *Chin. J. Inf. Traditional Chin. Med.* 16 (3), 16–18.

Huang, B., Shao, W., Dong, M., Tu, J., and Wang, L. (2008). Association between traditional Chinese medicine syndromes in cerebral infarction and angiotensinogen gene M235T polymorphism. *Med. J. Wuhan Univ.* 29 (4), 482–484+507.

Huo, Q., and Tan, F. (2016). Study on traditional Chinese medicine syndromes of cerebral infarction and fibrinogen related gene polymorphism. *Chin. J. Mod. Drug Appl.* 10 (12), 80–81.

Islam, M., Chen, B., Spraggins, J. M., Kelly, R. T., and Lau, K. S. (2020). Use of single-cell -omic technologies to study the gastrointestinal tract and diseases, from single cell identities to patient features. *Gastroenterology* 159 (2), 453–466.e1. e1. doi:10.1053/j.gastro.2020.04.073

Jia, N., You, J., and Huang, P. (2008). Relationship between ACE gene polymorphism and initial traditional Chinese medicine syndrome of acute ischemic stroke. *Liaoning J. traditional Chin. Med.* 35 (4), 481–483.

Jiang, M., Lu, C., Zhang, C., Yang, J., Tan, Y., Lu, A., et al. (2012). Syndrome differentiation in modern research of traditional Chinese medicine. *J. Ethnopharmacol.* 140 (3), 634–642. doi:10.1016/j.jep.2012.01.033

Lazaridis, K. N., and Petersen, G. M. (2005). Genomics, genetic epidemiology, and genomic medicine. *Clin. Gastroenterol. Hepatol.* 3 (4), 320–328. doi:10.1016/s1542-3565(05)00085-6

Li, J., Chen, Z., Ma, Y., Wu, D., Hu, Y., and Li, J. (2022). Analysis of biomarkers of ischemic stroke with Yang-deficiency syndrome based on GC-TOF-MS combined with metabolomics. *Hunan J. traditional Chin. Med.* 38 (1), 6–10.

Li, S., Wang, F., Li, P., Zhao, H., Zhang, W., and Wang, Y. (2014). Preliminary study on proteomics of Blood-stasis syndrome in ischemic stroke. *China J. Traditional Chin. Med. Pharm.* 29 (12), 3977–3980.

Li, S., Zhang, Z. Q., Wu, L. J., Zhang, X. G., Li, Y. D., and Wang, Y. Y. (2007). Understanding ZHENG in traditional Chinese medicine in the context of neuro-endocrine-immune network. *IET Syst. Biol.* 1 (1), 51–60. doi:10.1049/iet-syb:20060032

Li, Y., Xu, H., Wang, J., Zheng, F., Deng, L., Li, J., et al. (2019). Analysis of bacterial flora structure of patients with cerebral hemorrhage due to Hyperactive liver-yang syndrome by 16S rRNA gene sequencing technique. *Chin. J. Exp. Traditional Med. Formulae* 25 (8), 83–88.

Liao, J., Liu, Y., and Wang, J. (2016). Identification of more objective biomarkers for Blood-Stasis syndrome Diagnosis. *BMC Complement. Altern. Med.* 16 (1), 371. doi:10.1186/s12906-016-1349-9

Lindon, J. C., and Nicholson, J. K. (2008). Spectroscopic and statistical techniques for information recovery in metabonomics and metabolomics. *Annu. Rev. Anal. Chem.* 1, 45–69. doi:10.1146/annurev.anchem.1.031207.113026

Liu, L., Gao, Y., and Ma, B. (2014). Exploring molecular mechanism underlying Chinese medicine syndrome: A study on correlation between Chinese medicine syndrome and biomarkers for ischemic stroke. *Chin. J. Integr. Med.* 20 (1), 11–18. doi:10.1007/s11655-013-1194-8

Liu, W., Li, G., He, C., Qiao, L., Shen, X., Cheng, X., et al. (2019). Analysis of serum transcriptome characteristics of patients with Yin syndrome and Yang syndrome of acute ischemic stroke. *Chin. J. Exp. Traditional Med. Formulae* 25 (15), 122–130.

Lu, Y., Fang, Z., Zeng, T., Li, M., Chen, Q., Zhang, H., et al. (2019). Chronic hepatitis B: Dynamic change in traditional Chinese medicine syndrome by dynamic network biomarkers. *Chin. Med.* 14, 52. doi:10.1186/s13020-019-0275-4

Lu, Y., Zhou, C., Zhu, M., Fu, Z., Shi, Y., Li, M., et al. (2021). Traditional Chinese medicine syndromes classification associates with tumor cell and microenvironment heterogeneity in colorectal cancer: A single cell RNA sequencing analysis. *Chin. Med.* 16 (1), 133. doi:10.1186/s13020-021-00547-7

Manzoni, C., Kia, D. A., Vandrovcova, J., Hardy, J., Wood, N. W., Lewis, P. A., et al. (2018). Genome, transcriptome and proteome: The rise of omics data and their integration in biomedical sciences. *Brief. Bioinform.* 19 (2), 286–302. doi:10.1093/bib/bbw114

Montaner, J., Ramiro, L., Simats, A., Tiedt, S., Makris, K., Jickling, G. C., et al. (2020). Multilevel omics for the discovery of biomarkers and therapeutic targets for stroke. *Nat. Rev. Neurol.* 16 (5), 247–264. doi:10.1038/s41582-020-0350-6

Mutz, K. O., Heilkenbrinker, A., Lonne, M., Walter, J. G., and Stahl, F. (2013). Transcriptome analysis using next-generation sequencing. *Curr. Opin. Biotechnol.* 24 (1), 22–30. doi:10.1016/j.copbio.2012.09.004

Rong, L., and Li, Y. (2020). Study on biomarkers of Phlegm-dampness syndrome in ischemic stroke based on metabonomics. *J. Guangzhou Univ. Traditional Chin. Med.* 37 (2), 195–200.

Shang, Y., Bai, J., Shi, C., Li, T., Feng, Q., Zheng, H., et al. (2012). Correlation between platelet membrane glycoprotein Iba gene polymorphism and traditional Chinese medicine syndromes of arteriosclerotic cerebral infarction. *Lishizhen Med. Materia Medica Res.* 23 (8), 1994–1996.

Shen, T., Gu, L., Chen, Q., Liang, B., and Yan, Y. (2015). Association study on rs2107595 polymorphism identified by GWAS and ischemic stroke of Qi-deficiency syndrome and Blood-stasis syndrome. *J. Guangxi Univ. Traditional Chin. Med.* 18 (4), 5–8.

Su, W., Du, Y., Lian, F., Wu, H., Zhang, X., Yang, W., et al. (2022). Standards for collection, preservation, and transportation of fecal samples in TCM clinical trials. *Front. Cell. Infect. Microbiol.* 12, 783682. doi:10.3389/fcimb.2022.783682

Ussher, J. R., Elmariah, S., Gerszten, R. E., and Dyck, J. R. (2016). The emerging role of metabolomics in the diagnosis and prognosis of cardiovascular disease. *J. Am. Coll. Cardiol.* 68 (25), 2850–2870. doi:10.1016/j.jacc.2016.09.972

Wang, H., and Xu, A. (2014). Zheng: A systems biology approach to diagnosis and treatments. *Science* 346 (6216), S13–S15.

Wang, L., Liang, Q., Chen, X., Yang, L., Tang, K., Liu, Q., et al. (2012). A comparative study on proteomics of cerebral infarction with Liver-yang transforming into wind syndrome and Wind-stirring due to yin-deficiency syndrome. *J. Hunan Univ. traditional Chin. Med.* 32 (7), 54–57.

Wang, T., and Dong, J. (2017). What is "zheng" in traditional Chinese medicine? *J. Traditional Chin. Med. Sci.* 4 (1), 14–15. doi:10.1016/j.jtcms.2017.08.005

Wang, W., Huang, J., Tan, J., Chen, Q., Xie, J., Yang, J., et al. (2016). Toll like receptor 5 polymorphism is significantly associated with ischemic stroke with Wind-phlegm stagnation syndrome. *Liaoning J. traditional Chin. Med.* 43 (12), 2495–2497.

Wang, X., Wu, M., Lai, X., Zheng, J., Hu, M., Li, Y., et al. (2020). Network pharmacology to uncover the biological basis of spleen qi deficiency syndrome and herbal treatment. *Oxid. Med. Cell. Longev.* 2020, 2974268. doi:10.1155/2020/2974268

Wei, L., Xie, D., Zhang, J., Bao, Y., Huang, X., Jin, S., et al. (2019). Investigation of the correlation between traditional Chinese medicine syndromes and MTHFR C677T polymorphism of methylenetetrahydrofolate reductase in post-stroke cognitive impairment. *J. Liaoning Univ. Traditional Chin. Med.* (2), 95–98.

Wu, G., Zhao, J., Zhao, J., Song, N., Zheng, N., Zeng, Y., et al. (2021). Exploring biological basis of Syndrome differentiation in coronary heart disease patients with two distinct Syndromes by integrated multi-omics and network pharmacology strategy. *Chin. Med.* 16 (1), 109. doi:10.1186/s13020-021-00521-3

Xiao, M., Liang, Q., Xiong, X., Zeng, N., Qu, J., Zhang, Y., et al. (2008). Study of peripheral blood mononuclear cells of hypertension intracerebral hemorrhage patients with Liver-yang transforming into wind syndrome by proteomics technology. *Pract. Prev. Med.* 15 (3), 623–627.

Xie, J., Gu, L., Chen, Q., Wu, G., Yan, Y., and Su, L. (2013). Correlation study on 12p13 single nucleotide polymorphism rs12425791 and Chinese medical syndrome types in ischemic stroke patients of the Han nationality. *Chin. J. Integr. Traditional West. Med.* 33 (1), 47–50.

Xiong, X., Chen, J., Liang, Q., Fan, R., Zeng, Q., Qu, J., et al. (2011). Proteomics study on the essence of wind syndrome caused by gan-yang hyperactivity in Chinese medicine. *Chin. J. Integr. Traditional West. Med.* 31 (7), 913–920.

Xiong, X., Liang, Q., Hou, J., Chen, J., Liu, A., Yan, D., et al. (2007). Study on serum proteomics of hypertensive intracerebral hemorrhage patients with Liver-yang transforming into wind syndrome and Hyperactive liver-yang syndrome. *Pract. Prev. Med.* 14 (6), 1649–1652.

Yang, B., Liang, Q., Xiong, X., Chen, J., and Xiao, M. (2014). A proteomic comparative study of hypertensive cerebral hemorrhage in acute stage of Liver-yang transforming into wind syndrome and in recovery stage of Wind-stirring due to yin-deficiency syndrome. *J. Hunan Univ. Traditional Chin. Med.* 34 (10), 34–38+65.

Yang, G., He, H., Dong, Y., Duan, L., Chen, H., and Wang, J. (2021). Research progress and reflection on omics studies on coronary heart disease with binding of Phlegm-stasis syndrome. *J. Tradit. Chin. Med.* 62 (3), 189–194.

Yang, X., Gao, J., Zhang, N., Yang, S., Yang, D., Yu, M., et al. (2019). Biomarkers of the pathogenesis of Stasis-heat syndrome in acute intracerebral hemorrhage based on the plasma differential metabonomics. *Mod. Traditional Chin. Med. Materia Materia-World Sci. Technol.* 21 (10), 2062–2072.

You, L., Zhang, S., Li, T., Sang, X., Li, K., Wang, W., et al. (2021). Integrated analyses of miRNA and mRNA profiles in leukocytes and serums in traditional Chinese medicine (TCM)-defined Pi-qi-deficiency syndrome and Pi-wei damp-heat syndrome resulting from chronic atrophic gastritis. *Chin. Med.* 16 (1), 4. doi:10.1186/s13020-020-00416-9

Zeng, N., Liang, Q., Xiong, X., Qu, J., Xiao, M., Zhang, Y., et al. (2008). Proteromics analysis and identification on peripheral blood lymphocyte of Liver-yang transforming into wind syndrome of cerebral infarction. *Chin. J. Inf. Traditional Chin. Med.* 15 (4), 11–15.

Zeng, X., Zhang, Y., Kwong, J. S., Zhang, C., Li, S., Sun, F., et al. (2015). The methodological quality assessment tools for preclinical and clinical studies, systematic review and meta-analysis, and clinical practice guideline: A systematic review. *J. Evid. Based. Med.* 8 (1), 2–10. doi:10.1111/jebm.12141

Zhao, F., Huang, Y., Wu, M., Li, G., and Wu, M. (2018). Expressions of spectrum of inflammation-related and clotting-related genes in hemorrhagic stroke patients with Stasis-heat syndrome. *J. Tradit. Chin. Med.* 59 (20), 1753–1757.

Zhang, N., Tian, T., Yu, M., and Li, G. (2019). Differential proteomics analysis of pathogenic unit of Stasis-heat syndrome for acute intracerebral hemorrhage. *Chin. J. Integr. Traditional West. Med.* 39 (6), 675–680.

Zhang, Y., Wang, Q., Ding, Q., Wang, S., Zhu, K., Wang, J., et al. (2020). Correlation between CYP2C19 gene polymorphism and traditional Chinese medicine syndromes distribution in 70 patients with cerebral infarction. *Chin. J. Hosp. Pharm.* 40 (9), 1033–1037.

Zhao, H., Liu, P., Xu, C., Li, G., Gao, L., and Luo, Y. (2019). Unique MicroRNAs signature of lymphocyte of yang and yin syndromes in acute ischemic stroke patients. *Chin. J. Integr. Med.* 25 (8), 590–597. doi:10.1007/s11655-018-2843-3

Zhao, Y., Liang, Q., Xiong, X., Fan, R., Liang, X., Yang, B., et al. (2008). Effect of Zhengan Xifeng decoction on proteomics of peripheral blood mononuclear cell in intracerebral hemorrhage patients with Liver-yang transforming into wind syndrome. *China J. Traditional Chin. Med. Pharm.* 23 (10), 885–889.

Zhou, H., Chen, H., Zhou, X., Wang, M., and Wu, M. (2012). Proteomics is the important technology platform of Chinese medicine pathogenesis research. *Chin. J. Integr. Traditional West. Med.* 32 (7), 990–993.

Zhou, M., Wang, H., Zeng, X., Yin, P., Zhu, J., Chen, W., et al. (2019). Mortality, morbidity, and risk factors in China and its provinces, 1990-2017: A systematic analysis for the global burden of disease study 2017. *Lancet* 394 (10204), 1145–1158. doi:10.1016/S0140-6736(19)30427-1

Zhu, H., Bilgin, M., and Snyder, M. (2003). Proteomics. *Annu. Rev. Biochem.* 72, 783–812. doi:10.1146/annurev.biochem.72.121801.161511

Zhu, Q., Wu, G., Li, G., Meng, S., Liao, W., and Cai, Y. (2019). Association of HDAC9 gene single nucleotide polymorphism locus rs2240419 with ischemic stroke and susceptibility to traditional Chinese medicine syndromes in Guangdong Han Chinese. *Chin. J. Clin.* 47 (1), 35–40.

frontiers | Frontiers in Pharmacology

TYPE Original Research
PUBLISHED 30 September 2022
DOI 10.3389/fphar.2022.972351

OPEN ACCESS

EDITED BY
Xian-Jun Fu,
Shandong University of Traditional Chinese Medicine, China

REVIEWED BY
Pei Liu,
Nanjing University of Chinese Medicine, China
Loh Teng Hern Tan,
Monash University Malaysia, Malaysia

*CORRESPONDENCE
Jian Liang,
ljian1010@163.com
Jing Zhong,
zhongjing1212@163.com
Ming-Kun Liang,
liangmingkun13@163.com

SPECIALTY SECTION
This article was submitted to Ethnopharmacology, a section of the journal Frontiers in Pharmacology

RECEIVED 18 June 2022
ACCEPTED 30 August 2022
PUBLISHED 30 September 2022

CITATION
Liang X-Q, Mai P-Y, Qin H, Li S, Ou W-J, Liang J, Zhong J and Liang M-K (2022), Integrated 16S rRNA sequencing and metabolomics analysis to investigate the antidepressant role of Yang-Xin-Jie-Yu decoction on microbe-gut-metabolite in chronic unpredictable mild stress-induced depression rat model.
Front. Pharmacol. 13:972351.
doi: 10.3389/fphar.2022.972351

Integrated 16S rRNA sequencing and metabolomics analysis to investigate the antidepressant role of Yang-Xin-Jie-Yu decoction on microbe-gut-metabolite in chronic unpredictable mild stress-induced depression rat model

Xing-Qiu Liang[1,2], Peng-Yu Mai[2], Hui Qin[3], Sen Li[4], Wen-Juan Ou[4], Jian Liang[1]*, Jing Zhong[4]* and Ming-Kun Liang[2]*

[1]Medical College, Guangxi University, Nanning, China, [2]Department of Science and Technology, Ruikang Hospital Affiliated to Guangxi University of Chinese Medicine, Nanning, China, [3]Guangxi International Zhuang Medicine Hospital, Nanning, China, [4]School of Basic Medical Sciences, Guangxi University of Chinese Medicine, Nanning, China

Objectives: Our goals were to evaluate the antidepressant efficacy of Yang-Xin-Jie-Yu Decoction (YXJYD) in Chronic Unpredictable Mild Stress (CUMS)-induced depression rat model and to investigate the underlying mechanisms.

Design: We used CUMS-induced depression rat model to evaluate whether oral administration of YXJYD with different doses (2.1 g/kg, 1.05 g/kg and 0.525 g/kg, respectively) improve the depressive-like symptoms, and then performed UHPLC-Q-TOF-MS to explore the active ingredients of YXJYD. Subsequently, rat's cecal contents, serum, and urine were collected from the control group, CUMS model group, and YXJYD high-dose (2.1 g/kg) treatment group. The 16S rRNA sequencing was performed on the cecal contents, based on Illumina MiSeq platform, and ANOVA analysis were used to analyze the composition variety and screen differential expression of gut bacteria in the three groups. ^{1}H Nuclear Magnetic Resonance (NMR) analysis was used for analyzing the metabolites obtained from cecal contents, serum, and urine, and KEGG enrichment analysis was used to identify pathways of differential metabolites. An integrated 16S rRNA sequencing and metabolomic data were conducted to characterize the underlying mechanisms of YXJYD

Results: The gut microbial communities, and serum, cecal content, urine metabolic compositions were significantly significantly altered in CUMS-induced depressive rats, while YXJYD effectively ameliorated the CUMS-

associated gut microbiota dysbiosis, especially of *Monoglobus,* and alleviated the disturbance of serum, cecal content, urine metabolome and reversed the changes of key depressive and gut microbiota-related metabolites, such as succinic acid, taurine, hippuric acid, melatonin. With an integrated study of the gut microbiota and metabolomes, we identified the pathway of tricarboxylic acid cycle (TCA cycle) and propanoate metabolism as the regulated target of YXJYD on host-microbiome interaction.

Conclusion: Our findings further confirmed the imbalance of metabolism and intestinal microbial is closely related to CUMS-induced depression. YXJYD regulates gut microbiome to affect body metabolomes and then produce antidepressant-like effect in CUMS-induced depressive rats while its molecular mechanism possibly be increased *Monoglobus* abundance in gut microbiota and regulated the TCA cycle pathway and propanoate metabolism in host.

KEYWORDS

gut microbiota, metabolism, Traditional Chinese Medicine, adolescent depression, microbiota-gut-brain axis

1 Introduction

The prevalence of adolescent depression increased at a faster pace than adult depression due to it is unique period of physical development along with severe lifestyle changes (Mojtabai, Olfson, and Han 2016; Twenge et al., 2018; Simkin 2019). It has been observed a strong link between depression and suicide, and that finally lead to a ninefold rise in the incidence of suicidal thoughts among teenagers, particularly in females (Lara et al., 2018; Simkin 2019). The above grim situation highlighted the limits of available treatments. According to the data reported by several meta-analyses, most antidepressants do not provide obvious benefits above placebo for adolescents (Cipriani et al., 2016; Ignaszewski and Bruce, 2018). Moreover, another comprehensive meta-analysis indicated that the efficacy of medications for children and adolescents with MDD were far from satisfactory and also indicated that venlafaxine might increase the risk for suicidality (suicidal behavior or ideation) in young people (Cipriani et al., 2016). What's more, depression in adolescence predicts depression and anxiety in adulthood, and most of the affected adults had their first depressive episode during adolescence (Simkin 2019). Worsely, due to the particularity of physical development, the side effects of antidepressant drug, such as headache, stomach discomfort, drowsiness or sleeplessness, and dry mouth, are more prevalent in adolescence than in adults. This lead to the antidepressants choice for youth is highly restricted and also might eventually bring about drug withdrawal. Given all, there is an urgent need to find effective antidepressants but without adverse effects for teenage depression.

Adolescent depression is not a unified syndrome, in which multiple underlying mechanism also coexist. Thus, the best therapy strategy is to identify the unique cause for each individual patient and then employ a tailored treatment to address not just depression, but also the body's malfunction that causes depressive symptoms (Zhang and Cheng 2019; Li et al., 2020). Growing evidence has demonstrated that the gut microbiota disruption is closely associated with a variety of mental diseases, which mainly showed in changes of gut microbiota diversity and composition (P. Zheng et al., 2016; Yang et al., 2020). Comparing with healthy people, the phylum of *Bacteroidetes, Proteobacteria, Firmicutes* showed a higher proportion in major depressive disorder (MDD), while the phylum of *Actinobacteria* showed a lower. Moreover, the abundance of the genus *Bacteroides* was increased in MDD patients, while that of the genera *Blautia* and *Eubacterium* were decreased (Yang et al., 2020). The specific features of gut microbiota in different populations distinguish adolescents from adults. Thus, targeting on the gut microbiota may provide a manageable and personalized therapy for adolescent depression.

Up until now, Traditional Chinese Medicine (TCM) has been utilized to treat depression. Its holistic, multidrug, and multitarget character aligns well with the therapeutic concept of systemic medicine in the treatment of teenage depression. Yang-Xin-Jie-Yu decoction (YXJYD) is an empirical botanical drug prescription for adolescent depression made up of ten commonly used plants: *Panax ginseng* C.A.Mey., *Ophiopogon japonicus* (Thunb.) Ker Gawl., *Schisandra chinensis* (Turcz.) Baill., *Epimedium sagittatum* (Siebold & Zucc.) Maxim., *Allium chinense* G.Don, *Rosa rugosa* Thunb., *Albizia julibrissin* Durazz., *Curcuma aromatica* Salisb., *Acorus calamus L.*, and *Citrus* × *aurantium* L. It should be noted that *Panax ginseng* C.A.Mey., *Ophiopogon japonicus* (Thunb.) Ker Gawl., and *Schisandra chinensis* (Turcz.) Baill. are compositions of Sheng Mai Yin (SMY) prescription, which has traditionally been used to protect the heart from a variety of cardiac illnesses.

In both humans and rats, modern pharmacology discovered that SMY might enhance coronary blood flow, improve myocardial tolerance to hypoxia, and act as a stimulant similar to interrenalin (Z. Chen et al., 2018). Besides, the plants of *Epimedium sagittatum* (Siebold & Zucc.) Maxim. (Wu et al., 2013; Liu et al., 2015), *Allium chinense* G.Don (Yin et al., 2019), *Rosa rugosa* Thunb. (Fekadu, Shibeshi, and Engidawork 2016; Mingkun et al., 2021), *Albizia julibrissin* Durazz. (Chunlei, Yongquan, and Xueli 2012; Xueli et al., 2013), *Curcuma aromatica* Salisb. (Haibing, Yi, and Guojun 2012), *Acorus calamus L.* (Tengfei et al., 2012), and *Citrus* × *aurantium* L. (Li et al., 2013; Chengfu et al., 2014) are commonly used for antidepressant single or complex by multiple anti-depression mechanism. *Acorus calamus L.* was also shown to have an antidepressant effect on CUMS rats via modulating the expression of monoamine neurotransmitters and their receptors (Tengfei et al., 2012), while *Curcuma aromatica* Salisb. alleviated the depressive symptoms by affecting on the neuroplasticity of hippocampus neurons (Haibing, Yi, and Guojun 2012).

It is generally recognized that a TCM botanical drug formula is more effective than single botanical drug molecules or botanical drugs in clinical practice, and YXJYD shown notable antidepressant effect on teenagers with depression when compared to any other single botanical drugs in clinical practice (Hsiao and Liang, 2010). Moreover, patient comments revealed that YXJYD boosted their appetite and alleviated several digestive problems. We postulated that YXJYD's antidepressant impact was related to repair gut microbiota dysbiosis and subsequently regulating the body's metabolism. To test this hypothesis, we explored the effect of YXJYD on cecal content, urine, and serum metabolites in CUMS-induced depression rat model by untarget metabolomics, and then investigated the effect of YXJYD on cecal microbiome in CUMS-induced depression rats by 16S rRNA sequencing. We effectively demonstrated that the antidepressant mechanism of YXJYD was intimately related with the gut microbiota and body's metabolism, and that YXJYD had holistic, multidrug, and multitarget qualities that make it a potential medication for depression.

2 Materials and methods

2.1 Experimental reagents

Fluoxetine hydrochloride (Patheon France, France, production batch number: 21201A) was provided by Ruikang hospital affiliated to guangxi university of Chinese medicine. The ELISA assay kit for cortisol (202112) was purchased from the Shanghai Enzyme-linked Biotechnology Co., Ltd. (Shanghai, China). QlAamp DNA Stool Mini Kit (50) was purchased from Shanghai Canspec Scientific Instruments Co., Ltd. (catalog [cat.] no. 51604; Qiagen, Germany). Qubit dsDNA HS ASSAY Kit was obtained from Invitrogen and Life technologies company (CA, United States). DL2000 DNA Maker was obtained from Takara Bio INC. (Kyoto, Japan). The 50×TAE buffer was obtained from Shanghai Shenggong Bioengineering Co., Ltd. (Shanghai, China). UPLC-Q-TOF/MS grade acetonitrile and HPLC grade acetonitrile, formic acid, were provided by Merck & Co., Inc. (Merck, Germany). Animals Male Sprague-Dawley (SD) rats were obtained from the Laboratory Animal Center of Guangxi Medical University (license number: SCXK Gui 2020-0003). The rats were maintained at the Guangxi Medical University Animal Center with a 12 h light-dark cycle and fed for 1 week before to the experiment to minimize the stress reaction (22 ± 3°C with a relatively constant humidity of 55 ± 15%). Except during the study period, rats were fed and water freely. All animal experiments were in accordance with the Guide for the Care and Use of Laboratory Animals approved by the Institutional Animal Care and Use Committee at Guangxi Medical University (license number: SYXK Gui 2020-0004).

2.2 Drug preparation

Yang Xin Jie Yu decoction is composed as follows: *Panax ginseng* C.A.Mey. (15 g, Batch number: 210901), *Ophiopogon japonicus* (Thunb.) Ker Gawl. (15 g, Batch number: 210901), *Schisandra chinensis* (Turcz.) Baill. (15 g, Batch number: 210501), *Epimedium sagittatum* (Siebold & Zucc.) Maxim. (15 g, Batch number: 210501), *Allium chinense* G.Don (15 g, Batch number: 210501), *Rosa rugosa* Thunb. (15 g, Batch number: 210801), *Albizia julibrissin* Durazz. (He Huan Hua), *Curcuma aromatica* Salisb. (15 g, Batch number: 210901), *Acorus calamus L.* (15 g, Batch number: 210901), and *Citrus* × *aurantium* L (10 g, Batch number: 210901). (Details are showed in Table 1). All medicinal materials were provided by the Ruikang hospital affiliated to Guangxi university of Chinese medicine. The certificate specimens of each botanical drugs were identified by the pharmacy, and quality inspection reports were provided. All medicinal materials were soaked with water for 30 min at a solid liquid ratio of 1:8 (g/ml), and were then extracted three times under reflux for 2 h. All the supernates were mixed, and the solvents were then removed by using a rotary evaporator at 60°C to obtain YXJYD extracts, and subsequently freeze-dried and smashed into granules (total weight 31.30 g) for experimental use. The lyophilized YXJYD granule was thoroughly dissolved in 100 ml distilled water to make a solution containing 1.45 g raw drugs /mL for the future study.

2.3 The component analysis of YXJYD

The solution of YXJYD granules was filtered out by 0.22 μm membrane-filter and injected into an Ultra-High Performance Liquid Chromatography analytical system (Waters Corp.,

TABLE 1 Details of the herbal pieces in YXJYD.

Botanical plant name	Family and plant part used	English name	Chinese name	Dry weight of crude drugs in YXJYD (g)
Panax trifolius L.	*Araliaceae*, root	*Ginseng*	Ren-shen	15
Ophiopogon japonicus (Thunb.) Ker Gawl.	*Liliaceae*, root	*Ophiopogonis Radix*	Mai-dong	15
Schisandra chinensis (Turcz.) Baill.	*Schisandraceae*, fruit	Schisandrae Chinensis Fructus	Wu-wei-zi	15
Epimedium rotundatum K.S.Hao	*Berberidaceae*, Leaves basal and cauline	Epimedii Folium	Yin Yang Huo	15
Allium macrostemon Bunge	*Liliaceae*, root	Bulbus Allii Macrostemonis	Xie Bai	15
Rosa Abyssinica Lindley (Rosaceae)	*Rosaceae*, flower	Flos Rosae Rugosae	Mei Gui Hua	15
Acacia julibrissin (Durazz.) Willd	*Leguminosae, flower*	Flos Albiziae	He Huan Hua	15
Curcuma aeruginosa Roxb	*Zingiberaceae*, root	Radix Curcumae	Yu Jin	15
Acori Tatarinowii Rhizoma	*Araceae*, root	Acori Tatarinowii Rhizoma	Shi Chang Pu	15
Pericarpium Citri Reticulatae Viride	*Rutaceae*, fruit	Green Tangerine Peel	Qing Pi	10

Milford, MA, United States) with ACQUITY UPLC HSS T3 C18 column (100mm×2.1 mm, 1.8 μm i.d., Waters, Unites States) at the column temperature: 30°C. The mobile phases were 1% formic acid in water (A) and acetonitrile (B), and the elution conditions were: 0–0.5 min: 98%A; 0.5–5.0 min: 98%-70%A; 5.0–15.0 min: 70%-60%A; 15.0–20.0 min: 60%-40%A; 20.0–21.0 min: 40%-15%A; 21.0–23.0 min: 15%-60%A; 24.0–25.0 min: 60%-98%A.

Mass data was obtained from a XEVO-G2-S-QTOF-MS mass spectrometer equipped with an electrospray ionization source (ESI) (Waters Corp., Massachusetts, United States). The MS detection parameters were set as follows: collision voltage (capillary voltage): 3.0 kV (negative ion: 1.8 kV); sample and extraction cone voltage: 40 V (negative ion: 40 V) and 4.0 V; desolvation gas rate and temperature (negative ion: 4.0 V): 600 L/h and 350°C (negative ions: 150°C); cone gas rate: 50 L/h; ion source temperature: 100°C (negative ions: 100°C); scan time: 0.2 s; scan interval delay (interscan delay): 0.02 s. The leucine-enkephalin (mass-to-charge ratio in positive ion mode: 556.2771, mass-to-charge ratio in negative ion mode: 554.2615) was selected as the real-time calibration substance, and its concentration and flow rate were 500 ng/ml and 10 μL/min, respectively. The mass-to-charge ratios of the primary mass spectrometry data ranged from 100 to 1,500, whereas the secondary mass spectrometry data ranged from 50 to 1,500 Hz.

2.4 Drug administration

After 1 week of acclimatization, 90 SD rats (6 weeks old) were randomly divided into six groups: control group (n = 15, distilled water administrated, 0.01 ml/g), model group (n = 15, distilled water administrated, 0.01 ml/g), positive control group (n = 15, Fluoxetine Hydrochloride treated, 2.1 mg/kg), YXJYD high-, medium-, and low-dose group (n = 15 per group, YXJYD administrated, 2.1 g/kg, 1.05 g/kg and 0.525 g/kg, respectively). These dosages were calculated from the clinical dosages for adolescents and the equivalent conversion of the body surface area between animals and humans. The experimental design is showed in Figure 1. Drug administration was performed a week before CUMS.

2.5 Chronic unpredictable mild stress

The rats were placed individually and subjected to mild stress for 5 weeks except the control group. The stresses were as follows: 45 cage tilt for 24 h from 10 to 10 am in the next day, bound for 3 h, water deficiency for 24 h, fasted for 24 h, 200 r/min shaking for 15 min, tail-clamping for 5 min, wet bedding for 24 h (200 ml water/100 g bedding), swimming in cold water for 5 min (the temperature was below 10°C), light and shape reversed, lightening throughout the night (100 W light for 36 h), and so on.

2.6 Behavioral tests

2.6.1 Sucrose preference test

72 h before the test, rat were trained to adapt to 1% sucrose solution (W/V). Two bottles were placed in each cage, both were 1% sucrose solution for 24 h, next one bottle was 1% sucrose solution and another was water for 24 h, and the last 24 h were deprived of water and food. During the test, rats were housed in individual cages and had free access to two bottles with sucrose solution (100 ml, 1%, W/V) and tap water

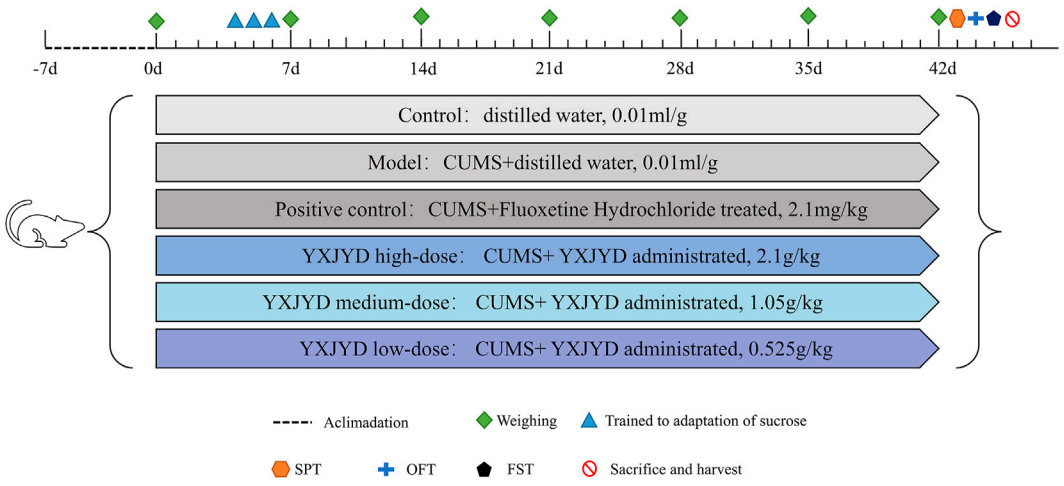

FIGURE 1
Animal experimental designed.

(100 ml), respectively. Twelve hours later, sucrose and water consumption (ml) were recorded, and the sucrose preference was calculated as following:

$$\text{sucrose preference}(\%) = \frac{\text{sucrose consumption volume (ml)}}{\text{sucrose consumption volume (ml)} + \text{water consumption volume (ml)}} \times 100\%$$

2.6.2 Open field test

The rats were left alone in a self-made PC box (50 cm × 50 cm × 50 cm) with the arena's floor split into 100 equal squares (5 cm × 5 cm) and allowed rats explore freely. Each rat was placed individually in the center of the arena in a calm room, allowing for 5 min of unfettered exploration. A camera was placed above the open box to record locomotor activity during the experiment. A 5-min test was used to determine the overall distance traveled and time spent in the center region. Before using another animal, the test apparatus was cleaned completely with 75% ethanol.

2.6.3 Forced swimming test

The experiment was carried out in a self-made cylindrical container (50 cm height; 30 cm in diameter) filled to a depth of 40 cm with water (at a temperature of 24°C). During the last 5 min of the experiment, the rat's immobility was assessed. Immobility was defined as having the limbs fixed or the forelimbs floating slightly (but the body remained immobile). Immobility was defined as their passive floating in the water during the test. Replacement of clean water before introducing new rats to avoid tainting the findings due to a waste water quality issue created by the prior.

2.7 Blood sampling collection

Blood was collected after behavior test by ntraperitoneal injection with 20% urethane to anaesthetize the rat. Blood was collected in rat aortic blood immediately, and then sampled into 5 ml blood collection tubes. After standing in the room temperature for 2 h, the serum was obtained following a 10 min centrifugation at 3,000 g (Hermle Z 300 K) at 4 °C, and stored at -80°C.

2.8 Determination of cortisol levels in the serum by ELISA

The determination of cortisol level were performed by using a commercial enzyme immunoassay kit (Shanghai Enzyme-linked Biotechnology Co., Ltd.) according to the manufacturer's instructions. All samples were tested in duplicate.

2.9 Urine, serum, and cecum contents collection

The night before sacrificed, rats' urine was collected for 24 h, and cecum contents was taken from the cecum after they were sacrificed. Blood samples were collected after the behavioral test. The rats were anesthetized and blood was immediately collected from the abdominal aorta in 5 ml of vacuum blood collection tubes without anticoagulant, left at room temperature for 2 h, centrifuged at 4°C for 10 min at 3,000 rpm, and the supernatant was collected in new centrifuge tubes. After the rats were

sacrificed, the contents of the cecum were collected. All samples were stored in the refrigerator at -80 °C.

2.10 ^{1}H NMR analysis for metabolomics

2.10.1 Preparation of urine, serum, and cecum content for ^{1}H NMR analysis

Cecum content samples: 100 mg cecum content samples were suspended in 1 ml PBS (0.1 mol /L, pH 7.4). The samples were homogenated in an ice bath for 2 times, 15 s at a time, and then stood for 10 s. After ultrasonicating for 30 min, centrifuging to remove deposition (14000 g, 15 min, 4°C). Afterward, 450 μL of the supernatant was added with 50 μl of D_2O containing 0.0025% (mass to volume ratio) TMSP. After being mixed by vortexing for 1 min, the mixture was transferred into a 5 mm NMR tube.

Urine sample: 500 μl urine sample were taken to 2 ml EP tube. After centrifuging to remove deposition (3,500 rpm, 15 min, 4°C), 450 μl of the supernatant were added in 50 μl PBS (0.1 mol /L, pH 7.4), and then vortexed for 1 min, centrifuging to remove deposition (12000 rpm, 15 min, 4°C). Afterward, 450 μL of the supernatant was added with 50 μl of D_2O containing 0.0025% (mass to volume ratio) TMSP. After being mixed by vortexing for 1 min, the mixture was transferred into a 5 mm NMR tube.

Serum sample: After thawing, 250 μl serum sample were taken in 2 ml EP tube, and 250 μl PBS (0.1 mol /L, pH 7.4) were added. After vortexing for 1 min, the mixture were centrifuged to remove deposition (14000 g, 15 min, 4°C). Afterward, 450 μl of the supernatant was added with 50 μl of D2O containing 0.0025% (mass to volume ratio) TMSP. After being mixed by vortexing for 1 min, the mixture was transferred into a 5 mm NMR tube.

2.10.2 ^{1}H NMR measurement

^{1}H NMR was performed on the Bruker 600 MHz AVANCE III NMR instrument (Karlsruhe, Germany) at the operating temperature of 25°C. The ^{1}D CPMGpr1d Bruker standard sequence was applied for feacal sample and serum sample to scan 64 times, while the NOSEY gppr1d Bruker standard sequence was for urine sample to scan 32 times. Fixed receiver gain, the detection spectrum width was 0.3 Hz, the pulse width was 20 ppm, and the relaxation delay was 5 s.

2.10.3 ^{1}H NMR data analysis

The raw ^{1}H NMR data were adjusted using MestReNova 11.0 (Santiago, Spain) to set TSP peaks at 0 ppm, shear water peaks (stool (4.24–6.00 ppm), urine (4.28–6.00 ppm), serum (4.12–7.08 ppm), baseline and peak extraction, and peak integration automation. To reduce baseline noise being identified as variable information, total area normalization was subsequently performed and peak area cut-offs that were performed at 0.04 ppm intervals. The processed data exported as .txt format files, while the identified fractions were used as variables for the differential substances to be screened, edited in a fixed format and imported into SIMCA-P 14.1 software for multivariate statistical analysis, including principal component analysis (PCA), partial least squares-discriminant analysis (PLS-DA) and orthogonal partial least squares-discriminant analysis (OPLS-DA). For the OPLS-DA mathematical model developed for potential biomarker screening, after 200 permutation tests to confirm that the model was not overfitted, the results were used for potential biomarker screening with the absolute value of Variable importance on projection (VIP) > 1 and $p < 0.05$. The peaks at different ppm were identified using Chenomx NMR suite 8.6 software, and the identification results were verified using ^{1}H-^{1}H coupling on the compounds and 2D NMR spectra with ^{1}H-^{1}H COSY coupling information.

2.11 Analysis of gut microbiota by 16S rRNA sequencing

Cecal contents were collected from the cecum, and total DNA was extracted from stool samples using the QIAmp DNA microbiome kit (Qiagen, German) according to the manufacturer's protocol. After determining the DNA concentration and integrity, an amplicon sequencing library was constructed based on the PCR-amplified V3–V4 variable region of 16S rRNA. Then, qualified libraries was used on the Illumina MiSeq platform for paired-end sequencing according to the manufacturer's instructions. The software of Trimmomatic, FLASH, and QIIME software were used to filter the original sequencing data. UPARSE software was used to cluster the clean readings into operational taxonomic units (OTUs) with the threshold of 97%. Then, QIIME package was used to select the representative reads from each OUT, and RDP Classifier software v.2.13 was used to annotate and classify representative OTU sequences against the SILVA 138 16S rRNA database using a confidence threshold of 70%. Alpha diversity and beta diversity analysis were performed by R software (version 3.3.1). Bray-Curtis dissimilarity matrix was developed with the normalized sequences. Hierarchical cluster analysis (HCA), principal coordinates analysis (PCoA), and distance between two groups were performed by the Bray-Curtis dissimilarity matrix. The linear discriminant analysis (LDA) effect size (LEfSe) method was applied to reveal the effect of each differentially abundant taxon and distinguish the key phenotypes responding to the YXJYD treatment, with a set logarithmic LDA score of 2.0. Functional classification schemes of KEGG (Kyoto Encyclopedia of Genes and Genomes) Orthology were predicted by Tax4Fun.

2.12 Statistical analysis

The results of behavioral tests and cortisol levels determination were compared among using one-way ANOVA by GraphPad Prism (9.0.0). Pairwise comparison of microbiome composition was conducted using Metastats based on the

A

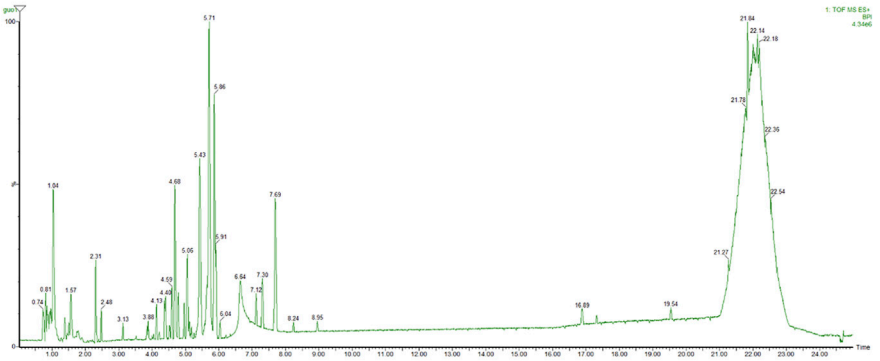

Number	Compound name	RT(min)	Precursor m/z	Adduct	ppm	Formula	Fragment ions
1	DL-Arginine	0.85	175.1184	$[M+H]^+$	4	$C_6H_{14}N4O_2$	175.1187、158.0911、130.0965
2	Synephrine	1.56	150.0909	$[M+H-H_2O]^+$	2.6	$C_9H_{13}NO_2$	135.0671、107.0479、91.0524、77.0362
3	Magnoflorine	4.67	343.1735	$[M+H]^+$	4.7	$C_{20}H_{24}INO_4$	343.1734、297.1122
4	Naringenin	5.63	273.0754	$[M+H]^+$	1.5	$C_{15}H_{12}O_5$	273.0755、153.0169
5	Quercetin	5.86	303.0495	$[M+H]^+$	7.6	$C_{15}H_{10}O_7$	303.0486、229.0485
6	Baohuoside V	7.12	831.2666	$[M+Na]^+$	8	$C_{38}H_{48}O_{19}$	831.2682
7	Epimedin B	7.12	809.2855	$[M+H]^+$	1.1	$C_{38}H_{48}O_{19}$	369.1329、313.0704
8	Epimedin C	7.3	823.2997	$[M+H]^+$	1.8	$C_{39}H_{50}O_{19}$	677.2455、531.1870、369.1331
9	Icariin	7.69	531.1851	$[M+H-C_6H_{10}O_4]^+$	2	$C_{33}H_{40}O_{15}$	369.1323、313.0699
10	Icariside II	8.23	369.1326	$[M+H-C_6H_{10}O_4]^+$	1.9	$C_{27}H_{30}O_{10}$	369.1322、313.0702
11	Gardenin	8.95	419.1327	$[M+H]^+$	2.3	$C_{21}H_{22}O_9$	419.1332
12	Isoanhydroicaritin	15.87	369.1322	$[M+H]^+$	5.9	$C_{21}H_{20}O_6$	369.1340、313.0714
13	Schizandrol A	16.88	455.2033	$[M+Na]^+$	4	$C_{24}H_{32}O_7$	455.2038、415.2103
14	Schizandrin	16.88	415.2106	$[M+H-H_2O]^+$	2.1	$C_{24}H_{32}O_7$	415.2103
15	Nobiletin	15.86	403.1371	$[M+H]^+$	1.7	$C_{21}H_{22}O_8$	403.1348

B

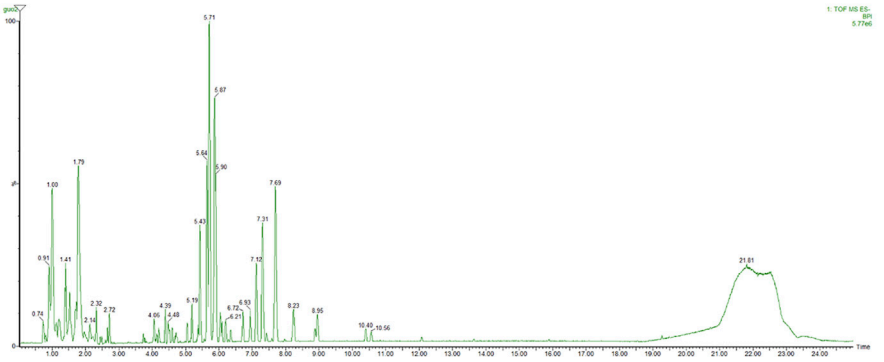

Number	Compound name	RT(min)	Precursor m/z	Adduct	ppm	Formula	Fragment ions
1	Eriodictyol-7-O-rutinoside	5.16	595.1669	$[M-H]^-$	0.2	$C_{27}H_{32}O_{15}$	595.1673、287.0559
2	Hyperoside	5.38	463.0903	$[M-H]^-$	4.5	$C_{21}H_{20}O_{12}$	463.0905、301.0346
3	Isoquercetrin	5.42	463.089	$[M-H]^-$	1.8	$C_{21}H_{20}O_{12}$	463.0889、301.0335、300.0272
4	Naringenin-7-O-rutinoside	5.63	579.171	$[M-H]^-$	1.5	$C_{27}H_{32}O_{14}$	579.1703、313.0699、271.0594
5	Epimedin B	7.12	843.2484	$[M+Cl]^-$	9.3	$C_{38}H_{48}O_{19}$	645.2135、367.1136
6	Epimedin C	7.3	857.2636	$[M+Cl]^-$	0.5	$C_{39}H_{50}O_{19}$	659.236
7	Icariin	7.69	721.2367	$[M+FA-H]^-$	2.5	$C_{33}H_{40}O_{15}$	721.2343、513.1752、367.1168
8	Icariside II	7.69	513.1769	$[M-H]^-$	0.7	$C_{27}H_{30}O_{10}$	513.1752、367.1168
9	Icariside I	7.69	529.1722	$[M-H]^-$	1.3	$C_{27}H_{30}O_{11}$	529.1699、409.1277、367.1168
10	Ginsenoside Rf	9.12	845.4906	$[M+FA-H]^-$	0.2	$C_{42}H_{72}O_{14}$	799.4833
11	Ginsenoside Rb1	10.39	1153.6045	$[M+FA-H]^-$	3.1	$C_{54}H_{92}O_{23}$	945.5486
12	Ginsenoside Rg3	10.57	829.4966	$[M+FA-H]^-$	1.3	$C_{42}H_{72}O_{13}$	829.5008、783.4954

FIGURE 2
(A) Base peak chromatograms and recognized main compounds of YXJYD extract in ESI (+) mode. **(B)** Base peak chromatograms and recognized main compounds of YXJYD extract in ESI (–) mode.

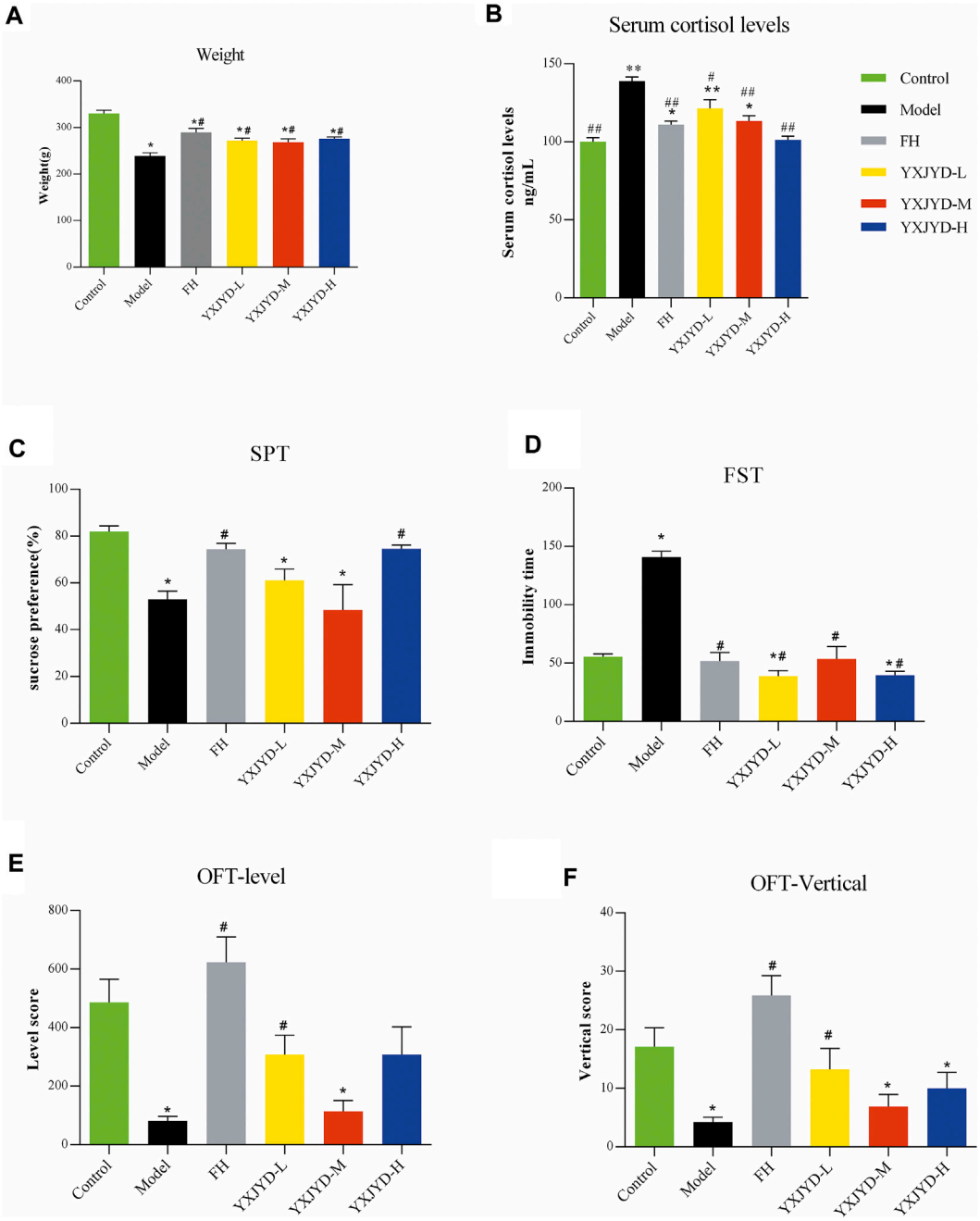

FIGURE 3
The effect of YXJYD administration on CUMS-induced depressive behaviors. Behavioral tests results. **(A)** Effect of YXJYD on the rats' weight; **(B)** Effect of YXJYD on the rats' serum cortisol levels; **(C)** the sugar preference test after YXJYD administration; **(D)** the forced swimming test after YXJYD administration; **(E)** the level score of open field test after YXJYD administration; **(F)** the vertical score of open field test after YXJYD administration. vs. control group, $^{*}p < 0.05$, $^{**}p < 0.01$, $^{***}p < 0.001$; vs. model group, $^{\#}p < 0.05$, $^{\#\#}p < 0.01$; $^{\#\#\#}p < 0.001$. (Rat for behavioral tests, n; Control = 14, Model = 14, FH = 13, YXJYD-L = 12, YXJYD-M = 8, YXJYD-L = 13). YXJYD-L, low-dose administration of YXJYD; YXJYD-M, medium-dose administration of YXJYD; YXJYD-H, high-dose administration of YXJYD; FH, Fluoxetine Hydrochloride treated; SPT, sugar preference test; FST, forced swimming test; OFT, open field test.

Majorbio Cloud Platform (https://cloud.majorbio.com/page/tools/). The Spearman correlation coefficient was used to analyze the correlations. $p < 0.05$ or FDR < 0.05 was considered statistically significant. For alpha diversity, the Wilcoxon rank-sum test $p < 0.05$ was considered statistically significant. For beta diversity, distance of PcoA between two groups were performed based on the Bray-Curtis dissimilarity matrix and ANOSIM test (permutations = 999, $p < 0.001$). The linear discriminant analysis (LDA) efect size (LEfSe, https://huttenhower. sph.harvard.edu/galaxy/) was used to identify biomarker taxa responsible for discrimination. Random forest (RF) analysis was performed by the R package "randomForest", and the mean decrease accuracy (MDA) score was used to determine the importance ranking of key taxa for classifcation (Statnikov et al., 2013; Miao et al., 2022).

3 Results

3.1 The chemical constituents of YXJYD

UPLC-Q-TOF/MS was used to characterize the chemical composition of YXJYD in positive and negative ion modes, and the characteristic chromatogram and results of YXJYD were shown in Figure 2 and Supplementary Figures S2–S3. There were fifteen chemicals discovered in the positive ion mode and twelve compounds detected in the negative ion mode.

3.2 Exposure to chronic unpredictable mild stress is sufficient to induce depressive-like behaviors

To create an adolescent depressive rat model, we employed chronic unpredictable mild stress to stimulate the rats (6 weeks old) to induce depressive-like behaviors. In comparison with control group, CUMS model rats displayed expected behavioral alterations, such as reduced exploratory activity in OFT ($p < 0.05$), decreased sucrose preference in SPT ($p < 0.05$), and prolonged immobility time in FST ($p < 0.05$) (details showed in Figure 3.). Likewise, the defeated rats' food intake was also reduced, and their body weights were considerably lower when compared pre- and post-social defeat exposure.

3.3 YXJYD alleviated depressive-like behaviors in CUMS rats

To validate the antidepressant effect of YXJYD, different concentrations of YXJYD were tested in CUMS-induced depression rats and asssessed the effectiveness by SPT, OFT, and FST. As showed in Figure 3 and Supplementary Table S1, YXJYD improved the CUMS rats' preference for sucrose in SPT significantly ($p < 0.05$), increased the spontaneous locomotor activity in OFT ($p < 0.05$), and decreased the immobility duration in FST ($p < 0.05$) when compared with the CUMS model group. Along with the decreasing of cortisol in the serum after YXJYD treatment, it is clear that YXJYD had an striking antidepressant effect.

In clinical, it is commonly found adolescent with depression are also suffer from decreasing appetite and losing weight. The weight of model rats in our study was dramatically reduced after 5 weeks of stimulation, which is consistent with similar symptoms in adolescents' depression. Interestingly, YXJYD treatment help CUMS rats to gain weight significantly ($p < 0.05$), and the rats had a stronger desire to eat after treating with YXJYD. These findings prompted us to investigate the effects of YXJYD on the gut microbiota and metabolites in CUMS-induced depression rats.

3.4 Cecal content metabolic profiling and biomarker identification

Multivariate analysis was performed to assess and compare the changes between control group and CUMS model group to detect biomarker metabolites that associated with the depression. Initially, the unsupervised PCA analysis produced a solution with two significant components explaining 93.4% of the total variance in the data, but the separations between the control group and model group were not obvious. To eliminate the irrelevant noise, we further performed orthogonal partial least-squares discriminant analysis (OPLS-DA) to filter irrelevant information, and obtained a clear separation between the control group and CUMS model group. The internal validation was perfomed to assess the predictive ability of the corresponding OPLS-DA model ($R^2 = 0.996$), suggesting that the model was a good fit. To futher evaluate the validity of this model, a random permutation test (200 times) was performed, indicating no overfitting. Then, we calculated the variable importance in the projection (VIP) of the OPLS-DA model to identify the potential biomarkers (Figure 4 and Supplementary Figure S9). The threshold of $|VIP|>1$, $p < 0.05$, and log Fold change > 2 or <0.05 was used to screen candidate metabolites that linked to the development of depression. Finally, the metabolites of L-isoleucine and succinic acid were identified, belonging to energetic metabolism (citrate cycle, propanoate metabolism), amino acid metabolism (Valine, leucine and isoleucine biosynthesis), and genetic information processing (aminoacyl-tRNA biosynthesis) (Figures 4A,B and Table 2). As showed in Figure 4C, compared with the control group, the relative abundance of L-isoleucine in the CUMS model rats was decreased, while that of succinic acid was increased. This is consistent with previous finding reported by Xing et al. (Xing et al., 2015). Interestingly, the abundance of L-isoleucine was increased, and the abundance of succinic acid was decreased after YXJYD treated, suggesting that succinic acid and L-isoleucine may be therapeutic targets of YXJYD.

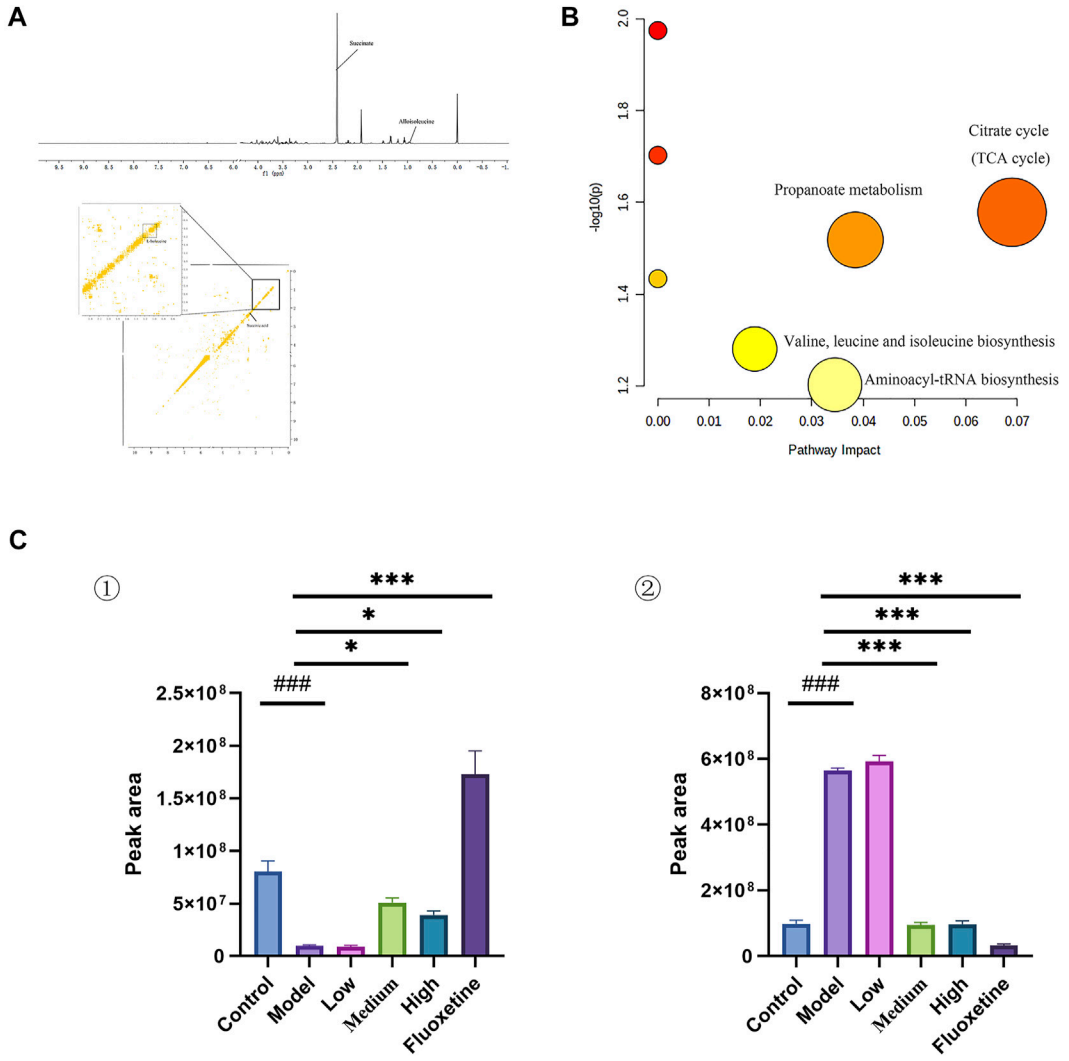

FIGURE 4
(A) 1D and 2D ^{1}H-^{1}H COSY identification results of different groups of cecal content differential metabolites; **(B)** Enrichment results of metabolic pathways associated with cecal contents; **(C)** Histogram of relative abundance of fecal differential metabolites in depressed rats [L-Isoleucine (①), Succinic acid (②)] (Control: Blank group, Model: Model group, Low: Formulation pellet low dose group, Middle: Formulation pellet medium dose group, High: Formulation pellet high dose administration group. Fluxetine: fluoxetine group) Note: Compared with blank group: $^{\#}p < 0.05$, $^{\#\#}p < 0.01$, $^{\#\#\#}p < 0.001$; Compared with model group: $^{*}p < 0.05$, $^{**}p < 0.01$, $^{***}p < 0.001$.

TABLE 2 Qualitative results of potential biomarkers of fecal metabolomics in rats with depression.

No.	Metabolites	Chemical shift (ppm)	VIP	HMDBID	KEGGID
1	L-Isoleucine	0.94(m)	1.13	HMDB0000172	C00407
		1.3(m)	0.69		
2	Succinic acid	2.39(s)	3.46	HMDB0000254	C00042

3.5 Urinary metabolic profiling and biomarker identification

In order to determine if the difference in the urine metabolome composition can be linked to the action of YXJYD on the gut microbiome, or if they are associated with development of depression, we further to characterize the urinary metabolic profiling and identify biomarker metabolites. Multivariate analytical methods performed on urinary samples were similar to cecal content samples (Supplementary Figure S9). In comparison with control group, nine

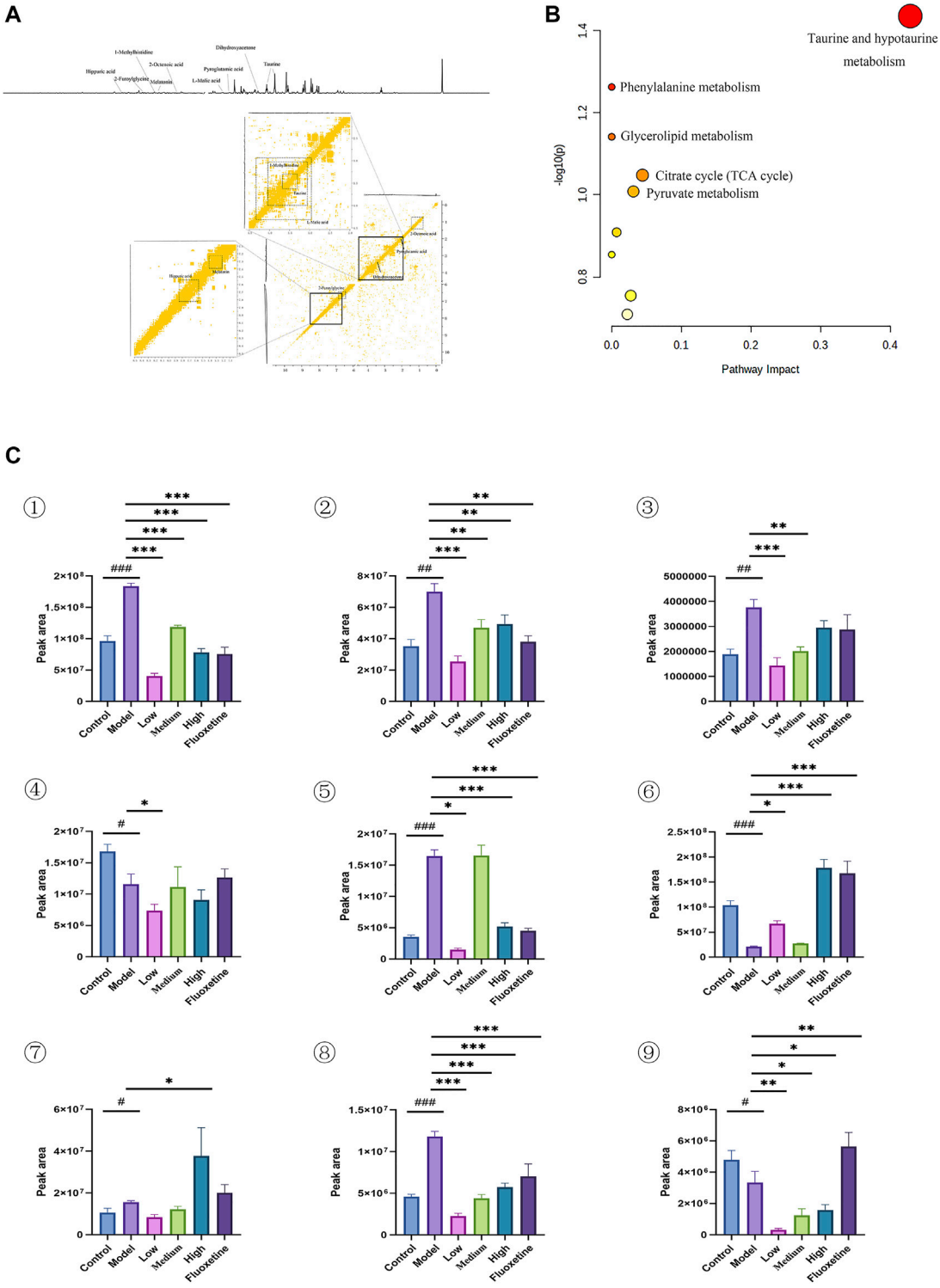

FIGURE 5
(A) 1D and 2D ^{1}H-^{1}H COSY identification results of different groups of urine differential metabolites; **(B)** Enrichment results of metabolic pathways associated with urine; **(C)** Histogram of relative abundance of urinary differential metabolites in depressed rats [Taurine (1), Dihydroxyacetone (2), L-Malic acid (3), 2-Octenoic acid (4), 1-Methylhistidine (5), Hippuric acid (6) Pyroglutamic acid (7), 2-Melatonin (8), Dimethylglycine (9)] (Control: blank group, Model: model group, Low: formulation pellet low dose group, Middle: formulation pellet medium dose group, High: formulation pellet high dose administration group. Fluxetine: fluoxetine group) Note: Compared with blank group: $^{\#}p < 0.05$, $^{\#\#}p < 0.01$, $^{\#\#\#}p < 0.001$; Compared with model group: $^{*}p < 0.05$, $^{**}p < 0.01$, $^{***}p < 0.001$.

TABLE 3 Qualitative results of potential biomarkers of urinary metabolomics in rats with depression.

No.	Metabolites	Chemical shift(ppm)	VIP	HMDBID	KEGGID
1	Taurine	3.28(t)	0.86	HMDB0000251	C00245
		3.41(t)	1.2		
2	Dihydroxyacetone	3.55(s)	1.28	HMDB0001882	C00184
		2.37(t)	0.59		
3	L-Malic acid	2.67(d)	0.67	HMDB0000156	C00149
		4.28(d)	2.09		
		0.86(t)	0.46		
4	2-Octenoic acid	2.13(q)	0.66	HMDB0000392	NA
		6.64(m)	1.55		
5	1-Methylhistidine	7.03(s)	1.39	HMDB0000001	C01152
		7.80(s)	1.04		
		3.95(d)	0.85		
6	Hippuric acid	7.54(t)	1.18	HMDB0000714	C01586
		7.63(t)	1.1		
		7.82(d)	1.05		
		2.03(m)	0.68		
7	Pyroglutamic acid	2.40(t)	0.64	HMDB0000267	C01879
		2.50(t)	0.61		
		4.14(t)	1.7		
		3.92(s)	0.61		
8	2-Furoylglycine	6.62(s)	1.64	HMDB0000439	NA
		7.17(d)	1.35		
		7.66(s)	1.07		
		1.89(s)	0.71		
		2.93(m)	0.63		
9	Melatonin	3.88(s)	0.98	HMDB0001389	C01598
		6.91(d)	1.48		
		7.21(d)	1.35		
		7.42(d)	1.34		

altered metabolites were identified in serum samples in CUMS model group, including taurine, dihydroxyacetone, L-malic acid, 2-octenoic acid, 1-methylhistidine, hippuric acid, pyroglutamic acid, 2-furoylglycine, melatonin (Figure 5A and Table 3). These metabolites are generated by some microorganisms through energetic metabolism (citrate cycle, pyruvate metabolism, glycerolipid metabolism) and amino acid metabolism (taurine and hypotaurine metabolism, phenylalanine metabolism, glutathione metabolism, tryptophan metabolism) (Figure 5B). Compared with control group, the relative abundance of taurine, dihydroxyacetone, L-malic acid, 1-methylhistidine, pyroglutamic acid, and 2-furoylglycine were upregulated significantly in the CUMS group, while that of 2-octenoic acid, hippuric acid, and melatonin were downregulated significantly in the CUMS group (Figure5C). These findings were consistent with previous researches on comparing depressive persons with healthy person (J. jun Chen et al., 2018). Coincided with our expectation, compared to the CUMS group, the abundance of taurine, dihydroxyacetone, L-malic acid, 1-methylhistidine, and 2-furoylglycine were downregulated significantly after YXJYD treated, while that of hippuric acid and melatonin were upregulated significantly after YXJYD treated. Notably, hippuric acid (also a metabolite of phenylalanine) could be produced by bacterial metabolism in the gut, highlighting the potential involvement of gut microbiota disturbance in the development of depression. These results showed that taurine, dihydroxyacetone, L-malic acid, 1-methylhistidine, 2-furoylglycine, hippuric acid and melatonin were important therapeutic targets of YXJYD.

3.6 Serum metabolic profiling and biomarker identification

In the serum metabolites, we performed the same multivariate analytical method to identify three significantly altered metabolites

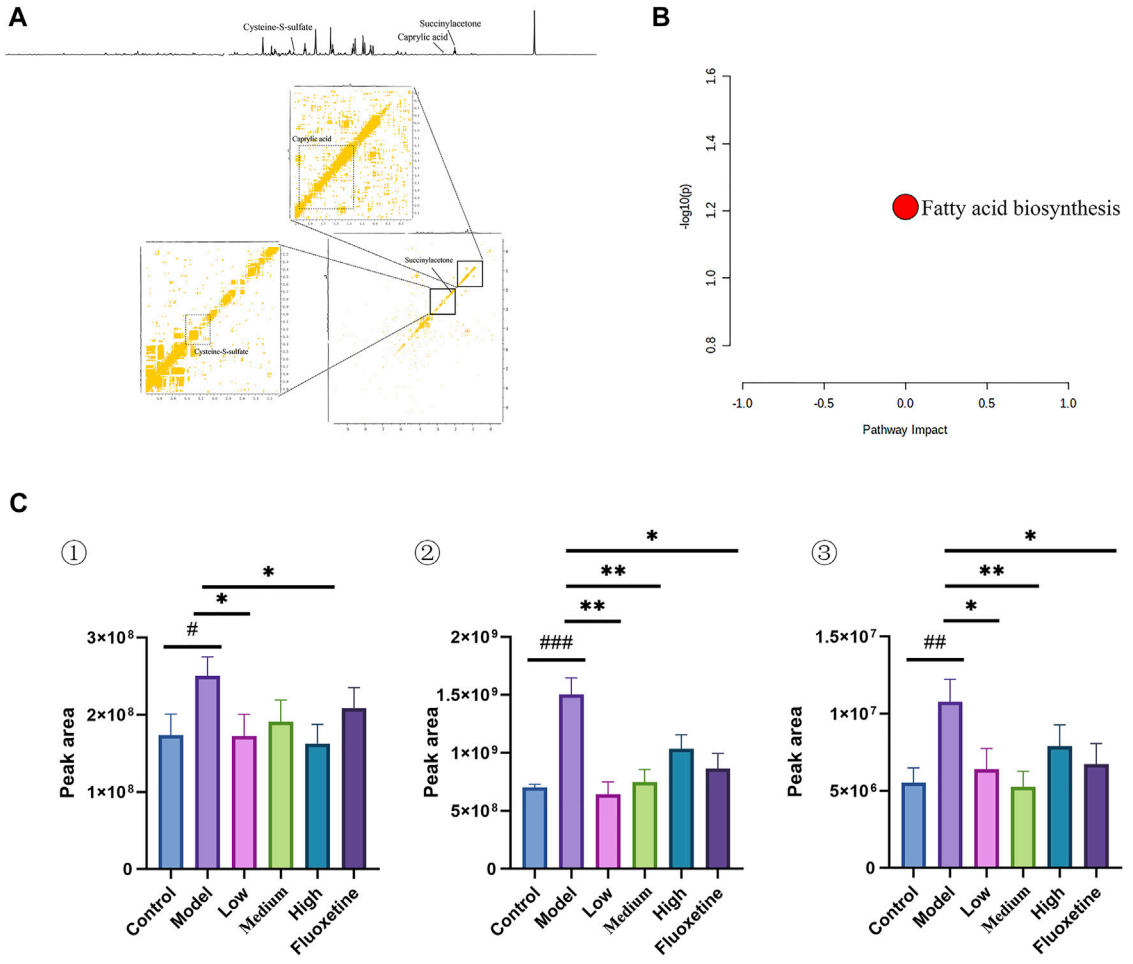

FIGURE 6
(A) 1D and 2D ^{1}H-^{1}H COSY identification results of different groups of serum differential metabolites; **(B)** Enrichment results of metabolic pathways associated with serum; **(C)** Histogram of relative abundance of serum differential metabolites in depressed rats [Cysteine-S-sulfate (1), Caprylic acid (2), Succinylacetone (3)] (Control: blank group, Model: model group, Low: formulation pellet low dose group, Middle: formulation pellet medium dose group, Fluxetine: fluoxetine group) dose group, High: formulation pellet high dose administration group, Fluxetine: fluoxetine group) Note: Compared with blank group: $^{\#}p < 0.05$, $^{\#\#}p < 0.01$, $^{\#\#\#}p < 0.001$; Compared with model group: $^{*}p < 0.05$, $^{**}p < 0.01$, $^{***}p < 0.001$.

between CUMS group and control group, which including caprylic acid, S-sulfo-L-cysteine (cysteine-S-sulfate), and succinylacetone (as showed in Figures 6A,C, and Table 4). These altered metabolites enriched in the pathway of fatty acid biosynthesis (Figure 6B). This result consistent with the finding that fatty acid metabolism is associated with the occurrence and development of depression (Robertson et al., 2017).

3.7 Effect of YXJYD treatment on gut microbiota diversity in CUMS-induced depression rats

The distribution of gut microbiota in different groups was compared by sequencing on the bacteria V3-V4 region of the 16S rRNA gene. A total of 1,391,894 reads were generated from twenty-four samples (8 samples per group, respectively). According to the rarefaction curves of all samples, the sequencing data volume is adequate to cover nearly all of microorganisms (Supplementary Figure S4). The Ace and Chao index were calculated to evaluate the α-diversity metrics in different groups (Figure 7A and Supplementary Table S2). As showed in the Figure 7, the index of Ace and Chao were showed markedly difference between control group and model group ($p < 0.001$), whereas showed no significant difference between control group and YXJYD-treated group ($p = 0.96$ and 0.78, respectively). Furtherly, compared with the control group, the Ace index and Chao index were decreased in the CUMS model rats, but that was reversed after YXJYD treated. It is indicated that YXJYD increased microbial richness and diversity, while CUMS caused microbial richness and diversity decreased.

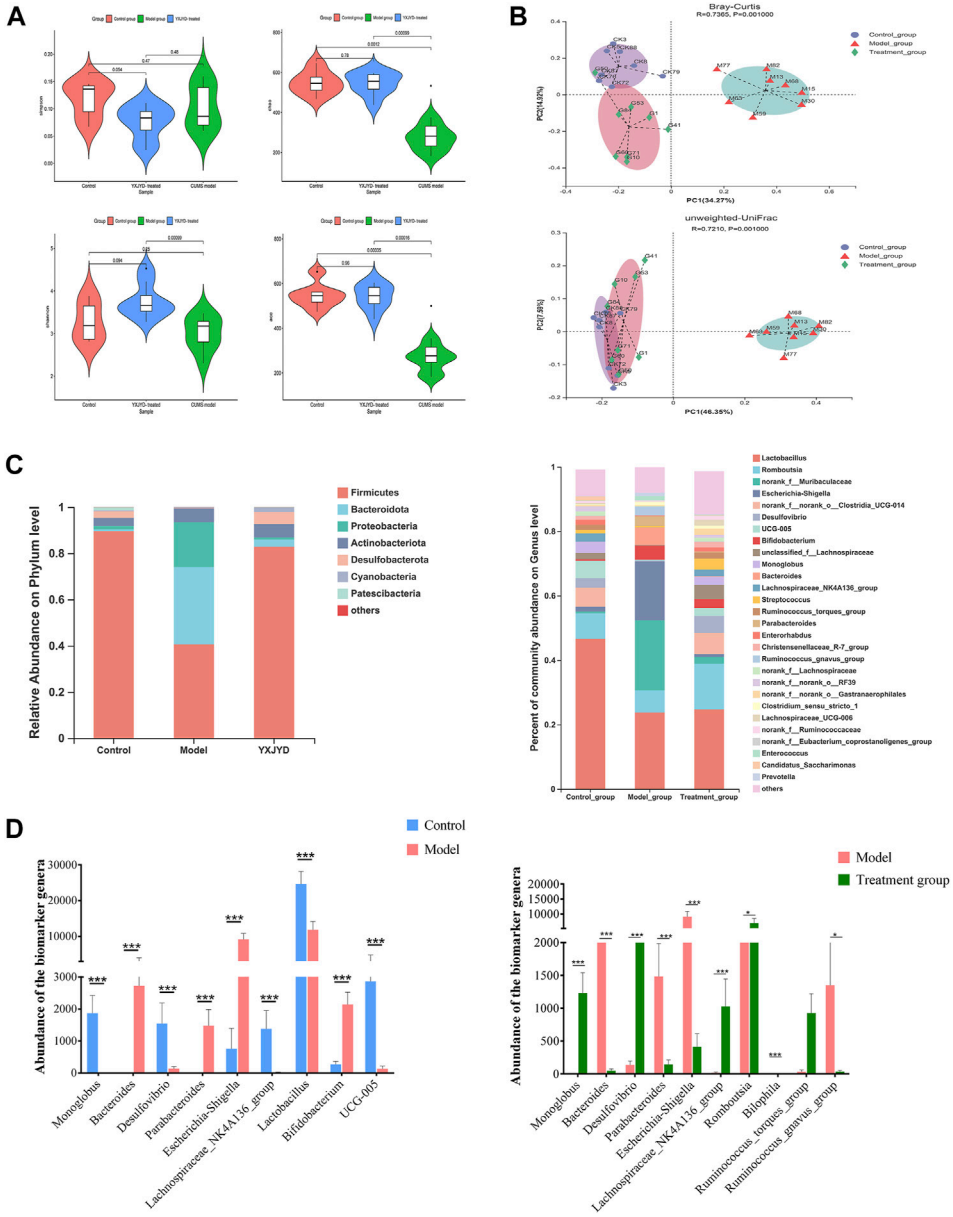

FIGURE 7
(A) Changes in the alpha diversity index (Simpson, Chao, Shannon, Ace) for different groups. Outliers were analyzed based on the Tukey outlier method **(B)** Features of the beta diversity index (Bray–Curtis, unweighted UniFrac) of samples in different groups. **(C)** Gut microbiota abundance of each sample at phylum level and genus level. **(D)** Potential biomarkers of the gut microbiome based on LEfSe analysis among the control, model, and YXJYD groups. (Cecal contents, n; Control = 8, Model = 8, YXJYD = 8).

To evaluate the difference of gut microbial composition by pairwise comparison, we performed the beta diversity and principal coordinate analysis (PCoA). The beta diversity analysis revealed that the microbiota of the model group differed considerably between the control group and the YXJYD treatment group (2.1 g/kg). The PCoA plot showed that the model group exhibited significant separation from the other two groups markedly (Figure 7B), indicating a significant difference of gut microbiota composition between model group and control group, whereas YXJYD treatment reduced the difference. The value on the axis records the percentage of results interpreted by each dimension.

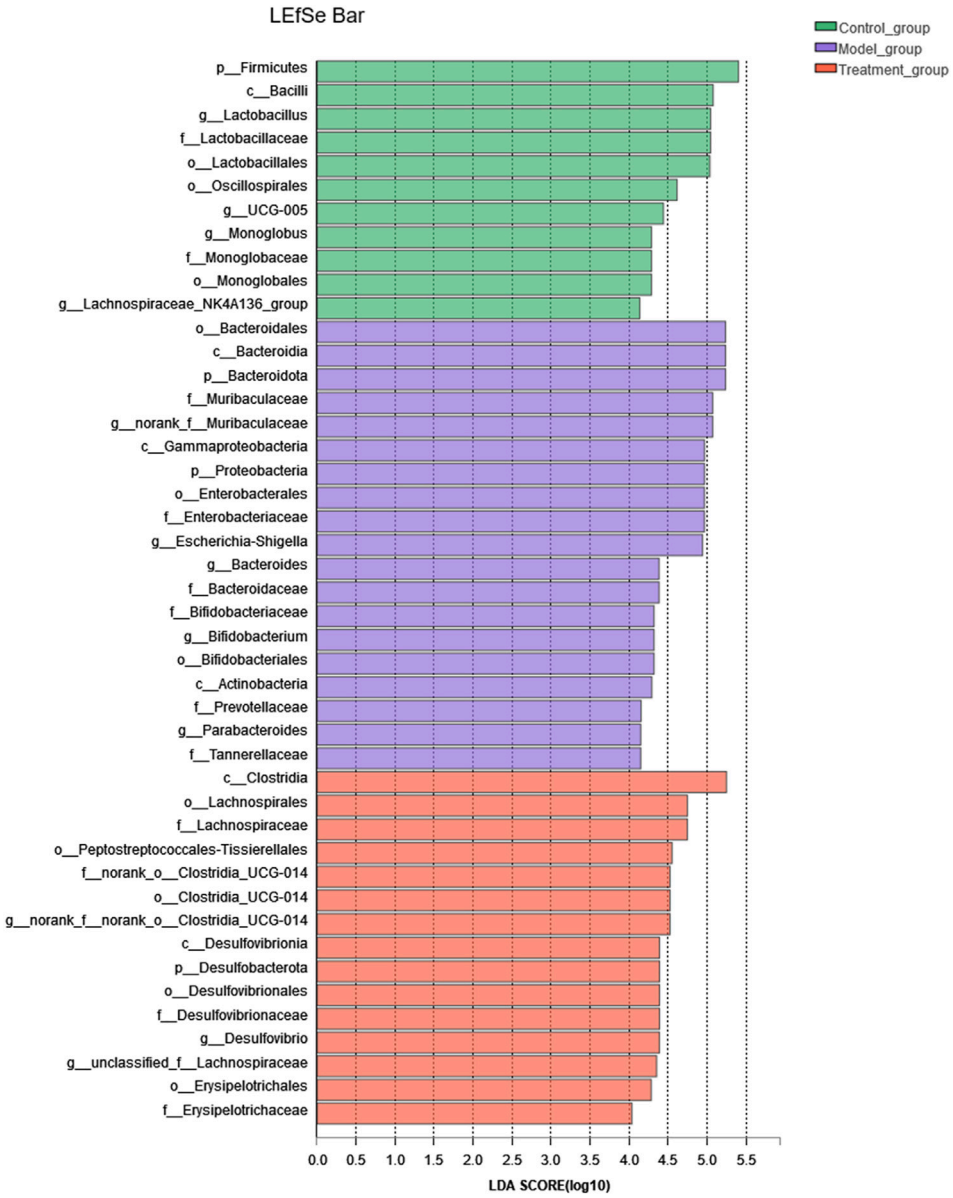

FIGURE 8
LEfSe analysis of relative abundance of gut microbiome among Control, Model and YXJYD-treatment groups. The larger of the LDA score represents the stronger effect of the species abundance on the differentiation. The Cut-off values were $p < 0.01$ and LDA > 4.

3.8 Regulation of YXJYD on the microbial distribution at the phylum levels

At the phylum level, the microbiota was dominated by *Firmicutes*, *Bacteroidetes*, *Proteobacteria*, *Actinobacteria*, *Desulfobacterota*, *Cyanobacteria* and *Patescibacteria*, and showed notable differences across control group, model group, and YXJYD high-dose treated group. The community bar plot at the phylum level showed the distributions of the top seven most abundant phyla (Figure 7C). Compared to control group, *Firmicutes* phylum was obviously decreased, while *Bacteroidota* increased in model group, but there is no difference between control group and YXJYD treatment group. Furthermore, Figure 7C demonstrated that CUMS increased the number of *Proteobacteria* and *Actinobacteria* while decreased the abundance of *Desulfobacterota, Cyanobacteria,* and *Patescibacteria*. Notably, a high dosage of YXJYD restored bacterial abundance, and the rats displayed a similar microbial distribution to the control group after YXJYD treatment.

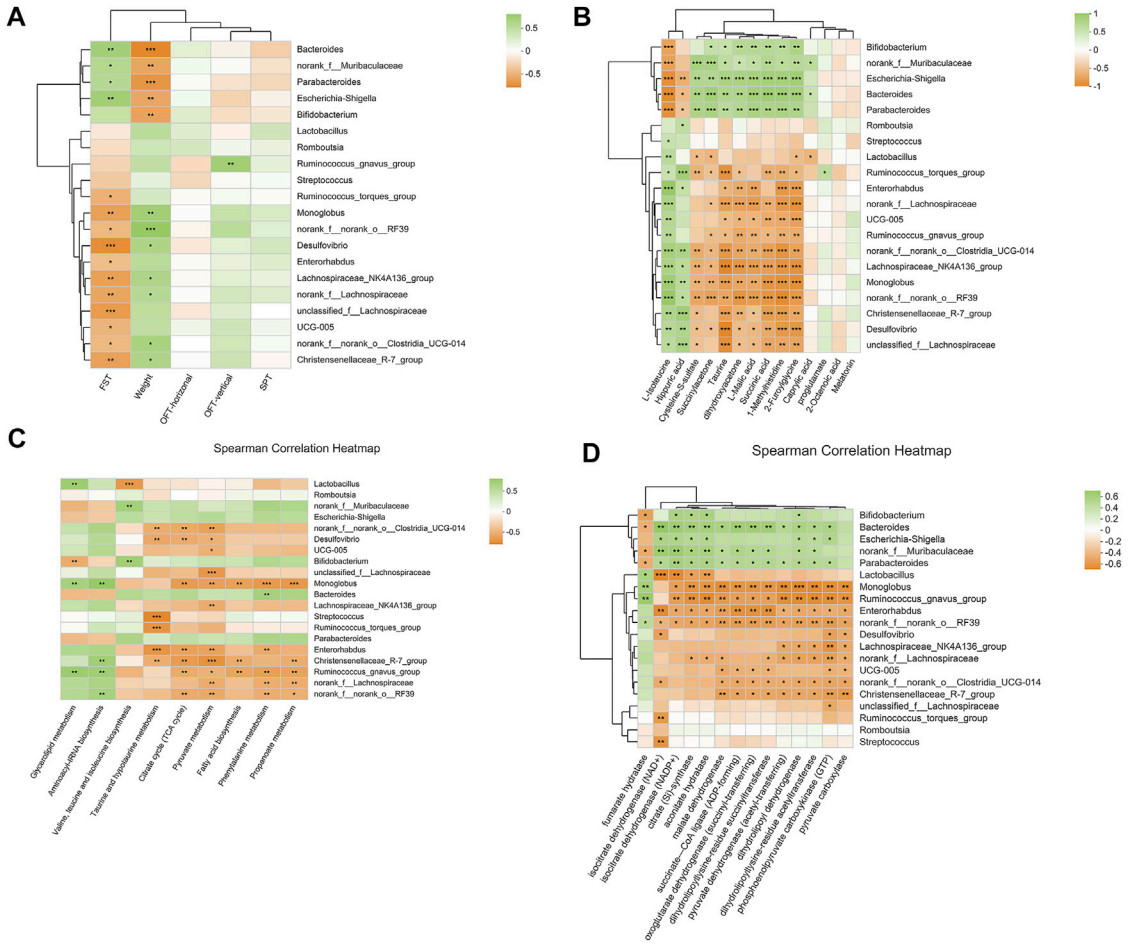

FIGURE 9
(A) Heat map for correlation analysis of intestinal differential microorganisms (relative abundance were rank top of 20) with behaviors; **(B)** Heat map for correlation analysis of intestinal differential microorganisms (relative abundance were rank top of 20) with differential metabolites of urine, cecal content, and serum; **(C)** Heat map for correlation analysis of intestinal differential microorganisms (relative abundance were rank top of 20) with metabolic pathways; **(D)** Heat map for correlation analysis of intestinal differential microorganisms (relative abundance were rank top of 20) with microbial enzymes. *$p < 0.05$; **$p < 0.01$; ***$p < 0.001$. FST, Forced Swimming Test results; OFT, Open Field Test results; SPT, Sucrose Preference Test results.

3.9 Identified biomarker microbiome at the genus level

At the genus level, a variety of microbiotas showed significantly different between model group and control group, including *Lactobacillus*, *Monoglobus*, *Desulfovibrio*, Lachnospiraceae*_NK4A136_group*, *Romboutsia*, *Ruminococcus_torques_group*, and so on (as showed in Figures 7C,D). We further used the method of LEfSe analysis to compare the difference between three groups at the genus level. While performed the LefSe analysis among three groups, with the threshold of logarithmic LDA score 4.0, and $p < 0.01$, the LefSe analysis revealed the genus of *Lactobacillus, Monoglobus, UCG-005,* and Lachnospiraceae*_NK4A136_group* were enriched in the control group, the genus of *Escherichia-Shigella*, *Bifidobacterium, Bacteroides, Parabacteroides* were enriched in the model group (as showed in Figure 8). Besides, as showed in the Supplementary Table S4 from the RF analysis (MDA score > 2.5), 11 key genera for classification were found. Given the results of these two analyses, we identified *Monoglobus*, *Bifidobacterium*, *Bacteroides*, *Parabacteroides*, and Lachnospiraceae*_NK4A136_group* were the biomarker genus of depression as well as YXJYD-treatment alteration of microbiota composition. Compared with the control group, *Monoglobus* and Lachnospiraceae*_NK4A136_group* were significantly decreased, while *Bifidobacterium, Bacteroides, Parabacteroides* were significantly increased in the model group. Whereas, compared with the model group, the abundance of *Monoglobus* and

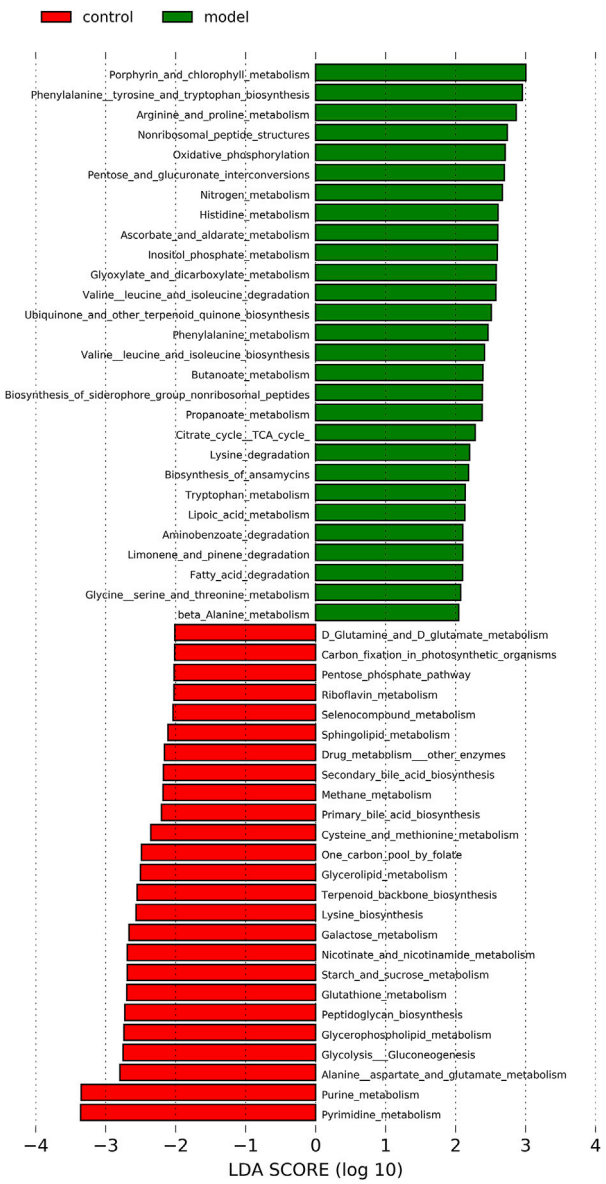

FIGURE 10
LEfSe analysis of functional metabolism pathways between Control and Model groups. The larger of the LDA score represents the stronger effect of the species abundance on the differentiation. The Cut-off values were $p < 0.01$ and LDA > 2.0.

Lachnospiraceae_*NK4A136_group* were significantly increased in the YXJYD-treatment group, while that of *Bifidobacterium, Bacteroides, Parabacteroides* were significantly decreased in the YXJYD-treatment group. Furthermore, the abundance of *Monoglobus* was closely correlated with the improvement of behavior symptoms, the variation of metabolites, and hosted metabolic pathways (Figure 9). Based on the above results, we considered that the variation of *Monoglobus* was the most important biomarker genus in the YXJYD-affected alteration of microbiota composition.

3.10 Microbial functional predictions and host-microbe interactions

253 differential pathways were predicted by Tax4Fun from levels 3 KEGG orthologs, which included metabolism (53.36%), organismal systems (13.44%), human diseases (16.21%), genetic information processing (7.90%), environmental information processing (4.74%), and cellular processes (4.35%). Among these pathways, we were interested in metabolic pathways, which were linked to depression pathophysiology. To detect the key pathways, LEfSe analysis and RF analysis were performed between the control and model groups. Based on the logarithmic LDA score of 2.0 as the cutoff (Kruskal-Wallis test, p-value < 0.01), 54 pathways were identified as significantly differential pathways relevant to depression (Figure 10). In addition, as showed in the plot from the RF analysis (MDA score >2.0) (Supplementary Table S10), 18 key pathways associated with depression were found. Given the results of these two results and the above metabolites related hosted metabolic pathway, citrate cycle and propanoate metabolism were identified as the key metabolic pathways that associated with the occurrence and development of depression. Moreover, 42 enzymes displayed significantly different in the YXJYD-treated groups (Supplementary Table S9). In the propanoate metabolism, there were four enzymes differentially expressed in the YXJYD-treatment group ((p < 0.01, LDA > 2)), including alpha-ketoisocaproate dehydrogenase (EC 1.2.4.4), acetyl-CoA synthetase (EC 6.2.1.1), dihydrolipoyl dehydrogenase (EC 1.8.1.4), and L-lactate dehydrogenase (EC 1.1.1.27) (showed in Figure 11A). In the tricarboxylic acid cycle (TCA cycle), there were five differentially expressed enzymes, which included pyruvate dehydrogenase E1 component alpha subunit [EC:1.2.4.1], dihydrolipoamide dehydrogenase [EC:1.8.1.4], pyruvate carboxylase [EC:6.4.1.1], aconitate hydratase [EC:4.2.1.3], and pyruvate dehydrogenase E2 component (dihydrolipoamide acetyltransferase) [EC:2.3.1.12] (showed in Figure 11B).

4 Discussion

The present study provided evidence that YXJYD increases the abundance of *Monoglobus* and upregulates four potential metabolic enzymes involvement in propanoate metabolism and five enzymes in TCA cycle. At present, the important role of gut microbiome in the central nervous system development has attracted more and more attention, and accepted by majority that gut microbiome play a critical role in the onset and development of depression via the "microbiota-gut-brain" axis. Thus, target on regulating of gut microbiome may be an effective way for antidepressant. However, available antidepressant drugs may lead, instead, to

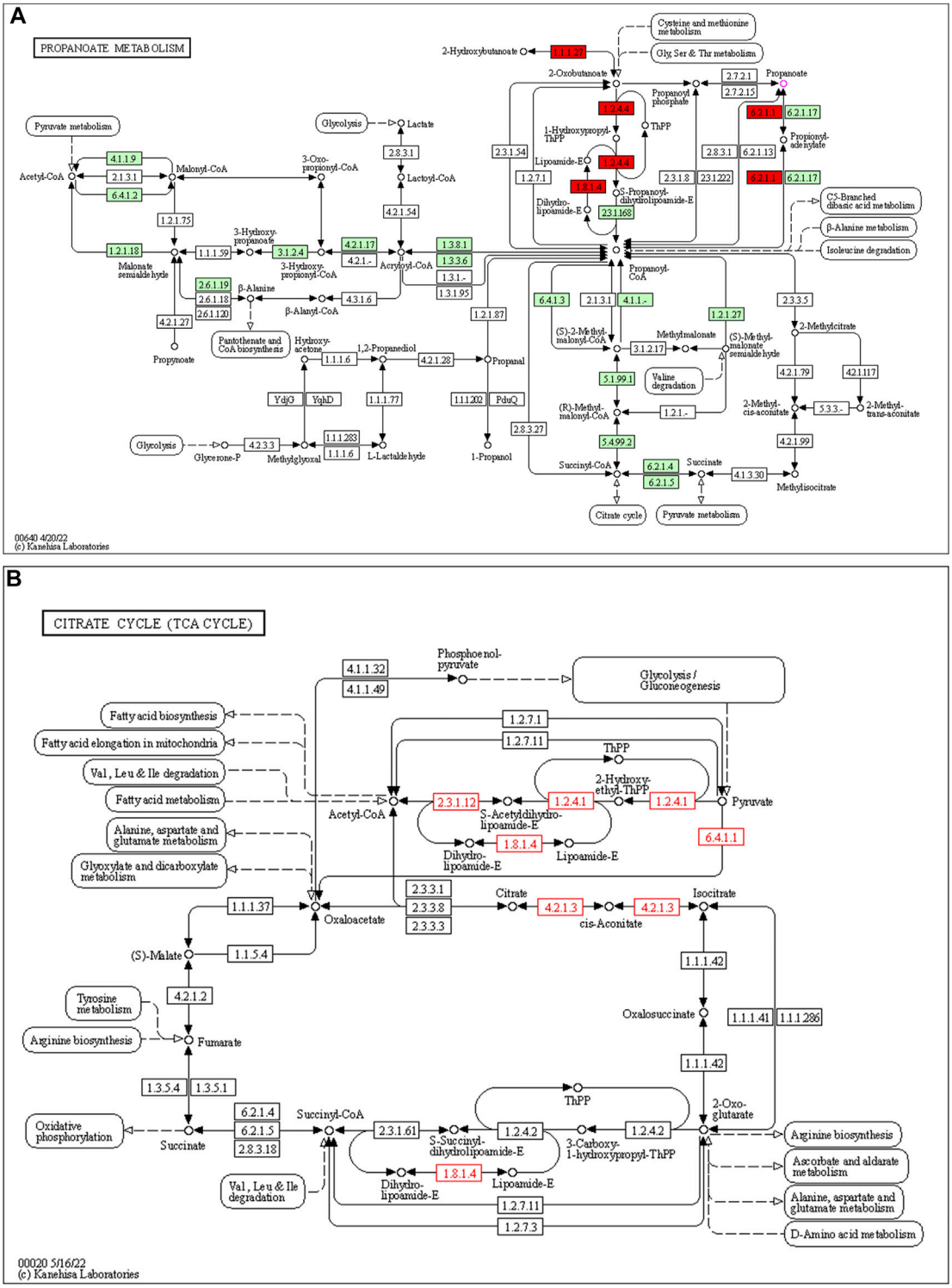

FIGURE 11
Propanoate metabolism pathway **(A)** and TCA cycle **(B)**. The target enzymes were marked red.

adverse effect of gastrointestinal disturbances. Hence, how the microbiome is involved in the development of depression has not been systematically investigated.

YXJYD is an empirical prescription for adolescents'depression, and was found to increase appetite and eliminate some digestive disorders from the feedback of adolescents'depressive patients

clinically. These feedbacks led us hypothesize that the antidepressant effect of YXJYD may associated with gut microbiota.With an integrated study of the gut microbiota and cecal content, serum, and urine metabolomes, we found that changes in microbiota abundance of the cecal contents significantly contribute to changes in the serum and urine metabolomes, and are linked with reducing depressive-like symptoms in CUMS rats. Our results verified the involvement of gut microbiota metabolism in the effects of YXJYD. Furthermore, the findings demonstrated that the disrupted metabolism was consistent with the pathway enrichment of the changed metabolomes and the projected functional profile of the altered cecal content microbiota in animal models. These findings supported the use of YXJYD as a valuable medication to treat depression in teenagers by modulating their gut microbiotas and host metabolism.

TCM combines well with the healing principle of systemic medicine in the treatment of difficult disorders, such as depression, because of its multi-target and multi-channel characteristics (Maes, Kubera, and Leunis 2008; Maes et al., 2012). Consistent with our expectation, our study indicated that YXJYD improved the behavioral symptoms of depression-like rats in a nondose-dependent manner, and seems superiored to fluoxetine hydrochloride. In addition, 16S rRNA sequencing on the gut microbiota revealed that CUMS decreased the richness and diversity of gut microbiotas significantly, as shown by the Chao and ACE indices. However, it is important to note that the CUMS-induced disruption of gut microorganisms was repaired after treatment with YXJYD. We hypothesized that the antidepressant role of YXJYD may be explained by regulating the "microbiota–gut–brain axis" and then to improve appetite. Evidence is mounting that the gut microbiota plays a critical role in a range of neuropsychiatric illnesses, including depression, schizophrenia, Parkinson's disease, and autism (Sampson et al., 2016; Sun et al., 2018; Sharon et al., 2019; Zheng et al., 2019). Further, the experimental of transplantation 'depressed microbiota' from a depressive patient to healthy animals would induce depressive-like behaviors that offers a foundation for exploring the connections between gut microorganisms and depression. Otherwise, Cai et al. revealed that transferring a healthy person's fecal microbiota to a depressed patient might alleviate depression-related symptoms by restoring or reconstructing the intestinal microbiota's composition (Cai et al., 2019). In our study, we found that the richness of *Firmicutes, Cyanobacteria* and *Desulfobacteria* were higher and the richness of *Bacteroidota, Proteobacteria,* and *Actinobacteria* were lower in CUMS model group than that in the control group, which were in agreement with Jiang et al. (H. Jiang et al., 2015) reported that the phylum of *Bacteroidetes, Proteobacteria,* and *Actinobacteria* were positively correlated with depression, while *Firmicutes phylum* was negatively related with depression. Moreover, it is reported that the microbiome members of *Bacteroidete* and *Firmicutes* play crucial roles in modulating host inflammation and immune balance, and a higher F/B ratio is positively associated with the homeostasis of the gut microbiome (Chang et al., 2015). In our study, we observed that *Bacteroidete* and *Firmicutes* were the two major phylas in our samples, and the ratio of *Firmicutes*/*Bacteroidota* in the CUMS model group was significantly lower than that in control group, while there is no significant difference between control group and YXJYD-treated group. It is indicated that CUMS may disturb the balance of the gut microbiota and that finally lead to depression. Otherwise, the ratio of Firmicutes/Bacteroidota was recovered in YXJYD group, indicating that the antidepressant effect of YXJYD was relevant to regulate gut microbiome disturbance.

With further analysis, we identified *Monoglobus* as the key biomarker genera. The abundance *Monoglobus* was decreased in the CUMS model group, but was enriched in the YXJYD-treatment group. We speculate that this genera may be associated with the development of depression. The protective role of *Monoglobus* are supported by previous studies. *Monoglobus* have been shown to be involved in dietary fiber fermentation and associated with healthy communities (C. C. Kim et al., 2019). Moreover, the genus of *Bacteroides, Parabacteroides, Escherichia-Shigella, Bifidobacterium,* and *Ruminococcus_gnavus_group* were significantly downregulated in the YXJYD group, while *Lactobacillus, Desulfovibrio,* Lachnospiraceae_*NK4A136_group, Romboutsia, Bilophila,* and *Ruminococcus_torques_group* were not. Consistent with this finding, higher abundance of *Bacteroides* and lower abundance of *Lactobacillus* were also found in the feces from

TABLE 4 Qualitative results of potential biomarkers of serum metabolomics in rats with depression.

NO.	Metabolites	Chemical shift(ppm)	VIP	HMDBID	KEGGID
1	Cysteine-S-sulfate	3.4(s) 3.68(d) 4.1(s) 0.89(s)	1.03 2.44 3.15 1.65	HMDB0000731	C05824
2	Caprylic acid	1.28(t) 1.5(s) 2.16(s) 2.26(s)	4.01 0.81 0.87 1.2	HMDB0000482	C06423
3	Succinylacetone	2.41(s) 2.81(s)	1.09 0.51	HMDB0000635	NA

patients with major depressive disorders (MDD), and previous investigations widely reported that upregulation of *Bacteroides* linked with higher peripheral cytokine levels and increased inflammation in MDD (Yang et al., 2020). The highest LDA score of *Lactobacillus* indicated that the reduced *Lactobacillus* was the most prominent biomarker genus in the CUMS-induced alteration of microbiota composition. Reduced level of gut *Lactobacillus* has also been observed in people with MDD, and that partly because stressor exposure associated with the colonic mucosa, reducing *Lactobacillus* abundance (Heym et al., 2019). Moreover, the anti-inflammatory activity of the *Lactobacillus* genus has been shown to improve cognitive function (Aizawa et al., 2016; J. K. Kim et al., 2020). Alternatively, our study also observed a higher *Bifidobacterium* in CUMS-induced depressive rats. Previous studies have been reported mono-colonisation of mice with human *Bifidobacterium*-rich microbiota had higher proinflammatory Th17 intestinal cells compared to mice colonised with *Bifidobacterium*-depleted microbiota (Ang et al., 2020) (Wang et al., 2014). Furthermore, a higher abundance of *Romboutsia* and *Bilophila* were also displayed in our study. *Romboutsia,* known SCFA producers, has been confirmed to be strongly correlated with the butyrate levels, while fecal butyrate was negatively correlated with depressive symptoms in PD patients.

It may be explained that YXJYD could affect several pathogenic targets concurrently with multiple botanical drugs. We performed HPLC-MS/MS to analyze the chemical compounds of YXJYD and identified 23 compounds enriched in the YXJYD. The majority of the compounds were found to have considerable antidepressant properties. Ginsenoside Rb1, for example, has been shown to have potential antidepressant-like effects in depression model mice by increasing BDNF signaling and encouraging hippocampus neurogenesis. (N. Jiang et al., 2021); Ginsenoside Rg3 was also reported to be effective in ameliorating depressive-like behavior by regulating microglia activation and nuclear factor kappa B (NF-κB) pathway (Kang et al., 2017); Ginsenoside Rf significantly restored depression-like behavioral abnormalities by increasing glial fibrillary acidic protein (GFAP) expression and decreasing Ki-67 expression in the PFC, as well as reducing astroglial changes in the hippocampus (Y. Kim et al., 2020); Magnoflorine has been shown to have an antidepressant effect in brain tissue by increasing the expression of lysine specific demethylase 1 (LSD1), despite its poor liposolubility and low permeability (Barua et al., 2018). Because YXJYD contains numerous components, each of which exerts a separate mechanism, determining the antidepressant mechanism of YXJYD is difficult.

Metabolite is the end products of biological processes, and it may display physiological circumstances directly due to its "downstream" regulatory relationships with the genome, transcriptome, and proteome levels (Bi et al., 2021). Furthermore, metabolites serve as important messengers between the gut microbiota and the host. Previous research has shown that the gut microbiota influences the onset and development of depressive-like behaviors via a metabolic route regulated by the host (P. Zheng et al., 2016). Therefore, we sought to uncover the metabolic mechanism behind the flow of metabolites from gut to brain for reliving depressive mood and behaviors by analyzing the changes of metabolites in serum, urine, and cecal contents. According to the previous metabonomic researches on depression, remarkable changes of metabolites were mostly enriched in energy metabolism, amino acid metabolism, gut microflora metabolism and amino acid neurotransmitters (S. Zheng et al., 2010; Xing et al., 2015; Gao et al., 2014). Consistent with these reports, a number of amino acid neurotransmitters and their derivatives, including taurine, pyroglutamic acid, 2-furoylglycine, and hippuric acid, were considerably changed in urine between CUMS model rats and control rats. Moreover, we found that these altered amino acid neurotransmitters enriched in the amino acid metabolism pathway of taurine and hypotaurine metabolism, phenylalanine metabolism, and glutathione metabolism. These results are in line with the findings of a systematic analyse that indicated abnormalities of amino acid neurotransmitters in depression models (Pu et al., 2021).

Meanwhile, a significant lower level of melatonin was found in CUMS-induced depression rats and was upregulated after treatment with YXJYD. Melatonin is a hormone generated by the pineal gland from serotonin (5-HT) as a precursor via tryptophan metabolism. Other authors using different classes of antidepressants have also found that antidepressants increased melatonin levels, included imipramine (Miller et al., 2001), clomipramine (Rabe-Jabłońska and Anna, 2001), desipramine (Kennedy and Brown 1992), clorgyline, tranylcypromine and phenelzine (Carvalho et al., 2009). Therefore, increased of melatonin levels seems to be an indicator of effective antidepressant. The level of melatonin was elevated in rats after treating with YXJYD. It is suggesting that the antidepressant effect of YXJYD may be associated with regulation of tryptophan metabolism. In comparison with control group, lower levels of succinic acid and L-malic acid were found in CUMS model rats, which are significant biological molecules and crucial intermediates in the TCA cycle linked to glycometabolism and energy metabolism. This is also consistent with our final results that we identified the pathway of TCA cycle and propanoate metabolism as the key pathways relevant to YXJYD treatment. Furthermore, succinic acid is a short-chain fatty acid that is essential for energy transmission and the Krebs cycle. Succinic acid levels was rose following CUMS, which was consistent with earlier research (Xing et al., 2015). As a result, these changed metabolites suggested that antidepressant effect of YXJYD may be linked to correct energy metabolism imbalances, as previously described, and that providing extra creatine or ATP may have antidepressant action (Cao et al., 2013; Cunha et al., 2018). Besides, succinic acid is crucial for energy transportation and is also an important factor in fatigue, as well as hippuric acid (HA) is the metabolite of phenylalanine (Phe) metabolized by the gut microflora, suggested that there was a significant effect on the gut by YXJYD treatment and then improved the fatigue as feedback from adolescents'depressive patients in clinical (Ladep et al., 2006).

Furthermore, the current findings revealed that L-isoleucine levels were reduced in the depression model and that YXJYD considerably increased L-isoleucine levels. It is reported that L-isoleucine affected the mammalian central nervous system (CNS) by two ways. Firstly, isoleucine can be used as a

significant amino group donor for the creation of brain glutamate, a crucial CNS neurotransmitter, after it has quickly crossed the blood–brain barrier (Ni et al., 2008). Impaired glutamate homoeostasis and glutamatergic neurotransmission have been identified as the primary causes of depression's incidence and progression (Shao et al., 2013; G. Chen et al., 2015). Second, the dipeptide glutamine–isoleucine has been found to greatly enhance locomotor activity in rats by injecting this neuropeptide into the ventral tegmental region of the rat midbrain, which transmits afferent GABAergic and glutamatergic projections to the PFC (Berberian, Sanchez, and Celis 2002). Isoleucine acts as essential ketogenic and glucogenic amino acid to play a significant role in energy metabolism. Isoleucine may be transformed into succinyl-CoA via transamination with alpha-ketoglutarate during the tricarboxylic acid cycle (TCA) oxidation process, or it can be turned into oxaloacetate for gluconeogenesis. These findings revealed that modulating L-isoleucine levels and TCA oxidation or gluconeogenesis might be a promising treatment target for depression, and the antidepressant mechanism of YXJYD was connected with regulating neurotransmitter biosynthesis and energy metabolism (G. Chen et al., 2015).

5 Conclusion

Our current results demonstrated that antidepressant effect of YXJYD was evident in CUMS rats and it's mechanism possibly be associated with increasing the abundance of *Monoglobus* and upregulating enzymes involvement in propanoate metabolism and in TCA cycle. In comparison to other antidepressant drugs, the concentration of YXJYD is lesser but showed a striking effect. Coupling with the efficacy for adolescents in clinical, YXJYD would be a promising antidepressants for further study. This work will make a great contribution to the development and application of YXJYD for the treatment on adolescents' depression. Moreover, there are still some limitations in this study. First of all, the microbiology we used can only comprehend the relative abundance of intestinal microbiota, not the exact composition. Secondly, the potential molecular mechanism of the effect of YXJYD on gut microbiota in this study needs to be further validated. Finally, this study only involved the regulation of gut microbiota and body's metabolites by YXJYD, and the linked between gut and brain that can be described was limited. It is valuable for us to explore the molecular mechanism of YXJYD by the gut-brain axis in further study.

Data availability statement

The datasets presented in this study can be found in online repositories. The names of the repository/repositories and accession number(s) can be found below: NCBI BioProject, PRJNA862250.

Ethics statement

The animal study was reviewed and approved by Animal Ethics Committee of Guangxi Medical University (permit number: SYXK Gui 2020-0004).

Author contributions

Conceived and designed the experiments: JL, JZ, and ML. Performed the experiments: XL, PM, HQ, SL, and WO. Analyzed the data: XL, PM, and HQ. Contributed to the writing of the manuscript: XL, ML, JZ, and PM. All authors contributed to the article and approved the submitted version.

Funding

This work was supported by the National Natural Science Foundation of China (81960807), Guangxi Traditional Chinese Medicine Appropriate Technology Development and Promotion Project (Gzsy22-37), and Guangxi Xinglin young talents project of Guangxi University of Traditional Chinese medicine.

Conflict of interest

The authors declare that the research was conducted in the absence of any commercial or financial relationships that could be construed as a potential conflict of interest.

Publisher's note

Supplementary material

The Supplementary Material for this article can be found online at: https://www.frontiersin.org/articles/10.3389/fphar.2022.972351/full#supplementary-material

References

Aizawa, E., Tsuji, H., Asahara, T., Takahashi, T., Teraishi, T., Yoshida, S., et al. (2016). Possible association of Bifidobacterium and Lactobacillus in the gut microbiota of patients with major depressive disorder. *J. Affect. Disord.* 202, 254–257. doi:10.1016/j.jad.2016.05.038

Ang, Q. Y., Alexander, M., Newman, J. C., Yuan, T., Cai, J., Upadhyay, V., et al. (2020). Ketogenic diets alter the gut microbiome resulting in decreased intestinal Th17 cells. *Cell* 181, 1263–1275. doi:10.1016/j.cell.2020.04.027

Barua, C. C., Saikia, B., Ren, X., Elancheran, R., Pathak, D. C., Tamuli, S., et al. (2018). Zanthoxylum alatum attenuates lipopolysaccharide-induced depressive-like behavior in mice Hippocampus. *Pharmacogn. Mag.* 14, 673. doi:10.4103/pm.pm_606_17

Berberian, V., Sanchez, M. S., and Ester Celis, M. (2002). Participation of the cholinergic system in the excessive grooming behavior induced by neuropeptide (N) glutamic acid (E) isoleucine (I) amide (NEI). *Neurochem. Res.* 27, 1713–1717. doi:10.1023/A:1021655631754

Bi, T., Feng, R., Zhan, L., Ren, W., and Lu, X. (2021). ZiBuPiYin recipe prevented and treated cognitive decline in ZDF rats with diabetes-associated cognitive decline via microbiota–gut–brain Axis dialogue. *Front. Cell Dev. Biol.* 9, 651517. doi:10.3389/fcell.2021.651517

Cai, T., Shi, X., Yuan, L. Z., Tang, D., and Wang, F. (2019). Fecal microbiota transplantation in an elderly patient with mental depression. *Int. Psychogeriatr.* 31, 1525–1526. doi:10.1017/S1041610219000115

Cao, X., Li, L. P., Wang, Q., Wu, Q., Hu, H. H., Zhang, M., et al. (2013). Astrocyte-derived ATP modulates depressive-like behaviors. *Nat. Med.* 19, 773–777. doi:10.1038/nm.3162

Carvalho, L. A., Gorenstein, C., Moreno, R., Pariante, C., and Markus, R. P. (2009). Effect of antidepressants on melatonin metabolite in depressed patients. *J. Psychopharmacol.* 23, 315–321. doi:10.1177/0269881108089871

Chang, C. J., Lin, C. S., Lu, C. C., Martel, J., Ko, Y. F., Ojcius, D. M., et al. (2015). Ganoderma lucidum reduces obesity in mice by modulating the composition of the gut microbiota. *Nat. Commun.* 6, 7489. doi:10.1038/ncomms8489

Chen, G., Yang, D., Yang, Y., Li, J., Cheng, K., Tang, G., et al. (2015). Amino acid metabolic dysfunction revealed in the prefrontal cortex of a rat model of depression. *Behav. Brain Res.* 278, 286–292. doi:10.1016/j.bbr.2014.05.027

Chen Jj, J. J., Bai, S. J., Li, W., Zhou, C. J., Zheng, P., Fang, L., et al. (2018). Urinary biomarker panel for diagnosing patients with depression and anxiety disorders. *Transl. Psychiatry* 8, 192. doi:10.1038/s41398-018-0245-0

Chen Z, Z., Wang, Z., Xu, Q., and Wang, B. (2018). Shengmai formula and its major survey of study on pharmacological effects of drugs in the treatment of cardiovascular disease. *Chin. J. Integr. Med. Cardio-Cerebrovascular Dis.* 16 (14), 3.

Chengfu, L., Chen, X., Chen, S., Yi, L., and Liu, Q. (2014). Extracts from pericarpium citri improve behaviors and hippocampal BDNFin mice exposed to chronic mild unpredictable stress. *China J. Exp. Traditional Med. Formulae* 20 (19), 151–155.

Chunlei, J., Zhang, Y., and Shi, X. (2012). Acacia flower clinical study on treatment of depression. *Guangxi J. Traditional Chin. Med.* 35 (6), 3.

Cipriani, A., Zhou, X., Del Giovane, C., Hetrick, S. E., Qin, B., Craig, W., et al. (2016). Comparative efficacy and tolerability of antidepressants for major depressive disorder in children and adolescents: A network meta-analysis. *Lancet* 388, 881–890. doi:10.1016/S0140-6736(16)30385-3

Cunha, M. P., Pazini, F. L., Lieberknecht, V., and Rodrigues, A. L. S. (2018). Subchronic administration of creatine produces antidepressant-like effect by modulating hippocampal signaling pathway mediated by FNDC5/BDNF/akt in mice. *J. Psychiatr. Res.* 104, 78–87. doi:10.1016/j.jpsychires.2018.07.001

Fekadu, N., Shibeshi, W., and Engidawork, E. (2016). Evaluation of the antidepressant-like activity of the crude extract and solvent fractions of Rosa abyssinica lindley (rosaceae) using rodent models of depression. *Clin. Exp. Pharmacol.* 6 (3), 1000207. doi:10.4172/2161-1459.1000207

Gao, X., Guo, B., Yang, L., Liu, J., Zhang, X., Qin, X., et al. (2014). Selection and dynamic metabolic response of rat biomarkers by metabonomics and multivariate statistical analysis combined with GC-MS. *Pharmacol. Biochem. Behav.* 117, 85–91. doi:10.1016/j.pbb.2013.12.013

Haibing, Q., Wang, Y., and Huang, G. (2012). Effect of wen Yu kim chui on post-stroke depression in rats. *Lishizhen Med. Materia Medica Res.* 23 (7), 3.

Heym, N., Heasman, B. C., Hunter, K., Blanco, S. R., Wang, G. Y., Siegert, R., et al. (2019). The role of microbiota and inflammation in self-judgement and empathy: Implications for understanding the brain-gut-microbiome Axis in depression. *Psychopharmacology* 236, 1459–1470. doi:10.1007/s00213-019-05230-2

Hsiao, W. L., and Liang, L. (2010). The role of traditional Chinese herbal medicines in cancer therapy from TCM theory to mechanistic insights. *Planta Med.* 76, 1118–1131. doi:10.1055/s-0030-1250186

Ignaszewski, M. J., and Bruce, W. (2018). Update on randomized placebo-controlled trials in the past decade for treatment of major depressive disorder in child and adolescent patients: A systematic review. *J. Child. Adolesc. Psychopharmacol.* 28, 668–675. doi:10.1089/cap.2017.0174

Jiang, H., Ling, Z., Zhang, Y., Mao, H., Ma, Z., Yin, Y., et al. (2015). Altered fecal microbiota composition in patients with major depressive disorder. *Brain Behav. Immun.* 48, 186–194. doi:10.1016/j.bbi.2015.03.016

Jiang, N., Huang, H., Zhang, Y., Lv, J., Wang, Q., He, Q., et al. (2021). Ginsenoside Rb1 produces antidepressant-like effects in a chronic social defeat stress model of depression through the BDNF–trkb signaling pathway. *Front. Pharmacol.* 12, 680903. doi:10.3389/fphar.2021.680903

Kang, A., Tong, X., Dong, Z., Shan, J., Di, L., and Zheng, X. (2017). Suppressive effect of Ginsenoside Rg3 against lipopolysaccharide-induced depression-like behavior and neuroinflammation in mice. *J. Agric. Food Chem.* 65, 6861–6869. doi:10.1021/acs.jafc.7b02386

Kennedy, S. H., and Brown, G. M. (1992). Effect of chronic antidepressant treatment with adinazolam and desipramine on melatonin output. *Psychiatry Res.* 43, 177–185. doi:10.1016/0165-1781(92)90132-M

Kim, C. C., Healey, R., Kelly, W. J., Patchett, M. L., Jordens, Z., Tannock, G. W., et al. (2019). Genomic insights from Monoglobus pectinilyticus: A pectin-degrading specialist bacterium in the human colon. *ISME J.* 13, 1437–1456. doi:10.1038/s41396-019-0363-6

Kim Jk, J. K., Lee, K. E., Ah Lee, S., Jang, H. M., and Kim, D. H. (2020). Interplay between human gut bacteria Escherichia coli and Lactobacillus mucosae in the occurrence of neuropsychiatric disorders in mice. *Front. Immunol.* 11, 273. doi:10.3389/fimmu.2020.00273

Kim Y, Y., Lee, H. Y., Choi, Y. J., and Cho, S. H. (2020). Antidepressant effects of Ginsenoside Rf on behavioral change in the glial degeneration model of depression by reversing glial loss. *J. Ginseng Res.* 44, 603–610. doi:10.1016/j.jgr.2019.08.005

Ladep, N. G., Obindo, T. J., Audu, M. D., Okeke, E. N., and Malu, A. O. (2006). Depression in patients with irritable bowel syndrome in jos, Nigeria. *World J. Gastroenterol.* 12, 7844–7847. doi:10.3748/wjg.v12.i48.7844

Lara, G. A. G., Zúñiga, J. O., Pérez, O. C., Solís, S. H., Jiménez, C. E. P., and Méndez, M. C. (2018). Predictors of suicidal ideation and depressive symptoms among adolescents in chiapas, Mexico. *Cien. Saude Colet.* 23, 1089–1096. doi:10.1590/1413-81232018234.14492016

Li, C., Huang, J., Cheng, Y. C., and Zhang, Y. W. (2020). Traditional Chinese medicine in depression treatment: From molecules to systems. *Front. Pharmacol.* 11, 586. doi:10.3389/fphar.2020.00586

Li, C., Rong, L., Wu, Q., and Wu, T. (2013). Effect of hesperidin on behavior and HPA Axis of rat model ofchronic stress-induced depression. *China J. Chin. Materia Medica* 38 (2), 5.

Liu, B., Xu, C., Wu, X., Liu, F., Du, Y., Sun, J., et al. (2015). Icariin exerts an antidepressant effect in an unpredictable chronic mild stress model of depression in rats and is associated with the regulation of hippocampal neuroinflammation. *Neuroscience* 294, 193–205. doi:10.1016/j.neuroscience.2015.02.053

Maes, M., Kubera, M., Leunis, J. C., and Berk, M. (2012). Increased IgA and IgM responses against gut commensals in chronic depression: Further evidence for increased bacterial translocation or leaky gut. *J. Affect. Disord.* 141, 55–62. doi:10.1016/j.jad.2012.02.023

Maes, M., Kubera, M., and Leunis, J. C. (2008). The gut-brain barrier in major depression: Intestinal mucosal dysfunction with an increased translocation of LPS from gram negative enterobacteria (leaky gut) plays a role in the inflammatory pathophysiology of depression. *Neuro Endocrinol. Lett.* 29, 117–124.

Miao, S., Tang, W., Li, H., Li, B., Yang, C., Xie, W., et al. (2022). Repeated inflammatory dural stimulation-induced cephalic allodynia causes alteration of gut microbial composition in rats. *J. Headache Pain* 23 (1), 71. doi:10.1186/s10194-022-01441-9

Miller, H. L., David Ekstrom, R., Mason, G. A., Bruce Lydiard, R., and Golden, R. N. (2001). Noradrenergic function and clinical outcome in antidepressant pharmacotherapy. *Neuropsychopharmacology* 24, 617–623. doi:10.1016/S0893-133X(00)00232-3

Mingkun, L., Yuting, W., Liang, X., Qin, H., and Zhong, J. (2021). Effects of rose granules on behavior and serum 5-HT in depressed mice. *J. Shaanxi Univ. Sci.* 39 (1), 5.

Mojtabai, R., Olfson, M., and Han, B. (2016). National trends in the prevalence and treatment of depression in adolescents and young adults. *Pediatrics* 138, e20161878. doi:10.1542/peds.2016-1878

Ni, Y., Su, M., Lin, J., Wang, X., Qiu, Y., Zhao, A., et al. (2008). Metabolic profiling reveals disorder of amino acid metabolism in four brain regions from a rat model of chronic unpredictable mild stress. *FEBS Lett.* 582, 2627–2636. doi:10.1016/j.febslet.2008.06.040

Pu, J., Liu, Y., Gui, S., Lu, T., Yue, Y., Song, X., et al. (2021). Metabolomic changes in animal models of depression: A systematic analysis. *Mol. Psychiatry* 26, 7328–7336. doi:10.1038/s41380-021-01269-w

Rabe-Jabłońska, J., and Anna, S. (2001).Diurnal profile of melatonin secretion in the acute phase of major depression and in remission. USA, NY: INT Scientific Literature Inc *Med. Sci. Monit.* 7 (5), 946–952.

Robertson, R. C., Oriach, C. S., Murphy, K., Moloney, G. M., Cryan, J. F., Dinan, T. G., et al. (2017). Omega-3 polyunsaturated fatty acids critically regulate behaviour and gut microbiota development in adolescence and adulthood. *Brain Behav. Immun.* 59, 21–37. doi:10.1016/j.bbi.2016.07.145

Sampson, T. R., Debelius, J. W., Thron, T., Janssen, S., Shastri, G. G., Esra Ilhan, Z., et al. (2016). Gut microbiota regulate motor deficits and neuroinflammation in a model of Parkinson's disease. *Cell* 167, 1469–1480. doi:10.1016/j.cell.2016.11.018

Shao, W. H., Song, H. F., Yang, L., Yao, G. E., Chen, J. J., Zhou, J., et al. (2013). Metabolomic identification of molecular changes associated with stress resilience in the chronic mild stress rat model of depression. *Metabolomics* 9, 433–443. doi:10.1007/s11306-012-0460-2

Sharon, G., Cruz, N. J., Kang, D. W., Gandal, M. J., Wang, B., Kim, Y. M., et al. (2019). Human gut microbiota from autism spectrum disorder promote behavioral symptoms in mice. *Cell* 177, 1600–1618. doi:10.1016/j.cell.2019.05.004

Simkin, D. R. (2019). Microbiome and mental health, specifically as it relates to adolescents. *Curr. Psychiatry Rep.* 21, 93. doi:10.1007/s11920-019-1075-3

Statnikov, A., Henaff, M., Narendra, V., Konganti, K., Li, Z., Yang, L., et al. (2013). A comprehensive evaluation of multicategory classification methods for microbiomic data. *Microbiome* 1, 11. doi:10.1186/2049-2618-1-11

Sun, M. F., Zhu, Y. L., Zhou, Z. L., Jia, X. B., Xu, Y. D., Yang, Q., et al. (2018). Neuroprotective effects of fecal microbiota transplantation on MPTP-induced Parkinson's disease mice: Gut microbiota, glial reaction and TLR4/TNF-α signaling pathway. *Brain Behav. Immun.* 70, 48–60. doi:10.1016/j.bbi.2018.02.005

Tengfei, L., Sun, X., Gao, J., Liu, X., and Liu, H. (2012). Antidepressant effect of the water extract of acori tatarinowii rhizoma in the learned helplessness rat mode. *Chin. J. Exp. Traditional Med. Formulae* 18 (2), 132–135.

Twenge, J. M., Joiner, T. E., Rogers, M. L., and Martin, G. N. (2018). Increases in depressive symptoms, suicide-related outcomes, and suicide rates among U.S. Adolescents after 2010 and links to increased new media screen time. *Clin. Psychol. Sci.* 6, 3–17. doi:10.1177/2167702617723376

Wang, W., Chen, L., Zhou, R., Wang, X., Lu, S., Huang, S., et al. (2014). Increased proportions of Bifidobacterium and the Lactobacillus group and loss of butyrate-producing bacteria in inflammatory bowel disease. *J. Clin. Microbiol.* 52, 398–406. doi:10.1128/JCM.01500-13

Wu, X., Wu, J., Xia, S., Li, B., and Dong, J. (2013). Icaritin opposes the development of social aversion after defeat stress via increases of GR MRNA and BDNF MRNA in mice. *Behav. Brain Res.* 256, 602–608. doi:10.1016/j.bbr.2013.09.034

Xing, H., Zhang, K., Zhang, R., Zhang, Y., Gu, L., Shi, H., et al. (2015). Determination of depression biomarkers in rat plasma by liquid chromatography-mass spectrometry for the study of the antidepressant effect of zhi-zi-hou-Po decoction on rat model of chronic unpredictable mild stress. *J. Chromatogr. B Anal. Technol. Biomed. Life Sci.* 988, 135–142. doi:10.1016/j.jchromb.2015.02.037

Xueli, S., Du, Z., Xia, M., Zhao, X., Wu, C., and Guo, C. (2013). Study on antidepressant effect of albizzia julibrissin flower total flavonoidson the expression of BDNF and TrkB in TheHippocampus CA3 of rats with depression. *Traditional Chin. Drug Res. Clin. Pharmacol.* 25 (018), 198–201.

Yang, J., Zheng, P., Li, Y., Wu, J., Tan, X., Zhou, J., et al. (2020). Landscapes of bacterial and metabolic signatures and their interaction in major depressive disorders. *Sci. Adv.* 6, eaba8555. doi:10.1126/sciadv.aba8555

Yin, W., Hu, C., Wang, L., and Guo, Z. (2019). Effects of gualou xiebai banxia decoction and wendan decoction on the level of seruminflammatory factors and neurotransmitters in coronary heart disease combinedwith depression patients. *Chin. J. Basic Med. Traditional Chin. Med.* 25 (12), 4.

Zhang, Y. W., and Cheng, Y. C. (2019). Challenge and prospect of traditional Chinese medicine in depression treatment. *Front. Neurosci.* 13, 190. doi:10.3389/fnins.2019.00190

Zheng, P., Zeng, B., Liu, M., Chen, J., Pan, J., Han, Y., et al. (2019). The gut microbiome from patients with schizophrenia modulates the glutamate-glutamine-GABA cycle and schizophrenia-relevant behaviors in mice. *Sci. Adv.* 5, eaau8317. doi:10.1126/sciadv.aau8317

Zheng, P., Zeng, B., Zhou, C., Liu, M., Fang, Z., Xu, X., et al. (2016). Gut microbiome remodeling induces depressive-like behaviors through a pathway mediated by the host's metabolism. *Mol. Psychiatry* 21, 786–796. doi:10.1038/mp.2016.44

Zheng, S., Yu, M., Lu, X., Huo, T., Lin, G., Yang, J., et al. (2010). Urinary metabonomic study on biochemical changes in chronic unpredictable mild stress model of depression. *Clin. Chim. Acta.* 411, 204–209. doi:10.1016/j.cca.2009.11.003

frontiers | Frontiers in Pharmacology

TYPE Original Research
PUBLISHED 05 October 2022
DOI 10.3389/fphar.2022.1007274

OPEN ACCESS

EDITED BY
Kah Keng Wong,
Universiti Sains Malaysia Health Campus, Malaysia

REVIEWED BY
Guang-Bo Ge,
Shanghai University of Traditional Chinese Medicine, China
Waijiao Tang,
Southern Medical University, China
Chengwu Song,
Hubei University of Chinese Medicine, China

*CORRESPONDENCE
Yan Qi,
qiyankm@ynutcm.edu.cn
Xuefang Li,
lixuef100@126.com
Jie Yu,
cz.yujie@gmail.com

†These authors have contributed equally to this work

SPECIALTY SECTION
This article was submitted to Ethnopharmacology, a section of the journal Frontiers in Pharmacology

RECEIVED 30 July 2022
ACCEPTED 05 September 2022
PUBLISHED 05 October 2022

CITATION
He J, Yang Y, Zhang F, Li Y, Li X, Pu X, He X, Zhang M, Yang X, Yu Q, Qi Y, Li X and Yu J (2022), Effects of Poria cocos extract on metabolic dysfunction-associated fatty liver disease via the FXR/PPARα-SREBPs pathway. *Front. Pharmacol.* 13:1007274. doi: 10.3389/fphar.2022.1007274

Effects of *Poria cocos* extract on metabolic dysfunction-associated fatty liver disease *via* the FXR/PPARα-SREBPs pathway

Jinbiao He†, Yu Yang†, Fan Zhang, Yanjuan Li, Xiaosi Li, Xuemei Pu, Xudong He, Mei Zhang, Xinxing Yang, Qiuman Yu, Yan Qi*, Xuefang Li* and Jie Yu*

College of Pharmaceutical Science, School of Clinical Medicine, Yunnan Key Laboratory of Southern Medicinal Utilization, Yunnan University of Chinese Medicine, Kunming, Yunnan, China

Despite the increase in the global prevalence of metabolic dysfunction-associated fatty liver disease (MAFLD), no approved drug currently exists for the disease. *Poria cocos* (Schw.) Wolf (*P. cocos*) is a medicinal mushroom belonging to a family of polyporaceae widely used in TCM clinics to protect the liver and treat obesity. However, its efficacy, practical components, and underlying mechanism against MAFLD are yet to be determined. In this study, we evaluated the effects of *Poria cocos (P. cocos)* ethanol extract (EPC) on hepatic dyslipidemia, steatosis, and inflammation by both bioinformatics analysis and MAFLD rats induced by HFD feeding. We found EPC treatment dramatically reduced lipid accumulation, inflammatory cell infiltration, and liver injury. EPC reduced serum TC, TG levels, and hepatic TG, TBA, and NEFA contents. UHPLC Q-Trap/MS examination of BA profiles in serum and feces showed that EPC increased fecal conjugated BAs, decreased free BAs, and improved BA metabolism in HFD-fed rats. Western blot and RT-qPCR analysis showed that EPC could activate hepatic FXR and PPARα expression and reduce CYP7A1 and SREBP-1c expression. Systemic pharmacology combined with molecular docking suggested that poricoic acid B and polyporenic acid C, the major active compounds in EPC, could ameliorate lipid homeostasis by activating the nuclear receptor PPARα. We further confirmed their inhibition effects of lipid droplet deposition in steatized L-02 hepatocytes. In summary, EPC alleviated HFD-induced MAFLD by regulating lipid homeostasis and BA metabolism *via* the FXR/PPARα-SREBPs signaling pathway. *P. cocos* triterpenes, such as poricoic acid

Abbreviations: CYP7A1, cholesterol 7α-hydroxylase; FXR, farnesoid X receptor; FGF 15, fibroblast growth factor15; HFD, high-fat diet; MAFLD, metabolic dysfunction-associated fatty liver disease; NEFA, nonesterified free fatty acids; PPARα, peroxisome proliferator-activated receptor α; SREBP-1c, sterol regulatory element binding protein 1c; TCM, traditional Chinese medicine; TC, cholesterol; TBA, total bile acid; UHPLC Q-Trap/MS, ultra-high performance liquid chromatography coupled with hybrid triple quadrupole linear ion trap mass spectrometer; UPLC Q-TOF/MS: ultraperformance liquid chromatography quadrupole time-of-flight mass spectrometry.

B and polyporenic acid C, were the characteristic substances of *P. cocos* for the treatment of MAFLD.

KEYWORDS

MAFLD (metabolic-associated fatty liver disease), Poria cocos (Schw.) Wolf., bile acid metabolism, FXR/PPARα-SREBP pathway, lipid homeostasis, UPLC Q-TOF/MS

Introduction

Metabolic dysfunction-associated fatty liver disease (MAFLD), formerly known as non-alcoholic fatty liver disease (NAFLD) (Wong and Lazarus, 2021), is the most common liver disease worldwide, affecting 25% of the global population (Younossi et al., 2016). In Asia, the prevalence of MAFLD is projected to increase to 20–35% over the next 10 years (Eslam et al., 2020). It is strongly associated with metabolic disorders, such as obesity, hypertension, dyslipidemia, and type 2 diabetes mellitus (de Alwis and Day, 2008). MAFLD is characterized by excessive accumulation of lipids in the liver, called steatosis (Byrne and Targher, 2015), which can develop into non-alcoholic fatty liver hepatitis, fibrosis, cirrhosis, and hepatocellular carcinoma, ultimately leading to necrosis (Michelotti et al., 2013; Zhu et al., 2016). At present, the MAFLD therapeutic targets are mainly focused on nuclear receptor agonists involved in steatosis, inflammation, or fibrogenesis, such as the farnesoid X receptor (FXR, NR1H4), peroxisome proliferator-activated receptor α (PPARα, NR1C1), as well as analogs of enterohepatic hormones, including fibroblast growth factor (FGF)19 in humans, FGF15 in rodents and FGF21 (Michelotti et al., 2013). Due to the complex pathogenesis of MAFLD, the critical regulatory issues and valid drug targets are unclear. Therefore, developing effective and safe drugs to prevent and treat MAFLD has become an essential issue in the global medical field.

When the rate of lipid influx and ab initio synthesis exceeds the rate of lipid oxidation and release, excess lipids accumulate in hepatocytes, leading to the development of MAFLD (Machado and Diehl, 2016). Hence, a central pathological characteristic of MAFLD is the accumulation of excess TG in the hepatic (de Alwis and Day, 2008). Recent research has shown that promoting *PPARα* gene expression can inhibit the expression of TG synthesis gene *HMGCR* and *SREBP-1c*, thereby reducing lipid accumulation in the hepatic and suppressing MAFLD in mice (Wu et al., 2019). In addition, activation of FXR inhibits the BA rate-limiting enzyme CYP7A1 and the TC synthesis rate-limiting enzyme *SREBP-1c* to regulate BA synthesis, reduce hepatic lipogenesis, and inhibit inflammatory and fibrotic responses to treat MAFLD (Moris et al., 2017; Jiao et al., 2022).

Poria cocos (Schw.) Wolf (*P. cocos*) is a medicinal mushroom belonging to a family of polyporaceae, also called Fuling, Tuckahoe, Hoelen, or Indian bread (Lindner and Banik, 2008), is a trophozoite mushroom found in the wilting skins and roots of pine trees in China, Korea, Japan, and North America (Ríos, 2011). In Asian medicine, it has been widely employed as a component of many preparations and as a medicinal and edible species (Lindner and Banik, 2008; Ríos, 2011). According to the ancient Chinese medical masterpieces "Sheng Nong's herbal classic (AD220–280)," "Jin Kui Yao Lue (AD198–201)," "Tai Ping Hui Min He Ji Ju Fang (AD1208)" and "Shang Han Lun (AD198.201)," *P. cocos* has been used in TCM for more than 2,000 years with multiple functions (Esteban, 2009; Li et al., 2019; Nie et al., 2020). Because of its liver-protective, anti-inflammatory, anti-oxidant, and anti-diabetic effects, *P. cocos* has been widely used to treat insomnia, neurological disorders, chronic edema, kidney disease, and heart disease. It has been described as "nine out of ten prescriptions (Ding et al., 2019). The chemical constituents of *P. cocos* are primarily triterpenoids, polysaccharides, and steroids (Qian et al., 2018). Research on chemical composition shows that the foremost effective compounds of *P. cocos* triterpenes are pachymic acid, dehydropachymic acid, polyporenic acid C, dehydrotrametenolic acid, poricoic acid A, poricoic acid B, and so on (Tian et al., 2019). Recent studies have demonstrated that *P. cocos* may alleviate hyperlipidemia and obesity, and *P. cocos* triterpenes have anti-inflammatory, anti-oxidant, diuretic, and hepatoprotective effects (Miao et al., 2016). Both eburicoic acid and dehydroeburicoic acid protect the hepatic against CCl_4-induced liver injury by anti-oxidant and pro-inflammatory mechanisms (Huang et al., 2013). However, whether *P. cocos* prevents MAFLD and its underlying material basis and mechanism are unclear.

This study aimed to ascertain the effects of *P. cocos* on the etiopathogenesis of MAFLD, including its impact on lipid heterogeneity, lipid accumulation, hepatic damage, and inflammation. Based on the unclear relationship between *P. cocos* on MAFLD, we used the TCM network pharmacology analysis system to establish the gene co-association between *P. cocos* and MAFLD. Subsequently, we evaluated the effects of *P. cocos* ethanol extract (EPC) on hepatic dyslipidemia, steatosis, BA metabolism, and inflammation in MAFLD rats induced by HFD feeding. And finally, the virtual screening combined with UPLC Q-TOF/MS technology and *in vitro* experiments hypothesized that *P. cocos* triterpenes, such as poricoic acid B and polyporenic acid C, were the characteristic substances of *P. cocos* for the treatment of MAFLD. Hence, we explored the pharmacological effects and mechanism of *P. cocos* from lipid homeostasis and BA metabolism through the FXR/PPARα-

SREBPs signaling pathway in rats with high-fat diet (HFD)-induced MAFLD.

Materials and methods

Reagents

The HFD containing 1% cholesterol, 10% refined lard, 10% egg yolk, and 79% basic feed was provided by Beijing Keaoxieli Feed Co. Ltd. (Beijing, China). The control diet consisted only of basic feed. Fenofibrate capsules (FC) were purchased from Abbott Laboratories (Chicago, IL, United States). The routine biochemical kits were obtained from Jiancheng Bioengineering Institute (Nanjing, China). Enzyme-linked immunosorbent assay (ELISA) kits for rat TBA, TNF-α, IL-1β, IL-6, and Insulin Receptor (IR) were purchased from Jiangsu Zeyu Biotechnology Co., Ltd., (Jiangsu, China, 31200). A sodium dodecyl-sulfate polyacrylamide gel electrophoresis matching kit (cat. no. P0012A) and the BCA protein assay kit (cat. no. P0012) were purchased from Beyotime Biotech Inc. (Shanghai, China). Primers were designed by General Biotech Co. Ltd. (Shanghai, China). Total ribonucleic acid (RNA) extraction kits (cat. no. DP419) were obtained from the Tiangen Biochemical Department, Technology Co., Ltd. (Beijing, China). TaKaRa PrimeScript RT Master Mix (cat. no. RR036A), and TaKaRa TB Green Premix Ex Taq II (cat. no. RR820A) was purchased from Bao Biological Engineering Co. (Dalian, China).

Anti-SCD1 (cat. no. ab9535) and anti-p-NF-κB (cat. no. ab6302) were purchased from Abcam (Cambridge, United Kingdom). Anti-CYP19A1 (cat. no. DF6884), anti-CYP7A1 (DF2612), anti-FGF15 (cat. no. DF2651), anti-PPARα (cat. no. AF5301), anti-p-AMPK (cat. no. AF3423), and anti-SHP1 (cat. no. AF3244) was purchased from Affinity Biosciences (Shanghai, China). Anti-FXR1 (cat. no. 13194-1-AP), anti-NR3C1 (cat. no. 24050-1-AP), anti- fatty acid synthase (FASN) (cat. no. 10624-2-AP), anti-AMPKα (cat. no. 10929-2-AP), anti-NF-κB (cat. no. 10745-1-AP), anti-ERK1/2 (cat. no. 51068-1-AP), anti-p-ERK1/2 (cat. no. 28733-1-AP), anti-JNK (cat. no. 24164-1-AP), anti-p-JNK (cat. no. 80024-1-RP) were purchased from Proteintech (Wuhan, China). Anti-β-actin (cat. no. YT0099) was purchased from ImmunoWay Biotechnology Company (Beijing, China). IRDye®680RD Goat anti-Rabbia IgG Secondary Antibody (cat. no. 926-68071) as purchased from LI-COR Biotechnology (Hong Kong, China).

Medicinal material identification, extraction, and measurement

The identification of *P. cocos*. *P. cocos* was purchased from Puer, Yunnan, China. The samples were authenticated by Professor Jie Yu (Professor at the Yunnan University of Chinese Medicine), and voucher specimens were deposited in the Key Laboratory of Preventing Metabolic Diseases of TCM, Yunnan University of Chinese Medicine (Kunming, China).

Preparation and content determination of EPC. Taking 30 Kg of *P. cocos* add 3 times the volume of 75% ethanol, boiled 2 h, and filtered. Added 2 times the volume of 75% ethanol to the filtered residue, continued to boil for 2 h and filtered. The filtrates were combined twice, filtered, and then concentrated under reduced pressure at 65°C using a rotary evaporator. The extract was frozen at −80°C, then transferred to a lyophilizer and lyophilized to obtain 537 g of EPC. Taking 100 mg of EPC, adding 75% ethanol to 25 ml volumetric flask, and taking 1 ml of solution into 100 ml volumetric flask, using vanillin-glacial acetic acid color displayed method to detect the purity of *P. cocos* triterpenes, its purity is calculated as 57.43%.

Network pharmacological analysis

Co-associations between MAFLD genes and *P. cocos* targets were analyzed in the TCMNPAS (http://54.223.75.62:3838/) by entering MAFLD (MCID: NNL005) and *P. cocos*, then selecting the HIT, TCMID, STITCH, and TCMSP databases. The drug activity index QED was set to 0.2, the drug association threshold was 400, and the compound target significance was $p < 0.05$ (Ma et al., 2021). Next, based on the absorption, distribution, metabolism, and excretion (ADME) and with the oral availability (OB) set to ≥ 30% and drug similarity (DL) ≥ 0. 18, the active components and targets of *P. cocos* were retrieved from the TCMSP database (http://tcmspw.com/index.php). Supplement and back-predicted active ingredients were not found for the target using the PharmMapper database search. (http://www.lilab-ecust.cn/pharmmapper/). The targets corresponding to each active component were corrected using the Uniport Database (http://www.uniprot.org/). Meanwhile, "MAFLD" was entered into the GeneCards website (https://www.genecards.org/), OMIM (https://omim.org/), and DrugBank databases (https://https://go.drugbank.com/) as a search term to collect related target information. Duplicate values were merged and deleted. The targets of the active components of *P. cocos* and MAFLD-related targets were introduced into venny 2.1.0 on the website (https://bioinfogp.cnb.csic.es/tools/venny/), and the intersection was regarded as the target protein of *P. cocos* in treating MAFLD. In addition, the protein-protein interaction network was constructed using the STRING database (https://string-db.org/), minimum interaction (score = 0.4), and the associated interaction network was visualized by Cytoscape 3.8.2 software. Finally, pathways associated with the predicted genes were annotated using DAVID (https://david.ncifcrf.gov/), and gene ontology-cellular component (GO-CC), Gene ontology-biological process (GO-BP), Gene ontology-molecular function (GO-MF), and Kyoto

Encyclopedia of Genes and Genomes (KEGG) enrichment analyses were carried out ($p \leq 0.0001$, count >5) and exported.

Target organ analysis

The key genes determined to be core targets of *P. cocos* in the treatment of MAFLD were imported into the BioGPS database (http://biogps.org/). Statistical analyses were then used on each result to determine the target organs by setting the target to a level higher than the average score. Cytoscape 3.8.2 was employed to construct the target-organ localization direct relationship network.

In vivo experimental design

Sprague–Dawley male rats (220 ± 20 g) were purchased from Dashuo Biotech Co. (SLAC, Hunan, China). All the rats were maintained in a pathogen-free environment with controlled conditions of 24 ± 2°C, 45 ± 10% humidity, and a 12 h light/dark cycle. Rats were acclimated to the environment on a control chow diet administered *ad libitum* for 1 week and were then randomly divided into five groups (n = 10 per group) as follows: 1) normal diet control group (CON, containing 10% kcal fat), 2) high-fat diet group (MOD, containing 60% kcal fat), 3) 20 mg/kg FC group, 4) low dose (56.3 mg/kg) and 5) high dose (168.9 mg/kg) of EPC group (EPC-L and EPC-H). The dosage of EPC-L used in rat experiments was calculated according to the known *P. cocos* dose of humans (10 g/day/person), which was recorded in the Chinese Pharmacopoeia (2020). Rats were treated daily from the first week to the end of the experiment (which lasted 12 weeks). The food intake of all the rats was recorded daily, and body weights were recorded weekly. At the end of this experiment, the rats were anesthetized using 1% pentobarbital sodium. Samples of blood, heart, liver, lung and adipose tissues were collected for hematoxylin and eosin (H&E) staining or liquid nitrogen flash freezing, followed by refrigerator storage at −80°C for later analysis.The liver tissue was fixed with 4% paraformaldehyde for 24 h and then sectioned by dehydration, embedded in paraffin, cut into 5–7 μm sections, stained with H&E, and examined under a light microscope (Thermo, Waltham, MA, United States) at 200× magnification. Five animals in each group were observed under the microscope in four fields of view, for changes in liver tissue.

Determination of serum and liver biochemical parameters

Serum samples (200 μL) were analyzed using a biochemical analyzer (Beckman CX4, Roche, Germany) to measure the levels of triglyceride (TG), total cholesterol (TC), high-density lipoprotein cholesterol (HDL-C), Low-density lipoprotein cholesterol (LDL-C), aspartate aminotransferase (AST), alanine aminotransferase (ALT), and glucose (GLU). Precisely 80 mg of rat liver tissue was weighed and placed into 720 μL of physiological saline, then homogenized. The supernatant was collected by centrifugation at 12004 ×*g* for 15 min at 4°C, and the protein concentration was determined using BCA kits. Determination of TG, TC, LDL-C, HDL-C, AST, ALT, and nonesterified free fatty acids (NEFA) levels in the liver was performed according to the standard operating instructions of the kit.

Measurement of inflammatory factors

Precisely 80 mg of rat liver tissue was weighed and placed into 720 μL of phosphate-buffered saline buffer (pH 7.4), then homogenized. The supernatant was collected by centrifugation at 12004 ×*g* for 15 min at 4°C, and the protein concentration was determined using BCA kits. According to the manufacturer's protocol, total bile acid (TBA), indirect bilirubin (IBIL), insulin receptor (IR), interleukin -1β (IL-1β), interleukin -6 (IL-6), and tumor necrosis factor-α (TNF-α) were quantified by ELISA kits.

Quantitative analysis of serum and ileal fecal BAs

50 mg were accurately weighted, and then add 400 μL of extraction solution (methanol: water = 4:1), grind at 4°C for 6 min, then grind with a freezer grnder for 6 min (−10°C, 50 Hz). An ultrasound (5°C, 40 kHz) for 30 min, centrifuged at 13000 ×*g* for 15 min at 4°C. Finally, the supernatant was injected into the LC-MS/MS system for analysis. 50 μL was accurately weighted, and then add 100 μL methanol by good vortexing for the 30 s, ultrasound (5°C, 40 kHz) for 30 min, standing for 30 min, and centrifuged at 13000 ×*g* for 15 min at 4°C. Afterward, 100 μL of supernatant were collected and blown dry with a nitrogen blower. Then the residue was reconstituted with 100 μL 25% acetonitrile solution. Finally, the supernatant (1 μL) was injected into the LC-MS/MS system for analysis. The analysis was performed using an UHPLC Q-Trap/MS for the sample's qualitative and quantitative detection of the target substances. Analyte compounds were separated with a Waters BEH C18 (150*2.1 mm, 1.7 μm) Liquid chromatography column (AB SCIEX). The mobile phases consisted of 0.1% formic acid—water solution (solvent A) and 0.1% formic acid—acetonitrile solution (solvent B), delivered at a flow rate set to 0.35 ml/min. The solvent gradient changed according to the following conditions: from 0 to 6 min, 31% A to 31% A, 29% B to 29% B; from 6 to 22 min, 31% A to 25% A, 29% B to 75% B; from 22 to 22.1 min, 25% A to 0% A, 75% B to 100% B; from 22.1 to 25 min, 0% A to 0% A, 100% B to 100% B for equilibrating the systems. The column temperature was maintained at 40°C. During the period of analysis, all these samples were stored at 4°C. Mass

spectrometry conditions: AB SCIEX QTRAP 6500+ with negative mode detection, Curtain Gas (CUR) of 35, Collision Gas (CAD) is Medium, IonSpray Voltage (IS) is −4500 V, Temperature (TEM) is 500°C, Ion Source Gas1 (GS1) is 40, Ion Source Gas2 (GS2) is 50.

Real-time quantitative PCR analysis

Total RNA was prepared from livers using Trizol reagent according to the manufacturer's instructions. RNA was equalized and converted to cDNA using a HiScript II reverse transcriptase kit. Gene expression was measured by RT-qPCR (Roche, Basel, Switzerland) using SYBR Green. A total of 1000 ng of cDNA template was used for PCR amplification using the primers listed in Supplementary Table S1. The total reaction volume was 20 μL, including SYBR Premix Ex TaqII (9 μL), Primer F (0.3 μL), Primer R (0.3 μL), cDNA (2 μL), and ddH_2O (8.4 μL). The PCR conditions were as follows: pre-denaturation at 95°C for 30 s, denaturation at 95°C for 5 s, annealing and extension for 20 s at 62°C, and amplification for 40 cycles. Glyceraldehyde-3-phosphate dehydrogenase (GAPDH) was used as an internal reference. Experiments were conducted in triplicate for each sample, and the $2^{-\Delta\Delta CT}$ method was used to determine the relative level of target gene expression.

Western blot analysis

Precisely 60 mg of rat liver tissue was weighed and placed into 300 μL of radio-immunoprecipitation assay buffer (Beyotime Technology, Shanghai, China) until completely lysed, and the supernatants were collected by centrifugation. The total protein concentration was determined using the BCA protein assay kit. Then, 5 μg/μL of protein was separated by gel electrophoresis and transferred onto a polyvinylidene difluoride membrane. The membrane was blocked with 5% skim milk for 2 h at 20–25 °C and then incubated with primary antibodies anti-CYP19A1 (1:1000), anti-CYP7A1 (1:1000), anti-FASN (1:2000), anti-SCD1 (1:1000), anti-FXR (1:1000), anti-FGF15 (1:1000), anti-SHP1 (1:1000), anti-AMPKα (1:2000), anti-p-AMPK (1:1000), anti-NR3C1 (1:4000), anti-JNK1 (1:5000), anti-p-JNK (1:2000), anti-ERK (1:1000), anti-p-ERK (1:5000), anti-NF-κB (1:2000), anti-p-NF-κB (1:1000), and anti-PPARα (1:1000) overnight at 4°C. Membranes were then washed and incubated with IRDye 680RD Goat anti-Rabbit for 2 h at 20–25°C, and the signal was detected using an enhanced immunofluorescence substrate. Immunoreactive bands were quantified using the ImageJ software.

Molecular docking analysis

Poricoic acid C, polyporenic acid C, poricoic acid B, dehydroeburicoic acid, eburicoic acid, dehydrotumulosic acid, (22E)-ergosta-7, dehydropachymic acid, poricoic acid A, 16 alpha-hydroxydehydrotrametenolic acid, and 22-diene-3β-ol were used as ligands. FXR, TNF, PPARα, CYP19A1, PPARγ, NR1H3, RXRα, HMGCR, FASN, and NR3C1 were used as protein receptors. The PubChem database (https://pubchem.ncbi.nlm.nih.gov/) was used to download ligands' two-dimensional (2D) structures. It was processed and transformed into PDB format through Chem3D (Chem3D 18.0.0.231) and saved in PDBQT format. The X-ray crystal structures of the targets (http://www.rcsb.org/), including TNF (PDB ID: 1FT4), FXR (PDB ID: 6A5G), PPARα (PDB ID: 6L37), CYP19A1 (PDB ID: 4KQ8), PPARγ (PDB ID: 6T6B), NR1H3 (PDB ID: 6AVI), RXRα (PDB ID: 6JNO), HMGCR (PDB ID: 3CD0), FASN (PDB ID: 6NNA), and NR3C1 (PDB ID: 6DXK), were obtained from the PDB database (https://www.pdbus.org/). Subsequently, the protein receptor files were processed and converted to PDBQT format using AutoDock Tools 1.5.6. Finally, Autodock Vina v.1.1.2 was run to perform molecular docking. The conformation with the best affinity was selected as the final docking conformation, and the results of the best binding energy were visualized using PyMOL 2.5.0. Moreover, hydrogen and hydrophobic bonds were analyzed for ligand and receptor binding using the PLIP (https://plip-tool.biotec.tu-dresden.de/).

Analysis and identification of EPC by UPLC Q-TOF/MS

Identification of the main active ingredients was performed by the Agilent UPLC Q-TOF/MS liquid mass spectrometer (Agilent Technologies, Inc., California, United States). Chromatographic column Agilent Zorbax SB-C18 (50*2.1 mm, 1.8 μm); column temperature 30°C; mobile phase: acetonitrile for A, water for B; flow rate 0.3 mL/min; detection wavelength 203nm; injection volume 5 μL; and running time 70 min. The solvent gradient changed according to the following conditions: from 0 to 5 min, 5% A to 5% A, 90% B to 85% B; from 20 to 30 min, 15% A to 25% A, 895% B to 75% B; from 30 to 40 min, 25% A to 45% A, 75% B to 55% B; from 40 to 50 min, 45% A to 70% A, 55% B to 30% B; from 50 to 60 min, 70% A to 100% A, 30% B to 0% B; from 60 to 70 min,100% A to 100% A, 0% B to 0% B; from 70 to 70.1 min, 100% A to 5% A, 0% B to 95% B. Mass spectrometry with positive and negative ion scan mode detection; ion source was ESI; the temperature was 350°C; collision gas and drying gas flow rate was 8 L/min; capillary voltage: 3.5 kV; atomization pressure: 30 psi; mass range *m/z*: ~100–1,200 ppm; and collision energy: 10, 20, 30, 40, 50 msec.

In vitro experiments

In vitro experiments were performed using L-02 hepatocytes cultured in RPMI 1640 medium at 37 °C with 10% fetal bovine serum, 1% penicillin-streptomycin, and 5% CO_2. Cells were

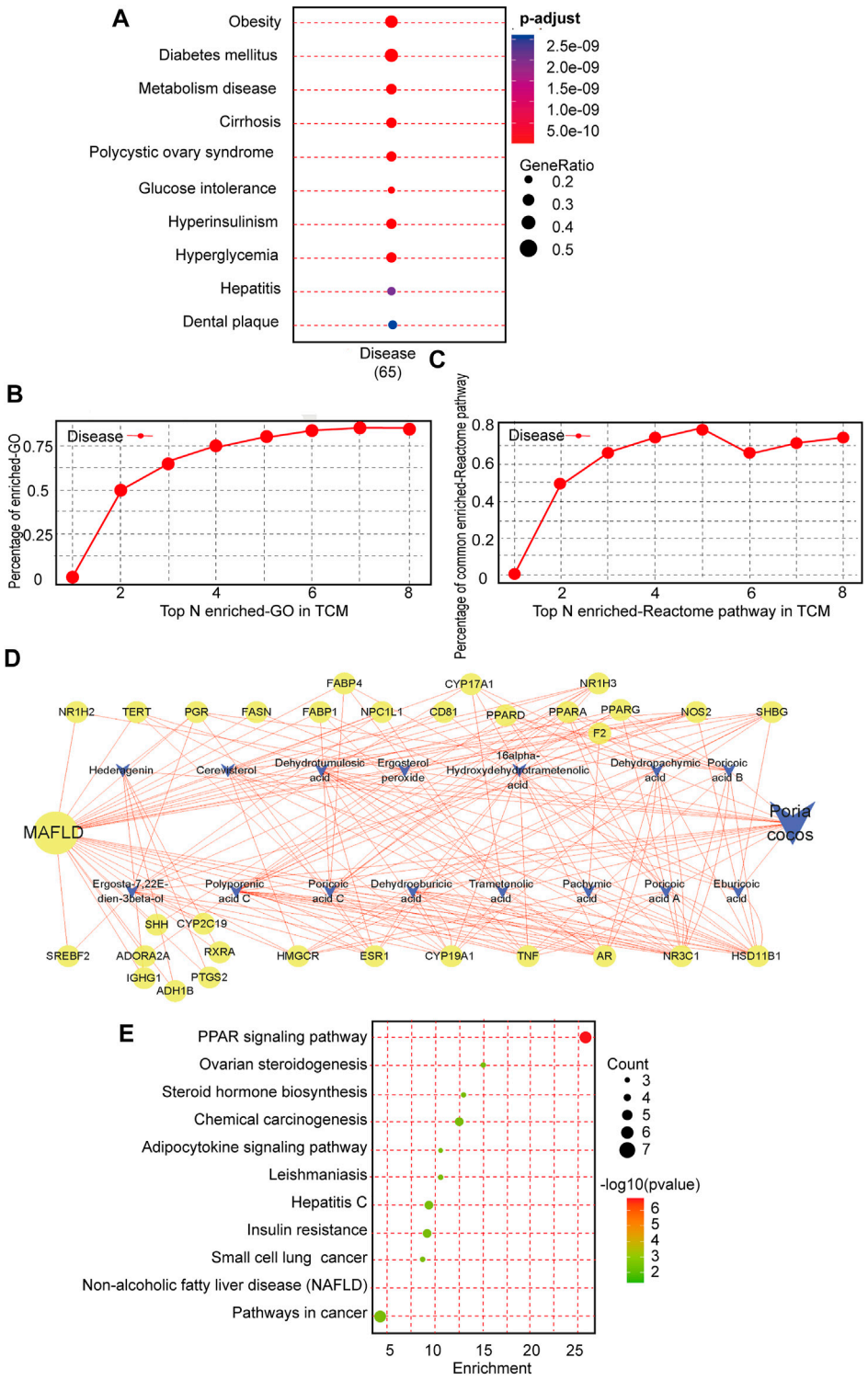

FIGURE 1
Intrinsic association and active compound identification of *Poria cocos* (*P. cocos*) for the treatment of MAFLD. **(A)** Metabolic dysfunction-associated fatty liver disease (MAFLD) Gene ontology (GO) enrichment. **(B)** Similarity of co-associated GO terms between *P. cocos* and MAFLD. The similarity between the co-associated GO terms of *P. cocos* and MAFLD was 0.87, and the area under the curve (AUC) of the top 30 of these terms was 4.84. **(C)** Similarity of co-associated Reactome pathways between *P. cocos* and MAFLD. The similarity between co-associated Reactome pathways of *P. cocos* and MAFLD was 0.78, and the AUC of the top 30 of these pathways was 4.47. **(D)** MAFLD-*Poria cocos*-target relationship network diagram. Nodes of higher degree value are indicated by a larger diameter and darker color. Stronger interactions between nodes are indicated with thicker edges and darker colors. Green represents the targets, orange represents the compound, and blue represents the disease. The circle represents the target and "V" represents the active component of *P. cocos*.**(E)** The Kyoto encyclopedia of genes and genomes (KEGG) pathway enrichment analysis of key targets.

seeded into 6-well plates at a density of 3×10^5 cells per well; upon reaching 80-90% confluency, they were starved in 0.2% serum for 12 h, exposed to 5% fat emulsion for 24 h, and then cultured with medium containing poricoic acid B (25, 50, and 100 μmol/L), polyporenic acid C (25, 50, and 100 μmol/L), eburicoic acid (25, 50, and 100 μmol/L), and FC (150 μmol/L) or separate medium (CON group) for 24 h and harvested. The levels of TG, TC, AST, and ALT in the cell supernatant were measured according to the manufacturer's instructions. In addition, the extent of lipid accumulation in L-02 hepatocytes was determined by Oil Red O staining according to the manufacturer's instructions. Briefly, replicate the hepatic L-02 cell steatosis model after administration of drug stimulation for 24 h. Washed twice with PBS, then added 2 mL of 4% paraformaldehyde per well for 30 min to fix and then aspirate and discard paraformaldehyde. Added 2 mL of 60% isopropanol to each well for 5 min, uniformly added 2 mL of Oil Red O staining working solution slowly along the wall of each well for 35 min, then rinse twice carefully with PBS, then add 1 ml of hematoxylin staining solution slowly along the wall of each well for 2 min, and rinse 3 times with PBS again. The Cx31 Olympus imaging system (Olympus, Tokyo, Japan) was used to capture images.

Statistical analysis

Statistical analyses were performed using SPSS version 21.0 (IBM, Armonk, NY, United States). Measurement data were expressed as the mean ± standard deviation. Paired *t*-tests were adopted for comparisons of the paired data between two groups with normal distribution and homogeneity of variance, while unpaired *t*-tests were performed for comparisons of unpaired data. One-way analysis of variance (ANOVA) or repeated-measures ANOVA was conducted for multiple group comparisons, followed by Tukey's post hoc test. Pearson's correlation was used to analyze the correlation of the observed indexes. A value of $p < 0.05$ was considered statistically significant.

Result

Intrinsic association and active compound identification of *P. cocos* for the treatment of metabolic dysfunction-associated fatty liver disease

To investigate whether there is a relationship between *P. cocos* and MAFLD, we used the TCMNPAS database to establish gene co-associations between the MAFLD and *P. cocos*. MAFLD was found to be related mainly to obesity, diabetes mellitus, metabolic diseases, cirrhosis, polycystic ovary syndrome, glucose intolerance, fatty liver, as well as other diseases. This was consistent with the results of clinical and laboratory studies and provided evidence for further questions addressed in this study (Figure 1A). Similarity of co-associated Reactome pathways and GO terms between *P. cocos* and MAFLD is shown in Figures 1B,C.

According to the ADME analysis, 15 main active (Supplementary Table S2) ingredients of *P. cocos* were screened and collated to obtain 125 potential targets. Screening according to a 2-fold degree (DC ≥ 8) revealed that poricoic acid C, polyporenic acid C, poricoic acid B, dehydroeburicoic acid, eburicoic acid, dehydrotumulosic acid, dehydropachymic acid, poricoic acid A, 16 α-hydroxydehydrotrametenolic acid, and (22E)-ergosta-7, 22-diene-3β-ol might be the key active components of *P. cocos* (Figure 1D). The above suggested that the total triterpenes of *P. cocos* may be one of the active ingredients in the treatment of MAFLD.

Enrichment analysis of key pathways and organs

Subsequently, in order to screen the key organs and pathways of *P. cocos* for the treatment of MAFLD. A total of 1397 MAFLD targets were obtained through data filtration, and 31 cross-over genes with *P. cocos* were identified (Supplementary Figures S1A–S1B). The most significant terms in the GO-BP, GO-MF, and GO-CC categories at $p < 0.0001$ with a count >5 are displayed in supplementary material Figure 1C. There are 11 signaling pathways screened by KEGG pathway enrichment analysis (Figure 1E). Among them, the top three signaling pathways are the metabolic signaling pathway, PPAR signaling pathway, and cancer signaling pathway. This suggested that the treatment of MAFLD by *P. cocos* may be related to the PPARα signaling pathway. Furthermore, the 31 intersecting genes of *P. cocos* and MAFLD were entered into the BioGPS database. Taking the above-average level as the screening standard for gene localization in tissues and organs, the main target tissues and organs were the pineal gland, liver, lung, heart, and intestine (Supplementary Figure S1D).

Effects of EPC on metabolic dysfunction-associated fatty liver disease in HFD-induced rats

To investigate the role of EPC in MAFLD, we prepared MAFLD rat models by HFD induction for 12 weeks and simultaneously administered EPC to receive different doses of treatment (Figure 2A). At the end of week 12, we weighed the body, liver, lung, heart and inguinal white adipose tissue (iWAT), perirenal white adipose tissue (pWAT), and epididymal white adipose tissue (eWAT) of the rats. In addition, H&E and Oil Red

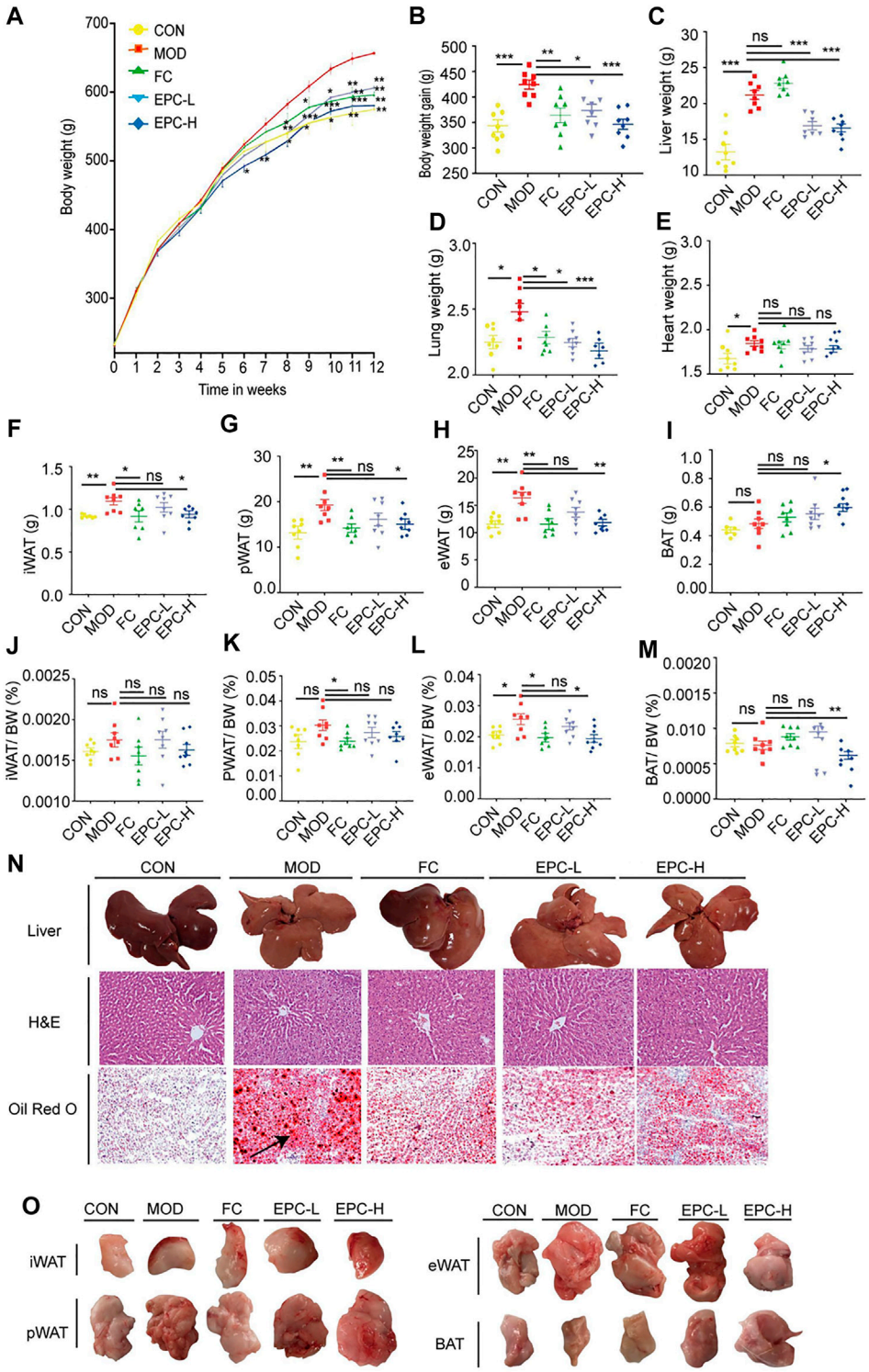

FIGURE 2
EPC ameliorated MAFLD in rats. **(A)** Body weight (BW). **(B)** BW gain. **(C-E)** Organ wet weight. **(F)** Inguinal white adipose tissue (iWAT). **(G)** Perirenal white adipose tissue (pWAT). **(H)** Epididymis white adipose tissue (eWAT). **(I)** Brown adipose tissue (BAT). **(J)** iWAT/BW ratio. **(K)** pWAT/BW ratio. **(L)** eWAT/BW ratio. **(M)** BAT/BW ratio. **(N)** Representative rat liver images of hematoxylin and eosin (H&E) and Oil Red O staining per group (X200). **(O)** Representative iWAT, pWAT, eWAT, BAT. **(N)** Brown adipose tissue (BAT). One-way analysis of variance (ANOVA) was conducted for the group comparison. $n = 8$, data are presented as mean ± SEM. $^{*}p < 0.05$, $^{**}p < 0.01$, $^{***}p < 0.001$ *vs* MOD group. EPC, *P. cocos* ethanol extract; CON, normal diet control group; MOD, high-fat diet group; FC, Fenofibrate capsules; EPC-L, low-dose *P. cocos* ethanol extract; EPC-H, high-dose *P. cocos* ethanol extract.

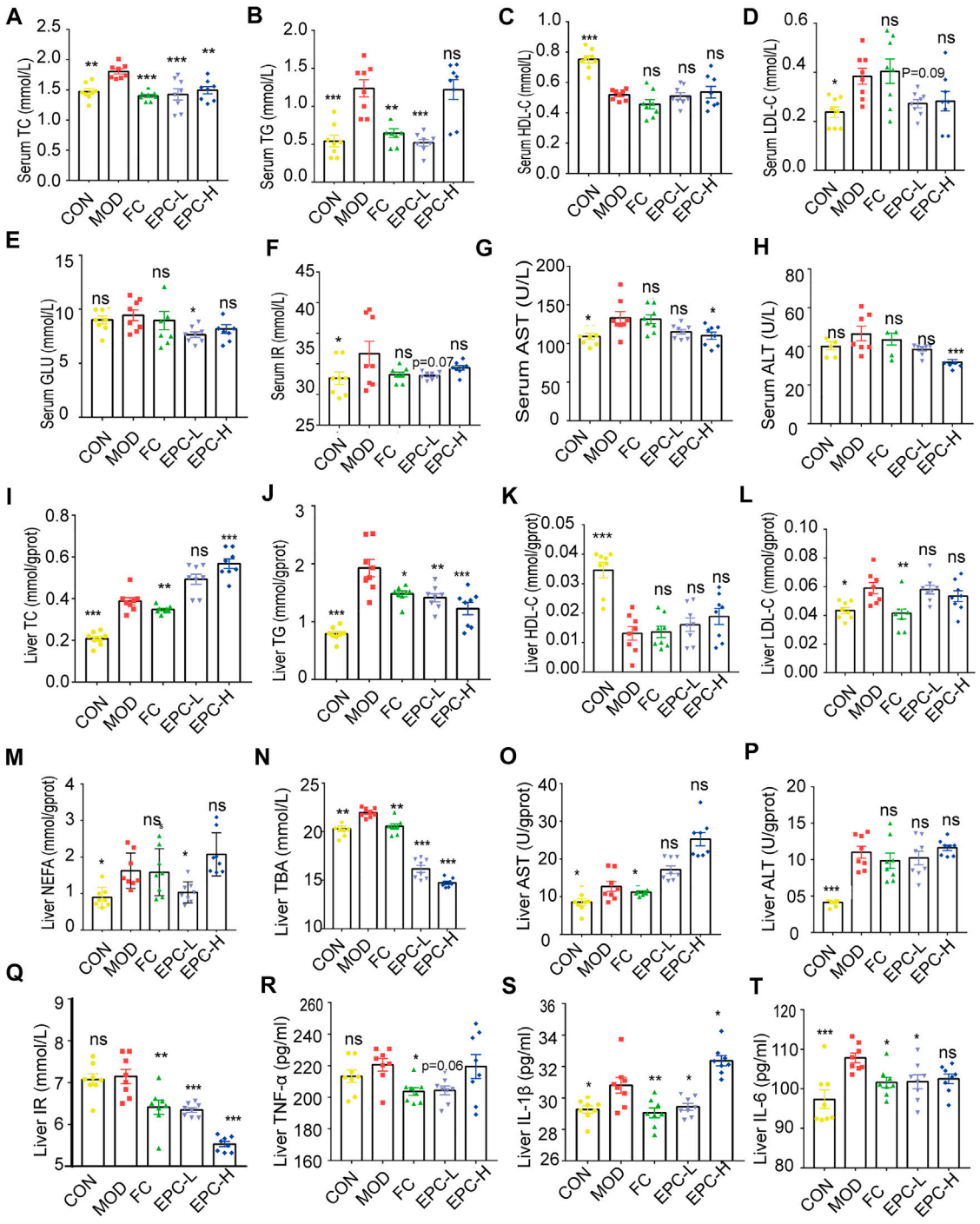

FIGURE 3
EPC administration improved lipid metabolism in HFD-fed rats. **(A–H)** Serum concentrations of TC, TG, HDL, LDL, GLU, IR, AST, and ALT in the rat. **(I–T)** Liver concentrations of TC, TG, HDL, LDL, NEFA, TBA, AST, ALT, IR, TNF-α, IL-1β, and IL-6. One-way analysis of variance (ANOVA) was conducted for the group comparison. $n = 8$, data are presented as mean ± SEM. $^{*}p < 0.05$, $^{**}p < 0.01$, $^{***}p < 0.001$ *vs* MOD group. TC, cholesterol; TG, triglyceride; BA, bile acid; TBA, total bile acid; NEFA, nonesterified free fatty acids; ALT, alanine transaminase; AST, aspartate transaminase; NEFA, nonesterified free fatty acid; LDL-C, low-density lipoprotein cholesterol; HDL-C, high-density lipoprotein cholesterol; TNF-α, tumor necrosis factor-α; IL-1β, Interleukin -1β; IL-6, Interleukin -6; IR, Insulin Receptor; GLU, glucose.

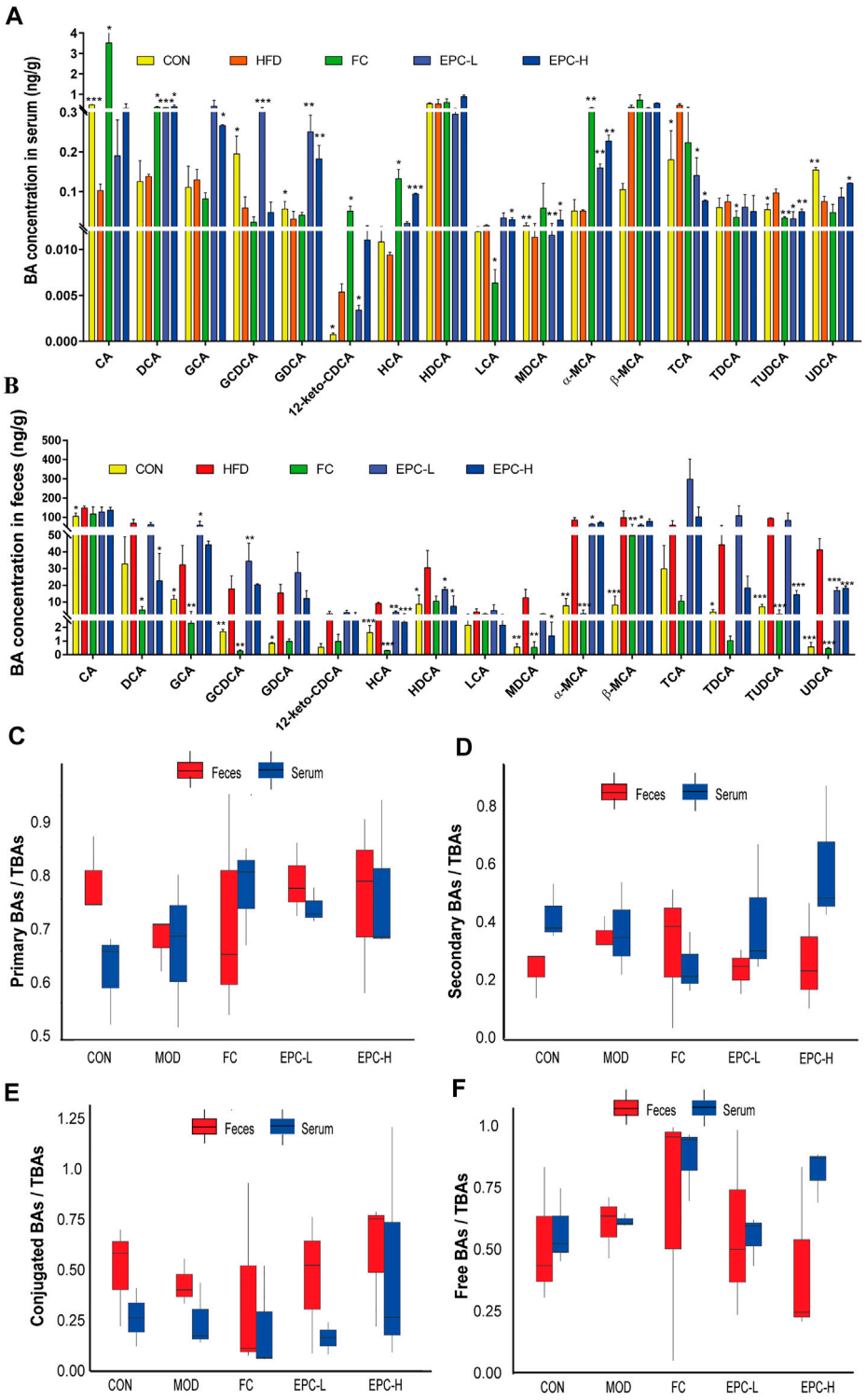

FIGURE 4
Effect of EPC on bile acid profiles in serum and feces. **(A)** BAs concentration in serum. **(B)** BAs concentration in feces. **(C)** Serum and fecal primary BAs concentration/serum and fecal TBAs concentration box chart. **(D)** Serum and fecal secondary BAs concentration/serum and fecal BAs concentration box chart. **(E)** Serum and fecal concentrations of conjugated BAs/serum and fecal TBAs concentrations box chart. **(F)** Free BAs concentration in serum and feces/serum and fecal BAs concentration box chart. $n = 3$, data are presented as mean ± SEM. CA, 12-keto-CDCA, HDCA, MDCA, and TCA in serum and GDCA, MDCA, HDCA, TDCA in feces by Tukey's post hoc test. The rest of the data were tested using paired Student's *t*-tests. $^{*}p < 0.05$, $^{**}p < 0.01$, $^{***}p < 0.001$ *vs* MOD group. CA, cholic acid; GCDCA, glycine (G)-chenodeoxycholic acid; GDCA, G-deoxycholic acid; MDCA, murideoxycholic acid; UDCA, ursodeoxycholic acid; TUDCA, taurine (T)-UDCA; HCA, hyocholic acid; HDCA, hyodeoxycholic acid.

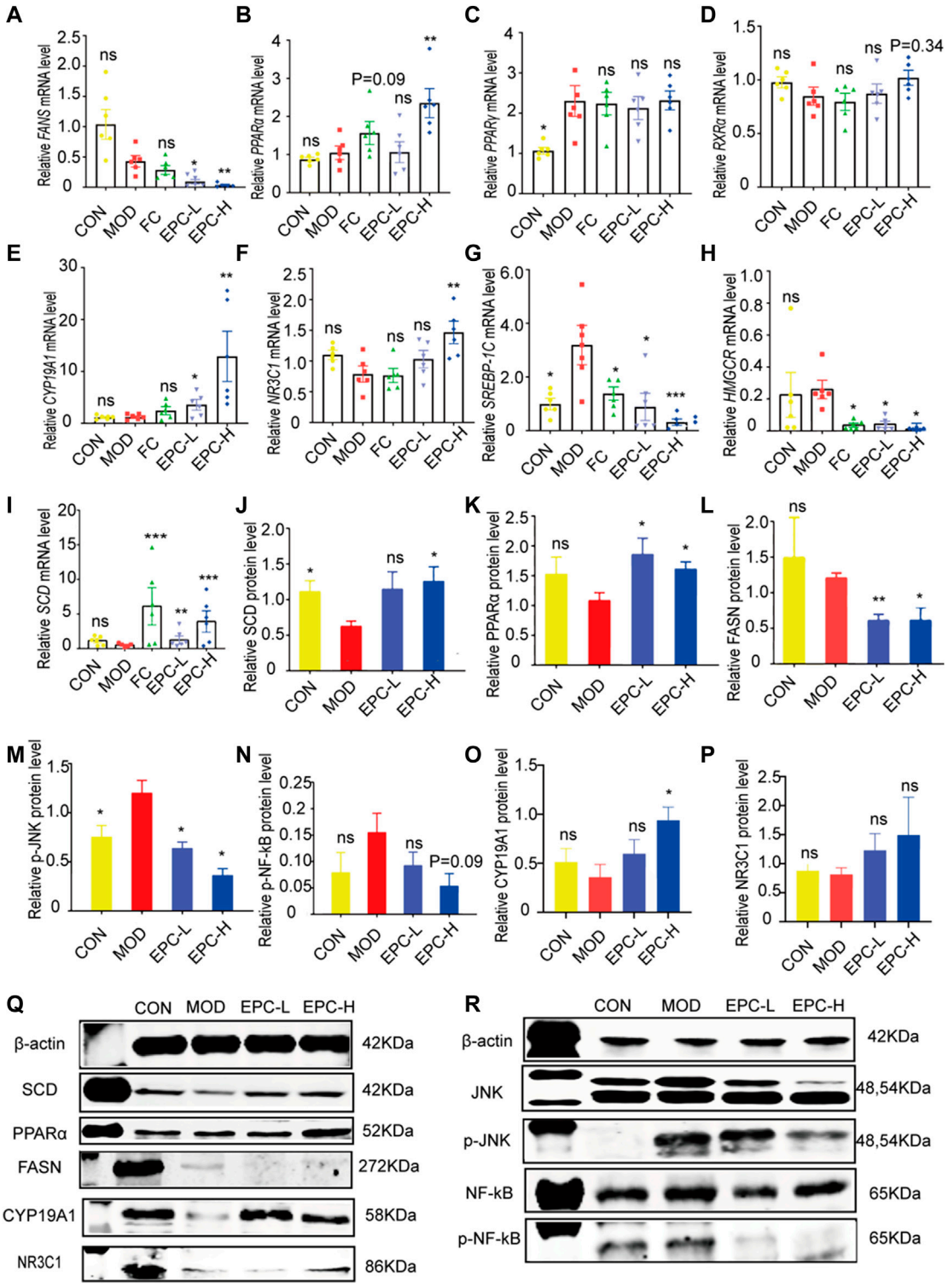

FIGURE 5
EPC regulated the lipid metabolism-related genes and proteins inMAFLD rats. **(A)** mRNA abundances of *FASN*. **(B)** mRNA abundances of *PPARα (PPARA)*. **(C)** mRNA abundances of *PPARγ (PPARG)*. **(D)** mRNA abundances of *RXRα*. **(E)** mRNA abundances of *CYP19A1*. **(F)** mRNA abundances of *NR3C1*. **(G)** mRNA abundances of *SREBP-1c*. **(H)** mRNA abundances of *HMGCR*. **(I)** mRNA abundances of *SCD*. $n = 6$; **(J)** Relative expression of protein SCD. **(K)** Relative expression of protein PPARα. **(L)** Relative expression of protein FASN. **(M)** Relative expression of protein p-JNK. **(N)** Relative expression of protein p-NF-κB. **(O)** Relative expression of protein CYP19A1. **(P)** Relative expression of protein NR3C1. **(Q-R)** Representative immunoblotting images of β-actin, SCD, PPARα, FASN,CYP19A1, NR3C1, JNK, p-JNK, NF-κB, pNF-κB; $n = 4$, data are presented as mean ± SEM. One-
(*Continued*)

FIGURE 5 (Continued)
way analysis of variance (ANOVA) was conducted for the group comparison. *$p < 0.05$, **$p < 0.01$, ***$p < 0.001$ *vs* MOD group. FASN, fatty acid synthase; PPARα/γ, peroxisome proliferator-activated receptor alpha/gamma; RXRa, retinoic acid receptor alpha; SREBP-1c, sterol regulatory element binding protein 1c; HMGCR, 3-hydroxy-3-methylglutaryl-coenzyme A reductase; SCD, Stearoyl-CoA desaturase; p-JNK, phosphorylation (p) -stress-activated protein kinase JNK; NF-κB, nuclear factor kappa B.

O staining images of the liver suggested MAFLD rat models were successfully induced in this study.

FC and EPC had significantly lower body weight and weight gain compared to the HFD rats ($p < 0.01$) (Figures 2A,B). Similar to the trend in body weight gain, EPC-L and EPC-H reduced liver weight gain ($p < 0.001$) (Figure 2C). Following the organ localization results, we also weighed the lungs and hearts of the rats and found that EPC-L reduced the wet weight of the lungs ($p < 0.001$), but EPC had no significant effect on the weight of the heart (Figures 2D,E). Treatment with EPC significantly reduced iWAT, pWAT, and eWAT (Figures 2F–H) and markedly increased the content of brown adipose tissue (BAT) ($p < 0.05$) (Figures 2I,O). The iWAT, pWAT, eWAT, and BAT to body weight in the MAFLD rats ($p < 0.05$) are displayed in Figures 2J–M. In addition, H&E and Oil Red O staining showed that FC and EPC-L/H treatment reduced lipid accumulation (Figure 2N). The above results indicated that EPC ameliorated MAFLD formation in HFD-induced rats.

Effects of EPC on blood lipid levels in rats

To determine the protective effect of EPC on MAFLD, we tested several conventional indicators (Figure 3). The serum levels of TC, TG, LDL, AST, and IR were significantly higher in MAFLD rats. Similarly, the levels of TC, TG, LDL, AST, ALT, NEFA, IR, TNF-α, IL-1β, IL-6, and TBA in their livers were remarkably higher. Moreover, HFD feeding also reduced HDL levels in the liver and serum of rats. Conversely, EPC-L/H can reverse the elevation of TC and TG in serum due to HFD (Figures 3A,B). EPC-H decreased liver and serum TG levels by 30% and 38%, respectively, but did not reduce hepatic TC levels (Figures 3I,J). Also, EPC did not noticeably increase HDL or reduced LDL levels in serum and liver (Figures 3C,D and Figures 3K–L), and the differences in serum AST and ALT levels showed that EPC had a protective effect against liver injury caused by the HFD (Figures 5G,H). Besides, EPC also regulated glucose metabolism disorder caused by the HFD (Figures 3E,F). After the administration of EPC, the NEFA, TBA, TNF-α ($p = 0.056$), IL-1β, and IL-6 levels in rat livers (Figures 3M–T) were significantly decreased. These results suggested that EPC restored abnormal blood lipid levels in HFD-induced rats.

Effect of EPC on the concentration of BAs in serum and feces of metabolic dysfunction-associated fatty liver disease rats

To determine the effect of EPC on BAs in MAFLD rats, we used UHPLC Q-Trap/MS to examine the BA profile in serum and feces. The concentrations of cholic acid (CA), glycine (G)-chenodeoxycholic acid (GCDCA), G-deoxycholic acid (GDCA), murideoxycholic acid (MDCA), and ursodeoxycholic acid (UDCA) in serum and ileal feces of MAFLD rats were significantly decreased (Figures 4A,B). Using the ratios of total primary, total secondary, total conjugated, and total free BAs to the corresponding TBAs in serum and feces, we found the EPC-H exhibited higher levels of conjugated BAs, and the EPC-L group showed lower levels of serum-free BAs. Fecal concentrations of primary and conjugated BAs were elevated and secondary BAs, and free BAs were reduced (Figures 4C–E). Specifically, EPC substantially increased serum concentration of deoxycholic acid (DCA), GDCA, muricholic acid (MCA), and α-MCA and dramatically decreased the concentration of taurine (T)-UDCA (TUDCA), and TCA in MAFLD rats (Figure 4A). In addition, the EPC-L notably increased the levels of GCA, GCDCA, and restored the levels of hyocholic acid (HCA), hyodeoxycholic acid (HDCA), α-MCA, β-MCA, and UDCA in ileal feces. EPC-H emphatically reduced the ileum's DCA, HCA, HDCA, MDCA, and UDCA levels (Figure 4B).

Effects of EPC on metabolic dysfunction-associated fatty liver disease formation by regulating the expression of genes and proteins related to lipid metabolism

To explore the mechanism of the action of EPC in lipid metabolism, we examined the expression of several genes and proteins related to lipid metabolism. As shown in Figure 5, administration of EPC prominently increased the expression levels of *CYP19A1*, *NR3C1*, *PPARα* ($p < 0.01$), and *SCD* mRNA and significantly decreased the expression levels of *FASN*, *SREBP-1c*, and *HMGCR* mRNA (Figures 5A–I). Relative to the MOD group, the protein expression levels of CYP19A1, NR3C1, PPARα ($p < 0.01$), and SCD increased markedly (Figures 5J,K,O–P). The FASN ($p < 0.05$), p-JNK/

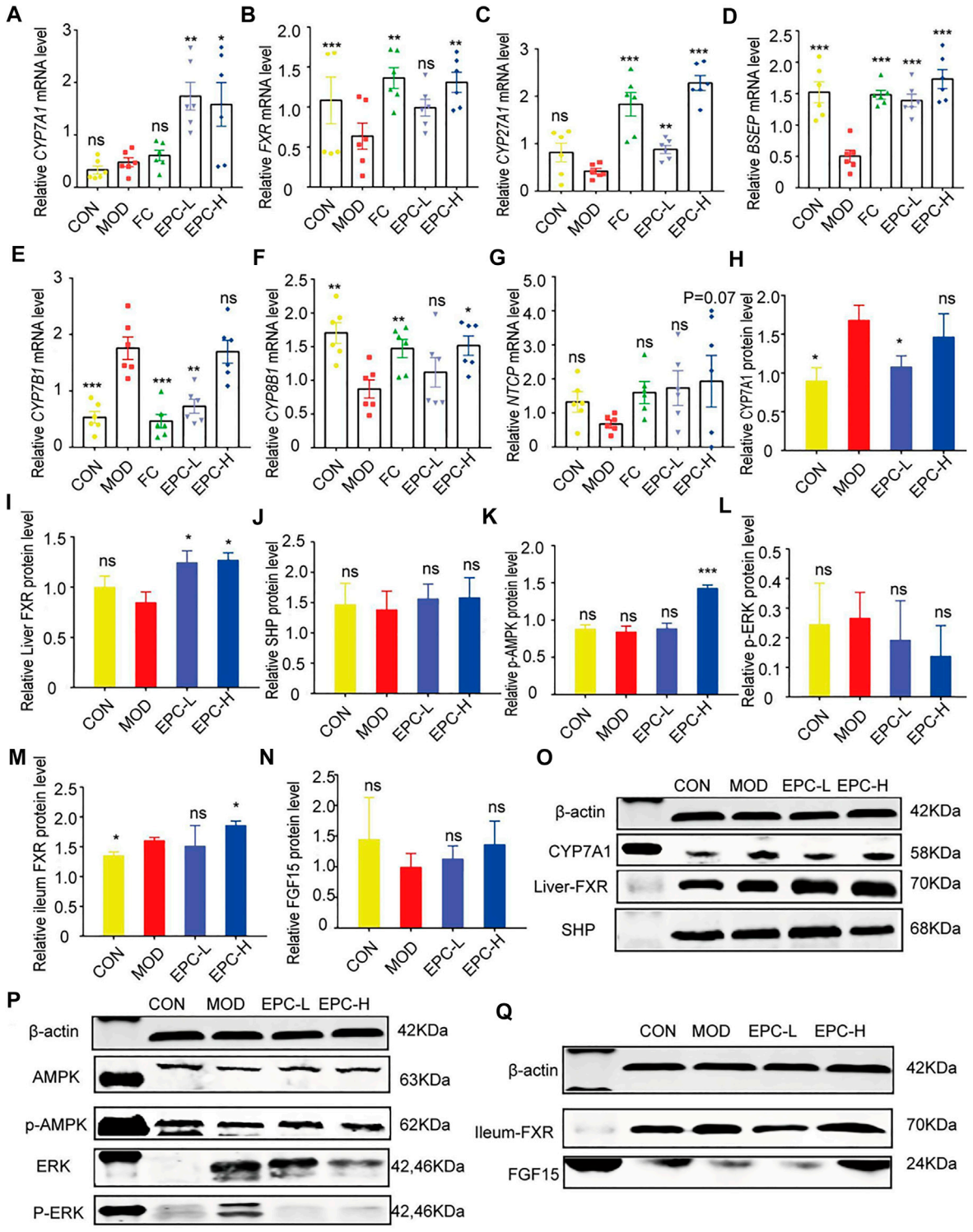

FIGURE 6
EPC ameliorated MAFLD formation in rats by regulating BA metabolism. **(A–G)** Relative expression of *CYP7A1, FXR, CYP27A1, BSEP, CYP7B1, CYP8B1, NTCP* mRNA in liver, n = 6; **(H–L)** Relative expression of protein CYP7A1, FXR, SHP, p-AMPK, and p-ERK in the liver, n = 4; **(M–N)** Relative expression of protein FXR and FGF15 in the ileum, *n* = 4. **(O–P)** Representative immunoblotting images of CYP7A1, FXR, SHP, p-AMPK,and p-ERK in the liver. **(Q)** Representative immunoblotting images of FXR and FGF15 in the ileum. Data are presented as mean ±SEM. One-way analysis of variance (ANOVA) was conducted for the group comparison. *$p < 0.05$, **$p < 0.01$, ***$p < 0.001$ *vs* MOD group. CYP7A1, cholesterol 7α-hydroxylase; FXR, farnesoid X receptor; CYP27A1, sterol 27-hydroxylase; BSEP, bile salt export protein; CYP7B1, oxysterol 7α-hydroxylase; CYP8B1, sterol 12α-hydroxylase; NTCP, Na^+-taurocholate co-transporting polypeptides; SHP, small heterodimer partner; AMPK, 5′-AMP-activated protein kinase; ERK, Extracellular signal-regulated kinase.

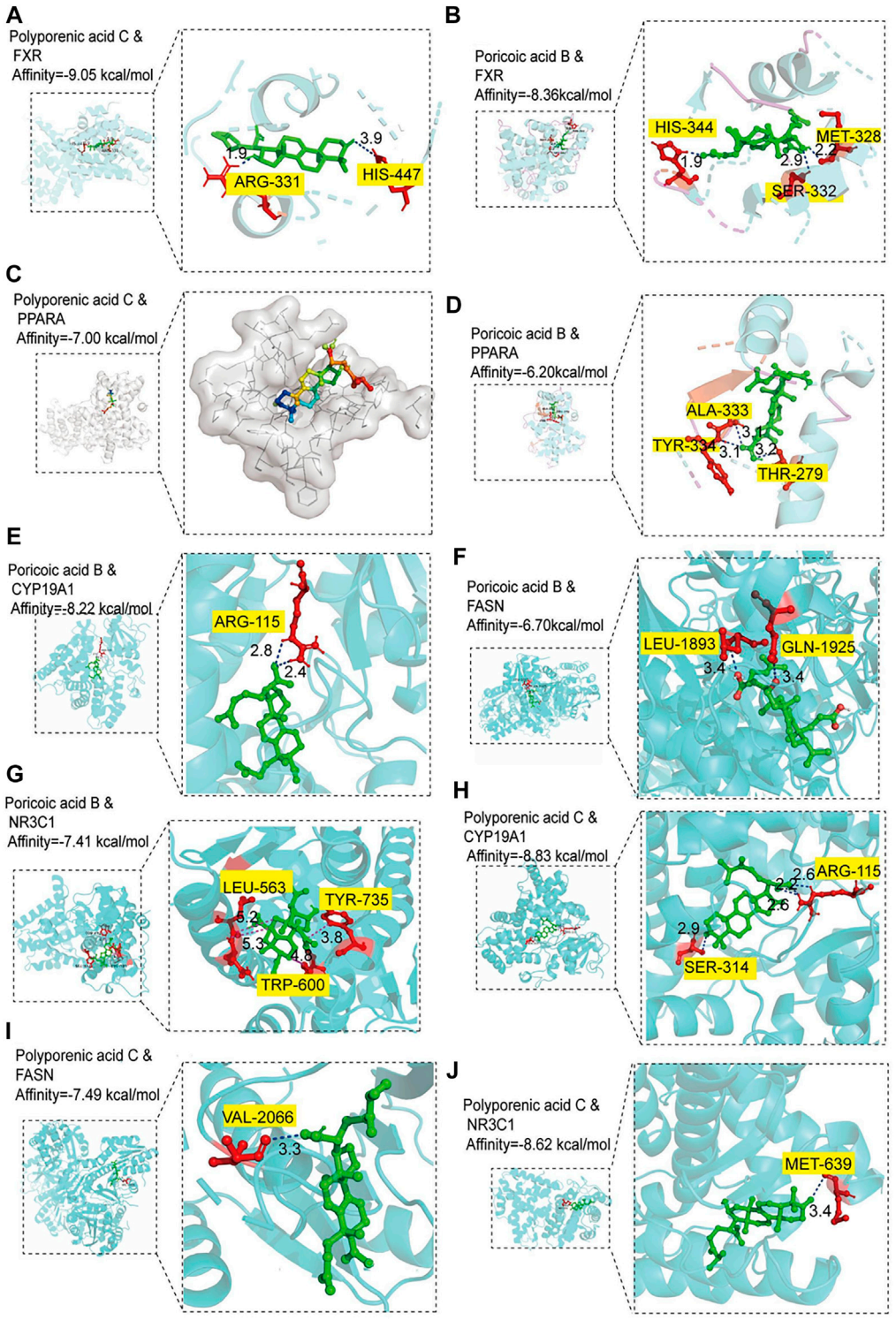

FIGURE 7
Molecular docking analysis. **(A–B)** Molecular docking of polyporenic acid C and Poricoic acid B to farnesoid X receptor (FXR). **(C-D)** Molecular docking of polyporenic acid C and Poricoic acid B to peroxisome proliferator-activated receptor α (PPARA, PPARα). **(E–G)** Molecular docking of poricoic acid B to aromatase (CYP19A1), fatty acid synthase (FASN), and glucocorticoid receptor (NR3C1). **(H–J)** Molecular docking of polyporenic acid C to CYP19A1, FASN, and NR3C1. CYP19A1, aromatase; NR3C1, Glucocorticoid receptor.

JNK ($p < 0.05$), and p-NF-κB/NF-κB($p = 0.089$) decreased dramatically after EPC treatment (Figures 5L–N).

Effects of EPC on metabolic dysfunction-associated fatty liver disease formation by regulating the expression of genes and proteins related to BA metabolism

To explore the mechanism of the action of EPC in BA metabolism, we examined the expression of several known related genes and proteins (Figure 6). In MAFLD rats, the expression of FXR, BSEP, and CYP8B1 mRNA was significantly downregulated in the liver. Conversely, EPC dramatically reversed the downregulation of *FXR*, *BSEP*, and *CYP8B1* mRNA downregulation after HFD feeding. In addition, EPC also remarkably upregulated *CYP7A1*, *CYP27A1*, and *NTCP* mRNA expression downregulated *CYP7B1* and *HMGCR* expression (Figures 6A–G). At protein expression level, CYP7A1 and p-ERK are significantly increased in the liver for HFD-fed rats, and the expression of CYP7A1 is visibly reduced after administration of EPC (Figures 6H,L). In addition, EPC significantly upregulated the expression of FXR and p-AMPK and downregulated the expression of p-ERK but had no significant effect on the relative expression of SHP (Figures 6I–K). In the ileum, we also found that EPC-H upregulated the relative expression of FXR ($p < 0.05$) and FGF15 ($p > 0.05$) (Figures 6M,N).

Screening of the binding ability of active ingredients to proteins

To further investigate the material basis of *P. cocos* for treating MAFLD and explore its mechanism. One hundred molecular dockings were performed based on the screened critical active ingredients and targets (Supplementary Table S3). It is generally accepted that binding energy < 0 kcalmol^{-1} indicates that the ligand and receptor can react spontaneously (Meng et al., 2011) (Supplementary Table S4). The more negative the Vina score, the more stable the compound binds to the protein (Supplementary Figure S2). FXR and PPARA have excellent binding activity with polyporenic acid C and poricoic acid B (Figures 7A–D). The binding energies were -9.05 kcal/mol, −8.36 kcal/mol, −7.0 kcal/mol, −6.20 kcal/mol. A binding energy ≤ −8.0 kcal/mol indicates a robust critical activity between the ligand and the receptor (Clyne et al., 2020). In addition, we also docked FXR and PPARA upstream and downstream proteins, and the results as shown in Figures 7E–J. Poricoic acid B formed two H-bonds with CYP19A1 ARG 115 (Score = −8.22 kcal/mol). Polyporenic acid C began four H-bonds with CYP19A1, SER 314, and ARG 115 (Score = −8.83 kcal/mol) and one H-bond with NR3C1 MET 639 (Score = −8.62 kcal/mol).

Identification of poricoic acid B and polyporenic acid C

Based on the molecular docking, according to the precise molecular mass and fragmentation information from previous reports, poricoic acid B and polyporenic acid C in the EPC were identified through the UPLC Q-TOF/MS. Analysis showed that the retention time of poricoic acid B in $[M-H]^-$ mode was 44.6758 min; Primary mass spectrum (m/s) was 483.312; Secondary ion fragments (ms/ms) were 467.2808, 421.3058, and 439.3169; And mass error was −4.58 ppm (Figure 8A). The retention time of polyporenic acid C in $[M-H]^-$ mode was 49.8359 min; The primary mass spectrum (m/s) was 481.3351; The secondary ion fragments (ms/ms) were 421.3074, 271.1652, and 435.8855; And mass error was −5.73 ppm (Figure 8B).

Poricoic acid B and polyporenic acid C reduced the level of L-02 adipocytes

Finally, Network pharmacology combined with UPLC Q-TOF/MS analysis showed that poricoic acid B and polyporenic acid C are the higher contributing compounds in treating MAFLD by EPC (Figures 1, 8). Besides, it is known from the literature that the content of poricoic acid B in *P. cocos* is ~0.3578%–0.8619%, and the content of polyporenic acid C is ~0.2369%–0.669% (Fu et al., 2018). In this study, we identified poricoic acid B and polyporenic acid C as 6.7% and 28.1% of EPC, respectively. Pharmacological studies showed that porcine acid B has a strong anti-inflammatory effect (Zhang et al., 2021). Polyporenic acid C potentiates insulin and induces differentiation of ST-13 preadipocytes (Yang et al., 2021). Based on the above findings, we chose poricoic acid B and polyporenic acid C to determine whether triterpenic acid could alleviate the damage to L-02 hepatocytes in a 5% fatty emulsion. After treatment with poricoic acid B and polyporenic acid C, we observed a reduction in intracellular lipid droplets (Figure 8G) and a significant decrease in TC, TG, ALT, and AST levels compared with that in the MOD group (Figures 8C–F).

Discussion

Currently, exercise and dietary intraventures remain the key treatment recommendations for patients with MAFLD and its progressive stages (Pang et al., 2022). However, this can be a challenging lifestyle for patients owing to social, mental, physical, and phylogenetic reasons (Worm, 2020). Therefore, it is imperative to find pharmacological treatments for MAFLD. In China, TCM has taken a tremendous role in the prevention and treatment of MAFLD because of its unique theory, pathogenesis, diagnosis, and treatment of MAFLD, such as the theory of "Hepatic and Spleen Co-

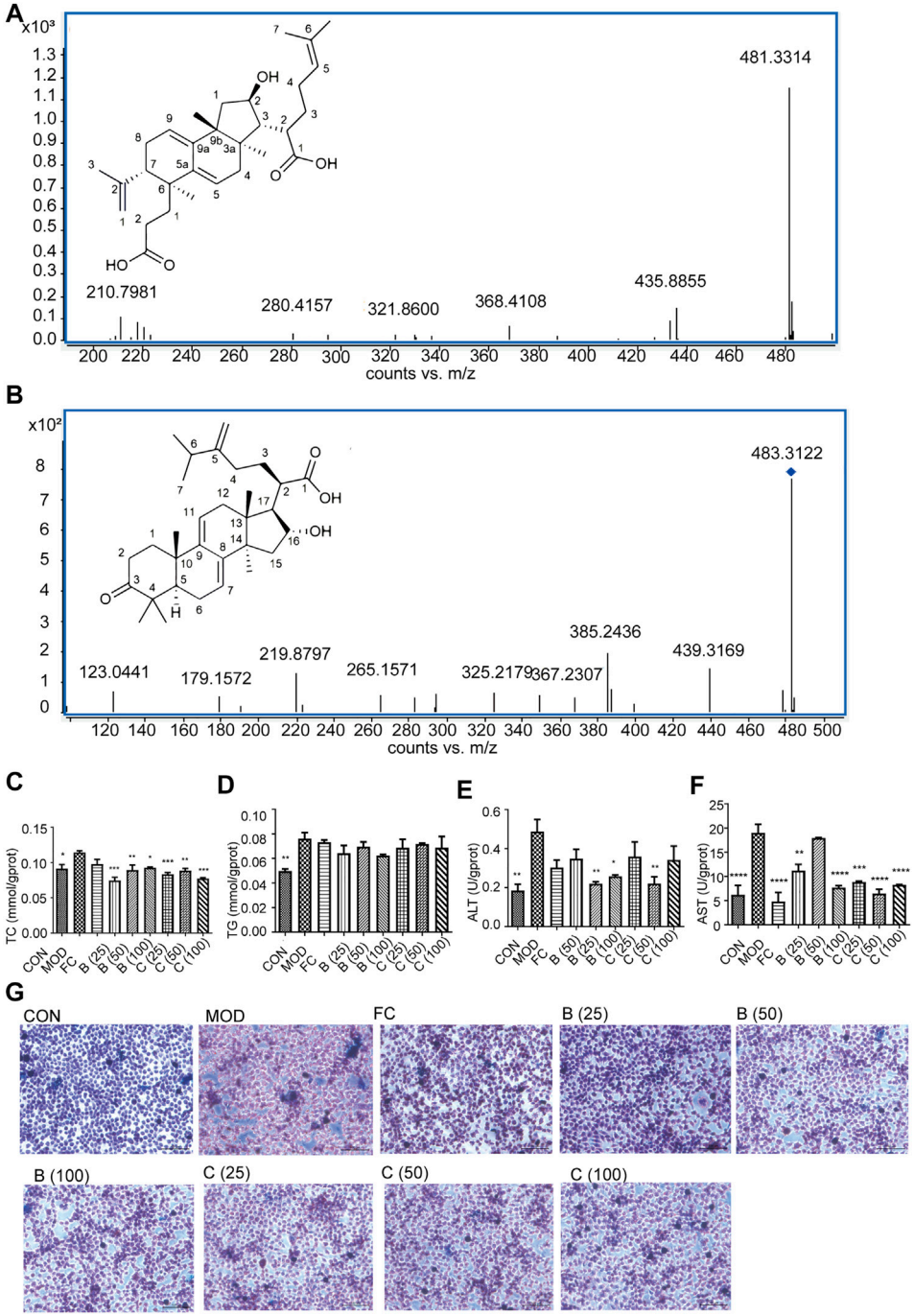

FIGURE 8
Identification of poricoic acid B and polyporenic acid C. **(A)** Characteristic ion peak and 2D structure of poricoic acid B. **(B)** Characteristic ion peak and 2D structure of polyporenic acid C. **(C-F)** Cell levels of TC, TG, ALT, AST. **(G)** Fat accumulation in cells were evaluated under a light microscope (×200) after Oil Red O staining dose (25, 50, and 100 μmol/L) of poricoic acid B group (B (25), B (50), and B (100)), dose (25, 50, and 100 μmol/L) of polyporenic acid C group (C (25), B (50), and B (100)), and FC (150 μmol/L) or separate medium (CON group). $n = 3$, data are presented as mean ± SEM. One-way analysis of variance (ANOVA) was conducted for the group comparison. *$p < 0.05$, **$p < 0.01$, ***$p < 0.001$, ****$p < 0.0001$ *vs* MOD).

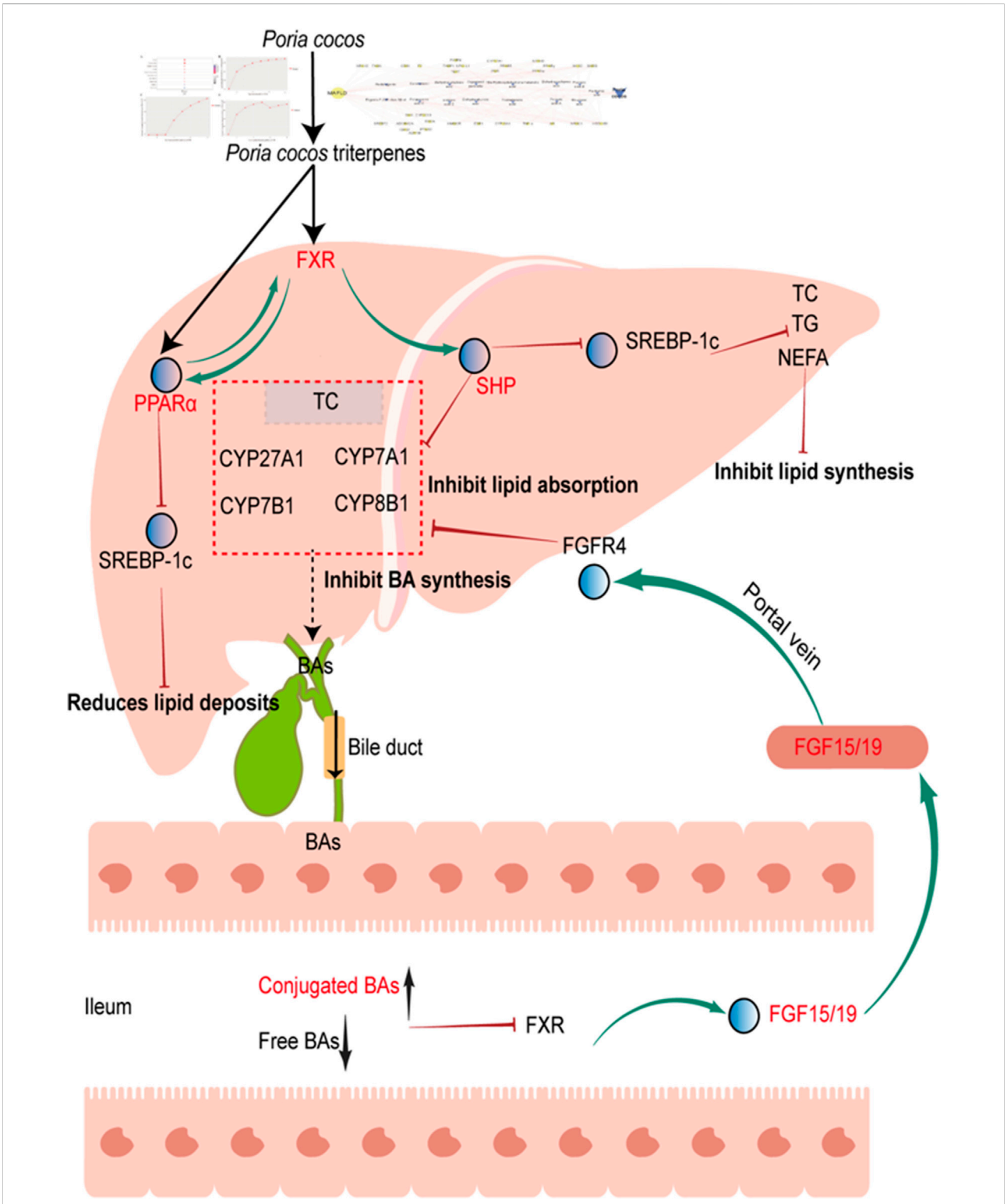

FIGURE 9
Proposed mechanism for *P. cocos* on MAFLD. *Poria cocos* activation of hepatic FXR, which can activate PPARα, inhibit SREBP-1c, reduces lipid deposits. Activation of hepatic FXR, which can activate SHP, inhibit SREBP-1c, reduce TC, TG, NEFA levels and inhibit lipid synthesis. Activation of hepatic FXR, which can activate SHP, reduce CYP7A1 expression and inhibit BA synthesis and lipid absorption; In addition, decreased free bile acids and increased bound bile acids in the intestine can inhibit FXR expression, promote FGF15/19 expression, and reduced bile acid absorption by binding to FGFR4 and inhibiting CYP7A1 expression. FGF15/19, fibroblast growth factor FGF15/19. FGFR4, fibroblast growth factor receptor 4.

treatment" and the system of hepatic-based metabolic balance regulation (Yao et al., 2016; Ding et al., 2019). In recent years, there has been a rapidly growing amount of evidence that herbal medicines have beneficial effects in treating MAFLD, such as Pu-erh tea and mulberry leaves (Huang et al., 2019; Zhong et al., 2020). To elucidate the relationship between *P. cocos* on MAFLD, we used the TCM network pharmacology analysis system to establish the gene co-association between *P. cocos* and MAFLD. UPLC Q-TOF/MS combined with *in vitro* and *in vivo* experiments showed that *P. cocos* triterpenes were the characteristic substances of *P. cocos* for treating MAFLD.

MAFLD is initiated by excessive intake of nutrients. Although most fat is consumed through muscle oxidation, a portion is stored in adipose tissue (Lan et al., 2022). The fat stored in iWAT is further converted to fatty acids through lipolysis. Overconsumption of fatty acids leads to the accumulation of abundant TG in hepatocytes and induces hepatic steatosis (Blüher, 2013). In the present study, EPC reduced HFD-induced hepatic lipid deposition and promoted the browning of eWAT, iWAT, and pWAT white fat. The SREBP transcription factor performs an essential function within lipid metabolism and has three isoforms, SREBP-1a, SREBP-1c, and SREBP-2 (Wu et al., 2019). The *SREBP-1c* high expression can promote fatty acid synthesis into TC, leading to hepatic lipid deposition. HMGCR is the rate-limiting enzyme for TC synthesis, and the *HMGCR* gene also regulates the expression of SREBP-2 at the transcriptional level (Wu et al., 2019). Additionally, HFD and excess energy intake have been shown to reduce (Wu et al., 2019)AMPK activity, thereby increasing the expression of lipid synthesis-related genes, including *ACC*, *SREBP-1c*, and *HMGCR*, ultimately leading to increased synthesis of fatty acids, TG and TC (Chen et al., 2018). In our study, EPC inhibited the expression of *FASN*, *SREBP-1c, and HMGCR* and promoted the expression of p-AMPKα and PPARα. The above suggested that EPC may reduce hepatic fat accumulation and steatosis and inhibit spontaneous fat synthesis and fatty acid uptake while accelerating fatty acid β-oxidation.

Persistent inflammation within the liver is thought to be a key cause of further MAFLD progression, such as inhibition of NF-κB and JNK activation can reduce inflammation and thus protect the liver (Lan et al., 2022). In our research, EPC inhibited the expression of p-NF-κB, p-ERK1/2, and p-JNK in liver tissue and decreased the secretion of the pro-inflammatory cytokines IL-6 and IL-1β under metabolic stress. Furthermore, disturbances in BA metabolism occur during the progression of MAFLD when hepatic BA production is increased or metabolism is slowed down, resulting in BA stasis and thus inducing inflammation (Jiao et al., 2022). In the clinic, in patients with MAFLD, the content of primary and free BAs increased, while that of secondary and conjugated BAs decreased (Michelotti et al., 2013; Zhu et al., 2016; Jiao et al., 2022). In this study, EPC-H reduced the fecal-free BAs induced by HFD by 16.36%, and fecal concentrations of conjugated BAs were elevated. In addition, higher levels of CA, LCA, and DCA were observed in the feces of HFD-induced MAFLD rats (Michelotti et al., 2013; Zhu et al., 2016; Jiao et al., 2022); In our study, EPC not only reduced TBA and IBIL levels in rat liver but also decreased CA, DCA, and LCA levels in feces. Suggested that EPC inhibits the development of MAFLD by suppressing the release of hepatic inflammatory factors and an improved BA metabolism.

PPARa signaling pathway participates in the control of BA metabolism and lipid metabolism (Michelotti et al., 2013; Lan et al., 2022). FXR is an upstream protein expressed in the SHP and PPARα signaling pathways during MAFLD disease progression (Li et al., 2013). Also, FXR inhibits the expression of SREBP-1c by synergizing with SHP, thereby suppressing the expression of fatty acid synthase, acetyl coenzyme A carboxylase, and other key enzymes of fatty acid ab initio synthesis, and ultimately inhibiting hepatic TG synthesis. In addition, FXR activation can negatively feedback and inhibit the expression of CYP7A1 and CYP8B1, the rate-limiting enzymes of BA synthesis, thereby reducing BA synthesis and lipid absorption (Li et al., 2022; Zeng et al., 2016). In our study, EPC remarkably increased the expression of FXR and PPARα. Interestingly, EPC also substantially reduced CYP7A1 and SREBP-1c of hepatic expression. FXR agonists CDCA and GW4064 cause upregulation of PPARα expression, mainly through FXR binding to the PPARα promoter region, enhancing the expression of the PPARα target gene *CPT1*, promoting fatty acid β-oxidation, and reducing hepatic TG accumulation (Miyata et al., 2014). Furthermore, the regulatory effect of PPARα on BA metabolism is being reported extensively (Mencarelli et al., 2013; Xie et al., 2019). It has been shown that PPARα can be activated by affecting the expression of CYP7A1, NTCP, and BSEP, thereby reducing the synthesis of BAs. FXR and PPARα regulate energy homeostasis in the hepatic mainly through the activation of PPARα to promote fatty acid oxidation and through the activation of FXR to control BA homeostasis (Xie et al., 2019).

Conclusion

In summary, EPC alleviated HFD-induced MAFLD through the regulation of lipid homeostasis and BA metabolism. *P. cocos* triterpenes, such as poricoic acid B and polyporenic acid C, are the characteristic substances of *P. cocos* for the treatment of MAFLD, and its mechanism may be *via* the FXR/PPARα-SREBPs signaling pathway (Figure 9).

Data availability statement

The raw data supporting the conclusions of this article will be made available by the authors, without undue reservation.

Ethics statement

The animal study was reviewed and approved by the intramural Committee on the Ethical and Humane Treatment of Experimental Animals of Yunnan TCM hospital/Medical ethics committee of the First Affiliated Hospital of Yunnan University of Chinese Medicine (Application No: SD2021-001).

Author contributions

Conceptualization: JY and YQ; Data curation: JH and XY; Formal analysis: XL and MZ; Funding acquisition: JY, MZ, and XY; Investigation: YQ and YY; Methodology: XL and FZ; Project administration: JY and FZ; Resources: JY and YQ; Software: JH and XP; Supervision: JY and YQ; Validation: XP and XH; Visualization: FZ; Roles/Writing—original draft: JH, and YL; Writing—review and Editing: JY. All the authors contributed to the article revision, read, and approved the submitted version.

Funding

This work was supported by the Application and Basis Research Project of Yunnan China (No. 2019IB009, 202002AA100007, 202001AZ070001-043, 202201AW070016, 2022Y345, 202105AG070012), National Natural Science Foundation of China (No. 82160748, 82104381), High-level TCM talents (reserve talents) project of Yunnan (2021. No1).

Acknowledgments

We thank Shanghai Majorbio Bio-Pharm Technology Co., Ltd., for the technical support of our serum and fecal bile acid profile.

Conflict of interest

The authors declare that the research was conducted in the absence of any commercial or financial relationships that could be construed as a potential conflict of interest.

Publisher's note

All claims expressed in this article are solely those of the authors and do not necessarily represent those of their affiliated organizations, or those of the publisher, the editors and the reviewers. Any product that may be evaluated in this article, or claim that may be made by its manufacturer, is not guaranteed or endorsed by the publisher.

Supplementary material

The Supplementary Material for this article can be found online at: https://www.frontiersin.org/articles/10.3389/fphar.2022.1007274/full#supplementary-material

References

Blüher, M. (2013). Adipose tissue dysfunction contributes to obesity related metabolic diseases. *Best. Pract. Res. Clin. Endocrinol. Metab.* 27 (2), 163–177. doi:10.1016/j.beem.2013.02.005

Byrne, C. D., and Targher, G. (2015). Nafld: A multisystem disease. *J. Hepatol.* 62, S47–S64. doi:10.1016/j.jhep.2014.12.012

Chen, Q., Liu, M., Yu, H., Li, J., Wang, S., Zhang, Y., et al. (2018). Scutellaria baicalensis regulates FFA metabolism to ameliorate NAFLD through the AMPK-mediated SREBP signaling pathway. *J. Nat. Med.* 72, 655–666. doi:10.1007/s11418-018-1199-5

Clyne, A., Yang, L., Yang, M., May, B., and Yang, A. (2020). Molecular docking and network connections of active compounds from the classical herbal formula Ding Chuan Tang. *PeerJ* 8, e8685. doi:10.7717/peerj.8685

de Alwis, N. M., and Day, C. P. (2008). Non-alcoholic fatty liver disease: The mist gradually clears. *J. Hepatol.* 48, S104–S112. doi:10.1016/j.jhep.2008.01.009

Ding, J., Zhang, B., Wang, P. J., He, G. N., Wei, D. M., Ding, J. L., et al. (2019). Analysis on mechanisms and medication rules of herbal prescriptions for nonalcoholic fatty liver disease based on methods of data mining and biological information. *Zhongguo Zhong Yao Za Zhi* 44, 1689–1695. doi:10.19540/j.cnki.cjcmm.20190110.001

Eslam, M., Sarin, S. K., Wong, V. W., Fan, J. G., Kawaguchi, T., Ahn, S. H., et al. (2020). The Asian Pacific Association for the Study of the Liver clinical practice guidelines for the diagnosis and management of metabolic associated fatty liver disease. *Hepatol. Int.* 14 (6), 889–919. doi:10.1007/s12072-020-10094-2

Esteban, C. I. (2009). Medicinal interest of *Poria cocos* (= Wolfiporia extensa). *Rev. Iberoam. Micol.* 26 (2), 103–107. doi:10.1016/S1130-1406(09)70019-1

Fu, M., Wang, L., Wang, X., Deng, B., Hu, X., and Zou, J. (2018). Determination of the five main terpenoids in different tissues of wolfiporia cocos. *Molecules* 23 (8), E1839. doi:10.3390/molecules23081839

Huang, F., Zheng, X., Ma, X., Jiang, R., Zhou, W., Zhou, S., et al. (2019). Theabrownin from Pu-erh tea attenuates hypercholesterolemia *via* modulation of gut microbiota and bile acid metabolism. *Nat. Commun.* 10 (1), 4971. doi:10.1038/s41467-019-12896-x

Huang, G. J., Deng, J. S., Huang, S. S., Lee, C. Y., Hou, W. C., Wang, S. Y., et al. (2013). Hepatoprotective effects of eburicoic acid and dehydroeburicoic acid from Antrodia camphorata in a mouse model of acute hepatic injury. *Food Chem.* 141 (3), 3020–3027. doi:10.1016/j.foodchem.2013.03.061

Jiao, T. Y., Ma, Y. D., Guo, X. Z., Ye, Y. F., and Xie, C. (2022). Bile acid and receptors: Biology and drug discovery for nonalcoholic fatty liver disease. *Acta Pharmacol. Sin.* 43 (5), 1103–1119. doi:10.1038/s41401-022-00880-z

Lan, T., Jiang, S., Zhang, J., Weng, Q., Yu, Y., Li, H., et al. (2022). Breviscapine alleviates NASH by inhibiting TGF-β-activated kinase 1-dependent signaling. *Hepatology* 76 (1), 155–171. doi:10.1002/hep.32221

Li, L., Zuo, Z. T., and Wang, Y. Z. (2022). The traditional usages, chemical components and pharmacological activities of wolfiporia cocos: A review. *Am. J. Chin. Med.* 50 (2), 389–440. doi:10.1142/S0192415X22500161

Li, X., Ma, L., and Zhang, L. (2019). Molecular basis for *Poria cocos* mushroom polysaccharide used as an antitumor drug in China. *Prog. Mol. Biol. Transl. Sci.* 163, 263–296. doi:10.1016/bs.pmbts.2019.02.011

Li, Y., Jadhav, K., and Zhang, Y. (2013). Bile acid receptors in non-alcoholic fatty liver disease. *Biochem. Pharmacol.* 86 (11), 1517–1524. doi:10.1016/j.bcp.2013.08.015

Lindner, D. L., and Banik, M. T. (2008). Molecular phylogeny of Laetiporus and other Brown rot polypore genera in North America. *Mycologia* 100 (3), 417–430. doi:10.3852/07-124r2

Ma, S., Zheng, L., Lin, X., Feng, Y., Yang, M., and Shen, L. (2021). Network pharmacology and metabolomics studies on antimigraine mechanisms of da chuan xiong Fang (DCXF). *Evid. Based. Complement. Altern. Med.* 2021, 6665137. doi:10.1155/2021/6665137

Machado, M. V., and Diehl, A. M. (2016). Pathogenesis of nonalcoholic steatohepatitis. *Gastroenterology* 150 (8), 1769–1777. doi:10.1053/j.gastro.2016.02.066

Mencarelli, A., Cipriani, S., Renga, B., D'Amore, C., Palladino, G., Distrutti, E., et al. (2013). FXR activation improves myocardial fatty acid metabolism in a rodent model of obesity-driven cardiotoxicity. *Nutr. Metab. Cardiovasc. Dis.* 23 (2), 94–101. doi:10.1016/j.numecd.2011.06.008

Meng, X. Y., Zhang, H. X., Mezei, M., and Cui, M. (2011). Molecular docking: A powerful approach for structure-based drug discovery. *Curr. Comput. Aided. Drug Des.* 7 (2), 146–157. doi:10.2174/157340911795677602

Miao, H., Zhao, Y. H., Vaziri, N. D., Tang, D. D., Chen, H., Chen, H., et al. (2016). Lipidomics biomarkers of diet-induced hyperlipidemia and its treatment with Poria cocos. *J. Agric. Food Chem.* 64 (4), 969–979. doi:10.1021/acs.jafc.5b05350

Michelotti, G. A., Machado, M. V., and Diehl, A. M. (2013). NAFLD, NASH and liver cancer. *Nat. Rev. Gastroenterol. Hepatol.* 10 (11), 656–665. doi:10.1038/nrgastro.2013.183

Miyata, M., Hata, T., Yamazoe, Y., and Yoshinari, K. (2014). SREBP-2 negatively regulates FXR-dependent transcription of FGF19 in human intestinal cells. *Biochem. Biophys. Res. Commun.* 443 (2), 477–482. doi:10.1016/j.bbrc.2013.11.126

Moris, D., Giaginis, C., Tsourouflis, G., and Theocharis, S. (2017). Farnesoid-X receptor (FXR) as a promising pharmaceutical target in atherosclerosis. *Curr. Med. Chem.* 24 (11), 1147–1157. doi:10.2174/0929867324666170124151940

Nie, A., Chao, Y., Zhang, X., Jia, W., Zhou, Z., and Zhu, C. (2020). Phytochemistry and pharmacological activities of wolfiporia cocos (F.A. Wolf) ryvarden & gilb. *Front. Pharmacol.* 11, 505249. doi:10.3389/fphar.2020.505249

Pang, Y., Kartsonaki, C., Lv, J., Millwood, I. Y., Fairhurst-Hunter, Z., Turnbull, I., et al. (2022). Adiposity, metabolomic biomarkers, and risk of nonalcoholic fatty liver disease: A case-cohort study. *Am. J. Clin. Nutr.* 115 (3), 799–810. doi:10.1093/ajcn/nqab392

Qian, Q., Zhou, N., Qi, P., Zhang, Y., Mu, X., Shi, X., et al. (2018). A UHPLC-QTOF-MS/MS method for the simultaneous determination of eight triterpene compounds from *Poria cocos* (Schw.) Wolf extract in rat plasma: Application to a comparative pharmacokinetic study. *J. Chromatogr. B Anal. Technol. Biomed. Life Sci.* 1102, 110334–110344. doi:10.1016/j.jchromb.2018.10.011

Ríos, J. L. (2011). Chemical constituents and pharmacological properties of *Poria cocos*. *Planta Med.* 77 (7), 681–691. doi:10.1055/s-0030-1270823

Tian, S. S., Liu, X. Q., Feng, W. H., Zhang, Q. W., Yan, L. H., Wang, Z. M., et al. (2019). Quality evaluation of Poria based on specific chromatogram and quantitative analysis of multicomponents. *Zhongguo Zhong Yao Za Zhi* 44 (7), 1371–1380. doi:10.19540/j.cnki.cjcmm.20181220.005

Wong, V. W., and Lazarus, J. V. (2021). Prognosis of MAFLD vs. NAFLD and implications for a nomenclature change. *J. Hepatol.* 75 (6), 1267–1270. doi:10.1016/j.jhep.2021.08.020

Worm, N. (2020). Beyond body weight-loss: Dietary strategies targeting intrahepatic fat in NAFLD. *Nutrients* 12, E1316. doi:10.3390/nu12051316

Wu, Q., Wang, Q., Fu, J., and Ren, R. (2019). Polysaccharides derived from natural sources regulate triglyceride and cholesterol metabolism: A review of the mechanisms. *Food Funct.* 10 (5), 2330–2339. doi:10.1039/c8fo02375a

Xie, C., Takahashi, S., Brocker, C. N., He, S., Chen, L., Xie, G., et al. (2019). Hepatocyte peroxisome proliferator-activated receptor α regulates bile acid synthesis and transport. *Biochim. Biophys. Acta. Mol. Cell Biol. Lipids* 1864, 1396–1411. doi:10.1016/j.bbalip.2019.05.014

Yang, M., Zhao, Y., Qin, Y., Xu, R., Yang, Z., and Peng, H. (2021). Untargeted metabolomics and targeted quantitative analysis of temporal and spatial variations in specialized metabolites accumulation in Poria cocos (schw.) wolf (fushen). *Front. Plant Sci.* 12, 713490. doi:10.3389/fpls.2021.713490

Yao, H., Qiao, Y. J., Zhao, Y. L., Tao, X. F., Xu, L. N., Yin, L. H., et al. (2016). Herbal medicines and nonalcoholic fatty liver disease. *World J. Gastroenterol.* 22 (30), 6890–6905. doi:10.3748/wjg.v22.i30.6890

Younossi, Z. M., Koenig, A. B., Abdelatif, D., Fazel, Y., Henry, L., and Wymer, M. (2016). Global epidemiology of nonalcoholic fatty liver disease-Meta-analytic assessment of prevalence, incidence, and outcomes. *Hepatology* 64 (1), 73–84. doi:10.1002/hep.28431

Zeng, T., Zhou, J., He, L., Zheng, J., Chen, L., Wu, C., et al. (2016). Blocking nuclear factor-kappa B protects against diet-induced hepatic steatosis and insulin resistance in mice. *PLoS One* 11 (3), e0149677. doi:10.1371/journal.pone.0149677

Zhang, L., Yin, M., Feng, X., Ibrahim, S. A., Liu, Y., and Huang, W. (2021). Anti-inflammatory activity of four triterpenoids isolated from poriae cutis. *Foods* 10, 3155. doi:10.3390/foods10123155

Zhong, Y., Song, B., Zheng, C., Zhang, S., Yan, Z., Tang, Z., et al. (2020). Flavonoids from mulberry leaves alleviate lipid dysmetabolism in high fat diet-fed mice: Involvement of gut microbiota. *Microorganisms* 8, 860. doi:10.3390/microorganisms8060860

Zhu, Y., Liu, H., Zhang, M., and Guo, G. L. (2016). Fatty liver diseases, bile acids, and FXR. *Acta Pharm. Sin. B* 6 (5), 409–412. doi:10.1016/j.apsb.2016.07.008

frontiers | Frontiers in Pharmacology

TYPE Original Research
PUBLISHED 17 November 2022
DOI 10.3389/fphar.2022.1027628

OPEN ACCESS

EDITED BY
Xian-Jun Fu,
Shandong University of Traditional Chinese Medicine, China

REVIEWED BY
Yuzhu Tan,
Chengdu University of Traditional Chinese Medicine, China
Feng Zhao,
Shandong University of Traditional Chinese Medicine, China

*CORRESPONDENCE
Yu Zhao,
cathy150@139.com
Yiyang Hu,
yyhuliver@163.com

†These authors have contributed equally to this work

SPECIALTY SECTION
This article was submitted to Ethnopharmacology, a section of the journal Frontiers in Pharmacology

RECEIVED 25 August 2022
ACCEPTED 07 November 2022
PUBLISHED 17 November 2022

CITATION
Pan Y, Guo J, Hu N, Xun Y, Zhang B, Feng Q, Chen S, Li X, Liu Q, Hu Y and Zhao Y (2022), Distinct common signatures of gut microbiota associated with damp-heat syndrome in patients with different chronic liver diseases. *Front. Pharmacol.* 13:1027628. doi: 10.3389/fphar.2022.1027628

Distinct common signatures of gut microbiota associated with damp-heat syndrome in patients with different chronic liver diseases

Yuqing Pan[1†], Jianchun Guo[2†], Na Hu[1†], Yunhao Xun[2], Binbin Zhang[1], Qin Feng[1], Si Chen[1], Xiaojing Li[1], Qiaohong Liu[1], Yiyang Hu[3*] and Yu Zhao[1*]

[1]Key Laboratory of Liver and Kidney Diseases (Ministry of Education), Shanghai Key Laboratory of Traditional Chinese Clinical Medicine, Institute of Liver Diseases, Shuguang Hospital Affiliated to Shanghai University of Traditional Chinese Medicine, Shanghai, China, [2]Department of Integrative Medicine, Hangzhou Xixi Hospital, Hangzhou, China, [3]Institute of Clinical Pharmacology, Shuguang Hospital Affiliated to Shanghai University of Traditional Chinese Medicine, Shanghai, China

Background: Chronic hepatitis B (CHB) and non-alcoholic fatty liver disease (NAFLD) are prevalent in China. According to traditional Chinese medicine (TCM) theory, damp-heat (DH) syndrome is common in chronic liver disease. However, the biological characteristics related to quantitative diagnosis remain to be determined. This study aimed to identify the consistent alterations in the gut microbiota associated with DH syndrome in patients with CHB or NAFLD.

Methods: A total of 405 individuals were recruited, of which 146 were participants who met the consistent TCM diagnosis by three senior TCM physicians and were typical syndromes. All participants were required to provide fresh stool and serum samples. The gut microbiota was assessed by fecal 16S rRNA gene sequencing, and the serum metabolite profiles of participants were quantified by an ultra-performance liquid chromatography coupled to tandem mass spectrometry (UPLC-MS/MS) system. DH syndrome-related bacteria taxa were identified based on the 146 individuals with typical syndromes and validated in all 405 volunteers.

Results: The results showed that CHB and NAFLD patients with typical TCM DH syndrome had consistently elevated serum total bile acid (TBA) levels. Significant alterations in microbial community were observed according to TCM syndromes identification. A total of 870 microbial operational taxonomic units and 21 serum metabolites showed the same variation trends in both the CHB and NAFLD DH syndrome groups. The functional analysis predicts consistent dysregulation of bile acid metabolism. Five genera (*Agathobacter, Dorea, Lachnospiraceae_NC2004_group, Subdoligranulum,* and *unclassified_c__Clostridia*) significantly decreased in abundance in patients with DH syndrome. We utilize these five genera combined with TBA to construct a random forest classifier model to predict TCM diagnosis. The diagnostic receiver-operator characteristic (ROC) areas for DH syndrome

were 0.818 and 0.791 in internal tenfold cross-validation and the test set based on all 405 individuals, respectively.

Conclusion: There are common signatures of gut microbiota associated with DH syndrome in patients with different chronic liver diseases. Serum TBA combined with DH-related genera provides a good diagnostic potential for DH syndrome in chronic liver disease.

KEYWORDS

traditional Chinese medicine, damp-heat syndrome, gut microbiota, chronic hepatitis B, non-alcoholic fatty liver disease

Introduction

Chronic hepatitis B (CHB) and non-alcoholic fatty liver disease (NAFLD) are currently the most prevalent forms of chronic hepatitis in China (Wang et al., 2014; Zhou et al., 2020). Traditional Chinese medicine (TCM) is widely used in China, as well as in the treatment of chronic liver disease. TCM is advanced at alleviating clinical symptoms and improving liver function in patients with liver diseases (Zhang et al., 2010). TCM prescription based on *Zheng* pattern identification. "*Zheng*", also known as TCM syndrome, is a term that generalizes the pathological properties and changes associated with certain stages of TCM disease. The TCM practitioner identifies the patient's syndrome diagnosis by a comprehensive symptom-based approach according to observation, auscultation, inquiry, and palpation. However, the symptoms that TCM syndrome pattern diagnosis relies on are subtle and unquantifiable (such as fatigue and thirst). TCM diagnosis may differ depending on the subjective observations and clinical experience of the TCM practitioner. The same condition of a patient may be diagnosed differently by different TCM clinicians, the inconsistency hinders the repeatability of TCM, and even spark a potential argument about TCM as a medical system. Therefore, it is essential to explore the quantitative and valid biological scientific foundation of TCM syndromes to enhance TCM diagnosis and modernization (Jiang et al., 2012).

Damp-heat (DH) syndrome is a status of disharmony that often occurs when dampness binds with heat evil. DH syndrome can be seen in a variety of modern medical diseases and is a common syndrome pattern in chronic liver disease. This pattern often results from the internal accumulation of damp heat and is characterized by distending pain/masses in the subcostal region, thirst, and a bitter mouth. The tongue is red with a yellow, greasy coating. The pulse is slippery and rapid. DH syndrome is very common in patients with chronic liver diseases, which is accounting for 21.9% of NAFLD patients (Li et al., 2019; Zhou et al., 2022). According to a systematic review based on 20,106 participants, DH occurs in 32.2% of all patients with CHB (Zeng et al., 2011). A crucial concept in TCM theory is that "different diseases have the same syndrome". CHB is a liver infection caused by persistent hepatitis B virus (HBV) (Seto et al., 2018), and NAFLD is characterized by excessive fat accumulation in the hepatocytes (Loomba et al., 2021). However, the prescriptions against DH syndrome may be similar for patients with either CHB or NAFLD in TCM. For example, *Yinchenhao* decoction is a classic Chinese medicine prescription, widely used in various liver diseases accompanied by dampness-heat syndrome and jaundice. Therefore, DH syndrome may share a common biological basis in different liver diseases.

In recent years, multi-omics have linked TCM and biomolecular changes. Our previous study showed that CHB and NAFLD patients with DH syndrome have certain common urinary metabolic disorders (Dai et al., 2013). According to TCM theory, DH syndrome reflects systemic changes in the entire body but mainly indicates dysfunction in digestive tract organs, such as the stomach, intestines, and liver. The human gastrointestinal system contains trillions of microorganisms. Gut microbiota strongly influences host homeostasis (Fan and Pedersen, 2021). Certain TCM herbal formulations and compounds are found to clear damp heat evil by modulating gut microbiota (Wu et al., 2020; Xu et al., 2020). However, the relationship between the gut microbiota and DH syndrome in patients with chronic liver diseases remains to be determined. In the present study, we investigated the distinct signatures common to CHB and NAFLD associated with DH syndrome on the basis of patient intestinal microbiota and serum metabolites.

Methods

Patient recruitment

From July 2019 to November 2020, patients with CHB or NAFLD who met the established inclusion and exclusion criteria were enrolled in this study. Healthy volunteers were enrolled as healthy control. Volunteers in this study originated from Shuguang Hospital affiliated with Shanghai University of Traditional Chinese Medicine (Shanghai, China), Shanxi Provincial Hospital of Traditional Chinese medicine (Taiyuan, China), and Hangzhou Xixi Hospital (Hangzhou, China). All

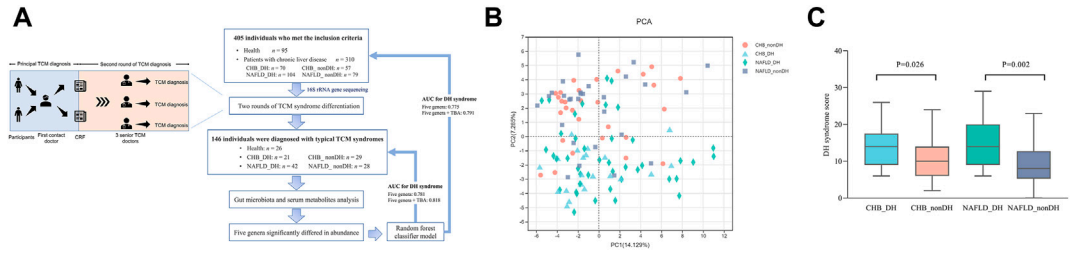

FIGURE 1
Analysis of TCM information for 146 individuals. **(A)** Flowchart of this study; **(B)** PCA analysis based on TCM diagnostic parameters; **(C)** DH syndrome score comparison.

participants were required to provide fresh stool and serum samples and basic information, be tested for disease-related laboratory indices and fill out TCM syndrome and diet questionnaires. The present study was conducted following the Declaration of Helsinki and was approved by the institutional review board (IRB) of Shuguang Hospital (No. 2019-662-17-01).

CHB was diagnosed based on the criteria of "Chinese guidelines on prevention and treatment of chronic hepatitis B" (2015 version) (GuiQiang, 2015). NAFLD was diagnosed according to the "Chinese guidelines on diagnosis and treatment of non-alcoholic fatty liver disease" (2010 version) (Fan Jiangao, 2010). Briefly, CHB diagnosis comprised a thorough examination and routine laboratory tests including liver function, hepatitis B virus (HBV) replication markers, and abdominal ultrasound. NAFLD diagnosis required confirmation of significant hepatic steatosis by imaging or histology and the absence of any secondary causes of hepatic steatosis.

Eligible patients with chronic liver diseases included those who were diagnosed with CHB or NAFLD, were 18–65 years of age, and signed an informed consent form. Those who were diagnosed with other chronic liver diseases such as other viral hepatitis, alcoholic fatty liver disease, cirrhosis, liver cancer, and NAFLD co-infected with HBV were excluded. Those with serious primary disease or malignant tumor, who had undergone gastrointestinal bariatric surgery or taken weight loss drugs within the past 3 months, who had taken antibiotics or proton pump inhibitors within the past month, or were pregnant or lactating were also excluded. Healthy controls were defined as individuals with normal routine laboratory tests, no diagnosis of chronic liver disease, and no abnormal TCM symptoms.

TCM syndrome diagnosis

TCM syndrome was diagnosed by "Guidelines for clinical research on new drugs of traditional Chinese medicine" (Xiaoyu, 2002). We performed two independent rounds of syndrome pattern identification to ensure the quality. As seen in Figure 1A, the first contact doctor received the participant, collected the participant's TCM symptom information, took tongue images, recorded in the case report form (CRF), and gave the principal TCM diagnosis in the CRF based on the information obtained at the consultation. The second round of diagnosis was conducted by three senior doctors practicing TCM for over 30 years independently according to the TCM symptom information recorded in the CRF.

The CRF contained 55 items of conventional TCM symptoms derived from the four diagnostic methods. Most symptom is divided into grades of none, mild, general, severe, and intolerable according to the frequency or degree. Each pulse item was recorded as present or absent. The TCM syndrome score of DH syndrome is based on the combination and degree of DH symptom-related positive items by the "Guidelines for clinical research on new drugs of traditional Chinese medicine" (Xiaoyu, 2002). For the different degrees of each item (none, mild, general, severe, and intolerable), the main symptoms were assigned a score of 0, 2, 4, 6, and eight; corresponding to secondary symptoms of 0, 1, 2, 3, 4, respectively.

Diet history questionnaire

Since diet has a considerable effect on intestinal microecology, we required all participants to fill out a dietary questionnaire, which accounts for the consumption of any seafood, tea, or wine during the day before stool collection. We also inquired about the forms, regularity, and colors of stool in the questionnaire.

Stool sample collection, fecal 16S rRNA sequencing and data processing

Before fecal sample collection, volunteers were required to avoid the consumption of drugs, seafood, strong tea, alcohol, and any other foods that significantly influence gut microbiota.

Researchers distributed the stool collection kits before enrollment and informed the subjects of the sampling process and precautions. Subjects collected fecal samples between 20: 00 on the night before enrollment and the morning of enrollment. The samples were placed in transport boxes with ice packs. Upon receipt, the samples were immediately frozen at −80°C.

The following steps were performed at Majorbio Bio-Pharm Technology Co. Ltd. (Shanghai, China). Total microbial community DNA was extracted according to the instructions of an E.Z.N.A.® Soil DNA kit (Omega Bio-tek, Norcross, GA, United States). DNA extract quality was determined using 1% agarose gel electrophoresis. DNA concentration and purity were determined with a NanoDrop2000 spectrophotometer (Thermo Fisher Scientific, Waltham, MA, United States). PCR amplification of the V3-V4 region of the 16S rRNA gene was performed using the primers 338F (5′-ACTCCTACGGGAGGC AGCAG-3′) and 806R (5′-GGACTACHVGGGTTWTCTAAT-3′). The PCR products from the same sample were pooled, recovered with 2% agarose gel, purified with an AxyPrep DNA Gel Extraction Kit (Axygen Biosciences, Union City, CA, United States), and detected using 2% agarose gel electrophoresis. The recovered product was detected and quantified with a Quantus™ fluorometer (Promega, Madison, WI, United States). The libraries were constructed with a NEXTFLEX® Rapid DNA-Seq kit (PerkinElmer, Waltham, MA, and United States). Sequencing was performed on the Illumina MiSeq platform (Shanghai Majorbio Bio-Pharm, Shanghai, and China). Fastp (https://github.com/OpenGene/fastp) was used for quality control of the original sequence and FLASH (http://ccb.jhu.edu/software/FLASH/) was used for splicing. Uparse v. 7.0.1090 (http://drive5.com/uparse/) was used to cluster the sequences by operational taxonomic unit (OTU) and according to a 97% similarity threshold. Chimeras were eliminated.

Data processing was performed at Majorbio Bio-Pharm Technology Co. Ltd. (Shanghai and China; https://cloud.majorbio.com). Based on the Silva 16S rRNA database (v. 138; https://www.arb-silva.de), the RDP classifier Bayesian algorithm (https://sourceforge.net/projects/rdp-classifier/) was used to annotate the representative OTU sequences with 97% similarity. A confidence threshold of 0.7 was set to obtain the species taxonomy annotation results. The alpha diversity index of the intestinal microbiota was analyzed using mothur (v. 1.30.2; https://mothur.org/wiki/calculators/) (Schloss et al., 2009). Principal co-ordinate analysis (PCoA) and partial least squares discriminant analysis (PLS_DA) were used to compare OTU-level gut microbiota compositions. Significantly altered bacteria and metabolites were identified by Wilcoxon's rank-sum test at a significance level of $p < 0.05$. Biomarker's taxa were identified with Linear discriminant analysis (LDA) effect size (LEfSe) using the Majorbio online platform (Shanghai and China; https://cloud.majorbio.com). PICRUST2 (https://github.com/picrust/picrust2) was used for functional predictions. Multivariate association analysis was performed using the MaAsLin2 R package to identify specific taxa associated with the host phenotype without the influence of other metadata. We adjusted for age, sex, and BMI as fixed variables. $p < 0.05$ were considered significant. We built Gaussian mixture models using MATLAB (v. 9.0.0) (The MathWorks Inc., Natick, MA, and United States). To evaluate the potential diagnostic ability of DH-associated bacterial genera for DH syndrome, we constructed random forest models and yielded receiver operating characteristic (ROC) curves using Weka (v. 3.8.6) (Machine Learning Group, University of Waikato, Hamilton, and NZ). Raw data were uploaded to the National Center for Biotechnology Information (NCBI) under Sequence Read Archive (SRA) No. SRP361117 (https://www.ncbi.nlm.nih.gov/sra/?term=PRJNA809132).

Serum metabolite analysis

Metabolomics analysis was performed using a Q300 Kit (Metabo-Profile, Shanghai, and China). All target metabolites were quantitatively analyzed using ultraperformance liquid chromatography coupled to tandem mass spectrometry (UPLC/MS) (ACQUITY UPLC-Xevo TQ-S, Waters Corp., Milford, MA, United States, and Metabo-Profile Biotechnology (Shanghai) Co. Ltd). Blood samples were collected from the peripheral veins after the volunteers fasted for 8 h. The blood was centrifuged at 3,500 × *g* and 4°C for 15 min and the supernatant was collected and immediately stored at −80°C. The samples were thawed on an ice bath to minimize degradation. Serum (20 μl) was added to each well of a 96-well plate. The plate was transferred to an Eppendorf epMotion Workstation (Eppendorf GmbH, Hamburg, and Germany). Then, 120 μl ice-cold methanol including partial internal standards was automatically added to each sample and the mixtures were vortexed for 5 min. The plate was centrifuged (Allegra X15R, Beckman Coulter, Inc., Indianapolis, IN, and United States) at 4,000 × *g* for 30 min and returned to the workstation. Then 30-μl supernatant was transferred to a clean 96-well plate and 20 μl of freshly prepared derivatizing reagent mixture was added to each well. The plate was sealed and derivatized at 30°C for 60 min. Then 330 μl ice-cold 50% (v/v) methanol solution was added to each well. The plate was then stored at −20°C for 20 min and centrifuged at 4,000 × *g* and 4°C for 30 min. Then 135 μl of supernatant was transferred to each well of a fresh 96-well plate. Each well contained 10 μl of internal standards. Serial dilutions of the derivatized stock standards were added to the left-side wells. Raw data files generated by UPLC-MS/MS were processed using MassLynx v.4.1 (Waters Corp.) for peak integration, calibration, and quantitation of each metabolite. The plate was then sealed for the LC-MS analysis. All targeted metabolite standards were obtained from Sigma-Aldrich (St. Louis, MO, and United States), Steraloids Inc. (Newport, RI, United States), and TRC Chemicals (Toronto, ON, Canada).

TABLE 1 The basic information of participants.

Characteristic	H (n = 26)	CHB_DH (n = 21)	CHB_nonDH (n = 29)	Statistical value	p-value*	NAFLD_DH (n = 42)	NAFLD_nonDH (n = 28)	Statistical value	p-value#
Gender (Male/Female)	10/16	16/5	17/12	0.851[a]	0.196	30/12	17/11	0.711[a]	0.350
Age (years)	29.69 ± 5.01	41.04 ± 12.63	38.34 ± 9.81	1.676[b]	0.399	44.61 ± 12.78	42.46 ± 11.83	0.874[b]	0.479
BMI (kg/m^2)	21.65 ± 1.74	22.32 (5.16)	21.14 (5.53)	−1.032[c]	0.302	27.42 (4.20)	26.25 ± 2.94	−1.547[c]	0.121
TBiL (μmol/L)	15.17 ± 5.41	14.50 (10.55)	12.60 (8.90)	−0.748[c]	0.188	12.70 (7.38)	13.33 (3.28)	1.041[a]	0.701
DBiL (μmol/L)	3.4 (2.38)	4.95 (4.18)	4.30 (2.75)	−0.248[a]	0.107	3.25 (1.65)	2.94 (1.03)	0.414[a]	0.388
ALT (U/L)	12.1 (9.38)	28.80 (148.35)	19.80 (13.65)	0.548[a]	0.014	30.15 (39.83)	28.80 (25.94)	−1.273[a]	0.976
AST (U/L)	17 (7.5)	28.80 (53.75)	22.70 (10.50)	−1.317[c]	0.007	24.55 (14.55)	25.45 (14.33)	−0.384[c]	0.824
GGT (U/L)	15.3 (9.21)	28.80 (71.24)	17.37 (10.69)	−1.612[c]	0.017	33.54 (27.14)	34.41 (25.54)	−0.864[c]	0.769
ALP (U/L)	65.48 ± 19.04	105 (45.35)	83.27 ± 21.35	−2.447[c]	0.026	85.27 ± 21.97	86.68 ± 12.37	−0.030[c]	0.733
ALB (g/L)	44.91 ± 2.86	42.04 ± 4.22	45.38 ± 3.69	−2.713[c]	0.005	44.79 ± 3.63	45.52 ± 2.33	−0.222[c]	0.315
TBA (μmol/L)	1.30 (0.99)	3.20 (6.65)	1.0 (1.15)	−2.389[c]	0.001	1.60 (1.23)	0.80 (1.16)	−0.294[c]	0.006
FBG (mmol/L)	4.78 ± 0.33	4.55 ± 0.79	4.81 ± 0.42	−2.231[c]	0.176	4.97 (1.53)	5.28 (1.02)	−0.342[a]	0.557
HDL (mmol/L)	1.36 ± 0.24	1.19 ± 0.25	1.31 ± 0.34	−2.971[a]	0.193	1.00 (0.31)	1.05 ± 0.22	−1.013[a]	0.746
LDL (mmol/L)	2.64 ± 0.57	2.52 ± 0.47	2.65 ± 0.65	−3.474[c]	0.435	3.10 ± 0.75	3.29 ± 0.64	−2.754[c]	0.291
TC (mmol/L)	4.52 ± 0.69	4.37 ± 0.69	4.33 ± 0.91	−1.387[a]	0.896	4.92 ± 0.90	5.18 ± 0.87	−0.588[c]	0.233
TG (mmol/L)	0.82 (0.52)	1.09 (0.50)	0.91 (0.66)	−1.321[a]	0.157	2.12 (1.57)	1.64 (1.56)	−0.324[c]	0.479
LSM score (kPa)	5.13 (1.15)	7.85 (2.23)	5.50 (1.55)	−0.787[a]	0.004	5.99 ± 1.73	5.60 (2.43)	−1.063[a]	0.353
CAP score (db/m)	224.0 (16.75)	217.36 (8.23)	210.21 ± 33.00	0.132[a]	0.192	301.21 ± 35.60	295.00 (31.75)	−1.202[a]	0.359

*p-value denotes differences between CHB_DH, and CHB_nonDH.

#p-value denotes differences between NAFLD_DH, and NAFLD_nonDH.

[a]Student's t test.

[b]Chi-square χ^2 test.

[c]Mann-Whitney U test. Abbreviations: TBiL, total bilirubin; DBiL, direct bilirubin; ALT, alanine aminotransferase; AST, aspartate aminotransferase; GGT, gamma-glutamyl transferase; ALP, alkaline phosphatase; ALB, albumin; TBA, total bile acid; FBG, fasting blood glucose; TC, total cholesterol; TG, triglycerides; HDL-C, high-density lipoprotein cholesterol; LDL-C, low-density lipoprotein cholesterol; LSM, hepatic fibrosis index-liver stiffness measurement; CAP, hepatic steatosis index-controlled attenuation parameter.

10.3389/fphar.2022.1027628

The data were analyzed with iMAP v. 1.0 (Metabo-Profile). Partial least-squares discriminant analysis (PLS_DA) was established to visualize differences in metabolite profiles. Metabolite enrichment analysis was performed on Metaboanalyst v. 5.0 (https://www.metaboanalyst.ca/). |Fold change (FC)| > 1.2 and p values in Wilcoxon's rank-sum test were used to estimate the significance of each metabolite.

Statistics

Clinical data was expressed as means ± standard deviation, median (interquartile range), or number (%) depending on the distribution. Student's *t*-test, Mann-Whitney *U* test, or Chi-square test was used to analyze significant differences between groups using SPSS (v. 26.0) (IBM Corp., Armonk, NY, and United States). A p-value less than 0.05 was considered statistically significant. The Spearman's rank or Pearson's correlation test was used for correlation analysis using Origin (v.9.8.0.200) (OriginLab, Northampton, MA, and United States). Images were plotted using GraphPad Prism (v. 9.0.0) (GraphPad Software, La Jolla, CA, and United States) or R (v. 4.2.0) (R Core team, Vienna, and Austria).

Results

Serum total bile acid expression increased in CHB and NAFLD patients with DH syndrome

The present study included 405 volunteers (95 healthy controls, and 310 patients with chronic liver disease). After two rounds of syndrome differentiation, 146 participants were diagnosed consistently with typical TCM syndrome. Among them, 26 were healthy volunteers (H group) and 120 were patients diagnosed with CHB (41.7%) and NAFLD (58.3%). We combined the other syndromes commonly observed in chronic liver diseases, such as spleen deficiency, liver-kidney Yin deficiency, and blood stasis syndromes, into the non_DH syndrome group. We diagnosed 21 CHB and 42 NAFLD volunteers with typical DH syndrome (CHB_DH and NAFLD_DH, respectively); and 29 CHB and 28 NAFLD patients without DH syndrome were identified as the non_DH syndrome groups (CHB_nonDH and NAFLD_nonDH, respectively) (Figure 1A).

There was no significant difference between patients with and without DH syndrome in terms of their basic information ($p > 0.05$; Table 1). A principal component analysis (PCA) based on TCM symptom data showed patients with chronic liver diseases with DH syndrome had a separation trend from the non_DH groups (Figure 1B). The DH syndrome scores based on TCM symptoms also differed significantly between patients with and without DH syndrome ($p < 0.05$; Figure 1C). Compared with the CHB_nonDH group, the patients with CHB DH syndrome exhibited elevated serum aspartate aminotransferase (AST), alkaline phosphatase (ALP), TBA, and FibroScan liver stiffness measurement (LSM) scores but decreased serum albumin (ALB) ($p < 0.05$). The trends for these clinical markers in NAFLD-DH patients were consistent, especially the serum TBA exhibited a consistent statistical difference between patients with and without DH syndrome ($p < 0.05$) (Table 1).

Patients with DH syndrome are accompanied by significant alterations in the gut microbial community

There were no differences in seafood, tea, wine consumption between groups (Supplementary Table S1). A total of 19,601,356 high-quality sequences (48,398.4 ± 9,426.31 reads) and 2,156 operational taxonomic units (OTUs) from 405 samples were obtained. The value of the good's coverage estimator showed that the sequencing depth was enough (Supplementary Figure S1A). Alpha-diversity based on the fecal samples of 146 participants showed that compared with the non_DH syndrome group, the CHB_DH and NAFLD_DH groups had lower gut microbiota abundance and diversity. The Sobs, Ace, and Shannon indices significantly differed between the NAFLD_DH and NAFLD_nonDH groups ($p < 0.05$) (Figures 2A–C). The trends in the whole 405 individuals were the same (Supplementary Figures S1B–D).

An OTU-level PCoA based on the Bray-Curtis dissimilarity index showed that the gut microbiota community compositions significantly differed between the patients in CHB_DH and CHB_nonDH ($p = 0.006$) and between those in NAFLD_DH and NAFLD_nonDH groups ($p = 0.01$) (Figures 2D,E). To clarify the correlation between the gut microbiota and the TCM syndromes, we combined CHB_DH and NAFLD_DH groups into the DH syndrome group and the patients without DH syndrome into the non_DH group. The PLS_DA analysis based on the gut microbiota OTUs disclosed that the DH syndrome and non_DH syndrome groups separated in the first component (COMP1) (Figure 2F). The PLS_DA analysis based on the TCM symptoms also revealed a separation trend between the DH syndrome and non_DH syndrome groups in COMP1 (Figures 2F,G). We built finite Gaussian mixture models to fit the COMP1 parameters in Figures 2F,G, respectively. They conformed to two normal distributions corresponding to the TCM syndrome groupings (Figures 2H,I). Both COMP1 parameters were significantly correlated ($p < 0.001$) (Figure 2J).

Aberrant bile acid metabolism in patients with DH syndrome based on microbial and serum metabolite functional analysis

The clinical analysis demonstrated that the TBA concentration of patients in the CHB_DH group was

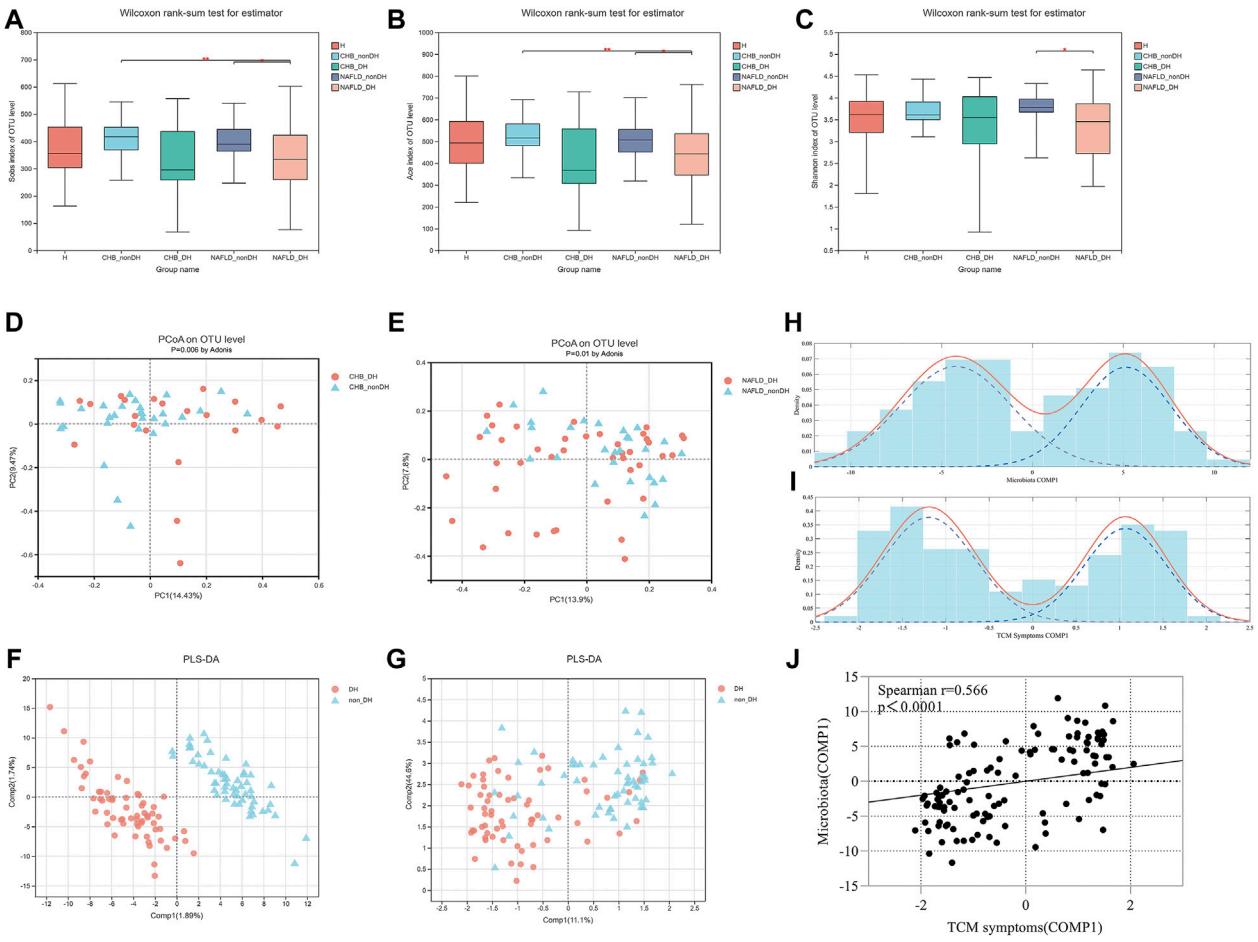

FIGURE 2
Comparison of α diversity and β diversity of gut microbial communities in patients with and without DH syndrome. **(A)** Sobs index; **(B)** Ace index; **(C)** Shannon index; PCoA with Bray-Curtis distance at OTU level based on **(D)** CHB_DH and CHB_nonDH individuals and **(E)** NAFLD_DH and NAFLD_nonDH individuals; **(F)** Score plot of PLS_DA analysis based on gut microbiota OTUs in patients with and without DH syndrome (the R^2Y and Q^2 values for the model were 0.988 and 0.469, respectively); **(G)** Score plot of PLS_DA analysis based on TCM symptoms in patients with and without DH syndrome (the R^2Y and Q^2 values for the model were 0.448 and 0.275, respectively); Finite Gaussian mixture models of parameters of **(H)** COMP1 in Figures 2F, **(I)** COMP1 in Figure 2G; **(J)** Spearman's correlation analysis of both COMP1 parameters.

significantly higher than those in the CHB_nonDH group, and the trend for the patients with NAFLD was consistent (Table 1). To investigate the underlying biological functions commonly associated with DH syndrome in patients with CHB and NAFLD, we performed functional analyses based on the microbiota and metabolites co-altered in DH syndrome (CHB_DH *vs.* CHB_nonDH and NAFLD_DH *vs.* NAFLD_nonDH, respectively).

There were 870 OTUs with the same expression trends for DH syndrome and non_DH syndrome. We used PICRUST2 to predict the biological functions of the foregoing 870 OTUs. Eight pathways were enriched at level-3 KOs with the same variation trend. Compared with the non_DH syndrome groups, flagellar assembly, cancer microRNAs, and autophagy-yeast were decreased in the DH syndrome groups. However, ether lipid metabolism, plant hormone signal transduction, bile secretion, gastric cancer, and retrograde endocannabinoid signaling were predicted increased in the DH syndrome groups ($p < 0.05$) (Figure 3A, Supplementary Table S2).

We also quantified 300 serum metabolites and detected 197 of them. A multivariate control chart of the samples indicated good QC (Supplementary Figure S2A). The most detected metabolites were carbohydrates, organic acids, amino acids, and fatty acids (Supplementary Figure S2B). We used the criterion |Fold change (FC)| > 1.2 to explore the metabolites with the same expression trends between CHB_DH and CHB_nonDH and between NAFLD_DH and NAFLD_nonDH groups. We screened out 21 metabolites. The DH syndrome volunteers had lower serum fatty acids and carnitines and higher serum BAs (glycochenodeoxycholic acid, iso-ursodeoxycholic

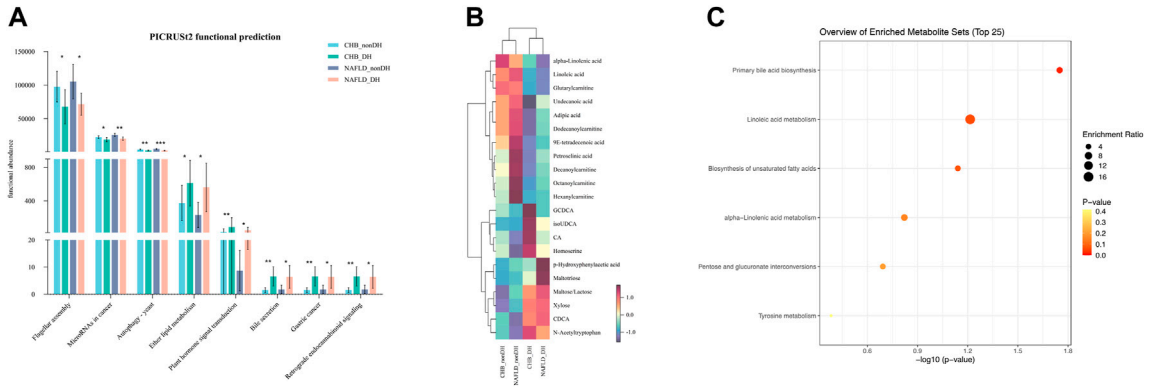

FIGURE 3
Patients with DH syndrome are associated with aberrant BA metabolism. **(A)** Functional pathways with the same trend predicted based on 870 OTUs, $*p < 0.05$, $**p < 0.01$, $***p < 0.001$; **(B)** heatmap of 21 metabolites with the same expression trends in DH syndrome groups; **(C)** functional enrichment analysis based on the 21 metabolites.

acid, chenodeoxycholic acid, and cholic acid) and carbohydrates trends than that of patients with the non_DH syndrome (Figure 3B). All 21 metabolites only enriched in the primary BA biosynthesis pathway ($p < 0.05$; Figure 3C).

Five genera significantly decreased in abundance in patients with DH syndrome

We then analyzed the compositional differences between the DH syndrome and non_DH syndrome groups at various taxonomic levels. There was no phylum-level compositional difference between the DH and non_DH syndrome groups in patients with CHB or NAFLD (Figure 4A). At the genus level, a total of 30 genera statistically differed between the CHB_DH and CHB_nonDH, and 16 genera differed between the NAFLD_DH and NAFLD_nonDH groups ($p < 0.05$) (Figures 4B,C). Of these, six genera overlapped and had the same trend. We adopted LEfSe to explore the variation of taxonomy in classification. These six genera also significantly differed between CHB and NAFLD patients with and without DH syndrome ($p < 0.05$, LDA score >2.0) (Figures 4D,E).

Compared with the non_DH syndrome group, the relative abundances of the *Agathobacter, Dorea, Lachnospiraceae_NC2004_group, Subdoligranulum,* and *unclassified_c__Clostridia* communities were decreased, while the relative abundance of *Ruminococcus_gnavus_group* was increased in the patients with DH syndrome adjusted for age, sex, and BMI ($p < 0.05$) (Figure 5A). We further analyzed the relative expression of the six genera across all 310 patients with CHB or NAFLD. Except for *Ruminococcus_gnavus_group,* the other five genera showed a consistent statistical difference between DH syndrome and non_DH syndrome groups (Figure 5B). We consider these five genera as DH syndrome-related stool genera. Integrative correlation analysis of the five DH-related genera, serum metabolites, and clinical indicators revealed that the serum TBA concentrations negatively correlated with the abundances of the DH-related genera, four of these genera had statistical significance (*unclassified_c__Clostridia, Subdoligranulum, Agathobacter,* and *Lachnospiraceae_NC2004_group* genera) (Figure 5C). This result indicates patients with DH syndrome lack genera that are negatively correlated with serum TBA concentrations. However, TBA concentrations were significantly positively correlated with the circulating cholic acid (CA) and glycochenodeoxycholic acid (GCDCA) levels. Especially GCDCA was strongly positively correlated with several clinical indices reflecting liver damage (Figure 5D).

Five genera have diagnostic potential for patients with DH syndrome

We constructed a random forest model to identify the potential utility of these five genera for indicating of DH syndrome according to the relative expression of the five genera in the 146 patients with typical TCM syndromes (Figure 1A, train set). Based on tenfold cross-validation, the model precision for the DH syndrome group was 71%, and the area under the ROC curve (AUC) was 0.781. We then adopted the classifier model to predict DH syndrome in a test set based on all patients with CHB or NAFLD. The classifier precision for DH syndrome was 78.5% with an AUC of 0.775 (Figure 5E, Supplementary Table S3).

In addition, considering the serum TBA levels differed between patients with and without DH syndrome, we also constructed a random forest model combing these five genera with TBA. The addition of TBA to these DH-related stool genera

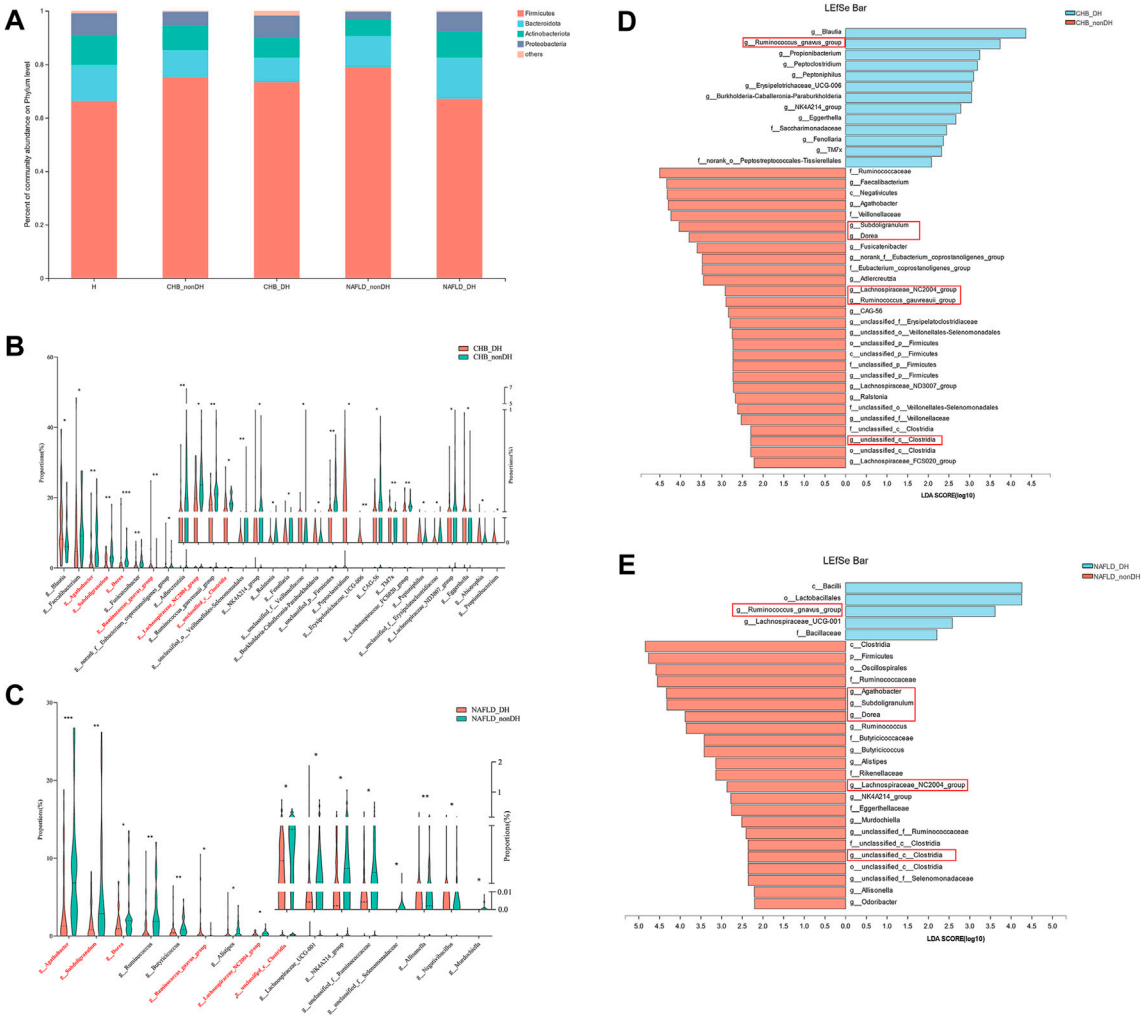

FIGURE 4
Comparison of the gut microbiome in patients with and without DH syndrome. **(A)** Phylum-level gut microbial composition; **(B)** the relative abundance of 30 different bacterial genera between CHB_DH and CHB_nonDH patients; **(C)** the relative abundance of 16 different bacterial genera between NAFLD_DH and NAFLD_nonDH patients; LEfSe analysis between **(D)** CHB_DH and CHB_nonDH groups; **(E)** NAFLD_DH and NAFLD_nonDH groups.

enhanced the diagnostic power with an improved model precision of 79.7% and 78.5% in the internal tenfold cross-validation and the expanded validation, respectively. The related AUC for typical DH syndrome was 0.818, The cut-off value of the model was 0.535, and its true positive rate (TPR) was 0.746. The AUC for DH syndrome in the test set was 0.791 (Figure 5F, Supplementary Table S3).

Discussion

TCM syndrome is the cornerstone of clinical TCM practice. However, this theory lacks an interpretation from the current biomedical perspective. The present study investigated the characteristics of the gut microbiota and serum metabolites of patients presenting with CHB or NAFLD as well as DH syndrome. We found significant alterations in the microbial community in TCM DH syndrome subjects with different chronic liver diseases such as CHB and NAFLD. DH syndrome is characterized by common alterations in gut microbiota and serum metabolites associated with aberrant bile acid metabolism. Furthermore, we verified five genera as candidate biomarkers for indicating DH syndrome in patients with CHB or NAFLD.

TCM theory believes DH syndrome is clinically common and caused by dysfunction of the spleen and stomach in TCM viscera. Patients with DH syndrome often present with gastrointestinal symptoms such as a bitter taste in the

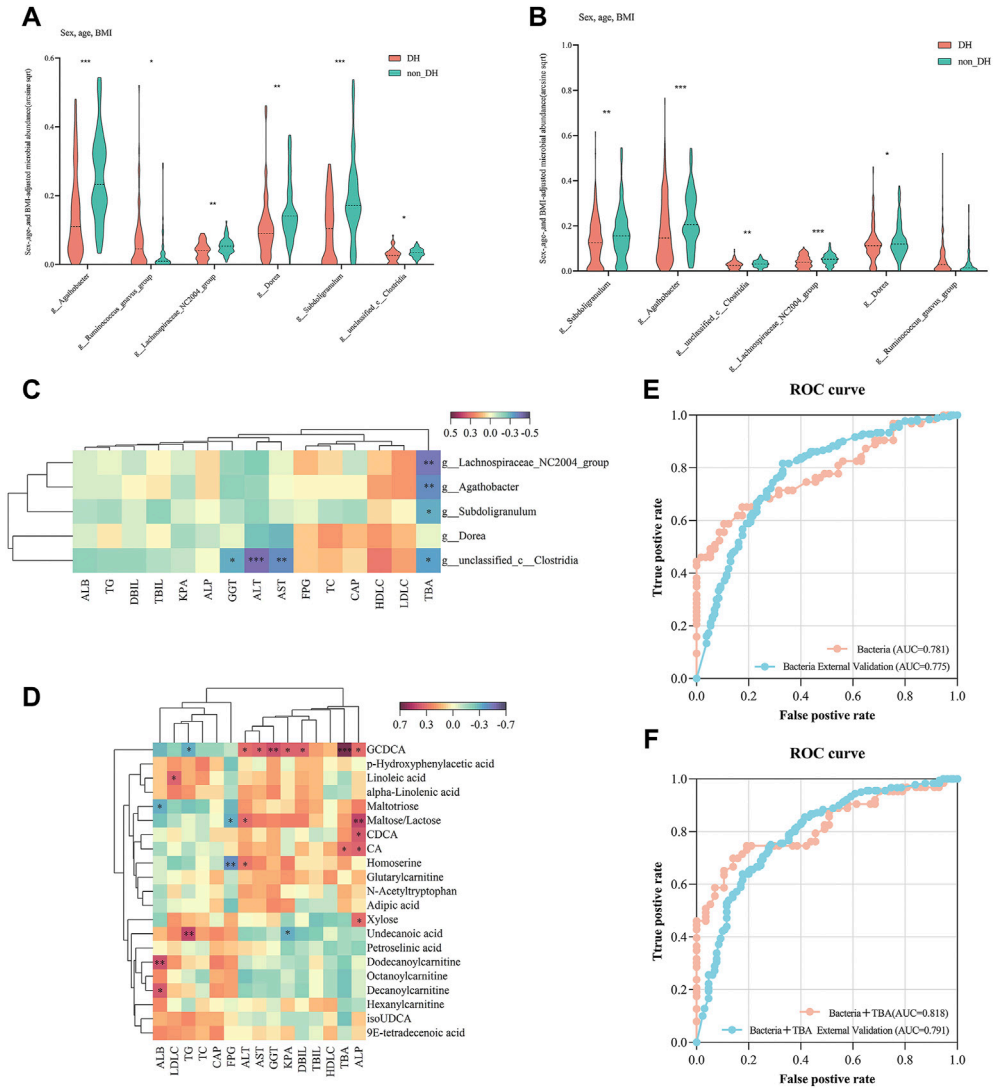

FIGURE 5
Five genera have diagnostic potential for DH syndrome. Relative expression of six bacterial genera in **(A)** 146 individuals with and without typical DH syndrome and **(B)** all chronic liver disease individuals with and without DH syndrome adjusted for age, sex, and BMI; **(C)** Correlation analysis of DH syndrome-associated gut genera and clinical indices; **(D)** correlation analysis of DH syndrome co-altered trends metabolites and clinical indices; ROC curves were plotted for the diagnosis of DH syndrome in 10-fold cross-validation and test set validation (310 patients with CHB or NAFLD) using the combination of **(E)** five genera, and **(F)** five genera combined with serum TBA. The areas under the ROC curves (AUCs) were calculated.

mouth, thirst, halitosis, sticky stool, or constipation (Kang et al., 2015; Zhao et al., 2017). Furthermore, the gut-liver axis has been widely recognized in liver disease, and a healthy intestinal microbial community is vital for maintaining gut and liver homeostasis (Albillos et al., 2020). Thus, there may be some common gut microbiota in the various chronic liver diseases associated with DH syndrome. That is, why we investigated the biological characteristics of DH syndrome for its association with the gut microbiome in the present study.

In TCM syndrome diagnosis, the symptoms have subjective somatosensory differences. The conclusive diagnosis may bias by the experience of the TCM physician. A reliable TCM diagnosis is the premise of follow-up research. Therefore, we employed two rounds of TCM syndrome identification and explored DH syndrome-associated alterations based on the typical participants with consistent TCM diagnosis. The DH syndrome score differed significantly between patients with and without DH syndrome, which indicates the reliability of TCM syndrome diagnosis in the study. We observed significant

differences in the changes of gut microbiota according to TCM diagnosis between DH and non_DH syndrome subjects. To further explore the correlation between gut microbiota alteration and DH syndrome, we fitted Gaussian mixture models to the first component of bacterial PLS_DA analysis (Figure 2F; COMP1) and TCM symptomatic PLS_DA analysis (Figure 2G; COMP1), respectively. Both models yielded two normal distributions corresponding to the TCM syndrome groupings. This approach indicates a significant positive correlation between TCM symptoms and intestinal microbiota related to DH syndrome grouping with objective data.

Syndrome diagnosis in TCM and disease diagnosis in Western medicine overlap and complement each other. TCM theory believes that various diseases with the same syndrome may coexist ("Yi Bing Tong Zheng"). Patients with CHB and NAFLD may develop DH syndrome regardless of the difference in pathogenesis between these conditions. Therefore, we sought the intersection of variations with similar trends between the DH and non_DH syndromes in patients with CHB and NAFLD. We found that patients with DH syndrome had relatively higher trends of liver function indices and significantly higher circulating TBA, which was consistent with our previous study. We have retrospectively analyzed the relationships between clinical indices and TCM syndromes in 999 patients with CHB. Patients with CHB and DH syndrome may present with more severe and persistent liver damage than patients without DH syndrome (Liu et al., 2020). Dysregulation of BA metabolism is common in liver disease. Increases in TBA pools are widely observed in metabolic and viral liver diseases and are associated with disease progression (Chavez-Talavera et al., 2017; Sang et al., 2021). BA accumulation in the hepatocytes mediates hepatotoxicity. In this study, patients with DH syndrome presented with elevated trend serum CDCA and GCDCA levels. Treatment of hepatocytes with CDCA upregulates the expression of proinflammatory genes and promotes hepatic inflammation (Allen et al., 2011). GCDCA is synthesized by conjugating CDCA with glycine and induces hepatocyte apoptosis (Vrenken et al., 2008; Cai et al., 2017).

We also found that 870 microbial OTUs and 21 serum metabolites had the same variation trends in both the CHB and NAFLD DH syndrome groups, and the related functional analysis predicted consistent dysregulation of bile acid metabolism. Dysregulation of BA metabolism in patients with DH syndrome aligns with TCM theory. DH syndrome is particularly prominent in TCM jaundice disease. Yin-Chen-Hao decoction is a classical TCM formula for the treatment of DH syndrome. It has been administered in China for ca. 2,000 years and is renowned for its efficacy in regulating bile acid metabolism and treating cholestasis (Cai et al., 2018; Shi et al., 2021). BAs are important bioactive mediators of gut-liver crosstalk (Schneider et al., 2018; Giuliani, 2019; Farooqui et al., 2022), the integrative correlation analysis disclosed that patients with DH syndrome had consistently low abundances of TBA-negative bacterial genera. BAs are directly enzymatically modified by gut bacteria. However, the mechanism associated with gut microbiota and BA metabolism in patients with DH syndrome lacks report and requires further clarification.

In recent years, systematic biology methods have been applied to explore the diagnostic markers of TCM syndromes (Wang and Chen, 2013). For example, an integrated metabonomic and proteomic study on the diagnosis of kidney-yin deficiency syndrome (Jiang et al., 2015). The implementation of metabolomics technology in a large-scale, multi-center urine biomarker identification study on different TCM syndromes (Zhou et al., 2019). Stool microbial profiles have immense potential as diagnostic or prognostic biomarkers for TCM syndromes as the properties of non-invasive and obtainable. A recent study validated two genera in the diagnosis in patients of lung adenocarcinoma-related Qi-Yin deficiency syndrome. However, TCM diagnosis based on gut microbiota is limited and not reported in liver diseases. In this study, we found five significant genera with the same trend in DH and non_DH syndrome groups. *Subdoligranulum, unclassified_c__Clostridia, Agathobacter,* and *Dorea* are implicated in short-chain fatty acid (SCFA) biosynthesis (Jiao et al., 2018; Che et al., 2019; Liu et al., 2019; Lloyd-Price et al., 2019), SCFAs maintain intestinal barrier function and are anti-inflammatory (Maslowski et al., 2009; Macia et al., 2015). A decrease in the relative abundance of *Subdoligranulum* positively correlated with intestinal inflammation (Kim et al., 2021). Hence, patients with DH syndrome are prone to this condition. We explored and verified the diagnostic potential of these five genera for DH syndrome. The AUC of the random forest-based classifier for DH syndrome was 0.781 and 0.775 in the 10-fold cross-validation and test set validation, respectively. To improve the diagnostic efficiency, we combined these five genera with serum TBA, the related diagnostic AUCs for DH syndrome were 0.818 and 0.791, respectively. Therefore, these bacterial genera may be candidates for the diagnosis of TCM DH syndrome. The combination of gut microbiota and serum TBA may be a better diagnostic tool for diagnosing DH syndrome in subjects with chronic liver diseases such as CHB and NAFLD.

We acknowledge several limitations of this study. First, we found increased serum TBA expression and aberrant BA metabolism in individuals with DH syndrome with CHB or NAFLD. However, the causality of DH-associated microbiota, metabolites, and BA metabolism remains unclear. Second, we explored common changes in gut microbiota according to TCM diagnosis in patients with DH syndrome. We validated five genera with diagnostic potential for DH syndrome in patients with chronic liver disease. However, the external test set and training set have overlap (38.7% of the test set). Given the possible overfitting error of the random forest model, future research should replicate this study using a larger sample size of individuals with DH syndrome. Third, the gut microbiota in this study was assessed by 16S rRNA gene sequencing, lacking the quantitative range of these five genera. We

hope to modify the diagnostic model with more accurate values in the future, such as Shotgun metagenomic sequencing data. DH syndrome is not common in healthy individuals. In this study, none of the healthy individuals was diagnosed with typical DH syndrome according to the same criteria in patients with CHB or NAFLD. Therefore, the changes in gut microbiota and serum TBA in healthy volunteers with and without DH syndrome cannot be determined yet. We hope to observe the correlated variation in healthy volunteers in larger sample data in the future.

Conclusion

This study addresses common microbial signatures of TCM DH syndrome in patients with CHB or NAFLD. We explored and validated five DH-specific genera combined with serum TBA as a non-invasive tool for diagnosing DH syndrome in patients with chronic liver disease. The results of this study contribute to the understanding and diagnosis of DH syndrome based on gut microbiota.

Data availability statement

The datasets presented in this study can be found in online repositories. The names of the repository/repositories and accession number(s) can be found below: NCBI BioProject, PRJNA809132.

Ethics statement

The studies involving human participants were reviewed and approved by the institutional review board (IRB) of Shuguang Hospital. The patients/participants provided their written informed consent to participate in this study.

Author contributions

YP and YZ: analysis and writing. JG, NH, YX, BZ, SC, XL, and QL: sample collection. QF: TCM diagnosis. YH and YZ: study design and manuscript revision. All authors contributed to the articles and approved the submitted version.

Funding

This work was supported by the National Natural Science Foundation of China, No. 81830119, 82174249; The Clinical Research Plan of SHCD, No. SHDC2020CR 2049B; The Shanghai Science and Technology Commission, No. 19401970300, and No. 20Y21901700.

Acknowledgments

We thank all subjects and sample collectors who participated in this study for their cooperation and assistance.

Conflict of interest

The authors declare that the research was conducted in the absence of any commercial or financial relationships that could be construed as a potential conflict of interest.

Publisher's note

Supplementary material

The Supplementary Material for this article can be found online at: https://www.frontiersin.org/articles/10.3389/fphar.2022.1027628/full#supplementary-material

References

Albillos, A., de Gottardi, A., and Rescigno, M. (2020). The gut-liver axis in liver disease: Pathophysiological basis for therapy. *J. Hepatol.* 72 (3), 558–577. doi:10.1016/j.jhep.2019.10.003

Allen, K., Jaeschke, H., and Copple, B. L. (2011). Bile acids induce inflammatory genes in hepatocytes: A novel mechanism of inflammation during obstructive cholestasis. *Am. J. Pathol.* 178 (1), 175–186. doi:10.1016/j.ajpath.2010.11.026

Cai, F. F., Wu, R., Song, Y. N., Xiong, A. Z., Chen, X. L., Yang, M. D., et al. (2018). Yinchenhao decoction alleviates liver fibrosis by regulating bile acid metabolism and TGF-β/smad/ERK signalling pathway. *Sci. Rep.* 8 (1), 15367. doi:10.1038/s41598-018-33669-4

Cai, S. Y., Ouyang, X., Chen, Y., Soroka, C. J., Wang, J., Mennone, A., et al. (2017). Bile acids initiate cholestatic liver injury by triggering a hepatocyte-specific inflammatory response. *JCI Insight* 2 (5), e90780. doi:10.1172/jci.insight.90780

Chavez-Talavera, O., Tailleux, A., Lefebvre, P., and Staels, B. (2017). Bile acid control of metabolism and inflammation in obesity, type 2 diabetes, dyslipidemia, and nonalcoholic fatty liver disease. *Gastroenterology* 152 (7), 1679–1694. doi:10.1053/j.gastro.2017.01.055

Che, L., Hu, Q., Wang, R., Zhang, D., Liu, C., Zhang, Y., et al. (2019). Inter-correlated gut microbiota and SCFAs changes upon antibiotics exposure links with rapid body-mass gain in weaned piglet model. *J. Nutr. Biochem.* 74, 108246. doi:10.1016/j.jnutbio.2019.108246

Dai, J., Sun, S., Cao, J., Zhao, Y., Cao, H., Zheng, N., et al. (2013). Similar connotation in chronic Hepatitis B and nonalcoholic Fatty liver patients with dampness-heat syndrome. *Evid. Based. Complement. Altern. Med.* 2013, 793820. doi:10.1155/2013/793820

Fan, Jiangao (2010). Guidelines for diagnosis and treatment of nonalcoholic fatty liver disease (revised in 2010). *Chin. J. liver Dis.* 03, 163–166.

Fan, Y., and Pedersen, O. (2021). Gut microbiota in human metabolic health and disease. *Nat. Rev. Microbiol.* 19 (1), 55–71. doi:10.1038/s41579-020-0433-9

Farooqui, N., Elhence, A., and Shalimar (2022). A current understanding of bile acids in chronic liver disease. *J. Clin. Exp. Hepatol.* 12 (1), 155–173. doi:10.1016/j.jceh.2021.08.017

Giuliani, C. (2019). The flavonoid quercetin induces AP-1 activation in FRTL-5 thyroid cells. *Antioxidants (Basel)* 8 (5), E112. doi:10.3390/antiox8050112

GuiQiang, W. (2015). Guidelines for the prevention and treatment of chronic Hepatitis B_ 2015 Vision. *Chin. J. liver Dis.* 7(03), 1–18. doi:10.3969/j.issn.1674-7380.2015.03.001

Jiang, M., Zhang, C., Zheng, G., Guo, H., Li, L., Yang, J., et al. (2012). Traditional Chinese medicine zheng in the era of evidence-based medicine: A literature analysis. *Evid. Based. Complement. Altern. Med.* 2012, 409568. doi:10.1155/2012/409568

Jiang, N., Liu, H. F., Li, S. D., Zhou, W. X., Zhang, Y. X., Zhang, Q., et al. (2015). An integrated metabonomic and proteomic study on Kidney-Yin Deficiency Syndrome patients with diabetes mellitus in China. *Acta Pharmacol. Sin.* 36 (6), 689–698. doi:10.1038/aps.2014.169

Jiao, N., Baker, S. S., Nugent, C. A., Tsompana, M., Cai, L., Wang, Y., et al. (2018). Gut microbiome may contribute to insulin resistance and systemic inflammation in obese rodents: A meta-analysis. *Physiol. Genomics* 50 (4), 244–254. doi:10.1152/physiolgenomics.00114.2017

Kang, H., Zhao, Y., Li, C., Chen, Y., Tang, K., Yang, L., et al. (2015). Integrating clinical indexes into four-diagnostic information contributes to the Traditional Chinese Medicine (TCM) syndrome diagnosis of chronic Hepatitis B. *Sci. Rep.* 5, 9395. doi:10.1038/srep09395

Kim, E. S., Tarassishin, L., Eisele, C., Barre, A., Nair, N., Rendon, A., et al. (2021). Longitudinal changes in fecal calprotectin levels among pregnant women with and without inflammatory bowel disease and their babies. *Gastroenterology* 160 (4), 1118–1130.e3. e1113. doi:10.1053/j.gastro.2020.11.050

Li, M. Q., Lin, Y., Xiang, L., Piao, S. H., and Guo, J. (2019). Study on the TCM syndrome distribution of non-alcoholic fatty liver disease based on clinical data. *World Chin. Med.* 14 (01), 6–11.CNKI:SUN:SJZA.0.2019-01-002

Liu, Q. H., Zhang, B. B., Xu, L., Shen, X. P., Hai, Y. M., Hu, Y. Y., et al. (2020). Comparative analysis of clinical and medication information between chronic hepatitis B patients with damp heat syndrome and spleen deficiency syndrome. *Evid. Based. Complement. Altern. Med.* 2020, 8846637. doi:10.1155/2020/8846637

Liu, Y., Ajami, N. J., El-Serag, H. B., Hair, C., Graham, D. Y., White, D. L., et al. (2019). Dietary quality and the colonic mucosa-associated gut microbiome in humans. *Am. J. Clin. Nutr.* 110 (3), 701–712. doi:10.1093/ajcn/nqz139

Lloyd-Price, J., Arze, C., Ananthakrishnan, A. N., Schirmer, M., Avila-Pacheco, J., Poon, T. W., et al. (2019). Multi-omics of the gut microbial ecosystem in inflammatory bowel diseases. *Nature* 569 (7758), 655–662. doi:10.1038/s41586-019-1237-9

Loomba, R., Friedman, S. L., and Shulman, G. I. (2021). Mechanisms and disease consequences of nonalcoholic fatty liver disease. *Cell* 184 (10), 2537–2564. doi:10.1016/j.cell.2021.04.015

Macia, L., Tan, J., Vieira, A. T., Leach, K., Stanley, D., Luong, S., et al. (2015). Metabolite-sensing receptors GPR43 and GPR109A facilitate dietary fibre-induced gut homeostasis through regulation of the inflammasome. *Nat. Commun.* 6, 6734. doi:10.1038/ncomms7734

Maslowski, K. M., Vieira, A. T., Ng, A., Kranich, J., Sierro, F., Yu, D., et al. (2009). Regulation of inflammatory responses by gut microbiota and chemoattractant receptor GPR43. *Nature* 461 (7268), 1282–1286. doi:10.1038/nature08530

Sang, C., Wang, X., Zhou, K., Sun, T., Bian, H., Gao, X., et al. (2021). Bile acid profiles are distinct among patients with different etiologies of chronic liver disease. *J. Proteome Res.* 20 (5), 2340–2351. doi:10.1021/acs.jproteome.0c00852

Schloss, P. D., Westcott, S. L., Ryabin, T., Hall, J. R., Hartmann, M., Hollister, E. B., et al. (2009). Introducing mothur: Open-source, platform-independent, community-supported software for describing and comparing microbial communities. *Appl. Environ. Microbiol.* 75 (23), 7537–7541. doi:10.1128/AEM.01541-09

Schneider, K. M., Albers, S., and Trautwein, C. (2018). Role of bile acids in the gut-liver axis. *J. Hepatol.* 68 (5), 1083–1085. doi:10.1016/j.jhep.2017.11.025

Seto, W.-K., Lo, Y.-R., Pawlotsky, J.-M., and Yuen, M.-F. (2018). Chronic Hepatitis B virus infection. *Lancet* 392 (10161), 2313–2324. doi:10.1016/s0140-6736(18)31865-8

Shi, K., Wen, J., Zeng, J., Guo, Y., Hu, J., Li, C., et al. (2021). Preclinical evidence of Yinchenhao decoction on cholestasis: A systematic review and meta-analysis of animal studies. *Phytother. Res.* 35 (1), 138–154. doi:10.1002/ptr.6806

Vrenken, T. E., Buist-Homan, M., Kalsbeek, A. J., Faber, K. N., and Moshage, H. (2008). The active metabolite of leflunomide, A77 1726, protects rat hepatocytes against bile acid-induced apoptosis. *J. Hepatol.* 49 (5), 799–809. doi:10.1016/j.jhep.2008.07.019

Wang, F. S., Fan, J. G., Zhang, Z., Gao, B., and Wang, H. Y. (2014). The global burden of liver disease: The major impact of China. *Hepatology* 60 (6), 2099–2108. doi:10.1002/hep.27406

Wang, P., and Chen, Z. (2013). Traditional Chinese medicine ZHENG and omics convergence: A systems approach to post-genomics medicine in a global world. *OMICS* 17 (9), 451–459. doi:10.1089/omi.2012.0057

Wu, J., Wei, Z., Cheng, P., Qian, C., Xu, F., Yang, Y., et al. (2020). Rhein modulates host purine metabolism in intestine through gut microbiota and ameliorates experimental colitis. *Theranostics* 10 (23), 10665–10679. doi:10.7150/thno.43528

Xiaoyu, Z. (2002). *Guiding principles for clinical research of new traditional Chinese medicine*. China Medical Science and Technology Press, Beijing, China, 147–372.

Xu, X., Gao, Z., Yang, F., Yang, Y., Chen, L., Han, L., et al. (2020). Antidiabetic effects of gegen qinlian decoction via the gut microbiota are attributable to its key ingredient berberine. *Genomics Proteomics Bioinforma.* 18 (6), 721–736. doi:10.1016/j.gpb.2019.09.007

Zeng, X. X., Bian, Z. X., Wu, T. X., Fu, S. F., Ziea, E., and Woon, W. T. (2011). Traditional Chinese medicine syndrome distribution in chronic Hepatitis B populations: A systematic review. *Am. J. Chin. Med.* 39 (6), 1061–1074. doi:10.1142/S0192415X11009408

Zhang, L., Wang, G., Hou, W., Li, P., Dulin, A., and Bonkovsky, H. L. (2010). Contemporary clinical research of traditional Chinese medicines for chronic Hepatitis B in China: An analytical review. *Hepatology* 51 (2), 690–698. doi:10.1002/hep.23384

Zhao, Y., Kang, H., Peng, J. H., Xu, L., Cao, Z. W., and Hu, Y. Y. (2017). Key symptoms selection for two major syndromes diagnosis of Chinese medicine in chronic Hepatitis B. *Chin. J. Integr. Med.* 23 (4), 253–260. doi:10.1007/s11655-016-2253-3

Zhou, H., Li, L., Zhao, H., Wang, Y., Du, J., Zhang, P., et al. (2019). A large-scale, multi-center urine biomarkers identification of coronary heart disease in TCM syndrome differentiation. *J. Proteome Res.* 18 (5), 1994–2003. doi:10.1021/acs.jproteome.8b00799

Zhou, J., Zhou, F., Wang, W., Zhang, X. J., Ji, Y. X., Zhang, P., et al. (2020). Epidemiological features of NAFLD from 1999 to 2018 in China. *Hepatology* 71 (5), 1851–1864. doi:10.1002/hep.31150

Zhou, Z., Zhang, J., You, L., Wang, T., Wang, K., Wang, L., et al. (2022). Application of herbs and active ingredients ameliorate non-alcoholic fatty liver disease under the guidance of traditional Chinese medicine. *Front. Endocrinol.* 13, 1000727. doi:10.3389/fendo.2022.1000727

frontiers | Frontiers in Pharmacology

TYPE Original Research
PUBLISHED 17 November 2022
DOI 10.3389/fphar.2022.1032741

OPEN ACCESS

EDITED BY
Yiider Tseng,
Shandong University of Traditional Chinese Medicine, China

REVIEWED BY
Yisheng He,
The Chinese University of Hong Kong, Shenzhen, China
Dong-Sheng Zhao,
Shandong University of Traditional Chinese Medicine, China

*CORRESPONDENCE
Luyong Zhang,
lyzhang@cpu.edu.cn
Zhenzhou Jiang,
beaglejiang@cpu.edu.cn

SPECIALTY SECTION
This article was submitted to Ethnopharmacology, a section of the journal Frontiers in Pharmacology

RECEIVED 31 August 2022
ACCEPTED 07 November 2022
PUBLISHED 17 November 2022

CITATION
Miao Y, Zhang Q, Yuan Z, Wang J, Xu Y, Chai Y, Du M, Yu Q, Zhang L and Jiang Z (2022), Proteomics analysis reveals novel insights into the mechanism of hepatotoxicity induced by *Tripterygium wilfordii* multiglycoside in mice. *Front. Pharmacol.* 13:1032741. doi: 10.3389/fphar.2022.1032741

Proteomics analysis reveals novel insights into the mechanism of hepatotoxicity induced by *Tripterygium wilfordii* multiglycoside in mice

Yingying Miao[1], Qin Zhang[1], Zihang Yuan[1], Jie Wang[1], Yunxia Xu[1], Yuanyuan Chai[1], Min Du[1], Qinwei Yu[1], Luyong Zhang[1,2]* and Zhenzhou Jiang[1,3]*

[1]New Drug Screening Center, Jiangsu Center for Pharmacodynamics Research and Evaluation, State Key Laboratory of Natural Medicines, China Pharmaceutical University, Nanjing, China, [2]Center for Drug Research and Development, Guangdong Pharmaceutical University, Guangzhou, China, [3]Key Laboratory of Drug Quality Control and Pharmacovigilance, Ministry of Education, China Pharmaceutical University, Nanjing, China

Tripterygium wilfordii multiglycoside (GTW), extracted and purified from the peeled roots of *T. wilfordii* Hook.f. (TwHF), is a well-known traditional Chinese medicine and applied to various autoimmune diseases clinically. However, it has been reported to cause severe liver injury. At present, the mechanism underlying GTW-induced hepatotoxicity remain poorly defined. Here, we evaluated the effects of GTW on mouse liver and elucidated the associated mechanisms *via* label-free proteomics combined with bioinformatics analysis. Male C57BL/6J mice were randomly divided into normal group, a low-dose GTW (70 mg/kg) group and a high-dose GTW (140 mg/kg) group. After 1-week administration, GTW dose-dependently induced hepatotoxicity. Further analysis showed that GTW could act on the intestinal immune network for IgA production pathway, which plays an important role in maintaining intestinal homeostasis and influences the crosstalk between gut and liver. Western blots confirmed that GTW could decrease pIgR protein expression in the liver and ileum, and, as a result, the secretion of IgA into gut lumen was reduced. Further validation showed that intestinal barrier integrity was impaired in GTW-treated mice, promoting bacteria transferring to the liver and triggering proinflammatory response. Our study demonstrated that gut-liver axis may play a vital part in the progression of GTW-induced hepatotoxicity, which provides guidance for basic research and clinical application of GTW.

KEYWORDS

***Tripterygium wilfordii* multiglycoside, hepatotoxicity, label-free proteomics, intestinal immune network for IgA production, gut-liver axis**

1 Introduction

Drug-induced hepatotoxicity is one of the major reasons for liver injury, the most serious of which is acute liver failure characterized by severe hepatocyte death (Andrea Iorga, 2017). Herbal drugs, with complex and diverse constituents, are effect triggers of liver injury leading to acute and chronic liver diseases (Stournaras and Tziomalos, 2015). *Tripterygium wilfordii* multiglycoside (GTW) is a well-known Chinese herbal medicine that is extracted and purified from the peeled roots of *T. wilfordii* Hook.f. (TwHF) and mostly used as tablets in clinical. The clinical dosage of GTW tablets is 1–1.5 mg/kg/day for adults (Gong et al., 2020). According to the standard of GTW tablets (WS3–B-33350-98-2011), stipulated by National Medical Products Administration (China), the contents of triptolide and wilforlide A in each GTW tablet (10 mg) shall not exceed and not less than10 μg, respectively (Dai et al., 2022). Because of its anti-inflammatory and immune-suppressive effects, GTW has been widely applied to various autoimmune diseases, for example, systemic lupus erythematosus (Zhou et al., 2018), nephrotic syndrome (Xu and Jiang, 2009) and rheumatoid arthritis (Tao et al., 2001; Marks, 2011). However, the adverse effects of GTW, especially liver injury, restrict its clinical application (Zhang et al., 2016; Liu et al., 2018). Since the liver is responsible for metabolism and detoxification, it is imperative to explore the mechanisms of GTW-induced liver injury for its safe clinical use.

Although studies have reported that GTW could cause liver damage when administered chronically or at very high doses (Zhang et al., 2012; Peng et al., 2021), generally, investigations on GTW-induced hepatotoxicity and associated molecular mechanisms are still few. Therefore, the effects of GTW on liver and the underlying mechanisms require further investigation.

Proteomics currently emerges as a comprehensive and powerful tool for detecting functional proteins and discovering molecular targets, therefore, it is more and more widely used to explore the pharmacological and toxicological mechanisms of herbal medicine (Bennett and Devarajan, 2018; Zhang et al., 2022). Numerous studies on drug-induced liver injury have been reported to identify differentially expressed proteins (DEPs) and explore associated mechanisms *via* label-free proteomics (Satoh et al., 2014; Dragoi et al., 2018). Although a previous study has used proteomics to detect DEPs in the livers of mice administered triptolide (TP), an essential bioactive but toxic component of TwHF (Li et al., 2017), at present, there are almost no investigations on liver proteome changes in GTW-induced hepatotoxic models.

In the present study, we evaluated the effects of GTW on mice livers and elucidated the associated mechanisms *via* label-free proteomics combined with bioinformatics analysis. By analyzing the identified DEPs and enriched functional pathways between the control and GTW groups, we found that GTW could act on the intestinal immune network for IgA production pathway, suggesting an important role of gut-liver axis in mediating GTW-induced hepatotoxicity. To our knowledge, our research was the first indication of the effects of GTW on mice liver proteome, which is expected to provide more insights into the mechanism of GTW-induced hepatotoxicity.

TABLE 1 The instrumental conditions of HPLC.

Catalog	Instrumental conditions
Colum	Agilent Zorbax SB-C18 (4.6 × 100 mm, 3.5 μm)
Mobile phase	Water containing acetonitrile (A)
Flow rate	0.75 ml/min
Elution	0–10 min: 20% A
	10–15 min: from 20% to 30% A
	15–40 min: 30% A
	40–50 min: from 30% to 40% A
	50–60 min: from 40% to 55% A
	60–90 min: from 55% to 85% A
	90–100 min: from 85% to 20% A
	100–110 min: 20% A
Injection volume	10 μl
Analytical wavelength	218 nm

2 Materials and methods

2.1 HPLC analysis of *T. wilfordii* multiglycoside

GTW (>98%, Batch No. 1507702) was obtained from Zhejiang DND Drug Factory (Zhejiang, China). The chemical profile of GTW was determined by HPLC. Standard chemicals including triptolide, triptonide, celastrol, and wilforlide A were purchased from National Institute for Food and Drug Control (Beijing, China), and wilforgine and wilforine were obtained from Chengdu Push Bio-technology Co., Ltd. (Sichuan, China). The conditions of HPLC were listed in Table 1.

2.2 Animals and experimental protocols

Male C57BL/6J mice (6–8 weeks) were supplied by Shanghai SLAC Laboratory Animal Co., Ltd. (Shanghai, China). Mice were housed in conditions with controlled light (12 h light/dark cycle), temperature (24 ± 2°C), and humidity (50%–60%) and had adequate food and tap water. All experiments on mice were performed under the guidelines of Ethical Committee of China Pharmaceutical University (Ethics approval No. 2022-05-003).

GTW in powder was suspended in 0.5% CMC-Na and administered to mice by gavage. Based on the resource equation method (Charan and Kantharia, 2013), one of the methods of sample size calculation in animal studies, 18 male C57BL/6J mice were randomly divided into the control group, GTW-L and GTW-H groups, with 6 mice in each group. The dosage and dosing time of GTW administration were chosen based on our previous studies (Zhang et al., 2012; Miao et al., 2019; Yuan et al., 2019). The doses selected for GTW in animal experiments were 70 mg/kg (GTW-L) and 140 mg/kg (GTW-H), which are approximately 5 times and 10 times mouse equivalent dosage (mouse equivalent dose was 9.1–13.65 mg/kg/day), respectively. After GTW administration for 1 week, mice were sacrificed.

2.3 Biochemical and histopathological examinations

Serum ALT, AST, and ALP detection kits were obtained from Whitman Biotech (Nanjing, China). All examinations were performed in accordance with the protocols.

Fragments from mice tissues were fixed in 4% paraformaldehyde overnight, embedded in paraffin, and then sliced for H&E and immunohistochemistry (IHC) staining to observe the pathological changes.

2.4 Immunofluorescence

Mouse tissue sections were fixed in 4% paraformaldehyde for 15 min, washed in PBS and permeabilized with 0.1% Triton X-100 for 10 min. After blocked with 5% goat serum for 1 h at room temperature, they were incubated with primary antibodies at 4°C overnight. Then, samples were incubated with secondary antibodies and DAPI (1: 1000) at room temperature for 1 h, and further imaged with a confocal laser scanning microscope (Olympus, Lake Success, LY). The following antibodies were used: mouse anti-occludin (1:200, #33-1500, Thermo Fisher), APC anti-mouse F4/80 antibody (1:50, #123115, BioLegend), Alexa Fluor 488-conjugated anti-mouse IgG (1:1000, ab150113, abcam).

2.5 Label-free quantitative proteomics and bioinformatics analysis

Label-free proteomics analysis of liver samples from the control and GTW-H (140 mg/kg) groups was performed with the help of Novogene Co., Ltd. (Beijing, China). The experimental procedures and methods were listed in Supplementary Materials and Methods.

TABLE 2 Primer sequences used for real-time PCR.

Gene		Primer sequence (5′ to 3′)
16S rRNA	Forward	AGAGTTTGATCCTGGCTCAG
	Reverse	TGCTGCCTCCCGTAGGAGT
Tlr2	Forward	ACAGCAAGGTCTTCCTGGTTCC
	Reverse	GCTCCCTTACAGGCTGAGTTCT
Tlr4	Forward	AGCTTCTCCAATTTTTCAGAACTTC
	Reverse	TGAGAGGTGGTGTAAGCCATGC
Tnfα	Forward	GGTGCCTATGTCTCAGCCTCTT
	Reverse	GCCATAGAACTGATGAGAGGGAG
β-actin	Forward	CATTGCTGACAGGATGCAGAAGG
	Reverse	TGCTGGAAGGTGGACAGTGAGG

Gene Ontology (GO) annotation analysis of the identified DEPs was performed using Database for Annotation, Visualization and Integrated Discovery (DAVID) (version 6.8) (Huang et al., 2009). Kyoto Encyclopedia of Genes and Genomes (KEGG) enrichment analysis of the DEPs was performed using KEGG Orthology-Based Annotation System (KOBAS) (version 3.0) (Bu et al., 2021), and the connection between pathways were visualized using Cytoscape with ClueGO and CluePedia applications (Bindea et al., 2009; Mlecnik and Bindea, 2013). p-value less than 0.05 was considered statistically significant.

The Search Tool for the Retrieval of Interacting Genes (STRING) database (http://www.string-db.org/) was used to establish protein-protein interaction (PPI) network of the DEPs (Szklarczyk et al., 2017). After visualization of the network by Cytoscape, the densely connected protein modules in the PPI network was detected using Molecular Complex Detection (MCODE) app with default parameter settings (Bader and Hogue, 2003). Furthermore, bioinformatics analysis for the top cluster, including biological process annotation and KEGG enrichment pathway analysis, was conducted according to the above-mentioned methods.

2.6 Western blot analysis

Mouse tissue samples were homogenized in RIPA buffer (Beyotime, China) supplemented with protease and phosphatase inhibitors (Bimake, China). After protein quantification assayed with a BCA method (Beyotime, China), the lysis was mixed with loading buffer (Bio-Rad, CA, United States) and denatured by heat. Then, protein was separated on SDS–PAGE and subsequently transferred onto PVDF membranes by electroblotting. Next, the membrane was blocked with 5% bovine serum albumin for 1 h at room temperature, followed by incubating with primary antibody at

TABLE 3 FISH probes.

Probe	Fluorochrome	Sequence (5′ to 3′)
EUB338 I	FAM	GCTGCCTCCCGTAGGAGT
EUB338 II	FAM	GCAGCCACCCGTAGGTGT
EUB338 III	FAM	GCTGCCACCCGTAGGTGT
Non-EUB	CY3	ACTCCTACGGGAGGCAGC

4°C overnight. Finally, the membrane was incubated with HRP-conjugated polyclonal secondary antibody at room temperature for 1 h, and further visualized using an ECL detection kit (Tanon, Shanghai, China). The antibodies used in the study are as follows: rabbit anti-β-ACTIN (AC026, ABclonal), rabbit anti-pIgR (A6130, ABclonal), mouse anti-Occludin (#33-1500, Thermo Fisher).

2.7 Real-time quantitative PCR

Mouse tissue samples were homogenized in Trizol reagent for RNA extraction. Approximately 1 μg of RNA was converted to cDNA after quantification with Nanodrop 2000 (Thermo, DE, United States). Target genes were analyzed by real-time PCR (RT-PCR) using SYBR Green on Stepone Plus (Thermo, DE, United States) with specific primers. Primers used were listed on Table 2, and the β-actin gene was used for normalization.

2.8 Enzyme-linked Immunosorbent assay (ELISA)

2.8.1 Detection of IgA in feces and serum

Mouse fecal samples were suspended in PBS containing protease inhibitor, and centrifuged at 12,000 × g for 15 min. After centrifugation, the supernatant was collected and diluted 1/1000 for fecal IgA ELISA. Serum was diluted 1/2000 for IgA ELISA. Mouse IgA ELISA kit was obtained from Neobioscience Technology Co., Ltd. (Shenzhen, China).

2.8.2 Serum TNFα detection

Mouse serum TNFα concentration was measured using commercially available ELISA kits according to the manufacturer's protocols. Mouse TNFα ELISA kit was obtained from Neobioscience Technology Co., Ltd. (Shenzhen, China).

2.9 Fluorescence *in situ* hybridization detection of bacteria in liver

Fluorescence *in situ* hybridization (FISH) analysis was conducted according to the protocol from GenePharma (Shanghai, China). Briefly, liver frozen sections were fixed in 4% paraformaldehyde for 15 min, washed in PBS, and incubated with proteinase K for 15 min. Then, slices were washed and incubated with 5 ng/μl of probes at 37°C for 12–16 h. After incubation, slices were washed in PBS and then stained with DAPI at room temperature for 20 min, and further imaged with a confocal laser scanning microscope (Olympus, Lake Success, LY). A mix of probes was synthesized by GenePharma, as shown in Table 3. The non-Eub probe was used as a negative control.

2.10 Statistical analysis

Data are presented as mean ± SEM. The differences between two groups were analyzed using Student's *t*-test, and the differences among multiple groups were analyzed using one-way analysis of variance (ANOVA). Statistical analysis and graphing were performed using GraphPad Prism 9 software (GraphPad Software, Inc., San Diego, CA, United States). *p*-value less than 0.05 was considered statistically significant.

3 Results

3.1 Fingerprint analysis of *T. wilfordii* multiglycoside by HPLC

In this study, the fingerprint of GTW was determined by an HPLC method, and components including triptolide, triptonide, wilforgine, celastrol, wilforine, and wilforlide A were detected and quantified (Figure 1). According to Table 4, the contents of triptolide and wilforlide A meted the quality standards of GTW (WS3-B-3350-98-2011).

3.2 *T. wilfordii* multiglycoside dose-dependently caused hepatotoxicity in mice

The body weights of experimental mice were recorded during 1-week administration of GTW. Compared with the control, GTW-H could prevent mice weight gain (Figure 2A). Meanwhile, liver tissue index of 140 mg/kg GTW-treated mice was slightly increased (Figure 2B). Serum aminotransferase levels were measured to evaluate whether GTW caused liver injury. As shown in Figures 2C–E, only 140 mg/kg GTW caused a significant increase in serum ALT and AST levels, suggesting hepatocellular injury. The effects of GTW on liver structure were examined by histopathological evaluation. Compared with the normal group, nuclear pyknosis was observed in the liver sections of GTW-H group (Figure 2F), suggesting apoptotic cell death. In addition, increased MPO immunopositive areas revealed

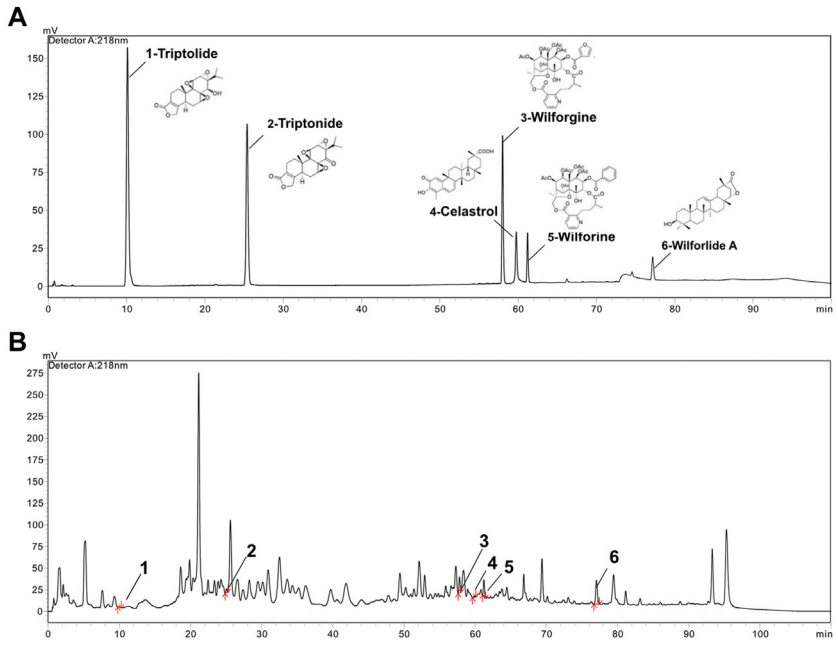

FIGURE 1
HPLC analysis of standard mixture and GTW. **(A)** The chromatograph of triptolide, triptonide, wilforgine, celastrol, wilforine, and wilforlide A standard mixture. **(B)** The HPLC chromatograph of GTW.

TABLE 4 Content assay of six components in GTW.

Name	Content (μg/g)	Content (‰)	Ct (min)	Standard (‰)
Triptolide	5.25	0.005	10	≤1
Triptonide	83.75	0.084	26	—
Wilforgine	479.75	0.480	57.8	—
Celastrol	67	0.067	60.1	—
Wilforine	1870.75	1.871	60.9	—
Wilforlide A	4460.75	4.461	77.4	≥1

recruitment and infiltration of neutrophils in GTW-H treated liver (Figure 2G). Taken together, these results demonstrate that GTW administration could induce hepatotoxicity in a dose-dependent manner.

3.3 Label-free quantification of mouse liver proteins after *T. wilfordii* multiglycoside administration

To obtain a comprehensive overview of the mechanism underlying GTW-induced hepatotoxicity, label-free quantitative proteomics was performed to identify the DEPs between the control group and GTW-H (hereinafter referred to as GTW) group. After three replicated biological analyses with high reliability, 3,670 proteins were recognized, of which 2,641 proteins were identified in both groups (Supplementary Table S1). Meanwhile, the proteomics profile of GTW group showed a clear separation from the control group (Figure 3A). Next, we screened DEPs by comparing protein abundance between the groups (fold change (FC) ≥ 2 and ≤ 0.5; p-value < 0.05) and identified 155 DEPs with 46 upregulated and 109 downregulated proteins (Figure 3B; Supplementary Table S2). The accuracy of the selected DEPs was measured by cluster analysis. As shown in Figure 3C, the identified DEPs were clearly distinguished between the two groups, suggesting that these DEPs may represent key changes in mice livers after GTW administration.

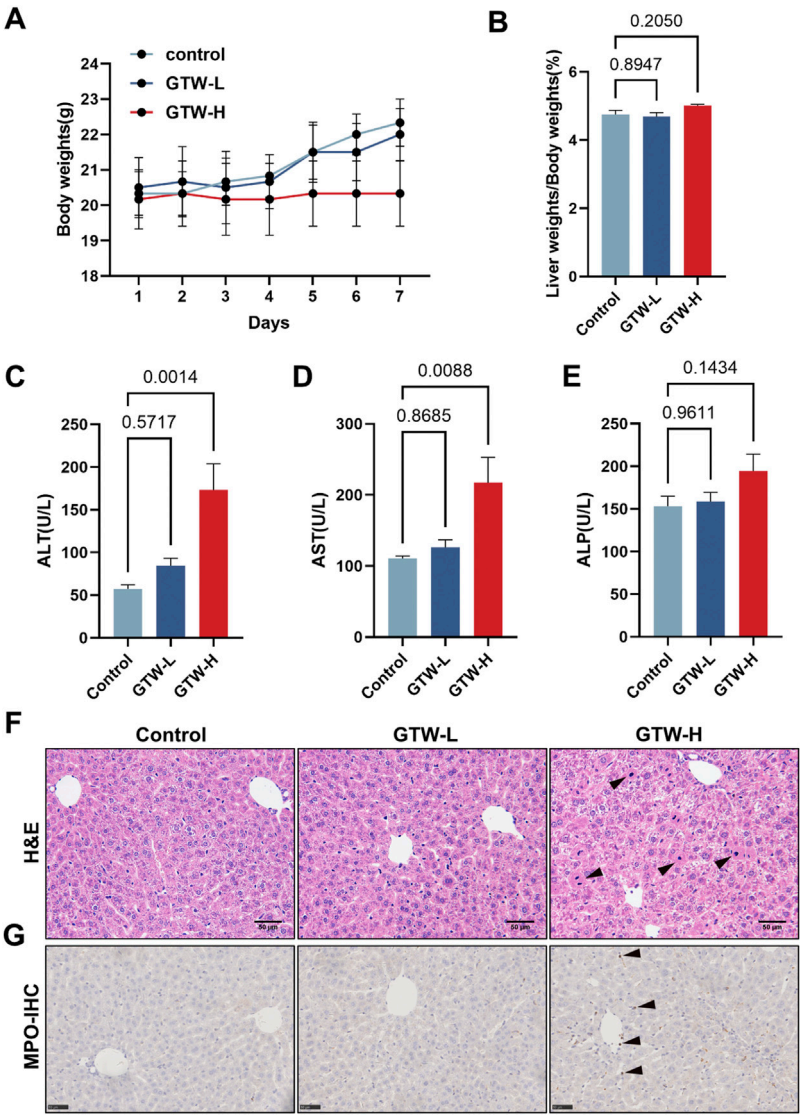

FIGURE 2
GTW administration caused liver injury in mice. **(A)** Changes in body weights (n = 6). **(B)** Liver tissue index calculated by tissue and body weights (n = 6). **(C–E)** Serum aminotransferase levels, including ALT, AST, and ALP (n = 6). **(F)** Representative H&E staining images of liver sections (scale bar = 50 μm), and nuclear pyknosis was pointed with black arrows. **(G)** Representative immunohistochemical measurements of liver in each group (scale bar = 50 μm). MPO positive areas were pointed with black arrows. Data are presented as mean ± SEM. $p < 0.05$ was considered statistically significant.

3.4 Bioinformatics analysis of differentially expressed proteins

3.4.1 Gene ontology annotation analysis

The GO annotation analysis on DEPs was carried out and classified into three GO terms: biological process (BP), cellular component (CC), and molecular function (MF). According to BP results (Figure 3D1), lipid metabolic process (16.2%), immune system process (14.9%), and translation (12.2%) were the top three processes. In CC analysis (Figure 3D2), the largest proportions of DEPs were assigned to the cytoplasm (22.5%), nucleus (18.3%), and cytosol (13.2%). In MF analysis (Figure 3D3), protein binding (29.1%), transferase activity (12.1%), nucleotide binding (11.5%), and RNA binding (11.5%) accounted for the major proportions.

3.4.2 Kyoto encyclopedia of genes and genomes pathway enrichment analysis

To better understand the functional categories, KEGG pathway analysis of DEPs was conducted. The top

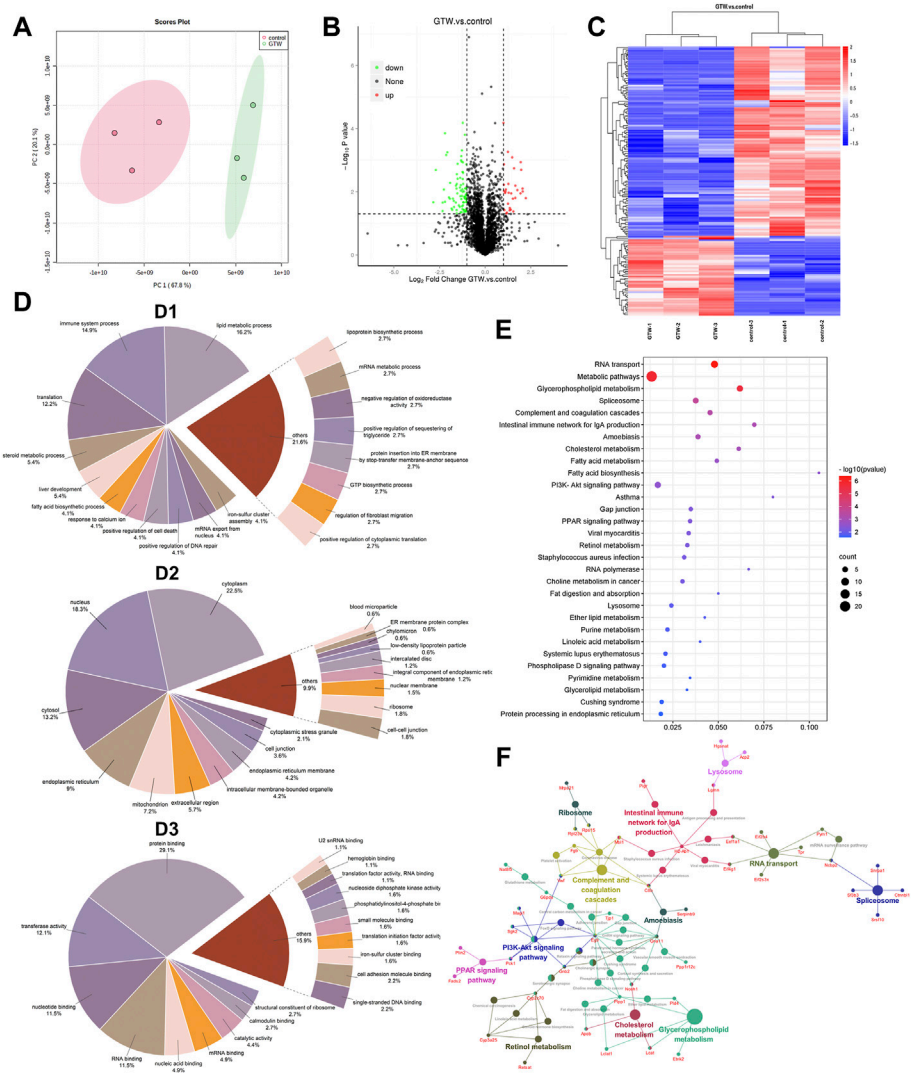

FIGURE 3
Results of proteomics combined with bioinformatics analysis of mice livers after GTW exposure. **(A)** PCA analysis of identified proteins. **(B)** Volcano plot. Proteins upregulated or downregulated were presented as red or green points, respectively, and black points represented proteins with no significant changes ($|log2FC| \geq 1$ and $p < 0.05$). **(C)** Heatmaps of DEPs. Rows represented DEPs and columns represented samples with three biological replicates. The signal values of DEPs were shown as colored bars, that is, the high expressed DEPs were colored in red, and the low expressed proteins were colored in blue. **(D)** GO annotation classification analysis of DEPs. (D1: Biological process. D2: Cellular component. D3: Molecular function.) **(E)** KEGG enrichment analysis of DEPs ($p < 0.05$). The ordinate represented the pathway term, and the abscissa represented the ratio of DEP numbers involved in a KEGG pathway to all identified protein numbers annotated in this pathway. The number of DEPs was represented by dot size, and the *p*-value was indicated by dot color. **(F)** The connection between pathways.

30 pathways were shown in Figure 3E, including RNA transport, glycerophospholipid metabolism, spliceosome, complement and coagulation cascade, and intestinal immune network for IgA production. Figure 3F shows the connection between them.

3.4.3 Protein-protein interaction analysis and significant cluster identification

To further determine the key pathways involved in GTW-induced hepatotoxicity, PPI analysis and significant cluster identification were performed. By using the STRING database, PPI network of the DEPs was conducted to explore their interactions. We observed that a total of 114 nodes and 432 edges showed interconnectivity (Figure 4A). The significant interconnected regions in this PPI network were analyzed, and the top three clusters were recognized (Figures 4B–D; Supplementary Table S3). Cluster 1 (Figure 4B) had the highest score, indicating that it would play an important role in regulating this PPI network, thus, BP annotation and KEGG

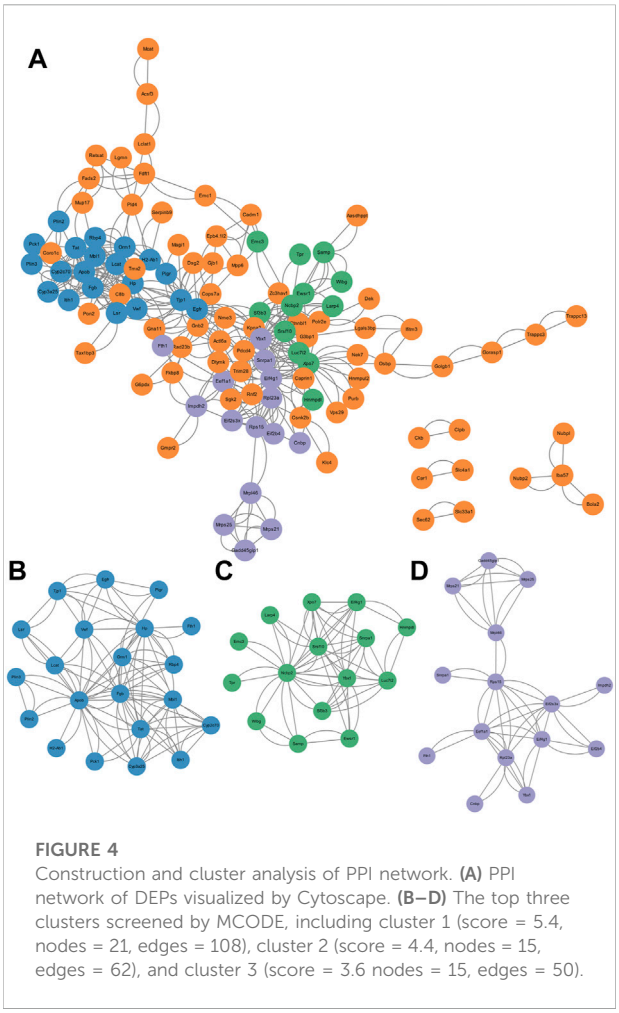

FIGURE 4
Construction and cluster analysis of PPI network. **(A)** PPI network of DEPs visualized by Cytoscape. **(B–D)** The top three clusters screened by MCODE, including cluster 1 (score = 5.4, nodes = 21, edges = 108), cluster 2 (score = 4.4, nodes = 15, edges = 62), and cluster 3 (score = 3.6 nodes = 15, edges = 50).

pathway analysis were performed. According to Table 5, cluster 1 was closely related to immune system process, response to lipopolysaccharide, and response to bacterium, suggesting that abnormal immune response would be the main reason for GTW-induced hepatotoxicity. Further KEGG analysis showed that intestinal immune network for IgA production pathway would be involved in the liver toxicity.

IgA, transported by polymeric immunoglobulin receptor (pIgR), is a major immunoglobulin isotype in the gut and plays a crucial role in maintaining gut barrier (Gutzeit et al., 2014). The interaction between gut and liver makes liver vulnerable to disrupted intestinal homeostasis (Seki and Schnabl, 2012). Intestinal barrier dysfunction could promote bacterial translocation to the liver and trigger proinflammatory response, contributing to the development of liver diseases (Wang et al., 2015; Tripathi et al., 2018). Thus, we assumed that GTW should affect the intestinal immune network for IgA production pathway and disturb intestinal homeostasis, contributing to abnormal immune response in livers of GTW-treated mice.

3.5 *T. wilfordii* multiglycoside acted on the intestinal immune network for IgA production pathway

Next, we evaluate the effects of GTW on the intestinal immune network for IgA production pathway. Results from proteomics indicated that GTW could downregulate pIgR protein expression (Figure 5A). Immunoblots confirmed that pIgR protein in liver was decreased in GTW group (Figure 5B). In addition, we assessed the expression of pIgR in gut and found that pIgR protein expression was reduced in the ileum but not significantly changed in the colon after GTW exposure (Figure 5B). As a consequence, the reduction of pIgR resulted in a decreased secretion of IgA into the gut lumen (Figure 5C), and a buildup of serum IgA compared to the normal group (Figure 5D). These results suggest that GTW could inhibit intestinal immune network for IgA production pathway *via* disturbing pIgR/IgA system.

TABLE 5 GO_BP annotation and KEGG pathway analysis of nodes in cluster 1.

Category	Term	Count	*p*-value
GOTERM_BP	Liver development	3	0.005
GOTERM_BP	Steroid metabolic process	3	0.007
GOTERM_BP	Immune system process	4	0.014
GOTERM_BP	Response to lipopolysaccharide	3	0.015
GOTERM_BP	Response to bacterium	3	0.033
KEGG_pathway	Complement and coagulation cascades	3	0.000
KEGG_pathway	Intestinal immune network for IgA production	2	0.000
KEGG_pathway	Cholesterol metabolism	2	0.000
KEGG_pathway	Linoleic acid metabolism	2	0.000
KEGG_pathway	Adherens junction	2	0.000
KEGG_pathway	PI3K-AKT signaling pathway	3	0.000

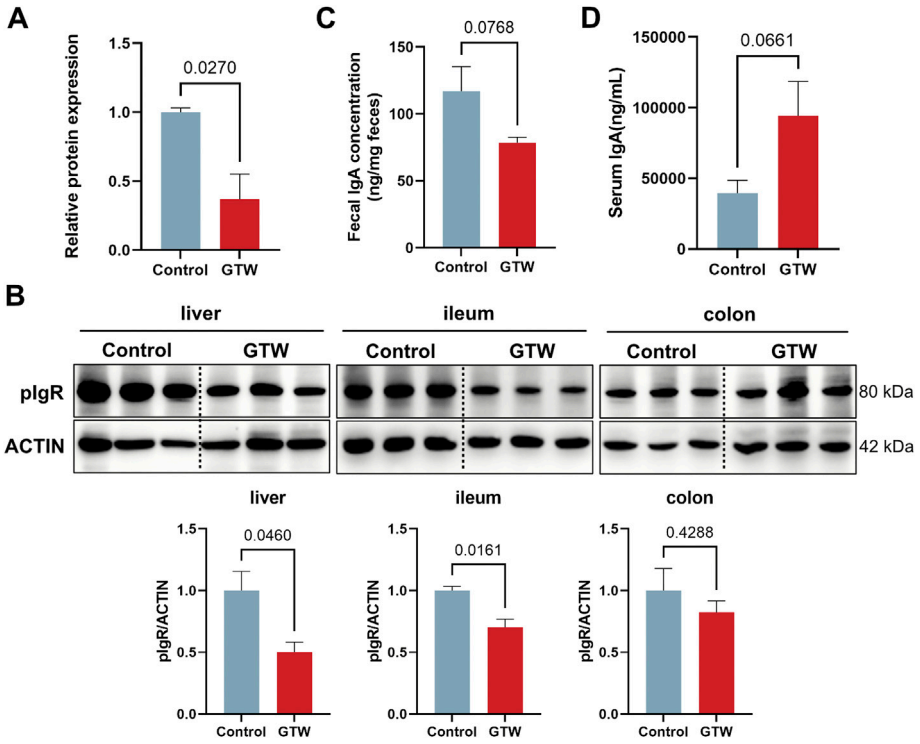

FIGURE 5
GTW affected the activation of intestinal immune network for IgA production pathway. **(A)** Relative pIgR protein expression according to proteomics results (n = 3). **(B)** The protein levels of pIgR in liver, ileum and colon were determined by western blot (n = 3). **(C)** IgA levels in feces (n = 5) and **(D)** serum (n = 5) were measured after GTW treatment. The band density was calculated using ImageJ software. Data are presented as mean ± SEM. $p < 0.05$ was considered statistically significant.

3.6 *T. wilfordii* multiglycoside-treated mice displayed intestinal barrier impairment

The intestinal immune network for IgA production pathway plays a crucial role in maintaining mucosal homeostasis and gut barrier (Brown and Kloppel, 1989; Mantis et al., 2011). Therefore, we assessed whether the intestinal barrier was altered in GTW-treated mice. Histopathological examination showed that in GTW-treated mice ileum, the villi were sparse and broken and the crypt depth was reduced (Figure 6A). In addition, GTW could damage the colon, manifested by extensive loss of epithelial cells, destruction of crypts, and inflammatory cell infiltration (Figure 6B). As a reliable sign of intestinal barrier disruption, we further analyzed the expression of tight junction protein occludin in the ileum and colon. As shown in Figure 6C, the ileal and colonic protein levels of occludin were decreased. Consistently, the fluorescence intensity of intestinal epithelial occludin was much lower in GTW-treated mice than in control mice (Figure 6D). These results point towards impaired intestinal barrier integrity and show consistency with disrupted pIgR/IgA system.

3.7 Intestinal barrier impairment contributed to *T. wilfordii* multiglycoside-induced hepatotoxicity

The liver, a key immune organ, is positioned to receive gut-derived products *via* the portal vein, implying that it could be severely affected by a disrupted intestinal homeostasis (Schnabl, 2013; Wang et al., 2021). The disruption of gut barrier allows bacterial translocation (Albillos et al., 2020). We thus detected bacteria in the liver. The 16S rRNA gene expression in GTW-treated mice livers were significantly increased (Figure 7A), in addition, FISH analysis confirmed that bacterial invasion to the liver was promoted after GTW exposure (Figure 7B). In agreement with this result, clear signs of inflammatory response in GTW-treated mice livers were observed, with an increase of F4/80 labeled macrophages (Figure 7C) and of hepatic TLR2 and TLR4 mRNA levels (Figure 7D). In addition, increased mRNA levels of proinflammatory cytokine TNFα (Figure 7E) and increased serum TNFα concentration (Figure 7F) further confirmed liver inflammation. Thus, these findings suggest that GTW-caused intestinal barrier impairment could increase bacterial translocation to the liver and trigger hepatic

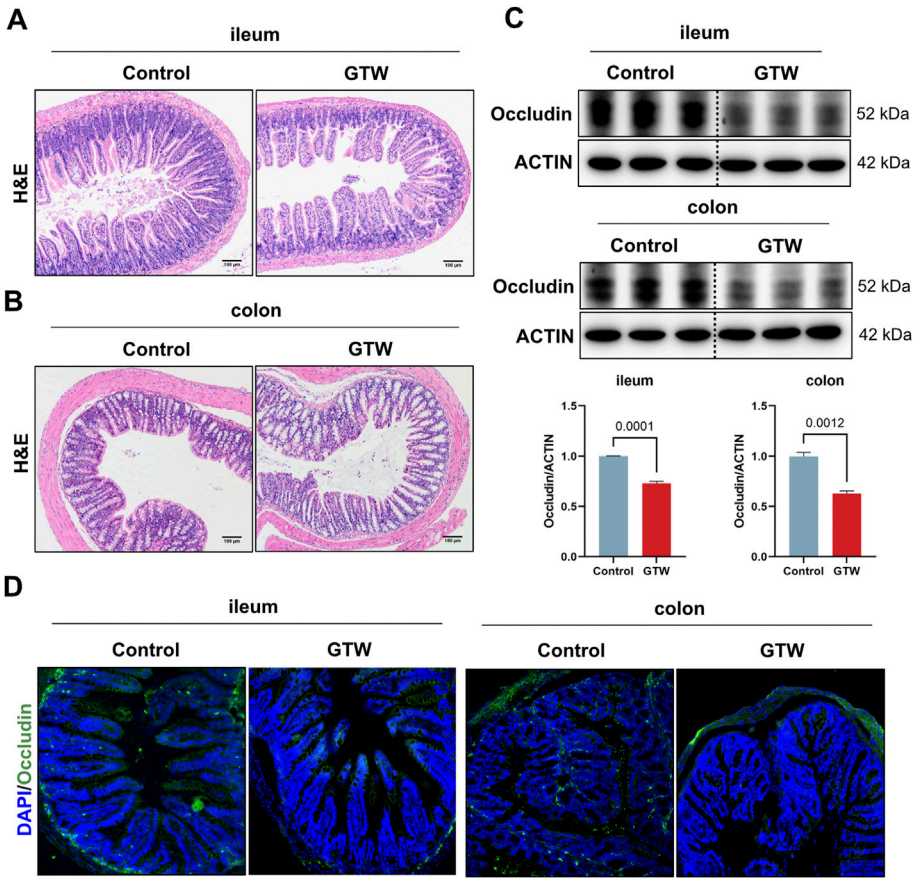

FIGURE 6
The effects of GTW on intestinal barrier integrity. **(A,B)** Representative H&E staining images of ileum and colon tissues (scale bar = 100 μm). **(C)** The protein levels of occludin in the ileum and colon were determined by western blot (n = 3). **(D)** Representative images of immunofluorescent staining of occludin (green) in ileum and colon sections (20x). The nuclei were visualized with DAPI (blue). The band density was calculated using ImageJ software. Data are presented as mean ± SEM. $p < 0.05$ was considered statistically significant.

inflammation, which may contribute to GTW-induced liver toxicity.

4 Discussion

GTW is a stable extract purified from the peeled roots of TwHF and extensively applied for autoimmune diseases in China. Three major ingredients, including diterpenoids (e.g., triptolide and triptonide), sesquiterpene alkaloids (e.g., wilforgine and wilforine), and triterpenoids (e.g., celastrol and wilforlide A), are thought to be contributed to the pharmacodynamics activities of GTW (Luo et al., 2016). In the study, we used an HPLC method to characterize the fingerprint of GTW, and calculated the contents of 6 representative components. It was found that among them, wilforlide A showed the highest content (the mean value was 4460.75 μg/g) while triptolide showed the lowest (the mean value was 5.25 μg/g). These results meted the quality standards of GTW (WS3-B-3350-98-2011) and showed consistency with previous studies (Luo et al., 2016).

The clinical application of GTW is restricted due to its adverse effects, especially liver injury. TP is concerned as an essential bioactive but toxic component of TwHF (Li et al., 2014b). Previous studies demonstrated that liver damage caused by TP was mainly associated with mitochondrial dysfunction (Fu et al., 2011), oxidative stress (Li et al., 2014a), abnormal lipid and glucose metabolism (Wang et al., 2013; Jiang et al., 2016), and inflammation (Wang et al., 2014). Compared to TP, studies about GTW-induced liver injury are few and associated signaling mechanisms remain poorly understood. In addition, to study the toxic effects of GTW, it is more appropriate to take GTW as a whole than to focus only on TP. In this study, we conducted experiments in male C57BL/6J mice to evaluate GTW-induced hepatotoxicity. ALT and AST are two reliable

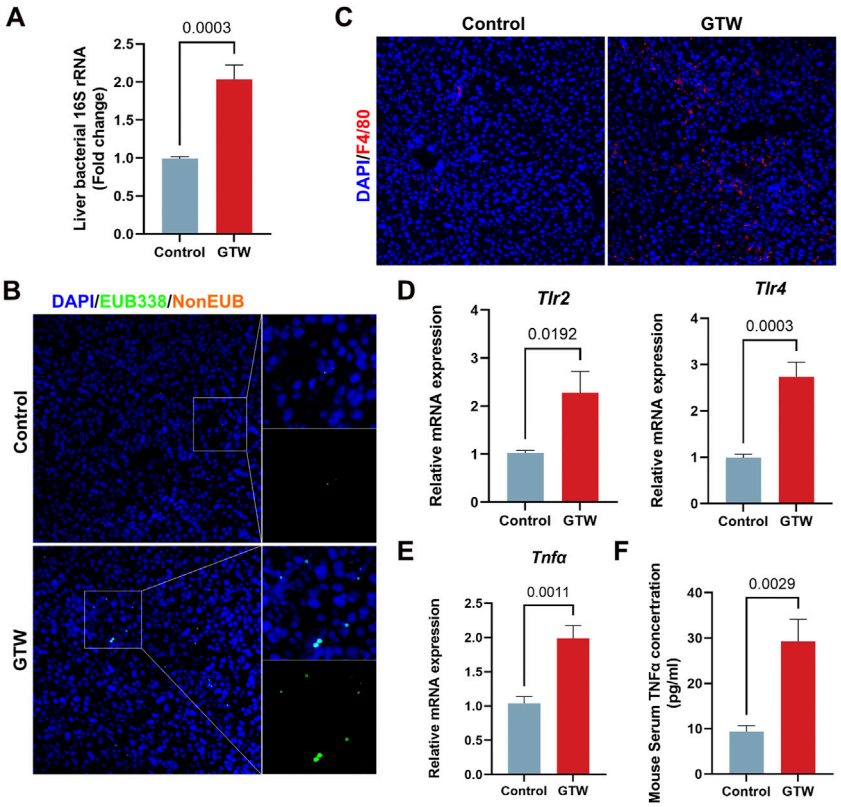

FIGURE 7
GTW administration promoted bacterial translocation to the liver and triggered hepatic inflammation. **(A)** Liver bacterial 16S rRNA expression measured by RT-PCR (n = 6). **(B)** Bacteria detected in the liver using FISH with probes EUB338 targeting eubacteria 16S rRNA region (20x). The nuclei were stained with DAPI (blue) and bacteria stained with EUB338 (green). **(C)** Representative images of immunofluorescent staining of F4/80 (red) in liver (20x). DAPI was used to visualize nuclei (blue). **(D)** Hepatic TLR2 and TLR4 mRNA expression levels were detected by RT-PCR (n = 6). **(E)** The expression levels of proinflammatory cytokine TNFα in liver were measured using RT-PCR analysis (n = 6). **(F)** Serum TNFα concentration in GTW-treated mice were detected by ELISA (n = 6). Data are presented as mean ± SEM. $p < 0.05$ was considered statistically significant.

markers reflecting hepatocellular injury while ALP reflects the extent of cholestasis (Cockeram, 1998). After 1-week administration, GTW at high dose significantly increased serum ALT and AST levels but had minor effects on ALP, indicating hepatocellular damage. Further examinations confirmed that GTW could cause hepatocyte apoptosis and liver inflammation. Similar to our results, a recent study reported that GTW induced hepatotoxicity in zebrafish *via* increased inflammation and enhanced apoptosis (DUAN et al., 2021). In fact, we also investigated the hepatotoxic effects of GTW on female mice. By detecting serum aminotransferase levels, we found that whereas there was no significant gender difference, the hepatotoxic effects of GTW showed a better dose-dependent manner in male mice than in female (Supplementary Figure S1).

Based on label-free proteomics combined with bioinformatics analysis, intestinal immune network for IgA production pathway was predicted to be involved in GTW-induced liver toxicity. IgA is a major immunoglobulin isotype in the gut and plays a crucial role in maintaining intestinal homeostasis (Mantis et al., 2013). Transport of IgA from the lamina propria to the mucosal surface and the release of secretory IgA onto the gut lumen require pIgR, a protein expressed on mucosal epithelial cells (Kaetzel et al., 1991; Schneeman et al., 2005). Besides lamina propria-produced IgA, liver-derived IgA is also an important source of total gut IgA in mouse, which is secreted to bile by pIgR on hepatocytes and cholangiocytes (Brown and Kloppel, 1989; Turula and Wobus, 2018). Secretory IgA has been reported to favor the maintenance of gut barrier by regulating microbiota composition, preventing bacteria invasion, and downregulating immune responses in the intestinal mucosal (Strugnell and Wijburg, 2010; Mantis et al., 2011). Deficiency in secretory IgA would alter gut microbiome and increase intestinal permeability (Inamine and Schnabl, 2018). Accumulating evidence indicates that controlling gut microbial composition is critical for maintaining intestinal homeostasis (Albillos et al., 2020). Gut bacterial dysbiosis can

lead to a direct interaction between the microbiota and epithelial cells, promoting inflammatory response and enhancing gut permeability, thereby increasing bacterial translocation and affecting the development of chronic liver diseases, including ALD, NAFLD and NASH(Mao et al., 2015; Cheng et al., 2018; Wang et al., 2020; Wang et al., 2021). Results from our study demonstrate that GTW could significantly reduce pIgR protein expression in the liver and ileum, as a result, a reduction in fecal IgA was observed. In agreement with reduced fecal IgA levels, serum IgA concentration was increased, which was consistent with previous study (Shimada et al., 1999). These findings suggest that GTW could act on intestinal immune network for IgA production pathway *via* inhibiting pIgR/IgA system, it raises the possibility that GTW would disrupt intestinal homeostasis, which might be associated with altered microbiota composition, and as a consequence, the increased intestinal inflammation, the impaired gut barrier integrity and the enhancement of intestinal permeability.

We thus assess whether GTW caused intestinal barrier dysfunction. Histopathological analysis showed that GTW administration caused damage to ileum and colon, in addition, obvious inflammation was observed in the colon of GTW-treated mice. Tight junctions, sealing adjacent intestinal epithelial cells together, play a central role in gut barrier maintenance (Chelakkot et al., 2018; Lee et al., 2018). Numerous studies have reported that damage to tight junctions contributes to intestinal barrier dysfunction (Lee, 2015; Chen et al., 2017). In our study, we found that the expression of tight junction protein occludin in the ileum and colon were decreased after GTW exposure, indicating impaired intestinal barrier integrity. The liver, the first organ for receiving gut-derived products through the portal vein, is vulnerable to disrupted intestinal homeostasis (Inamine and Schnabl, 2018). Gut barrier disruption enhances intestinal permeability and promotes bacteria and/or bacterial products (e.g., lipopolysaccharides) transferring to the liver, triggering a proinflammatory cascade, thereby inducing or exacerbating a range of hepatic diseases (Albillos et al., 2020; Ghosh et al., 2020). In our study, increased bacteria were found in the livers of GTW-treated mice while livers of control mice were harboring few bacteria. Toll-like receptors (TLR) have been shown to recognize microbial pattern recognition receptors and stimulate immune response (Kawasaki and Kawai, 2014), we thus assessed hepatic TLR2 and TLR4 expression. In agreement with increased bacterial translocation, TLR2 and TLR4 mRNA levels in GTW-treated mice livers were significantly elevated. In addition, F4/80 immunofluorescent staining revealed more macrophages in the livers of GTW-treated mice, and MPO immunohistochemical staining revealed increased recruitment and infiltration of neutrophils. The proinflammatory response was further confirmed by the increase of hepatic TNFα mRNA expression and of serum TNFα concentration. Taken together, our study suggests that GTW could disrupt intestinal barrier integrity, promoting the translocation of bacteria to the liver and increasing hepatic inflammation. Furthermore, our findings suggest a key role of gut-liver axis in GTW-induced liver injury. In fact, according to clinical reports, GTW has the highest incidence of gastrointestinal upset, ranging from diarrhea, nausea, vomiting, and even colitis (Zhang et al., 2016), it raises the possibility that GTW could disrupt gut barrier and thereby affect the progression of liver toxicity. However, the effects of GTW on gut microbiome and the role of intestinal microbiota dysbiosis in GTW-induced hepatotoxicity require validation in our further study, in addition, our study just did a preliminary exploration, more experiments need to be conducted to investigate the crosstalk between gut and liver in GTW-induced hepatotoxic model and to identify potential molecular targets.

Outcomes obtained from this study reveal novel insights into the mechanism of GTW-induced hepatotoxicity, but, inevitably, there are limitations. First, these findings were based on the analysis of livers in mice, which may have inconsistencies with clinical results. Second, the effects of GTW on gut microbiome and the crosstalk between gut and liver injury required further exploration. Third, in addition to the gut-liver axis, other functional pathways and targets related to GTW-induced hepatotoxicity need to be validated. Furthermore, potential ingredients and/or toxic core structures, contributing to hepatotoxicity, need to be explored to promote the clinical application of GTW.

5 Conclusion

Our findings demonstrate that GTW could induce liver injury. Based on label-free proteomics combined with bioinformatics analysis, we found that GTW may act on intestinal immune network for IgA production pathway and impair intestinal barrier integrity, therefore, the bacterial translocation to the liver and hepatic inflammation were increased. In summary, our study reveals a novel insight into the mechanism of GTW-induced hepatotoxicity that the crosstalk between gut and liver may play a crucial part in the progression of GTW-induced liver toxicity. However, more experimental data are needed to verify this.

Data availability statement

The datasets of proteomics analysis presented in this study can be found in ProteomeXchange Consortium with the dataset identifier PXD038084.

Ethics statement

The animal study was reviewed and approved by Ethical Committee of China Pharmaceutical University.

Author contributions

Conceptualization, YM and ZJ; methodology, YM and ZY; validation, QZ and MD; investigation, JW, YX, and YC; writing—original draft preparation, YM; writing—review and editing, ZJ; supervision, QY; project administration, LZ and ZJ; funding acquisition, LZ and ZJ.

Funding

This research was funded by the National Natural Science Foundation of China (82074114, 81973562, 81773995); the Innovation Team Projects in Universities of Guangdong Province (No. 2018KCXTD016); "Double First-Class" University project (CPU2018GY33); the Postgraduate Research Practice Innovation Program of Jiangsu Province (KYCX20_0669).

Conflict of interest

The authors declare that the research was conducted in the absence of any commercial or financial relationships that could be construed as a potential conflict of interest.

Publisher's note

All claims expressed in this article are solely those of the authors and do not necessarily represent those of their affiliated organizations, or those of the publisher, the editors and the reviewers. Any product that may be evaluated in this article, or claim that may be made by its manufacturer, is not guaranteed or endorsed by the publisher.

Supplementary material

The Supplementary Material for this article can be found online at: https://www.frontiersin.org/articles/10.3389/fphar.2022.1032741/full#supplementary-material

References

Albillos, A., Gottardi, A. D., and Rescigno, M. (2020). The gut-liver axis in liver disease: Pathophysiological basis for therapy. *J. Hepatol.* 72, 558–577. doi:10.1016/j.jhep.2019.10.003

Andrea Iorga, L. D., and Kaplowitz, N. (2017). Drug-induced liver injury: Cascade of events leading to cell death, apoptosis or necrosis. *Int. J. Mol. Sci.* 18, E1018. doi:10.3390/ijms18051018

Bader, G. D., and Hogue, C. W. V. (2003). An automated method for finding molecular complexes in large protein interaction networks. *BMC Bioinforma.* 4, 2–27. doi:10.1186/1471-2105-4-2

Bennett, M. R., and Devarajan, P. (2018). The future role of proteomics in the understanding of acute kidney injury. *Expert Rev. Proteomics* 15, 191–192. doi:10.1080/14789450.2018.1443007

Bindea, G., Mlecnik, B., Hackl, H., Charoentong, P., Tosolini, M., Kirilovsky, A., et al. (2009). ClueGO : A Cytoscape plug-in to decipher functionally grouped gene ontology and pathway annotation networks. *Bioinformatics* 25, 1091–1093. doi:10.1093/bioinformatics/btp101

Brown, W. R., and Kloppel, T. M. (1989). The liver and IgA: Immunological, cell biological and clinical implications. *Hepatology* 9, 763–784. doi:10.1002/hep.1840090518

Bu, D., Luo, H., Huo, P., Wang, Z., Zhang, S., and He, Z., (2021). KOBAS-i: Intelligent prioritization and exploratory visualization of biological functions for gene enrichment analysis. *Nucleic Acids Res.* 49, W317–W325. doi:10.1093/nar/gkab447

Charan, J., and Kantharia, N. (2013). How to calculate sample size in animal studies? *J. Pharmacol. Pharmacother.* 4, 303–306. doi:10.4103/0976-500X.119726

Chelakkot, C., Ghim, J., and Ryu, S. H. (2018). Mechanisms regulating intestinal barrier integrity and its pathological implications. *Exp. Mol. Med.* 50, 103. doi:10.1038/s12276-018-0126-x

Chen, W. Y., Wang, M., Zhang, J., Barve, S. S., McClain, C. J., and Joshi-Barve, S. (2017). Acrolein disrupts tight junction proteins and causes endoplasmic reticulum stress-mediated epithelial cell death leading to intestinal barrier dysfunction and permeability. *Am. J. Pathol.* 187, 2686–2697. doi:10.1016/j.ajpath.2017.08.015

Cheng, C., Tan, J., Qian, W., Zhang, L., and Hou, X. (2018). Gut inflammation exacerbates hepatic injury in the high-fat diet induced NAFLD mouse: Attention to the gut-vascular barrier dysfunction. *Life Sci.* 209, 157–166. doi:10.1016/j.lfs.2018.08.017

Cockeram, A. W. (1998). Canadian association of gastroenterology Practice guidelines: Evaluation of dysphagia. *Can. J. Gastroenterol.* 12, 409–413. doi:10.1155/1998/303549

Dai, M., Peng, W., Zhang, T., Zhao, Q., Ma, X., and Cheng, Y., (2022). Metabolomics reveals the role of PPARα in Tripterygium Wilfordii-induced liver injury. *J. Ethnopharmacol.* 289, 115090. doi:10.1016/j.jep.2022.115090

Dragoi, D., Benesic, A., Pichler, G., Kulak, N. A., Bartsch, H. S., and Gerbes, A. L. (2018). Proteomics analysis of monocyte-derived hepatocyte-like cells identifies integrin beta 3 as a specific biomarker for drug-induced liver injury by Diclofenac. *Front. Pharmacol.* 9, 699–710. doi:10.3389/fphar.2018.00699

Duan, X. Y., Ma, R. J., Hsiao, C. Der, Jiang, Z. Z., Zhang, L. Y., and Zhang, Y., (2021). Tripterygium wilfordii multiglycoside-induced hepatotoxicity via inflammation and apoptosis in zebrafish. *Chin. J. Nat. Med.* 19, 750–757. doi:10.1016/S1875-5364(21)60078-X

Fu, Q., Huang, X., Shu, B., Xue, M., Zhang, P., and Wang, T., (2011). Inhibition of mitochondrial respiratory chain is involved in triptolide-induced liver injury. *Fitoterapia* 82, 1241–1248. doi:10.1016/j.fitote.2011.08.019

Ghosh, S. S., Wang, J., Yannie, P. J., and Ghosh, S. (2020). Intestinal barrier function and metabolic/liver diseases. *Liver Res.* 4, 81–87. doi:10.1016/j.livres.2020.03.002

Gong, L., Wang, L., Cao, Y., and Li, C. (2020). Rapid induction of clinical remission in sapho syndrome using high-dose Tripterygium glycosides: A case report. *Med. Baltim.* 99, e21102. doi:10.1097/MD.0000000000021102

Gutzeit, C., Magri, G., and Cerutti, A. (2014). Intestinal IgA production and its role in host-microbe interaction. *Immunol. Rev.* 260, 76–85. doi:10.1111/imr.12189

Huang, D. W., Sherman, B. T., and Lempicki, R. A. (2009). Systematic and integrative analysis of large gene lists using DAVID bioinformatics resources. *Nat. Protoc.* 4, 44–57. doi:10.1038/nprot.2008.211

Inamine, T., and Schnabl, B. (2018). Immunoglobulin A and liver diseases. *J. Gastroenterol.* 53, 691–700. doi:10.1007/s00535-017-1400-8

Jiang, Z., Huang, X., Huang, S., Guo, H., Wang, L., and Li, X., (2016). Sex-related differences of lipid metabolism induced by triptolide: The possible role of the LXRα/

SREBP-1 signaling pathway. *Front. Pharmacol.* 7, 87–10. doi:10.3389/fphar.2016.00087

Kaetzel, C. S., Robinson, J. K., Chintalacharuvu, K. R., Vaerman, J. P., and Lamm, M. E. (1991). The polymeric immunoglobulin receptor (secretory component) mediates transport of immune complexes across epithelial cells: A local defense function for IgA. *Proc. Natl. Acad. Sci. U. S. A.* 88, 8796–8800. doi:10.1073/pnas.88.19.8796

Kawasaki, T., and Kawai, T. (2014). Toll-like receptor signaling pathways. *Front. Immunol.* 5, 461–468. doi:10.3389/fimmu.2014.00461

Lee, B., Moon, K. M., and Kim, C. Y. (2018). Tight junction in the intestinal epithelium: Its association with diseases and regulation by phytochemicals. *J. Immunol. Res.* 2018, 2645465. doi:10.1155/2018/2645465

Lee, S. H. (2015). Intestinal permeability regulation by tight junction: Implication on inflammatory bowel diseases. *Intest. Res.* 13, 11–18. doi:10.5217/ir.2015.13.1.11

Li, J., Shen, F., Guan, C., Wang, W., Sun, X., and Fu, X., (2014). Activation of Nrf2 protects against triptolide-induced hepatotoxicity. *PLoS One* 9, e100685. doi:10.1371/journal.pone.0100685

Li, M., Hu, T., Tie, C., Qu, L., Zheng, H., and Zhang, J. (2017). Quantitative proteomics and targeted fatty acids analysis reveal the damage of triptolide in liver and kidney. *Proteomics* 17, 1700001–1700025. doi:10.1002/pmic.201700001

Li, X. J., Jiang, Z. Z., and Zhang, L. Y. (2014b). Triptolide: Progress on research in pharmacodynamics and toxicology. *J. Ethnopharmacol.* 155, 67–79. doi:10.1016/j.jep.2014.06.006

Liu, L., Zhao, H., Sun, X., Zheng, Q., Luo, Y., and Ru, Y., (2018). Efficacy and safety of Tripterygium wilfordii hook F for chronic urticaria: A systematic review and meta-analysis. *BMC Complement. Altern. Med.* 18, 243–312. doi:10.1186/s12906-018-2305-7

Luo, H., Wu, X., Huang, H., Chen, S., Yang, W., and Zhang, L., (2016). Simultaneous determination of triptolide, tripterifordin, celastrol and nine sesquiterpene alkaloids in Tripterygium preparations using high-performance liquid chromatography-triple quadrupole mass spectrometry. *J. Pharm. Biomed. Anal.* 117, 195–204. doi:10.1016/j.jpba.2015.08.043

Mantis, N. J., Rol, N., and Corthésy, B. (2013). Secretory IgA's complex roles in immunity and mucosal homeostasis in the gut. *Mucosal Immunol.* 4, 603–611. doi:10.1038/mi.2011.41

Mantis, N. J., Rol, N., and Corthésy, B. (2011). Secretory IgA's complex roles in immunity and mucosal homeostasis in the gut. *Mucosal Immunol.* 4, 603–611. doi:10.1038/mi.2011.41

Mao, J., Tang, H., Zhao, T., Tan, X., Bi, J., and Wang, B., (2015). Intestinal mucosal barrier dysfunction participates in the progress of nonalcoholic fatty liver disease. *Int. J. Clin. Exp. Pathol.* 8, 3648–3658.

Marks, W. H. (2011). Tripterygium wilfordii hook F. Versus sulfasalazine in the treatment of rheumatoid arthritis: A well-designed clinical trial of a botanical demonstrating effectiveness. *Fitoterapia* 82, 85–87. doi:10.1016/j.fitote.2010.11.024

Miao, Y. Y., Luo, L., Shu, T., Wang, H., Jiang, Z. Z., and Zhang, L. Y. (2019). Study on difference of liver toxicity and its molecular mechanisms caused by Tripterygium wilfordii multiglycoside and equivalent amount of triptolid in rats. *Zhongguo Zhong Yao Za Zhi* 44, 3468–3477. doi:10.19540/j.cnki.cjcmm.20190301.002

Mlecnik, B., and Bindea, G. (2013). Systems biology CluePedia Cytoscape plugin : Pathway insights using integrated experimental and in silico data. *Bioinformatics*, 29, 661–663. doi:10.1093/bioinformatics/btt019

Peng, W., Dai, M. Y., Bao, L. J., Zhu, W. F., and Li, F. (2021). FXR activation prevents liver injury induced by Tripterygium wilfordii preparations. *Xenobiotica.* 51, 716–727. doi:10.1080/00498254.2021.1900626

Satoh, S., Otsuka, Y., Ozeki, Y., Itoh, K., Hashiguchi, A., and Yamazaki, K., (2014). Label-free visualization of acetaminophen-induced liver injury by high-speed stimulated Raman scattering spectral microscopy and multivariate image analysis. *Pathol. Int.* 64, 518–526. doi:10.1111/pin.12206

Schnabl, B. (2013). Linking intestinal homeostasis and liver disease. *Curr. Opin. Gastroenterol.* 29, 264–270. doi:10.1097/MOG.0b013e32835ff948

Schneeman, T. A., Bruno, M. E. C., Schjerven, H., Johansen, F.-E., Chady, L., and Kaetzel, C. S. (2005). Regulation of the polymeric ig receptor by signaling through TLRs 3 and 4: Linking innate and adaptive immune responses. *J. Immunol.* 175, 376–384. doi:10.4049/jimmunol.175.1.376

Seki, E., and Schnabl, B. (2012). Role of innate immunity and the microbiota in liver fibrosis: Crosstalk between the liver and gut. *J. Physiol.* 590, 447–458. doi:10.1113/jphysiol.2011.219691

Shimada, S., Kawaguchi-Miyashita, M., Kushiro, A., Sato, T., Nanno, M., and Sako, T., (1999). Generation of polymeric immunoglobulin receptor-deficient mouse with marked reduction of secretory IgA. *J. Immunol.* 163, 5367–5373. Available at: http://www.ncbi.nlm.nih.gov/pubmed/10553061.

Stournaras, E., and Tziomalos, K. (2015). Herbal medicine-related hepatotoxicity. *World J. Hepatol.* 7, 2189–2193. doi:10.4254/wjh.v7.i19.2189

Strugnell, R. A., and Wijburg, O. L. C. (2010). The role of secretory antibodies in infection immunity. *Nat. Rev. Microbiol.* 8, 656–667. doi:10.1038/nrmicro2384

Szklarczyk, D., Morris, J. H., Cook, H., Kuhn, M., Wyder, S., and Simonovic, M., (2017). The STRING database in 2017: Quality-controlled protein-protein association networks, made broadly accessible. *Nucleic Acids Res.* 45, D362–D368. doi:10.1093/nar/gkw937

Tao, X., Cush, J. J., Garret, M., and Lipsky, P. E. (2001). A phase I study of ethyl acetate extract of the Chinese antirheumatic herb Tripterygium wilfordii Hook F in rheumatoid arthritis. *J. Rheumatol.* 28, 2160–2167.

Tripathi, A., Debelius, J., Brenner, D. A., Karin, M., Loomba, R., and Schnabl, B., (2018). The gut-liver axis and the intersection with the microbiome. *Nat. Rev. Gastroenterol. Hepatol.* 15, 397–411. doi:10.1038/s41575-018-0011-z

Turula, H., and Wobus, C. E. (2018). The role of the polymeric immunoglobulin receptor and secretory immunoglobulins during mucosal infection and immunity. *Viruses* 10, 2377–E315. doi:10.3390/v10050237

Wang, F., Cui, Q., Zeng, Y., and Chen, P. (2020). Gut microbiota-an important contributor to liver diseases. *Nan Fang. Yi Ke Da Xue Xue Bao* 40, 595–600. doi:10.12122/j.issn.1673-4254.2020.04.23

Wang, J., Jiang, Z., Ji, J., Wang, X., Wang, T., and Zhang, Y., (2013). Gene expression profiling and pathway analysis of hepatotoxicity induced by triptolide in Wistar rats. *Food Chem. Toxicol.* 58, 495–505. doi:10.1016/j.fct.2013.04.039

Wang, L., Llorente, C., Hartmann, P., Yang, A. M., Chen, P., and Schnabl, B. (2015). Methods to determine intestinal permeability and bacterial translocation during liver disease. *J. Immunol. Methods* 421, 44–53. doi:10.1016/j.jim.2014.12.015

Wang, R., Tang, R., Li, B., Ma, X., Schnabl, B., and Tilg, H. (2021). Gut microbiome, liver immunology, and liver diseases. *Cell. Mol. Immunol.* 18, 4–17. doi:10.1038/s41423-020-00592-6

Wang, X., Jiang, Z., Cao, W., Yuan, Z., Sun, L., and Zhang, L. (2014). Th17/Treg imbalance in triptolide-induced liver injury. *Fitoterapia* 93, 245–251. doi:10.1016/j.fitote.2014.01.006

Xu, G., Jiang, D., and Xu, C. (2009). Tripterygium wilfordii hook F treatment for idiopathic refractory nephrotic syndrome in adults : A meta-analysis. *Nephron. Clin. Pract.* 111 (4), c223–c228. doi:10.1159/000208990

Yuan, Z., Zhang, H., Hasnat, M., Ding, J., Chen, X., and Liang, P., (2019). A new perspective of triptolide-associated hepatotoxicity: Liver hypersensitivity upon LPS stimulation. *Toxicology* 414, 45–56. doi:10.1016/j.tox.2019.01.005

Zhang, C., Sun, P. P., Guo, H. T., Liu, Y., Li, J., and He, X. J., (2016). Safety profiles of Tripterygium wilfordii hook F: A systematic review and meta-analysis. *Front. Pharmacol.* 7, 402–408. doi:10.3389/fphar.2016.00402

Zhang, M., Guo, F., Li, X., Xian, M., Wang, T., and Wu, H., (2022). Yi-Xin-Shu capsule ameliorates cardiac hypertrophy by regulating RB/HDAC1/GATA4 signaling pathway based on proteomic and mass spectrometry image analysis. *Phytomedicine.* 103, 154185. doi:10.1016/j.phymed.2022.154185

Zhang, Y., Jiang, Z., Xue, M., Zhang, S., Wang, Y., and Zhang, L. (2012). Toxicogenomic analysis of the gene expression changes in rat liver after a 28-day oral Tripterygium wilfordii multiglycoside exposure. *J. Ethnopharmacol.* 141, 170–177. doi:10.1016/j.jep.2012.02.015

Zhou, Y. Y., Xia, X., Peng, W. K., Wang, Q. H., Peng, J. H., and Li, Y. L., (2018). The effectiveness and safety of Tripterygium wilfordii hook. F extracts in rheumatoid arthritis: A systematic review and meta-analysis. *Front. Pharmacol.* 9, 356–410. doi:10.3389/fphar.2018.00356

frontiers | Frontiers in Pharmacology

TYPE Original Research
PUBLISHED 24 November 2022
DOI 10.3389/fphar.2022.1036589

OPEN ACCESS

EDITED BY
Kah Keng Wong,
Universiti Sains Malaysia Health Campus, Malaysia

REVIEWED BY
Jianing Mi,
Guangdong Provincial Hospital of Chinese Medicine, China
Richou Han,
Guangdong Institute of Applied Biological Resources, China

*CORRESPONDENCE
Li Zhou,
zhouli_jerry@whu.edu.cn
Sheng Li,
lisheng-znyy@whu.edu.cn
Hankun Hu,
huhankun@whu.edu.cn

†These authors have contributed equally to this work

SPECIALTY SECTION
This article was submitted to Ethnopharmacology, a section of the journal Frontiers in Pharmacology

RECEIVED 04 September 2022
ACCEPTED 14 November 2022
PUBLISHED 24 November 2022

CITATION
Guo S, Lin M, Xie D, Zhang W, Zhang M, Zhou L, Li S and Hu H (2022), Comparative metabolic profiling of wild *Cordyceps* species and their substituents by liquid chromatography-tandem mass spectrometry. *Front. Pharmacol.* 13:1036589. doi: 10.3389/fphar.2022.1036589

Comparative metabolic profiling of wild *Cordyceps* species and their substituents by liquid chromatography-tandem mass spectrometry

Shan Guo[1†], Manting Lin[2,3†], Di Xie[2], Wenqing Zhang[2], Mi Zhang[2], Li Zhou[4*], Sheng Li[1,5,6*] and Hankun Hu[2,7*]

[1]Department of Biological Repositories, Zhongnan Hospital of Wuhan University, Wuhan, Hubei, China, [2]Department of Pharmacy, Zhongnan Hospital of Wuhan University, Wuhan, Hubei, China, [3]Department of Pharmacy, Xiamen Maluan Bay Hospital, Xiamen, Fujian, China, [4]Animal Biosafety Level III Laboratory, Wuhan University School of Basic Medical Sciences, Wuhan, Hubei, China, [5]Department of Urology, Zhongnan Hospital of Wuhan University, Wuhan, Hubei, China, [6]Tumor Precision Diagnosis and Treatment Technology and Translational Medicine, Hubei Engineering Research Center, Wuhan, Hubei, China, [7]School of Pharmaceutical Sciences, Wuhan University, Wuhan, Hubei, China

Cordyceps is a genus of ascomycete fungi and used widely in fungal drugs. However, in-depth studies of the metabolites of wild *Cordyceps* species and their substituents are lacking. In this study, a liquid chromatography-tandem mass spectrometry (LC-MS/MS)-based metabolomics analysis was carried out to comprehensively profile the metabolites in wild Chinese *Cordyceps* species (*Ophiocordyceps sinensis* (Berk.) G.H. Sung, J.M. Sung, Hywel-Jones and Spatafora 2007) from Naqu (NCs) and Yushu (YCs) and their substituents including artificially cultivated *Cordyceps* species (CCs) and mycelia. A total of 901 metabolites were identified in these samples, including lipids, amino acids, nucleosides, carbohydrates, organic acids, coenzymes, vitamins, alkaloids and their derivatives. Univariate and multivariate statistical analyses revealed remarkable differences and significantly different metabolites among them. Seventy amino acid-relevant metabolites were analyzed quantitatively in four samples for the first time. The four samples contained abundant L-glutamic acid and oxidized glutathione as well as multiple unique amino acid-relevant metabolites (e.g., 3-chloro-L-tyrosine, 6-aminocaproic acid, L-theanine, anserine, γ-glutamyl-cysteine). Collectively, our study provides rich metabolic information of wild *Cordyceps* species and their substituents, which could facilitate their quality control and optimal utilization.

KEYWORDS

wild *Cordyceps* species, cultivated *Cordyceps* species, mycelia, metabolic profiling, liquid chromatography-tandem mass spectrometry

Introduction

Cordyceps is a genus of ascomycete fungi. *Cordyceps* species are highly valued tonic foods and well-known fungal drugs. Studies have demonstrated the diverse pharmaceutical effects of *Cordyceps* species-based products (Kuo et al., 1996; Zhang et al., 2005; Hsu et al., 2008; Yang et al., 2011; Zhang et al., 2014; Mi et al., 2018; Cheng et al., 2020) and revealed various chemical constituents, such as nucleosides, lipids, saccharides, mannitol, and amino acids (Zhao et al., 2014; Liu et al., 2015).

However, *Cordyceps* species are rarely found in the wild, and their substituents are desired (Li et al., 2019). The fermented mycelia of wild *Cordyceps* species are popular, and have been made into medical and functional products in the forms of capsules, tablets, or granulations (Dong et al., 2015; Zhao et al., 2020). Besides, Sunshine Lake Pharma (Dongguan, China) has undertaken artificial cultivation of Chinese *Cordyceps* species. *Ophiocordyceps sinensis* (Berk.) G.H. Sung, J.M. Sung, Hywel-Jones & Spatafora 2007 (known previously as *Cordyceps sinensis*) is a fungus that grows on insects in the family Ophiocordycipitaceae (Li et al., 2019). *O. sinensis* is a form of wild *Cordyceps* species. The annual yield of cultured *Cordyceps* species (CCs) reaches tens of tons, accounting for ≥20% of the total natural resource (Li et al., 2019). However, whether wild *Cordyceps* species (e.g., *O. sinensis*) and such substituents have chemical homogeneity is controversial.

Metabolomics analysis has become a powerful approach for large-scale study of metabolites in biological samples (Patti et al., 2012). In general, two analytical methods are used to conduct metabolomics analysis: nuclear magnetic resonance (NMR) spectroscopy and mass spectrometry (MS) (Perez et al., 2021). Compared with MS, NMR provides unique structural information. Nonetheless, it has limited sensitivity when measuring a large number of metabolites with a wide dynamic range (Lu et al., 2019; Perez et al., 2021). With regard to MS-based metabolic profiling, gas chromatography (GC) and liquid chromatography (LC) are hyphenated to MS for more accurate identification of metabolites. GC-MS often requires further derivatization of metabolites, and makes them more volatile and more thermally stable (Smart et al., 2010; Zhang et al., 2020). Nevertheless, LC-MS can detect thermally labile metabolites directly without derivatization, and is used more widely for metabolite profiling. LC-MS-based metabolomics analysis has been applied to analyze a certain class of metabolites (e.g., lipid, nucleoside, nucleobase, nucleotide, protein) (Fan et al., 2006; Mi et al., 2016; Cheng et al., 2017; Zhang et al., 2018; Jia et al., 2019; Lin et al., 2022) or dozens of metabolites (Wang et al., 2015; Zhang et al., 2015; Chen et al., 2018; He et al., 2019; Yao et al., 2019) in wild *Cordyceps* species and/or their substituents. However, few studies have profiled hundreds of metabolites in wild *Cordyceps* species or cultivated *Cordyceps* species and their mycelia for more comprehensive assessment of their chemical composition and alterations.

In this study, we leveraged liquid chromatography-electrospray ionization-tandem mass spectrometry (LC-ESI-MS/MS) to comprehensively survey metabolites in wild *Cordyceps* species (*O. sinensis*) from Naqu (Tibet, China; NCs) and Yushu (Qinghai, China; YCs), CCs (*O. sinensis*), and mycelia (*Hirsutella sinensis* X.J. Liu, Y.L. Guo, Y.X. Yu & W. Zeng 1989) from Bailing capsules (BLs). Using univariate and multivariate statistical analyses, chemical differences among NCs, YCs, CCs, and BLs were evaluated. Furthermore, differential metabolites among four samples were screened out and enrichment analysis using the Kyoto Encyclopedia of Genes and Genomes (KEGG) database was undertaken. Besides, 70 amino acid-relevant metabolites in these four samples were analyzed quantitatively. Taken together, this work provides a holistic insight into the metabolic differences in wild *Cordyceps* species and their substituents.

Materials and methods

Materials and reagents

Wild *Cordyceps* species (*O. sinensis* (Berk.) G.H. Sung, J.M. Sung, Hywel-Jones & Spatafora 2007), from Naqu (NCs) and Yushu (YCs) were acquired from Hubei Tianji Pharmaceuticals (Hubei, China) and Qinghai Yuanzu Biological Technology (Qinghai, China), respectively. Artificially cultivated *Cordyceps* species (*O. sinensis*; catalog number = 200111-I01) was purchased from Sunshine Lake Pharma (Guangdong, China). BLs containing *H. sinensis* X.J. Liu, Y.L. Guo, Y.X. Yu & W. Zeng 1989 (1911355) were obtained from Zhongmei East China Pharmaceuticals (Zhejiang, China). Methanol (I1069707004) and acetonitrile (JA095830) were sourced from Merck (Darmstadt, Germany). Formic acid (RH208519) was purchased from Aladdin (Shanghai, China). Standards for quantitative analysis of amino acid-relevant metabolites are shown in Supplementary Table S1. [2H2]L-threonine [IsoReag (Shanghai, China); 21J161-G1] was used as an internal standard and added to calibrate as-prepared *Cordyceps* samples, compensating for losses during sample preparation or variability during analytical determination.

Liquid chromatography-tandem mass spectrometry for metabolic profiling of wild and cultivated species of *Cordyceps* and mycelia

To extract metabolites, 50 mg of each sample was first weighed and homogenized with steel balls at 30 Hz for 3 min. Then, 1 ml of a methanol:water mixture (7:3) was added, and the mixture was vortex-mixed for 5 min followed by centrifugation (12,000 rpm, 10 min, 4°C). Subsequently, the supernatant

(400 μl) was collected and stored at −20°C overnight. Finally, the supernatant was centrifuged again (12,000 rpm, 3 min, 4°C), and 200 μl of supernatant pipetted for LC-MS.

Chromatographic separation was undertaken on a Shim-pack CBM30A ultra-high-pressure liquid chromatography (UPLC) system (Shimadzu, Kyoto, Japan). An Acquity HSS T3 C18 column (2.1 mm × 100 mm, 1.8 μm; Waters, Milford, MA, United States) was used for LC and its temperature were maintained at 40°C. Mobile phase A was H_2O with 0.1% formic acid. Mobile phase B was acetonitrile with 0.1% formic acid. Gradient elution was: 0–10 min, 5%–90% B; 10–11 min, 90% B; 11–11.1 min, 90%–5% B; 11.1–14 min, 5% B. The flow rate was 0.35 ml/min and the injection volume was 2 μl.

A Triple Quad™ 6500+ MS (Sciex, Framingham, MA, United States) instrument was operated in electrospray ionization in positive (ESI+) and negative (ESI−) modes with the following parameters: positive ion spray voltage, 5500 V; negative ion spray voltage, −4500 V; source temperature, 500°C; ion source gas 1, 50 psi; ion source gas 2, 50 psi; curtain gas, 25 psi; collision gas, high. A specific set of multiple reaction monitoring (MRM) transitions was recorded for each period according to the metabolites eluted within this period.

Liquid chromatography-tandem mass spectrometry for quantifying amino acid-relevant metabolites

Similarly, 50 mg of each sample was weighed and homogenized with steel balls at 30 Hz for 3 min. Then, 500 μl of a methanol:water (7:3) mixture containing [2H2]L-threonine was added. The mixture was vortex-mixed for 5 min followed by centrifugation (12,000 rpm, 10 min, 4°C). Subsequently, the supernatant (300 μl) was collected and stored at −20°C for 30 min. Finally, the supernatant was centrifuged again (12,000 rpm, 10 min, 4°C) and 200 μl of the supernatant was pipetted for LC-MS.

Chromatographic separation was achieved on an ExionLC AD UPLC system (Sciex) with an Acquity BEH Amide column (2.1 mm × 100 mm, 1.7 μm). The column temperature was maintained at 40°C. Mobile phase A was H_2O with ammonium acetate (2 mM) and 0.04% formic acid. Mobile phase B was acetonitrile with ammonium acetate (2 mM) and 0.04% formic acid. Gradient elution was: 0–1.2 min, 90% B; 1.2–9 min, 90%–60% B; 9–10 min, 60%–40% B; 10–11 min, 40% B; 11–15 min, 40%–90% B. The flow rate was 0.35 ml/min, and the injection volume was 2 μl.

Acquisition of MS data was undertaken on a Triple Quad™ 6500+ MS system (Sciex) in MRM mode with the following parameters: positive ion spray voltage, 5500 V; negative ion spray voltage, −4500 V; source temperature, 550°C; ion source gas 1, 50 psi; ion source gas 2, 50 psi; curtain gas, 35 psi; collision gas, medium.

Data processing

Metabolites were identified by matching the retention time, precursor ions/product ions, and MS/MS spectra to the self-compiled MetWare database (MetWare Biological Science and Technology, Wuhan, China) and public databases [METLIN (https://massconsortium.com/), Human Metabolome Database (HMDB; https://hmdb.ca/), KEGG (www.genome.jp/)] using Analyst 1.6.3 (Sciex). The integration and calibration of chromatographic peaks were done with MultiQuant 3.0.3 (Sciex).

Statistical analyses

Principal component analysis (PCA) and orthogonal partial least squares-discriminant analysis (OPLS-DA) were conducted in R (R Institute for Statistical Computing, Vienna, Austria) using the statistics function "prcomp" and "MetaboAnalystR" package, respectively. Hierarchical clustering analysis (HCA) and the Pearson correlation coefficient were carried out by the R package "ComplexHeatmap."

Results and discussion

Liquid chromatography-tandem mass spectrometry-based wide-targeted metabolomics analysis for the characterization of metabolites in wild *Cordyceps* species and their substituents

LC-MS-based strategies for metabolomics analysis can be targeted or untargeted (Patti et al., 2012). Untargeted metabolomics analysis is dependent upon high-resolution MS to measure metabolites without bias. Typically, targeted metabolomics analysis uses MRM on MS/MS to analyze *a priori* defined metabolites with high sensitivity and quantitative reproducibility. In this work, a LC-MS/MS-based wide-targeted metabolomics analysis was employed to comprehensively identify metabolites and assess their alterations in wild Chinese *Cordyceps* species (*O. sinensis* (Berk.) G.H. Sung, J.M. Sung, Hywel-Jones & Spatafora 2007; NCs and YCs) and their substituents, including artificially cultivated *Cordyceps* species (CCs) and fermented mycelia (BLs). Total ion chromatographs of sample metabolomic analysis in ESI+ and ESI− modes are shown in Supplementary Figure S1. A total of 901 metabolites were detected in pooled quality control (QC) samples comprising extracts of NCs, YCs,

TABLE 1 Metabolites detected in pooled QC samples comprising extracts of NCs, YCs, CCs, and BLs.

Classes	Subclasses	Number	Total
Lipids	Glycerophospholipids	63	181
	Glycerolipids	10	
	Sphingolipids	1	
	Oxidized lipids	28	
	Fatty acyls	79	
Amino acid and its derivatives	Amino acids	36	210
	Amino acid derivatives	92	
	Small peptides	82	
Nucleotide and its derivatives	Nucleotide and its derivatives	83	83
Carbohydrate and its derivatives	Phosphate sugars	13	51
	Sugar alcohols	7	
	Sugars	22	
	Sugar acids	6	
	Sugar derivatives	3	
Organic acid and its derivatives	Sulfonic acids	6	135
	Phosphoric acids	7	
	Organic acid and its derivatives	122	
Coenzyme and vitamins	Coenzyme and vitamins	23	23
Alkaloids	Alkaloids	1	1
Others	Benzene and substituted derivatives	69	217
	Alcohols and amines	54	
	Heterocyclic compounds	49	
	Aldehyde, ketones, and esters	24	
	Tryptamines, cholines, and pigments	6	
	Hormones and hormone related compounds	4	
	Others	11	

CCs, and BLs. Table 1 shows that the chemical constituents of samples included lipids, amino acids, nucleotides, carbohydrates, organic acids, vitamins, and their derivatives or other small molecules. Notably, more lipids, amino acids, organic acids, and their derivatives were detected.

Specifically, in ESI + mode, 453, 466, 453, and 452 metabolites were detected in NCs, YCs, CCs, and BLs, respectively. In ESI− mode, 389, 385, 379, and 382 metabolites were detected in NCs, YCs, CCs, and BLs, respectively (Figure 1). Detailed information of metabolites detected in NCs, YCs, CCs, and BLs is displayed in Supplementary Table S2. A Venn diagram highlighted that 753 out of 901 metabolites were detected in these four samples (Figure 1B). Importantly, some widely used bioactive constituents or biomarkers were identified in all samples, such as nucleosides (e.g., cordycepin, adenosine), ergosterol, D-mannitol, and amino acids (e.g., tryptophan, glutamic acid) (Li et al., 2006; Yue et al., 2013; Zhao et al., 2014; Liu et al., 2015). Besides, 1, 2, 2, and 29 metabolites were only detected in NCs, YCs, CCs, and BLs, respectively (Figure 1B; Table 2). Collectively, we detected a wide variety of metabolites with large amounts in wild and cultivated *Cordyceps* species and mycelia, which facilitated comprehensive assessment of their differences.

Multivariate statistical analyses for assessment of differences between wild *Cordyceps* species and their substituents

To characterize differences between wild *Cordyceps* species and their substituents comprehensively, multivariate statistical analyses (PCA, OPLS-DA, clustering analysis, correlation analysis) were employed. Metabolites measured in QC samples with relative standard deviation <30% were used for subsequent analyses (Supplementary Table S2). Results of PCA (Figure 2A) and OPLS-DA (Figures 2B–F) clearly showed distinct sample clusters corresponding to NCs, YCs, CCs, and BLs, respectively. Besides, clustering analyses (Figure 2G) and correlation analyses (Figure 2H) indicated differential metabolites among NCs, YCs, CCs, and BLs. Notably, the differences between CCs and wild *Cordyceps* species

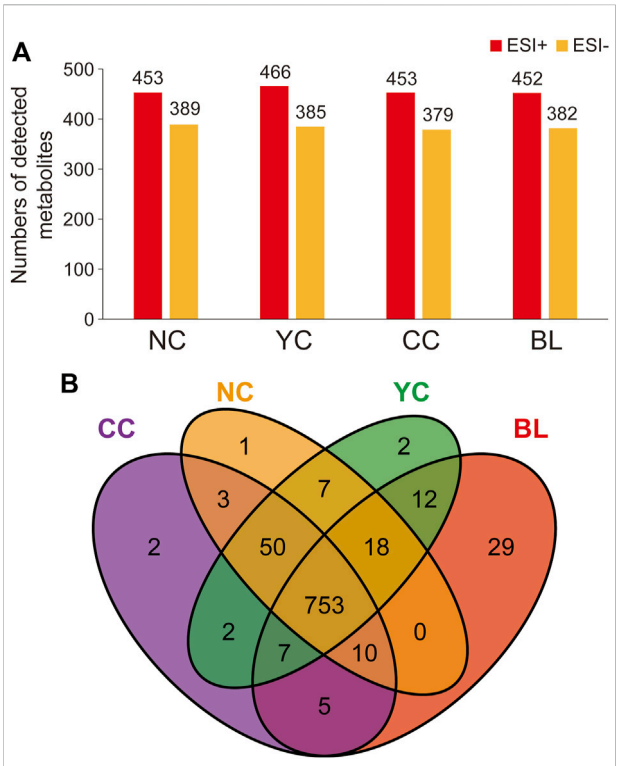

FIGURE 1
Metabolites identified in NCs, YCs, CCs, and BLs. **(A)** Numbers of metabolites detected from NCs, YCs, CCs, and BLs in ESI+ and ESI- modes, respectively. **(B)** Venn diagram of metabolites detected from NCs, YCs, CCs, and BLs.

(NCs and YCs) were less than those between BLs and wild *Cordyceps* species. The similarity between CCs and NCs was higher than that between CCs and YCs (Figure 2H). Taken together, these results suggested that metabolic differences were present among NCs, YCs, CCs, and BLs.

Differential metabolites between *Cordyceps* from Naqu and Yushu

Molecular features with variable importance in projection (VIP) ≥1 and fold change (FC) ≥2 or ≤0.5 were defined as significantly differential metabolites between two samples of *Cordyceps* species. A total of 365 differential metabolites (183 were up-regulated and 182 were down-regulated) between NCs and YCs were documented (Figure 3A). Furthermore, except for one alkaloid, all detected metabolite classes had an upward or downward trend in level (Supplementary Table S3). Furthermore, enrichment analysis using the KEGG database displayed that more differential metabolites between NCs and YCs were associated with biosynthesis of cofactors (Figure 3B). However, nine glycerolipids (MG (18:2 (9Z, 12Z)/0:0/0:0) [rac], glycidyl oleate, MAG (16:1) isomer, MAG (16:1), MG (20:5) isomer, MG (18:1 (9Z)/0:0/0:0) [rac], glycine linoleate, (±) 1,2-sebacyl glycerol (10:0), 2-palmitoyl-rac-glycerol) and one sphingolipid (Sphinganine 1-phosphate) were detected in both types of wild *Cordyceps* species. Besides, the contents of bioactive cordycepin (i.e., 3′-deoxyadenosine) and D-mannitol (i.e., cordycepic acid) were higher in NCs than YCs. Collectively, these data suggested that wild *Cordyceps* species from different habitats had some differential metabolites, indicating that local unique ecological factors may affect the chemical constituents of wild *Cordyceps* species.

Differential metabolites between wild and cultivated species of *Cordyceps*

Similarly, 356 significant differential metabolites (95 were up-regulated and 261 were down-regulated) were found between CCs and NCs, and 452 remarkably altered metabolites (147 were up-regulated and 305 were down-regulated) were found between CCs and YCs (VIP ≥1 and FC ≥ 2 or ≤0.5) (Figures 4A,B). Among them, there were 258 overlapped differential metabolites (including lipids, amino acids, nucleotides) between CCs and wild *Cordyceps* species (Figure 4C) and they are emboldened in Supplementary Tables S4, S5. Of note, the content of ergosterol was lower in CCs than in both types of wild *Cordyceps* species. Besides, six sugar acids (D-glucoronic acid, L-gulonolactone, D-glucarate, L-arabinonic acid-1,4-lactone, mucic acid, gluconic acid), and two sugar derivatives (N-acetyl-D-glucosamine, methyl beta-D-galactopyranoside) detected in wild and cultivated species of *Cordyceps* displayed no differences. Moreover, enrichment analyses using the KEGG database clearly showed that more significant differential metabolites between CCs and wild *Cordyceps* species were associated mainly with purine metabolism (Figures 4D,E). These results showed that CCs and wild *Cordyceps* species had different chemical constituents. On the one hand, this finding will provide promising indicators to discriminate artificially cultivated *Cordyceps* species from wild *Cordyceps* species (Zhang et al., 2015). On the other hand, this finding may encourage study of whether these differential metabolites between CCs and wild *Cordyceps* species are relevant to differences in their pharmacology.

Differential metabolites between bailing capsules and wild *Cordyceps* species

Compared with NCs, 625 metabolites were altered significantly in BLs (VIP ≥1; FC ≥ 2 or ≤0.5; 334 were up-regulated; 291 were down-regulated) (Figure 5A; Supplementary Table S6). Besides, 598 significantly different metabolites (324 were up-regulated and 274 were down-regulated) were found between BLs and YCs (Figure 5B; Supplementary Table S7). Figure 5C shows 522 overlapped differential metabolites between BLs and wild

TABLE 2 Metabolites found unique to NCs, YCs, CCs, and BLs, respectively.

Cordyceps samples	Unique metabolites	Subclasses
NC	3-Ketosphingosine	Alcohols and amines
YC	18-Hydroxyoleate	Fatty acyls
	N′-Formylkynurenine	Amino acid derivatives
CC	Carnitine C5:DC	Fatty acyls
	α-Cyclopiazonic acid	Benzene and substituted derivatives
BL	1-O-Palmitoyl-2-O-acetyl-sn-glycerol-3-phosphate choline	Glycerophospholipids
	1-(1Z-Hexadecenyl)-sn-glycero-3-phosphocholine	Glycerophospholipids
	LPA (18:2)	Glycerophospholipids
	(±)16-HETE	Oxidized lipids
	20-HETE	Oxidized lipids
	Xanthurenic acid	Amino acid derivatives
	S-(Indolylmethylthiohydroximoyl)-L-cysteine	Amino acid derivatives
	γ-Glutamyl-L-putrescine	Amino acid derivatives
	Histidyl-threoninyl-lysine	Small peptides
	Threoninyl-tyrosyl-lysine	Small peptides
	Glutaminyl-valine	Small peptides
	L-Alanyl-L-valine	Small peptides
	2-Amino-4,6-pteridinediol	Nucleotide and its derivatives
	Creatinine	Organic acid and its derivatives
	Indole-3-pyruvic acid	Organic acid and its derivatives
	3-Methoxyphenylacetic acid	Organic acid and its derivatives
	5-Methyltetrahydrofolate	Organic acid and its derivatives
	Methyl nicotinate	Coenzyme and vitamins
	4-Acetamidobutanoyl-CoA	Coenzyme and vitamins
	Acetaminophen glucuronide	Alcohols and amines
	5,7,22,24 (28)-Ergostatetraenol	Alcohols and amines
	1,3-Diphenylguanidine	Alcohols and amines
	N-Butylaniline	Alcohols and amines
	Isoxanthopterin	Heterocyclic compounds
	3-Indolepropionic acid	Heterocyclic compounds
	1-Methyl-hydantoin	Heterocyclic compounds
	α-[3-[(Hydroxymethyl)nitrosoamino]propyl]-3-pyridinemethanol	Heterocyclic compounds
	Methyl propyl disulfide	Others
	8,8a-Deoxy oleane	Others

Cordyceps species, and they are emboldened in Supplementary Tables S6, S7. There were more differential metabolites (including lipids, amino acids, nucleotides) between BLs and wild *Cordyceps* species (Figures 5A,B) than those between CCs and wild *Cordyceps* species (Figures 4A,B). For the well-known bioactive constituents, the cordycepin content was higher in BLs than in wild *Cordyceps* species, whereas the ergosterol content was lower in BLs. Likewise, these differential metabolites between BLs and wild *Cordyceps* species could facilitate discrimination of adulteration in the processed products of wild *Cordyceps* species (Zhang et al., 2020). Besides, enrichment analyses using the KEGG database showed that differential metabolites between BLs and NCs and between BLs and YCs were located to different pathways (Figures 5D,E), which indicated that wild *Cordyceps* species from different habitats had metabolomic differences.

Quantitative analyses of amino acid-relevant metabolites in wild *Cordyceps* species and their substituents

Amino acids are important chemical and bioactive constituents in *Cordyceps* species (Zhang et al., 1991; Liu et al., 2015; Zhang et al., 2022) but have not been

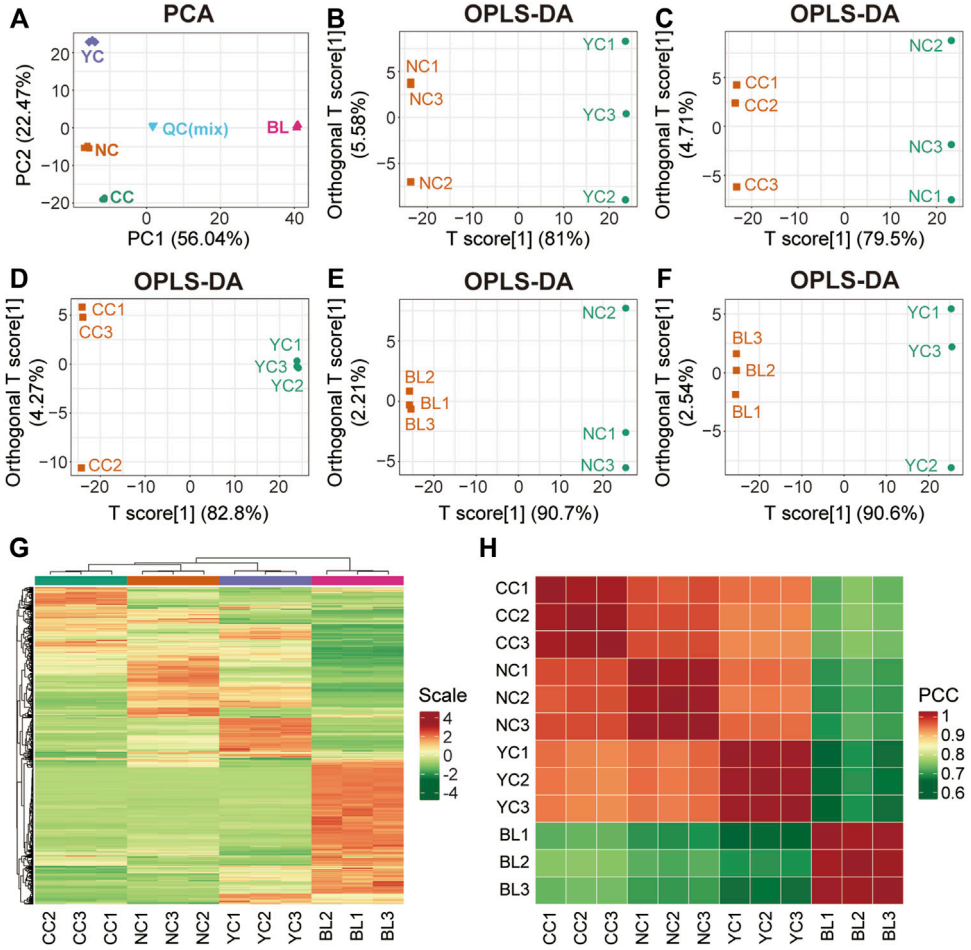

FIGURE 2
Multivariate statistical analyses of metabolites detected in NCs, YCs, CCs, and BLs. **(A)** PCA result. **(B–F)** Plots showing OPLS-DA scores. **(G)** Heatmap of hierarchical clustering analysis. **(H)** Heatmap of correlation analysis. PCC, Pearson's correlation coefficient.

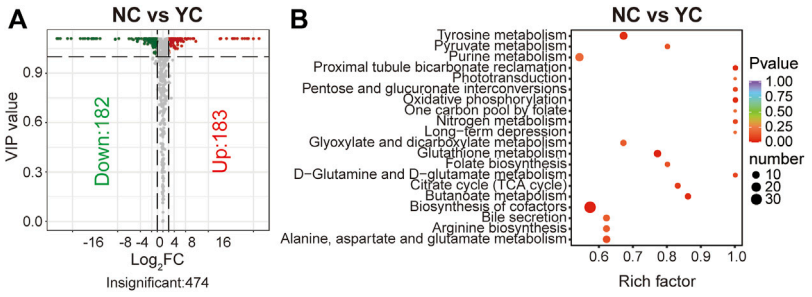

FIGURE 3
Differential analyses between NCs and YCs. **(A)** Volcano plot of differential metabolites between NCs and YCs. Differential metabolites were screened based on VIP ≥1 and FC ≥ 2 or ≤0.5. The fold change was the ratio of NCs to YCs. **(B)** Enrichment analysis of differential metabolites between NCs and YCs using the KEGG database. The top-20 enriched metabolic pathways (with *p*-values) are displayed.

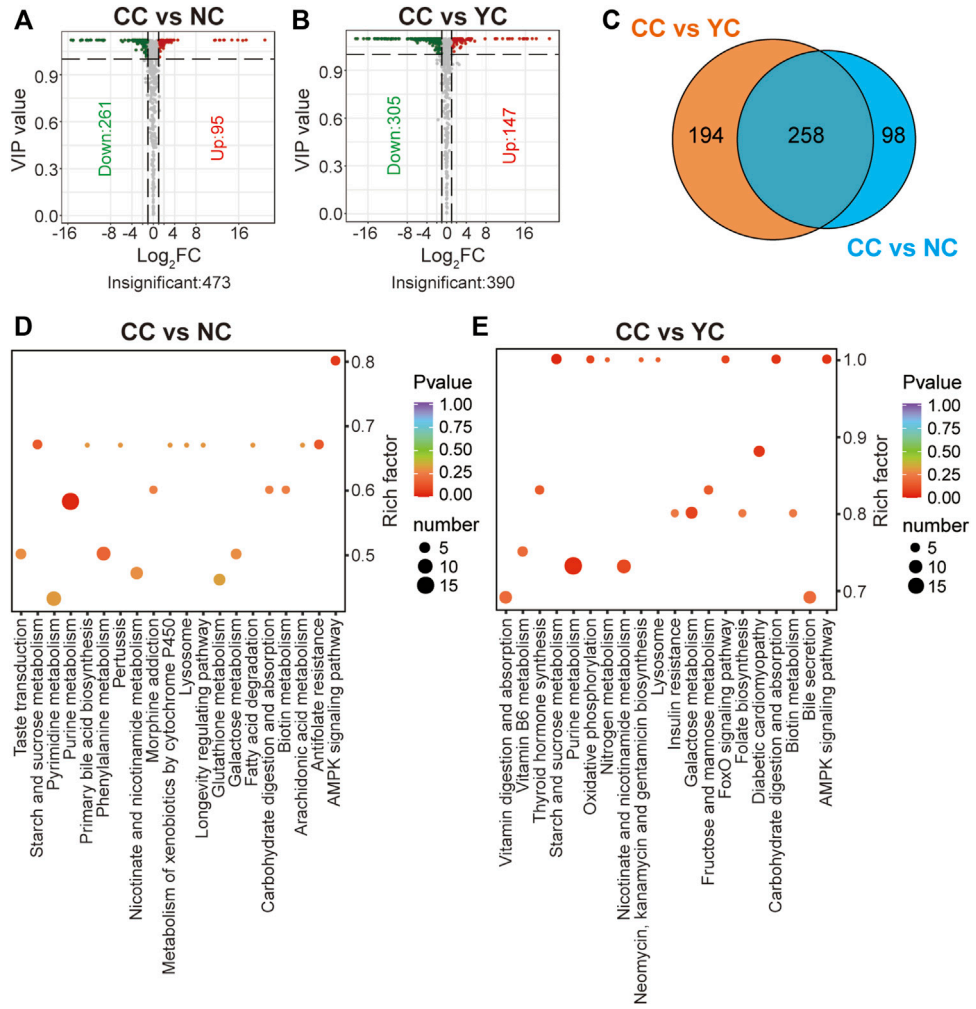

FIGURE 4
Differential analyses between CCs and wild *Cordyceps* species. **(A)** Volcano plot of differential metabolites between CCs and NCs. Differential metabolites were screened based on VIP ≥1 and FC ≥ 2 or ≤0.5. The fold change was the ratio of CCs to NCs. **(B)** Volcano plot of differential metabolites between CCs and YCs. Differential metabolites were screened based on VIP ≥1 and FC ≥ 2 or ≤0.5. The fold change was the ratio of CCs to YCs. **(C)** Venn diagram of differential metabolites between CCs and wild *Cordyceps* species. **(D)** Enrichment analysis of differential metabolites between CCs and NCs using the KEGG database. The top-20 KEGG enriched metabolic pathways (with *p*-values) are displayed. **(E)** Enrichment analysis of differential metabolites between CCs and YCs using the KEGG database. The top-20 KEGG enriched metabolic pathways (with *p*-values) are displayed.

characterized comprehensively previously. Here, 70 amino acids and their relevant metabolites in four samples were analyzed quantitatively. Figures 6A,B show the quantitative results of some amino acids and their derivatives. Figure 6C displays the quantitative results of 11 small peptides. Compared with widely targeted metabolic analyses (Supplementary Figure S2), most of these amino acid-relevant metabolites detected by targeted quantitative analyses showed consistent trends in alteration across four samples (Figure 6). However, 11 amino acids and their derivatives were not detected by widely targeted metabolic analysis (nicotinuric acid, 5-hydroxy-tryptophan, homoserine, 3-iodo-L-tyrosine, 3-chloro-L-tyrosine, N-acetylaspartate, L-leucine, L-theanine, argininosuccinic acid, 2-aminobutyric acid, 4-acetamidobutyric acid) (Supplementary Figures S2A,B). Targeted quantitative analyses showed such undetected metabolites with relatively low abundance (Figures 6A,B).

Additionally, absolute quantitative results showed that L-glutamic acid and oxidized glutathione had a high level in wild and cultivated species of *Cordyceps* and mycelia (Figures 6B,C). Notably, the content of L-glutamine and L-ornithine was significantly higher in wild and cultivated species of *Cordyceps* than that in BLs (Figure 6A). Furthermore, some unique amino acid-relevant metabolites were noted: 1) 3-chloro-L-tyrosine was not

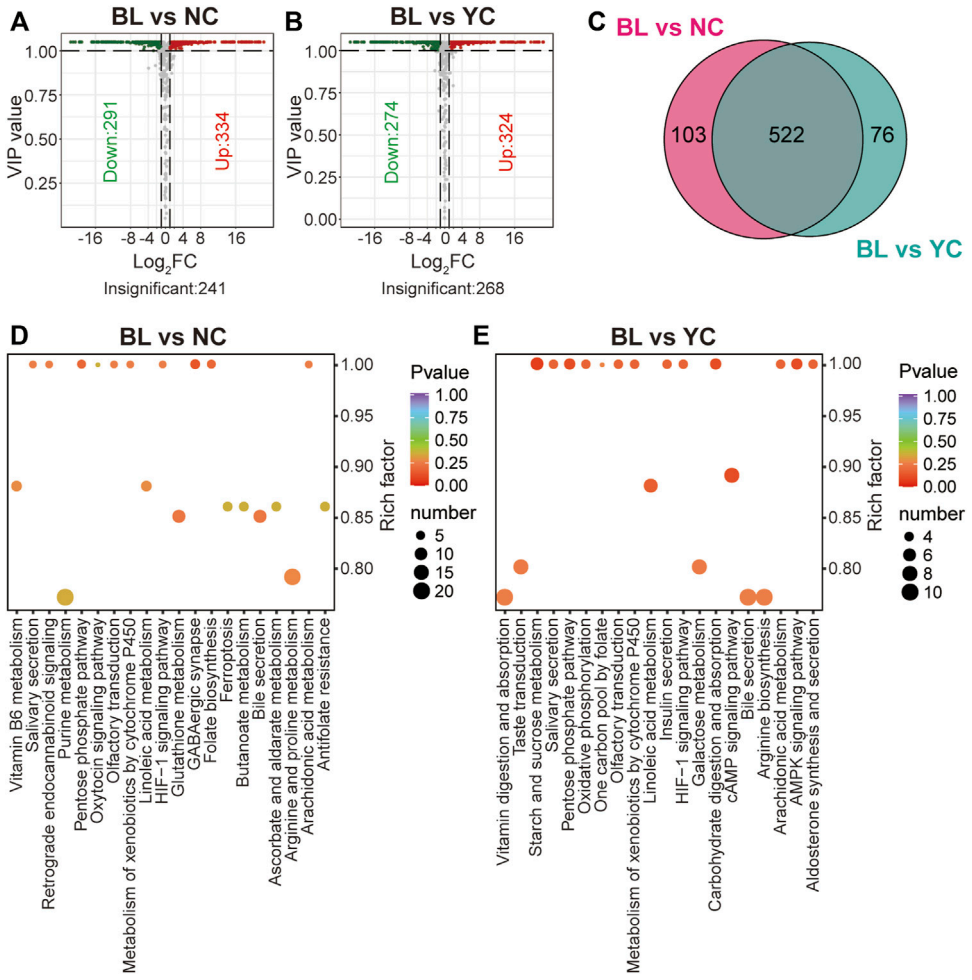

FIGURE 5
Differential analyses between BLs and wild *Cordyceps* species **(A)** Volcano plot of differential metabolites between BLs and NCs. Differential metabolites were screened based on VIP ≥1 and FC ≥ 2 or ≤0.5. The fold change was the ratio of BLs to NCs. **(B)** Volcano plot of differential metabolites between BLs and YCs. Differential metabolites were screened based on VIP ≥1 and FC ≥ 2 or ≤0.5. The fold change was the ratio of BLs to NCs. **(C)** Venn diagram of differential metabolites between BLs and wild *Cordyceps* species. **(D)** Enrichment analysis of differential metabolites between BLs and NCs using the KEGG database. The top-20 enriched pathways (with *p*-values) are displayed. **(E)** Enrichment analysis of differential metabolites between BLs and YCs using the KEGG database. The top-20 enriched pathways (with *p*-values) are displayed.

detected in CCs and BLs, but was present in wild *Cordyceps* species (Figure 6A); 2) 6-aminocaproic acid was not detected in YCs but was present in NCs, CCs, and BLs (Figure 6B); 3) L-theanine was not detected in wild and cultivated species of *Cordyceps* but was present in BLs (Figure 6B); 4) anserine and γ-glutamyl-cysteine were not detected in CCs and BLs, respectively (Figure 6C).

Conclusion

In summary, this work performed a comparative metabolic profiling to comprehensively characterize metabolites and assess their alterations in wild *Cordyceps* species (*O. sinensis* (Berk.) G.H. Sung, J.M. Sung, Hywel-Jones & Spatafora 2007) and their substituents. LC-MS/MS-based widely targeted approach measured 901 metabolites in *Cordyceps* samples, including lipids, amino acids, nucleosides, carbohydrates, organic acids, coenzymes, vitamins, alkaloids and their derivatives. Univariate and multivariate statistical analyses revealed metabolic differences among wild *Cordyceps* species from different habitats, cultivated *Cordyceps* species, and mycelia, and covered all the detected metabolite classes. Enrichment analyses using the KEGG database clearly showed differential metabolic pathways among four samples. Importantly, some amino acid-relevant metabolites were found to be unique to wild *Cordyceps* species (e.g., 3-chloro-L-tyrosine) or their substituents (e.g., L-theanine). These differences revealed among wild and cultivated *Cordyceps*

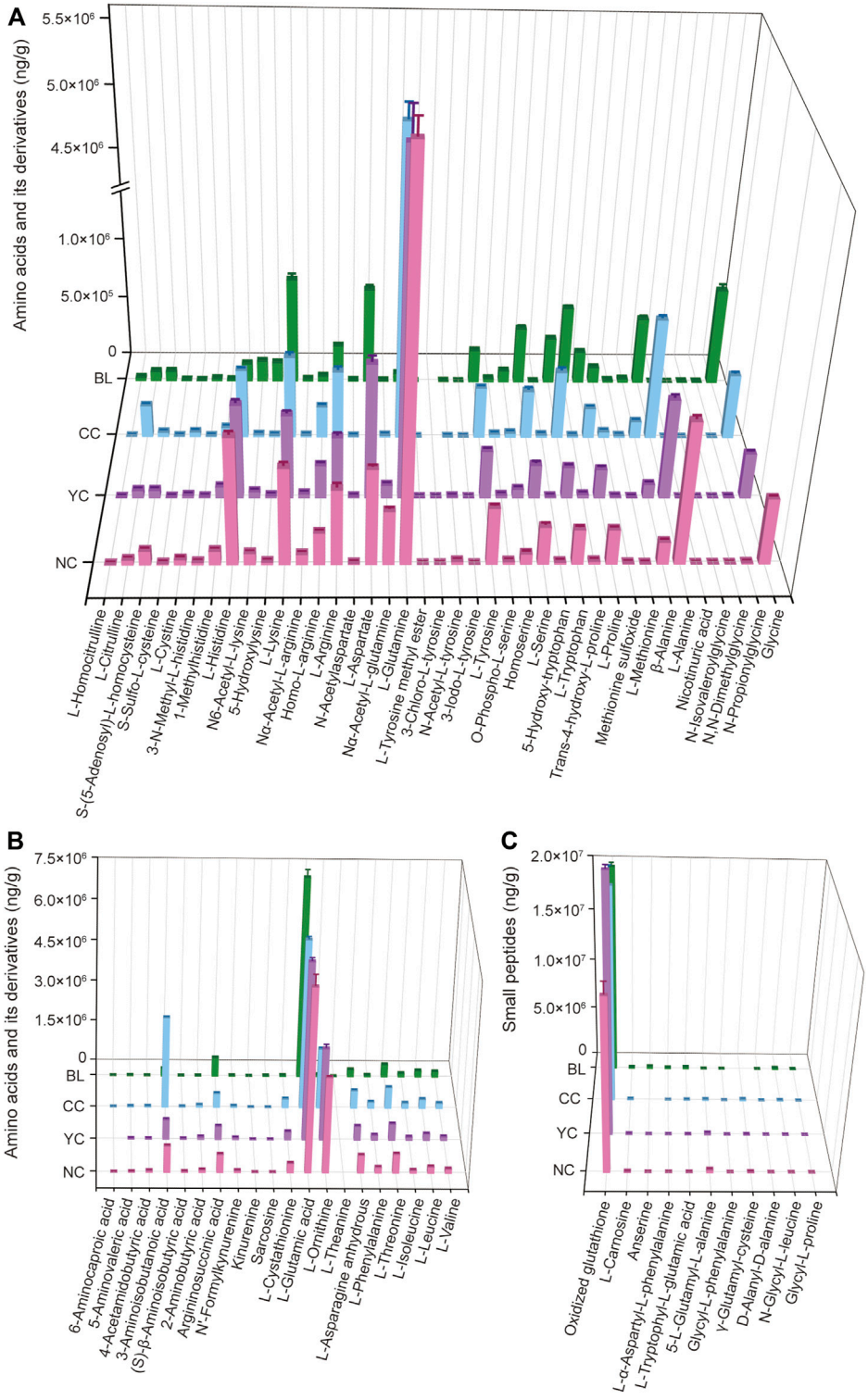

FIGURE 6
Absolute quantitative results of some amino acids and their derivatives **(A,B)** and small peptides **(C)** in wild and cultivated *Cordyceps* species and BLs.

species and mycelia could facilitate rational utilization and better QC.

Data availability statement

The original contributions presented in the study are included in the article/Supplementary Material, further inquiries can be directed to the corresponding authors.

Author contributions

SG and ML designed the experiments, analyzed the data, and prepared the manuscript. DX, WZ, and MZ carried out the experiments and recorded the data. LZ optimized the language of the manuscript. SL and HH revised the manuscript. All authors agreed to submission of the final version of the manuscript.

Funding

This work was supported by the Traditional Chinese Medicine Research Project of Hubei Provincial Health Commission (ZY 2019M033), Science and Technology Innovation Cultivation Fund of Zhongnan Hospital of Wuhan University (znpy2019093), and Program of Excellent Doctoral (Postdoctoral) of Zhongnan Hospital of Wuhan University (ZNYB2019015).

Conflict of interest

The authors declare that the research was conducted in the absence of any commercial or financial relationships that could be construed as a potential conflict of interest.

Publisher's note

All claims expressed in this article are solely those of the authors and do not necessarily represent those of their affiliated organizations, or those of the publisher, the editors and the reviewers. Any product that may be evaluated in this article, or claim that may be made by its manufacturer, is not guaranteed or endorsed by the publisher.

Supplementary material

The Supplementary Material for this article can be found online at: https://www.frontiersin.org/articles/10.3389/fphar.2022.1036589/full#supplementary-material

SUPPLEMENTARY FIGURE S1
Total ion chromatograms of LC-MS/MS-based metabolic analysis of *Cordyceps* samples in positive and negative ion modes.

SUPPLEMENTARY FIGURE S2
Peak areas of amino acids and their derivatives **(A,B)** and small peptides **(C)** detected in NCs, YCs, CCs, and BLs.

References

Chen, L., Liu, Y., Guo, Q., Zheng, Q., and Zhang, W. (2018). Metabolomic comparison between wild *Ophiocordyceps sinensis* and artificial cultured *Cordyceps militaris*. *Biomed. Chromatogr.* 32, e4279. doi:10.1002/bmc.4279

Cheng, W., Zhang, X., Song, Q., Lu, W., Wu, T., Zhang, Q., et al. (2017). Determination and comparative analysis of 13 nucleosides and nucleobases in natural fruiting body of *Ophiocordyceps sinensis* and its substitutes. *Mycology* 8 (4), 318–326. doi:10.1080/21501203.2017.1385546

Cheng, J., Song, J., Wei, H., Wang, Y., Huang, X., Liu, Y., et al. (2020). Structural characterization and hypoglycemic activity of an intracellular polysaccharide from *Sanghuangporus sanghuang* mycelia. *Int. J. Biol. Macromol.* 164, 3305–3314. doi:10.1016/j.ijbiomac.2020.08.202

Dong, C., Guo, S., Wang, W., and Liu, X. (2015). *Cordyceps* industry in China. *Mycology* 6 (2), 121–129. doi:10.1080/21501203.2015.1043967

Fan, H., Li, S., Xiang, J., Lai, C., Yang, F., Gao, J., et al. (2006). Qualitative and quantitative determination of nucleosides, bases and their analogues in natural and cultured *Cordyceps* by pressurized liquid extraction and high performance liquid chromatography–electrospray ionization tandem mass spectrometry (HPLC–ESI–MS/MS). *Anal. Chim. Acta X.* 567 (2), 218–228. doi:10.1016/j.aca.2006.03.032

He, Y., Zhang, W., Peng, F., Lu, R., Zhou, H., Bao, G., et al. (2019). Metabolomic variation in wild and cultured cordyceps and mycelia of *Isaria cicadae*. *Biomed. Chromatogr.* 33 (4), e4478. doi:10.1002/bmc.4478

Hsu, C. H., Sun, H. L., Sheu, J. N., Ku, M. S., Hu, C. M., Chan, Y., et al. (2008). Effects of the immunomodulatory agent *Cordyceps militaris* on airway inflammation in a mouse asthma model. *Pediatr. Neonatol.* 49 (5), 171–178. doi:10.1016/S1875-9572(09)60004-8

Jia, W., Shi, L., Zhang, F., Chang, J., and Chu, X. (2019). High-throughput screening of the nucleosides and nucleotides using characteristic structural fragments fusion. *J. Pharm. Biomed. Anal.* 175, 112787. doi:10.1016/j.jpba.2019.112787

Kuo, Y. C., Tsai, W. J., Shiao, M. S., Chen, C. F., and Lin, C. Y. (1996). *Cordyceps sinensis* as an immunomodulatory agent. *Am. J. Chin. Med.* 24 (2), 111–125. doi:10.1142/S0192415X96000165

Li, S. P., Yang, F. Q., and Tsim, K. W. K. (2006). Quality control of *Cordyceps sinensis*, a valued traditional Chinese medicine. *J. Pharm. Biomed. Anal.* 41 (5), 1571–1584. doi:10.1016/j.jpba.2006.01.046

Li, X., Liu, Q., Li, W., Li, Q., Qian, Z., Liu, X., et al. (2019). A breakthrough in the artificial cultivation of Chinese *cordyceps* on a large-scale and its impact on science, the economy, and industry. *Crit. Rev. Biotechnol.* 39 (2), 181–191. doi:10.1080/07388551.2018.1531820

Lin, M., Guo, S., Xie, D., Li, S., and Hu, H. (2022). Lipidomic profiling of wild *cordyceps* and its substituents by liquid chromatography-electrospray ionization-tandem mass spectrometry. *Lwt-Food Sci. Technol.* 163, 113497. doi:10.1016/j.lwt.2022.113497

Liu, Y., Wang, J., Wang, W., Zhang, H., Zhang, X., and Han, C. (2015). The chemical constituents and pharmacological actions of *Cordyceps sinensis*. *Evid. Based. Complement. Altern. Med.* 2015, 575063. doi:10.1155/2015/575063

Lu, Y., Zhi, Y., Miyakawa, T., and Tanokura, M. (2019). Metabolic profiling of natural and cultured *Cordyceps* by NMR spectroscopy. *Sci. Rep.* 9 (1), 7735. doi:10.1038/s41598-019-44154-x

Mi, J. N., Wang, J. R., and Jiang, Z. H. (2016). Quantitative profiling of sphingolipids in wild *Cordyceps* and its mycelia by using UHPLC-MS. *Sci. Rep.* 6, 20870. doi:10.1038/srep20870

Mi, J., Han, Y., Xu, Y., Kou, J., Li, W. J., Wang, J. R., et al. (2018). Deep profiling of immunosuppressive glycosphingolipids and sphingomyelins in wild *cordyceps*. *J. Agric. Food Chem.* 66 (34), 8991–8998. doi:10.1021/acs.jafc.8b02706

Patti, G. J., Yanes, O., and Siuzdak, G. (2012). Innovation: Metabolomics: The apogee of the omics trilogy. *Nat. Rev. Mol. Cell Biol.* 13 (4), 263–269. doi:10.1038/nrm3314

Perez, D. S. L., Alseekh, S., Scossa, F., and Fernie, A. R. (2021). Ultra-high-performance liquid chromatography high-resolution mass spectrometry variants for metabolomics research. *Nat. Methods* 18 (7), 733–746. doi:10.1038/s41592-021-01116-4

Smart, K. F., Aggio, R. B., Van Houtte, J. R., and Villas-Boas, S. G. (2010). Analytical platform for metabolome analysis of microbial cells using methyl chloroformate derivatization followed by gas chromatography-mass spectrometry. *Nat. Protoc.* 5 (10), 1709–1729. doi:10.1038/nprot.2010.108

Wang, J., Kan, L., Nie, S., Chen, H., Cui, S. W., Phillips, A. O., et al. (2015). A comparison of chemical composition, bioactive components and antioxidant activity of natural and cultured *Cordyceps sinensis*. *LWT - Food Sci. Technol.* 63 (1), 2–7. doi:10.1016/j.lwt.2015.03.109

Yang, M. L., Kuo, P. C., Hwang, T. L., and Wu, T. S. (2011). Anti-inflammatory principles from *Cordyceps sinensis*. *J. Nat. Prod.* 74 (9), 1996–2000. doi:10.1021/np100902f

Yao, C. L., Qian, Z. M., Tian, W. S., Xu, X. Q., Yan, Y., Shen, Y., et al. (2019). Profiling and identification of aqueous extract of *Cordyceps sinensis* by ultra-high performance liquid chromatography tandem quadrupole-orbitrap mass spectrometry. *Chin. J. Nat. Med.* 17 (8), 631–640. doi:10.1016/S1875-5364(19)30066-4

Yue, K., Ye, M., Zhou, Z., Sun, W., and Lin, X. (2013). The genus *cordyceps*: A chemical and pharmacological review. *J. Pharm. Pharmacol.* 65 (4), 474–493. doi:10.1111/j.2042-7158.2012.01601.x

Zhang, S. S., Zhang, D. S., Zhu, T. J., and Chen, X. Y. (1991). A pharmacological analysis of the amino acid components of *Cordyceps sinensis* Sacc. *Yao Xue Xue Bao* 26 (5), 326–330. doi:10.16438/j.0513-4870.1991.05.002

Zhang, W., Yang, J., Chen, J., Hou, Y., and Han, X. (2005). Immunomodulatory and antitumour effects of an exopolysaccharide fraction from cultivated *Cordyceps sinensis* (Chinese caterpillar fungus) on tumour-bearing mice. *Biotechnol. Appl. Biochem.* 42, 9–15. doi:10.1042/BA20040183

Zhang, H. W., Lin, Z. X., Tung, Y. S., Kwan, T. H., Mok, C. K., Leung, C., et al. (2014). *Cordyceps sinensis* (a traditional Chinese medicine) for treating chronic kidney disease. *Cochrane Database Syst. Rev.* 12, CD008353. doi:10.1002/14651858.CD008353.pub2

Zhang, J., Wang, P., Wei, X., Li, L., Cheng, H., Wu, Y., et al. (2015). A metabolomics approach for authentication of *Ophiocordyceps sinensis* by liquid chromatography coupled with quadrupole time-of-flight mass spectrometry. *Food Res. Int.* 76, 489–497. doi:10.1016/j.foodres.2015.07.025

Zhang, X., Liu, Q., Zhou, W., Li, P., Alolga, R. N., Qi, L. W., et al. (2018). A comparative proteomic characterization and nutritional assessment of naturally- and artificially-cultivated *Cordyceps sinensis*. *J. Proteomics* 181, 24–35. doi:10.1016/j.jprot.2018.03.029

Zhang, J., Yu, H., Li, S., Zhong, X., Wang, H., and Liu, X. (2020). Comparative metabolic profiling of *Ophiocordyceps sinensis* and its cultured mycelia using GC-MS. *Food Res. Int.* 134, 109241. doi:10.1016/j.foodres.2020.109241

Zhang, Y., Liu, J., Wang, Y., Sun, C., Li, W., Qiu, J., et al. (2022). Nucleosides and amino acids, isolated from *Cordyceps sinensis*, protected against cyclophosphamide-induced myelosuppression in mice. *Nat. Prod. Res.*, 1–4. doi:10.1080/14786419.2022.2043307

Zhao, J., Xie, J., Wang, L. Y., and Li, S. P. (2014). Advanced development in chemical analysis of *Cordyceps*. *J. Pharm. Biomed. Anal.* 87, 271–289. doi:10.1016/j.jpba.2013.04.025

Zhao, J., Shi, T., Zhu, W., Chen, L., Guan, Y., and Jin, C. (2020). Quality control method of sterols in fermented *Cordyceps sinensis* based on combined fingerprint and quantitative analysis of multicomponents by single marker. *J. Food Sci.* 85 (10), 2994–3002. doi:10.1111/1750-3841.15412

frontiers | Frontiers in Pharmacology

TYPE Review
PUBLISHED 25 November 2022
DOI 10.3389/fphar.2022.1031051

OPEN ACCESS

EDITED BY
Yiider Tseng,
Shandong University of Traditional Chinese Medicine, China

REVIEWED BY
Xiaofei Zhang,
Shaanxi University of Chinese Medicine, China
Hua Yang,
China Pharmaceutical University, China

*CORRESPONDENCE
Ronghua Yang,
yrh96183@163.com
Hong Bai,
baihong@hust.edu.cn
Kang Ning,
ningkang@hust.edu.cn

†These authors have contributed equally to this work

SPECIALTY SECTION
This article was submitted to Ethnopharmacology, a section of the journal Frontiers in Pharmacology

RECEIVED 29 August 2022
ACCEPTED 15 November 2022
PUBLISHED 25 November 2022

CITATION
Zhu X, Yao Q, Yang P, Zhao D, Yang R, Bai H and Ning K (2022), Multi-omics approaches for in-depth understanding of therapeutic mechanism for Traditional Chinese Medicine. *Front. Pharmacol.* 13:1031051. doi: 10.3389/fphar.2022.1031051

Multi-omics approaches for in-depth understanding of therapeutic mechanism for Traditional Chinese Medicine

Xue Zhu[1†], Qi Yao[1†], Pengshuo Yang[1], Dan Zhao[1], Ronghua Yang[2*], Hong Bai[1*] and Kang Ning[1*]

[1]Key Laboratory of Molecular Biophysics of the Ministry of Education, Hubei Key Laboratory of Bioinformatics and Molecular-imaging, Center of AI Biology, Department of Bioinformatics and Systems Biology, College of Life Science and Technology, Huazhong University of Science and Technology, Wuhan, Hubei, China, [2]Dovetree Synbio Company Limited, Shenyang, China

Traditional Chinese Medicine (TCM) is extensively utilized in clinical practice due to its therapeutic and preventative treatments for various diseases. With the development of high-throughput sequencing and systems biology, TCM research was transformed from traditional experiment-based approaches to a combination of experiment-based and omics-based approaches. Numerous academics have explored the therapeutic mechanism of TCM formula by omics approaches, shifting TCM research from the "one-target, one-drug" to "multi-targets, multi-components" paradigm, which has greatly boosted the digitalization and internationalization of TCM. In this review, we concentrated on multi-omics approaches in principles and applications to gain a better understanding of TCM formulas against various diseases from several aspects. We first summarized frequently used TCM quality assessment methods, and suggested that incorporating both chemical and biological ingredients analytical methods could lead to a more comprehensive assessment of TCM. Secondly, we emphasized the significance of multi-omics approaches in deciphering the therapeutic mechanism of TCM formulas. Thirdly, we focused on TCM network analysis, which plays a vital role in TCM-diseases interaction, and serves for new drug discovery. Finally, as an essential source for storing multi-omics data, we evaluated and compared several TCM databases in terms of completeness and reliability. In summary, multi-omics approaches have infiltrated many aspects of TCM research. With the accumulation of omics data and data-mining resources, deeper understandings of the therapeutic mechanism of TCM have been acquired or will be gained in the future.

KEYWORDS

traditional Chinese medicine, multi-omics approaches, quality control, pharmacodynamic effects, network pharmacology analysis, TCM databases

Introduction

Traditional Chinese Medicine (TCM) has a long history of treating a variety of diseases around the world (Lan et al., 2015; Xiang et al., 2019; Runfeng et al., 2020). The most critical concerns of TCM are the quality of TCM formulas, as well as the effectiveness of TCM formulas, both of which have been extensively studied by researchers and physicians (Jia et al., 2017; Xin et al., 2018a; Xin et al., 2018b; Bai et al., 2019; Xiang et al., 2019; Ding et al., 2020; Liu et al., 2020; Chandrasekara et al., 2021). Western medications are typically prescribed individually for a specific effect with a single component. In contrast, classical TCM formulas, following TCM theory and the principle of "King, Vassal, Assistant, and Delivery servant," are comprehensive systems with "multiple ingredients, multiple targets, and multiple pathways" to exert the synergistic effect in the prevention and treatment of diseases (Yi and Chang, 2004; Wang and Zhang, 2017). Their complexity in terms of components (especially for these structurally similar components), metabolites, and bioactivities, also hampered research into the therapeutic mechanism of TCM in treating various diseases. With the development of high-throughput sequencing technology, system biology-driven omics approaches meet the needs of TCM research, which could be applied to decoding complex components, targets, and drug-disease interactions (Subramanian et al., 2020). The multi-omics approaches refer to a series of research methods based on high-throughput analysis in modern biological research systems, which mainly include genomics, transcriptomics, metagenomics, metabolomics, epigenomics, and proteomics (Olivier et al., 2019; Subramanian et al., 2020). From the perspective of omics approaches, TCM could be considered as a combination of small molecules. Thus, a single TCM could treat multiple diseases by combining the small molecules with their respective gene/protein targets. After thousands of years of therapeutic practice in China, researchers have found a vast number of TCM formulas that are utilized for treating numerous diseases based on multi-omics approaches and clinical experiments, contributing to new drug discovery and therapeutic mechanisms (Buriani et al., 2012; Olivier et al., 2019; Guo et al., 2020), as well as advancing TCM towards precision medicine (Olivier et al., 2019).

While TCM has been extensively used in the treatment of various kinds of acute and chronic diseases worldwide (Bai et al., 2015; Kim et al., 2010; Miryala et al., 2018; Yang M. and Lao), several limitations have hindered the development of TCM research, including TCM formula quality control, multi-omics approaches on TCM analysis, and data resources for TCM research. Firstly, the quality control of TCM formulas is highly contentious (Yao et al., 2022). Thus, much attention should be paid to its ingredients and production process to ensure its safety and efficacy. Only if the ingredients of TCM formula are safe and lawful, TCM could exert its power in clinics worldwide, laying the groundwork for further studying the therapeutic mechanism, bioactive compounds, targets, and drug discovery to benefit humans. Moreover, TCM research is primarily experience-based and experiment-based methods, in which the small molecules of TCM and the specific targets for the treatment of diseases have not been thoroughly investigated, which impedes the modernization of TCM. Furthermore, the regulating principles of TCM formulas in human body behind the treatment of various diseases remain largely unclear.

Luckily, with the development of sequencing technology and system biology-driven omics approaches, TCM research has also advanced (Zhang et al., 2019b). The mechanisms of TCM and side-effects of TCM formulas were further deciphered at the molecular level (Buriani et al., 2012; Cai et al., 2018; Subramanian et al., 2020), leading to new therapeutic directions (Yang and Lao, 2019; Guo et al., 2020). These efforts are potentially accelerating TCM towards modernization (Qiu, 2007), and enhancing the applicability of the TCM formulas for personalized treatment (Aronson and Rehm, 2015; Jameson and Longo, 2015; Miryala et al., 2018). The concept of network pharmacology analysis is proposed to ascertain which bioactive compounds and targets are effective in treating various diseases. This approach entails deciphering a "compound-protein/gene-disease" network for TCM formulas and elucidating the regulatory principles of small molecules in a high-throughput manner. Furthermore, TCM-associated databases have been developed to meet the needs of TCM research, serving as a repository for TCM formula, herbal ingredients, bioactive compounds, targets, and TCM-disease interactions, and feedback for more comprehensive analysis of the network pharmacology analysis and omics research. These efforts would accelerate the internationalization and digitization of TCM formulas. However, to digitalize all TCM-related resources and fully excavate these resources for deeper understanding of TCM materials and formulas, the help of bioinformaticians would be important. In contrast, bioinformaticians need to better understand TCM research (Gómez-López et al., 2019).

In this review, we have reviewed and summarized the recent progress of multi-omics approaches in deciphering the mechanism of TCM against various diseases (Figure 1). We first discussed the currently widely used quality control methods of the TCM formula. Chemical and biological ingredients (Figure 1A) are both indispensable components for TCM, and we could assess TCM quality by detecting these ingredients using fingerprint-based chemical methods and DNA-sequencing-based biological methods (Figure 1B). Secondly, we emphasized the importance of integrating multi-omics in decoding the mechanism of TCM formulas in treating various diseases (Figure 1C). Thirdly, we also discussed the interaction of bioactive compounds and disease targets from the perspective of network analysis (Figure 1D). Finally, we compared different TCM databases based on their basic properties and search results (Figure 1E). These initiatives may help unravel the "black box" of

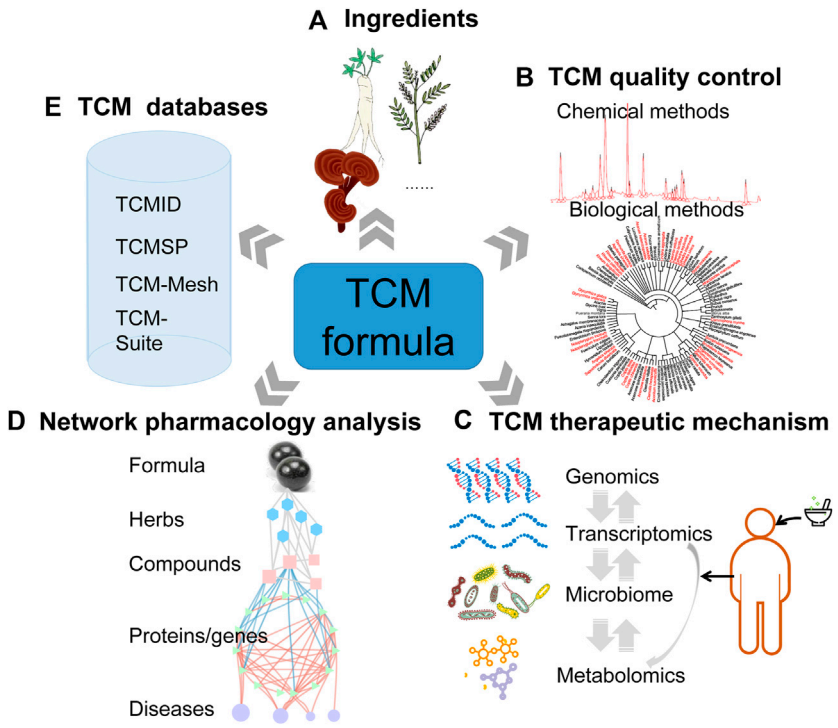

FIGURE 1
Systems biology-driven omics approaches have boosted TCM research from multiple perspectives. **(A)** Prescribed ingredients of TCM formula recorded in Chinese Pharmacopoeia (2020 edition). **(B)** The TCM quality control (fingerprint-based chemical ingredients analysis methods and genomics-related biological ingredients analysis methods). **(C)** Multi-omics approaches including genomics, transcriptomics, microbiome, and metabolomics could be utilized for investigating the therapeutic mechanism of the TCM formula for treating various diseases. **(D)** Network pharmacology analysis for screening the bioactive compounds and potential targets for TCM formulas in treating various diseases. **(E)** The databases for TCM research. The current databases serve as a link across TCM formulas, ingredients, bioactive compounds, targets (proteins/genes), and various diseases.

the therapeutic mechanisms of the TCM formula, provide the best practices of contemporary bioinformatics analysis for TCM formulas, as well as contribute to the TCM toward digitalization, internationalization, and precision medicine. Of course, to translate these advances and fully excavate these resources, the routine clinical practice needs a bioinformatician with good training in clinics, which will help multi-omics approaches and datasets be of importance in better understanding the TCM towards precision therapeutics.

Omics approaches for TCM formula quality control: Biological and chemical ingredient analysis

Omics approaches, including fingerprint-based chemical ingredients analytical methods and DNA-sequencing-based biological ingredients analytical methods (related to genomics approaches), are essential for the quality assessment of TCM formulas. With the popularity of TCM, its quality control methods have become an important research topic to ensure its safety and effectiveness and thus promote the modernization and internationalization of TCM (Cheng et al., 2014; Baing et al., 2019; Yao et al., 2022). Although standards for the quality control of botanical drugs, processed products, TCM extracts, and TCM formulas have been documented in the Chinese Pharmacopoeia (ChP, 2020 edition) (Xu et al., 2021), the methods recorded in ChP are capable of discriminating substances from morphological, chemical, and physical characteristics, they are not precise enough to distinguish the ingredients from genetically related or hybrid species (Cheng et al., 2014).

The methods for chemical ingredient analysis

Currently, the most extensively utilized methods for TCM quality control are fingerprint-based methods (Cheng et al., 2014; Bai et al., 2019), such as thin-layer chromatographic scanning (TLCS), high-performance liquid chromatography (HPLC), gas chromatography (GC), and mass spectrometry (MS), which are focused on the bioactive compounds of the TCM formula. Among

TABLE 1 The candidate DNA barcodes for identifying ingredients of TCM formulas.

DNA barcodes	Abbreviation	Gene type	Characteristic	Application	Sensitivity (%)	References
Internal transcribed spacer 1	ITS1	Nucleus gene	High inter-specific and intra-specific divergence, but poor PCR amplification	Plant barcode	52~88.2	(Luo K. et al., 2010; Chen et al., 2010)
Internal transcribed spacer 2	ITS2		High inter-specific and intra-specific divergence with high species identification ability	Core plant barcode	92.7	Chen et al. (2010)
psbA-trnH	*psbA-trnH*	Chloroplast gene	High variation and species identification ability	Core plant barcode	75~100	(Jia et al., 2017; Zhang P. et al., 2019a)
Chloroplast genome trnL (UAA) intron	*trnL*		Short fragment; multiple internal conserved primer sites and easily amplified in heavily degraded DNA samples; not applicable for fungi	Plant barcode	44.4~100	(Coghlan et al., 2012; Cheng et al., 2014; Yao Q. et al., 2022)
maturase K	*matK*		High variation and species identification ability, but lacks universally conserved primer-binding sites	Plant barcode	~72	(Group, 2009; DUNNING and SAVOLAINEN, 2010; Chen et al., 2010)
rbcL	*rbcL*		High discriminatory power in the cryptogam; ambiguous species identification	Plant barcode	35.6~87	(Chen et al., 2010; Kolter and Gemeinholzer, 2021)
ropB	*ropB*		Low variation and low identification ability	Plant barcode	<50	(Group, 2009; Chen et al., 2010)
Cytochrome oxidase I	COI	Mitochondrial gene	Standard DNA barcode for animals	Core animal barcode	~90	(Vences et al., 2005; Zhang P. et al., 2019a)

them, HPLC is characterized by high separation efficiency, high selectivity, high detection sensitivity, and rapid analysis, which is broadly applicated and usually coupled with other chromatographic methods in assessing the chemical ingredients of TCM formula (Heinisch and Rocca, 2009). For example, liquid chromatography-mass spectrometry (LC-MS)-based metabolic method has been utilized to detect the bioactive compounds of Kaixin Powder (KXP) in treating mentally depressed diseases (Zhu et al., 2010). They have found several bioactive compounds: ginsenosides, 3,6′-disinapoyl sucrose, α/β-asarone, and pachymic acid for *Ginseng Radix* et Rhizoma, *Polygalae Radix*, *Acori Tatarinowii* Rhizoma, and *Poria* in KXP based on LC-MS, respectively (Zhu et al., 2010). Apart from these five compounds, Wang et al. (2021), have firstly found two novel bioactive compounds of KXP (dehydrotrametenolic and dehydrotumulosic acids) from KXP using HPLC-DAD and HPLC-QTOF-MS/MS. These efforts have also resulted in the widespread use of chromatographic methods for TCM formula quality assessment (Liu et al., 2016b; Fan et al., 2021; Zeng et al., 2021).

The methods for biological ingredient analysis

On the other hand, biological ingredients are also indispensable components for TCM formulas, which could be identified through DNA barcoding-based approach. Out of the plenty of DNA barcodes (Table 1), ITS2, *trnL*, and *psbA-trnH* are the most frequently used herbal DNA barcodes, while COI is a well-known standard DNA barcode for animal materials detection (Coghlan et al., 2012; Li et al., 2018; Zhang et al., 2019a). Numerous studies have also used these representative barcodes to assess the biological ingredients of TCM formulas by detecting their prescribed species using high-throughput sequencing, which has detected 44.4%–100% of the prescribed ingredients of TCM formulas, suggesting the high universality, sensitivity, and specificity of this approach (Cheng et al., 2014; Jia et al., 2017; Joseph and Pe'er, 2021; Li et al., 2018; Xin et al., 2018a; Yao et al., 2022). In addition, DNA barcoding could also be applied to detect whether the prescribed ingredients are replaced by similar ingredients, such as the *Arisaematis Rhizoma* is replaced by *Pinellia pedatisecta* in the Ruyi Jinhuang Powder (Li et al., 2018). This approach could also be applied in auditing whether TCM formulas contain derivatives of protected species, especially for these endangered, trade-restricted species of plants and animals (Coghlan et al., 2012; Chen et al., 2015), which could promote the protection of wild species. Taken together, the DNA-barcoding approach innovatively identifies the prescribed ingredients of TCM at molecular level. It breaks away from the traditional morphological identification methods that heavily rely on long-term experience or experiment results, providing the "gene identity card" for TCM materials, and contributing to the standardization of the TCM industry.

However, there are also some limitations and challenges in fully utilizing the methods for TCM quality assessment. Firstly,

the methods for chemical ingredients analysis were unable to discriminate the ingredients with comparable or unambiguous peaks (Wolfender et al., 2003). Secondly, fixating on chemical ingredients overlooks the biological characteristics that are also indispensable components of TCM formula (Cheng et al., 2014; Bai et al., 2015; Bai et al., 2019). Thirdly, though DNA barcoding-based approaches, the prescribed ingredients (recorded in ChP) of TCM formula could be detected (Table 1), they are unable to detect all prescribed ingredients of TCM formula. For example, *trnL* is incompatible with detecting fungal ingredients in TCM formulas (Cheng et al., 2014), and *rbcL* is a well-characterized barcode in GenBank, but this barcode is limited in identifying species from the same genera (Newmaster et al., 2006; Besse et al., 2021). Thus, more DNA barcode candidates should be considered for TCM biological ingredients assessment. Fourthly, the referenced prescribed species in the GeneBank are not enough for species identification. Further studies should take more databases into consideration, such as the DDBJ, EMBL, and PDB databases (Coghlan et al., 2012), TCM-suite (Yang et al., 2022), as well as tcmbarcode (Chen et al., 2014), and other databases. Finally, the genomics-based DNA barcoding approach could not detect the mineral ingredients. At the same time, the fingerprint-based chemical methods could overcome this drawback, and thus combining the methods for chemical ingredients analysis and the biological ingredients analysis could yield a more comprehensive and reliable assessment for TCM. Collectively, these efforts will benefit the safety issues of TCM formulas and accelerate the digitalized management process and internationalization of the TCM industry.

Omics techniques for understanding the therapeutic mechanism of TCM in treating various diseases

Omics approaches could be used to explain the complicated therapeutic mechanism of TCM against diseases from multiple levels (Xin et al., 2019; Guo et al., 2020), which could help us comprehend the relationship between TCM and human health. In the recent 20 years, high-throughput sequencing techniques have evolved at a breakneck pace. As omics technologies become mature, the multi-omics approaches are indispensable strategies for further understanding the therapeutic mechanism of TCM formulas (Buriani et al., 2012; Aronson and Rehm, 2015). In this review, we have summarized the omics approaches in TCM research, such as the prevalent chronic and metabolic diseases (i.e., diabetes), cancer (a leading cause of death worldwide, such as colorectal cancer, breast cancer, and lung cancer) (Fan et al., 2017; Lehmann et al., 2021; Sun et al., 2021), and infectious diseases (i.e., COVID-19, a global public health event) (Runfeng et al., 2020; Wu et al., 2021b; Chen et al., 2021), as well as the corresponding TCM formulas as examples to illustrate the critical role of multi-omics approaches for elucidating the therapeutic mechanism of TCM formulas in treating diseases (Figure 2).

Intestinal microbiota-mediated anti-diabetic effects of berberine

Berberine as an extract of TCM formula from *Berberis*, *Coptis*, and *Hydrastis* (Habtemariam, 2020), is an excellent treatment for chronic and metabolic disorders diseases (Lan et al., 2015; Heindel et al., 2017). Its anti-diabetic function has been demonstrated by plenty of studies. Through metabolomics analysis, the researchers have found that berberine has improved glycometabolism (Dong et al., 2016; Yao et al., 2020) (Figure 2A). Zhang et al. (2010), used transcriptomics, proteomics, and found berberine increased the expression of InsR messenger RNA and protein in various human cells. They lowered the metabolites such as glycaemic levels, hemoglobin A, triglyceride levels, and increased insulin levels in type 2 diabetic (T2D) patients. As known, berberine exhibits poor oral bioavailability (Liu Chang-Shun et al., 2016a). While the intestinal microbes, which contain a specific enzyme called nitroreductase (NTR), are reported as the mediators that could convert berberine into absorbable molecule dihydroberberine (five times more absorption compared to berberine) for host, and then oxidize them back to berberine after absorption in the intestine (Chen et al., 2016; Feng et al., 2018) (Figure 2A). Zhang et al. (2020b), have used metagenomics and metabolomics data from the berberine treatment T2D patients, and found berberine reduced the glycaemic level by inhibiting deoxycholic acid species biotransformation by *Ruminococcus bromii*. Thus, the interactions between intestinal microbes and bioactive compounds of TCM formulas highlight the critical role of TCM and intestinal microbes in human health (Zhang et al., 2020a), implying that the intestinal microbes might be considered as potential targets for designing the drug delivery system.

Multi-omics analysis for understanding the anti-cancer effects of *C. chinensis* Franch. (Ranunculaceae)

Based on the genomics approach (Figure 2B), Chen *et al.*, have used genomics approaches to analyze the genome of the *C. chinensis* Franch. (Ranunculaceae) and revealed the diversification of protoberberine-type alkaloids (Liu et al., 2021). They also discovered that the gene *cyp719* is involved in berberine biosynthesis through encoding the enzyme called (S)-canadine synthase. Through metabolome and transcriptome analysis, researchers have found the bioactive compounds of *C. chinensis* Franch. (Ranunculaceae) such as berberine could downregulate the expression of eukaryotic translation initiation factor 4A isoform 2 (*eif4a2*) gene (Lv et al., 2016; Chou et al., 2017; Wang et al., 2019) (Figure 2B), which indirectly

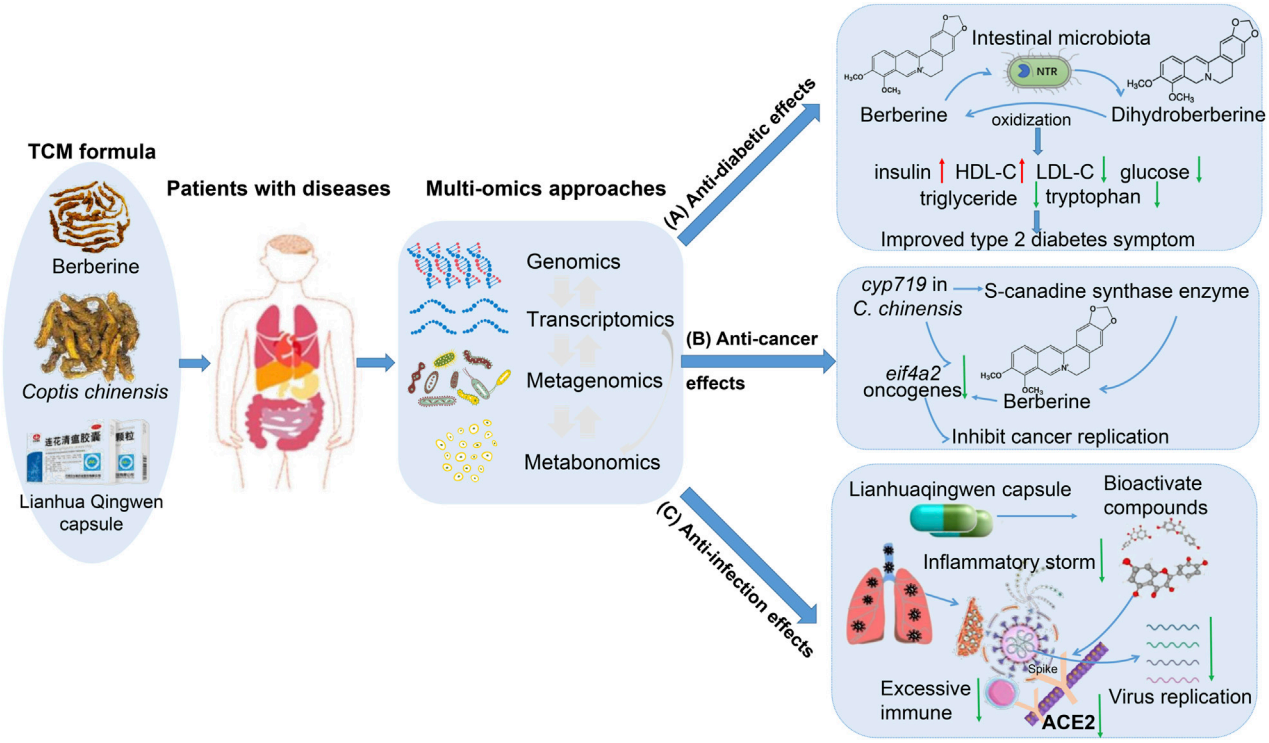

FIGURE 2
Multi-omics approaches are applicable for investigating the therapeutic mechanism of TCM in treating diseases. In this review, we used berberine, *C. chinensis* Franch. (Ranunculaceae), and Lianhua qingwen capuse as examples to illustrate the critical role of multi-omics approaches in elucidating the therapeutic mechanism of TCM. **(A)** Multi-omics analysis for berberine in treating type 2 diabetes mellitus. In this case study, intestinal microbes converted berberine as host absorbable molecule dihydroberberine to improve diabetes. NTR: nitroreductase. **(B)** Multi-omics analysis of *C. chinensis* Franch. (Ranunculaceae) for anti-cancer effect. Through multi-omics analysis, the functional genes (i.e., *cyp719*) and bioactive compounds (i.e., berberine) of *C. chinensis* Franch. (Ranunculaceae) have suppressed the eukaryotic translation initiation factor 4A isoform 2 (*eif4a2*) expression, and thus blocked cancer replication. **(C)** Multi-omics analysis for the potential therapeutic mechanism of Lianhua Qingwen capsule in COVID-19 patients. Through multi-omics analysis, the bioactive compounds of Lianhua Qingwen capsule could inhibit the combination of the viral target Spike and human target ACE2, thus preventing the viruses' invasion and attachment to host cells and inhibiting the virus replication and pro-inflammatory cytokine levels (i.e., IL6, TNF-α), and chemokine levels, and thereby improving the symptoms of COVID-19 patients.

emphasized the important role of *cyp719* gene of *C. chinensis* Franch. (Ranunculaceae) in anti-cancer effect. While *eif4a2* gene is considered a novel target for cancer therapy and anti-cancer drug discovery (Lv et al., 2016; Chou et al., 2017; Wang et al., 2019), its inhibition prevents the cooperation between *eif4a2* and oncogenes (Lindqvist and Pelletier, 2009), and thus effectively inhibits the replication of cancer and tumor (Lindqvist and Pelletier, 2009; Slaine et al., 2017).

Multi-omics analysis for understanding the potential anti-infection effects of Lianhua Qingwen capsule

TCM formula may exert comprehensive influences, enhancing the host's ability to resist viral infection (Yuan and Lin, 2000; Jiang, 2005) (Figure 2C). Among numerous infectious diseases, COVID-19 is a well-known global public health event, which brings trouble to our daily life and huge burden worldwide. Researchers have found numerous TCM formulas that may achieve therapeutic outcomes for COVID-19 patients through multiple pathological pathways and TCM-disease targets across stages (Ren et al., 2020; Wu et al., 2021b). Chai *et al.*, have analyzed the alteration of genetics, DNA methylation, and RNA expression for samples from COVID-19 patients, and found that during viral infection, angiotensin-converting enzyme 2 (ACE2) is identified as a membrane-binding receptor to the fusion and invasion process of the COVID-19 and host cells (Chai et al., 2020). And the COVID-19' S protein (also called Spike protein; Figure 2C) could recognize and combine with the human cell protein ACE2, then use the host genetics to replicate new COVID-19 viruses (Hoffmann et al., 2020). These novel COVID-19 viruses were released and disseminated in the bloodstream. They then bind the ACE2 of other cells in COVID-19 patients, disrupting their equilibrium, and threatening other organs, such as the intestine, kidney, and

heart of COVID-19 patients (Leung et al., 2020). Thus, the potential therapeutic effect of the TCM formula is to find the bioactive compounds to bind to host receptors such as ACE2, to prevent or inhibit the invasion/attachment of the virus to host cells (Figure 2C).

Lianhua Qingwen capsule is a classic patent TCM, which consists of 13 ingredients, including *Forsythia suspensa* (Thunb.) Vahl (Oleaceae; 255 g), *Lonicera japonica* Thunb. (Caprifoliaceae; 255 g), *Prunus armeniaca* L. (Rosaceae; 85 g), *Ephedra sinica* Stapf (Ephedraceae; 85 g), *Isatis indigotica* Fort. (Cruciferae; 255 g), *Dryopteris crassirhizoma* Nakai (Polypodiaceae; 255 g), *Rheum palmatum* L. (Polygonaceae; 51 g), *Houttuynia cordata* Thunb. (Saururaceae; 255 g), *Pogostemon cablin* (Blanco) Benth. (Blanco; 85 g), *Rhodiola crenulata* (Hook.f. and Thomson) H. Ohba (Crassulaceae; 85 g), *Mentha haplocalyx* Briq. (Lamiaceae; 7.5 g), *Gypsum Fibrosum* (255 g), *Glycyrrhiza uralensis* Fisch. ex DC. (Fabaceae; 85 g) (Xiao et al., 2020). This TCM is an innovative drug with potential therapeutic effects on respiratory diseases (Hu et al., 2022). Li *et al.*, have assessed the antiviral effectiveness of Lianhua Qingwen capsule against SARS-CoV-2 in Vero E6 cells and human hepatocellular carcinoma cells using cytopathic effect inhibition assay, plaque reduction assay, and real-time quantitative PCR analysis (Runfeng et al., 2020). They have found that TCM formula Lianhua Qingwen could block the replication and expression of proinflammatory cytokines (i.e., IL6, TNF-α). and chemokine (i.e., CXCL-10, IP-10) caused by COVID-19, and thus considerably alleviating the symptoms and the development of the COVID-19 in patients (Runfeng et al., 2020; Wu et al., 2021b) (Figure 2C). Chen *et al.* found 132 bioactive metabolites in Lianhua Qingwen capsule in treating COVID-19 (Chen et al., 2021). Among them, five compounds (forsythoside I, forsythoside A, rhein, neochlorogenic acid, and its isomers) were further identified with high inhibitory effects on ACE2 receptor of host cells, implying that they could inhibit the invasion of the virus to the host cells, and thus improved the symptoms of COVID-19 patients (Chen et al., 2021). Collectively, these efforts provided insight into the molecular mechanisms of therapeutic effects of Lianhua Qingwen capsule in treating COVID-19, thereby confirming the applicability and vital significance of the TCM formula in infectious illness treatment.

Multi-omics approaches for TCM network analysis research

One of the most successful applications of omics approaches is network pharmacology analysis. TCM formulas typically incorporate various ingredients and multi-targets for synergistic anti-disease effects (Figure 3), which coincides with the concept of network pharmacology analysis (Zhang et al., 2019b; Yang et al., 2022). Network pharmacology analysis is presented to clarify which compounds of TCM formula exert effects in treating diseases and which targets could be exploited for drug design (Boezio et al., 2017; Wu et al., 2018; Zhang et al., 2019b), which has developed into a powerful method for leveraging the "ingredients-compounds-proteins/genes-diseases" network for TCM research (Zhang et al., 2019b; Yang et al., 2022). Multi-omics such as transcriptomics, genomics, epigenomics, and proteomics could be used to determine the ingredients, proteins, and/or genes of TCM formulas, whereas electrochemical method, HPLC, real-time qPCR, and other quantified methods can be used to determine and quantify the content of bioactive compounds (Wolfender et al., 2003; Zhu et al., 2010; Wang et al., 2021). While network pharmacology analysis could facilitate the integration of ingredients, bioactive compounds, and proteins/genes into a network, providing an effective resolution for exploring the TCM-disease interaction (Zhang et al., 2019b).

Network pharmacology analysis in decoding the roles of LDW in treating type 2 diabetes

T2D is a chronic metabolic disease that affects approximately affecting nearly 425 million people around global, leading to poor health status and massive economic outputs (Lin et al., 2015; Gan et al., 2019), causing substantial damage to the blood vessels, heart, and brain with long-time hyperglycemic status (Adeshara et al., 2016; Areosa Sastre et al., 2017). It was reported that Liuwei Dihuang Wan (LDW) is a patented TCM formula for treating T2D (Cheng et al., 2014; He et al., 2019). Based on the bioactive compounds recorded in TCMSP (30,069 bioactive compounds; http://sm.nwsuaf.edu.cn/lsp/tcmsp.php), BATMAN (25,210 bioactive compounds; http://bionet.ncpsb.org/batman-tcm/), and TCM Database@Taiwan (351 bioactive compounds; http://tcm.cmu.edu.tw/) databases, He et al. (2019), used the network pharmacology analysis and found 45 active compounds of LDW ingredients, which exert their pharmacological effects on T2D. As known, people with T2D were identified to have higher levels of inflammatory cytokines, such as IL-1B and IL-6, and lower levels of IL-10 (Kologrivova et al., 2014; Fathy et al., 2019), and the inflammatory cytokines disorder were also reported as biomarkers for early T2D diagnosis (Senthilkumar et al., 2018; Fathy et al., 2019). While the bioactive compounds of LDW, such as beta-sitosterol, isofucosterol, quercetin, are enriched in anti-inflammatory, anti-oxidative stress responses pathway by interacting with the target genes (i.e., *akt1*, *ptgs2*), which could decrease the inflammatory and remove oxidative stress and reactive oxygen species (Chasseaud, 1979; Sheehan et al., 2001), thus improved the symptoms in T2D patients. These findings imply that LDW may play an important role in treating T2D through the bioactive compounds interacting with the key or central genes in the development of T2D.

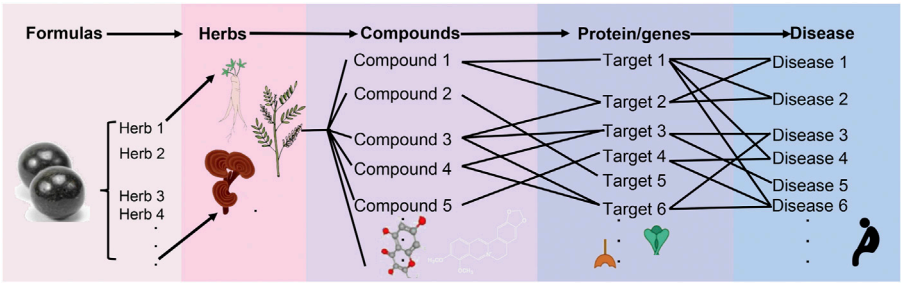

FIGURE 3
TCM network pharmacology analysis is proposed for leveraging the "ingredients-compounds-proteins/genes-diseases" network for TCM research. A TCM formula is made according to the Chinese Pharmacopoeia, herbal ingredients were the major prescribed ingredients in most TCM formulas. While based on network pharmacology analysis, chromatography, and high-throughput sequencing technology, we could decode the relationship between TCM formulas-species ingredients-compounds-targets-diseases. By looking at the bioactive compounds in the prescribed ingredients, we could learn more about the herb, the bioactive compounds, the target proteins, and the genes in treating diseases. This would help us understand how TCM works to treat different diseases.

Network pharmacology analysis in decoding the roles of TCM in treating the cardiovascular and cerebrovascular diseases

Cardiovascular and cerebrovascular disease (CCVD) is a term that refers to an illness that affects the heart, brain, or blood vessels (Tao et al., 2013; Wang et al., 2020). According to the WHO, this disease contributes to 32% of fatalities worldwide [https://www.who.int/news-room/fact-sheets/detail/cardiovascular-diseases-(cvds)]. Through network pharmacology analysis, Wang et al. (2020) have found and experimentally verified superoxide dismutase, glutathione peroxidase, malondialdehyde, and nitric oxide synthase of Safflower and Salvia as promising therapeutic targets for treating cerebral and myocardial infarction in. Safflower can decrease the cerebral infarction rate, cerebral cell edema, glial cell proliferation, and inflammatory cell infiltration, as well as increase the content of superoxide dismutase and glutathione peroxidase, and decrease the content of malondialdehyde and nitric oxide synthase (Wang et al., 2020). Moreover, Tao et al. (2013), incorporated the chemical compounds including the chemical structure and pharmacological information, as well as biological functional data of TCM formula *Radix Curcumae*, and found 58 bioactive compounds and 32 potential targets for the prevention and/or treatment of CCVD. In summary, network pharmacology analysis sheds fresh light on the TCM-disease interactions, providing potential therapeutic targets for drug discovery.

Network pharmacology analysis in decoding the roles of TCM in treating cancer

With the advancement of multi-omics approaches, many TCM formulas have been mined for cancer prevention and treatment (Fan et al., 2017; Xiang et al., 2019; Lehmann et al., 2021; Sun et al., 2021). In this review, we took CRC as an example to elucidate the omics approaches underlying the mechanisms of TCM against cancer. CRC is diagnosed as the third major malignant tumor worldwide, which contributes to the fourth leading cause of cancer death (Arnold et al., 2017). Using network analysis to integrate multiple-omics data, researchers have found that the bioactive compounds in the TCM formula Huang Lian-Gan Jiang (Gingerenone C, Obaculactone, and Isogingerenone B) could interact with the main targets of CRC (i.e., PDE5A, TGFBR2, HRAS) to regulate the signaling pathways (i.e., DAP12, NGF, AKT signaling pathway), contributing to therapeutic effects for CRC patients (Gong et al., 2019). Among these targets, FGFR4 has been confirmed with the ability to inhabit CRC cell proliferation, promote apoptosis, and disrupt the cell cycle, which could be a novel target for drug design and new therapeutic direction (Jiang et al., 2017). In addition, Shaoyao decoction was verified to increase the survival rate and decrease the occurrence of colonic neoplasms in the mice model (Lin et al., 2014). Moreover, through network pharmacology analysis, the bioactivate compounds Zuojinwan: quercetin, baicalein, and wogonin combined with the target genes *akt1*, *jun*, and thus activate the

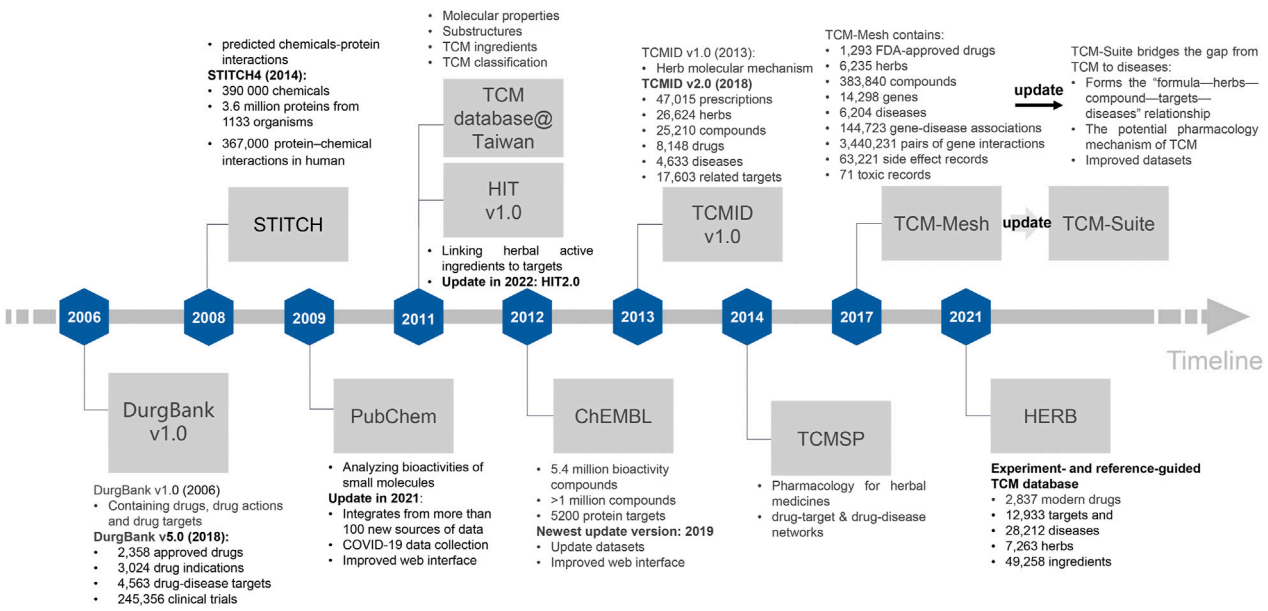

FIGURE 4
The development of commonly used TCM-disease databases along the timeline. We described the TCM databases based on their initial and most recent updated versions, respectively, which highlighted the primary composition, function, and characteristics of these databases along the timeline. The updated version of a database is highlighted in bold font of the description.

important pathway such as PI3K-Akt signaling pathway to induce apoptosis to exert anti-cancer effects in CRC patients (Huang et al., 2020). Relevant scientific research also demonstrated that the *Ampelopsis ethanolic* extract could inhibit *stat3* and Src phosphorylation, and downregulate the expression of their target genes, such as *bcl-xL*, *mmp*-2 in CRC patients (Sun et al., 2021). These curative or preventative effects of TCM for various diseases have been demonstrated in rodent or human studies (Sun et al., 2021). The candidate bioactive compounds and targets screened by network pharmacology analysis could guide new drug discovery and therapeutic direction.

Databases and analytical resources for TCM research

The TCM-associated databases are repositories for storing omics data, including ingredients, compounds, genes, targets, and diseases. Based on a comprehensive screening analysis of TCM-associated databases, the network pharmacology analysis has further deepened the therapeutic effects of TCM. Numerous efforts have also been put into the establishment of TCM-associated databases. In this section, we present the most frequently used databases, and then use the well-studied ingredients to assess the properties of these TCM-associated databases.

Current TCM-associated database for TCM research

Currently, numerous TCM databases have emerged in response to the need for different aspects of TCM-disease studies (Mendez et al., 2019; Fang et al., 2021). In this review, we processed the development of the most frequently used TCM databases and their updated versions during our evaluation (Figure 4).

DurgBank (http://www.drugbank.ca) was initially reported in 2006, and has been updated continuously over the past years (Wishart David S. et al., 2006). The most recent version is DurgBank 5.0, which comprises 2,358 FDA-approved small molecular pharmaceuticals and 4,964 experimental drugs, as well as 7,129 unique drug targets and other drug-associated informantion (Wishart et al., 2018) (Figure 4). STITCH is primarily concerned with decoding chemical-protein interactions (Kuhn et al., 2008), its most recent version STITCH4 has 390,000 chemicals and 3.6 million proteins from 1,133 organisms, and 367,000 protein–chemical interactions in human (Kuhn et al., 2014). PubChem (http://pubchem.ncbi.nlm.nih.gov) is used to search for the 2D and 3D bioactivities of small molecules (Wang et al., 2009), which was updated in 2021. The updated version of PubChem has integrated more than 100 Corona Virus Disease 2019 (COVID-19) datasets, such as chemical, physical property, and patent associated information, and supports various types

of structure search (such as identity, similarity, substructure, and superstructure searches) *via* its web interfaces (Kim et al., 2021) (Figure 4). TCM Database@Taiwan (http://tcm.cmu.edu.tw/) is one of the largest non-commercial TCM databases for drug screening that launched in 2011 and contains over 20,000 pure compounds derived from 453 TCM ingredients (Chen, 2011). HIT (Herb Ingredients' Targets, http://lifecenter.sgst.cn/hit/) is a database that connects herbal active ingredients to targets (Ye et al., 2011), which is updated in 2022 (HIT2.0). HIT2.0 has 10,031 compound-target activity pairs with quality indicators between 2,208 targets and 1,237 ingredients from more than 1,250 reputable herbal materials (Yan et al., 2022). ChEMBL (https://www.ebi.ac.uk/chembldb) contains 5. 4 million bioactivity compounds for more than 1 million compounds and 5,200 protein targets (Mendez et al., 2019), and the most recent upgraded version is in 2019 with the improved dataset and web interfaces (Mendez et al., 2019). TCMID database (Traditional Chinese Medicine Integrated Database, http://www.megabionet.org/tcmid/) integrates the molecular mechanism of herbal materials (Xue et al., 2013). Its updated version TCMID2.0 is more comprehensive and contains 18,203 herbal ingredients, 15 prescriptions, 82 associated targets, 1,356 drugs, 842 diseases, and 170 herbal materials associated with mass spectrometry spectra (Huang et al., 2018). TCMSP (http://sm.nwsuaf.edu.cn/lsp/tcmsp.php) has considered the pharmacodynamics and pharmacokinetics for systemic pharmacology research, such as the bioactive compounds and compound-related targets screening (Ru et al., 2014), which includes 499 herbal materials with 29,384 ingredients, 3,311 targets, and 837 associated diseases in ChP, as well as 12 important absorptions, distribution, metabolism, and excretion related properties (Ru et al., 2014). TCM-Mesh (http://mesh.tcm.microbioinformatics.org/) was established based on the concept of the "TCM formula-compounds-proteins/genes-diseases" network to elucidate the regulatory mechanisms governing tiny molecules in TCM formula, as well as recording their side-effects (Zhang et al., 2017). Since pharmacotranscriptomics has become a powerful method for assessing the therapeutic efficacy of drugs, and identifying novel drug targets, HERB (high-throughput experiment- and reference-guided database of TCM, http://herb.ac.cn/) is built based on manually curated 1,241 gene targets and 494 modern diseases for 473 herbal materials, linking with 12,933 targets and 28,212 diseases to 7,263 herbs and 49,258 ingredients (Fang et al., 2021). To solve the problem of lacking holistic and systematical analysis of TCM formula, the newest database named TCM-suite (http://tcm-suite.aimicrobiome.cn/) was built (Yang et al., 2022). This database is a holistic pipeline that connects TCM biological and chemical ingredient identification and downstream network pharmacology analysis. It establishes a detailed "TCM formula-ingredients-compounds-proteins/genes-diseases" relationship. It enables users to identify components of a TCM formula and investigate its potential pharmacology mechanism and side effects simultaneously. These databases with different usages have provided the opportunity to explore the potential pharmacology mechanism of TCM formula at the molecular level in the treatment of numerous diseases.

Comparing the properties of frequently used TCM database

The frequently used TCM databases also have different focuses and comprehensiveness. In this work, the databases (Google Scholar citations: as of April 2022: TCMSP: 1748, TCMID: 580, TCM-Mesh: 114), as well as TCM-Suite (http://tcm-suite.aimicrobiome.cn/) were chosen for comparison of their properties (Table 2). By comparing the results from different databases, we found that although the bioactive compounds recorded in the TCM-Suite database were fewer than those in other TCM-associated databases, the data of compound-target associations and target-disease associations were more abundant in this database. Additionally, we have discovered TCM-Suite database is more comprehensive in terms of the compound-target associations and target-disease associations. Most of the ingredients, with fewer bioactive compounds being collected in this database, were matched with more hits in bioactive compound-target associations and target-disease associations. The fewer bioactive compounds in TCM-Suite are probably because the TCM-Suite database removes the ambiguous bioactive compounds of TCM formulas.

Discussion

While numerous works have evaluated the multi-omics approaches in TCM research, this is the first systematic and comprehensive review of omics approaches in TCM research from a holistic standpoint. In this review, we have summarized the recent progress of multi-omics approaches in deciphering the mechanism of TCM against various diseases as compared to the previous research and discussed the advantages and limitations, as well as the future direction of multi-omics applied to the field of TCM. With the development of systems biology-driven omics analysis, TCM research has profoundly advanced (Wu et al., 2019; Wu al., 2021a; Gao et al., 2021), which means that TCM studies have already undergone a paradigm shift from the traditional biochemical and molecular analysis approaches to the data-driven omics analysis approaches (Figure 5). Analytical chemistry and biology approaches have pushed forward the development of TCM research and laid the groundwork for applying omics approaches (Zeng et al., 2019). In contrast, the omics approaches have the potential to significantly supplement the traditional analysis approach with more precise and

TABLE 2 Comparing the properties of four representative TCM databases based on the selected ingredients reported in the previous study (Zhang R. et al., 2019b).

Ingredients	TCMID			TCMSP			TCM-mesh			TCM-suite		
	C	C-T	T-D	C	C-T	T-D	C	C-T	T-D	C	C-T	T-D
Ganoderma lucidum (Leyss. ex Fr.) Karst (Polyporaceae)	160	1,164	771	32	150	238	484	543	365	40	1,477	9,860
Panax ginseng C. A. Mey (Araliaceae)	293	4,820	2,913	153	4,144	2,970	380	748	486	134	7,045	19,400
Codonopsis pilosula (Franch.) Nannf. (Campanulaceae)	187	2,531	1,631	104	2,493	2,211	268	911	556	97	4,158	12,373
Astragalus membranaceus Bunge. (Fabaceae)	70	1,832	1,186	35	2,426	2,376	174	953	605	53	5,737	12,463
Dioscorea oppositifolia L. (Dioscoreaceae)	42	1,004	655	20	959	1,307	142	851	451	20	1,722	10,726
Panax notoginseng (Burk.) F.H.Chen (Araliaceae)	157	900	635	71	1,104	1,591	238	716	506	2	3	24
Polygonum multiflorum Thunb. (Polygonaceae)	73	618	599	—	—	—	24	513	888	14	1,155	7,728
Radix *Angelicae dahuricae* (Hoffm.) Benth. and Hook.f. ex Franch. and Sav. (Apiaceae)	135	406	289	446	1,408	454	80	362	477	7	107	1,947
C. chinensis Franch. (Ranunculaceae)	30	238	231	96	596	513	23	142	274	33	453	5,261
Cordyceps sinensis (BerK.) Sacc. (Ophiocordycipitaceae)	37	1,010	519	76	369	483	21	919	944	37	2,169	8,663

Notes, the numbers in the table indicate the search results in the corresponding databases. C: the number of the bioactive compounds; C-T: the number of compound-target associations; T-D: the number of target-disease associations. Though TCM-Suite (http://tcm-suite.aimicrobiome.cn/) is the newest version of TCM-Mesh, this database is a comprehensive and holistic platform for TCM composition identification and network pharmacology analysis. For the first time, this database constructed a holistic pipeline to interconnect TCM biological ingredient identification and downstream network pharmacology analysis, which also allows users to identify components of a TCM formula and investigate its potential pharmacology mechanism. The names of these ingredients were recorded in Chinese Pharmacopoeia (ChP) and/or validated taxonomically in http://mpns.kew.org/mpns-portal/or http://www.plantsoftheworldonline.org (Rivera et al., 2014).

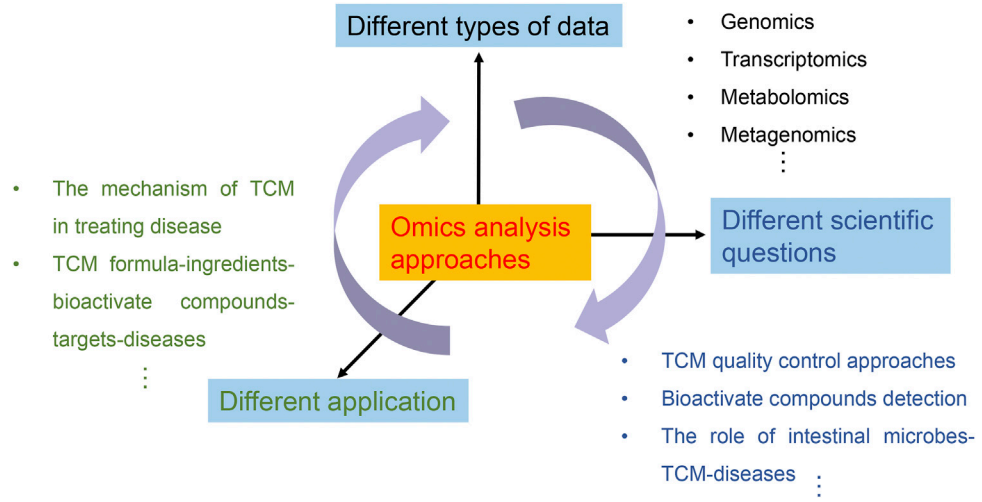

FIGURE 5
TCM research in the omics age has utilized different types of omics data to address different scientific questions, and meet the needs of different applications. With the development of sequencing technology, different types of data including genomics, transcriptomics, metabolomics, and metagenomics data could be gathered to address various scientific topics. The molecular mechanism of TCM formula in treating various diseases is gradually exposed by omics analysis approaches, and the relationship of TCM bioactive compounds-targets-diseases is constructed, providing suggestions for drug-target design. These scientific questions in turn contribute to the practical value of TCM materials, and the different applications will also create different types of data. This bidirectional interaction reinforces the clinical use of TCM and drives its modernization.

comprehensive approaches, which has undoubtedly made a significant contribution to deciphering the mechanism of TCM from various aspects (bioactive compounds, TCM-drug targets, pharmacodynamic effects, and therapeutic mechanisms). This accomplishment has also sparked various anxieties and concerns for TCM, given the volume of heterogeneous data on issues that may be solved using omics data for the TCM research areas (Figure 5).

In this review, we have evaluated the TCM formulas from four aspects to address several anxieties and concerns about TCM. Firstly, the inconsistent quality control methods make TCM disputable (Yao Q. et al., 2022). Based on the advancement of sequencing and chromatographic technologies, researchers have combined chemical methods (i.e., HPLC, TLC) (Wolfender et al., 2003; Zhu et al., 2010; Wang Binbin et al., 2021) and biological methods (DNA fragments: ITS2, *trnL*, *trnH-psbA*, and COI) (Vences et al., 2005; Jia et al., 2017; Xin et al., 2018a; Xin Tianyi et al., 2018b; Zhang et al., 2019a; Chandrasekara et al., 2021) for quality control of TCM formula through detecting their prescribed ingredients. These initiatives have also yielded significant results in terms of evaluating the quality control of TCM formulas[18-20], which would push forward the digital management of TCM. These advancements are inseparable from the database with the storage of referenced materials and the omics approaches, which ensure the legality and therapeutic efficiency of TCM formulas (Newmaster et al., 2006; Chen et al., 2014; Cheng et al., 2014; Guo et al., 2020; Subramanian et al., 2020; Besse et al., 2021).

Secondly, omics analysis approaches would provide clues for clinical applications of TCM formulas, thereby deepening our understanding of the therapeutic mechanism of TCM formulas. Numerous forms of data for TCM research have been analyzed to understand the therapeutic effects of TCM formulas on human diseases (Wang et al., 2015; Dong et al., 2016; Subramanian et al., 2020). Because the majority of the TCM formulas are administered orally, which typically come into contact with intestinal microbes and are transformed into host absorbable molecules under microbes, allowing for optimal utilization of TCM formulas (Feng et al., 2015; Chen Feng et al., 2016; Feng et al., 2018). Through the omics approach, TCM formulas have also been applied in the treatment of certain diseases, and show outstanding anti-diseases, such as cancer (Xiang et al., 2019; Liu et al., 2020), COVID-19 (Fan et al., 2020; Leung et al., 2020), and chronic diseases (Deng, 2010; Dong et al., 2016; Yang et al., 2019; Guo et al., 2020). All of these findings, which are based on omics datasets and approaches, have allowed for the identification of the mechanism underlying significant therapeutic effects (Feng et al., 2015; Liu et al., 2016a; Chen et al., 2016; Feng et al., 2018; Zhang et al., 2020a).

Thirdly, with its notion of integrity, comprehensiveness, and systematic approach, network analysis offers new strategies and approaches for researching TCM formulas, as it may transform TCM from an experience-based to an evidence-based medical system. From a network view based on different types of omics datasets and approaches, we can decode the molecular mechanism of the complicated TCM formulas (Tao et al., 2013; Li et al., 2014). That is, the relationship between TCM formulas and diseases could be divided into prescribed ingredients, bioactive compounds of prescribed ingredients, compounds-targets, and diseases-targets interactions (Zhang et al., 2017), which confirms the advantages of multi-compound, multi-target and multi-pathway characteristics of TCM formula and providing a reliable solution for systemic analyzing the clinical efficacy of TCM formula (Luo et al., 2020). These efforts will benefit target discovery, bioactive compound screening, toxicity evaluation, and the mechanism elucidation of TCM. These efforts may deepen our understanding of how TCM formulas could treat diseases. Based on these advantages, future applications of multi-omics approach in TCM research could be focused on drug mining, drug design, drug re-purposing, and therapeutic mechanisms investigation to make contributions to the modernization of TCM. Network pharmacology analysis is a systems biology-based approach, which selects specific signal nodes for multi-target drug molecule design to uncover the molecular mechanisms underlying the pharmacodynamic effects (Luo et al., 2020). This analytical approach largely depends on the high volume of data, while the current resources including medicines, genes, proteins, *etc.* are not exhaustive (Yang et al., 2022). It cannot be assured that the databases on TCM, bioactive compounds of TCM, and TCM-related gene targets are accurate and comprehensive. Moreover, no suitable calculation methods have been developed to calculate the correlations in network analysis. Network pharmacology analysis employs computer network screening for target selection, and these correlations were calculated without considering the distribution character of TCM data. Hence, influenced by cascade amplification, the number of disease targets and medication target proteins is gradually expanding, and the interpretation of data cannot keep up with the growth of data. Additionally, the network pharmacology analysis in TCM, such as new targets, or drug mechanism discovery, is still qualitative, and the scientific and mechanism discovery of TCM through network analysis still needs critical and extensive clinical trials. Furthermore, the dose-efficacy relationship between the TCM formula and disease remains further explored and quantified. Last but not least, human disease is dynamic changes, so the course of disease development and treatment efficacy process should be considered in further studies.

Fourthly, the TCM-associated databases provide plenty of TCM-related data, which were created and are continuously updated with the demand for TCM research. We proposed the TCM-Suite database (http://tcm-suite.aimicrobiome.cn/) (Yang et al., 2022), which overcomes the limitations of the currently available databases for network analysis and other omics analysis, and serves as a bridge for integrating the prescribed ingredients of TCM formulas, the bioactive compounds of prescribed ingredients, compounds-targets, and disease-targets as a holistic concept. This database establishes the foundation for the systemic investigation of the therapeutic effects from a network analysis perspective, facilitating the clinical application value and drug development. Given the importance of intestinal microbes in assisting the host's absorption of bioactive compounds

(Feng et al., 2015; Chen et al., 2016; Feng et al., 2018), further database developments should take the interaction between intestinal microbes, TCM formulas, and human symptoms into consideration for building up more complete and exhaustive databases, making the TCM research more concise and convenient. With the need for TCM research, various TCM-related databases have emerged, but the query of these databases is quite different. For example, the herbal material "*C. chinensis* Franch." could be accessed by searching "huang lian" or "*Coptidis*" in TCMID (Huang et al., 2018), "huanglian" in TCMSP (Ru et al., 2014), whereas in the TCM-Suite database (Yang et al., 2022), this herbal material could be accessed by searching "huang lian" or "C. *chinensis*." And thus, a platform considering the various official name/ID or a standard platform for TCM research is needed, which could make the databases more concise and available, enabling the researchers to make full use of the resources.

Collectively, systems biology and data-driven omics analysis approaches, including genomics, proteomics, metagenomics, transcriptomics, and metabolomics, play an indispensable role in decoding the interactions of TCM and diseases, which could comprehensively and deeply decode the therapeutic mechanisms of the TCM formula. These efforts have hastened the translation of TCM from fundamental research to a broad spectrum of applications, particularly in clinical applications.

However, apart from the aforementioned limitations for each part of TCM analyses, there are also several limitations of the multi-omics approach applied to TCM. Consider network analyses is still at a very preliminary level of evidence and might often be used misleadingly. Firstly, the high dimensionality, high complexity, and high volume of heterogeneous data make it difficult for TCM analysis. Secondly, there is a lack of data resources for in-depth interpretation of TCM preparations: from identifying herbal ingredients and their bioactive compounds to understanding how small molecules in herbal formulas interact with genes and proteins in the human body. And the high chemical complexity of TCM makes it challenging to characterize their bioactive compounds and investigate systemic actions in humans. Thirdly, the limited knowledge of biochemistry has constrained our further understanding of TCM pharmacological and toxicological effects. Fourthly, even under the idea of "homology of medicine and food" (Hou and Jiang, 2013; Gong et al., 2020), there is limited knowledge about the medicinal value and mechanism of medicinal and edible plants and their effects on human health. A deeper understanding of these medical homologous plants will help people adjust their health according to their daily diet. Fifthly, even though multi-omics have been extensively used in TCM research and clinical practices, more digital information, including protein structure information, biological images, as well as electronic medical records, could be integrated for better understanding of the TCM-disease relationships. Finally, the application of omics approaches in new drug discovery still has a long way to go, pharmacodynamic effects of the new drugs should perform with critical clinical trials. In the future research, it will be useful to highlight the current pitfalls in these approaches and how they can be overcome.

To achieve this, a bioinformatician with good clinical training should act as a bridge to translate multi-omics approaches and datasets into routine clinical practice to assist with clinical diagnosis. We believe these efforts are beneficial for the process of TCM towards modernization, internationalization, and digitalization in the treatment of a variety of complicated diseases.

Conclusions

In this review, we have summarized the recent progress of multi-omics approaches in deciphering the mechanism of TCM against various diseases as compared to the previous research and discussed the advantages and limitations, as well as the future direction of multi-omics applied to the field of TCM. With the development of systems biology-driven omics analysis. And we suggested combing the chemical and biological ingredients analytical methods to get a more objective and comprehensive assessment of TCM quality. Moreover, with the help of bioinformaticians, omics analysis approaches would accelerate the unveiling of the mystery of TCM, and move it towards internationalization. Besides, assisted by network analysis, the link between TCM and diseases could be visualized from ingredients to compounds to targets, which could enhance our understanding of the relationship between TCM and diseases. Furthermore, with heterogeneous TCM data, databases serve as a repository for these data, which promote the modernization and internationalization of TCM and potentially provide critical technological support for clinical diagnosis, drug development, and precision medicine. We believe under the guidance of bioinformaticians, these efforts are advantageous for the TCM process including modernization, internationalization, and digitalization.

Author contributions

KN and HB designed the study. XZ performed the review. KN, HB, RY, XZ, PY, DZ, and QY revised and proofread the manuscript. All the authors have read and approved the final manuscript.

Funding

This work was partially supported by the National Science Foundation of China grant (Grant Numbers. 81774008, 81573702, 32071465, 31871334, and 31671374), the Ministry of Science and Technology's national key research and development program grant (Grant Number. 2018YFC0910502).

Conflict of interest

Author RY was employed by Dovetree Synbio Company Limited.

The remaining authors declare that the research was conducted in the absence of any commercial or financial relationships that could be construed as a potential conflict of interest.

Publisher's note

All claims expressed in this article are solely those of the authors and do not necessarily represent those of their affiliated organizations, or those of the publisher, the editors and the reviewers. Any product that may be evaluated in this article, or claim that may be made by its manufacturer, is not guaranteed or endorsed by the publisher.

References

Adeshara, A. K., Diwan, G. A., and Tupe, R. S. (2016). Diabetes and complications: Cellular signaling pathways, current understanding and targeted therapies. *Curr. Drug Targets* 17, 1309–1328. doi:10.2174/1389450117666151209124007

Areosa Sastre, A., Vernooij, R. W., Gonzalez-Colaco Harmand, M., and Martinez, G. (2017). Effect of the treatment of Type 2 diabetes mellitus on the development of cognitive impairment and dementia. *Cochrane Database Syst. Rev.* 6, CD003804. doi:10.1002/14651858.CD003804.pub2

Arnold, M., Sierra, M. S., Laversanne, M., Soerjomataram, I., Jemal, A., and Bray, F. (2017). Global patterns and trends in colorectal cancer incidence and mortality. *Gut* 66, 683–691. doi:10.1136/gutjnl-2015-310912

Aronson, S. J., and Rehm, H. L. (2015). Building the foundation for genomics in precision medicine. *Nature* 526, 336–342. doi:10.1038/nature15816

Bai, H., Li, X., Li, H., Yang, J., and Ning, K. (2019). Biological ingredient complement chemical ingredient in the assessment of the quality of TCM preparations. *Sci. Rep.* 9, 5853. doi:10.1038/s41598-019-42341-4

Bai, H., Ning, K., and Wang, C. y. (2015). Biological ingredient analysis of traditional Chinese medicines utilizing metagenomic approach based on high-throughput-sequencing and big-data-mining. *Acta Pharm. Sin. B* 50, 272–277. doi:10.1038/srep05147

Besse, P., Da Silva, D., and Grisoni, M. (2021). Plant DNA barcoding principles and limits: A case study in the genus vanilla. *Methods Mol. Biol.* 2222, 131–148. doi:10.1007/978-1-0716-0997-2_8

Boezio, B., Audouze, K., Ducrot, P., and Taboureau, O. (2017). Network-based approaches in pharmacology. *Mol. Inf.* 36, 1700048. doi:10.1002/minf.201700048

Buriani, A., Garcia-Bermejo, M. L., Bosisio, E., Xu, Q., Li, H., Dong, X., et al. (2012). Omic techniques in systems biology approaches to traditional Chinese medicine research: Present and future. *J. Ethnopharmacol.* 140, 535–544. doi:10.1016/j.jep.2012.01.055

Cai, F.-F., Zhou, W. J., Wu, R., and Su, S. B. (2018). Systems biology approaches in the study of Chinese herbal formulae. *Chin. Med.* 13, 65. doi:10.1186/s13020-018-0221-x

Chai, P., Yu, J., Ge, S., Jia, R., and Fan, X. (2020). Genetic alteration, RNA expression, and DNA methylation profiling of coronavirus disease 2019 (COVID-19) receptor ACE2 in malignancies: A pan-cancer analysis. *J. Hematol. Oncol.* 13, 43. doi:10.1186/s13045-020-00883-5

Chandrasekara, C., Naranpanawa, D. N. U., Bandusekara, B. S., Pushpakumara, D. K. N. G., Wijesundera, D. S. A., and Bandaranayake, P. C. G. (2021). Universal barcoding regions, rbcL, matK and trnH-psbA do not discriminate Cinnamomum species in Sri Lanka. *PLoS One* 16, e0245592. doi:10.1371/journal.pone.0245592

Chasseaud, L. F. (1979). The role of glutathione and glutathione S-transferases in the metabolism of chemical carcinogens and other electrophilic agents. *Adv. Cancer Res.* 29, 175–274. doi:10.1016/s0065-230x(08)60848-9

Chen, C. Y. C. (2011). TCM Database@Taiwan: The world's largest traditional Chinese medicine database for drug screening in silico. *PLoS One* 6, e15939. doi:10.1371/journal.pone.0015939

Chen, F., Wen, Q., Jiang, J., Li, H. L., Tan, Y. F., Li, Y. H., et al. (2016). Could the gut microbiota reconcile the oral bioavailability conundrum of traditional herbs? *J. Ethnopharmacol.* 179, 253–264. doi:10.1016/j.jep.2015.12.031

Chen, J., Jiang, Z., Li, C., Ping, X., Cui, S., Tang, S., et al. (2015). Identification of ungulates used in a traditional Chinese medicine with DNA barcoding technology. *Ecol. Evol.* 5, 1818–1825. doi:10.1002/ece3.1457

Chen, S., Pang, X., Song, J., Shi, L., Yao, H., Han, J., et al. (2014). A renaissance in herbal medicine identification: From morphology to DNA. *Biotechnol. Adv.* 32, 1237–1244. doi:10.1016/j.biotechadv.2014.07.004

Chen, X., Wu, Y., Chen, C., Gu, Y., Zhu, C., Wang, S., et al. (2021). Identifying potential anti-COVID-19 pharmacological components of traditional Chinese medicine Lianhuaqingwen capsule based on human exposure and ACE2 biochromatography screening. *Acta Pharm. Sin. B* 11, 222–236. doi:10.1016/j.apsb.2020.10.002

Chen, S., Yao, H., Han, J., Liu, C., Song, J., Shi, L., et al. (2010). Validation of the ITS2 region as a novel DNA barcode for identifying medicinal plant species. *PLoS One* 5, e8613. doi:10.1371/journal.pone.0008613

Cheng, X., Su, X., Chen, X., Zhao, H., Bo, C., Xu, J., et al. (2014). Biological ingredient analysis of traditional Chinese medicine preparation based on high-throughput sequencing: The story for Liuwei Dihuang wan. *Sci. Rep.* 4, 5147. doi:10.1038/srep05147

Chou, S. T., Hsiang, C. Y., Lo, H. Y., Huang, H. F., Lai, M. T., Hsieh, C. L., et al. (2017). Exploration of anti-cancer effects and mechanisms of Zuo-Jin-Wan and its alkaloid components *in vitro* and in orthotopic HepG2 xenograft immunocompetent mice. *BMC Complement. Altern. Med.* 17, 121. doi:10.1186/s12906-017-1586-6

Coghlan, M. L., Haile, J., Houston, J., Murray, D. C., White, N. E., Moolhuijzen, P., et al. (2012). Deep sequencing of plant and animal DNA contained within traditional Chinese medicines reveals legality issues and health safety concerns. *PLoS Genet.* 8, e1002657. doi:10.1371/journal.pgen.1002657

Deng, Z. (2010). TCM dietotherapy for hypertension. *J. Tradit. Chin. Med.* 30, 235–236. doi:10.1016/s0254-6272(10)60048-9

Ding, Z., Zhong, R., Yang, Y., Xia, T., Wang, W., Wang, Y., et al. (2020). Systems pharmacology reveals the mechanism of activity of Ge-Gen-Qin-Lian decoction against LPS-induced acute lung injury: A novel strategy for exploring active components and effective mechanism of TCM formulae. *Pharmacol. Res.* 156, 104759. doi:10.1016/j.phrs.2020.104759

Dong, Y., Chen, Y. T., Yang, Y. X., Zhou, X. J., Dai, S. J., Tong, J. F., et al. (2016). Metabolomics study of type 2 diabetes mellitus and the AntiDiabetic effect of berberine in zucker diabetic fatty rats using uplc-ESI-hdms. *Phytother. Res.* 30, 823–828. doi:10.1002/ptr.5587

Dunning, L. T., and Savolainen, V. (2010). Broad-scale amplification of matK for DNA barcoding plants, a technical note. *Bot. J. Linn. Soc.* 164, 1–9. doi:10.1111/j.1095-8339.2010.01071.x

Fan, H. H., Wang, L. Q., Liu, W. L., An, X. P., Liu, Z. D., He, X. Q., et al. (2020). Repurposing of clinically approved drugs for treatment of coronavirus disease 2019 in a 2019-novel coronavirus-related coronavirus model. *Chin. Med. J.* 133, 1051–1056. doi:10.1097/cm9.0000000000000797

Fan, J., Bao, Y., Meng, X., Wang, S., Li, T., Chang, X., et al. (2017). Mechanism of modulation through PI3K-AKT pathway about Nepeta cataria L.'s extract in non-small cell lung cancer. *Oncotarget* 8, 31395–31405. doi:10.18632/oncotarget.15608

Fan, W., Zhou, J., Wu, Z., Tan, G., Li, H., Mei, Q., et al. (2021). Analysis of antioxidants in Chrysanthemum indici flos by online gradient extraction and HPLC-FRAP. *Anal. Methods* 13, 2283–2289. doi:10.1039/d1ay00548k

Fang, S., Dong, L., Liu, L., Guo, J., Zhao, L., Zhang, J., et al. (2021). Herb: A high-throughput experiment- and reference-guided database of traditional Chinese medicine. *Nucleic Acids Res.* 49, D1197–d1206. doi:10.1093/nar/gkaa1063

Fathy, S. A., Mohamed, M. R., Ali, M. A. M., El-Helaly, A. E., and Alattar, A. T. (2019). Influence of IL-6, IL-10, IFN-γ and TNF-α genetic variants on susceptibility to diabetic kidney disease in type 2 diabetes mellitus patients. *Biomarkers* 24, 43–55. doi:10.1080/1354750x.2018.1501761

Feng, R., Shou, J. W., Zhao, Z. X., He, C. Y., Ma, C., Huang, M., et al. (2015). Transforming berberine into its intestine-absorbable form by the gut microbiota. *Sci. Rep.* 5, 12155. doi:10.1038/srep12155

Feng, R., Zhao, Z. X., Ma, S. R., Guo, F., Wang, Y., and Jiang, J. D. (2018). Gut microbiota-regulated pharmacokinetics of berberine and active metabolites in beagle dogs after oral administration. *Front. Pharmacol.* 9, 214. doi:10.3389/fphar.2018.00214

Gan, W. Z., Ramachandran, V., Lim, C. S. Y., and Koh, R. Y. (2019). Omics-based biomarkers in the diagnosis of diabetes. *J. Basic Clin. Physiol. Pharmacol.* 31. doi:10.1515/jbcpp-2019-0120

Gao, L., Cao, M., Li, J. Q., Qin, X. M., and Fang, J. S. (2021). Traditional Chinese medicine network pharmacology in cardiovascular precision medicine. *Curr. Pharm. Des.* 27, 2925–2933. doi:10.2174/1381612826666201112142408

Gómez-López, G., Dopazo, J., Cigudosa, J. C., Valencia, A., and Al-Shahrour, F. (2019). Precision medicine needs pioneering clinical bioinformaticians. *Brief. Bioinform.* 20, 752–766. doi:10.1093/bib/bbx144

Gong, B., Kao, Y., Zhang, C., Zhao, H., Sun, F., and Gong, Z. (2019). Exploring the pharmacological mechanism of the herb pair "HuangLian-GanJiang" against colorectal cancer based on network pharmacology. *Evid. Based. Complement. Altern. Med.* 2019, 2735050. doi:10.1155/2019/2735050

Gong, X., Ji, M., Xu, J., Zhang, C., and Li, M. (2020). Hypoglycemic effects of bioactive ingredients from medicine food homology and medicinal health food species used in China. *Crit. Rev. Food Sci. Nutr.* 60, 2303–2326. doi:10.1080/10408398.2019.1634517

Group, C. P. W. (2009). A DNA barcode for land plants. *Proc. Natl. Acad. Sci. U. S. A.* 106, 12794–12797. doi:10.1073/pnas.0905845106

Guo, R., Luo, X., Liu, J., Liu, L., Wang, X., and Lu, H. (2020). Omics strategies decipher therapeutic discoveries of traditional Chinese medicine against different diseases at multiple layers molecular-level. *Pharmacol. Res.* 152, 104627. doi:10.1016/j.phrs.2020.104627

Habtemariam, S. (2020). Berberine pharmacology and the gut microbiota: A hidden therapeutic link. *Pharmacol. Res.* 155, 104722. doi:10.1016/j.phrs.2020.104722

He, D., Huang, J. H., Zhang, Z. Y., Du, Q., Peng, W. J., Yu, R., et al. (2019). A network pharmacology-based strategy for predicting active ingredients and potential targets of LiuWei DiHuang pill in treating type 2 diabetes mellitus. *Drug Des. devel. Ther.* 13, 3989–4005. doi:10.2147/DDDT.S216644

Heindel, J. J., Blumberg, B., Cave, M., Machtinger, R., Mantovani, A., Mendez, M. A., et al. (2017). Metabolism disrupting chemicals and metabolic disorders. *Reprod. Toxicol.* 68, 3–33. doi:10.1016/j.reprotox.2016.10.001

Heinisch, S., and Rocca, J. L. (2009). Sense and nonsense of high-temperature liquid chromatography. *J. Chromatogr. A* 1216, 642–658. doi:10.1016/j.chroma.2008.11.079

Hoffmann, M., Kleine-Weber, H., Schroeder, S., Kruger, N., Herrler, T., Erichsen, S., et al. (2020). SARS-CoV-2 cell entry depends on ACE2 and TMPRSS2 and is blocked by a clinically proven protease inhibitor. *Cell.* 181, 271–280. e278. doi:10.1016/j.cell.2020.02.052

Hou, Y., and Jiang, J. G. (2013). Origin and concept of medicine food homology and its application in modern functional foods. *Food Funct.* 4, 1727–1741. doi:10.1039/c3fo60295h

Hu, C., He, B., Gong, F., Liang, M., Zhao, D., and Zhang, G. (2022). The adverse reactions of Lianhua qingwen capsule/granule compared with conventional drug in clinical application: A meta-analysis. *Front. Pharmacol.* 13, 764774. doi:10.3389/fphar.2022.764774

Huang, L., Xie, D., Yu, Y., Liu, H., Shi, Y., Shi, T., et al. (2018). Tcmid 2.0: A comprehensive resource for TCM. *Nucleic Acids Res.* 46, D1117-D1120–d1120. doi:10.1093/nar/gkx1028

Huang, S., Zhang, Z., Li, W., Kong, F., Yi, P., Huang, J., et al. (2020). Network pharmacology-based prediction and verification of the active ingredients and potential targets of zuojinwan for treating colorectal cancer. *Drug Des. devel. Ther.* 14, 2725–2740. doi:10.2147/dddt.S250991

Jameson, J. L., and Longo, D. L. (2015). Precision medicine-personalized, problematic, and promising. *N. Engl. J. Med.* 372, 2229–2234. doi:10.1056/NEJMsb1503104

Jia, J., Xu, Z., Xin, T., Shi, L., and Song, J. (2017). Quality control of the traditional patent medicine yimu wan based on SMRT sequencing and DNA barcoding. *Front. Plant Sci.* 8, 926. doi:10.3389/fpls.2017.00926

Jiang, D., Li, J., Li, J., Wang, M., Han, C., Wang, X., et al. (2017). Combination of FGFR4 inhibitor Blu9931 and 5-fluorouracil effects on the biological characteristics of colorectal cancer cells. *Int. J. Oncol.* 51, 1611–1620. doi:10.3892/ijo.2017.4143

Jiang, W. Y. (2005). Therapeutic wisdom in traditional Chinese medicine: A perspective from modern science. *Discov. Med.* 5, 455–461.

Joseph, T. A., and Pe'er, I. (2021). An introduction to whole-metagenome shotgun sequencing studies. *Methods Mol. Biol.* 2243, 107–122. doi:10.1007/978-1-0716-1103-6_6

Kim, H. J., Jee, E. H., Ahn, K. S., Choi, H. S., and Jang, Y. P. (2010). Identification of marker compounds in herbal drugs on TLC with DART-MS. *Arch. Pharm. Res.* 33, 1355–1359. doi:10.1007/s12272-010-0909-7

Kim, S., Chen, J., Cheng, T., Gindulyte, A., He, J., He, S., et al. (2021). PubChem in 2021: New data content and improved web interfaces. *Nucleic Acids Res.* 49, D1388–d1395. doi:10.1093/nar/gkaa971

Kologrivova, I. V., Suslova, T. E., Koshel'skaya, O. A., Vinnitskaya, I. V., and Trubacheva, O. A. (2014). System of matrix metalloproteinases and cytokine secretion in type 2 diabetes mellitus and impaired carbohydrate tolerance associated with arterial hypertension. *Bull. Exp. Biol. Med.* 156, 635–638. doi:10.1007/s10517-014-2413-4

Kolter, A., and Gemeinholzer, B. (2021). Plant DNA barcoding necessitates marker-specific efforts to establish more comprehensive reference databases. *Genome* 64, 265–298. doi:10.1139/gen-2019-0198

Kuhn, M., Szklarczyk, D., Pletscher-Frankild, S., Blicher, T. H., von Mering, C., Jensen, L. J., et al. (2014). Stitch 4: Integration of protein-chemical interactions with user data. *Nucleic Acids Res.* 42, D401–D407. doi:10.1093/nar/gkt1207

Kuhn, M., von Mering, C., Campillos, M., Jensen, L. J., and Bork, P. (2008). Stitch: Interaction networks of chemicals and proteins. *Nucleic Acids Res.* 36, D684–D688. doi:10.1093/nar/gkm795

Lan, J., Zhao, Y., Dong, F., Yan, Z., Zheng, W., Fan, J., et al. (2015). Meta-analysis of the effect and safety of berberine in the treatment of type 2 diabetes mellitus, hyperlipemia and hypertension. *J. Ethnopharmacol.* 161, 69–81. doi:10.1016/j.jep.2014.09.049

Lehmann, B. D., Colaprico, A., Silva, T. C., Chen, J., Ban, Y., Huang, H., et al. (2021). Multi-omics analysis identifies therapeutic vulnerabilities in triple-negative breast cancer subtypes. *Nat. Commun.* 12, 6276. doi:10.1038/s41467-021-26502-6

Leung, E. L.-H., Pan, H. D., Huang, Y. F., Fan, X. X., Wang, W. Y., He, F., et al. (2020). The scientific foundation of Chinese herbal medicine against COVID-19. *Engineering* 6, 1099–1107. doi:10.1016/j.eng.2020.08.009

Li, Q., Sun, Y., Guo, H., Sang, F., Ma, H., Peng, H., et al. (2018). Quality control of the traditional Chinese medicine Ruyi jinhuang powder based on high-throughput sequencing and real-time PCR. *Sci. Rep.* 8, 8261. doi:10.1038/s41598-018-26520-3

Li, S., Fan, T. P., Jia, W., Lu, A., and Zhang, W. (2014). Network pharmacology in traditional Chinese medicine. *Evid. Based. Complement. Altern. Med.* 2014, 138460. doi:10.1155/2014/138460

Lin, X., Yi, Z., Diao, J., Shao, M., Zhao, L., Cai, H., et al. (2014). ShaoYao decoction ameliorates colitis-associated colorectal cancer by downregulating proinflammatory cytokines and promoting epithelial-mesenchymal transition. *J. Transl. Med.* 12, 105. doi:10.1186/1479-5876-12-105

Lin, Y.-J., Ho, T. J., Yeh, Y. C., Cheng, C. F., Shiao, Y. T., Wang, C. B., et al. (2015). Chinese herbal medicine treatment improves the overall survival rate of individuals with hypertension among type 2 diabetes patients and modulates *in vitro* smooth muscle cell contractility. *PLoS One* 10, e0145109. doi:10.1371/journal.pone.0145109

Lindqvist, L., and Pelletier, J. (2009). Inhibitors of translation initiation as cancer therapeutics. *Future Med. Chem.* 1, 1709–1722. doi:10.4155/fmc.09.122

Liu, C.-S., Zheng, Y. R., Zhang, Y. F., and Long, X. Y. (2016a). Research progress on berberine with a special focus on its oral bioavailability. *Fitoterapia* 109, 274–282. doi:10.1016/j.fitote.2016.02.001

Liu, G. D., Huang, W. Z., Ma, S. P., and Wang, Z. Z. (2016b). Fingerprint of dazhu hongjingtian capsule by HPLC-DAD-QTOF-MS. *China J. Chin. Mater Med.* 41, 3022–3026. doi:10.4268/cjcmm20161613

Liu, Y., Wang, B., Shu, S., Li, Z., Song, C., Liu, D., et al. (2021). Analysis of the Coptis chinensis genome reveals the diversification of protoberberine-type alkaloids. *Nat. Commun.* 12, 3276. doi:10.1038/s41467-021-23611-0

Liu, Y., Yang, S., Wang, K., Lu, J., Bao, X., Wang, R., et al. (2020). Cellular senescence and cancer: Focusing on traditional Chinese medicine and natural products. *Cell. Prolif.* 53, e12894. doi:10.1111/cpr.12894

Luo, K., Chen, S., Chen, K., Song, J., Yao, H., Ma, X., et al. (2010). Assessment of candidate plant DNA barcodes using the Rutaceae family. *Sci. China. Life Sci.* 53, 701–708. doi:10.1007/s11427-010-4009-1

Luo, T. T., Lu, Y., Yan, S. K., Xiao, X., Rong, X. L., and Guo, J. (2020). Network pharmacology in research of Chinese medicine formula: Methodology, application and prospective. *Chin. J. Integr. Med.* 26, 72–80. doi:10.1007/s11655-019-3064-0

Lv, X., Li, Y., Tang, C., Zhang, Y., Zhang, J., and Fan, G. (2016). Integration of HPLC-based fingerprint and quantitative analyses for differentiating botanical species and geographical growing origins of Rhizoma coptidis. *Pharm. Biol.* 54, 3264–3271. doi:10.1080/13880209.2016.1223699

Mendez, D., Gaulton, A., Bento, A. P., Chambers, J., De Veij, M., Felix, E., et al. (2019). ChEMBL: Towards direct deposition of bioassay data. *Nucleic Acids Res.* 47, D930-D940–d940. doi:10.1093/nar/gky1075

Miryala, S. K., Anbarasu, A., and Ramaiah, S. (2018). Discerning molecular interactions: A comprehensive review on biomolecular interaction databases and network analysis tools. *Gene* 642, 84–94. doi:10.1016/j.gene.2017.11.028

Newmaster, S. G., Fazekas, A., and Ragupathy, S. (2006). DNA barcoding in land plants: Evaluation of rbcL in a multigene tiered approach. *Can. J. Bot.* 84, 335–341. doi:10.1139/b06-047

Olivier, M., Asmis, R., Hawkins, G. A., Howard, T. D., and Cox, L. A. (2019). The need for multi-omics biomarker signatures in precision medicine. *Int. J. Mol. Sci.* 20, E4781. doi:10.3390/ijms20194781

Qiu, J. (2007). China plans to modernize traditional medicine. *Nature* 446, 590–591. doi:10.1038/446590a

Ren, J. L., Zhang, A. H., and Wang, X. J. (2020). Traditional Chinese medicine for COVID-19 treatment. *Pharmacol. Res.* 155, 104743. doi:10.1016/j.phrs.2020.104743

Rivera, D., Allkin, R., Obon, C., Alcaraz, F., Verpoorte, R., and Heinrich, M. (2014). What is in a name? The need for accurate scientific nomenclature for plants. *J. Ethnopharmacol.* 152, 393–402. doi:10.1016/j.jep.2013.12.022

Ru, J., Li, P., Wang, J., Zhou, W., Li, B., Huang, C., et al. (2014). Tcmsp: A database of systems pharmacology for drug discovery from herbal medicines. *J. Cheminform.* 6, 13. doi:10.1186/1758-2946-6-13

Runfeng, L., Yunlong, H., Jicheng, H., Weiqi, P., Qinhai, M., Yongxia, S., et al. (2020). Lianhuaqingwen exerts anti-viral and anti-inflammatory activity against novel coronavirus (SARS-CoV-2). *Pharmacol. Res.* 156, 104761. doi:10.1016/j.phrs.2020.104761

Senthilkumar, G. P., Anithalekshmi, M. S., Yasir, M., Parameswaran, S., Packirisamy, R. M., and Bobby, Z. (2018). Role of omentin 1 and IL-6 in type 2 diabetes mellitus patients with diabetic nephropathy. *Diabetes Metab. Syndr.* 12, 23–26. doi:10.1016/j.dsx.2017.08.005

Sheehan, D., Meade, G., Foley, V. M., and Dowd, C. A. (2001). Structure, function and evolution of glutathione transferases: Implications for classification of non-mammalian members of an ancient enzyme superfamily. *Biochem. J.* 360, 1–16. doi:10.1042/0264-6021:3600001

Slaine, P. D., Kleer, M., Smith, N. K., Khaperskyy, D. A., and McCormick, C. (2017). Stress granule-inducing eukaryotic translation initiation factor 4A inhibitors block influenza A virus replication. *Viruses* 9, E388. doi:10.3390/v9120388

Subramanian, I., Verma, S., Kumar, S., Jere, A., and Anamika, K. (2020). Multi-omics data integration, interpretation, and its application. *Bioinform. Biol. Insights* 14, 1177932219899051. doi:10.1177/1177932219899051

Sun, Q., He, M., Zhang, M., Zeng, S., Chen, L., Zhao, H., et al. (2021). Traditional Chinese medicine and colorectal cancer: Implications for drug discovery. *Front. Pharmacol.* 12, 685002. doi:10.3389/fphar.2021.685002

Tao, W., Xu, X., Wang, X., Li, B., Wang, Y., Li, Y., et al. (2013). Network pharmacology-based prediction of the active ingredients and potential targets of Chinese herbal Radix Curcumae formula for application to cardiovascular disease. *J. Ethnopharmacol.* 145, 1–10. doi:10.1016/j.jep.2012.09.051

Vences, M., Thomas, M., Bonett, R. M., and Vieites, D. R. (2005). Deciphering amphibian diversity through DNA barcoding: Chances and challenges. *Philos. Trans. R. Soc. Lond. B Biol. Sci.* 360, 1859–1868. doi:10.1098/rstb.2005.1717

Wang, B., Feng, X., Liu, S., Qiu, F., Lu, X., and Li, Z. (2021). Comprehensive quality assessment of Kaixin powder by HPLC-DAD quantification and HPLC-QTOF-MS/MS confirmation. *ACS omega* 6, 11319–11326. doi:10.1021/acsomega.1c00289

Wang, J., Wang, L., Lou, G. H., Zeng, H. R., Hu, J., Huang, Q. W., et al. (2019). Coptidis rhizoma: A comprehensive review of its traditional uses, botany, phytochemistry, pharmacology and toxicology. *Pharm. Biol.* 57, 193–225. doi:10.1080/13880209.2019.1577466

Wang, W.-L., Xu, S. Y., Ren, Z. G., Tao, L., Jiang, J. W., and Zheng, S. S. (2015). Application of metagenomics in the human gut microbiome. *World J. Gastroenterol.* 21, 803–814. doi:10.3748/wjg.v21.i3.803

Wang, W. J., and Zhang, T. (2017). Integration of traditional Chinese medicine and Western medicine in the era of precision medicine. *J. Integr. Med.* 15, 1–7. doi:10.1016/s2095-4964(17)60314-5

Wang, Y., Shi, Y., Zou, J., Zhang, X., Liang, Y., Tai, J., et al. (2020). Network pharmacology exploration reveals a common mechanism in the treatment of cardio-cerebrovascular disease with Salvia miltiorrhiza Burge. and Carthamus tinctorius L. *BMC Complement. Med. Ther.* 20, 351. doi:10.1186/s12906-020-03026-y

Wang, Y., Xiao, J., Suzek, T. O., Zhang, J., Wang, J., and Bryant, S. H. (2009). PubChem: A public information system for analyzing bioactivities of small molecules. *Nucleic Acids Res.* 37, W623–W633. doi:10.1093/nar/gkp456

Wishart, D. S., Feunang, Y. D., Guo, A. C., Lo, E. J., Marcu, A., Grant, J. R., et al. (2018). DrugBank 5.0: A major update to the DrugBank database for 2018. *Nucleic Acids Res.* 46, D1074-D1082–d1082. doi:10.1093/nar/gkx1037

Wishart, D. S., Knox, C., Guo, A. C., Shrivastava, S., Hassanali, M., Stothard, P., et al. (2006). DrugBank: A comprehensive resource for *in silico* drug discovery and exploration. *Nucleic Acids Res.* 34, D668–D672. doi:10.1093/nar/gkj067

Wolfender, J. L., Ndjoko, K., and Hostettmann, K. (2003). Liquid chromatography with ultraviolet absorbance-mass spectrometric detection and with nuclear magnetic resonance spectroscopy: A powerful combination for the on-line structural investigation of plant metabolites. *J. Chromatogr. A* 1000, 437–455. doi:10.1016/s0021-9673(03)00303-0

Wu, G. S., Li, H. K., and Zhang, W. D. (2019). Metabolomics and its application in the treatment of coronary heart disease with traditional Chinese medicine. *Chin. J. Nat. Med.* 17, 321–330. doi:10.1016/s1875-5364(19)30037-8

Wu, G., Zhao, J., Zhao, J., Song, N., Zheng, N., Zeng, Y., et al. (2021a). Exploring biological basis of Syndrome differentiation in coronary heart disease patients with two distinct Syndromes by integrated multi-omics and network pharmacology strategy. *Chin. Med.* 16, 109. doi:10.1186/s13020-021-00521-3

Wu, X., Li, W., Qin, Z., Xue, L., Huang, G., Luo, Z., et al. (2021b). Traditional Chinese medicine as an adjunctive therapy for mild and common COVID-19: A systematic review and network meta-analysis. *Med. Baltim.* 100, e27372. doi:10.1097/md.0000000000027372

Wu, Z., Lu, W., Yu, W., Wang, T., Li, W., Liu, G., et al. (2018). Quantitative and systems pharmacology 2. *in silico* polypharmacology of G protein-coupled receptor ligands via network-based approaches. *Pharmacol. Res.* 129, 400–413. doi:10.1016/j.phrs.2017.11.005

Xiang, Y., Guo, Z., Zhu, P., Chen, J., and Huang, Y. (2019). Traditional Chinese medicine as a cancer treatment: Modern perspectives of ancient but advanced science. *Cancer Med.* 8, 1958–1975. doi:10.1002/cam4.2108

Xiao, M., Tian, J., Zhou, Y., Xu, X., Min, X., Lv, Y., et al. (2020). Efficacy of huoxiang zhengqi dropping pills and Lianhua qingwen granules in treatment of COVID-19: A randomized controlled trial. *Pharmacol. Res.* 161, 105126. doi:10.1016/j.phrs.2020.105126

Xin, T., Su, C., Lin, Y., Wang, S., Xu, Z., and Song, J. (2018a). Precise species detection of traditional Chinese patent medicine by shotgun metagenomic sequencing. *Phytomedicine* 47, 40–47. doi:10.1016/j.phymed.2018.04.048

Xin, T., Xu, Z., Jia, J., Leon, C., Hu, S., Lin, Y., et al. (2018b). Biomonitoring for traditional herbal medicinal products using DNA metabarcoding and single molecule, real-time sequencing. *Acta Pharm. Sin. B* 8, 488–497. doi:10.1016/j.apsb.2017.10.001

Xin, T., Zhang, Y., Pu, X., Gao, R., Xu, Z., and Song, J. (2019). Trends in herbgenomics. *Sci. China. Life Sci.* 62, 288–308. doi:10.1007/s11427-018-9352-7

Xu, X., Xu, H., Shang, Y., Zhu, R., Hong, X., Song, Z., et al. (2021). Development of the general chapters of the Chinese Pharmacopoeia 2020 edition: A review. *J. Pharm. Anal.* 11, 398–404. doi:10.1016/j.jpha.2021.05.001

Xue, R., Fang, Z., Zhang, M., Yi, Z., Wen, C., and Shi, T. (2013). Tcmid: Traditional Chinese Medicine integrative database for herb molecular mechanism analysis. *Nucleic Acids Res.* 41, D1089–D1095. doi:10.1093/nar/gks1100

Yan, D., Zheng, G., Wang, C., Chen, Z., Mao, T., Gao, J., et al. (2022). Hit 2.0: An enhanced platform for herbal ingredients' targets. *Nucleic Acids Res.* 50, D1238–d1243. doi:10.1093/nar/gkab1011

Yang, M., Lao, L., Yang, M., and Lao, L. (2019). Emerging applications of metabolomics in traditional Chinese medicine treating hypertension: Biomarkers, pathways and MoreEmerging applications of metabolomics in traditional Chinese medicine treating hypertension: Biomarkers, pathways and more. *Front. Pharmacol.* 10, 158. doi:10.3389/fphar.2019.00158

Yang, P. S., Lang, J., Li, H., Lu, J., Lin, H., Tian, G., et al. (2022). TCM-suite: A comprehensive and holistic platform for traditional Chinese medicine component identification and network pharmacology analysis. *iMeta* e47. doi:10.1002/imt2.47

Yang, X., Han, S., Zhang, X., Sun, Y., Xing, Y., et al. (2019). The role of traditional Chinese medicine in the regulation of oxidative stress in treating coronary heart disease. *Oxid. Med. Cell. Longev.* 2019, 3231424. doi:10.1155/2019/3231424

Yao, Q., Zhu, X., Han, M., Chen, C., Li, W., Bai, H., et al. (2022). Decoding herbal materials of TCM preparations with the multi-barcode sequencing approach. *Sci. Rep.* 12, 5988. doi:10.1038/s41598-022-09979-z

Yao, Y., Chen, H., Yan, L., Wang, W., and Wang, D. (2020). Berberine alleviates type 2 diabetic symptoms by altering gut microbiota and reducing aromatic amino acids. *Biomed. Pharmacother.* 131, 110669. doi:10.1016/j.biopha.2020.110669

Ye, H., Ye, L., Kang, H., Zhang, D., Tao, L., Tang, K., et al. (2011). Hit: Linking herbal active ingredients to targets. *Nucleic Acids Res.* 39, D1055–D1059. doi:10.1093/nar/gkq1165

Yi, Y. D., and Chang, I. M. (2004). An overview of traditional Chinese herbal formulae and a proposal of a new code system for expressing the formula titles. *Evid. Based. Complement. Altern. Med.* 1, 125–132. doi:10.1093/ecam/neh019

Yuan, R., and Lin, Y. (2000). Traditional Chinese medicine: An approach to scientific proof and clinical validation. *Pharmacol. Ther.* 86, 191–198. doi:10.1016/s0163-7258(00)00039-5

Zeng, K. W., Jiang, Y., Wang, J., Ye, M., Li, J., Ai, X. N., et al. (2019). TCM chemical biology-emerging interdiscipline of "TCM chemistry" and "biology. *China J. Chin. Mater Med.* 44, 849–860. doi:10.19540/j.cnki.cjcmm.20190222.011

Zeng, X., Zheng, Y., Liu, Y., and Su, W. (2021). Chemical composition, quality control, pharmacokinetics, pharmacological properties and clinical applications of fufang danshen tablet: A systematic review. *J. Ethnopharmacol.* 278, 114310. doi:10.1016/j.jep.2021.114310

Zhang, H., Wei, J., Xue, R., Wu, J. D., Zhao, W., Wang, Z. Z., et al. (2010). Berberine lowers blood glucose in type 2 diabetes mellitus patients through increasing insulin receptor expression. *Metabolism.* 59, 285–292. doi:10.1016/j.metabol.2009.07.029

Zhang, P., Liu, C., Zheng, X., Wu, L., Liu, Z., Liao, B., et al. (2019a). Full-length multi-barcoding: DNA barcoding from single ingredient to complex mixtures. *Genes.* 10, E343. doi:10.3390/genes10050343

Zhang, R., Gao, X., Bai, H., and Ning, K. (2020a). Traditional Chinese medicine and gut microbiome: Their respective and concert effects on healthcare. *Front. Pharmacol.* 11, 538. doi:10.3389/fphar.2020.00538

Zhang, R., Zhu, X., Bai, H., and Ning, K. (2019b). Network pharmacology databases for traditional Chinese medicine: Review and assessment. *Front. Pharmacol.* 10, 123. doi:10.3389/fphar.2019.00123

Zhang, R. Z., Yu, S. J., Bai, H., and Ning, K. (2017). TCM-Mesh: The database and analytical system for network pharmacology analysis for TCM preparations. *Sci. Rep.* 7, 2821. doi:10.1038/s41598-017-03039-7

Zhang, Y., Gu, Y., Ren, H., Wang, S., Zhong, H., Zhao, X., et al. (2020b). Gut microbiome-related effects of berberine and probiotics on type 2 diabetes (the PREMOTE study). *Nat. Commun.* 11, 5015. doi:10.1038/s41467-020-18414-8

Zhu, K. Y., Fu, Q., Xie, H. Q., Xu, S. L., Cheung, A. W. H., Zheng, K. Y. Z., et al. (2010). Quality assessment of a formulated Chinese herbal decoction, kaixinsan, by using rapid resolution liquid chromatography coupled with mass spectrometry: A chemical evaluation of different historical formulae. *J. Sep. Sci.* 33, 3666–3674. doi:10.1002/jssc.201000498

frontiers | Frontiers in Pharmacology

TYPE Original Research
PUBLISHED 29 November 2022
DOI 10.3389/fphar.2022.1022627

OPEN ACCESS

EDITED BY
Sheng Guo,
Nanjing University of Chinese Medicine, China

REVIEWED BY
Zhi Yong Du,
Beijing Anzhen Hospital, Capital Medical University, China
Kunming Qin,
Jiangsu Ocean Universiity, China

*CORRESPONDENCE
Jun Hu,
1398046131@qq.com
Jie Wang,
wangjie0103@126.com

†These authors have contributed equally to this work

SPECIALTY SECTION
This article was submitted to Ethnopharmacology, a section of the journal Frontiers in Pharmacology

RECEIVED 18 August 2022
ACCEPTED 14 November 2022
PUBLISHED 29 November 2022

CITATION
Yang G, Zhou S, He H, Shen Z, Liu Y, Hu J and Wang J (2022), Exploring the "gene–protein–metabolite" network of coronary heart disease with phlegm and blood stasis syndrome by integrated multi-omics strategy. *Front. Pharmacol.* 13:1022627. doi: 10.3389/fphar.2022.1022627

Exploring the "gene–protein–metabolite" network of coronary heart disease with phlegm and blood stasis syndrome by integrated multi-omics strategy

Guang Yang[1†], Siyuan Zhou[1†], Haoqiang He[1†], Zinuo Shen[2], Yongmei Liu[1], Jun Hu[1*] and Jie Wang[1*]

[1]Department of Cardiology, Guang'anmen Hospital, China Academy of Chinese Medical Sciences, Beijing, China, [2]School of traditional chinese medicine, Beijing University of Chinese Medicine, Beijing, China

Background: According to the theory of traditional Chinese medicine, phlegm and blood stasis (PBS) is the pathological basis for coronary heart disease (CHD). This study aimed to explore the biological basis of PBS syndrome in CHD.

Methods: Using a strategy that integrated RNA-seq, DIA-based proteomics, and untargeted metabolomics on 90 clinic samples, we constructed a "gene–protein–metabolite" network for CHD-PBS syndrome. We expanded the sample size and validated the differential genes and metabolites in the network through enzyme-linked immunosorbent assay.

Results: Our findings revealed that the "gene–protein–metabolite" network of CHD-PBS syndrome included 33 mRNAs, four proteins, and 25 metabolites. JNK1, FOS, CCL2, CXCL8, PTGS2, and CSF1 were all poorly expressed in the PBS group during the sequencing stage, whereas arachidonic acid (AA) was highly expressed. During the validation stage, JNK1, AP-1, CCL2, and CXCL8 were poorly expressed, whereas PTGS2, CSF1, and AA were highly expressed. The area under the receiver operating curve was as follows: CSF1 [0.9635, 95%CI (0.9295, 0.9976)] >JNK1 [0.9361, 95% CI (0.8749, 0.9972)] >CXCL8 [0.8953, 95% CI (0.8222, 0.9684)] > CCL2 [0.8458, 95% CI (0.7676, 0.9241)] >AP-1 [0.7884, 95%CI (0.6869, 0.8899)]. The logistic regression model composed of CSF1 and JNK1 showed the greatest diagnostic value and significance for PBS syndrome.

Abbreviations: AA, Arachidonic acid; ACS, Acute coronary syndrome; AUC, Area under the receiver operating curve; AUC, Area under the receiver operating curve; CHD, Coronary heart disease; DDA, Data dependent acquisition; DGs, Differential genes; DMs, Differential metabolites; DPs, Differential proteins; Elisa, Enzyme linked immunosorbent assay; FC, Fold change; HC, Healthy control; KEGG, Kyoto Encyclopedia of Genes and Genomes; LC-MS, Liquid chromatography tandem mass spectrometry; NPBS, Non phlegm and blood stasis syndrome; OPLS-DA, Orthogonal partial least-squares-discriminant analysis; PBS, Phlegm and Blood Stasis; PPI, Protein-protein interaction; ROC, Receiver operating characteristic curve; TCM, traditional Chinese medicine; VIP, Variable importance in the projection.

Conclusion: PBS syndrome is characterized by low levels of FOS, AP-1, CCL2, CXCL8, and JNK1 and elevated levels of PTGS2 and CSF1, implying that the AA metabolism is abnormal and that the JNK/AP-1 pathway is inhibited. PBS syndromes, as a subtype of CHD, may have unique molecular changes. Background. Globally, coronary heart disease (CHD) is the leading cause of death, and this would likely continue until 2030 (Mirzaei et al., 2009, 95, 740–746). According to the disease course, CHD can be classified as chronic stable CHD (or chronic coronary syndrome) and acute coronary syndrome (ACS) (Katus et al., 2017; Knuuti, 2019). Although stable CHD is not as lethal as ACS, it has a varied incidence range and patients with CHD have prolonged angina. Some symptoms of stable angina are alleviated with pharmacological therapy, but it cannot eliminate recurrent angina (Rousan et al., 2017). The clinical outcomes were not significantly improved in patients who underwent revascularization compared with those who received optimal pharmacological therapy (Shaw et al., 2008; Antman and Braunwald, 2020). A bottleneck appears to exist in CHD treatment, and traditional Chinese medicine (TCM) can act as a favorable complement. Because of its individualized treatment approach, TCM is widely practiced in eastern civilizations (Teng et al., 2016). TCM has become a principal complement in western countries (Wieland et al., 2013). Like "disease" is used in western medicine, "syndrome" is used in TCM to comprehend anomalous human conditions on the basis of patients' symptoms, tongue, and pulse (Li et al., 2012). On the basis of disease-syndrome diagnose, a TCM doctor can subclassify CHD patients into various categories, such as phlegm and blood stasis (PBS) syndrome, cold congealing and Qi stagnation syndrome, and Qi stagnation and blood stasis syndrome. PBS syndrome has recently emerged as a hot research topic in the TCM field. Objective diagnosis, expert consultations, and efficacy evaluation scales have been developed for PBS syndrome (Ren et al., 2020; Liu et al., 2021; Zheng et al., 2022). The concept of "omics" originates from the genome. It refers to the vocabulary generated by biological molecules at different levels to describe high-sequence molecular biological data resources (Dai and Shen, 2022). RNA, protein, and metabolites decipher the essence of complex etiologies, and the integration of transcriptomics, proteomics, and metabolomics are becoming a promising research mode (Pan et al., 2022). Multi-omics studies have revealed the biological characteristics of APOE transgenic mice, bronchopulmonary dysplasia, and plant tolerant to heavy metals (Singh et al., 2016; Lal et al., 2018; Mohler et al., 2020). Over the past few years, many academic achievements related to CHD-PBS syndrome have been accrued in the single-omic area. For example, Zhou identified the differential metabolites between PBS syndrome and Qi and Yin deficiency syndrome by using the urine samples of 1072 volunteers. Some of the specific metabolites of PBS syndrome are pyroglutamic acid, glutaric acid, glucose, mannitol, and xanthine (Zhou et al., 2019). Li's metabolomic study suggested that valine, leucine, isoleucine, and glycerol phospholipid metabolism could represent PBS syndrome (Zheng et al., 2022). Although some progress has been made in the understanding of PBS syndrome in CHD through the studies conducted, some issues still exist, such as a single-omics level, a lack of in-depth research, an inability to verify each other's research results, and a lack of validation of research conclusions. Overall, a systematic description of the biological foundation of PBS syndrome is lacking. Thus, the present study utilizes system biology methodologies and constructs a multi-omics network by integrating differential genes, proteins, and metabolites to systematically and comprehensively reveal the biological basis of CHD-PBS syndrome. The current

study explored 1) the characteristics of the transcriptome, proteome, and metabolome for CHD-PBS syndrome; 2) the "gene–protein–metabolite" network based on differential genes (DGs), differential proteins (DPs), and differential metabolites (DMs); 3) the key biological process and metabolic pathway most related to PBS syndrome; and 4) quantitative results and the diagnostic potential of biomarkers for PSB syndrome. Materials and methods. Multi-omics sequencing, bioinformatics analysis, and clinical validation research strategy. We collected the blood samples from healthy subjects as well as CHD patients with PBS and non-phlegm and blood stasis (NPBS) syndrome to compare the differences between them by subjecting the samples to the transcriptome, proteome, and metabolomics analyses. Bioinformatics analysis identified differential molecules as well as related biological processes and pathways. Next, the "gene–protein–metabolite" network was constructed using the MetaboAnalyst database, String database, and Cytoscape software. We selected molecules with strong centrality and biological association as potential PBS syndrome biomarkers and recruited more volunteers for further validation by enzyme-linked immunosorbent assay (ELISA). Finally, the ROC curve was utilized to assess the level and diagnostic efficacy of various molecules (Figure 1).

KEYWORDS

coronary heart disease, phlegm and blood stasis syndrome, traditional Chinese medicine, RNA-seq, proteomics, metabolomics

Participants recruitment

The RNA-seq-based transcriptomic analysis included 15 participants, five each with CHD-PBS syndrome and CHD-NPBS syndrome and five healthy controls (HC). The data-independent-acquisition (DIA) proteomic study included 18 participants, six each with CHD-PBS syndrome and CHD-NPBS syndrome and six HC. The metabolomic study included 30 patients each with CHD-PBS syndrome and CHD-NPBS syndrome and 30 HC. The diagnostic test included 94 participants, of which 64 patients had CHD-PBS syndrome and 30 were HC. The informed consent forms were signed voluntarily by all participants. The CHD patients were recruited from cardiovascular ward of Guang'anmen Hospital and outpatient clinic between August 2020 to March 2021. The healthy adults were enrolled when they showed normal physical examination. One Chief Physician of Cardiovascular Department in Guang'anmen Hospital (J Hu) determined whether patients met the inclusion criteria and Exclusion criteria, with verification by three assistants (G Yang, HQ He, and SY Zhou). The ethics committee of Guang 'anmen Hospital approved the study (No. 2019-225-KY).

Inclusion criteria

The inclusion criteria were as follows: patients diagnosed with CHD-PBS syndrome and CHD-NPBS syndrome; age 30–75 years; voluntary participation. The disease diagnosis was made with reference to the 2019 European Society of Cardiology Guidelines for the Diagnosis and Management of Chronic Coronary Syndromes (Knuuti, 2019). The syndrome diagnosis was referred to the Diagnostic Criteria for Syndrome Elements of Coronary Heart Disease Angina, as published by the Chinese Society of Traditional Chinese Medicine Cardiovascular Disease Branch in 2018 (Wang and Xing, 2018) (Supplementary Figure S1). One syndrome was diagnosed when the total symptom score was >8. PBS syndrome was diagnosed when both phlegm syndrome and blood stasis syndrome criteria were met. Otherwise, the condition was diagnosed as NPBS syndrome.

Exclusion criteria

Participants meeting any of the following criteria would be excluded from the study. 1) Patients with a history of unstable angina or acute myocardial infarction; other conditions that can cause chest pain, including congenital heart disease, valvular disease, and severe neurological disorders; arrhythmias; 2) Patients with the acute phase of cerebral infarction. 3) Patients with severe liver and kidney diseases; patients with alanine aminotransferase and aspartate aminotransferase 1.5 times higher than the normal upper limit; patients with abnormal renal function. 4) Infection acute within the past 2 weeks. 5) Patients with other life-threatening conditions requiring treatment (e.g., t hematological diseases, umors, diabetic complications, etc.)

RNA-seq-based transcriptomic study

Sample collection and RNA extraction

Fasting venous blood samples were collected from the subjects in the early morning and dispensed into 2 ml EDTA-containing anticoagulation tubes. The tubes were centrifuged for 15 min and the supernatant was discarded. The precipitate was then transferred into a 15-ml centrifuge tube, to which an erythrocyte lysate was added in a ratio of 1:3. The tube was allowed to sit for 10 min and centrifuged again. After the centrifugation, the supernatant was discarded and the erythrocyte lysate was added at a ratio of 1: 1 and centrifuged again. After centrifugation, the supernatant was discarded and the precipitate was transferred into a 2-ml lyophilization tube. To this tube, 1.5 ml of Trizol was added and the tube was placed in a −80°C refrigerator for freezing. Total RNA was extracted using the mirVana miRNA Isolation Kit (Ambion) as per the manufacturer's protocol. RNA purity and quantification were evaluated using the NanoDrop 2000 spectrophotometer. RNA integrity was assessed using the Agilent 2100 Bioanalyzer.

Library construction and sequencing

The RNA library was completed by Shanghai OE Biotech Co., Ltd. The libraries were constructed using the TruSeq Stranded mRNA LT Sample Prep Kit (Illumina, San Diego, CA, United States) according to the manufacturer's instructions. These libraries were then sequenced on the Illumina HiSeq X Ten platform to generate 150-bp paired-end reads. About 49 M raw reads for each sample were generated in all. Raw data (raw reads) in the fastq format were first processed using Trimmomatic and the low-quality reads were removed to obtain clean reads. Then, about 48.8 M clean reads for each sample were retained for subsequent analyses. The clean reads were mapped to the human genome (GRCh38) using HISAT2. FPKM of each gene was calculated using Cufflinks, and the read counts of each gene were obtained by HTSeqcount.

Differential gene expression analysis

Differential gene expression analysis was performed using the DESeq2 package for the R software. $p < 0.05$ and foldchange(FC) > 2 or foldchange <0.5 was set as the threshold for DGs. Hierarchical cluster analysis of DGs was performed to demonstrate the expression pattern of genes in different groups and samples. GO enrichment and KEGG pathway enrichment analysis of DGs were respectively performed using the R software based on the hypergeometric distribution.

Data-independent-acquisition-based proteomic study

Plasma protein extraction

Fasting venous blood samples of the participants were collected in the morning and subpacked into a 2-ml EDTA-containing anticoagulation tube for centrifugation. The supernatant was centrifuged at 3000 ×*g* at 4°C for 15 min and the fresh supernatant was collected into an Eppendorf tube. Proteins were extracted and identified by Shanghai OE Biotech Co., Ltd, followed by their labeling and storage in a refrigerator at −80°C. The total protein content in the sample was determined; half of the protein was subjected to protein concentration determination and SDS-PAGE detection, and the remaining half was subjected to trypsin enzymolysis. After desalting the enzymolysis peptide, the samples were identified by liquid chromatography-tandem mass spectrometry (LC-MS/MS).

Liquid chromatography-tandem mass spectrometry detection

All analyses were performed by using the Q-Exactive HF mass spectrometer (Thermo, United States) equipped with a Nanospray Flex source (Thermo). Before mass spectrometry detection, each sample was mixed according to the volume ratio iRT: sample to be tested = 1:10 as an internal standard. First, high-pH liquid-phase separation was performed. All samples after enzymatic hydrolysis were mixed with equal amounts of peptides. The Agilent 1100 HPLC system was used to separate the components in the mobile phase with pH = 10. A total of 10 components were collected and vacuum-freeze-dried until further analyses by mass spectrometry. The liquid in the storage ring was pushed into the analysis column connected with the mass spectrometer by a high-pressure pump at the flow rate of 1 μL/min and separated by the 30SPD method. The MS parameters of data-dependent acquisition (DDA) were set as follows: Capillary: 1.5 kV; Dry Temperature: 180°C; Dry Gas: 3.0 L/min. Mass Range: 100–1700 m/z; Ion Mobility: 0.6–1.6; Collision Energy: 20–59 EV. DIA mass spectrum scanning parameters were kept the same as for DDA.

Liquid chromatography-tandem mass spectrometry data analysis

The MS output was matched with the theoretical spectrogram generated by the fastA library. The original LC-MS/MS file was imported to Spectronaut Pulsar for library search and construction. The main parameters included Missed cleavage: two; Fixed modification: Carbamidomethyl (C); Variable modification: Oxidation (M); Enzyme: Trypsin/P; Protein FDR Cut Off: 0.01; Peptide FDR Cut Off: 0.01; PSM FDR Cut Off: 0.01; Database: Uniprot-REVIEWED -Homo sapiens (Human) -2020081. DIA raw data were processed using the Spectronaut Pulsar software. The key parameters were as follows: Precursor Qvalue cutoff: 0.01; Protein Qvalue

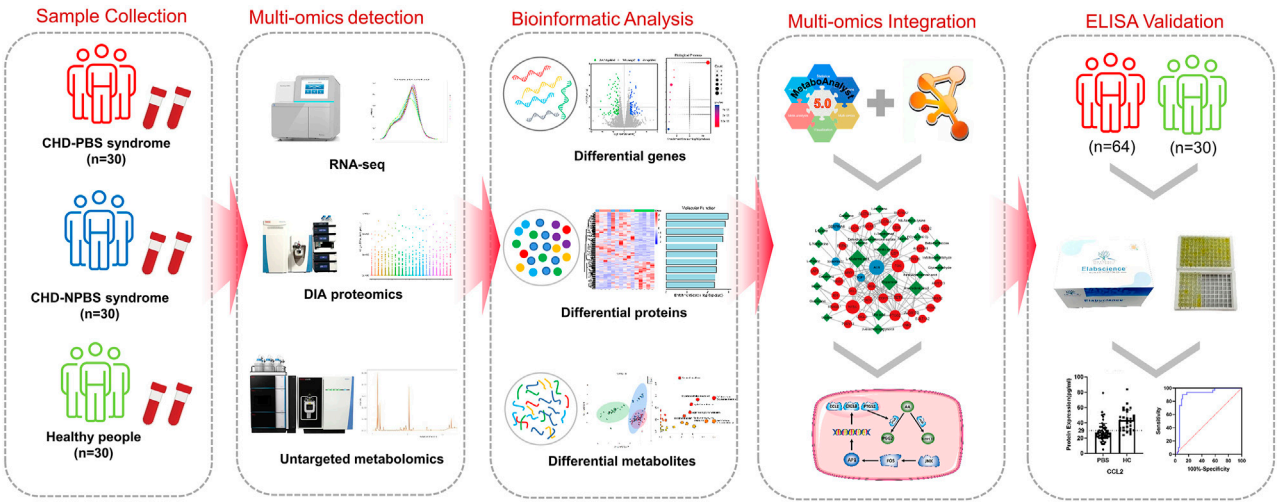

FIGURE 1
The flowchart of the integrated multi-omics strategy for PBS syndrome.

cutoff: 0.01; Normalization Strategy: Local Normalization; Quantity MS-Level: MS2.

Trusted protein analysis

The original data were retrieved from the database, and proteins whose expression value accounted for ≥50% were retained in any group of samples. Proteins with missing values ≤ 50% were filled with the mean value of the same group. The trusted proteins were obtained by Median Normalization and log2 conversion. Log2FC was obtained by subtracting the average value of the trusted proteins in different groups. The fold change was calculated from log2FC, and MS Excel was used to calculate the FC and *q*-value. The screening criteria were FC > 1.2 and *q*-value < 0.05, and the volcano map was drawn with the ggplot2 package of R software for visualization.

Untargeted metabolomic study

Sample preparation

Human fasting venous blood samples were collected from 08:00 AM to 10:00 AM, and the serum was obtained after centrifugation at 3000 ×*g* at 4°C for 10 min. The samples stored at −80°C were thawed at room temperature. Sample preparation and LC-MS detection were completed by Shanghai OE Biotech Co., Ltd. Briefly, 100 μL of the sample was added to a 1.5-ml Eppendorf tube containing 10 μl of 2-chloro-L-phenylalanine (0.3 mg/ml) dissolved in methanol as an internal standard, and the tube was vortexed for 10 s. Subsequently, 300 μl of an ice-cold mixture of methanol and acetonitrile (2/1, v/v) was added to the tube, and the mixture was vortexed for 1 min, ultrasonicated at ambient temperature (25°C–28°C) for 10 min, and stored at −20°C for 30 min. The extract was centrifuged at 13000 rpm, 4°C for 15 min. Then, 300 ml of the supernatant was collected in a brown glass vial and dried in a freeze-concentration centrifugal dryer. Then, 400 μl of a methanol and water mixture (1/4, vol/vol) was added to each sample, vortexed for 30 s, and placed at 4°C for 2 min. The samples were centrifuged at 13000 rpm/4°C for 5 min. The supernatants (150 μl) from each tube were collected using crystal syringes, filtered through 0.22-μm microfilters, and transferred into LC vials. These vials were stored at −80°C until LC/MS analyses.

Analysis conditions of LC/MS

The LC-MS system used was the Dionex U3000 UHPLC Ultra-High Performance Liquid and QE PLUS High-resolution Mass Spectrometer under the following chromatographic conditions: chromatographic column: ACQUITY UPLC HSS T3 (100 × 2.1 mm, 1.8 um); column temperature: 45°C; Mobile phase: A-water (containing 0.1% formic acid), B- acetonitrile (containing 0.1% formic acid); Flow rate: 0.35 ml/min; Injection volume: 2 μl. The MS conditions were as follows: Ion source: ESI; Positive and negative ion scanning mode was used to collect the MS signals. Mass spectrum parameters: Spray Voltage (V): 3800 (positive ion), -3000 (negative ion); MS parameters: Spray Voltage (V): 3800 (positive ion), -3000 (negative ion); Capillary Temperature (°C): 320; Aux gas heater temperature (°C): 350; Sheath Gas Flow Rate (Arb): 35; Aux gas flow rate (Arb): 8; S-lens RF level: 50; Mass range (m/z):

TABLE 1 Clinical characteristics of CHD patients with either PBS or NPBS syndrome.

Participants	CHD-PBS	CHD-NPBS	HC
RNA-seq			
sample size	5	5	5
Age	60.20 ± 13.63	63.20 ± 3.49	25.00 ± 1.87
Sex (male%)	4 (80.00%)	3 (60.00%)	3 (60.00%)
Hypertension (%)	4 (80.00%)	3 (60.00%)	0
Hyperlipidemia (%)	2 (40.00%)	5 (100.00%)	0
Diabetes (%)	3 (60.00%)	1 (20.00%)	0
DIA-based proteomics			
sample size	6	6	6
Age	59.33 ± 12.37	63.17 ± 3.13	25.00 ± 1.67
Sex (male%)	5 (83.33%)	4 (66.67%)	3 (50.00%)
Hypertension (%)	4 (66.67%)	3 (50.00%)	0
Hyperlipidemia (%)	3 (50.00%)	5 (83.33%)	0
Diabetes (%)	3 (50.00%)	2 (33.33%)	0
Metabolomics			
sample size	30	30	30
Age	60.04 ± 7.40	65.37 ± 3.91	25.03 ± 1.92
Sex (male%)	23 (76.67%)	15 (50.00%)	16 (53.33%)
Hypertension (%)	27 (90.00%)	20 (66.67%)	0
Hyperlipidemia (%)	22 (73.33%)	27 (90.00%)	0
Diabetes (%)	12 (40.00%)	11 (36.67%)	0
ELISA validation			
sample size	64	-	30
Age	60.99 ± 7.10	-	57.24 ± 5.51
Sex (male%)	41 (64.06%)	-	17 (53.33%)
Hypertension (%)	39 (60.94%)	-	0
Hyperlipidemia (%)	51 (79.69%)	-	0
Diabetes (%)	18 (28.13%)	-	0

100–1000; Full ms resolution: 70,000; MS/MS resolution: 17500; NCE/stepped NCE: 10, 20, 40.

Data preprocessing and statistical analysis

The acquired LC-MS raw data were analyzed by the progqenesis QI software (Waters Corporation, Milford, United States) using the following parameters: precursor tolerance set to 5 ppm, fragment tolerance set to 10 ppm, and retention time (RT) tolerance set to 0.02 min. Internal standard detection parameters were deselected for peak RT alignment, and the isotopic peaks were excluded for analysis, with the noise elimination level set at 10.00 and minimum intensity at 15% of the base peak intensity. The Excel file was obtained with 3-dimensional datasets, including m/z, peak RT, and peak intensities, and RT–m/z pairs were used as the identifier for each ion. The resulting matrix was further reduced by removing any peaks with a missing value (ion intensity = 0) in more than 50% of samples. The metabolites were identified by progenesis QI (Waters Corporation, Milford, United States) Data Processing Software, based on public databases and self-built databases. The positive and negative data were combined to obtain the combined data. Orthogonal partial least-squares-discriminant analysis (OPLS-DA) was conducted by the SIMCA software to visualize the metabolic alterations among the experimental groups. The differential metabolites were selected on the basis of a statistically significant threshold of variable influence on the projection (VIP) values obtained from the OPLS-DA model, where metabolites with VIP >1.0 and adj.p < 0.05 were considered DMs.

Multi-omics network construction and potential biomarkers selection

In order to investigate the biological links between the transcriptome/proteome and metabolome, we entered the DGs, DPs, and DMs into the "Network Analysis" module of the MetaboAnalyst database. The interactions between DGs and DPs were determined by using the String database. We integrated the relevant data in MS Excel and determined the genes, proteins, and metabolites that formed the network. The "gene–protein–metabolite" network of syndromes was further visualized by using the Cytoscape software. We selected genes and metabolites with high centrality and biological linkages as potential biomarkers for PBS syndrome, based on the literature and KEGG enrichment results.

ELISA validation

We enlarged the sample size by collecting serum from 64 CHD-PBS syndrome patients and 30 HC. To conduct the validation experiment, we purchased ELISA kits from Elabscience (China) and followed the manufacturer's instructions. First, we added 50 μl of a diluted standard and sample to a 96-well plate, immediately followed by the addition of 50 μl of the Biotinylated Detection Ab working solution to each well. The plate was covered with a sealer and incubated for 45 min at 37°C. The solution was then decanted and 350 μl of a wash buffer was added to each well. After repeating the washing step thrice, 100 μL of the HRP conjugate working solution was added to each well. The plate was covered with a new sealer and incubated for another 30 min at 37°C. The solution was then decanted from each well and the washing process was repeated 5 times. Then, 90 μl of the substrate reagent was added to each well. The plate was covered with a new sealer and incubated for about 15 min at 37°C. Finally, 50 μL of the stop solution was added to each well and the optical density (OD value) of each well was determined with the microplate reader (Tecan, Switzerland) at 450 nm.

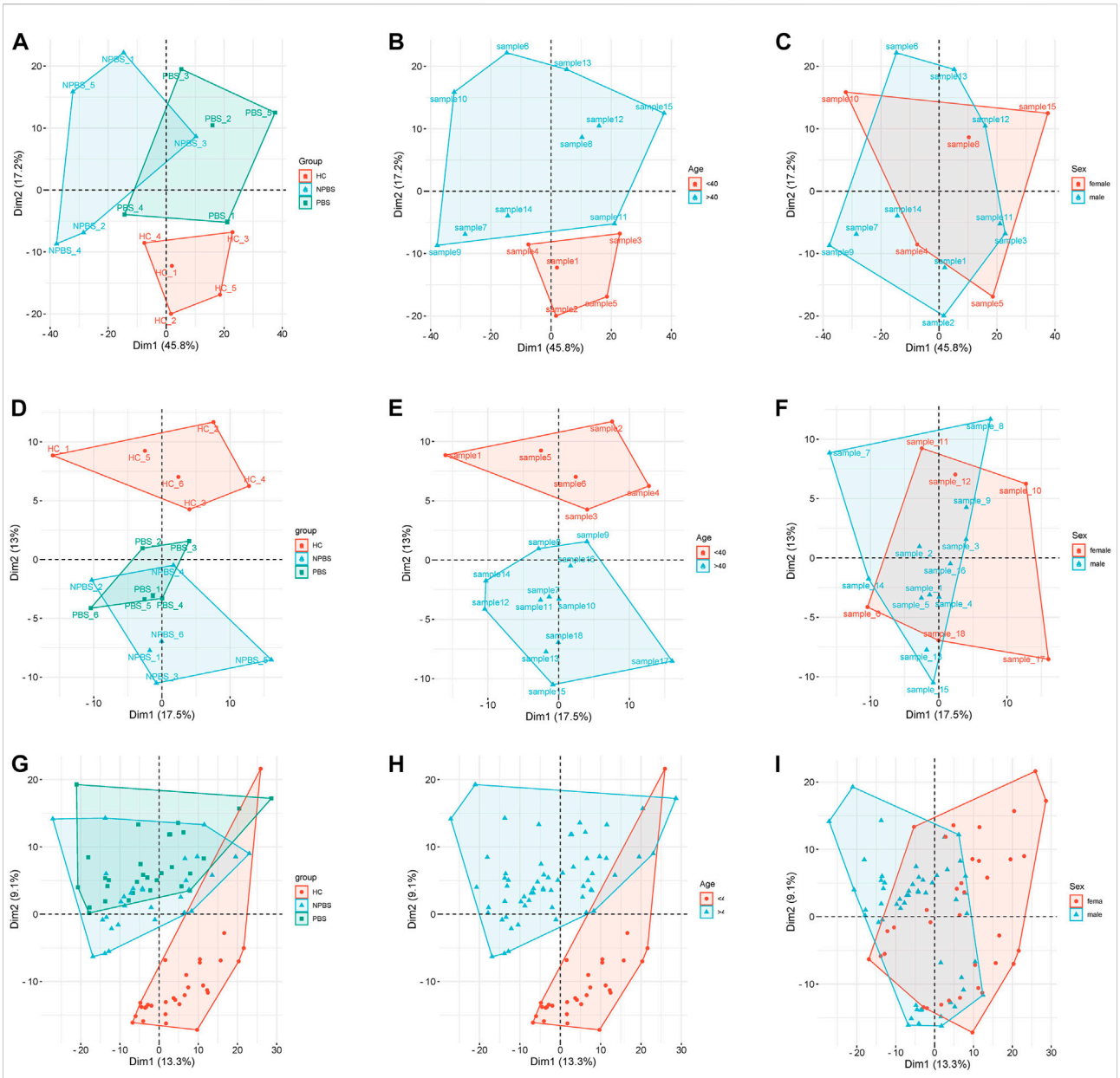

FIGURE 2
Principal component analysis for different clinical characteristics. **(A–C)** The influence of disease, age, and sex on transcriptome expression. **(D–F)** The influence of disease, age, and sex on proteome expression. **(G–I)** The influence of disease, age, and sex on metabolome expression.

Results

Clinical characteristics of coronary heart disease patients with phlegm and blood stasis or non-phlegm and blood stasis syndrome

Table 1 lists the demographic and clinical characteristics of participants. No significant differences in age, sex, and past medical history were observed between the CHD-PBS and CHD-NPBS groups. However, disparities in age and past medical history were observed between CHD patients and healthy adults (Table 1). We evaluated the influence of disease, age, and sex on transcriptome and proteome, and metabolome expression separately. Principal component analysis was performed using the selected top 1000 genes and metabolites, and all proteins. According to the results, disease status and age were the main factors resulting in changes in the transcriptome, proteome, and metabolome (Figures 2A–F). Obviously, significant differences are

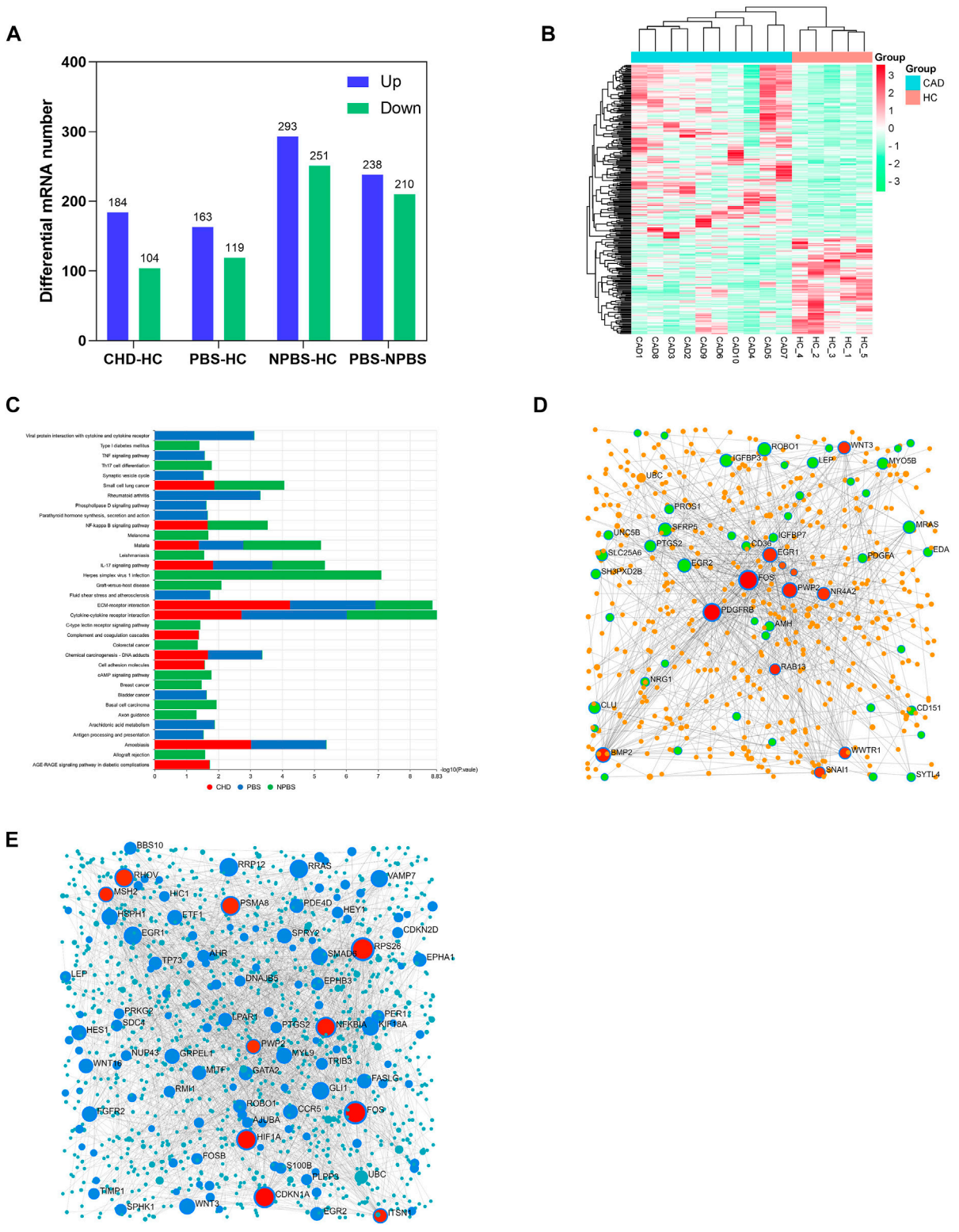

FIGURE 3
Transcriptomics characteristic of CHD-PBS syndrome. **(A)** The number of differentially expressed genes in each group. **(B)** Heat map of differential genes between CHD and HC groups. **(C)** Comparison of KEGG pathway in different groups. **(D)** Gene-gene interaction network for CHD-PBS syndrome. **(E)** Gene-gene interaction network for CHD-NPBS syndrome.

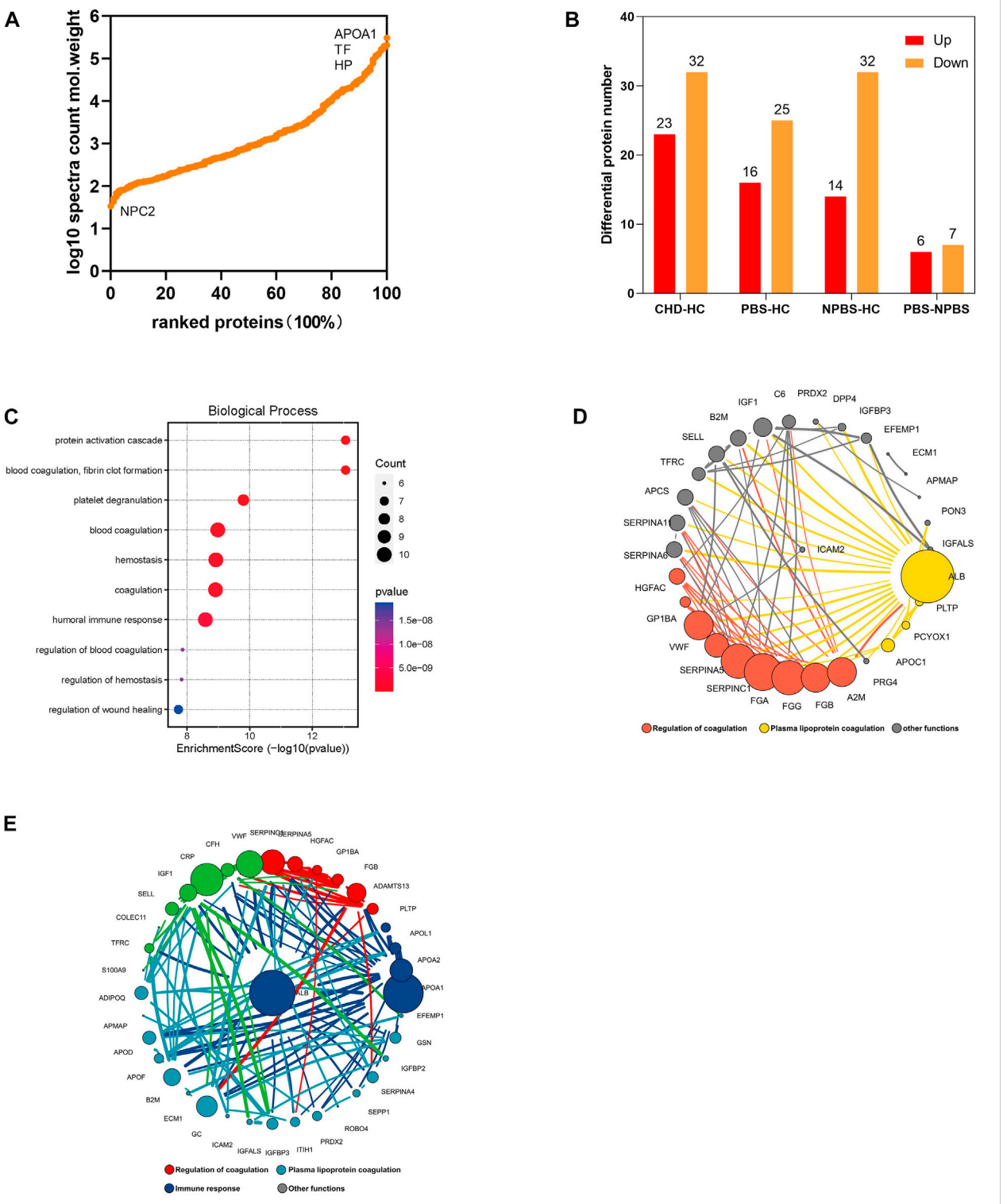

FIGURE 4
Proteomics characteristic of CHD patients with PBS syndrome. **(A)** Relative abundance of proteins spans five orders of magnitude. **(B)** The number of differential proteins in each group. **(C)** GO enrichment analysis of differential proteins in patients with CHD-PBS Syndrome. **(D)** Protein-protein interactions analysis of differential proteins in patients with CHD-PBS syndrome. **(E)** Protein-protein interactions analysis of differential proteins in patients with CHD-NPBS syndrome.

present in the expression of mRNA, proteins, and metabolites between patients with CHD-PBS syndrome, patients with CHD-NPBS syndrome, and healthy adults. In the following study, we will quantitatively describe this difference and determine the association between the different omics.

Transcriptomic characteristics of CHD-PBS syndrome

In a transcriptomics study, we identified the DGs of CHD-PBS syndrome. First, we assessed the quality of sequencing data. According to the quality assessment of raw data, 93%–96% of bases fulfilled the Q30 requirements for each sample, and the error rate of bases was <0.04%, which indicated that the sequence was stable (Supplementary Table S6). Supplementary Table S7 presents the results of the reference genome comparison. FPKMs can indirectly reflect gene expression. In total, over 20,000 functional genes were detected. The mean value of FPKMs was 15–18, and the FPKM homogeneity was good across individual samples, suggesting that the quality of each sample was good and reliable (Supplementary Table S8; Supplementary Figure S1). To identify the DGs, we performed a count-based DG expression analysis. In total, 288 DGs were identified between the CHD and HC groups, with 184 DGs upregulated and 104 DGs downregulated (Figure 3A). The heatmap revealed significant differences in gene expression between the CHD and HC groups (Figure 3B). Based on diagnostic criteria for syndromes, the samples were divided into two groups, as detailed in Supplementary Table S1. Compared with the HC group, the PBS group had 282 genes; of them, 163 genes were upregulated and 169 genes were downregulated. The NPBS group contained 544 genes, with 293 genes upregulated and 251 genes downregulated. In addition, 448 DGs were identified between the PBS and NPBS groups. Then, KEGG enrichment analysis was performed for DGs of CHD (q-value < 0.05). The results revealed that these DGs were enriched in the AGE-RAGE signaling pathway, complement and coagulation cascades, IL-17 signaling pathway, and NF-κB signaling pathway (Supplementary Figure S2A). The DGs of PBS syndrome were enriched in atherosclerosis, arachidonic acid (AA) metabolism, parathyroid hormone metabolism, the phospholipase D signal transduction pathway, the TNF signal transduction pathway, bladder cancer, and rheumatoid arthritis. The DGs of NPBS syndrome were enriched in the c-type lectin receptor signal transduction pathway, Th17 cell differentiation, and colorectal cancer (Supplementary Figure S2B,C). On summarizing the enrichment results of the aforementioned three groups, we found that DGs of PBS syndrome were enriched in the TNF signaling pathway, phospholipase D signaling pathway, and AA metabolism (Figure 3C). To further investigate the core genes expressed in patients with the two syndromes, we performed a network analysis of gene–gene interactions. Some of the hub genes for PBS syndrome are FOS, PDGFRB, PWP2, BMP2, and EGR1 (Figure 3D), whereas that for NPBS syndrome were FOS, CDKN1A, HIF, and NFKBIA (Figure 3E).

Proteomic characteristics of CHD-PBS syndrome

Next, we performed a DIA-based proteomic analysis to explore the differences in protein abundance among PBS syndrome and healthy adults. The average deviation and DIA data points of each sample satisfied the standards, demonstrating that this proteome quantification was accurate (Supplementary Figure S3, 4). For monitoring the stability of LC/MS data and the reliability of qualitative and quantitative data, QC samples were inserted into a certain number of samples at each interval in the sample queue. A correlation analysis was conducted, and the correlation coefficients were found to be all >0.9 (Supplementary Figure S5). In total, 3,690 peptides and 324 proteins were discovered in the plasma of 18 participants by using the DIA method. The relative abundance of proteins spanned five orders of magnitude. The highest protein expression level was observed for apolipoprotein A-I (APOA1), whereas the lowest was for NPC intracellular cholesterol transporter 2 (Figure 4A). According to the DP expression analysis, 23 plasma proteins were upregulated and 32 were downregulated in the CHD group compared with the HC group. The PBS syndrome group exhibited 41 DPs, and of them, 16 DPs were upregulated and 25 were downregulated. The NPBS syndrome group exhibited 46 DPs, of which 14 DPs were upregulated and 32 were downregulated compared with the HC group. Supplementary Figure S6 presents the volcano diagrams of the DPs. In addition, 13 DPs were identified between the PBS and NPBS groups, and of them, six were upregulated and seven were downregulated (Figure 4B). The plasma proteome of the two syndromes did not differ as much as the transcriptome. GO annotation analysis revealed that DPs for PBS syndrome were enriched in biological processes such as complement activation, platelet degranulation, humoral immune response, phagocytosis, receptor-mediated endocytosis, classical pathway, and immunoglobulin-mediated immune response (Figure 4C). Next, we determined the protein difference between the two syndromes of CHD. According to the PPI network and analysis of the biological function of core proteins, proteins expressed for PBS syndrome were primarily associated with coagulation and lipid metabolism (Figure 4D), whereas those expressed for NPBS syndrome were associated with coagulation, lipid metabolism, and inflammation (Figure 4E).

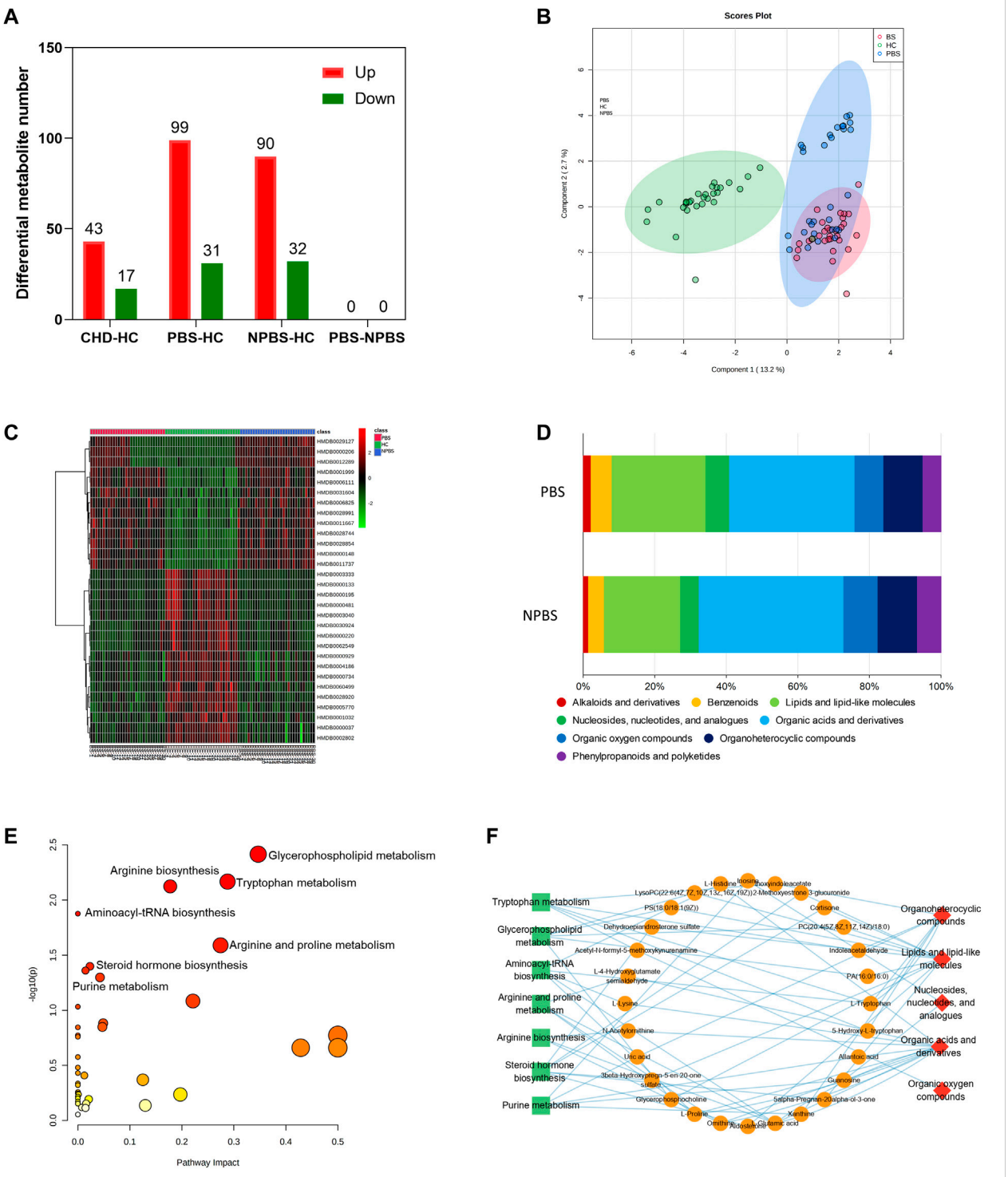

FIGURE 5
Metabolomics characteristic of CHD patients with PBS Syndrome. **(A)** Number of differential metabolites in each group. **(B)** OPLS-DA analysis of three groups. **(C)** Cluster heatmap analysis of three groups. **(D)** Metabolite type of different syndromes. **(E)** Functional enrichment analysis of identified DMs of PBS syndrome. **(F)** The network relationship of metabolites, species, and enrichment pathways.

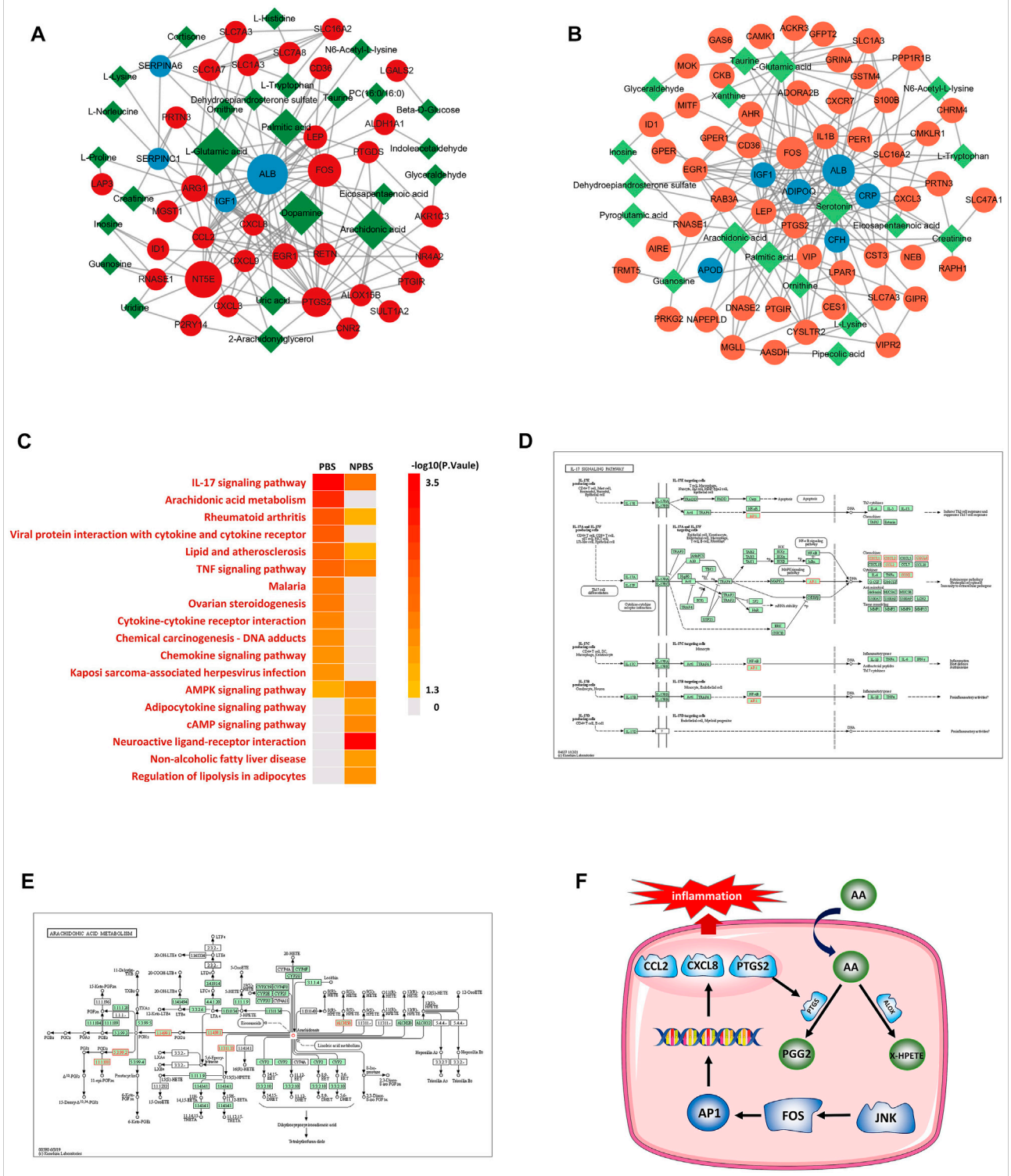

FIGURE 6
Transcriptome-proteome-metabolome integrated analysis and potential targets. **(A)** Network anlaysis of differential genes, proteins and metabolites for PBS Syndrome. **(B)** Network anlaysis of differential genes, proteins and metabolites for NPBS Syndrome. **(C)** KEGG enrichment analysis for the networks of two Syndromes. **(D)** IL-17 signaling pathway. **(E)** Arachidonic acid metabolism. **(F)** JNK-FOS-AP-1 pathway.

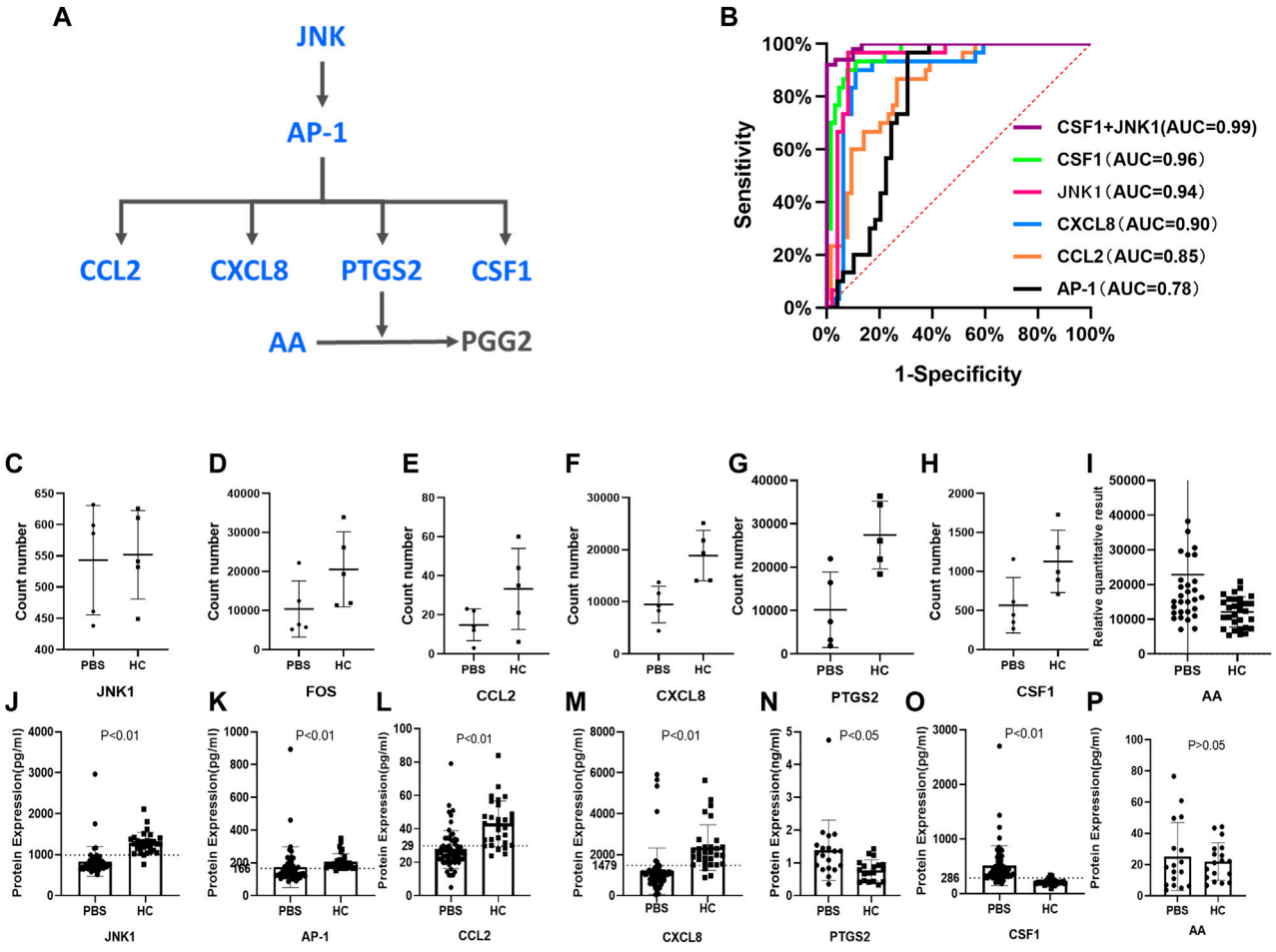

FIGURE 7
Validation by ELISA test. **(A)** JNK/AP-1 pathway and AA metabolism. **(B)** ROC curves for different molecules. **(C–I)** RNA-seq results of JNK1, FOS, CCL2, CXCL8, PTGS2, CSF1, AA. **(J–P)** ELISA results of JNK1, AP-1, CCL2, CXCL8, PTGS2, CSF1, and AA.

Metabolomic characteristics of CHD-PBS syndrome

Then, we investigated the serum metabolomic characteristics of CHD-PBS syndrome by using positive and negative ion scan data collected from patients and healthy participants through UPLC/MS (Supplementary Figure S7). QC samples were used to further evaluate detection stability. The PCA model diagram derived through 7-fold cross-validation and the Boxplot generated on the basis of the intensity of metabolites demonstrated that the QC samples were closely clustered, which indicated that the detection stability in this study was good (SupplementryFigures S8, 9). In total, 17,890 metabolites were discovered, of which 1385 were annotated in the HDMB database. We generated DMs through SIMCA software's OPLS-DA analysis, with the screening criteria of VIP >1 and *adj. p*-value < 0.05. Compared with the HC group, 130 (99 upregulated and 31 downregulated DMs) and 122 (90 upregulated and 32 downregulated DMs) metabolites were altered in the CHD-PBS and CHD-NPBS groups, respectively (Figure 5A). The OPLS-DA score and cluster heatmap revealed that the PBS, NPBS, and HC groups exhibited a clear trend of separation, whereas the PBS and NPBS groups somewhat overlapped (Figures 5B,C). On differentiating the two syndromes by the metabolite type, we found that the PBS group exhibited more lipid trends (Figure 5D). Next, we used the MetaboAnalyst platform to perform functional enrichment analysis. Several metabolic pathways related to PBS syndrome were identified (*p*-value < 0.05), including tryptophan metabolism, glycerophospholipid metabolism, aminoacyl-tRNA biosynthesis, arginine and proline metabolism, arginine biosynthesis, steroid hormone biosynthesis, and purine metabolism (Figure 5E). To further comprehend the relationship between the metabolites, their species, and

enrichment pathways, we edited the results using Cytoscape Software. Lipids and lipid-like molecules, organic acids and their derivatives, and organoheterocyclic compounds were the main species of these metabolites that are involved in the metabolic imbalance observed in patients with PBS syndrome, as depicted in Figure 5F.

Integrated analysis of DGs, DPs, and DMs

By integrating transcriptomics, proteomics, and metabolomic data, we established a "gene–protein–metabolite" network for the two syndromes. The multi-omics network of PBS syndrome consisted of 33 mRNAs, four proteins, and 25 metabolites (Figure 6A), while that of NPBS syndrome contained 64 mRNAs, nine proteins, and 23 metabolites (Figure 6B). Next, KEGG enrichment analysis performed for the two networks revealed that molecules in the PBS syndrome network were enriched in the IL-17 signaling pathway, rheumatoid arthritis, viral protein interaction with cytokine and cytokine receptor, Chagas disease, TNF signaling pathway, malaria, lipid and atherosclerosis, AA metabolism, and so forth (q-value > 0.05). Molecules in the NPBS syndrome network were only enriched in the neuroactive ligand–receptor interaction (q-value > 0.05) (Figure 6C). Finally, we sought the key targets of PBS syndrome. According to KEGG enrichment results, PBS syndrome was closely related to the IL-17 signaling pathway and AA metabolism. Some of the DGs encode the following key molecules of the MAPK signaling pathway, which was downstream of the IL-17 pathway: FOS (AP-1 in Figure 6E), CCL2, CXCL8, CXCL1, CXCL2, and PTGS2. Among the DGs and DMs, AA, PTGS2, ALOX15B, PTGDS, and AKR1C3 are the substrates and key enzymes of AA metabolism (Figure 6F). Moreover, the molecules in the network were ranked according to their degree and betweenness. We observed that CXCL8, CCL2, FOS, PTGS2, and AA had higher centrality (Supplementary Material). Consequently, owing to the biological association and statistical association, we further validated AA, AP-1, PTGS2, CCL2, and CXCL8 as potential targets of PBS syndrome (Figure 6D).

Validation by the enzyme-linked immunosorbent assay test

According to the results of the multi-omics network, the hub genes and metabolites for PBS syndrome were AP-1 (FOS), CCL2, CXCL8, PTGS2, and AA. These genes exhibited up–down regulatory relationships and are related to the MAPK pathway (Figure 7A). The FOS family is a subunit of the transcription factor AP-1. Activated JNK phosphorylates FOS and ultimately activates AP-1. Furthermore, CSF1, a downstream molecule of AP-1, was differentially expressed in our transcriptomics study. Based on the aforementioned biological links, AA, JNK1, AP-1, CCL2, PTGS2, CXCL8, and CSF1 were selected as candidate molecules for final validation by expanding the sample size. In the sequencing stage, the expression of JNK1, FOS, CCL2, CXCL8, PTGS2, and CSF1 was low in the PBS group, whereas that of AA was high (Figures 7C–I). In the validation stage, the expression of JNK1, AP-1, CCL2, and CXCL8 was low in the PBS group, whereas that of PTGS2, CSF1, and AA was high (Figure 7J–P). Except for AA, these indicators were all statistically significant ($p < 0.05$). JNK1, AP-1, CCL2, CXCL8, and CSF1 were assessed using the receiver operating characteristic (ROC) curve; these were validated using a large sample size. The bigger the area under the curve (AUC), the more effective the diagnostic value. The AUC of each molecule was as follows: CSF1 [0.9635, 95%CI (0.9295, 0.9976)] > JNK1 [0.9361, 95% CI (0.8749, 0.9972)] > CXCL8 [0.8953, 95% CI (0.8222, 0.9684)] > CCL2 [0.8458, 95% CI (0.7676, 0.9241)] > AP-1 [0.7884, 95%CI (0.6869, 0.8899)] (Figure 7B). Logistic regression analysis was conducted based on CSF1 and JNK1, and the regression equation was as follows: $p = 1/[1+ e^{-(0.042\times CSF1-0.008\times JNK1-2.146)}]$. The AUC of this logistic model was 0.992. Detecting CSF1 and JNK1 together was of the highest diagnostic value and significance for PBS syndrome. The Youden index was calculated by combining the specificity and sensitivity of the ROC curve. The cut-off value corresponding to the maximum Youden index was considered the best diagnostic point. The optimal diagnostic points of CSF1, JNK, CXCL8, CCL2, and AP-1 were 286.6, 992.7, 1479, 29.78, and 166.8 pg/ml, respectively.

Discussion

TCM is personalized medicine that investigates clinical diagnosis and treatment regularities. TCM can serve as a valuable complement to Western medicine's standardized treatment for CHD and related conditions (Zhou et al., 2014). Currently, multi-omics network research guided by the concept of systems biology, utilizing the most up-to-date high-throughput sequencing and high-resolution MS technology, and utilizing the method of non-targeted screening combined with targeted verification is advantageous in the study of biomarkers and biological foundations of TCM syndromes. For example, Wu explored the biological basis of two CHD syndromes using proteomics, metabolomics, and network pharmacology strategy. The study indicated that downregulated PON1 and ADIPOQ might be potential biomarkers of cold coagulation and blood stasis syndrome and that downregulated APOE and APOA1 might be biomarkers of Qi stagnation and blood stasis syndrome (Wu et al., 2021). Guo integrated untargeted and targeted metabonomics and

showed that Shi syndromes involved inflammation and anomalous levels of bioactive phospholipids and antioxidant molecules, while Xu syndromes involved long-chain unsaturated lipid ceramide metabolism and bile acid metabolism (Guo et al., 2021). Using human urine samples, Zhou identified 15 and 12 biomarkers of PBS syndrome and Qi and Yin deficiency syndrome, respectively (Zhou et al., 2019). In this study, we proposed a strategy integrating RNA-seq, proteomics, and metabolomics to explore the biological basis of CHD-PBS syndrome by constructing the "gene–protein–metabolite" network associated with this syndrome.

In the transcriptomics study, 282 mRNAs were identified as DGs for PBS syndrome. They were enriched in the TNF signaling pathway, phospholipase D signaling pathway, and AA metabolism. Forty-one proteins were identified as DPs for PBS syndrome in the proteomics study. They were enriched in the biological processes of complement activation, platelet degranulation, humoral immune response, phagocytosis, receptor-mediated endocytosis, *etc.* A total of 130 metabolites were identified as DMs for PBS syndrome in the metabonomics study. They were enriched in unsaturated fatty acid metabolism (AA metabolism, taurine, and hypotaurine metabolism), amino acid metabolism, and vitamin and sugar acid metabolism. The DGs, DPs, and DMs were integrated to construct a gene–protein–metabolite network. After the biological correlation and order of centrality were integrated, AA, JNK1, FOS, CCL2, CXCL8, PTGS2, and CSF1 were identified as potential biomarkers. ELISA results showed that JNK1, AP-1, CCL2, and CXCL8 levels were significantly lower in CHD-PBS patients than in healthy adults, whereas PTGS2 and CSF1 levels were significantly higher. Based on their AUC values, the combined detection of CSF1 and JNK1 had the greatest diagnostic value for PBS syndrome. The biological foundation of PBS syndrome is speculated to be associated with abnormal AA metabolism and inhibition of the JNK/AP-1 pathway.

AA metabolism and CHD-PBS syndrome

Previous metabolomics results have shown that glucose and glucose metabolism were significantly increased in patients with CHD-PBS syndrome (Zhou et al., 2019). High glucose levels activate the RAGE-ERK1/2-ICAM-1 pathway, resulting in accelerated atherosclerosis (Pertynska-Marczewska and Merhi, 2015). We here found that PBS syndrome was highly associated with AA metabolism, especially the PTGS2 and LOX-12/15 pathways. AA, the most widely distributed omega-6 polyunsaturated fatty acid in organisms, generates several different bioactive substances through three metabolic pathways: cyclooxygenase (COX/PTGS), lipoxygenase (ALOX12/15), and cytochrome P450 (CYP450) (Hanna and Hafez, 2018). Different enzymes mediate the production of different metabolites having different effects on the heart. For example, CYP450-mediated epoxyeicosatrienoic acids protect the heart, preventing LPS-induced cardiac dysfunction by inhibiting inflammatory molecules released by macrophages (Dai et al., 2015). 12/15-Lipoxygenase produced by ALOX12/15 promotes oxidative stress and myocardial ischemia/reperfusion injury (Zhang et al., 2021). COX-mediated prostaglandins have complex and controversial effects on the heart (Al-Kofahi et al., 2018) and may promote cardiac repair, possibly by interacting with different cells and prostaglandin receptors. Because AA metabolism is diverse and complex, we focused on AA levels and enzyme levels. Although the AA level did not change significantly, the enzyme levels were significantly upregulated in PBS patients. The levels of ALOX12X and 15-HETE increased during the sequencing stage and those of PTGS2 increased during the validation stage. Levels of beneficial AA products decreased, while those of detrimental products increased, leading to the rapid development of both CHD and PBS syndrome.

JNK/AP-1 signaling pathway and CHD-PBS syndrome

The JNK/AP-1 signaling pathway is supposed to be upregulated in CHD patients, whereas an opposite result was observed in our study, which may be an effect of PBS syndrome. JNK, also known as stress-activated protein kinase (SAPK), regulates the transcription and protein expression of apoptosis- and inflammation-related downstream genes in a transcription-dependent manner. Upon activation with stimulants, JNK moves from the cytoplasm to the nucleus and activates transcription factors such as AP-1 through phosphorylation. AP-1 is composed of FOS and JUN families and is a key transcription factor regulating cell proliferation, differentiation, apoptosis, transformation, migration, and inflammation. After signal regulation, AP-1 mediates the production of PTGS2, CCL2, CXCL8, and other pro-inflammatory cytokines and chemokines (Nakayama et al., 2022; Matsumoto et al., 2007; Du et al., 2020). The FOS family and AP-1 have a crucial role in atherosclerosis and myocardial ischemia. They have different pathogenic effects on vascular smooth muscle cells, endothelial cells, cardiomyocytes, and macrophages. For example, ox-LDL enhances the c-fos transcriptional activity to promote the expression of the low-density lipoprotein receptor, thereby promoting foam cell formation and atherosclerosis (Miao et al., 2022). AP-1 plays the main role in VSMC proliferation, differentiation, and migration and participates in AS formation (Meijer et al., 2012; Zhang et al., 2012). Ap-1 is also a key transcription factor that induces the apoptosis of endothelial cells and cardiomyocytes (Taimor et al., 2001; Li et al., 2021). Furthermore, AP-1 is a crucial player in the activation of macrophage-induced inflammatory responses (Hannemann et al., 2017). Many drugs inhibit AP-1 expression and thus improve atherosclerosis and ventricular remodeling after acute myocardial infarction (Yoshiyama et al., 2001; Lin et al., 2015; Chou et al., 2019; Yang et al., 2020). PTGS2, a downstream molecule of AP-1, is a key

enzyme in AA metabolism. PTGS2 metabolizes AA to produce prostaglandin and thromboxane, which influence platelet aggregation, vascular wall tension, and atherosclerosis. So far, the role of PTGS2 in cardiovascular diseases remains controversial. PTGS2 is generally accepted to promote atherosclerosis; however, it also protects against myocardial ischemia/reperfusion injury (Zhou et al., 2021; Zhuang et al., 2022). CCL2, or monocyte chemoattractant protein-1 (MCP-1), is a well-known CC chemokine that regulates the locomotion and recruitment of monocytes/macrophages to the injury site (Khambhati et al., 2018). CCL2/CCR2 is a key player in the formation, development, and instability of atherosclerotic plaques and has a crucial role in the reconstruction after myocardial infarcts (Dewald et al., 2005; Hernández-Aguilera et al., 2020). Moreover, plasma CCL2 levels have a prognostic value in the acute phase of ACS, with lower CCL2 levels possibly associated with a worse prognosis (Leocádio et al., 2019). Interleukin-8 (CXCL8) is a typical inflammatory mediator, mainly secreted by macrophages. CXCL8 binds to CXCR1 and CXCR2 to perform its role, which can chemotaxis neutrophils to regulate the inflammatory response (Roebuck, 1999). High plasma CXCL8 levels are associated with large infarct size, impaired recovery of left ventricular function, and adverse clinical outcomes (Orn et al., 2009). Furthermore, the CXCL8-induced neutrophil extracellular attractor increases atherosclerosis by activating NF-κB signaling and MAPK in macrophages (An et al., 2019). CSF1 (M-CSF) is a protein that regulates monocyte survival, differentiation, and function (Popova et al., 2011) and is produced in tissues and secreted into the blood. In blood, it recruits monocytes, which then differentiate into tissue macrophages (Roth and Stanley, 1992). Studies have shown that CSF1 deficiency decreases the number of monocytes in peripheral blood and tissues, enhances macrophage apoptosis, and significantly inhibits atherosclerosis (Shaposhnik et al., 2010).

In our study, both high-throughput sequencing and the ELISA test revealed that the JNK1, FOS, AP-1, CCL2, and CXCL8 levels in patients with PBS syndrome were significantly lower than those in healthy adults. This suggests that the JNK/AP-1 signaling pathway might be inhibited in these patients. This could be due to the medications that the patients were taking, such as aspirin and statin, which reduce these inflammatory markers. On the other hand, we are more inclined to conclude that FOS, AP-1, CCL2, CXCL8, and JNK1 were all downregulated by PBS syndrome. We speculate that there are different CHD subtypes, and patients with PBS syndrome exhibit a reduction in some inflammatory markers. We will continue to investigate PBS syndrome in animal models and conduct additional validation of syndrome-related biomarkers.On the other hand, despite the opposing changes in the CSF1 expression in the PBS group during the sequencing and validation stages, we selected CSF1 as an important biomarker as we value the outcomes of basic experiments. Omics research is merely a strategy or a method to determine the potential differential molecules and not to obtain final results. Numerous new directions have opened up through omics research, albeit its findings must be supported by fundamental studies. In our study, the sample size for ELISA verification was much larger than that for omics sequencing, which provided greater confidence in the ELISA results. In other words, we focused more on the implementation of clinical validation and the omics technology played an auxiliary role. Therefore, we consider the upregulation of CSF1 as the characteristic of PBS syndrome of coronary heart disease. In addition, we did not perform diagnostic tests of omics data of NPBS syndrome, which could have benefited in determining whether the biomarkers of CHD-PBS syndrome are altered in the CHD-NPBS syndrome. These are the limitations of the study. In summary, this study aimed to ascertain the biological foundation of CHD-PBS syndrome rather than the biological basis of the CHD-NPBS syndrome or the distinction between the two syndromes. In the future, we plan to conduct an in-depth analysis to look at the distinct molecules across diverse syndromes.

Conclusion

By integrating the clinical samples with multi-omics studies, the present study identified that 1) the "gene–protein–metabolite" network of CHD-PBS syndrome includes at least 33 mRNAs, four proteins, and 25 metabolites. 2) The disorder of AA metabolism and the inhibition of the JNK/AP-1 pathway may be the characteristics of PBS syndrome. 3) PBS syndrome exhibited decreased levels of FOS, AP-1, CCL2, CXCL8, and JNK1 and increased levels of PTGS2 and CSF1. 4) The diagnostic biomarkers of CHD-PBS syndrome included CSF1 (>286.6 pg/ml), PTGS2 (>992.7 pg/ml), and CXCL8 (>1479 pg/ml). This study provides a methodological reference for the analyses of the biological foundation of TCM under objective, quantitative, and accurate requirements and suggests that TCM syndromes, which are a subtype of diseases, may have unique molecular changes.

Data availability statement

The RNA-seq data have been deposited to the SRA database with the dataset identifier PRJNA871404. The mass spectrometry mics data have been deposited to the Xchange Consortium (http://partnerrepositorywiththedatasetcentral.proteomexchange.org) *via* XD036389.

Ethics statement

The studies involving human participants were reviewed and approved by the ethics committee of Guang'anmen Hospital. The patients/participants provided their written informed consent to participate in this study. Written informed consent was obtained from the individual(s) for the publication of any potentially identifiable images or data included in this article.

Author contributions

JW designed the study. GY, HH, SZ and ZS were responsible for the design of case report form and informed consent form, patient recruitment, and clinical data collation. YL is in charge of sample storage. GY was responsible for data analysis, ELISA test, and writing the manuscript. JH was responsible for revising the manuscript. All authors read and approved the final manuscript.

Funding

The work was supported by the National Natural Science Foundation of China (81974556), National Key Research and Development Plan (2020YFC2002701).

Acknowledgments

We thank the Shanghai Luming biological technology co., Ltd (Shanghai, China) for providing proteomics services. We thank all the reviewers who participated in the review and MJE ditor (www.mjeditor.com) for its linguistic assistance during the preparation of this manuscript.

Conflict of interest

The authors declare that the research was conducted in the absence of any commercial or financial relationships that could be construed as a potential conflict of interest.

Publisher's note

All claims expressed in this article are solely those of the authors and do not necessarily represent those of their affiliated organizations, or those of the publisher, the editors and the reviewers. Any product that may be evaluated in this article, or claim that may be made by its manufacturer, is not guaranteed or endorsed by the publisher.

Supplementary material

The Supplementary Material for this article can be found online at: https://www.frontiersin.org/articles/10.3389/fphar.2022.1022627/full#supplementary-material.

References

Al-Kofahi, M., Omura, S., Tsunoda, I., Sato, F., Becker, F., Gavins, F. N. E., et al. (2018). IL-1β reduces cardiac lymphatic muscle contraction via COX-2 and PGE2 induction: Potential role in myocarditis. *Biomed. Pharmacother. Biomedecine Pharmacother.* 107, 1591–1600. doi:10.1016/j.biopha.2018.08.004

An, Z., Li, J., Yu, J., Wang, X., Gao, H., Zhang, W., et al. (2019). Neutrophil extracellular traps induced by IL-8 aggravate atherosclerosis via activation NF-κB signaling in macrophages. *Cell Cycle* 18, 2928–2938. doi:10.1080/15384101.2019.1662678

Antman, E. M., and Braunwald, E. (2020). Invasive or conservative strategy for stable coronary disease. Reply. *N. Engl. J. Med.* 383, e66. doi:10.1056/NEJMc2024008

Chou, C.-C., Wang, C.-P., Chen, J.-H., and Lin, H.-H. (2019). Anti-atherosclerotic effect of Hibiscus leaf polyphenols against tumor necrosis factor-alpha-induced abnormal vascular smooth muscle cell migration and proliferation. *Antioxidants* 8, 620. doi:10.3390/antiox8120620

Dai, M., Wu, L., He, Z., Zhang, S., Chen, C., Xu, X., et al. (2015). Epoxyeicosatrienoic acids regulate macrophage polarization and prevent LPS-induced cardiac dysfunction. *J. Cell. Physiol.* 230, 2108–2119. doi:10.1002/jcp.24939

Dai, X., and Shen, L. (2022). Advances and trends in omics technology development. *Front. Med.* 9, 911861. doi:10.3389/fmed.2022.911861

Dewald, O., Zymek, P., Winkelmann, K., Koerting, A., Ren, G., Abou-Khamis, T., et al. (2005). CCL2/Monocyte chemoattractant protein-1 regulates inflammatory responses critical to healing myocardial infarcts. *Circ. Res.* 96, 881–889. doi:10.1161/01.RES.0000163017.13772.3a

Du, S., Li, Z., Xie, X., Xu, C., Shen, X., Wang, N., et al. (2020). IL-17 stimulates the expression of CCL2 in cardiac myocytes via Act1/TRAF6/p38MAPK-dependent AP-1 activation. *Scand. J. Immunol.* 91, e12840. doi:10.1111/sji.12840

Guo, N., Wang, P., Yang, J., Yang, X., van der Voet, M., Wildwater, M., et al. (2021). Serum metabolomic analysis of coronary heart disease patients with stable Angina pectoris subtyped by traditional Chinese medicine diagnostics reveals biomarkers relevant to personalized treatments. *Front. Pharmacol.* 12, 664320. doi:10.3389/fphar.2021.664320

Hanna, V. S., and Hafez, E. A. A. (2018). Synopsis of arachidonic acid metabolism: A review. *J. Adv. Res.* 11, 23–32. doi:10.1016/j.jare.2018.03.005

Hannemann, N., Jordan, J., Paul, S., Reid, S., Baenkler, H. W., Sonnewald, S., et al. (2017). The AP-1 transcription factor c-jun promotes arthritis by regulating cyclooxygenase-2 and arginase-1 expression in macrophages. *J. Immunol.* 198, 3605–3614. doi:10.4049/jimmunol.1601330

Hernández-Aguilera, A., Fibla, M., Cabre, N., Luciano-Mateo, F., Camps, J., Fernandez-Arroyo, S., et al. (2020). Chemokine (C-C motif) ligand 2 and coronary artery disease: Tissue expression of functional and atypical receptors. *Cytokine* 126, 154923. doi:10.1016/j.cyto.2019.154923

Katus, H., Ziegler, A., Ekinci, O., Giannitsis, E., Stough, W. G., Achenbach, S., et al. (2017). Early diagnosis of acute coronary syndrome. *Eur. Heart J.* 38, 3049–3055. doi:10.1093/eurheartj/ehx492

Khambhati, J., Engels, M., Allard-Ratick, M., Sandesara, P. B., Quyyumi, A. A., and Sperling, L. (2018). Immunotherapy for the prevention of atherosclerotic cardiovascular disease: Promise and possibilities. *Atherosclerosis* 276, 1–9. doi:10.1016/j.atherosclerosis.2018.07.007

Knuuti, J. (2019). 2019 ESC Guidelines for the diagnosis and management of chronic coronary syndromes the Task Force for the diagnosis and management of chronic coronary syndromes of the European Society of Cardiology (ESC). *Russ. J. Cardiol.* 25, 119–180. doi:10.15829/1560-4071-2020-2-3757

Lal, C. V., Bhandari, V., and Ambalavanan, N. (2018). Genomics, microbiomics, proteomics, and metabolomics in bronchopulmonary dysplasia. *Semin. Perinatol.* 42, 425–431. doi:10.1053/j.semperi.2018.09.004

Leocádio, P. C. L., Menta, P. L. D. R., Dias, M. T. S., Fraga, J. R., Goulart, A. C., Santos, I. S., et al. (2019). Low serum levels of CCL2 are associated with worse prognosis in patients with acute coronary syndrome: 2-year survival analysis. *Biomed. Pharmacother. Biomedecine Pharmacother.* 109, 1411–1416. doi:10.1016/j.biopha.2018.10.087

Li, G.-J., Yang, Q. H., Yang, G. K., Wan, J., Du, L. J., Li, Z. X., et al. (2021). MiR-137 regulates low-intensity shear stress-induced human aortic endothelial cell apoptosis via JNK/AP-1 signaling. *J. Physiol. Biochem.* 77, 451–460. doi:10.1007/s13105-021-00812-1

Li, G.-Z., Sun, S., You, M., Wang, Y.-L., and Liu, G.-P. (2012). Inquiry diagnosis of coronary heart disease in Chinese medicine based on symptom-syndrome interactions. *Chin. Med.* 7, 9. doi:10.1186/1749-8546-7-9

Lin, X., Wu, M., Liu, B., Wang, J., Guan, G., Ma, A., et al. (2015). Candesartan ameliorates acute myocardial infarction in rats through inducible nitric oxide synthase, nuclear factor-κB, monocyte chemoattractant protein-1, activator

protein-1 and restoration of heat shock protein 72. *Mol. Med. Rep.* 12, 8193–8200. doi:10.3892/mmr.2015.4432

Liu, R., Jiang, L. J., Yang, Y., Wang, C. C., Tong, X., Xu, W. M., et al. (2021). Study on syndrome differentiation strategy of phlegm and blood stasis syndromes of coronary heart disease based on expert consultation on medical cases. *Ann. Palliat. Med.* 10, 9940–9952. doi:10.21037/apm-21-2332

Matsumoto, N., Imamura, R., and Suda, T. (2007). Caspase-8- and JNK-dependent AP-1 activation is required for Fas ligand-induced IL-8 production. *FEBS J.* 274, 2376–2384. doi:10.1111/j.1742-4658.2007.05772.x

Meijer, C. A., Le Haen, P. A. A., van Dijk, R. A., Hira, M., Hamming, J. F., van Bockel, J. H., et al. (2012). Activator protein-1 (AP-1) signalling in human atherosclerosis: Results of a systematic evaluation and intervention study. *Clin. Sci.* 122, 421–428. doi:10.1042/CS20110234

Miao, G., Zhao, X., Chan, S. L., Zhang, L., Li, Y., Zhang, Y., et al. (2022). Vascular smooth muscle cell c-Fos is critical for foam cell formation and atherosclerosis. *Metabolism.* 132, 155213. doi:10.1016/j.metabol.2022.155213

Mirzaei, M., Truswell, A. S., Taylor, R., and Leeder, S. R. (2009). Coronary heart disease epidemics: Not all the same. *Heart* 95, 740–746. doi:10.1136/hrt.2008.154856

Mohler, E. G., Ried, J. S., Bahnassawy, L., Reinhardt, P., Curado, M. R., Bakker, M. H., et al. (2020). Proteomic, metabolomic, and transcriptomic examination of APOE transgenic mice. *Alzheimer's. &amp. Dement.* 16, e040533. doi:10.1002/alz.040533

Nakayama, M., Naito, M., Omori, K., Ono, S., Nakayama, K., and Ohara, N. (2022). Porphyromonas gingivalis gingipains induce cyclooxygenase-2 expression and prostaglandin E2 production via ERK1/2-activated AP-1 (c-Jun/c-Fos) and IKK/NF-κB p65 cascades. *J. I.* 208, 1146–1154. doi:10.4049/jimmunol.2100866

Orn, S., Breland, U. M., Mollnes, T. E., Manhenke, C., Dickstein, K., Aukrust, P., et al. (2009). The chemokine network in relation to infarct size and left ventricular remodeling following acute myocardial infarction. *Am. J. Cardiol.* 104, 1179–1183. doi:10.1016/j.amjcard.2009.06.028

Pan, Y., Lei, X., and Zhang, Y. (2022). Association predictions of genomics, proteinomics, transcriptomics, microbiome, metabolomics, pathomics, radiomics, drug, symptoms, environment factor, and disease networks: A comprehensive approach. *Med. Res. Rev.* 42 (1), 441–461. doi:10.1002/med.21847

Pertynska-Marczewska, M., and Merhi, Z. (2015). Relationship of advanced glycation end products with cardiovascular disease in menopausal women. *Reprod. Sci.* 22, 774–782. doi:10.1177/1933719114549845

Popova, A., Kzhyshkowska, J., Nurgazieva, D., Goerdt, S., and Gratchev, A. (2011). Pro- and anti-inflammatory control of M-CSF-mediated macrophage differentiation. *Immunobiology* 216, 164–172. doi:10.1016/j.imbio.2010.06.003

Ren, Q., Zhou, X. W., He, M. Y., Fang, G., Wang, B., Chen, X. L., et al. (2020). A quantitative diagnostic method for phlegm and blood stasis syndrome in coronary heart disease using tongue, face, and pulse indexes: An exploratory pilot study. *J. Altern. Complement. Med.* 26, 729–737. doi:10.1089/acm.2020.0008

Roebuck, K. A. (1999). Oxidant stress regulation of IL-8 and ICAM-1 gene expression: Differential activation and binding of the transcription factors AP-1 and NF-kappaB (review). *Int. J. Mol. Med.* 4, 223–230. doi:10.3892/ijmm.4.3.223

Roth, P., and Stanley, E. R. (1992). The biology of CSF-1 and its receptor. *Curr. Top. Microbiol. Immunol.* 181, 141–167. doi:10.1007/978-3-642-77377-8_5

Rousan, T. A., Mathew, S. T., and Thadani, U. (2017). Drug therapy for stable Angina pectoris. *Drugs* 77, 265–284. doi:10.1007/s40265-017-0691-7

Shaposhnik, Z., Wang, X., and Lusis, A. J. (2010). Arterial colony stimulating factor-1 influences atherosclerotic lesions by regulating monocyte migration and apoptosis. *J. Lipid Res.* 51, 1962–1970. doi:10.1194/jlr.M005215

Shaw, L. J., Berman, D. S., Maron, D. J., Mancini, G. B. J., Hayes, S. W., Hartigan, P. M., et al. (2008). Optimal medical therapy with or without percutaneous coronary intervention to reduce ischemic burden: Results from the clinical outcomes utilizing revascularization and aggressive drug evaluation (COURAGE) trial nuclear substudy. *Circulation* 117, 1283–1291. doi:10.1161/CIRCULATIONAHA.107.743963

Singh, S., Parihar, P., Singh, R., Singh, V. P., and Prasad, S. M. (2016). Heavy metal tolerance in plants: Role of transcriptomics, proteomics, metabolomics, and ionomics. *Front. Plant Sci.* 6, 1143. doi:10.3389/fpls.2015.01143

Taimor, G., Rakow, A., and Piper, H. M. (2001). Transcription activator protein 1 (AP-1) mediates NO-induced apoptosis of adult cardiomyocytes. *FASEB J. Off. Publ. Fed. Am. Soc. Exp. Biol.* 15, 2518–2520. doi:10.1096/fj.01-0353fje

Teng, L., Zu, Q., Li, G., Yu, T., Job, K. M., Yang, X., et al. (2016). Herbal medicines: Challenges in the modern world. Part 3. China and Japan. *Expert Rev. Clin. Pharmacol.* 9, 1225–1233. doi:10.1080/17512433.2016.1195263

Wang, J., and Xing, Y. W. (2018). Diagnostic criteria for syndrome elements of coronary heart disease angina. *J. Tradit. Chin. Med.* 59, 539–540.

Wieland, L. S., Manheimer, E., Sampson, M., Barnabas, J. P., Bouter, L. M., Cho, K., et al. (2013). Bibliometric and content analysis of the Cochrane Complementary Medicine Field specialized register of controlled trials. *Syst. Rev.* 2, 51. doi:10.1186/2046-4053-2-51

Wu, G., Zhao, J., Zhao, J., Song, N., Zheng, N., Zeng, Y., et al. (2021). Exploring biological basis of Syndrome differentiation in coronary heart disease patients with two distinct Syndromes by integrated multi-omics and network pharmacology strategy. *Chin. Med.* 16, 109. doi:10.1186/s13020-021-00521-3

Yang, X.-J., Liu, F., Feng, N., Ding, X. S., Chen, Y., Zhu, S. X., et al. (2020). Berberine attenuates cholesterol accumulation in macrophage foam cells by suppressing AP-1 activity and activation of the Nrf2/HO-1 pathway. *J. Cardiovasc. Pharmacol.* 75, 45–53. doi:10.1097/FJC.0000000000000769

Yoshiyama, M., Omura, T., TaKeuchi, K., Kim, S., Shimada, K., YamagisHi, H., et al. (2001). Angiotensin blockade inhibits increased JNKs, AP-1 and NF- kappa B DNA-binding activities in myocardial infarcted rats. *J. Mol. Cell. Cardiol.* 33, 799–810. doi:10.1006/jmcc.2001.1351

Zhang, H.-W., Zhang, T., Shen, B.-Z., Liu, M., and Liu, J.-R. (2012). Toxicological insight from AP-1 silencing study on proliferation, migration, and dedifferentiation of rat vascular smooth muscle cell. *Cardiovasc. Toxicol.* 12, 25–38. doi:10.1007/s12012-011-9135-x

Zhang, X.-J., Liu, X., Hu, M., Zhao, G. J., Sun, D., Cheng, X., et al. (2021). Pharmacological inhibition of arachidonate 12-lipoxygenase ameliorates myocardial ischemia-reperfusion injury in multiple species. *Cell Metab.* 33, 2059–2075. doi:10.1016/j.cmet.2021.08.014

Zheng, L., Mingxue, Z., Zeng, L., Yushi, Z., Yuhan, A., Yi, Y., et al. (2022). A landscape of metabonomics for intermingled phlegm and blood stasis and its concurrent syndromes in stable Angina pectoris of coronary heart disease. *Front. Cardiovasc. Med.* 9, 871142. doi:10.3389/fcvm.2022.871142

Zhou, H., Li, L., Zhao, H., Wang, Y., Du, J., Zhang, P., et al. (2019). A large-scale, multi-center urine biomarkers identification of coronary heart disease in TCM syndrome differentiation. *J. Proteome Res.* 18, 1994–2003. doi:10.1021/acs.jproteome.8b00799

Zhou, X., Li, Y., Peng, Y., Hu, J., Zhang, R., He, L., et al. (2014). Clinical phenotype network: The underlying mechanism for personalized diagnosis and treatment of traditional Chinese medicine. *Front. Med.* 8, 337–346. doi:10.1007/s11684-014-0349-8

Zhou, Y., Zhou, H., Hua, L., Hou, C., Jia, Q., Chen, J., et al. (2021). Verification of ferroptosis and pyroptosis and identification of PTGS2 as the hub gene in human coronary artery atherosclerosis. *Free Radic. Biol. Med.* 171, 55–68. doi:10.1016/j.freeradbiomed.2021.05.009

Zhuang, Y., Yu, M.-L., and Lu, S.-F. (2022). Purinergic signaling in myocardial ischemia-reperfusion injury. *Purinergic Signal.* doi:10.1007/s11302-022-09856-4

Frontiers in Pharmacology

Explores the interactions between chemicals and living beings

The most cited journal in its field, which advances access to pharmacological discoveries to prevent and treat human disease.

Discover the latest Research Topics

See more →

Frontiers

Avenue du Tribunal-Fédéral 34
1005 Lausanne, Switzerland
frontiersin.org

Contact us

+41 (0)21 510 17 00
frontiersin.org/about/contact